

# Rational design of small molecule 14-3-3 protein-protein interaction stabilizers

**Citation for published version (APA):**

Bosica, F. (2020). *Rational design of small molecule 14-3-3 protein-protein interaction stabilizers*. [Phd Thesis 1 (Research TU/e / Graduation TU/e), Biomedical Engineering]. Technische Universiteit Eindhoven.

**Document status and date:**

Published: 13/11/2020

**Document Version:**

Publisher's PDF, also known as Version of Record (includes final page, issue and volume numbers)

**Please check the document version of this publication:**

- A submitted manuscript is the version of the article upon submission and before peer-review. There can be important differences between the submitted version and the official published version of record. People interested in the research are advised to contact the author for the final version of the publication, or visit the DOI to the publisher's website.
- The final author version and the galley proof are versions of the publication after peer review.
- The final published version features the final layout of the paper including the volume, issue and page numbers.

[Link to publication](#)

**General rights**

Copyright and moral rights for the publications made accessible in the public portal are retained by the authors and/or other copyright owners and it is a condition of accessing publications that users recognise and abide by the legal requirements associated with these rights.

- Users may download and print one copy of any publication from the public portal for the purpose of private study or research.
- You may not further distribute the material or use it for any profit-making activity or commercial gain
- You may freely distribute the URL identifying the publication in the public portal.

If the publication is distributed under the terms of Article 25fa of the Dutch Copyright Act, indicated by the "Taverne" license above, please follow below link for the End User Agreement:

[www.tue.nl/taverne](http://www.tue.nl/taverne)

**Take down policy**

If you believe that this document breaches copyright please contact us at:

[openaccess@tue.nl](mailto:openaccess@tue.nl)

providing details and we will investigate your claim.

# Rational design of small molecule 14-3-3 protein-protein interaction stabilizers

PROEFSCHRIFT

ter verkrijging van de graad van doctor aan de Technische  
Universiteit Eindhoven, op gezag van de rector magnificus  
prof.dr.ir. F.P.T. Baaijens, voor een commissie  
aangewezen door het College voor Promoties, in het  
openbaar te verdedigen op vrijdag 13 november 2020 om  
11h00 uur

door

Francesco Bosica

geboren te Turijn, Italië

Dit proefschrift is goedgekeurd door de promotoren en de samenstelling van de promotiecommissie is als volgt:

voorzitter:	prof.dr. M. Merkx
1 <sup>e</sup> promotor:	dr. C. Ottmann
copromotor:	dr. G. O'Mahony (AstraZeneca)
leden:	prof.dr.ir. L. Brunsveld dr. A. Bach (University of Copenhagen) prof.dr. M. Waring (Newcastle University) prof.dr.ir. A.R.A. Palmans
adviseur:	dr. F. Eduati

*Het onderzoek of ontwerp dat in dit proefschrift wordt beschreven is uitgevoerd in overeenstemming met de TU/e Gedragscode Wetenschapsbeoefening.*





A catalogue record is available from the Eindhoven University of Technology Library  
ISBN: 978-90-386-5149-1

This research has been financially supported by the Innovative Training Network (ITN) called TASPPI (Targeted Small Molecule Stabilization of Protein-Protein Interactions), funded by the H2020 Marie Curie Actions of the European Commission under Grant Agreement 675179.

# TABLE OF CONTENTS

CHAPTER 1   Introduction .....	7
CHAPTER 2   Unravelling The Epibestatin Mystery: True Stabilizer Or Assay Artifact? .....	45
CHAPTER 3   Design Of Drug-Like Protein-Protein Interaction Stabilizers Guided By Chelation-Controlled Bioactive Conformation Stabilization .....	79
CHAPTER 4   Synthetic Strategies For The Development Of Six- Membered Bicyclic Rigid Analogues Of Pyrrolidone1 .....	151
CHAPTER 5   Optimization Of Pyrrolidone-Based Druglike Molecules For The Stabilization Of 14-3-3 Protein-Protein Interactions: Achieving Full-Length PPI Stabilization .....	177
CHAPTER 6   Epilogue.....	237
SUMMARY .....	247
BIOGRAPHY .....	251
LIST OF PUBLICATIONS .....	253
ACKNOWLEDGEMENTS.....	255



# CHAPTER 1

## Introduction

### **Abstract**

This chapter provides an introduction to the fundamental concepts of induced protein proximity, a common regulatory mechanism in biology. In fact, many biochemical processes are physiologically regulated by the selective and spatio-temporal controlled interaction between previously dispersed proteins, a concept also known as protein-protein interactions (PPIs). To understand the role of proximity, chemical inducers of proximity (CIPs) were developed. This technology platform has enabled researchers to successfully elucidate many biological dilemmas, finding applications that stretch as far as cell-based immunotherapies. Attention will be placed on CIPs that regulate pre-formed native protein complexes. Particularly, the modulation of the interactions of the 14-3-3 hub protein family will be discussed, with a major focus on their tractability with small molecules that are able to stabilize and enhance their activity.

## CHAPTER 1

### 1.1 A SHIFTING PARADIGM IN DRUG DISCOVERY

Over the last 50 years, the most common approach in drug discovery programs has been based on the “magic bullet” concept, first established by Ehrlich in 1900.<sup>1-2</sup> Most traditional drug design strategies rely on identifying a defined target and then developing a highly selective compound that binds exclusively to that target. Following this “one target, one drug” paradigm led to the development of hundreds of small molecule and biologic drugs.<sup>3</sup> Despite many success stories, this approach presents an inherent limitation: biological systems and diseases are considerably more complex than a two-variable equation (i.e. a drug and a target). Indeed, these drug modalities had allowed researchers to barely scratch the surface of the potential druggable targets, pointing the spotlight on a relatively small number of easily tractable targets, such as G-protein coupled receptors (GPCRs) and protein kinases, which represent a mere portion of the total estimated human genome.<sup>4</sup> The pharmaceutical industry, in fact, has not yet fully capitalized on the proteome information that became available with the human genome project in 2001.<sup>5</sup>

However, over the last decade, the classical view of drug action and therapeutic targets has started to change, shifting from a protein-centric view (single entity) towards a more holistic, proteome-centric view (network). The conceptual advantage of this paradigm shift is based on the fact that just as protein networks have helped researchers better understand both physiological and pathological mechanisms, they also promise to aid in the identification of novel drug targets.<sup>6</sup> Indeed, understanding the molecular basis of a disease (where and how the protein network fails) is crucial for developing an effective therapeutic strategy. Thinking in network terms expands the possibilities of drug discovery, as it may help to disentangle the mechanistic basis underlying complex pathological disorders, thus contributing to the identification of more easily druggable targets compared to the already established ones, which are known to be non-tractable through classic approaches.<sup>7</sup>

The study of protein-protein interactions (PPIs) for therapeutic purposes is still in its infancy, but holds great potential. The most recent figures reported for the “druggable genome” estimate 4479 (22%) of 20,300 protein-coding genes to be drugged or druggable,<sup>8</sup> whereas the size of the so-called human protein-protein “interactome” is around 130,000<sup>9</sup> up to 650,000<sup>10</sup> protein complexes. Needless to say, these figures make PPIs a tremendously attractive target to expand the druggable genome. PPIs have long been deemed to be undruggable for several reasons, such as larger contact surfaces areas, which are often shallow and featureless, lack of distinct recognition motifs, and high structural diversity and conformational flexibility in the unbound state.<sup>11</sup> However, one could argue that the challenges posed are very much correlated with the way of thinking that has largely permeated the small molecule drug discovery field, that is targeting the given enzyme/receptor, which carries the classical ligand binding pocket that specifically

## CHAPTER 1

evolved to accommodate small molecules.<sup>12</sup> These concerns are also very often related to inhibition of a target PPI, as inhibition is surely the predominant mode of action when it comes to modulation of classical drug targets. Conceptually, it is much easier to develop inhibitors of PPIs rather than stabilizers. While in stabilization simple binding to one of both protein partners does not necessarily correlate with a functional effect, inhibition is less demanding, as it can be accomplished by any means that effectively prevent the interaction.<sup>7</sup> However, new molecular targets require new strategic thinking.

The conceptual approach that will be discussed here is the chemical induction of PPIs, i.e. using compounds to physically bring two or more proteins in close proximity to achieve an enhanced or novel biological effect. Inspiration comes from Nature, which has evolved elegant mechanisms to regulate proximity between macromolecules to control a myriad of different biological functions. It is important to remember that despite differences in structure, source, activity and nomenclature, all the molecules that here will be discussed employ the same unifying strategy, which is altering the interactome by modulation of protein proximity.<sup>13-14</sup>

In this regard, in order to provide some clarity, a list of the common terms and their definition as intended in this chapter, is hereby provided:

- **CIP.** Chemically induced proximity or chemical inducers of proximity. Indicates the concept of bringing two (or more) molecular entities physically close together in order to elicit a biological effect. It is the most general term and applies to all of the categories below (i.e. CID, dimerizer, molecular glue, bifunctional molecule and stabilizer).
- **CID.** Chemically induced dimerization. It is the controlled dimerization (homo- or hetero-) of two proteins by means of a dimerizer. The term is used interchangeably with CIP. CID, however, does not refer to oligomerization, as more than two partners are involved in this case. The acronym is also used to refer directly to the dimerizer itself (see next definition).
- **Dimerizer (chemical inducer of dimerization, CID).** The molecular entity (for example a small molecule or antibody) responsible for inducing protein dimerization. Commonly also referred to as homo- or hetero-dimerizers, depending on the whether the molecule is symmetrical (and will therefore dimerize two identical protein monomers, forming a homodimer) or nonsymmetrical (will form a heterodimer). Synthetic dimerizers can be endowed with a linker of appropriate length that joins the two moieties together.
- **Molecular glue.** A molecule that nucleates a non-native or stabilizes a native protein-protein interaction. The term was first used by Schreiber<sup>15</sup> to describe the molecular mechanism of immunophilins, which induce the formation of a neo-complex that does not exist under natural circumstances. In this sense, the

## CHAPTER 1

compounds engage their multiple binding partners in a defined order such that the first binding event generates a new interface or induces a conformational change that promotes the binding of the second target. Many molecules discussed in this thesis such as FK506, cyclosporin, rapamycin and IMiDs fall under this category. The definition has been later extended to compounds that instead bind to pre-formed native complexes, thus stabilizing them and therefore enhancing their function. In this case, the molecule binds with only weak or undetectable affinity to the individual proteins, and usually have relatively low affinity for the complex, but still are able to elicit a strong biological effect. Examples are: brefeldin A, forskolin and fusicoccin A.

- **Bifunctional molecule.** The term designates a molecular entity that is able to bind two proteins. It is *de facto* a synonym of the term dimerizer. Indeed, bifunctional molecules can be classified in homobifunctional, if they bridge together the same protein monomers or heterobifunctional, in case proteins differ from each other. PROTACs, for example, are defined as heterobifunctional molecules.
- **Stabilizer.** A molecular glue that stabilizes and enhances a pre-formed native complex and, as such, falls within the “extended” definition of molecular glues.

### 1.2 PROTEIN-PROTEIN INTERACTIONS (PPIs) AND THE CONCEPT OF PROXIMITY

The advent of the “-omics” era (genomics, transcriptomics, proteomics) has enabled scientists to collect a great deal of information about the cell’s individual components such as proteins, DNA, RNA and small molecules.<sup>16</sup> However, systematic classification of all the molecules present in a cell (e.g. identification of the whole genome and the whole proteome) is not sufficient to fully elucidate the complex molecular machinery that governs cellular function.<sup>17</sup> In fact, a discrete biological function can with difficulty be attributed to only a single entity.<sup>18</sup> Instead, most biological processes are the result of intricate interactions among multiple cells’ components.<sup>18-19</sup> Within this framework, the protein-protein network, known as the “interactome”,<sup>16</sup> play a central role in the regulation and execution of many of the cell’s functions and, as such, its study represents a crucial aspect of the biochemical and biomolecular research.

A map of the human interactome can be visualized as a network: nodes (or hubs) represent proteins and edges correspond to the interactions between a given protein pair, where protein-protein interactions (PPIs) are defined as “*specific physical contacts between protein pairs that occur by selective molecular docking in a particular biological context*” (Figure 1.1a).<sup>20-21</sup> A complete interactome mapping will represent a major achievement in biomolecular research, as it will allow to define the

role of a protein within its PPI network, in a specific physiological or pathological context, thus aiding in the discovery of potential viable targets.<sup>17</sup>

The dynamic nature of the interactome is an important aspect when considering modulation of the interactome, as not all PPIs occur all the time at the same location under all conditions. In fact, cellular functions require the precise coordination of a large number of events to occur, and the identification of temporal and contextual signals underlying specific PPIs is pivotal for the understanding of such functions.<sup>22</sup>

Biology operates in crowded environment. It is estimated that between 5% and 40% of a cell's total volume is occupied by macromolecules.<sup>23</sup> In order to properly function in such congested landscape, a fine spatio-temporal control of protein localization is required, so nature has developed several approaches to promote meaningful interactions between proteins. Most of these methods involve the induction of protein proximity.<sup>14</sup>

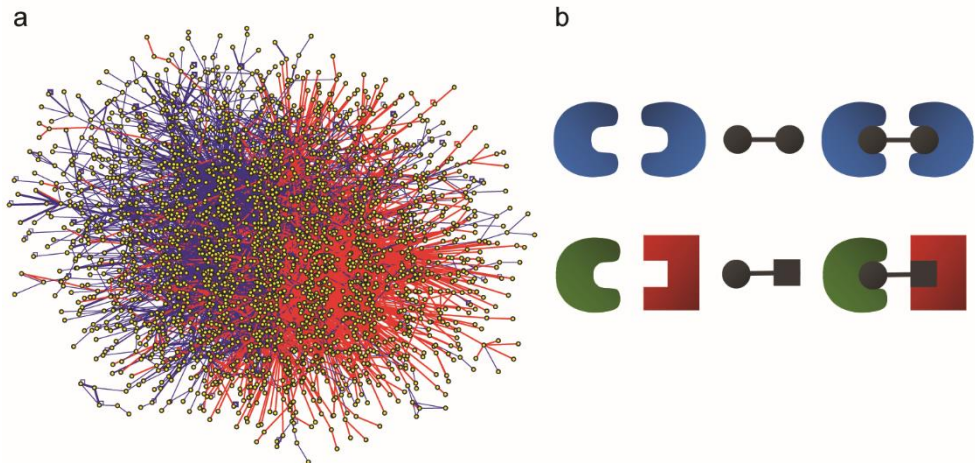


**Figure 1.1** | The human PPI network and the concept of induced protein proximity via dimerization. (a) Network graph of human interactome. Proteins are shown as yellow nodes (or hubs) and interactions are shown in red (CCSB-HI1) and blue (LCI). CCSB-HI1 (Center for Cancer Systems Biology Human Interactome version 1) and LCI (Literature-Curated Interactions) are two different databases. (b) Scheme representing the general concept of chemically induced dimerization (CID). In the presence of a homo- (top) or hetero- (bottom) bifunctional ligand, two proteins can be brought together to form a homo- or heterodimer, respectively. Figure in panel (a) was reprinted from ref.<sup>21</sup> with permission from Springer Nature.

Proximity, or the physical closeness of molecules, is a ubiquitous and essential mechanism in biology.<sup>13</sup> For example, most posttranslational modifications such as methylation, acetylation, ubiquitination instigate PPIs by recruiting target proteins to elicit a specific context-dependent function, which will determine the signalling fate of the given protein (e.g. activation, translocation or degradation).<sup>24</sup> Another common



## CHAPTER 1

phenomenon through which the cell regulates proximity is by inducing dimerization.<sup>25</sup> Dimerization (and oligomerization) can have different functional outcomes, such as improved stability, control over accessibility and specificity of active sites or increased structural complexity.<sup>25</sup> Induced dimerization or oligomerization is of particular relevance in the context of transmembrane receptor signal transduction (G-protein coupled receptors, tyrosine kinase receptors), enzyme complexes, ion channels and transcription factors. Also, different multi-protein complexes such as the proteasome, ribosome and nucleosome regulate some of their functions by self-assembling into homodimers.<sup>26</sup>

The concept of inducing proximity through dimerization (both homo- and hetero, Figure 1.1b) by the use of small molecules to study the role of PPIs *in vitro* was first

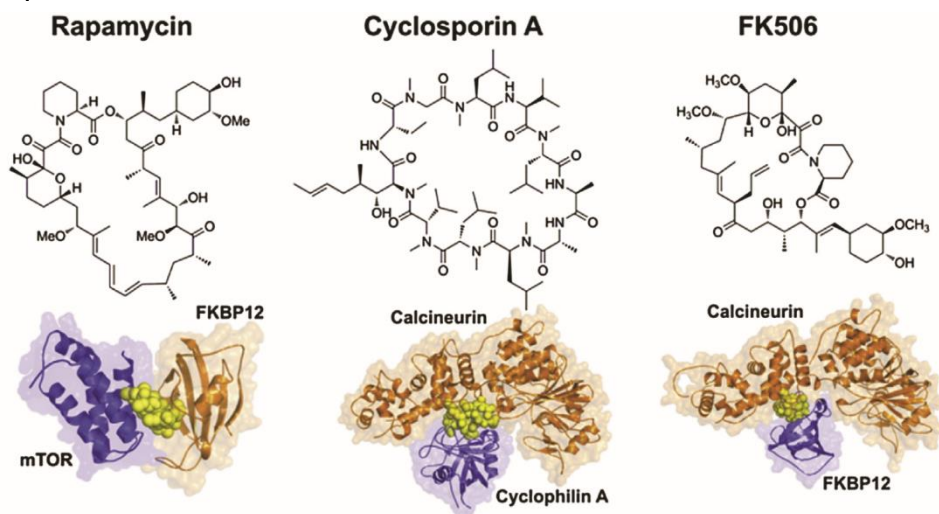


**Figure 1.2** | The first Chemical Inducers of Dimerization (CIDs) reported. Left: rapamycin (Rp, yellow) and its crystal structure in complex with mTOR (blue) and FKBP12 (orange). Centre: cyclosporin A (CsA, yellow) and relative crystal structure in complex with Cyclophilin A (CyP, blue) and calcineurin (orange). Right: FK506 (yellow) and its crystal structure in complex with FKBP12 (blue) and calcineurin (orange). Adapted from ref.<sup>31</sup>, reprinted with permission from Elsevier.

introduced in the early 1990s<sup>27</sup> (discussed in section 1.3), following the elucidation of the molecular mechanism through which immunosuppressant agents, namely FK506 (or tacrolimus), cyclosporin A (CsA) and rapamycin (Rp), exert their therapeutic effect (Figure 1.2). FK506, CsA and Rp are natural products that inhibit specific signal transduction pathways that lead to T-cells activation. To exert their activity, these molecules bind with high affinity to cytoplasmic receptors termed immunophilins (immunosuppressant binding proteins).<sup>28</sup> The CsA-binding receptor is cyclophilin (CyP), while the receptor for the structurally-related FK506 and Rp is is

## CHAPTER 1

FKBP12 (12 kDa FK506-binding protein). The newly-formed complexes of CyP/CsA or FKBP12/FK506 then bind to the enzyme calcineurin and block its phosphatase activity.<sup>29-30</sup> This event prevents the dephosphorylation and subsequent translocation to the nucleus of the cytoplasmic nuclear factor of activated T-cells (NF-ATc), which inhibits interleukin-2 (IL-2) associated gene transcription.

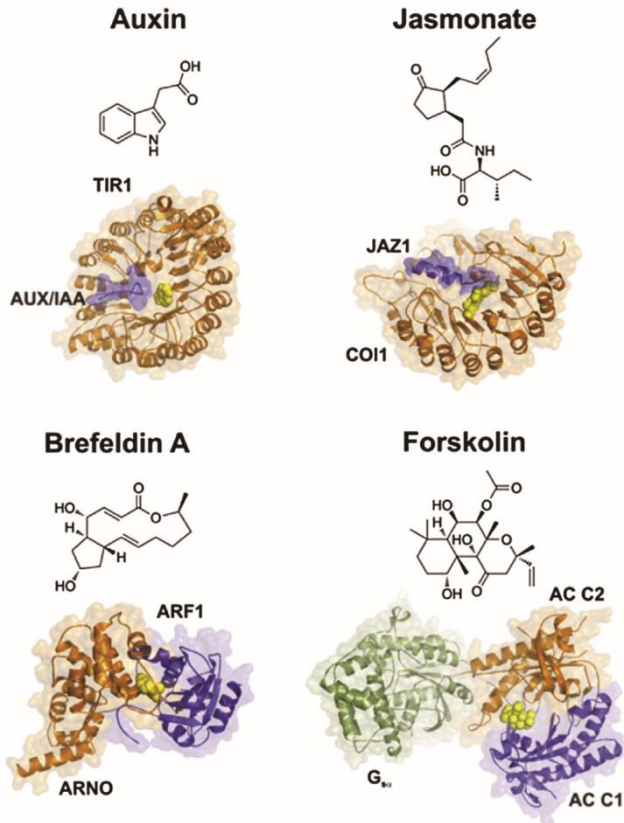


**Figure 1.3** | Chemical structures and X-ray ternary complexes of other natural compounds acting as molecular glues. Top left: auxin (IAA, yellow) in complex with TIR1 (orange) and AUX/IAA (blue). Top right: jasonate (JSS, yellow) and its crystal structure with COI1 (orange) and JAZ1 (blue). Bottom left: brefeldin A (BFA, yellow) and relative crystal structure with ARF1 (blue) and ARNO (orange). Bottom right: forskolin (FSK, yellow) stabilizing the complex between adenylyl cyclase subunits C1 (blue) and C2 (orange), with the stimulatory G protein subunit G<sub>s</sub>α shown in green. Adapted from ref.<sup>31</sup>, reprinted with permission from Elsevier.

Consequently, T-cells do not produce IL-2, which is necessary for full T-cell activation.<sup>32</sup> On the other hand, the complex Rp/FKBP12 does not target calcineurin but the FK506-rapamycin binding (FRB) domain of the serine-threonine protein kinase mTOR (mammalian target of rapamycin). mTOR is a component of two distinct complexes, mTOR complex 1 (mTORC1) and 2 (mTORC2). mTORC1 is the

## CHAPTER 1

major downstream component of the PI3K (phosphatidylinositol 3-kinase), and AKT (protein kinase B) pathway that controls cell growth and proliferation. Rp in complex with FKBP12, specifically blocks mTORC1 activity and inhibits cell growth.<sup>33-34</sup> Although it was initially thought that Rp only targets mTORC1 selectively, recent studies showed that chronic exposure to Rp can also inhibit mTORC2 in some cell types.<sup>35</sup> Despite similar modes of action, the recruitment and subsequent inhibition of different targets has profound influence on the therapeutic effect of these drugs. The ubiquitous tissue distribution and physiological role of calcineurin is the primary liability in the mechanism of action of CsA and FK506. In fact, they are associated with neurotoxicity and nephrotoxicity, thus limiting their use to immunotherapy.<sup>36</sup> Conversely, as these side effects have not been observed with Rp, it is also used in treating various cancers, due to its inhibitory effect on cell proliferation.<sup>33</sup> The elucidation of the mechanism of action of FK506, CsA and Rp suggested a new paradigm for the regulation of intracellular signalling, providing the first demonstration that it was possible to achieve a biological effect by bringing two proteins into close proximity. These natural products, often referred to as “molecular glues”, fall into a new class of “chemical inducers of dimerization” (CIDs).<sup>37</sup>

Following FK506, CsA and Rp, many other natural products were found to act as molecular glues, by promoting or enhancing the interaction between proteins. Among them, it is worth mentioning the plant hormones auxin (or indole-3-acetic acid, IAA)<sup>38-39</sup> and jasmonate (JS)<sup>40</sup> and the cell biology tool compounds brefeldin A (BFA)<sup>41</sup> and forskolin (FSK).<sup>42</sup> IAA acts by promoting the degradation of the Aux/IAA transcriptional repressors through the action of the ubiquitin protein ligase SCF<sup>TIR1</sup>. TIR1 (Transport Inhibitor Response 1) is a F-box protein that acts as an IAA receptor within the SFC ubiquitin ligase complex. Interaction of IAA with TIR1 creates a new binding interface that promotes the subsequent binding of Aux/IAA proteins (Figure 1.3, top left).<sup>39</sup> Similarly, JS binds to the substrate-recruiting F-box protein COI1 (Coronatine Insensitive 1), thus forming a new interface that allows recruitment and consequent degradation of the transcriptional repressor JAZ (Figure 1.3, top right). BFA is used for the analysis of membrane trafficking by stabilizing the complex of the small G protein ARF1 with the Sec7 domain of its guanine exchange factor ARF-GEF ARNO (Figure 1.3, bottom left).<sup>43</sup> FSK increases intracellular cAMP levels by stabilizing the heterodimer between the adenylyl cyclase subunits C1 and C2, thus increasing adenylyl cyclase enzymatic activity (Figure 1.3, bottom right).<sup>44</sup> Interestingly, both BFA and FSK bind to a preformed native complex and stabilize it, rather than promoting the formation of a neo-complex, such as the case for the aforementioned immunosuppressants and plant hormones.

## CHAPTER 1

### 1.3 CID SYSTEMS AS BIOLOGICAL TOOL TO STUDY PPIs

The scope of biology that can be modulated with natural products is, however, limited. In response, researchers have investigated whether proximity-based regulation of protein activity could be extended to synthetic compounds and non-natural PPIs.<sup>14</sup>

A typical CID system exploits a synthetic molecule to reproduce the ability of natural systems to use proximity as an activation switch. Initially, one protein component is localized and anchored at a specific cellular location (P1, Figure 1.4a), whereas the other component (P2) is fused (by protein engineering) to a protein of interest (POI). The small molecule, known as dimerizer (D), acts by bridging two proteins together (P1 and P2) and can be used to increase the effective concentration of two previously dispersed proteins, thus causing chemically induced proximity (CIP).<sup>45-46</sup>

CIDs have allowed researchers to probe the so-called “signalling paradox” or “black box”, that is, the gap between cell-membrane receptors and the nucleus and how the cell is able to switch between a very large number of signalling pathways using only a limited set of proteins and signalling molecules.<sup>46-47</sup> The key to unlock this black box lies in the ability of the cell to activate specific pathways, in a confined location, for a well-defined amount of time. CIDs enabled researchers to reproduce such localized events. Indeed, one of the main distinguishing features of small-molecule induced proximity systems relies on the ability to initiate a process mid-pathway rather than at the initial stage of a signalling cascade. The effect occurs rapidly, typically in the timescale of seconds to minutes. This provides minute-by-minute kinetic analysis, allowing a precise cause/effect correlation of a specific biochemical event to be established, without concern for delayed toxic effects of the dimerizer on much slower processes such as proliferation or transcription.<sup>13</sup>

As anticipated in section 1.2, the landmark study conducted by Crabtree and co-workers in 1993,<sup>27</sup> set the scene for the use of small molecules to study the role of PPIs *in vitro* was first introduced in by a landmark study by Crabtree and coworkers in 1993.<sup>27</sup> In their experiment, they used a non-toxic derivative of the immunosuppressant drug FK506, namely FK1012 (Figure 1.4b), as dimerizer. FK1012, a dimeric variant of FK506, was used to induce dimerization of the fusion protein FKBP/T-cell receptor (TCR)  $\zeta$ -chain, resulting in the activation of the signal transduction cascade (Figure 1.4c and d). From this pioneering work, the CID strategy was established as a versatile tool to investigate biological functions that were up to then otherwise difficult to study.

The FK1012-promoted homodimerization of FKBP12 proved to be a versatile CID system and was used for a number of investigative applications.<sup>48</sup> In parallel, the use

## CHAPTER 1

of heterodimerizers was also implemented. Among them we find FKCsA, a FK506-CsA fusion molecule (Figure 1.5, top), that brings together FKBP12 and CyP<sup>49</sup> and

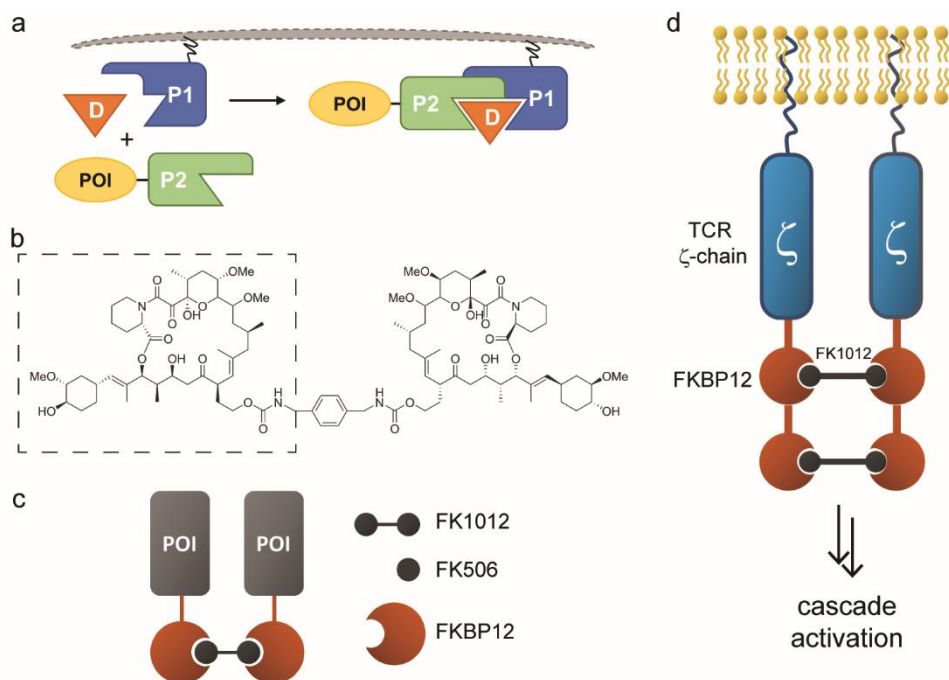


**Figure 1.4** | Expanding the CID toolkit: the first synthetic CID. (a) Schematic representation of the principles of CID applied to the study of PPIs. One protein (P1, blue) is localized at a precise cellular location, while the other (P2, green) is fused to the desired POI (yellow). In the presence of a dimerizer (D, orange) P1 and P2 are brought together, thus causing chemically induced proximity (CIP). (b) Chemical structure of FK1012, the first reported synthetic small molecule dimerizer, derived from FK506 (FK506 structure highlighted by dashed square). (c) Scheme illustrating the CID system developed by Schreiber, Crabtree and co-workers, based on FKBP12 (in red) protein fused to a POI (in grey) and FK1012 as dimeric variant of FK506. (d) Model for intracellular activation of the TCR-mediated signaling pathway. FKBP12 is fused to the  $\zeta$ -chain of the chimeric TCR and addition of FK1012 induces dimerization and subsequent cascade activation.

a number of Rp derivatives, known as “rapalogs”, which bridge FKBP and FRB. These heterodimerizers were used to investigate a myriad of different mechanisms, including glycosylation,<sup>50</sup> GTPase function,<sup>51</sup> caspase activation<sup>52</sup> and protein splicing.<sup>13, 48, 53</sup>

In the effort to expand the CIDs chemical repertoire and improve the biocompatibility (*i.e.* reducing off-target effects due to, for example, the dimerizer binding to naturally occurring proteins), non FKBP-based CIDs were also developed and found good use for applications both *in vitro* and *in vivo*.<sup>54</sup> The methotrexate (MTX) – dihydrofolate reductase (DHFR) is one of them, where MTX was used either

## CHAPTER 1

as homo- (*bisMTX1*) or hetero- bifunctional molecule and DHFR was the targeted protein (Figure 1.5, middle).<sup>55</sup> Another one exploited the ability of the non-toxic natural product coumermycin to dimerize bacterial DNA gyrase B (GyrB) domains due to its natural dimeric form (Figure 1.5 bottom). The use of this system provided, for example, first proof of Raf-1 activation independent of Ras. A chimeric Raf-1-

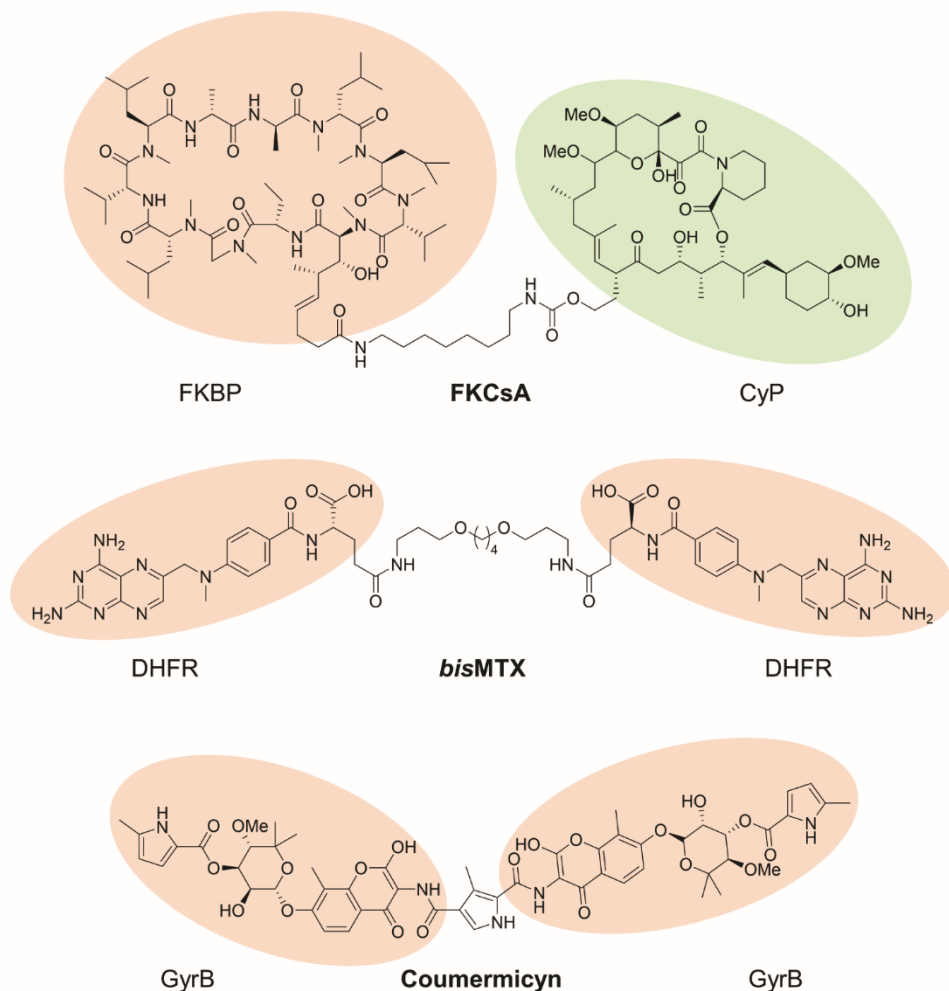


**Figure 1.5** | Examples of bifunctional molecules used as CIDs. Reported are the chemical structures of FKCsA, *bisMTX* and coumermycin, which cause the dimerization of FKBP12-CyP, DHFR and GyrB proteins. Colored shapes represent regions of each molecule binding to the corresponding fusion protein.

GyrB fusion protein on one side and a membrane-anchored form of GyrB on the other were initially generated and exposure to coumermycin alone was sufficient to activate Raf-1, in the absence of the canonical Ras-dependent membrane

## CHAPTER 1

localization.<sup>56</sup> Coumermycin-based CID systems also helped in elucidating several signaling pathways. In fact, CIDs offer a more specific control compared to traditional receptor activation-based techniques, which usually tend to feed into multiple pathways. For example, the coumermycin-based system has been used to study the mechanism of Janus kinase 2 (Jak2) activation and its role in signal transduction. For this, the authors envisaged a GyrB-Jak2 fusion proteins dimerization system. The addition of coumermycin induced GyrB-Jak2 dimerization and activation by GyrB-Jak2 autophosphorylation, which resulted in specific activation of Stat5, a member of the Stat family, known downstream substrates of Jak2.<sup>57</sup>

The aforementioned cases are examples of CIP systems that rely on fusion proteins to function. This strategy has clearly proven to be a valuable investigational tool, allowing to decipher previously unexplained biological quandaries. However, despite representing a valid proof of concept, protein engineering is often undesirable or impractical, especially when developing drug therapies. In this regard, the appeal of bifunctional small molecules that can exert their effect without genetic manipulation is based on the fact that we cannot readily genetically manipulate the cells of the patient. Researchers then shifted their attention towards the use of native proteins where the desired molecular glue is required to directly bind the native protein instead of a tagged fusion protein. On the one hand, this approach poses some major challenges: for native proteins, the risk of inhibiting their endogenous function must be considered. Reciprocally, sequestration of the CIP molecule by intrinsic proteins may prevent its activity. Although these factors are not unique to native proteins, in this context they have higher relevance and must be taken into account. As a consequence of this, each system will require extensive chemical optimization and the resulting CIPs will not be applicable to other targets. On the other hand, however, targeting native proteins is more likely to be physiologically and therapeutically relevant compared to proteins not found in humans. Also, the need for specificity will probably require rational design of small molecule-like compounds, thus removing the need for natural products, which are difficult to synthesize.<sup>14, 48, 54</sup>

### 1.4 EXPANDED CIP TOOLBOX: TOWARDS THERAPEUTIC APPLICATIONS

The natural product geldanamycin (GDM, Figure 1.6a) is one of the earliest examples of chemically induced proximity of native proteins. It targets the estrogen receptor (ER) by conferring selectivity to a compound that was previously known for its non-specific mode of action. GDM is a potent antitumor agent that binds to and inhibits the molecular chaperone heat shock protein 90 (HSP90), thus blocking the stabilizing activity of HSP90 towards key proteins involved in cell cycle regulation, apoptosis, oncogenesis, and cell growth and ultimately promoting their ubiquitin-

## CHAPTER 1

dependent proteasomal degradation.<sup>58-59</sup> ER and the androgen receptor (AR) are, for example, clients of HSP90. The pharmaceutical potential of GDM is, however, limited by its non-selective toxicity. A way to directly harness GDM activity towards a particular target was devised by Danishefsky and co-workers, who developed a series of geldanamycin-estradiol (GDM-E2) hybrids able to selectively induce the degradation of ER (Figure 1.6b).<sup>60</sup> A similar approach was then used with geldanamycin-testosterone hybrids to target AR for degradation.<sup>61</sup> Both ER and AR are well-known drivers of oncogenic signaling and have long been targeted for therapeutic purposes.<sup>62-63</sup> One of the strategies employed is, indeed, receptor downregulation through degradation, as represented by the successful drug classes known as selective estrogen receptor degraders (SERDs)<sup>64</sup> and selective androgen receptor degraders (SARDs)<sup>65</sup>, respectively.

Simultaneously, other groups attempted to achieve induced protein degradation by means of inhibitors that would target HSP90. Much of the excitement stemmed

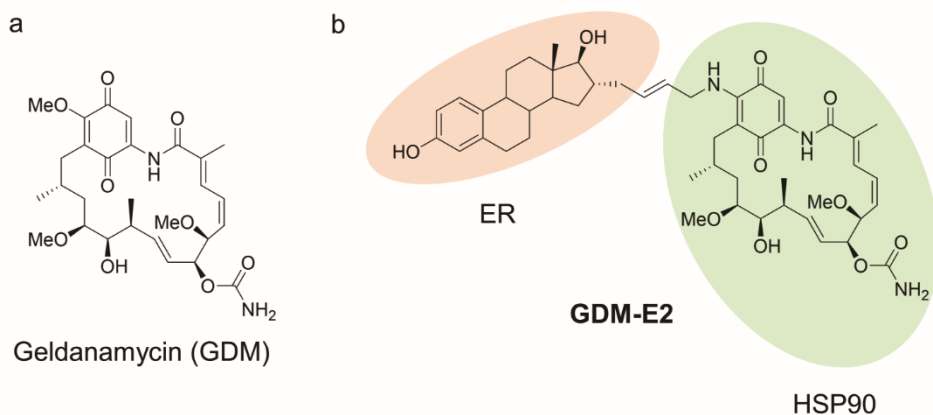


**Figure 1.6** | The geldanamycin (GDM) CID system. (a) Chemical structure of GDM. (b) Chemical structure of the GDM-E2 compound, a GDM-E2 heterodimerizer. Colored shapes represent regions of each molecule binding to the corresponding fusion protein.

from the observation that HSP90 is overexpressed in many cancers and that it is more sensitive to inhibition due to an overactive conformation only adopted in cancer cells. The first clinical candidate targeting HSP90 was released in 1999, and many others followed over the years. However, as of today, still none of them have been approved because of poor pharmacological properties and probable lack of specificity due to the large number of client partners. As a consequence, a more selective and predictable approach was desired.<sup>66</sup>

Protein degradation is a process that occurs physiologically in cells as part of maintain cellular homeostasis. One of the major pathways of protein degradation is



## CHAPTER 1

ubiquitin-dependent proteasomal proteolysis. Ubiquitination, the process of attaching ubiquitin units to lysine residues of the substrate proteins, is a posttranslational modification performed by three classes of enzymes that act

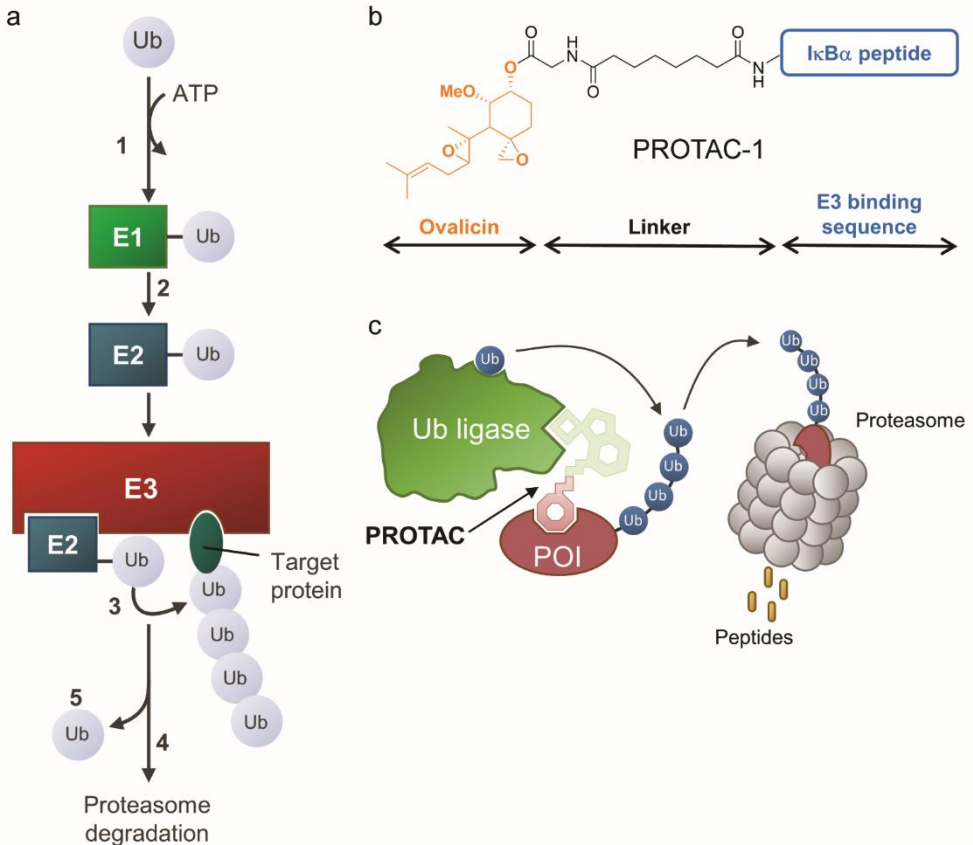


**Figure 1.7** | The ubiquitin-proteasome system and the proteolysis-targeting chimaera (PROTAC) technology (a) Main enzymatic steps of the ubiquitin-proteasome system. Ubiquitin (Ub) is activated by the ubiquitin-activating enzymes (E1, 1), followed by its transfer to a ubiquitin-conjugating enzyme (E2, 2). Both E2 and the target protein bind to a specific ubiquitin-protein ligase (E3) and the activated Ub is then transferred to the protein substrate (3). Subsequent rounds of ubiquitinylation generate a polyubiquitin chain that functions as a signal for the proteasome to induce promote substrate degradation (4). Reusable ubiquitin is released by deubiquitylating enzymes (5). (b) The first PROTAC, PROTAC-1 consisting of MetAP2 covalent inhibitor ovalicin linked via a linker to the decapeptide of IκBα that is recognized by SCF<sup>β-TRCP</sup>. (c) Scheme illustrating the principle of PROTAC function. PROTACs are heterobifunctional molecules comprising, on one end, an E3 ligand linked to a substrate protein of interest (POI) ligand. The chemical induced proximity between the E3 and the POI results in ubiquitination and proteasomal degradation of the latter.

sequentially: ubiquitin-activating enzymes (E1), ubiquitin-conjugating enzymes (E2) and ubiquitin-protein ligases (E3). E3 ligases bind directly to the substrate and hence confer the specificity of ubiquitination. Subsequent rounds of ubiquitination result in

## CHAPTER 1

the formation of a polyubiquitin chain which is then recognized by the proteasome, ultimately leading to protein degradation (Figure 1.7a).<sup>54, 66-67</sup> As E3 ligases must be able to interact with a high number of different substrates, it is not surprising that more than 600 E3s have been identified in the mammalian genome so far,<sup>68</sup> compared to only two E1s and about 40 E2s.<sup>69-70</sup>

The idea of harnessing the ubiquitin-proteasome machinery to rapidly and precisely modulate the cellular fate of proteins was initially reported by the Deshaies and Sakamoto laboratories in 2001, where the first so-called PROTeolysis-TARgeting Chimera (PROTAC) was developed.<sup>71</sup> In this proof-of-concept study, they sought to degrade methionine aminopeptidase-2 (MetAP-2) by recruiting the SCF <sup>$\beta$ -TRCP</sup> E3 complex (Skp-Cullin-F-box containing complex, where  $\beta$ -TRCP, beta-transducin repeat-containing protein, is a F-box protein). In order to do that, they designed a heterobifunctional molecule, PROTAC-1 (Figure 1.7b), consisting of a conjugate of ovalicin, a known binder of MetAP-2 and the E3 ligase binding sequence of IKK $\alpha$  joined by a linker moiety. Notably, MetAP-2 is not known to be ubiquitinated or substrate for any SFC complex, thus showing that degradation MetAP-2 is induced in a PROTAC-1-dependent manner.

The term PROTAC now designates any heterobifunctional molecule in which one end binds to the protein of interest (POI) and the other end is a recognition unit that recruits a specific E3 ligase. The two ends are connected to each other by means of a linker of variable length and nature. Functionally, PROTACs promote co-localization of a POI and a E3 ubiquitin ligase, therefore inducing the formation of a novel PPI with a new function (Figure 1.7c). This gain-of-function type of interaction can be considered to be a case of chemically induced proximity.

Arguably, validation of the PROTAC approach as potential therapeutic strategy came as a consequence of the elucidation of the mechanism of action of the immunomodulatory imide drug (IMiD) thalidomide and the closely related lenalidomide and pomalidomide (Figure 1.8a).<sup>66, 72</sup> Thalidomide was first marketed in 1957 to treat morning sickness in pregnant women but was then withdrawn after it was shown to cause birth defects.<sup>73</sup> It was later repurposed for treatment of multiple myeloma,<sup>74</sup> which later stimulated the development of lenalidomide and pomalidomide.<sup>75</sup> However, despite their widespread use, their MoA remained elusive for many years.

In 2010, a seminal study set out the basis for the elucidation of their mechanism of action, showing that thalidomide binds the Cereblon (CRBN) subunit of the E3 ubiquitin ligase complex with DDB1 (damaged DNA binding protein 1), Cul4A (Cullin-4A) and ROC1 (regulator of cullins 1) and subsequently inhibits the E3 function.<sup>76</sup> This observation allowed researchers to unravel the mechanistic basis underlying the effect of IMiDs against multiple myeloma. They act as molecular glues, inducing recruitment of the IKAROS family transcription factors IKZF1 and IKZF3 (which are



## CHAPTER 1

pathway for subsequent protein degradation.<sup>83</sup> Concomitantly, it was shown that delivery of proteins to the lysosome could be achieved also through the activation of autophagy by means of autophagy-targeting chimeras (AUTACs).<sup>84</sup> Finally, the concept of proximity-induced degradation could be extended beyond proteins by showing that ribonuclease-targeting chimeras (RIBOTACs) could eliminate a specific RNA by tethering it to a RNase.<sup>85-86</sup>

### 1.5 CIP AND IMMUNOTHERAPY APPLICATIONS

Moving outside the cell, CIP has also found wide application in immunotherapy. Multiple strategies can be used to hijack and redirect the immune system towards the desired target cell and, although they come under different names and formats, the governing principle remains the same: use bifunctional molecules to bring two separate entities together in a spatiotemporally controlled fashion.

One of the strategies encompasses the use of bispecific antibodies (BsAbs). BsAbs have a wide range of possible applications and uses but, in the context of immunotherapy, they redirect the cytotoxic activity of effector T cells to specifically eliminate tumor cells. In this approach, T cells are physically linked to tumor cells by means of a bifunctional antibody consisting of, on one side, a T cell-binding domain and, on the other side, a tumor-associated antigen (TAA), a domain that binds an antigen expressed on the surface of the cancer cell (Figure 1.9a).<sup>87-88</sup> This dual targeting concept led to the approval of two BsAbs, catumaxomab (now withdrawn) and blinatumomab, with many others currently at clinical stage.<sup>51-52</sup>

Another strategy is known as antibody-recruiting small molecules (ARMs)<sup>89</sup> and relies on the ability of synthetic, bifunctional ligands to induce endogenous antibody recruitment and binding to disease-relevant proteins, cells or organisms (Figure 1.9b). An ARM possesses an antibody-binding terminus, which recognizes the anti-hapten antibody and a target-binding terminus, which associates with the surface-exposed receptors. By inducing proximity of the antibody and the target-bearing cell, the ARM promotes the formation of a ternary complex which can subsequently elicit an immune effector response.<sup>89-90</sup> The original concept of ARMs has evolved during the years. In fact, great effort was put on trying to directly engage innate immune receptors such as the Fc receptors (Fc = fragment crystallizable, the antibody portion responsible for binding to the corresponding receptors present on immune cells), thus bypassing the need for antibody recruitment with what would be, essentially, a small molecule antibody mimic. This idea led to the development of the so-called synthetic antibody mimics (SyAMs).

SyAMs are bifunctional ligands that can bind both to a surface membrane antigen (overexpressed in a pathological context) and to a receptor present on immune cells, the Fc gamma receptors (Fc $\gamma$ Rs) (Figure 1.9c).<sup>91</sup> The advantages of SyAMs over

## CHAPTER 1

classic antibody therapies rely on their much smaller size (about 5% MW of an antibody) which potentially favors better tumor penetration, modular nature (enabling a quick redevelopment in the targeting of different antigens), and inherent simplification of production, purification and storage compared to biologics.<sup>90</sup>

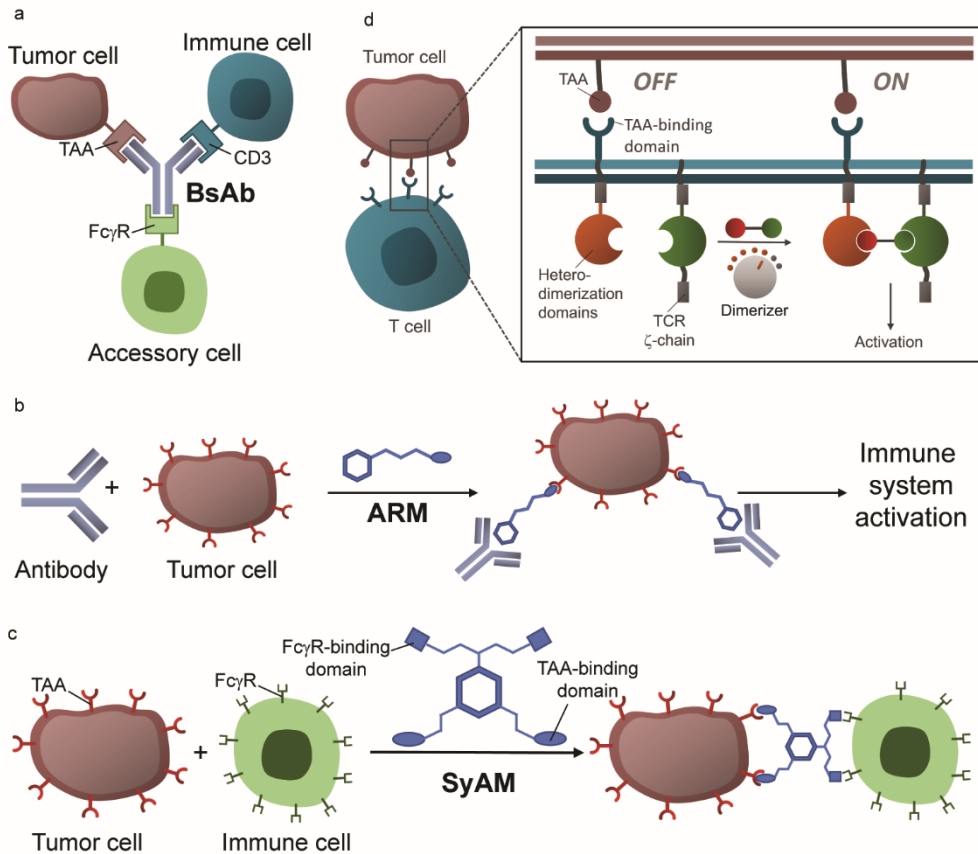


**Figure 1.9** | CIP strategy applied to immune cell therapies. (a) Bispecific antibodies (BsAbs) bind two different antigens: one located on the tumor cell (TAA) and the other on a T-cell (CD3 receptor complex), thus increasing their proximity. Concomitant recruitment of immune system accessory cells (e.g. natural-killer cells, macrophages) via their Fc $\gamma$  receptor, highly increase the immune response. (b) Antibody-recruiting small molecules (ARMs) are heterobifunctional small molecules designed to recognize on one end a disease-relevant target, while the other recruits and binds to antibody proteins, therefore triggering an immune response. (c) Synthetic antibody mimics (SyAMs) are heterobifunctional molecules that can bind to both a TAA and an effector domain present in immune cells such as the Fc $\gamma$ R, thus inducing selective degradation of the target cancer cell. (d) CAR-T cell safety switches rely on a binary input system, a TAA and a small molecule dimerizer. The intracellular portion of the CAR is split in two parts, each of them fused to a dimerizing domain. In the absence of dimerizer, the T cell cannot function, even in the presence of the appropriate TAA. Upon administration of dimerizer (and in the presence of TAA), the CAR regains function, leading to activation of the T-cell signaling cascade.

## CHAPTER 1

Cell-based therapies have shown encouraging results as treatment modality for diseases such as cancer<sup>92-93</sup> and autoimmunity.<sup>94</sup> Another field where CIP found application is in the activity control of T cells engineered to express chimeric antigen receptors (CARs), known as CAR T cells. Particularly, CAR T cells have proven to be effective against refractory B cell cancers in clinical trials.<sup>95</sup> Despite this promise, however, significant challenges persist, mainly related to off-target toxicity that eventually leads to killing of non-tumor cells. To mitigate these adverse effects, one of the approaches that have been pursued is to use small molecules as “safety switches”. The protein engineering goal here was to devise a split-input system, i.e. a CAR that requires two distinct inputs, a TAA and a small molecule, for T cell activation, that would allow regulation of CAR T cell activity in a temporal, titratable and reversible fashion.<sup>96</sup> To achieve this, a split receptor design was proposed, that is splitting the receptor into two separate subunits: the first, extracellular, features a TAA-binding domain while the second, intracellular, entails a downstream T-cell signaling element from the TCR  $\zeta$ -chain, which normally triggers the cascade of T-cell activation. Both subunits are fused to heterodimerization domains that can coalesce in the presence of an appropriate safety switch (Figure 1.9d). These safety switches are simply dimerizers that act via CIP, thus promoting chemically induced dimerization of the two CAR subunits. Unlike conventional CIP systems, however, here the addition of the safety switch is a necessary but not sufficient condition for T-cell activation, as it only acts as a priming factor, that is a precondition for antigen-triggered activation.<sup>96-97</sup> Notably, the authors made use of the well-known FKBP/FRB dimerization system (described in section 1.2), using a rapalog as inducer of dimerization.<sup>96</sup> A similar approach envisioned the use of a FKBP-caspase-9 fusion protein system, using another rapalog as safety switch to induce elimination of CAR-T cells in a dose-dependent manner.<sup>98</sup>

An extension of this principle is to use switches acting intercellularly, where the specificity of CAR T cells can be redirected by means of a bifunctional small molecule that acts as CIP. Unlike the previous approach, the extracellular domain of such CAR does not bind directly to any specific TAA, thus making these CAR T cells essentially inactive in the presence of healthy and cancer cells.<sup>99</sup> However, in the presence of the appropriate switch, that is specific for both the TAA and the CAR, the CAR T cell is redirected to target a specific cancer cell via induced proximity. These safety switches make the CAR T cell activity strictly dependent on the formation of a ternary complex between the CAR T cell, the switch, and tumor antigen. Therefore, titration or removal of the switch molecule can control or terminate CAR T cell response, respectively. It is worth pointing out that, as the CAR does not interact directly with the TAA on the cancer cell, this approach potentially enables the targeting of multiple TAAs with a single, “universal” CAR T cell.<sup>97, 99</sup>

## CHAPTER 1

### 1.6 CIP OF NATIVE PROTEIN COMPLEXES

The previous paragraphs have highlighted how cells control many of their functions by inducing proximity and how this simple and rather elegant concept can be applied to solve biological dilemmas as well as therapeutic challenges. As mentioned earlier, each of the molecules that have been discussed so far, fall under the category of chemical inducers of proximity. A peculiar case, however, is represented by BFA and FSK (Figure 1.3). In fact, these molecules act by stabilizing a preformed native PPI complex and thus increasing the binding affinity of the interaction partners. Such molecules have only very weak or null affinity for the individual protein components of the complex, but higher affinity for a binary complex formed from them. Moreover, despite showing marked physiological activity, their binding affinities for the binary complex are relatively low ( $EC_{50} > 10 \mu\text{M}$ ), suggesting that the uncompetitive nature of the interaction might play an important role.<sup>31</sup> Despite being also termed molecular glues, their mode of action is different compared to other molecular glues such as immunosuppressants FK506, CsA and Rp or IMiDs that first bind to one of the two proteins, thereby creating or modifying an interaction surface which then promotes the association with the second protein, and contrasts with bifunctional molecules like PROTACS, which bind individually to each protein partner with high affinity. The concept behind compounds like immunosuppressants or IMiDs is promotion of the formation of a neo-complex that does not exist under natural conditions, thus inducing a gain-of-function that results in a new functional effect that the individual partners do not possess.

As already widely discussed in the previous sections, the artificially induced formation of a neo-complex is a powerful tool for manipulating cellular functions. At the same time, exploiting what nature has already provided, that is stabilize native PPI complexes already endowed of a functional response, also represents an attractive opportunity for new potential therapeutic applications.

In this regard, our research has focused on the study of a particular class of PPIs, that is the interactome of the 14-3-3 proteins as subject for small molecule PPI stabilization.

### 1.7 14-3-3 PROTEINS AS PLATFORM FOR THE STUDY OF PPI STABILIZATION

14-3-3 proteins are a family of highly conserved adapter proteins which bind to phosphorylated client proteins that are found in all eukaryotic species.<sup>100</sup> First discovered in brain tissue in the late 1960s, the name was given based on the migration pattern following two-dimensional DEAE (diethylaminoethyl)-cellulose chromatography (14<sup>th</sup> fraction) and subsequent starch gel electrophoresis (fraction 3.3).<sup>101</sup> There are 7 known isoforms in mammals –  $\alpha/\beta$ ,  $\epsilon$ ,  $\eta$ ,  $\delta/\zeta$ ,  $\tau$  (also called  $\theta$ ),

## CHAPTER 1

$\gamma$  and  $\sigma$ , with  $\alpha$  and  $\delta$  representing the phosphorylated versions of  $\beta$  and  $\gamma$ , respectively.<sup>102-104</sup> Although each isoform is encoded by a separate gene, they all share a high degree of homology (70-90%) and, in general, are expressed ubiquitously.<sup>102, 105</sup>

14-3-3 proteins have a high tendency to form both homo- and hetero-dimers, with some isoform-specific preferences.<sup>106-108</sup> Each monomeric unit consists of nine anti-parallel  $\alpha$ -helices (H1-H9), organized into a N-terminal and C-terminal domain (Figure 1.10a). The latter represents the region where maximal sequence variability occurs<sup>107</sup>, while the most highly conserved regions are mainly found in the largely negatively charged channel that is formed by the two 14-3-3 subunits (Figure 1.10b).<sup>107, 109</sup> This channel is responsible for the recognition of consensus binding motifs on target proteins. In particular, the side chains of Arg56, Arg129, Tyr130, and Lys49 of the conserved amphipathic groove form the primary phospho-accepting pocket (Figure 1.11).<sup>107, 110</sup>

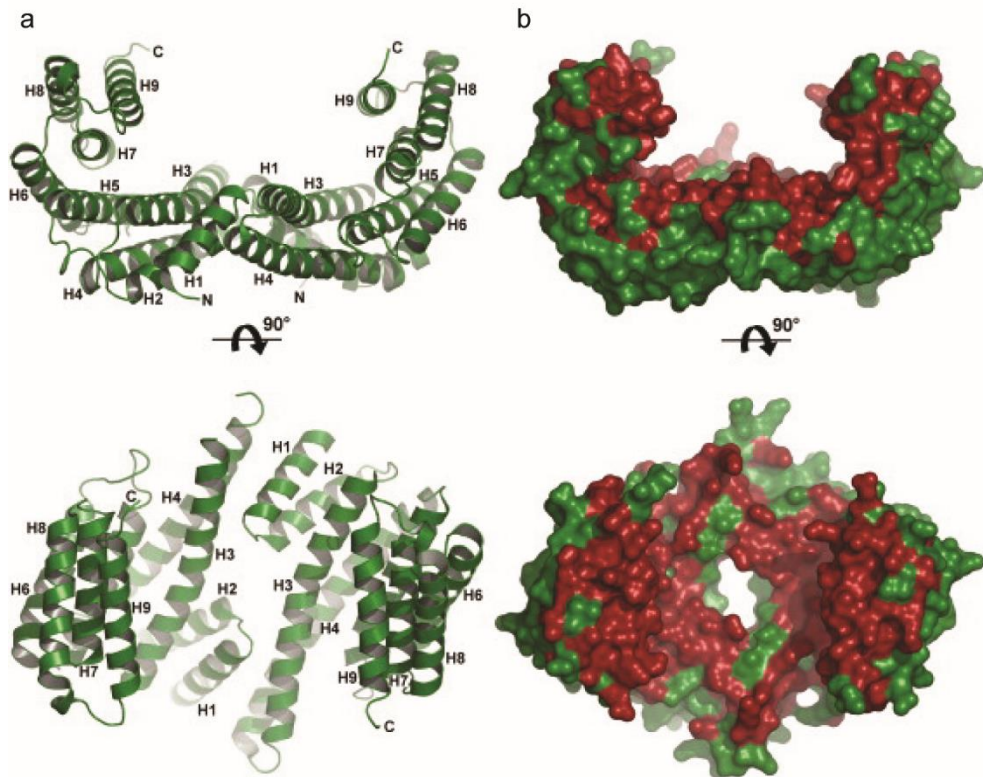


**Figure 1.10** | Crystal structure of the 14-3-3 protein (human  $\zeta$  isoform, PDB: 1QJB [29]). (a) Front and top view, ribbon representation. (b) Front and top view, surface representation. Residues that are totally conserved among all seven human isoforms are colored in red. Reprinted from ref.<sup>107</sup> with permission from Elsevier.



## CHAPTER 1

To date, three distinct binding motifs have been identified, all having a phosphorylated serine or threonine residue as common denominator: mode I (-RSXpS/TXP-), mode II (RXXXpS/TXP) (Figure 1.11a) and the C-terminal mode III (-pS/TX<sub>1-2</sub>-COOH, Figure 1.11b), where X is any amino acid (except for mode III where X is not a proline).<sup>100, 111</sup> The observation that partner protein phosphorylation is required for 14-3-3 binding is true for the vast majority of client partners. However, it is worth noting that cases of phosphorylation-independent binding have been reported (Figure 1.11c).<sup>112-114</sup> Through these motifs, 14-3-3 proteins are estimated to bind to more than 200 partners.<sup>115</sup> The 14-3-3 interactome has been shown to be involved in a myriad of biological processes such as cell cycle regulation, signalling, metabolism, protein synthesis, nucleic acid binding, chromatin structure, protein folding, proteolysis, nucleolar function, and nuclear transport.<sup>116-118</sup>

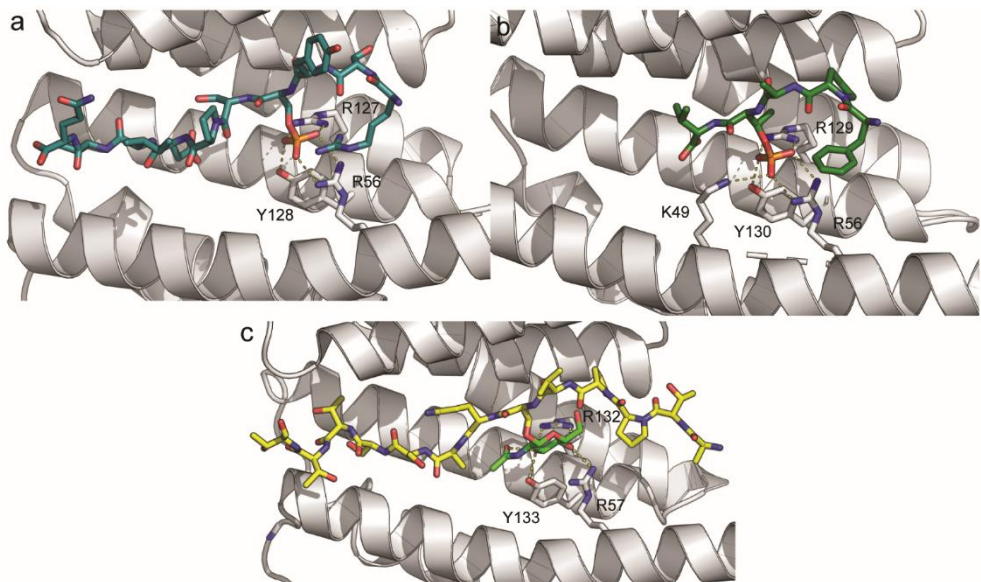


**Figure 1.11** | View of the interactions within the conserved 14-3-3 binding groove and common 14-3-3 recognition motifs. (a) Representative example of a mode I-II binding motif for the complex between ubiquitin specific protease 8 (USP8) pS<sup>718</sup> 13-mer peptide (teal sticks) and 14-3-3 $\zeta$  (PDB: 6F09). Highlighted, the conserved residues R56, R127 and Y128, responsible for the interaction with pS<sup>718</sup> (b) Representative example of a mode III binding motif for the complex between estrogen receptor alpha (ER $\alpha$ ) pT<sup>594</sup> 8-mer peptide (green sticks) and 14-3-3 $\sigma$  (PDB: 4JC3). Highlighted, the conserved residues K49, R56, R129 and Y130, responsible for the interaction with pT<sup>594</sup>. (c) Representative example of a phosphorylation-independent interaction between a 20-mer peptide (yellow sticks) containing a O-GlcNAcylated (N-acetylglucosamine, GlcNAc) serine residue (green sticks) and 14-3-3 $\gamma$  (PDB: 6BYJ). Highlighted, the conserved residues R57, R132 and Y133, responsible for the interaction with S-O-GlcNAc. In all panels, 14-3-3 protein is shown as white ribbons and H-bond contacts are shown as yellow dashed lines. Numbering of the conserved residues differs based on the different protein isoform used.

## CHAPTER 1

As the 14-3-3 proteins play such a central role in many physiological processes and bind to such a broad range of functionally important client partners, they are implicated in many human diseases. Diseases involving 14-3-3 proteins and the corresponding 14-3-3 binding partners include cancer<sup>119-121</sup> (e.g. p53, c-Raf, ER $\alpha$  BAD/BAX), neurodegeneration<sup>122-124</sup> (Tau,  $\alpha$ -synuclein) and cystic fibrosis (CFTR).<sup>125-126</sup> Hence, modulation of 14-3-3 PPIs represent a potential strategy for therapeutic intervention.<sup>127-128</sup>

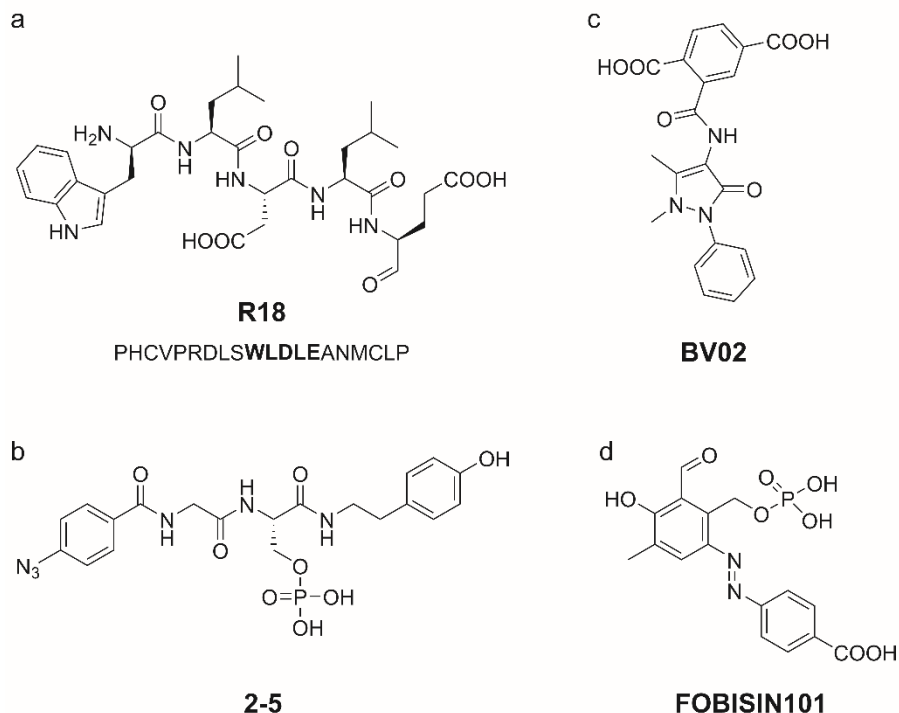


**Figure 1.12** | Examples of 14-3-3 PPI inhibitors. (a) R18 peptide sequence, with the structure of the WLDLE motif highlighted. The WLDLE motif binds in the phospho-binding pocket of 14-3-3 proteins. (b) Chemical structure of the small molecule-peptide hybrid 2-5. (c) Chemical structure of the 14-3-3 $\sigma$ /c-Abl inhibitor BV02. (d) Chemical structure of FOBISIN101, a phosphor-Ser/Thr mimic.

Physiological and pathological relevance for modulation of this PPI class by inhibition or stabilization requires careful investigation. Given that binding to 14-3-3 proteins is very often dependent on the recognition of a phosphorylated binding motif, phosphorylated peptides and small molecule phosphonates have been successfully used as inhibitors.<sup>129</sup> The first reported 14-3-3 PPI inhibitor, the peptide R18 (20 amino acidic residues), was identified by Fu and colleagues in a phage display approach (Figure 1.12a).<sup>130</sup> The Yao group used a fragment-based combinatorial small-molecule microarray (SMM) approach to identify compound 2-5,

## CHAPTER 1

a small molecule-peptide hybrid, which showed activity both *in vitro* and in cells (Figure 1.12b).<sup>131</sup> Different non-peptidic small molecule inhibitors have also been reported. Among these, we find BV02, which disrupts the 14-3-3 $\sigma$ /c-Abl interaction and was found to be active in human leukemia cells (Figure 1.12c),<sup>132</sup> and FOBISIN101, a phosphoSer/Thr-mimetic agent, which upon X-ray irradiation covalently binds to 14-3-3 (Figure 11d).<sup>133</sup>

Despite the numerous examples found in literature, inhibitors of 14-3-3 PPIs present an intrinsic limitation: due to sequence similarity between 14-3-3 isoforms, most of these compounds are non-isoform selective. In addition, they inhibit the PPIs of 14-3-3 with all client proteins, which is likely to have significant impact on overall cellular function given the central role and high abundance of 14-3-3 proteins in cells. While inhibitors might find some application, more selective modulators are desirable. To this end, implementation of stabilizers can potentially lead to selective modulation, as these stabilizers will be designed to specifically target one particular 14-3-3/client partner complex acting as molecular glues rather than simply binding to only one of the complex components.

A valuable example of 14-3-3 PPI stabilizers is represented by the fusicoccanes, of which fusicoccin A (Fc-A) is the most prominent member (Figure 1.13a). Fc-A is a diterpene glycoside, originally isolated from the plant pathogenic fungus *Phomopsis amigdalii*, causes plant death by causing stomata to open, leading to dehydration through increased transpiration. Fc-A operates by activating the plasma membrane proton pump PMA2, causing acidification of the cell wall and leading to irreversible opening of the stomata. Mechanistically, Fc-A binds to the preformed 14-3-3/PMA2 binary complex, hence stabilizing PMA2 in its active state, but has little to no affinity in respect to the individual protein partners.<sup>134-135</sup> Elucidation of the crystal structure of this Fc-A/14-3-3/PMA2 ternary complex provided a structural explanation for Fc-A's mechanism of action. Fc-A acts as a molecular glue, by binding at the rim-of-the-interface of the 14-3-3/PMA2 complex (from now on termed "Fc pocket") and closes the gap that remains in the 14-3-3 binding groove after the binding of PMA2, leading to mutual stabilization of both ligands (Figure 1.13b).<sup>136-137</sup> The discovery of Fc-A's mode of action set out its use as chemical biology tool compound for the study of 14-3-3 PPI stabilization. Fc-A has been shown to stabilize many 14-3-3 PPIs relevant in the context of diseases mentioned above, such as CFTR,<sup>126</sup> ER $\alpha$ ,<sup>138</sup> c-Raf,<sup>139</sup> TASK-3<sup>140</sup> and p53.<sup>141</sup>

In addition to their biological relevance, as well as that of their client partners, there are other important features to consider that make 14-3-3 proteins a viable platform for the study of the principles governing PPI stabilization: 1) 14-3-3 proteins are easily expressed and purified, which makes them readily available for crystallization and biophysical studies, 2) there is clear structural evidence for their mode of action, 3) the Fc pocket is well defined, making them conceptually simple

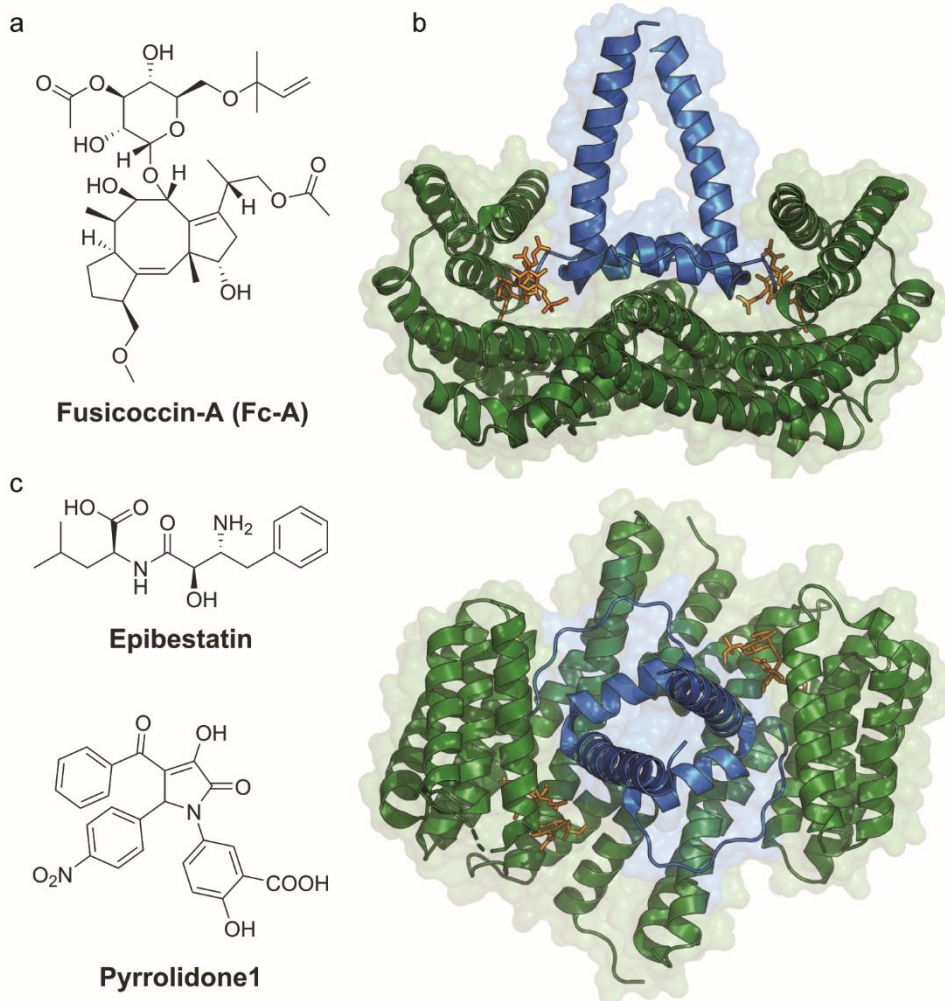


**Figure 1.13** | Known stabilizers of 14-3-3/PMA2 interaction. (a) Chemical structure of Fc-A. (b) Front (top panel) and top (bottom panel) view of Fc-A (orange sticks) in complex with T14-3-3 $\Delta$ C (tobacco 14-3-3, truncated of its 18 C-terminal residues, green ribbons) and PMA2-CT52 (C-terminal 52 amino acids, blue ribbons) dimer (PDB: 2O98). (c) Chemical structures of epibestatin (top) and pyrrolidone1 (bottom).

targets for small molecules, and 4) they are amenable to crystallization. Finally, two classes of small molecules, epibestatin and pyrrolidone1 (Figure 1.13c), have been reported to also stabilize the 14-3-3/PMA2 interaction,<sup>142</sup> providing more tractable starting points than Fc-A for medicinal chemistry to develop more potent, selective and drug-like 14-3-3 PPI stabilizer and investigation of SAR and selectivity principles.

## CHAPTER 1

### 1.8 AIM OF THE THESIS

A new paradigm has emerged in biopharmaceutical research, dictated by the need to surpass the conventional strategy of the “magic bullet” and “one target, one drug” paradigm, which is now reaching its limits. Previously considered “undruggable”, the human protein interactome has drawn the attention of the scientific community and now represents an attractive opportunity for therapeutic intervention.

As discussed in this chapter, targeting PPIs by the modulation of proximity – a mechanism commonly used by Nature to regulate biological functions - has proven to be a viable strategy. Despite the many promising examples, the study of PPIs as therapeutic target class is still at early stages and its success will depend on the inventiveness of scientists in developing efficient strategies and chemical tools that will allow us to overcome the many challenges that still lie ahead. Indeed, new targets will require an improvement of the way conventional drug discovery is conducted. For example, the compound libraries currently employed for screening campaigns will need to be revisited in terms of the chemical space probed, the physicochemical properties and three dimensionality (by increasing fraction of sp<sup>3</sup> carbon atoms), as most of the compounds have been developed with conventional drug targets in mind, while the molecular surfaces and binding sites in PPIs present much different features. Computational approaches can assist in this effort, but the relative paucity of available structural information and the complex dynamic equilibria governing PPIs has so far limited the viability of such approaches.

In this regards, the 14-3-3 proteins provide a useful platform, as they address already some of the issues here presented. The natural product Fc-A is a known stabilizer of many 14-3-3 PPIs, but its synthetic complexity and lack of selectivity makes it a less-than-ideal starting point for drug discovery purposes. On the other hand, epibestatin and pyrrolidone<sup>1</sup> represent more tractable chemical matter. Therefore, the aim of this thesis is to generate more potent and druglike compounds that will find use in elucidating the structural drivers and SAR principles governing 14-3-3 PPI stabilization.

**Chapter 2** describes the initial work performed on epibestatin, one of the two reported small molecule stabilizers of the 14-3-3/PMA2 PPI. Lack of consistent results in biochemical assays, raised the question whether the initial report was valid. A more detailed analysis of the related ternary complex crystal structure revealed that the electron density initially assigned to epibestatin was also present in crystals that grew in the absence of epibestatin, thus devalidating epibestatin as a 14-3-3 PPI stabilizer . It was hypothesized that the source of the density assigned to epibestatin belonged to one of the crystallization buffer components, namely *N*-cyclohexyl-2-aminoethanesulfonic acid (CHES). A library of 35 CHES derivatives

## CHAPTER 1

was synthesized in order to potentially improve its putative weak activity. However, none of the analogues resulted to be active. Taken together, the results indicated that the extra electron density observed is not attributable to a stabilizer of any sort.

**Chapter 3** analyzes the role of the other reported 14-3-3/PMA2 small molecule stabilizer, the racemic compound pyrrolidone1 (Pyr1). Pyr1 was found to be weakly active also towards the 14-3-3/estrogen receptor alpha ( $ER\alpha$ )-derived phosphopeptide PPI. Testing of Pyr1 enantiomers in biophysical assays showed that only one enantiomer contributes to PPI stabilisation activity. Protein- and ligand-based NMR experiments confirmed the active enantiomer as a true hit and identified the compound binding site as the Fc-A binding site. An X-ray crystal structure of the Pyr1 active enantiomer ternary complex with 14-3-3/ $ER\alpha$  was obtained, unambiguously assigning the (*R*) absolute configuration. In the complex, an unexpected, non-protein interacting  $Mg^{2+}$  ion chelated by (*R*)-Pyr1 was observed. Addition of bivalent metal ions afforded a ~100-fold increase in the apparent PPI stabilization potency of (*R*)-Pyr1. Computational and experimental work led to conclude that this was due to ligand-specific, chelation-controlled bioactive conformation stabilization. Mimicry of this by intramolecular H-bonds led to the first potent, drug-like 14-3-3 PPI stabilizers. Chelation has been associated with pan-assay interference compounds (PAINS) but, as in this case, can also lead to true potency gains and be exploited to guide medicinal chemistry optimization.

**Chapter 4** further describes the attempts made in trying to mimic the ligand-specific metal ion effect by synthesis of six-membered bicyclic rigid analogues of Pyr1. Different synthetic strategies were employed, involving either vinylogous carboxylic acids or vinylogous carboxylate esters and reactants such as urea, *O*-methylisourea and guanidine. The chemistry around this type of substrates is widely discussed and literature examples are provided. Of the multiple synthetic routes envisaged, the reaction of vinylogous carboxylate esters and urea under basic conditions was found to be the most promising one. Structural characterization of the putative six-membered bicyclic rigid analogue of Pyr1 was, however, puzzling and further experiments are still required to fully elucidate the synthesized compound and its underlying chemistry.

**Chapter 5** reports on a comprehensive structure-activity relationship study performed on 59 Pyr1 derivatives. Potency, stabilization effect and selectivity of the synthesized compounds was evaluated against two different 14-3-3 PPIs, namely 14-3-3/ $ER\alpha$  and 14-3-3/CaMKK2. One of these derivatives was found to be as potent and efficacious as Pyr1, while another one exhibited higher selectivity for CaMKK2 than Pyr1. Two derivatives were then selected for crystallization studies and a crystal structure of their respective ternary complexes with 14-3-3/ $ER\alpha$  was obtained. Both bind in the same binding conformation observed for (*R*)-Pyr1, and electron density associated with  $Mg^{2+}$  ion was also observed. Finally, the stabilization effect of (*R*)-

## CHAPTER 1

Pyr1 was evaluated in the 14-3-3/CaMKK2 PPI using full-length CaMKK2 protein. A 27-fold stabilization was measured, therefore demonstrating that phosphopeptides can be successfully used as surrogates of full-length proteins in the study of 14-3-3-mediated PPIs.

**Chapter 6** aims to provide an epilogue to the work here presented, with a perspective on the current status of 14-3-3 PPI stabilization. Issues on isoform-specificity, target-partner selectivity and the present knowledge on 14-3-3 PPI stabilizers are addressed. Finally, possible future plans and directions are outlined.

## CHAPTER 1

### 1.9 REFERENCES

1. Tan, S. Y.; Grimes, S. Paul Ehrlich (1854-1915): man with the magic bullet. *Singapore Med. J.* **2010**, *51* (11), 842-3.
2. Deshaies, R. J. Multispecific drugs herald a new era of biopharmaceutical innovation. *Nature* **2020**, *580* (7803), 329-338.
3. Jaeger, S.; Aloy, P. From protein interaction networks to novel therapeutic strategies. *IUBMB Life* **2012**, *64* (6), 529-537.
4. Hopkins, A. L.; Groom, C. R. The druggable genome. *Nat. Rev. Drug Discovery* **2002**, *1* (9), 727-730.
5. Ruffner, H.; Bauer, A.; Bouwmeester, T. Human protein–protein interaction networks and the value for drug discovery. *Drug Discovery Today* **2007**, *12* (17), 709-716.
6. Strong, M.; Eisenberg, D., The protein network as a tool for finding novel drug targets. In *Systems Biological Approaches in Infectious Diseases*, Boshoff, H. I.; Barry, C. E., Eds. Birkhäuser Basel: Basel, 2007; pp 191-215.
7. Gordo, S.; Giralt, E. Knitting and untying the protein network: Modulation of protein ensembles as a therapeutic strategy. *Protein Sci.* **2009**, *18* (3), 481-493.
8. Finan, C.; Gaulton, A.; Kruger, F. A.; Lumbers, R. T.; Shah, T.; Engmann, J.; Galver, L.; Kelley, R.; Karlsson, A.; Santos, R.; Overington, J. P.; Hingorani, A. D.; Casas, J. P. The druggable genome and support for target identification and validation in drug development. *Science Translational Medicine* **2017**, *9* (383), eaag1166.
9. Venkatesan, K.; Rual, J. F.; Vazquez, A.; Stelzl, U.; Lemmens, I.; Hirozane-Kishikawa, T.; Hao, T.; Zenkner, M.; Xin, X.; Goh, K. I.; Yildirim, M. A.; Simonis, N.; Heinzmann, K.; Gebreab, F.; Sahalie, J. M.; Cevik, S.; Simon, C.; de Smet, A. S.; Dann, E.; Smolyar, A.; Vinayagam, A.; Yu, H.; Szeto, D.; Borick, H.; Dricot, A.; Klitgord, N.; Murray, R. R.; Lin, C.; Lalowski, M.; Timm, J.; Rau, K.; Boone, C.; Braun, P.; Cusick, M. E.; Roth, F. P.; Hill, D. E.; Tavernier, J.; Wanker, E. E.; Barabasi, A. L.; Vidal, M. An empirical framework for binary interactome mapping. *Nat. Methods* **2009**, *6* (1), 83-90.
10. Stumpf, M. P.; Thorne, T.; de Silva, E.; Stewart, R.; An, H. J.; Lappe, M.; Wiuf, C. Estimating the size of the human interactome. *Proc. Natl. Acad. Sci. U. S. A.* **2008**, *105* (19), 6959-64.
11. Wells, J. A.; McClendon, C. L. Reaching for high-hanging fruit in drug discovery at protein-protein interfaces. *Nature* **2007**, *450* (7172), 1001-9.
12. Gao, M.; Skolnick, J. A comprehensive survey of small-molecule binding pockets in proteins. *PLoS Comput. Biol.* **2013**, *9* (10), e1003302-e1003302.
13. Stanton, B. Z.; Chory, E. J.; Crabtree, G. R. Chemically induced proximity in biology and medicine. *Science* **2018**, *359* (6380), eaao5902.
14. Gerry, C. J.; Schreiber, S. L. Unifying principles of bifunctional, proximity-inducing small molecules. *Nat. Chem. Biol.* **2020**, *16* (4), 369-378.
15. Schreiber, S. L. Immunophilin-sensitive protein phosphatase action in cell signaling pathways. *Cell* **1992**, *70* (3), 365-368.
16. Cusick, M. E.; Klitgord, N.; Vidal, M.; Hill, D. E. Interactome: gateway into systems biology. *Hum. Mol. Genet.* **2005**, *14* (suppl\_2), R171-R181.
17. De Las Rivas, J.; Fontanillo, C. Protein–protein interaction networks: unraveling the wiring of molecular machines within the cell. *Briefings Funct. Genomics* **2012**, *11* (6), 489-496.
18. Hartwell, L. H.; Hopfield, J. J.; Leibler, S.; Murray, A. W. From molecular to modular cell biology. *Nature* **1999**, *402* (6761), C47-C52.



## CHAPTER 1

19. Barabási, A.-L.; Oltvai, Z. N. Network biology: understanding the cell's functional organization. *Nat. Rev. Genet.* **2004**, *5* (2), 101-113.
20. De Las Rivas, J.; Fontanillo, C. Protein–Protein Interactions Essentials: Key Concepts to Building and Analyzing Interactome Networks. *PLoS Comput. Biol.* **2010**, *6* (6), e1000807.
21. Rual, J.-F.; Venkatesan, K.; Hao, T.; Hirozane-Kishikawa, T.; Dricot, A.; Li, N.; Berriz, G. F.; Gibbons, F. D.; Dreze, M.; Ayivi-Guedehoussou, N.; Klitgord, N.; Simon, C.; Boxem, M.; Milstein, S.; Rosenberg, J.; Goldberg, D. S.; Zhang, L. V.; Wong, S. L.; Franklin, G.; Li, S.; Albala, J. S.; Lim, J.; Fraughton, C.; Llamasas, E.; Cevik, S.; Bex, C.; Lamesch, P.; Sikorski, R. S.; Vandenhaute, J.; Zoghbi, H. Y.; Smolyar, A.; Bosak, S.; Sequerra, R.; Doucette-Stamm, L.; Cusick, M. E.; Hill, D. E.; Roth, F. P.; Vidal, M. Towards a proteome-scale map of the human protein–protein interaction network. *Nature* **2005**, *437* (7062), 1173-1178.
22. Przytycka, T. M.; Singh, M.; Slonim, D. K. Toward the dynamic interactome: it's about time. *Briefings Bioinf.* **2010**, *11* (1), 15-29.
23. Ellis, R. J.; Minton, A. P. Join the crowd. *Nature* **2003**, *425* (6953), 27-28.
24. Scott, J. D.; Pawson, T. Cell Signaling in Space and Time: Where Proteins Come Together and When They're Apart. *Science* **2009**, *326* (5957), 1220-1224.
25. Marianayagam, N. J.; Sunde, M.; Matthews, J. M. The power of two: protein dimerization in biology. *Trends Biochem. Sci.* **2004**, *29* (11), 618-625.
26. Ispolatov, I.; Yuryev, A.; Mazo, I.; Maslov, S. Binding properties and evolution of homodimers in protein-protein interaction networks. *Nucleic Acids Res.* **2005**, *33* (11), 3629-3635.
27. Spencer, D.; Wandless, T.; Schreiber, S.; Crabtree, G. Controlling signal transduction with synthetic ligands. *Science* **1993**, *262* (5136), 1019-1024.
28. Almawi, W. Y.; Melemedjian, O. K. Clinical and mechanistic differences between FK506 (tacrolimus) and cyclosporin A. *Nephrol., Dial., Transplant.* **2000**, *15* (12), 1916-1918.
29. Kunz, J.; Hall, M. N. Cyclosporin A, FK506 and rapamycin: more than just immunosuppression. *Trends Biochem. Sci.* **1993**, *18* (9), 334-338.
30. Liu, J.; Farmer, J. D.; Lane, W. S.; Friedman, J.; Weissman, I.; Schreiber, S. L. Calcineurin is a common target of cyclophilin-cyclosporin A and FKBP-FK506 complexes. *Cell* **1991**, *66* (4), 807-815.
31. Bier, D.; Thiel, P.; Briels, J.; Ottmann, C. Stabilization of Protein–Protein Interactions in chemical biology and drug discovery. *Prog. Biophys. Mol. Biol.* **2015**, *119* (1), 10-19.
32. Ho, S.; Clipstone, N.; Timmermann, L.; Northrop, J.; Graef, I.; Fiorentino, D.; Nourse, J.; Crabtree, G. R. The Mechanism of Action of Cyclosporin A and FK506. *Clin. Immunol. Immunopathol.* **1996**, *80* (3), S40-S45.
33. Tong, M.; Jiang, Y. FK506-Binding Proteins and Their Diverse Functions. *Current molecular pharmacology* **2015**, *9* (1), 48-65.
34. Li, J.; Kim, Sang G.; Blenis, J. Rapamycin: One Drug, Many Effects. *Cell Metabolism* **2014**, *19* (3), 373-379.
35. Laplante, M.; Sabatini, David M. mTOR Signaling in Growth Control and Disease. *Cell* **2012**, *149* (2), 274-293.
36. Dumont, F. J.; Su, Q. Mechanism of action of the immunosuppressant rapamycin. *Life Sci.* **1995**, *58* (5), 373-395.
37. Austin, D. J.; Schreiber, S. L.; Crabtree, G. R. Proximity versus allostery: the role of regulated protein dimerization in biology. *Chem. Biol.* **1994**, *1* (3), 131-136.
38. Gray, W. M.; Kepinski, S.; Rouse, D.; Leyser, O.; Estelle, M. Auxin regulates SCFTIR1-dependent degradation of AUX/IAA proteins. *Nature* **2001**, *414* (6861), 271-276.

## CHAPTER 1

39. Dharmasiri, N.; Dharmasiri, S.; Estelle, M. The F-box protein TIR1 is an auxin receptor. *Nature* **2005**, *435* (7041), 441-445.
40. Sheard, L. B.; Tan, X.; Mao, H.; Withers, J.; Ben-Nissan, G.; Hinds, T. R.; Kobayashi, Y.; Hsu, F.-F.; Sharon, M.; Browse, J.; He, S. Y.; Rizo, J.; Howe, G. A.; Zheng, N. Jasmonate perception by inositol-phosphate-potentiated COI1–JAZ co-receptor. *Nature* **2010**, *468* (7322), 400-405.
41. Chardin, P.; McCormick, F. Brefeldin A: The Advantage of Being Uncompetitive. *Cell* **1999**, *97* (2), 153-155.
42. Sunahara, R. K.; Dessauer, C. W.; Whisnant, R. E.; Kleuss, C.; Gilman, A. G. Interaction of G $\alpha$  with the cytosolic domains of mammalian adenylyl cyclase. *J. Biol. Chem.* **1997**, *272* (35), 22265-71.
43. Renault, L.; Guibert, B.; Cherfils, J. Structural snapshots of the mechanism and inhibition of a guanine nucleotide exchange factor. *Nature* **2003**, *426* (6966), 525-530.
44. Tesmer, J. J.; Sunahara, R. K.; Gilman, A. G.; Sprang, S. R. Crystal structure of the catalytic domains of adenylyl cyclase in a complex with G $\alpha$ -GTP $\gamma$ S. *Science* **1997**, *278* (5345), 1907-16.
45. Fegan, A.; White, B.; Carlson, J. C. T.; Wagner, C. R. Chemically Controlled Protein Assembly: Techniques and Applications. *Chem. Rev.* **2010**, *110* (6), 3315-3336.
46. DeRose, R.; Miyamoto, T.; Inoue, T. Manipulating signaling at will: chemically-inducible dimerization (CID) techniques resolve problems in cell biology. *Pflugers Arch. - Eur. J. Physiol.* **2013**, *465* (3), 409-417.
47. Crabtree, G. R.; Schreiber, S. L. Three-part inventions: intracellular signaling and induced proximity. *Trends Biochem. Sci.* **1996**, *21* (11), 418-422.
48. Gestwicki, J. E.; Marinec, P. S. Chemical control over protein-protein interactions: beyond inhibitors. *Comb Chem High Throughput Screen* **2007**, *10* (8), 667-75.
49. Belshaw, P. J.; Ho, S. N.; Crabtree, G. R.; Schreiber, S. L. Controlling protein association and subcellular localization with a synthetic ligand that induces heterodimerization of proteins. *Proc. Natl. Acad. Sci.* **1996**, *93* (10), 4604-4607.
50. Kohler, J. J.; Bertozzi, C. R. Regulating Cell Surface Glycosylation by Small Molecule Control of Enzyme Localization. *Chem. Biol.* **2003**, *10* (12), 1303-1311.
51. Inoue, T.; Heo, W. D.; Grimley, J. S.; Wandless, T. J.; Meyer, T. An inducible translocation strategy to rapidly activate and inhibit small GTPase signaling pathways. *Nat. Methods* **2005**, *2* (6), 415-418.
52. Mallet, V. O.; Mitchell, C.; Guidotti, J.-E.; Jaffray, P.; Fabre, M.; Spencer, D.; Arnoult, D.; Kahn, A.; Gilgenkrantz, H. Conditional cell ablation by tight control of caspase-3 dimerization in transgenic mice. *Nat. Biotechnol.* **2002**, *20* (12), 1234-1239.
53. Mootz, H. D.; Blum, E. S.; Tyszkiewicz, A. B.; Muir, T. W. Conditional Protein Splicing: A New Tool to Control Protein Structure and Function in Vitro and in Vivo. *J. Am. Chem. Soc.* **2003**, *125* (35), 10561-10569.
54. Corson, T. W.; Aberle, N.; Crews, C. M. Design and Applications of Bifunctional Small Molecules: Why Two Heads Are Better Than One. *ACS Chem. Biol.* **2008**, *3* (11), 677-692.
55. Kopytek, S. J.; Standaert, R. F.; Dyer, J. C. D.; Hu, J. C. Chemically induced dimerization of dihydrofolate reductase by a homobifunctional dimer of methotrexate. *Chem. Biol.* **2000**, *7* (5), 313-321.
56. Farrar, M. A.; Alberola-Ila, J.; Perlmutter, R. M. Activation of the Raf-1 kinase cascade by coumermycin-induced dimerization. *Nature* **1996**, *383* (6596), 178-181.

## CHAPTER 1

57. Mohi, M. G.; Arai, K.; Watanabe, S. Activation and functional analysis of Janus kinase 2 in BA/F3 cells using the coumermycin/gyrase B system. *Mol. Biol. Cell* **1998**, *9* (12), 3299-308.
58. Huryn, D. M.; Wipf, P., CHAPTER 5 - Natural product chemistry and anticancer drug discovery. In *Cancer Drug Design and Discovery*, Neidle, S., Ed. Academic Press: New York, 2008; pp 107-130.
59. Mimnaugh, E. G.; Xu, W.; Vos, M.; Yuan, X.; Isaacs, J. S.; Bisht, K. S.; Gius, D.; Neckers, L. Simultaneous inhibition of hsp 90 and the proteasome promotes protein ubiquitination, causes endoplasmic reticulum-derived cytosolic vacuolization, and enhances antitumor activity. *Mol. Cancer Ther.* **2004**, *3* (5), 551-566.
60. Kuduk, S. D.; Zheng, F. F.; Sepp-Lorenzino, L.; Rosen, N.; Danishefsky, S. J. Synthesis and evaluation of geldanamycin-estradiol hybrids. *Biorg. Med. Chem. Lett.* **1999**, *9* (9), 1233-1238.
61. Kuduk, S. D.; Harris, C. R.; Zheng, F. F.; Sepp-Lorenzino, L.; Ouerfelli, Q.; Rosen, N.; Danishefsky, S. J. Synthesis and evaluation of geldanamycin–testosterone hybrids. *Biorg. Med. Chem. Lett.* **2000**, *10* (11), 1303-1306.
62. Liang, J.; Shang, Y. Estrogen and Cancer. *Annual Review of Physiology* **2013**, *75* (1), 225-240.
63. Heinlein, C. A.; Chang, C. Androgen Receptor in Prostate Cancer. *Endocr. Rev.* **2004**, *25* (2), 276-308.
64. Dauvois, S.; Danielian, P. S.; White, R.; Parker, M. G. Antiestrogen ICI 164,384 reduces cellular estrogen receptor content by increasing its turnover. *Proc. Natl. Acad. Sci.* **1992**, *89* (9), 4037-4041.
65. Bradbury, R. H.; Hales, N. J.; Rabow, A. A.; Walker, G. E.; Acton, D. G.; Andrews, D. M.; Ballard, P.; Brooks, N. A. N.; Colclough, N.; Girdwood, A.; Hancox, U. J.; Jones, O.; Jude, D.; Loddick, S. A.; Mortlock, A. A. Small-molecule androgen receptor downregulators as an approach to treatment of advanced prostate cancer. *Biorg. Med. Chem. Lett.* **2011**, *21* (18), 5442-5445.
66. Cromm, P. M.; Crews, C. M. Targeted Protein Degradation: from Chemical Biology to Drug Discovery. *Cell Chem. Biol.* **2017**, *24* (9), 1181-1190.
67. Lai, A. C.; Crews, C. M. Induced protein degradation: an emerging drug discovery paradigm. *Nat. Rev. Drug Discovery* **2017**, *16* (2), 101-114.
68. Li, W.; Bengtson, M. H.; Ulbrich, A.; Matsuda, A.; Reddy, V. A.; Orth, A.; Chanda, S. K.; Batalov, S.; Joazeiro, C. A. P. Genome-Wide and Functional Annotation of Human E3 Ubiquitin Ligases Identifies MULAN, a Mitochondrial E3 that Regulates the Organelle's Dynamics and Signaling. *PLOS ONE* **2008**, *3* (1), e1487.
69. Jin, J.; Li, X.; Gygi, S. P.; Harper, J. W. Dual E1 activation systems for ubiquitin differentially regulate E2 enzyme charging. *Nature* **2007**, *447* (7148), 1135-1138.
70. Pelzer, C.; Kassner, I.; Matentzoglou, K.; Singh, R. K.; Wollscheid, H.-P.; Scheffner, M.; Schmidtke, G.; Groettrup, M. UBE1L2, a Novel E1 Enzyme Specific for Ubiquitin. *J. Biol. Chem.* **2007**, *282* (32), 23010-23014.
71. Sakamoto, K. M.; Kim, K. B.; Kumagai, A.; Mercurio, F.; Crews, C. M.; Deshaies, R. J. Protacs: Chimeric molecules that target proteins to the Skp1–Cullin–F box complex for ubiquitination and degradation. *Proc. Natl. Acad. Sci.* **2001**, *98* (15), 8554-8559.
72. Verma, R.; Mohl, D.; Deshaies, R. J. Harnessing the Power of Proteolysis for Targeted Protein Inactivation. *Molecular Cell* **2020**, *77* (3), 446-460.
73. Speirs, A. L. THALIDOMIDE AND CONGENITAL ABNORMALITIES. *The Lancet* **1962**, *279* (7224), 303-305.
74. Larkin, M. Low-dose thalidomide seems to be effective in multiple myeloma. *The Lancet* **1999**, *354* (9182), 925.

## CHAPTER 1

75. Muller, G. W.; Chen, R.; Huang, S.-Y.; Corral, L. G.; Wong, L. M.; Patterson, R. T.; Chen, Y.; Kaplan, G.; Stirling, D. I. Amino-substituted thalidomide analogs: Potent inhibitors of TNF- $\alpha$  production. *Biorg. Med. Chem. Lett.* **1999**, *9* (11), 1625-1630.
76. Ito, T.; Ando, H.; Suzuki, T.; Ogura, T.; Hotta, K.; Imamura, Y.; Yamaguchi, Y.; Handa, H. Identification of a Primary Target of Thalidomide Teratogenicity. *Science* **2010**, *327* (5971), 1345-1350.
77. Bandyopadhyay, S.; Duré, M.; Paroder, M.; Soto-Nieves, N.; Puga, I.; Macián, F. Interleukin 2 gene transcription is regulated by Ikaros-induced changes in histone acetylation in anergic T cells. *Blood* **2006**, *109* (7), 2878-2886.
78. Gandhi, A. K.; Kang, J.; Havens, C. G.; Conklin, T.; Ning, Y.; Wu, L.; Ito, T.; Ando, H.; Waldman, M. F.; Thakurta, A.; Klippel, A.; Handa, H.; Daniel, T. O.; Schafer, P. H.; Chopra, R. Immunomodulatory agents lenalidomide and pomalidomide co-stimulate T cells by inducing degradation of T cell repressors Ikaros and Aiolos via modulation of the E3 ubiquitin ligase complex CRL4CRBN. *Br. J. Haematol.* **2014**, *164* (6), 811-821.
79. Lu, G.; Middleton, R. E.; Sun, H.; Naniong, M.; Ott, C. J.; Mitsiades, C. S.; Wong, K.-K.; Bradner, J. E.; Kaelin, W. G. The Myeloma Drug Lenalidomide Promotes the Cereblon-Dependent Destruction of Ikaros Proteins. *Science* **2014**, *343* (6168), 305-309.
80. Krönke, J.; Udeshi, N. D.; Narla, A.; Grauman, P.; Hurst, S. N.; McConkey, M.; Svinkina, T.; Heckl, D.; Comer, E.; Li, X.; Ciarlo, C.; Hartman, E.; Munshi, N.; Schenone, M.; Schreiber, S. L.; Carr, S. A.; Ebert, B. L. Lenalidomide Causes Selective Degradation of IKZF1 and IKZF3 in Multiple Myeloma Cells. *Science* **2014**, *343* (6168), 301-305.
81. Buckley, D. L.; Gustafson, J. L.; Van Molle, I.; Roth, A. G.; Tae, H. S.; Gareiss, P. C.; Jorgensen, W. L.; Ciulli, A.; Crews, C. M. Small-Molecule Inhibitors of the Interaction between the E3 Ligase VHL and HIF1 $\alpha$ . *Angew. Chem. Int. Ed.* **2012**, *51* (46), 11463-11467.
82. Mullard, A. First targeted protein degrader hits the clinic. *Nat. Rev. Drug Discovery* **2019**, *18*, 237-239.
83. Steven, B.; Kayvon, P.; Simon, W.; Nicholas, R.; Carolyn, B. Lysosome Targeting Chimeras (LYTACs) for the Degradation of Secreted and Membrane Proteins. *ChemRxiv* **2019**.
84. Takahashi, D.; Moriyama, J.; Nakamura, T.; Miki, E.; Takahashi, E.; Sato, A.; Akaike, T.; Ito-Nakama, K.; Arimoto, H. AUTACs: Cargo-Specific Degradation Using Selective Autophagy. *Molecular Cell* **2019**, *76* (5), 797-810.e10.
85. Dey, S. K.; Jaffrey, S. R. RIBOTACs: Small Molecules Target RNA for Degradation. *Cell Chem. Biol.* **2019**, *26* (8), 1047-1049.
86. Costales, M. G.; Suresh, B.; Vishnu, K.; Disney, M. D. Targeted Degradation of a Hypoxia-Associated Non-coding RNA Enhances the Selectivity of a Small Molecule Interacting with RNA. *Cell Chem. Biol.* **2019**, *26* (8), 1180-1186.e5.
87. Sedykh, S. E.; Prinz, V. V.; Buneva, V. N.; Nevinsky, G. A. Bispecific antibodies: design, therapy, perspectives. *Drug Des., Dev. Ther.* **2018**, *12*, 195-208.
88. Labrijn, A. F.; Janmaat, M. L.; Reichert, J. M.; Parren, P. W. H. I. Bispecific antibodies: a mechanistic review of the pipeline. *Nat. Rev. Drug Discovery* **2019**, *18* (8), 585-608.
89. McEnaney, P. J.; Parker, C. G.; Zhang, A. X.; Spiegel, D. A. Antibody-Recruiting Molecules: An Emerging Paradigm for Engaging Immune Function in Treating Human Disease. *ACS Chem. Biol.* **2012**, *7* (7), 1139-1151.
90. McEnaney, P. J.; Parker, C. G.; Zhang, A. X., Antibody-Recruiting Small Molecules: Synthetic Constructs as Immunotherapeutics. In *Platform Technologies in Drug Discovery and Validation*, 2017; pp 481-518.

## CHAPTER 1

91. McEnaney, P. J.; Fitzgerald, K. J.; Zhang, A. X.; Douglass, E. F.; Shan, W.; Balog, A.; Kolesnikova, M. D.; Spiegel, D. A. Chemically Synthesized Molecules with the Targeting and Effector Functions of Antibodies. *J. Am. Chem. Soc.* **2014**, *136* (52), 18034-18043.
92. Stuckey, D. W.; Shah, K. Stem cell-based therapies for cancer treatment: separating hope from hype. *Nat. Rev. Cancer* **2014**, *14* (10), 683-691.
93. Rafei, H.; Mehta, R. S.; Rezvani, K. Editorial: Cellular Therapies in Cancer. *Front. Immunol.* **2019**, *10*, 2788-2788.
94. Arellano, B.; Graber, D. J.; Sentman, C. L. Regulatory T cell-based therapies for autoimmunity. *Discov. Med.* **2016**, *22* (119), 73-80.
95. Kochenderfer, J. N.; Rosenberg, S. A. Treating B-cell cancer with T cells expressing anti-CD19 chimeric antigen receptors. *Nat. Rev. Clin. Oncol.* **2013**, *10* (5), 267-276.
96. Wu, C.-Y.; Roybal, K. T.; Puchner, E. M.; Onuffer, J.; Lim, W. A. Remote control of therapeutic T cells through a small molecule-gated chimeric receptor. *Science* **2015**, *350* (6258), aab4077.
97. Ma, J. S. Y.; Kim, J. Y.; Kazane, S. A.; Choi, S.-h.; Yun, H. Y.; Kim, M. S.; Rodgers, D. T.; Pugh, H. M.; Singer, O.; Sun, S. B.; Fonslow, B. R.; Kochenderfer, J. N.; Wright, T. M.; Schultz, P. G.; Young, T. S.; Kim, C. H.; Cao, Y. Versatile strategy for controlling the specificity and activity of engineered T cells. *Proc. Natl. Acad. Sci.* **2016**, *113* (4), E450-E458.
98. Diaconu, I.; Ballard, B.; Zhang, M.; Chen, Y.; West, J.; Dotti, G.; Savoldo, B. Inducible Caspase-9 Selectively Modulates the Toxicities of CD19-Specific Chimeric Antigen Receptor-Modified T Cells. *Mol. Ther.* **2017**, *25* (3), 580-592.
99. Kim, M. S.; Ma, J. S. Y.; Yun, H.; Cao, Y.; Kim, J. Y.; Chi, V.; Wang, D.; Woods, A.; Sherwood, L.; Caballero, D.; Gonzalez, J.; Schultz, P. G.; Young, T. S.; Kim, C. H. Redirection of Genetically Engineered CAR-T Cells Using Bifunctional Small Molecules. *J. Am. Chem. Soc.* **2015**, *137* (8), 2832-2835.
100. Aitken, A. 14-3-3 proteins: A historic overview. *Semin. Cancer Biol.* **2006**, *16* (3), 162-172.
101. Moore, B. W.; Perez, V. J., In *Physiological and biochemical aspects of nervous integration*, Carlson, F. D., Ed. Englewood Cliffs, NJ: Prentice-Hall, 1967; pp 343-359.
102. Thomas, D.; Guthridge, M.; Woodcock, J.; Lopez, A., 9 - 14-3-3 Protein Signaling in Development and Growth Factor Responses. In *Current Topics in Developmental Biology*, Schatten, G. P., Ed. Academic Press: 2005; Vol. 67, pp 285-303.
103. Aitken, A. Functional specificity in 14-3-3 isoform interactions through dimer formation and phosphorylation. Chromosome location of mammalian isoforms and variants. *Plant Molecular Biology* **2002**, *50* (6), 993-1010.
104. Martin, H.; Patel, Y.; Jones, D.; Howell, S.; Robinson, K.; Aitken, A. Antibodies against the major brain isoforms of 14-3-3 protein: an antibody specific for the N-acetylated amino-terminus of a protein. *FEBS Lett.* **1993**, *331* (1), 296-303.
105. Takahashi, Y. The 14-3-3 Proteins: Gene, Gene Expression, and Function. *Neurochem. Res.* **2003**, *28* (8), 1265-1273.
106. Yang, X.; Lee, W. H.; Sobott, F.; Papagrigoriou, E.; Robinson, C. V.; Grossmann, J. G.; Sundström, M.; Doyle, D. A.; Elkins, J. M. Structural basis for protein-protein interactions in the 14-3-3 protein family. *Proc. Natl. Acad. Sci.* **2006**, *103* (46), 17237-17242.
107. Obsil, T.; Obsilova, V. Structural basis of 14-3-3 protein functions. *Seminars in Cell & Developmental Biology* **2011**, *22* (7), 663-672.
108. Gardino, A. K.; Smerdon, S. J.; Yaffe, M. B. Structural determinants of 14-3-3 binding specificities and regulation of subcellular localization of 14-3-3-ligand complexes: A comparison of

## CHAPTER 1

- the X-ray crystal structures of all human 14-3-3 isoforms. *Semin. Cancer Biol.* **2006**, *16* (3), 173-182.
109. Aitken, A.; Baxter, H.; Dubois, T.; Clokie, S.; Mackie, S.; Mitchell, K.; Peden, A.; Zemlickova, E. Specificity of 14-3-3 isoform dimer interactions and phosphorylation. *Biochem. Soc. Trans.* **2002**, *30* (4), 351-360.
110. Ballone, A.; Centorrino, F.; Ottmann, C. 14-3-3: A Case Study in PPI Modulation. *Molecules* **2018**, *23* (6), 1386.
111. Yaffe, M. B. How do 14-3-3 proteins work? – Gatekeeper phosphorylation and the molecular anvil hypothesis. *FEBS Lett.* **2002**, *513* (1), 53-57.
112. Johnson, C.; Crowther, S.; Stafford, Margaret J.; Campbell, David G.; Toth, R.; MacKintosh, C. Bioinformatic and experimental survey of 14-3-3-binding sites. *Biochem. J* **2010**, *427* (1), 69-78.
113. Ottmann, C.; Yasmin, L.; Weyand, M.; Veessenmeyer, J. L.; Diaz, M. H.; Palmer, R. H.; Francis, M. S.; Hauser, A. R.; Wittinghofer, A.; Hallberg, B. Phosphorylation-independent interaction between 14-3-3 and exoenzyme S: from structure to pathogenesis. *The EMBO Journal* **2007**, *26* (3), 902-913.
114. Toleman, C. A.; Schumacher, M. A.; Yu, S.-H.; Zeng, W.; Cox, N. J.; Smith, T. J.; Soderblom, E. J.; Wands, A. M.; Kohler, J. J.; Boyce, M. Structural basis of O-GlcNAc recognition by mammalian 14-3-3 proteins. *Proc. Natl. Acad. Sci.* **2018**, *115* (23), 5956-5961.
115. RUBIO, M. P.; GERAGHTY, K. M.; WONG, B. H. C.; WOOD, N. T.; CAMPBELL, D. G.; MORRICE, N.; MACKINTOSH, C. 14-3-3-affinity purification of over 200 human phosphoproteins reveals new links to regulation of cellular metabolism, proliferation and trafficking. *Biochem. J* **2004**, *379* (2), 395-408.
116. Chan, P. M.; Ng, Y.-W.; Manser, E. A Robust Protocol to Map Binding Sites of the 14-3-3 Interactome: Cdc25C Requires Phosphorylation of Both S216 and S263 to bind 14-3-3. *Molecular & Cellular Proteomics* **2011**, *10* (3), M110.005157.
117. Pozuelo Rubio, M.; Geraghty, K. M.; Wong, B. H.; Wood, N. T.; Campbell, D. G.; Morrice, N.; Mackintosh, C. 14-3-3-affinity purification of over 200 human phosphoproteins reveals new links to regulation of cellular metabolism, proliferation and trafficking. *Biochem. J* **2004**, *379* (Pt 2), 395-408.
118. Meek, S. E. M.; Lane, W. S.; Piwnica-Worms, H. Comprehensive Proteomic Analysis of Interphase and Mitotic 14-3-3-binding Proteins. *J. Biol. Chem* **2004**, *279*, 32046–32054.
119. Mhaweche, P. 14-3-3 proteins—an update. *Cell Research* **2005**, *15* (4), 228-236.
120. Wilker, E.; Yaffe, M. B. 14-3-3 Proteins—a focus on cancer and human disease. *Journal of Molecular and Cellular Cardiology* **2004**, *37* (3), 633-642.
121. De Vries-van Leeuwen, I. J.; da Costa Pereira, D.; Flach, K. D.; Piersma, S. R.; Haase, C.; Bier, D.; Yalcin, Z.; Michalides, R.; Feenstra, K. A.; Jimenez, C. R.; de Greef, T. F.; Brunsveld, L.; Ottmann, C.; Zwart, W.; de Boer, A. H. Interaction of 14-3-3 proteins with the estrogen receptor alpha F domain provides a drug target interface. *Proc. Natl. Acad. Sci. U. S. A.* **2013**, *110* (22), 8894-9.
122. Kaplan, A.; Fournier, A. Targeting 14-3-3 adaptor protein-protein interactions to stimulate central nervous system repair. *Neural Regeneration Research* **2017**, *12* (7), 1040-1043.
123. Steinacker, P.; Aitken, A.; Otto, M. 14-3-3 proteins in neurodegeneration. *Seminars in Cell & Developmental Biology* **2011**, *22* (7), 696-704.
124. Kaplan, A.; Ottmann, C.; Fournier, A. E. 14-3-3 adaptor protein-protein interactions as therapeutic targets for CNS diseases. *Pharmacol. Res.* **2017**, *125*, 114-121.

## CHAPTER 1

125. Liang, X.; Paula, A. C. D.; Bozóky, Z.; Zhang, H.; Bertrand, C. A.; Peters, K. W.; Forman-Kay, J. D.; Frizzell, R. A. Phosphorylation-dependent 14-3-3 protein interactions regulate CFTR biogenesis. *Mol. Biol. Cell* **2012**, *23* (6), 996-1009.
126. Stevers, L. M.; Lam, C. V.; Leysen, S. F. R.; Meijer, F. A.; van Scheppingen, D. S.; de Vries, R. M. J. M.; Carlile, G. W.; Milroy, L. G.; Thomas, D. Y.; Brunsveld, L.; Ottmann, C. Characterization and small-molecule stabilization of the multisite tandem binding between 14-3-3 and the R domain of CFTR. *Proc. Natl. Acad. Sci.* **2016**, *113* (9), E1152-E1161.
127. Aghazadeh, Y.; Papadopoulos, V. The role of the 14-3-3 protein family in health, disease, and drug development. *Drug Discovery Today* **2016**, *21* (2), 278-287.
128. Zhao, J.; Meyerkord, C. L.; Du, Y.; Khuri, F. R.; Fu, H. 14-3-3 proteins as potential therapeutic targets. *Seminars in Cell & Developmental Biology* **2011**, *22* (7), 705-712.
129. Stevers, L. M.; Sijbesma, E.; Botta, M.; MacKintosh, C.; Obsil, T.; Landrieu, I.; Cau, Y.; Wilson, A. J.; Karawajczyk, A.; Eickhoff, J.; Davis, J.; Hann, M.; O'Mahony, G.; Doveston, R. G.; Brunsveld, L.; Ottmann, C. Modulators of 14-3-3 Protein-Protein Interactions. *J. Med. Chem.* **2018**, *61* (9), 3755-3778.
130. Wang, B.; Yang, H.; Liu, Y.-C.; Jelinek, T.; Zhang, L.; Ruoslahti, E.; Fu, H. Isolation of High-Affinity Peptide Antagonists of 14-3-3 Proteins by Phage Display. *Biochemistry* **1999**, *38* (38), 12499-12504.
131. Wu, H.; Ge, J.; Yao, S. Q. Microarray-Assisted High-Throughput Identification of a Cell-Permeable Small-Molecule Binder of 14-3-3 Proteins. *Angew. Chem. Int. Ed.* **2010**, *49* (37), 6528-6532.
132. Corradi, V.; Mancini, M.; Manetti, F.; Petta, S.; Santucci, M. A.; Botta, M. Identification of the first non-peptidic small molecule inhibitor of the c-Abl/14-3-3 protein-protein interactions able to drive sensitive and Imatinib-resistant leukemia cells to apoptosis. *Biorg. Med. Chem. Lett.* **2010**, *20* (20), 6133-6137.
133. Zhao, J.; Du, Y.; Horton, J. R.; Upadhyay, A. K.; Lou, B.; Bai, Y.; Zhang, X.; Du, L.; Li, M.; Wang, B.; Zhang, L.; Barbieri, J. T.; Khuri, F. R.; Cheng, X.; Fu, H. Discovery and structural characterization of a small molecule 14-3-3 protein-protein interaction inhibitor. *Proc. Natl. Acad. Sci.* **2011**, *108* (39), 16212-16216.
134. Jahn, T.; Fuglsang, A. T.; Olsson, A.; Brüntrup, I. M.; Collinge, D. B.; Volkmann, D.; Sommarin, M.; Palmgren, M. G.; Larsson, C. The 14-3-3 protein interacts directly with the C-terminal region of the plant plasma membrane H<sup>+</sup>-ATPase. *The Plant Cell* **1997**, *9* (10), 1805-1814.
135. Oecking, C.; Piotrowski, M.; Hagemeyer, J.; Hagemann, K. Topology and target interaction of the fusicoccin-binding 14-3-3 homologs of *Commelina communis*. *The Plant Journal* **1997**, *12* (2), 441-453.
136. Wurtele, M.; Jelich-Ottmann, C.; Wittinghofer, A.; Oecking, C. Structural view of a fungal toxin acting on a 14-3-3 regulatory complex. *EMBO J.* **2003**, *22* (5), 987-994.
137. Ottmann, C.; Marco, S.; Jaspert, N.; Marcon, C.; Schauer, N.; Weyand, M.; Vandermeeren, C.; Duby, G.; Boutry, M.; Wittinghofer, A.; Rigaud, J.-L.; Oecking, C. Structure of a 14-3-3 Coordinated Hexamer of the Plant Plasma Membrane H<sup>+</sup>-ATPase by Combining X-Ray Crystallography and Electron Cryomicroscopy. *Molecular Cell* **2007**, *25* (3), 427-440.
138. De Vries-van Leeuwen, I. J.; da Costa Pereira, D.; Flach, K. D.; Piersma, S. R.; Haase, C.; Bier, D.; Yalcin, Z.; Michalides, R.; Feenstra, K. A.; Jiménez, C. R.; de Greef, T. F. A.; Brunsveld, L.; Ottmann, C.; Zwart, W.; de Boer, A. H. Interaction of 14-3-3 proteins with the Estrogen Receptor Alpha F domain provides a drug target interface. *Proc. Natl. Acad. Sci.* **2013**, *110* (22), 8894-8899.

## CHAPTER 1

139. Molzan, M.; Schumacher, B.; Ottmann, C.; Baljuls, A.; Polzien, L.; Weyand, M.; Thiel, P.; Rose, R.; Rose, M.; Kuhenne, P.; Kaiser, M.; Rapp, U. R.; Kuhlmann, J.; Ottmann, C. Impaired Binding of 14-3-3 to C-RAF in Noonan Syndrome Suggests New Approaches in Diseases with Increased Ras Signaling. *Mol. Cell. Biol.* **2010**, *30* (19), 4698-4711.
140. Anders, C.; Higuchi, Y.; Koschinsky, K.; Bartel, M.; Schumacher, B.; Thiel, P.; Nitta, H.; Preisig-Müller, R.; Schlichthörl, G.; Renigunta, V.; Ohkanda, J.; Daut, J.; Kato, N.; Ottmann, C. A Semisynthetic Fusicoccane Stabilizes a Protein-Protein Interaction and Enhances the Expression of K<sup>+</sup> Channels at the Cell Surface. *Chem. Biol.* **2013**, *20* (4), 583-593.
141. Doveston, R. G.; Kuusk, A.; Andrei, S. A.; Leysen, S.; Cao, Q.; Castaldi, M. P.; Hendricks, A.; Brunsveld, L.; Chen, H.; Boyd, H.; Ottmann, C. Small-molecule stabilization of the p53 – 14-3-3 protein-protein interaction. *FEBS Lett.* **2017**, *591* (16), 2449-2457.
142. Rose, R.; Erdmann, S.; Bovens, S.; Wolf, A.; Rose, M.; Hennig, S.; Waldmann, H.; Ottmann, C. Identification and structure of small-molecule stabilizers of 14-3-3 protein-protein interactions. *Angew. Chem. Int. Ed.* **2010**, *49* (24), 4129-32.



## CHAPTER 1

# CHAPTER 2

## Unravelling The Epibestatin Mystery: True Stabilizer Or Assay Artifact?

### **Abstract**

The natural product epibestatin has been reported to be a stabilizer of the interaction between 14-3-3 and the plant plasma membrane proton pump PMA2. Based on the initial publication, a 189 membered library of epibestatin derivatives had previously synthesized and tested, but none of the analogues resulted to be active. Additionally, difficulties in consistently reproducing the initial experiment were encountered. In fact, it appeared that - out of different batches of epibestatin (both commercially available and synthesized in-house) – only epibestatin purchased from Sigma-Aldrich showed some activity. Crystallographic studies revealed that the additional electron density, which was initially assigned to epibestatin, was indeed also present in crystals grown in the absence of it. The structurally similar buffer component CHES was proposed as a possible candidate, but no biophysical evidence of its activity could be given. Still, binding of CHES could be so weak to be under the detection threshold of the assay used. Hence, a small library of 35 CHES analogues was synthesized to investigate for potential increased binding affinity. However, no active compounds could be produced. Taken together, the results indicate that both epibestatin and CHES are not stabilizers of the 14-3-3/PMA2 interaction.

## 2.1 BACKGROUND

The natural product epibestatin (**2.1**, Figure 2.1) represents one of the first examples of a chemical entity found through a HTS campaign specifically designed to find PPI stabilizers. Epibestatin is a synthetic stereoisomer of bestatin,<sup>1-2</sup> a natural product first isolated from *Streptomyces olivoreticulithe*<sup>3</sup> and commonly used in proteomics research in protease inhibitor cocktails.<sup>2</sup> It was reported in 2010 by Rose *et al.*<sup>4</sup>, out of a 37,000-member library, in the attempt to find new chemical matter for the stabilization of 14-3-3 PPIs. For this purpose, the model system chosen was the complex between tobacco 14-3-3e (T14-3-3e) and the plant plasma membrane H<sup>+</sup>-ATPase 2 (PMA2), known to be stabilized by the diterpene fusicoccin A (Fc-A, Figure 2.1).<sup>5-6</sup>

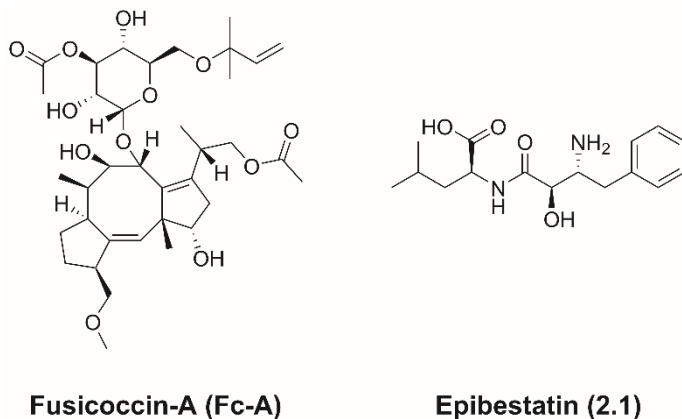
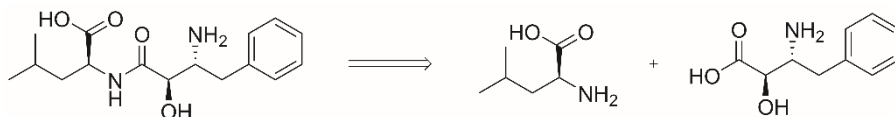


**Figure 2.1** | Structures of Fusicoccin-A (Fc-A) and epibestatin (**2.1**), two known stabilizers of the 14-3-3e:PMA2 interaction.

Compared to Fc-A, **2.1** clearly represents a synthetically more attractive starting point for the study of PPI stabilization. Despite containing three stereocenters, it can be efficiently synthesized via amide coupling between L-leucine and (2*R*,3*R*)-3-amino-2-hydroxy-4-phenylbutanoic acid (Scheme 2.1), for which an efficient enantioselective synthesis has already been reported.<sup>1-2</sup>

The reported crystal structure of the **2.1**-stabilized complex between T14-3-3e and the 30 C-terminal amino acids of PMA2 (PMA2-CT30),<sup>4</sup> shows how **2.1** occupies a different pocket compared to Fc-A, wedged between the T14-3-3e protein and the PMA2-CT30 peptide (Figure 2.2). This different binding pose is probably less efficient, as testified by a lower  $K_d$  for the 14-3-3/PMA2-CT30 complex (1.8  $\mu$ M, in the presence of 50  $\mu$ M of **2.1**) as compared to Fc-A (5.1 nM, in the presence of 5  $\mu$ M of compound). However, since Fc-A is known to be a non-selective 14-3-3 PPI

## CHAPTER 2



### 2.1

**Scheme 2.1** | Retrosynthetic scheme of **2.1**

stabilizer, the fact that **2.1** appeared to interact more extensively with PMA2 may suggest a potential higher selectivity. Additionally, the vacant Fc-A pocket could be exploited to gain potency by mimicry of Fc-A key interactions.

A library of 189 analogues of **2.1** was generated following the synthetic strategy depicted in Scheme 2.1 to investigate the potential stabilization activity of the **2.1** scaffold for the 14-3-3/PMA2 interaction. For the initial screen, a surface-based fluorescence format was used. Briefly, the assay detects the binding of enhanced green fluorescent protein (eGFP) fused with T14-3-3e to surface-immobilized glutathione S-transferase (GST) fused with PMA2-CT66 (the C-terminal 66 amino acids of PMA2). The primary screen yielded a few hits, which were however ruled out as false positives in the subsequent counter-screen based on

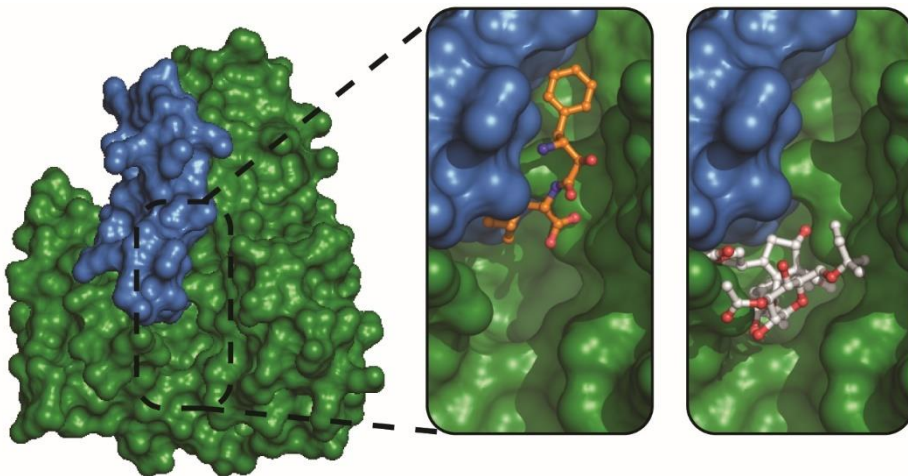


**Figure 2.2** | Crystal structures of T14-3-3e (green surface) and PMA2-CT30 (blue surface) in complex with different stabilizers. FC-A (white sticks) binds in a pocket formed upon 14-3-3/PMA2 complex formation, the so-called “Fc-binding pocket” (PDB: 2O98), while **2.1** (orange sticks) binds in a narrow channel in between the protein and the peptide (PDB: 3M50)

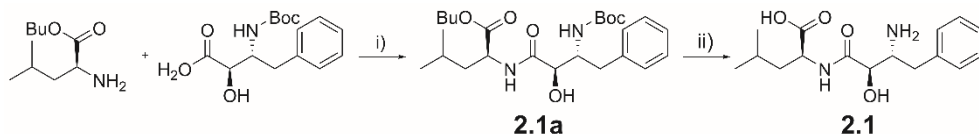
surface plasmon resonance (SPR). Interestingly though, in the primary screen, different batches of **2.1** yielded different results. In the initial assay optimization experiments, that were performed using **2.1** purchased from Sigma-Aldrich, a

## CHAPTER 2

moderate activity (~1.8-fold over DMSO negative control at 100  $\mu\text{M}$  vs ~5.3-fold of Fc-A at 2  $\mu\text{M}$ ) could be observed. On the contrary, **2.1** used as positive control in the screen, from Apollo Scientific, as well as a third sample (part of the 189-member screening library) did not show any stabilization.<sup>7</sup>

### 2.2 NMR AND SPR STUDIES ON EPIBESTATIN

In an attempt to investigate the why two different batches of **2.1** gave contradicting outcomes, a new batch was purchased from Sigma-Aldrich. Interestingly, we found out that this sample came from the single batch that was ever produced by Sigma-Aldrich. The product was so old that its origins could not be traced and hence, no additional information about the synthetic process could be retrieved. The product has been discontinued. An in-house batch was also produced in 45% yield, following a known literature procedure<sup>2</sup> (Scheme 2.2).



**Scheme 2.2** | Synthesis of **2.1**. i) PyBOP, DIPEA, DCM, RT, o/n, 70%. ii) HCl 4M in dioxane, DCM, RT, o/n, 45%.

First, NMR experiments were conducted. <sup>1</sup>H NMR spectra were recorded for **2.1** from Sigma-Aldrich (“Epi\_Sigma”, blue spectrum, Figure 2.3) and in-house made **2.1** (“Epi\_AZ”, green spectrum, Figure 2.3) separately, and then mixed together in equal molar amount (“Epi\_mix”, red spectrum). By comparison of the three spectra, it was clear that the two samples were identical (Figure 2.3). Notably, the <sup>1</sup>H NMR spectrum of Epi\_Sigma showed some small traces of impurities not present in Epi\_AZ and that could not be identified (for full spectra see Figure S2.1-S2.3). Overall, the three spectra do not show any significant difference, suggesting that the Epi\_AZ is indeed identical to Epi\_Sigma. **2.1** is a chiral molecule, so optical rotation was determined. Values obtained were in accordance with literature data:  $[\alpha]_{\text{D}}^{20}$  (*exp.*) = +10 (*c* 0.40, H<sub>2</sub>O) vs  $[\alpha]_{\text{D}}^{20}$  (*lit.*) = +5.9 (*c* 0.38, H<sub>2</sub>O), for **2.1** hydrochloride salt.<sup>2</sup>

Next, both samples were tested in a 14-3-3/PMA2 SPR assay. In the assay format used, a construct of the 52 C-terminal amino acids of PMA2 (PMA2-CT52) was immobilized on a CM5 chip, followed by subsequent injections of preincubated 14-3-3e (10  $\mu\text{M}$ ) and **2.1** (100  $\mu\text{M}$ ) or 1% DMSO (blank) in running buffer. Fc-A (10  $\mu\text{M}$ ) was used as positive control, yielding strong and fast association, followed by very slow dissociation (Figure 2.4a, blue, orange and grey curves). Precedent experience on the above-mentioned assay set-up, showed that traces of Fc-A still present in the flow system after the regeneration step would cause the subsequent

## CHAPTER 2

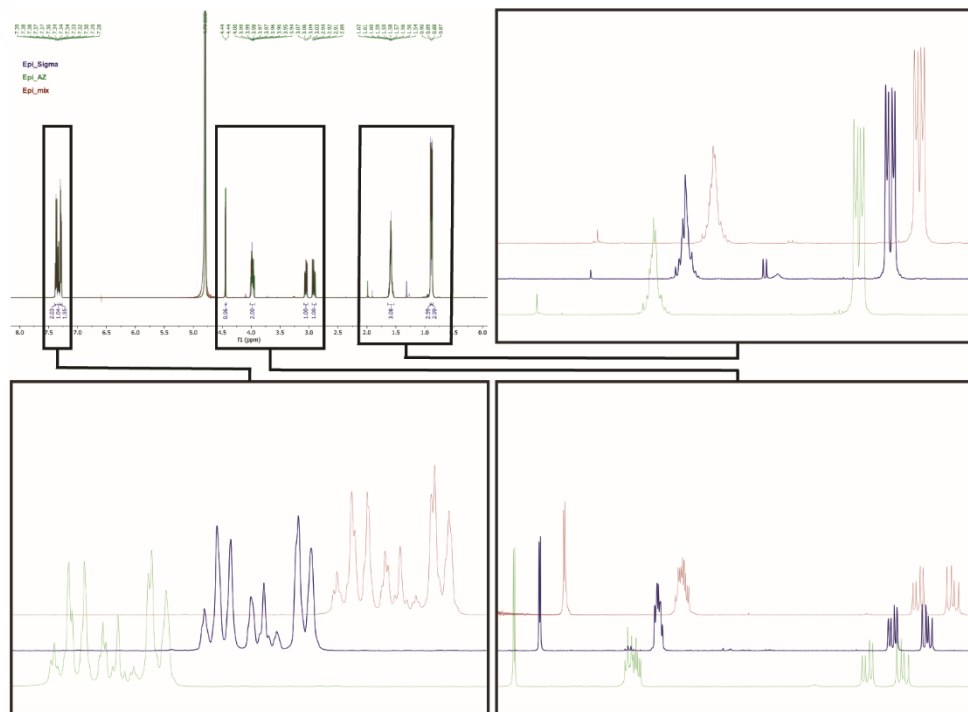


**Figure 2.3** |  $^1\text{H}$  NMR spectra comparison of Epi\_AZ (green spectrum, recorded at 500 MHz), Epi\_Sigma (blue spectrum, recorded at 600 MHz) and Epi\_mix (red spectrum, recorded at 500 MHz). Top left panel shows the three superimposed full spectra, while the other panels show enlarged regions, with the spectra staggered relative to each other. For full spectra see Figure S2.1-S2.3.

sample injection to look partially active, leading to potential false positives. Mindful of this, multiple DMSO injections were added in between the Fc-A injections and the **2.1** ones (Figure 2.4b). Injection of Epi\_Sigma (Figure 2.4c, yellow curve) resulted in a small but detectable binding, which became even more evident upon a second injection (Figure 2.4c, light blue curve), as opposed to Epi\_AZ (Figure 2.4c, green and dark blue curves), where no binding was observed. As the second round of injections yielded the same outcome, it was hypothesized that the observed signal from Epi\_Sigma could be due to unspecific binding and/or deposition effect on the surface. To confirm this in a subsequent experiment, DMSO controls (T14-3-3e + 1% DMSO) were added between each **2.1** injection (Figure 2.5). Injections of either 14-3-3 + Epi\_Sigma (green and blue curve) or Epi\_Sigma alone (orange and red curve) did not give a response above the assay noise, and indeed the highest signal appears to come from the second injection of Epi\_Sigma alone (red curve). This, together with the fact that none of the Epi\_AZ injections gave any appreciable signal, confirmed that our initial assessment of deposition/unspecific binding was specific to the Epi\_Sigma sample.

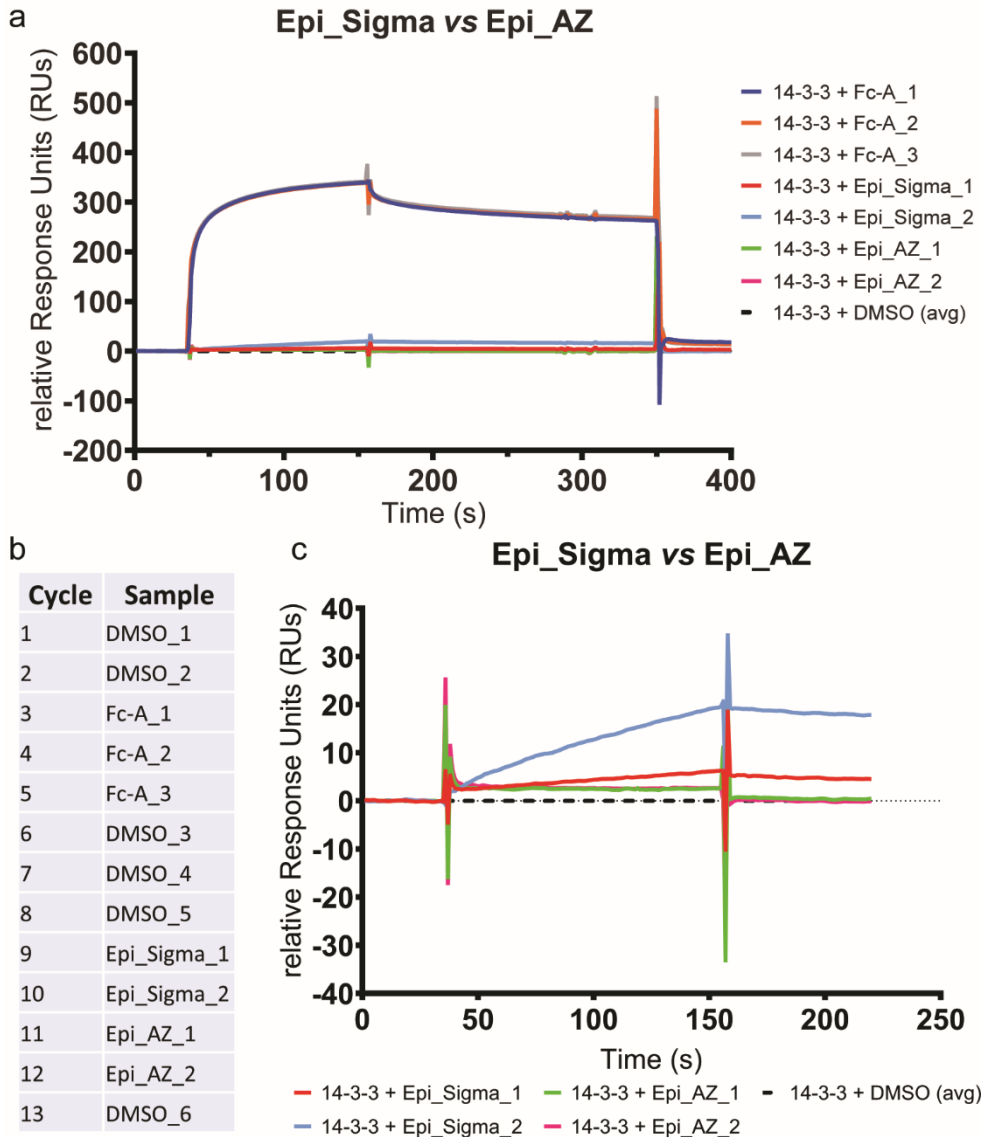


**Figure 2.4 |** SPR binding analysis evaluating the effect of Epi\_Sigma and Epi\_AZ against T14-3-3e:PMA2-CT52. (a) Representative example of an SPR sensorgram where a fixed concentration of T14-3-3e protein (10  $\mu$ M) and compound (100  $\mu$ M) were injected over a surface-immobilised PMA2-CT52 peptide. Fc-A (10  $\mu$ M) was used as positive control. (b) Table illustrating the injection order of the samples (co-injected with 10  $\mu$ M T14-3-3e). (c) Close-up view of the SPR curves from the different samples of 2.1. The “Relative signal” (expressed in Response Units, RUs) achieved (y-axes), relative to the DMSO control (blank), is presented as a function of time, in seconds (x-axes). The “DMSO” control curve (*i.e.* injection of T14-3-3e alone, hence representative of the T14-3-3e:PMA-CT52 binary interaction) corresponds to the median value for each time point of DMSO injections n° 2, 5 and 6 (cycles 2, 8 and 13, respectively), and has been reference-subtracted for each curve.

The fact that no binding signal was observed in the presence of Epi\_AZ may also indicate that the low levels of unidentified contaminants in the Epi\_Sigma batch (Figure 2.3) are responsible for its activity. However, without any further knowledge on the synthetic process used and since no conclusive characterization of the impurities observed in the  $^1\text{H}$  NMR spectrum of Epi\_Sigma was possible, only speculations in this regard could be made (potentially some residual metals or small traces of organics).

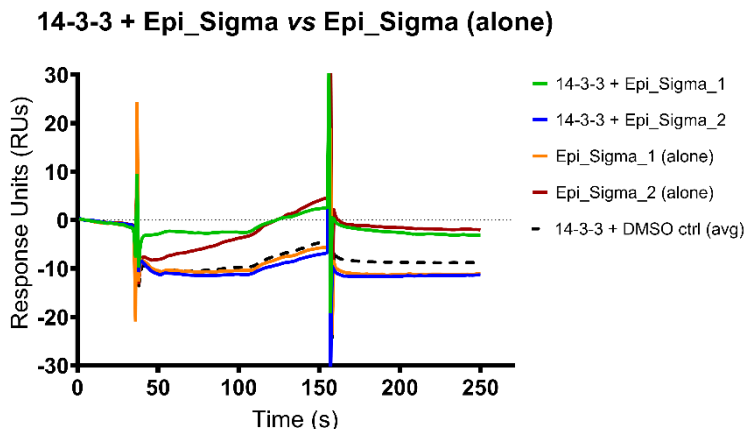


**Figure 2.5** | Analysis of possible unspecific binding and/or deposition of Epi\_Sigma. Epibestatin injections of 14-3-3 + Epi\_Sigma (green and blue curve) and Epi\_Sigma alone (orange and red curve) in are reported. 14-3-3 + DMSO control injections (blank, corresponding to 14-3-3 alone, reported as average value, black dashed curve) were added after each sample injection. Curves were not blank-subtracted.

## 2.3 IN-DEPTH CRYSTALLOGRAPHIC ANALYSIS AND THE CHES HYPOTHESIS

In an attempt to understand the results from different batches of **2.1** in the SPR assay, we decided to perform crystallography experiments. X-ray crystallography has been successfully employed in the study of low MW and low potency compounds, for example in fragment-based approaches<sup>8</sup>, and we wanted to investigate the possibility that **2.1** (MW = 308 Da) may have such low affinity that it was not detectable by SPR. A crystal structure of the T14-3-3e/PMA2-CT30 binary complex was obtained in the absence of **2.1**.



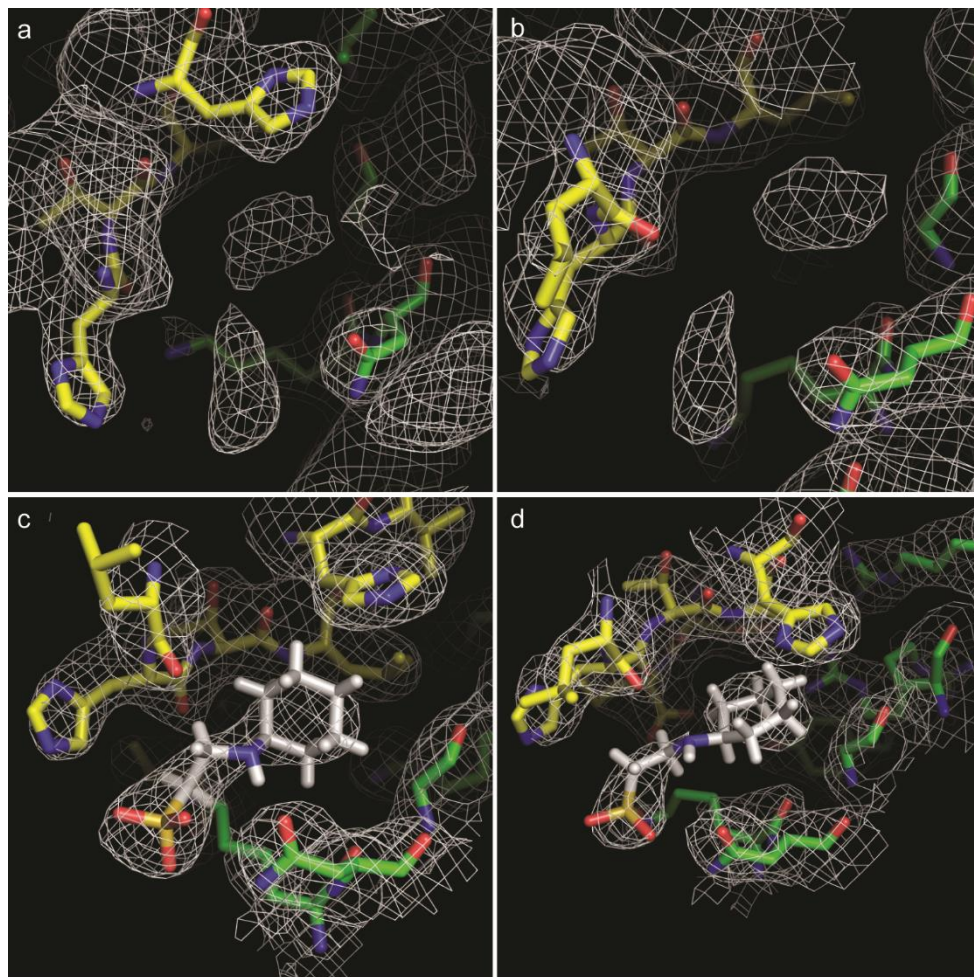


**Figure 2.6** | Detailed analysis of the additional electron density peaks found in the T14-3-3e/PMA2-CT30 crystal structures. (a) Published crystal structure (PDB 3M50), with **2.1** removed (resolution 2.6 Å). (b) Crystal structure obtained in the absence of **2.1** (resolution 2.9 Å) showing additional electron density in the same region as observed in pdb 3M50 (c and d) Corresponding crystal structures with the buffer component *N*-cyclohexyl-2-aminoethanesulfonic acid (CHES) modelled in. In all panels, T14-3-3e is shown in green and PMA2-CT30 in yellow. The 2Fo-Fc electron density is contoured at 1  $\sigma$  and displayed as a white mesh.

In this structure, additional electron density was observed at the interface between the PMA2-CT30 peptide and T14-3-3e corresponding to the same region where **2.1** was modelled in the original published structure (PDB 3M50)<sup>4</sup>, thus suggesting that this electron density did not originate from **2.1** binding at the interface (Figure 2.6). Due the poor resolution of both crystal structures (2.6 Å and 2.9 Å, respectively), it was not possible to unequivocally identify the source of these electron density peaks. Candidates included semi-ordered water molecules or metal

## CHAPTER 2

ions, or alternatively, a component of the crystallization buffer. In particular, one of the components of the crystallization buffer, namely *N*-cyclohexyl-2-aminoethanesulfonic acid (CHES, **2.2**), drew attention. **2.2** was an interesting candidate, as it structurally resembles **2.1** and could be reasonably modelled into the observed electron density (Figure 2.6c and 2.6d). Hence, to evaluate a possible role of **2.2** in stabilizing the T14-3-3e/PMA2-CT30 interaction an SPR assay was performed. The assay was set up using the same conditions described above for **2.1**. **2.2** was tested both as DMSO solution (500  $\mu$ M, orange curve, Figure 2.7a and 2.7b) and dissolved directly in running buffer (4 mM, blue curve, Figure 2.7c), with

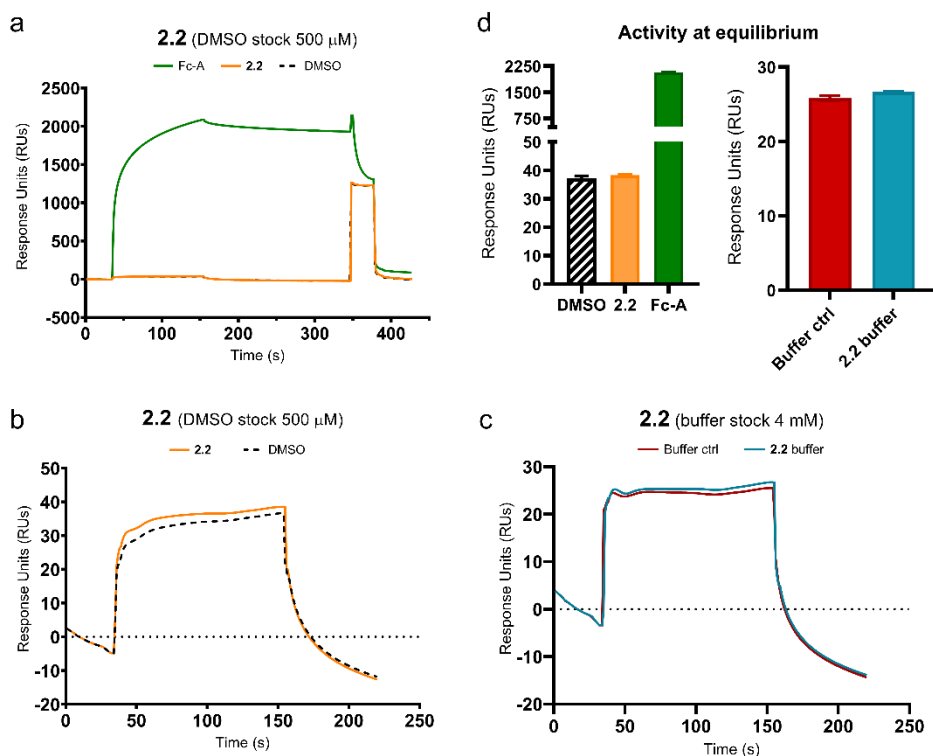


**Figure 2.7** | Test of **2.2** in SPR assay. (a) representative example of a SPR sensorgram in which fixed concentrations of Fc-A positive control (100  $\mu$ M, green curve), **2.2** (500  $\mu$ M in DMSO stock, orange curve) and DMSO control (1% v/v) in the presence of 10  $\mu$ M T14-3-3e were flowed over immobilized PMA2-CT52. (b) Close-up view of **2.2** and DMSO control curves. (c) Sensorgram comparing **2.2** (blue curve), injected as 4 mM buffer stock and control injection (i.e. T14-3-3e alone in buffer, red curve) over immobilized PMA2-CT52. (d) Histogram reporting values at equilibrium response (reported as means  $\pm$  SD,  $n = 3$ ).

Fc-A as positive control (green curve, Figure 2.7a), in the presence of 10  $\mu$ M T14-3-3e. In both setups, no measurable activity was observed for **2.2**, as reported in Figure 2.7d (values at equilibrium response). The lack of a positive response under the assay conditions used, does not exclude, however, that **2.2** may still bind at the 14-3-3/PMA2 interface, although so weakly that its affinity could not be detected by SPR.

In view of this, we hypothesized that an expansion from the original, fragment-like **2.2** scaffold towards the vacant Fc-A binding pocket, may lead to an increased and detectable overall affinity (Figure 2.8a). The library was designed by keeping the N-cyclohexylethylamino moiety constant, as it fitted rather well in the observed additional electron density and may presumably serve as an anchor point, and by varying linker type, spacer length and bulky lipophilic head (R groups, Tables 1-5). The linker type was chosen on the basis of conferring the right orientation to the lipophilic head towards the Fc-A pocket as well as maintaining the structural similarities of the sulfonate function. Therefore we opted for thioether, sulfoxide, sulfone, amide and sulfonamide linkers. The spacer should be long and flexible enough to allow to reach the vacant Fc-A pocket. Hence, we chose alkyl chains of varying length (two to four methylene groups). Finally, for the lipophilic head, we opted for phenyl rings (both substituted and unsubstituted), together with smaller alkyl groups (ethyl and isopropyl). We included the benzhydryl moiety in the library design as previous observations showed a high intrinsic affinity of this bulky group for the 14-3-3 protein surface, binding in the region of the Fc-A pocket.<sup>9-10</sup>

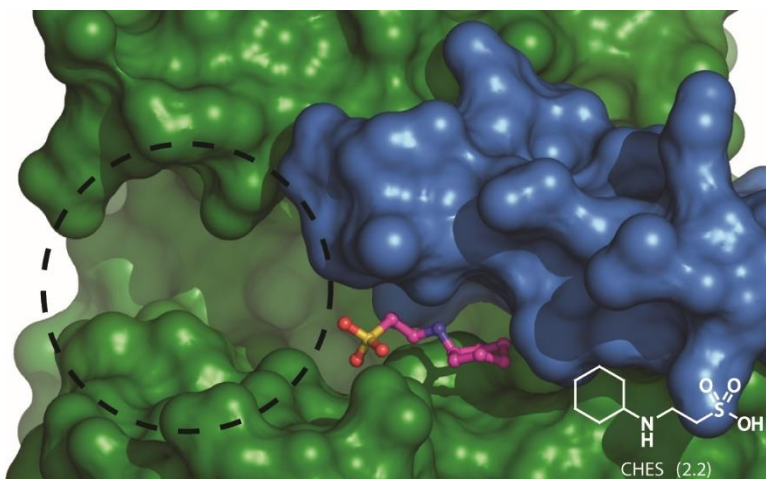
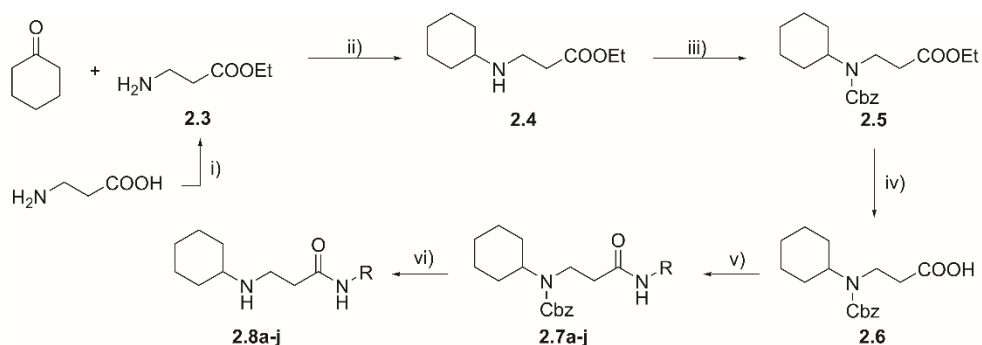


**Figure 2.8** | Crystal structure of the complex between T14-3-3e (green surface) and PMA2-CT30 (blue surface) with **2.2** modelled in pink sticks, highlighting the vacant Fc-A binding pocket (black dashed circle). The chemical structure of **2.2** (N-cyclohexyl-2-aminoethanesulfonic acid, **2.2**) is reported in white in the bottom right-hand corner.

## CHAPTER 2

The synthesis of the amide library started with the generation of the common *N*-cyclohexylpropanoic acid intermediate **2.6** (Scheme 2.3). 3-Aminopropanoic acid was reacted with ethanol to afford the corresponding ethyl ester (**2.3**), which was subsequently reductively aminated with cyclohexanone in the presence of sodium triacetoxyborohydride to afford the corresponding *N*-cyclohexylamino derivative (**2.4**). Cbz protection of the amino group followed by ester hydrolysis using lithium hydroxide afforded carboxylic acid **2.6**. Installation of the different substituents was carried out in parallel fashion by amide coupling using PyBOP and DIPEA (**2.7a-j**) which, upon catalytic hydrogenation to remove the Cbz group, yielded the desired amides (**2.8a-j**, Table 2.1). Compound **2.8b** was prepared from the corresponding 4-nitrophenylethylamine which gave the corresponding amine derivative under H<sub>2</sub> atmosphere.

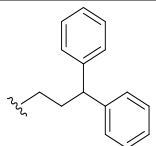
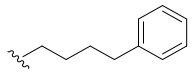
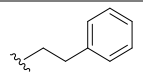
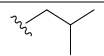
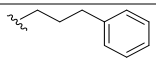
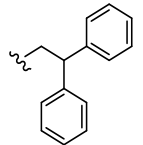
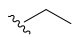
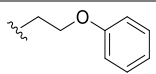


**Scheme 2.3** | Synthesis of the amide analogues of **2.2**. i) 3-Aminopropanoic acid, dry EtOH, SOCl<sub>2</sub>, 0 °C, 10 min, then reflux, 2 h (98%). ii) Cyclohexanone, Na[BH(OAc)<sub>3</sub>], MeOH/DCM 3:2, RT, on (66%). iii) CbzCl, TEA, dry DCM, 0 °C, then RT. iv) LiOH·H<sub>2</sub>O, EtOH/H<sub>2</sub>O 4:1, RT, 6 h (76%, two steps). v) RNH<sub>2</sub>, PyBOP, DIPEA, dry DMF, RT, on (9-77%). vi) H<sub>2</sub> (1 bar), 5% Pd/C in MeOH, RT, 12 h (24-64%).

**Table 2.1** | Amide derivatives of **2.2**<sup>a</sup>.

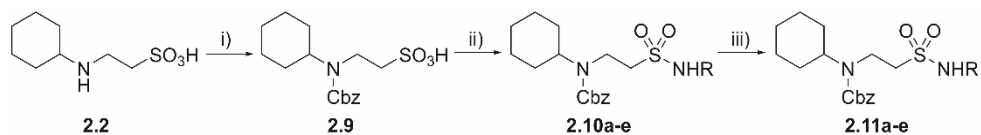
Compound	R group	Yield (%)
<b>2.8a</b>		24
<b>2.8b</b>		64

## CHAPTER 2

<b>2.8c</b>		32
<b>2.8d</b>		31
<b>2.8e</b>		31
<b>2.8f</b>		43
<b>2.8g</b>		37
<b>2.8h</b>		61
<b>2.8i</b>		55
<b>2.8j</b>		31

(a) Yields refer to final synthetic step

The sulfonamides **2.11a-e** were prepared from **2.2** (Scheme 2.4). Cbz protection was followed by coupling with the desired amine in the presence of oxalyl chloride to give the corresponding Cbz-protected sulfonamides **2.10a-e** in moderate yields over two steps. Final catalytic hydrogenation gave the resulting sulfonamides **2.11a-e** (Table 2.2).



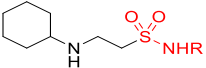
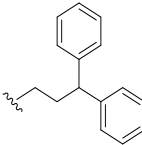
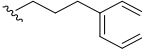
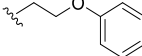
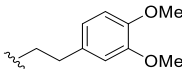
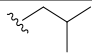
**Scheme 2.4** | Synthesis of the sulfonamide analogues. i)  $K_2CO_3$ , CbzCl,  $H_2O/1,4$ -dioxane 1:1,  $0\text{ }^\circ\text{C}$ , then RT, 5 h. ii)  $(COCl)_2$ , DMF drops, dry DCM, RT, on (12-51%, two steps). iii)  $H_2$  (1 bar), 5% Pd/C in MeOH, RT, 12 h (54-97%).

The sulfoxide and sulfone derivatives were synthesized as shown in Scheme 2.5. The non-commercially available alkyl bromides **2.12a-c** were prepared from the

## CHAPTER 2

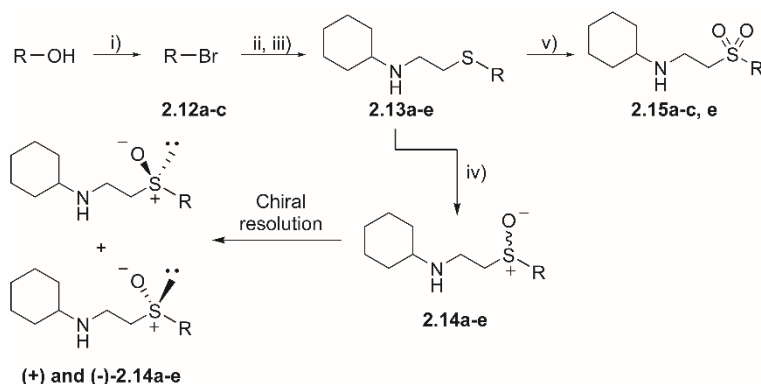
corresponding alcohols by reaction with  $\text{PBr}_3$ . The alkyl bromides were reacted with 2-mercaptoethanamine hydrochloride in degassed DMF under microwave heating and subsequently reductively aminated using cyclohexanone to give the desired thioethers (**2.13a-e**, Table 2.3). Oxidation of the thioethers using hydrogen peroxide in glacial acetic acid gave either the corresponding sulfoxides (**2.15a-c,e**, Table 2.4)

**Table 2.2** | Sulfonamide derivatives of **2.2<sup>a</sup>**.

		
Compound	R group	Yield (%)
<b>2.11a</b>		54
<b>2.11b</b>		81
<b>2.11c</b>		97
<b>2.11d</b>		96
<b>2.11e</b>		93

(a) Yields refer to final synthetic step

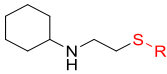
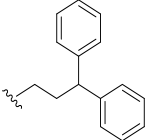
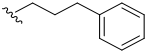
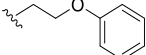
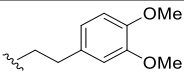
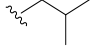
after 50 min reaction or the sulfones if allowed to react overnight (**2.14a-e**). The sulfoxides **2.14a-e** were subsequently chirally separated affording the pure enantiomers with good enantiomeric excess (95.4-99.8 %ee, Table 2.5).



## CHAPTER 2

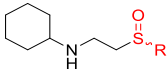
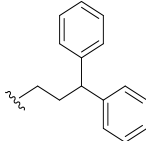
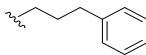
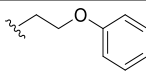
**Scheme 2.5** | Synthesis of the thioether, sulfoxide and sulfone analogues. i)  $\text{PBr}_3$ , dry DCM,  $0\text{ }^\circ\text{C}$ , 2 h, then RT, on (54-86%). ii)  $\text{HS}(\text{CH}_2)_2\text{NH}_2\cdot\text{HCl}$ , degassed DMF, MW,  $100\text{ }^\circ\text{C}$ , 10 min, (1 bar). iii) cyclohexanone,  $\text{Na}[\text{BH}(\text{OAc})_3]$ , dry MeOH/DCM 3:2, RT, on (4-25%). iv) 30%  $\text{H}_2\text{O}_2$  in glacial AcOH, RT, 50 min (55-98%). v) 30%  $\text{H}_2\text{O}_2$  in glacial AcOH, RT, on (8-40%).

**Table 2.3** | Thioether derivatives of **2.2<sup>a</sup>**.

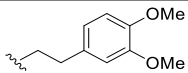
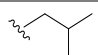
		
Compound	R group	Yield (%)
<b>2.13a</b>		4
<b>2.13b</b>		20
<b>2.13c</b>		4
<b>2.13d</b>		16
<b>2.13e</b>		25

(a) Yields refer to final synthetic step

**Table 2.4** | Sulfoxide derivatives of **2.2<sup>a</sup>**.

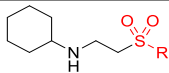
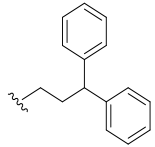
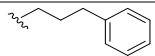
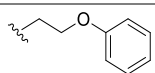
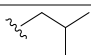
		
Compound	R group	Yield (%) and ee (%)
(+ and -) <b>2.14a</b>		75 99.8/95.4
(+ and -) <b>2.14b</b>		76 97.8/99.0
(+ and -) <b>2.14c</b>		98 93.0/97.0

## CHAPTER 2

(+ and -) <b>2.14d</b>		55 99.2/97.6
(-) and (+) <b>2.14e</b>		90 99.6/99.4

(a) Yields refer to final synthetic step

**Table 2.5** | Sulfone derivatives of **2.2**<sup>a</sup>.

Compound	R group	Yield (%)
		
<b>2.15a</b>		40
<b>2.15b</b>		7
<b>2.15c</b>		8
<b>2.15e</b>		32

(a) Yields refer to final synthetic step

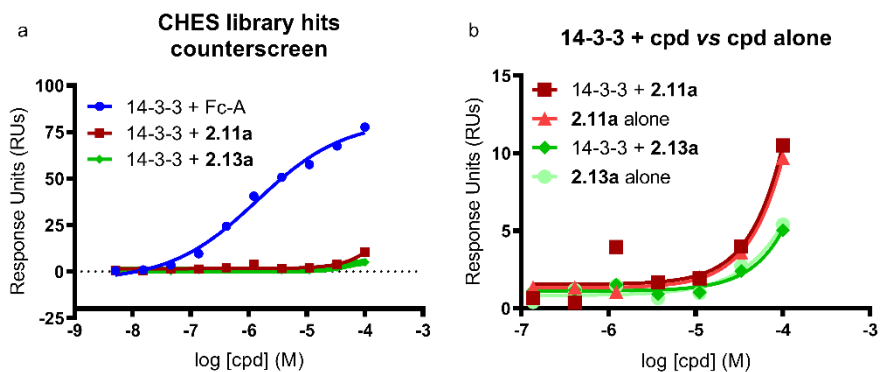


**Figure 2.9** | SPR counter-screening of **2.2** analogue hits from primary screen. (a) Concentration-response curves of compounds **2.10a** (red squares) and **2.12a** (green diamonds), with Fc-A as positive control (blue circles), in the presence of T14-3-3e (10  $\mu$ M), having PMA2-CT52 peptide immobilized on the surface (b) Concentration-response curves of **2.10a** and **2.12a** when tested in the presence (red squares and green diamonds) and in the absence (light red triangles and light green circles) of T14-3-3e. Concentration response experiments were performed in 1:3 dilution series, starting from a concentration of 100  $\mu$ M.



## CHAPTER 2

The compounds were then tested using the same surface-based fluorescence assay format, monitoring the binding of eGFP-T14-3-3e to surface-immobilized GST-PMA2-CT66. The first round of screening, conducted in single concentration (200  $\mu$ M), revealed two potential hits, **2.11a** (~ 2.1-fold over DMSO ctrl) and **2.13a** (~ 3.3-fold over DMSO ctrl).<sup>7</sup> These two compounds were counter-screened in our SPR assay in a concentration-response format, using Fc-A as positive control, monitoring the binding of T14-3-3e over immobilized PMA2-CT52 peptide (Figure 2.9a). Both compounds gave a small but detectable signal, which however was ruled out as unspecific binding to the peptide when the compounds were tested in the absence of protein (Figure 2.9b).

### 2.4 CONCLUSION

In summary, the reported 14-3-3/PMA2 PPI stabilization effect of **2.1** could not be reproduced. Despite being identical by NMR, only **2.1** purchased from Sigma-Aldrich (Epi\_Sigma), and not **2.1** synthesized in-house (Epi\_AZ), gave a signal in the SPR assay, thus indicating an unknown contamination of the commercial batch. Another factor that must be taken into account, that has probably misled the authors of the original work in the SPR data interpretation, is the presence of residual traces of Fc-A in the SPR system which made the following injection look partially active. Structural evidence of **2.1** binding to the T14-3-3e/PMA2-CT30 complex were also not conclusive, as the electron density peaks initially attributed to **2.1** were also present in crystals obtained in the absence of **2.1**. The resolution of the crystal structures was unfortunately too low to confidently determine what the origin of the density was, but the buffer component **2.2** was suggested to be a possible candidate. Biochemical evaluation of **2.2**, as well as a number of synthesized **2.2** analogues, did not provide any evidence of stabilization.

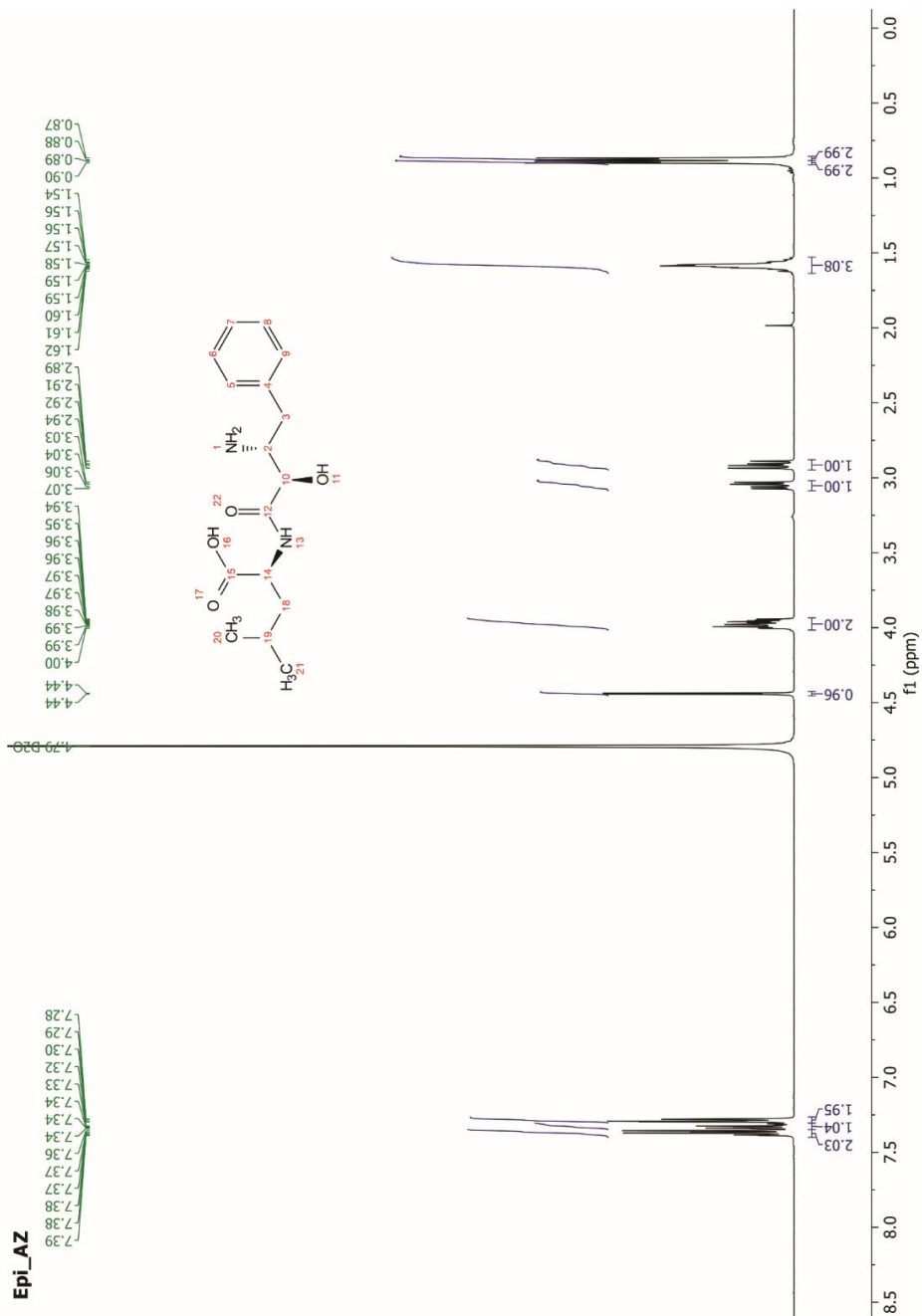
Taken together, the results in this chapter conclusively show that **2.1** is not a stabilizer of the 14-3-3/PMA2 interaction, but rather an artefact.

### Author contribution

The work in this chapter was performed in collaboration with Dr. Sebastian Andrei (background information, crystallographic data and initial testing of the CHES analogues). Dr. Anders Gunnarsson is thanked for his training and help with the SPR assay.

## 2.5 EXPERIMENTAL SECTION

## 2.5.1 Supporting Figures

Figure S2.1. <sup>1</sup>H NMR of "Epi\_AZ".

CHAPTER 2

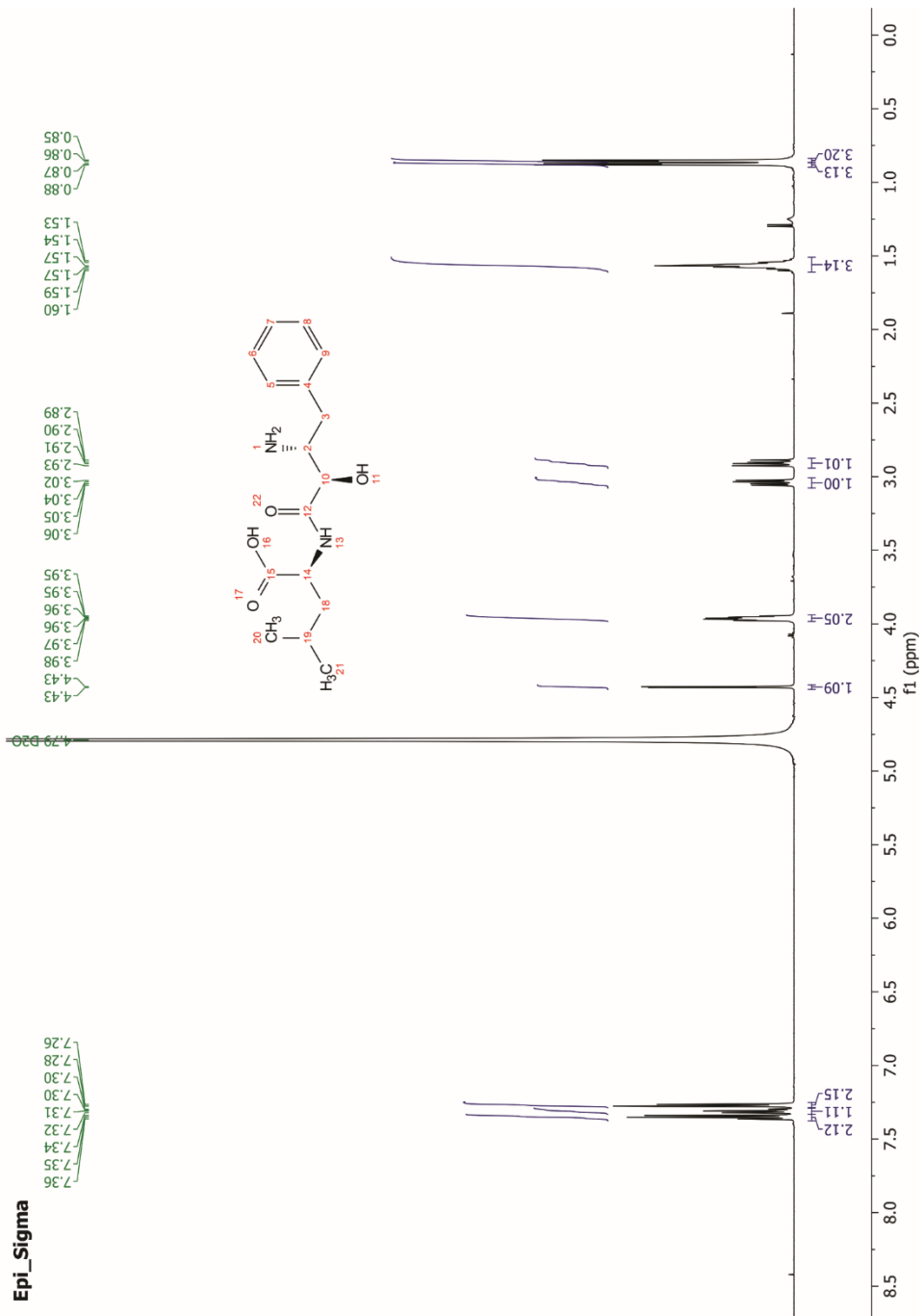


Figure S2.2. <sup>1</sup>H NMR of "Epi\_Sigma".

CHAPTER 2

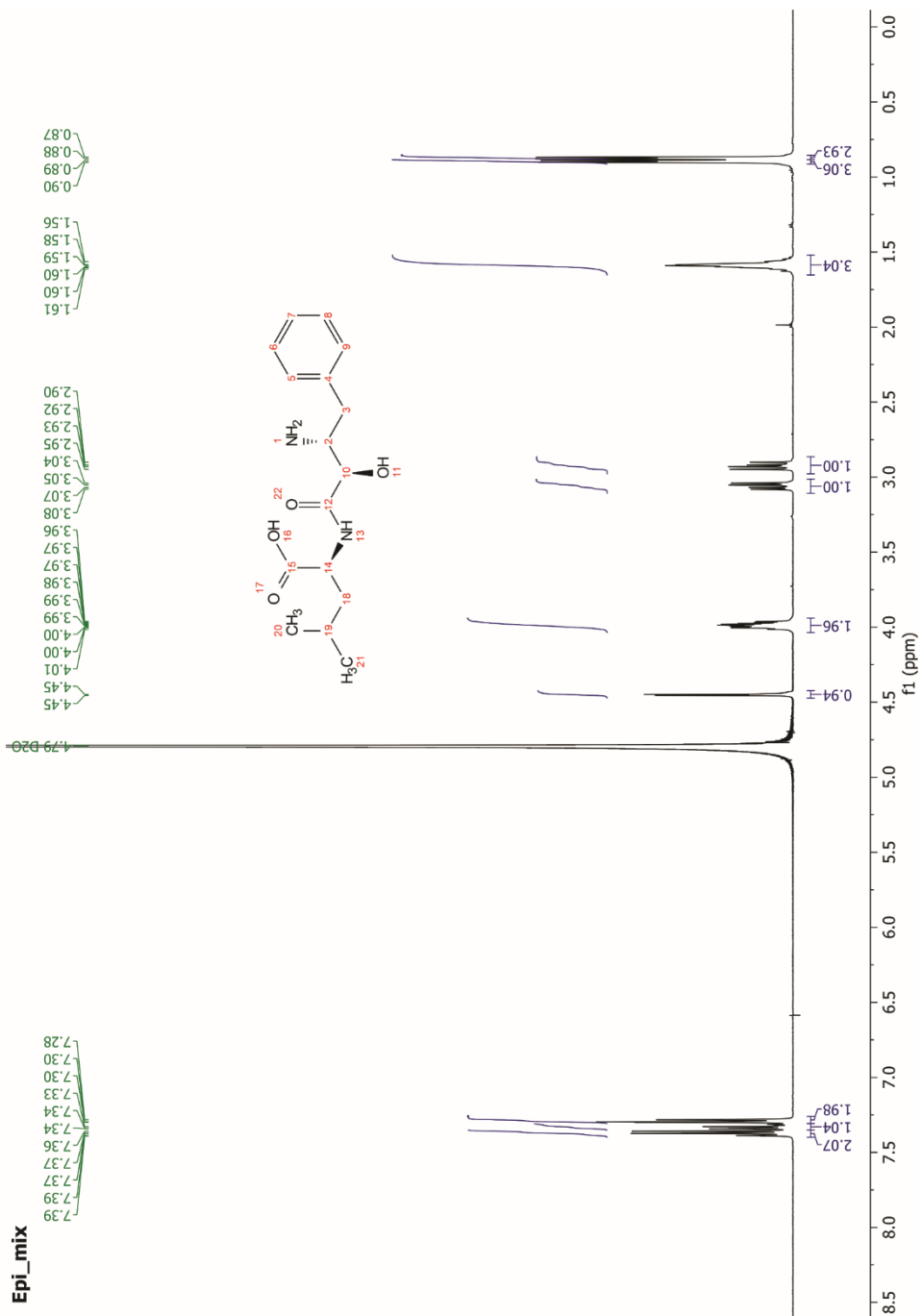


Figure S2.3. <sup>1</sup>H NMR of "Epi\_mix", a mixture of equimolar amount of Epi\_AZ and Epi\_Sigma.

### 2.5.2 Surface Plasmon Resonance (SPR)

Unless otherwise stated, SPR measurements were performed on a Biacore 3000 (GE Healthcare) using 10 mM HEPES, 150 mM NaCl, 0.05% TWEEN 20, pH 7.4 as running buffer. PMA2-CT52 was immobilized on a CMD500L Biacore Sensor Chip (XanTec Bioanalytics GmbH, Düsseldorf, Germany) at approximately 4000 RUs using EDC/NHS coupling chemistry (from a 10 mM solution in acetate buffer pH = 5.5). In subsequent experiments, T14-3-3e protein (10  $\mu$ M) was flowed in running buffer + 1% DMSO. Fc-A (10  $\mu$ M or 100  $\mu$ M) and test compounds (100  $\mu$ M) were dissolved in running buffer and prepared from 10 mM DMSO stock solution to achieve final test concentration and 1% final DMSO concentration. Compounds were either premixed with protein or injected alone directly at a flowrate of 20  $\mu$ L/min and 20 °C for 120 s or 150 s in running buffer. Regeneration step was performed with a 60 s pulse of 0.5 % SDS. All experiments were performed in triplicate (n = 3) unless otherwise stated. Sensograms were analyzed using BiaEvaluation software, data points were extracted and final curves were plotted using Microsoft Excel (Office 365). For the **2.2** analogues, in each curve the values at equilibrium response (*i.e.* binding coverage) were extracted and fitted using a four-parameter logistic model (4PL) using GraphPad Prism version 8.3.0 for Windows, GraphPad Software, San Diego, California USA, [www.graphpad.com](http://www.graphpad.com).

### 2.5.3 Protein and Peptide

The T14-3-3e used for crystallization and SPR studies was expressed and purified according to ref.<sup>11</sup> The PMA2-CT52 construct (C-terminal region encompassing amino acids 905-956), characterized by the C-terminal YDI-COOH phosphomimic (in place of native YpSV-COOH)<sup>11</sup>, was used for SPR studies.

Sequence: TNFNELNQLAEAKRRRAEIRQRELHTLKGHVESVVKLGLDIETIQQSYDI.

### 2.5.4 Chemistry

#### *General Information*

All solvents and reagents were obtained from commercially available sources and used without further purification. The microwave syntheses were performed in a Biotage Initiator with an external surface IR probe. Flash column chromatography was carried out on prepacked silica gel columns supplied by Biotage and using Biotage automated flash systems with UV detection.

UHPLC-MS experiments were performed using a Waters Acquity UHPLC system combined with a SQD mass spectrometer. The UHPLC system was equipped with both a BEH C<sub>18</sub> column 1.7  $\mu$ m 2.1×50 mm in combination with a 46 mM (NH<sub>4</sub>)<sub>2</sub>CO<sub>3</sub>/NH<sub>3</sub> buffer at pH 10 and a HSS C<sub>18</sub> column 1.8  $\mu$ m 2.1×50 mm in combination with 10 mM formic acid or 1 mM ammonium formate buffer at pH 3. The mass spectrometer used ESI<sup>+</sup>/– as ion source. UPLC was also carried out using a Waters UPLC fitted with Waters QDa mass spectrometer (Column temp 40 °C, UV = 190–400 nm, MS = ESI with pos/neg switching) equipped with a Waters Acquity BEH 1.7  $\mu$ m 2.1×100 mm in combination with either 0.1% formic acid in water, 0.05% TFA in water or 0.04% NH<sub>3</sub> in water. The flow rate was 1 mL/min.

Preparative HPLC was performed by Waters Fraction Lynx with ZQ MS detector on either a Waters Xbridge C<sub>18</sub> OBD 5  $\mu$ m column (19×150 mm, flow rate 30 mL/min or 30×150 mm, flow rate 60 mL/min) using a gradient of 5–95% MeCN with 0.2% NH<sub>3</sub> at pH 10 or a Waters SunFire C18 OBD 5  $\mu$ m column (19×150 mm, flow rate 30 mL/min or 30×150 mm, flow rate 60 mL/min) using a gradient of 5–95% MeCN with 0.1 M formic acid or on a Gilson Preparative HPLC with a UV/VIS detector 155 on a Kromasil C8 10  $\mu$ m column (20 × 250 mm, flow rate 19 mL/min, or 50 × 250 mm, flow rate 100 mL/min) using a varying gradient of ACN with 0.1% formic acid (FA) in water or 0.2%

## CHAPTER 2

ammonia (NH<sub>3</sub>) in water. Preparative SFC was performed on a Viridis BEH column (5 μm 250x30 mm) using a gradient of CO<sub>2</sub> in MeOH/H<sub>2</sub>O/NH<sub>3</sub> 97/3/50 mM buffer over 15 minutes. Molecular mass (HR-ESI-MS) was recorded using a Shimadzu LCMS-2020 instrument (ESI+). Purity of all test compounds was determined by LCMS.

General <sup>1</sup>H NMR spectra were recorded on a Bruker Avance II, III, AV300, AV400 or AVIII500 spectrometer at a proton frequency of 400, 500 or 600 MHz at 25 °C or at a temperature and frequency stated in each experiment. <sup>13</sup>C NMR spectra were recorded at 101 MHz or 126 MHz. The chemical shifts (δ) are reported in parts per million (ppm) with residual solvent signal used as a reference ((CD<sub>3</sub>)<sub>2</sub>SO at 2.50 ppm for <sup>1</sup>H NMR and 39.52 ppm for <sup>13</sup>C NMR, CDCl<sub>3</sub> at 7.26 ppm for <sup>1</sup>H NMR and 77.16 ppm for <sup>13</sup>C NMR, CD<sub>3</sub>OD at 3.31 ppm for <sup>1</sup>H NMR and 49.00 ppm <sup>13</sup>C NMR). Coupling constants (*J*) are reported as Hz. NMR abbreviations are used as follows: br = broad, s = singlet, d = doublet, t = triplet, q = quartet, m = multiplet. Protons on heteroatoms such as COOH protons are only reported when detected in NMR and can therefore be missing.

### *Synthetic procedures and compound characterization*

**Tert-butyl ((2*R*,3*R*)-3-((tert-butoxycarbonyl)amino)-2-hydroxy-4-phenylbutanoyl)-L-leucinate (2.1a)** was prepared as described by Richter *et al.*<sup>2</sup> to afford the title compound (83 mg, 70 %) as an orange solid. <sup>1</sup>H NMR (400 MHz, CDCl<sub>3</sub>) δ 7.24 – 7.33 (m, 2H), 7.16 – 7.24 (m, 3H), 5.38 (br, 1H), 5.05 (d, *J* = 6.9 Hz, 1H), 4.50 (m, 1H), 4.31 (br, 1H), 4.01 (br, 1H), 2.81 – 3.12 (m, 2H), 1.83 (s, 1H), 1.51 – 1.75 (m, 3H), 1.46 (s, 9H), 1.40 (s, 9H), 0.92 – 1 (m, 6H).

**((2*R*,3*R*)-3-Amino-2-hydroxy-4-phenylbutanoyl)-L-leucine (2.1).** In a RBF, to a solution of tert-butyl ((2*R*,3*R*)-3-((tert-butoxycarbonyl)amino)-2-hydroxy-4-phenylbutanoyl)-L-leucinate (**2.1a**) (83 mg, 0.18 mmol) in DCM (3.00 mL), hydrogen chloride (4M in dioxane) (3.36 mL, 13.45 mmol) and water (0.10 mL) were added. The mixture was allowed to stir at 40 °C overnight, after which the solvent was evaporated to dryness. The resulting slightly brown solid (61 mg) was triturated with Et<sub>2</sub>O, then the resulting white solid was collected by filtration and washed carefully with Et<sub>2</sub>O. The solid was dried under vacuum, to afford the title compound (28 mg, 45%) as HCl salt. [α]<sub>D</sub><sup>20</sup> = +10 (c 0.40, H<sub>2</sub>O). <sup>1</sup>H NMR (500 MHz, D<sub>2</sub>O) δ 7.35 – 7.4 (m, 2H), 7.31 – 7.35 (m, 1H), 7.26 – 7.3 (m, 2H), 4.44 (d, *J* = 3.2 Hz, 1H), 3.93 – 4.02 (m, 2H), 3.05 (dd, *J* = 14.4, 6.3 Hz, 1H), 2.91 (dd, *J* = 14.4, 8.8 Hz, 1H), 1.53 – 1.64 (m, 3H), 0.89 (d, *J* = 6.1 Hz, 3H), 0.87 (d, *J* = 6.1 Hz, 3H). HRMS (ESI) *m/z* [M + H]<sup>+</sup> calcd for C<sub>16</sub>H<sub>24</sub>N<sub>2</sub>O<sub>4</sub>: 309.1814, found: 309.1810. Purity: 99%.

**Ethyl 3-aminopropanoate hydrochloride (2.3)** In a RBF, to a suspension of 3-aminopropanoic acid (1.00 g, 11.22 mmol) in dry ethanol (25 mL), sulfurous dichloride (0.977 mL, 13.47 mmol) was added dropwise at 0 °C over 10 min. The reaction was refluxed until complete consumption of starting material (2h). After cooling to room temperature, solvent was removed under reduced pressure, to give the title compound as hydrochloric salt (1.698 g, 98%). <sup>1</sup>H NMR (400 MHz, DMSO) δ 8.25 (br, 3H), 4.09 (q, *J* = 7.1 Hz, 2H), 2.92 – 3.04 (m, 2H), 2.71 (t, *J* = 7.2 Hz, 2H), 1.19 (t, *J* = 7.1 Hz, 3H).

**Ethyl 3-(cyclohexylamino)propanoate (2.4)** was prepared as described by Yen *et al.*<sup>12</sup> to afford the title compound (1.118 g, 66%). <sup>1</sup>H NMR (400 MHz, DMSO) δ 4.04 (q, *J* = 7.1 Hz, 2H), 2.74 (t, *J* = 6.8 Hz, 2H), 2.28 – 2.41 (m, 3H), 1.72 – 1.82 (m, 2H), 1.6 – 1.69 (m, 2H), 1.48 – 1.58 (m, 1H), 1.04 – 1.27 (m, 6H), 0.9 – 1.02 (m, 2H).

**3-(((Benzyloxy)carbonyl)(cyclohexyl)amino)propanoic acid (2.6).** In a RBF, ethyl 3-(cyclohexylamino)propanoate (**2.4**, 4.167 g, 20.91 mmol) and triethylamine (3.50 mL, 25.09 mmol) were dissolved in DCM and the resulting solution was cooled to 0 °C, under inert atmosphere. Benzyl carbonochloridate (3.46 mL, 23.00 mmol) was slowly added, then the resulting mixture was allowed to warm up at room temperature and stirred until complete consumption of the SM was observed. The reaction was quenched with water. The resulting suspension was poured into a separatory funnel and the crude product was washed with water and brine. The organic layer was dried using a phase separator and solvent was removed under reduced pressure, to afford the title compound ethyl 3-(((benzyloxy)carbonyl)(cyclohexyl)amino)propanoate (**2.5**), used for the following step without further purification.

To a solution of **2.5** in EtOH (20 mL), a solution of lithium hydroxide hydrate (3.83 g, 91.32 mmol) in H<sub>2</sub>O (5 mL) was added. The resulting mixture was allowed to stir for 6h at room temperature. Volatiles were removed and the reaction mixture was acidified with aq. HCl (3 M) to pH ~ 1. The aq. mixture was extracted with EtOAc (3x), dried using a phase separator and the solvent removed under reduced pressure, to afford the title compound (4.859 g, 76%), as a off-white solid, over two steps. <sup>1</sup>H NMR (400 MHz, DMSO) δ 12.26 (br, 1H), 7.27 – 7.41 (m, 6H), 5.08 (s, 2H), 3.29 – 3.4 (m, 3H), 2.38 – 2.47 (m, 2H), 1.68 – 1.78 (m, 2H), 1.52 – 1.67 (m, 3H), 1.46 (qd, *J* = 12.3, 3.1 Hz, 2H), 1.16 – 1.32 (m, 2H), 0.98 – 1.13 (m, 1H). MS (ES<sup>+</sup>) *m/z* [M + H]<sup>+</sup> calcd for C<sub>17</sub>H<sub>23</sub>NO<sub>4</sub>: 306.2, found: 306.1

#### General procedure A for amide coupling (2.7a-j).

In a vial, to a solution of 3-(((benzyloxy)carbonyl)(cyclohexyl)amino)propanoic acid (**2.6**, 1.0 eq), N-ethyl-N-isopropylpropan-2-amine (1.2 eq) and the corresponding amine (1.1 eq) in dry DMF (3 mL), ((1H-benzo[d][1,2,3]triazol-1-yl)oxy)tri(pyrrolidin-1-yl)phosphonium hexafluorophosphate(V) (1.0 eq) was added. The mixture was stirred overnight at room temperature. After solvent removal, the mixture was dissolved in DCM (15 mL) and washed with aq HCl 0.5 M (10 mL), NaHCO<sub>3</sub> 5% (10 mL) and brine (10 mL) The organic layer was dried using a phase separator and solvent removed under reduced pressure. The crude product was purified by preparative HPLC (run time: 20 min; flow rate: 19 mL/min).

#### Benzyl cyclohexyl(3-((3,4-dimethoxyphenethyl)amino)-3-oxopropyl) carbamate (2.7a).

Compound **2.7a** was synthesized from 2-(3,4-dimethoxyphenyl)ethan-1-amine, according to general procedure A (purification conditions: 35-75% ACN in H<sub>2</sub>O/ACN/NH<sub>3</sub> 95/5/0.2 buffer) to afford the title compound (136 mg, 45%). <sup>1</sup>H NMR (500 MHz, CDCl<sub>3</sub>) δ 7.27 – 7.39 (m, 5H), 6.76 – 6.82 (m, 1H), 6.69 (br, 2H), 5.13 (s, 2H), 3.86 (d, *J* = 3.2 Hz, 6H), 3.44 (s, 4H), 2.70 (s, 2H), 2.39 (d, *J* = 62.9 Hz, 2H), 1.78 (d, *J* = 13.2 Hz, 2H), 1.65 (dd, *J* = 27.2, 12.0 Hz, 3H), 1.18 – 1.52 (m, 4H), 1.08 (dddd, *J* = 16.5, 13.0, 8.3, 3.5 Hz, 1H). <sup>13</sup>C NMR (126 MHz, CDCl<sub>3</sub>) δ 171.26, 156.50, 149.17, 147.83, 136.99, 131.39, 128.69, 128.15, 127.72, 120.73, 111.96, 111.43, 67.12, 56.28, 56.28, 56.06, 56.00, 40.86, 40.86, 40.25, 39.62, 38.05, 37.63, 35.37, 31.37, 31.05, 26.00, 25.47.

#### Benzyl cyclohexyl(3-((4-nitrophenethyl)amino)-3-oxopropyl) carbamate (2.7b).

Compound **2.7b** was synthesized from 2-(4-nitrophenyl)ethan-1-amine hydrochloride, according to general procedure A (purification conditions: 35-75% ACN in H<sub>2</sub>O/ACN/NH<sub>3</sub> 95/5/0.2 buffer) to afford the title compound (105 mg, 47%). <sup>1</sup>H NMR (400 MHz, CDCl<sub>3</sub>) δ 8.12 – 8.19 (m, 2H), 7.27 – 7.42 (m, 7H), 5.13 (s, 2H), 3.3 – 3.59 (m, 4H), 2.74 – 2.99 (m, 2H), 2.2 – 2.57 (m, 2H), 1.73 – 1.85 (m, 2H), 1.54 – 1.73 (m, 4H), 1.37 – 1.53 (m, 2H), 1.2 – 1.37 (m, 2H), 0.99 – 1.17 (m, 1H).

## CHAPTER 2

**Benzyl cyclohexyl(3-((2,2-diphenylethyl)amino)-3-oxopropyl) carbamate (2.7c).** Compound **2.7c** was synthesized from 2,2-diphenylethan-1-amine, according to general procedure A (purification conditions: 45-95% ACN in H<sub>2</sub>O/ACN/NH<sub>3</sub> 95/5/0.2 buffer) to afford the title compound (112 mg, 35%). <sup>1</sup>H NMR (500 MHz, CDCl<sub>3</sub>) δ 7.27 – 7.38 (m, 9H), 7.17 – 7.25 (m, 6H), 5.09 (s, 2H), 4.06 – 4.22 (m, 1H), 3.73 – 3.93 (m, 3H), 3.29 – 3.46 (m, 2H), 2.17 – 2.45 (m, 2H), 1.77 (d, *J* = 12.8 Hz, 2H), 1.57 – 1.69 (m, 3H), 1.35 – 1.5 (m, 2H), 1.2 – 1.35 (m, 2H), 1 – 1.14 (m, 1H). <sup>13</sup>C NMR (126 MHz, CDCl<sub>3</sub>) δ 170.85, 155.93, 141.88, 136.97, 128.79, 128.61, 128.11, 128.05, 126.91, 66.98, 56.30, 50.65, 43.78, 40.53, 37.35, 31.22, 25.95, 25.42.

**Benzyl cyclohexyl(3-oxo-3-((4-phenylbutyl)amino)propyl) carbamate (2.7d).** Compound **2.7d** was synthesized from 4-phenylbutan-1-amine, according to general procedure A (purification conditions: flash column chromatography. DCM/MeOH 100:0 to 80:20 over 25 CV) to afford the title compound (203 mg, 69%). <sup>1</sup>H NMR (400 MHz, CDCl<sub>3</sub>) δ 7.15 – 7.32 (m, 7H), 7.05 – 7.14 (m, 3H), 5.05 (s, 2H), 3.58 – 3.96 (m, 1H), 3.29 – 3.46 (m, 2H), 2.99 – 3.22 (m, 2H), 2.53 (t, *J* = 7.6 Hz, 2H), 2.15 – 2.46 (m, 2H), 1.66 – 1.75 (m, 2H), 1.48 – 1.65 (m, 5H), 1.31 – 1.46 (m, 4H), 1.12 – 1.3 (m, 2H), 0.92 – 1.08 (m, 1H). <sup>13</sup>C NMR (101 MHz, CDCl<sub>3</sub>) δ 170.88, 155.58, 142.13, 136.92, 128.61, 128.45, 128.39, 128.06, 125.88, 67.02, 56.33, 40.55, 39.77, 39.34, 37.81, 35.53, 31.18, 29.17, 28.70, 25.94, 25.40.

**Benzyl cyclohexyl(3-oxo-3-(phenethylamino)propyl) carbamate (2.7e).** Compound **2.7e** was synthesized from 2-phenylethan-1-amine, according to general procedure A (purification conditions: 45-85% ACN in H<sub>2</sub>O/ACN/NH<sub>3</sub> 95/5/0.2 buffer) to afford the title compound (149 mg, 62%). <sup>1</sup>H NMR (500 MHz, CDCl<sub>3</sub>) δ 7.27 – 7.4 (m, 7H), 7.02 – 7.25 (m, 3H), 5.12 (s, 2H), 3.68 – 4.01 (m, 1H), 3.35 – 3.53 (m, 4H), 2.67 – 2.84 (m, 2H), 2.21 – 2.54 (m, 2H), 1.78 (d, *J* = 13.1 Hz, 2H), 1.64 – 1.72 (m, 2H), 1.57 – 1.64 (m, 1H), 1.37 – 1.51 (m, 2H), 1.2 – 1.36 (m, 2H), 0.99 – 1.15 (m, 1H). <sup>13</sup>C NMR (126 MHz, CDCl<sub>3</sub>) δ 170.82, 156.28, 155.85, 138.87, 136.91, 128.76, 128.65, 128.59, 128.04, 127.59, 126.54, 66.98, 56.21, 40.62, 39.56, 37.89, 37.45, 35.69, 31.27, 30.94, 25.91, 25.38.

**Benzyl cyclohexyl(3-(isobutylamino)-3-oxopropyl)carbamate (2.7f).** Compound **2.7f** was synthesized from 2-methylpropan-1-amine, according to general procedure A (purification conditions: 40-80% ACN in H<sub>2</sub>O/ACN/NH<sub>3</sub> 95/5/0.2 buffer) to afford the title compound (125 mg, 69%). <sup>1</sup>H NMR (500 MHz, CDCl<sub>3</sub>) δ 7.27 – 7.41 (m, 5H), 5.13 (s, 2H), 3.66 – 4.05 (m, 1H), 3.35 – 3.56 (m, 2H), 2.85 – 3.09 (m, 2H), 2.27 – 2.61 (m, 2H), 1.77 (d, *J* = 13.3 Hz, 2H), 1.67 (d, *J* = 10.9 Hz, 3H), 1.60 (d, *J* = 13.1 Hz, 1H), 1.44 (m, 2H), 1.18 – 1.36 (m, 2H), 1.06 (m, 1H), 0.86 (m, 6H). <sup>13</sup>C NMR (126 MHz, CDCl<sub>3</sub>) δ 170.94, 156.37, 155.93, 136.92, 128.61, 128.06, 127.64, 67.04, 56.31, 46.86, 40.65, 39.77, 37.94, 37.73, 31.28, 31.00, 28.46, 25.93, 25.39, 20.16.

**Benzyl cyclohexyl(3-oxo-3-((3-phenylpropyl)amino)propyl)carbamate (2.7g).** Compound **2.7g** was synthesized from 3-phenylpropan-1-amine, according to general procedure A (purification conditions: 45-85% ACN in H<sub>2</sub>O/ACN/NH<sub>3</sub> 95/5/0.2 buffer) to afford the title compound (143 mg, 68%). <sup>1</sup>H NMR (500 MHz, CDCl<sub>3</sub>) δ 7.31 – 7.38 (m, 4H), 7.23 – 7.31 (m, 3H), 7.11 – 7.2 (m, 3H), 5.12 (s, 2H), 3.67 – 4.03 (m, 1H), 3.37 – 3.53 (m, 2H), 3.07 – 3.29 (m, 2H), 2.52 – 2.72 (m, 2H), 2.26 – 2.5 (m, 2H), 1.71 – 1.86 (m, 4H), 1.64 – 1.71 (m, 2H), 1.55 – 1.63 (m, 1H), 1.38 – 1.51 (m, 2H), 1.2 – 1.37 (m, 2H), 0.98 – 1.13 (m, 1H). <sup>13</sup>C NMR (126 MHz, CDCl<sub>3</sub>) δ 170.96, 156.33, 155.84, 141.43, 136.85, 128.56, 128.44, 128.35, 128.01, 127.56, 125.98, 66.98, 56.26, 40.51, 39.61, 39.10, 37.81, 37.56, 33.26, 31.13, 30.93, 25.88, 25.34.



## CHAPTER 2

**Benzyl cyclohexyl(3-((3,3-diphenylpropyl)amino)-3-oxopropyl)carbamate (2.7h).** Compound **2.7h** was synthesized from 3,3-diphenylpropan-1-amine, according to general procedure A (purification conditions: 45-95% ACN in H<sub>2</sub>O/ACN/NH<sub>3</sub> 95/5/0.2 buffer) to afford the title compound (316 mg, 77%). <sup>1</sup>H NMR (400 MHz, CDCl<sub>3</sub>) δ 7.11 – 7.42 (m, 15H), 5.14 (s, 2H), 3.66 – 4.1 (m, 2H), 3.31 – 3.56 (m, 2H), 3 – 3.27 (m, 2H), 2.12 – 2.51 (m, 4H), 1.78 (d, *J* = 13.0 Hz, 2H), 1.55 – 1.72 (m, 3H), 1.44 (q, *J* = 11.6 Hz, 2H), 1.18 – 1.37 (m, 2H), 1 – 1.16 (m, 1H). <sup>13</sup>C NMR (101 MHz, CDCl<sub>3</sub>) δ 170.87, 156.37, 156.14, 144.24, 136.89, 128.60, 128.03, 127.76, 126.41, 66.99, 56.28, 49.11, 40.19, 39.61, 38.44, 37.62, 35.21, 31.04, 25.90, 25.36.

**Benzyl cyclohexyl(3-(ethylamino)-3-oxopropyl)carbamate (2.7i).** Compound **2.7i** was synthesized from ethanamine, according to general procedure A (purification conditions: 35-75% ACN in H<sub>2</sub>O/CAN/NH<sub>3</sub> 95/5/0.2 buffer) to afford the title compound (164 mg, 75%). <sup>1</sup>H NMR (400 MHz, CDCl<sub>3</sub>) δ 7.29 – 7.41 (m, 5H), 5.15 (s, 2H), 3.80 (s, 1H), 3.37 – 3.55 (m, 2H), 3.07 – 3.34 (m, 2H), 2.19 – 2.62 (m, 2H), 1.74 – 1.84 (m, 2H), 1.65 – 1.73 (m, 2H), 1.56 – 1.65 (m, 1H), 1.38 – 1.54 (m, 2H), 1.19 – 1.38 (m, 2H), 0.93 – 1.19 (m, 4H).

**Benzyl cyclohexyl(3-oxo-3-((2-phenoxyethyl)amino)propyl)carbamate (2.7j).** Compound **2.7j** was synthesized from 2-phenoxyethan-1-amine, according to general procedure A (purification conditions: 35-75% ACN in H<sub>2</sub>O/ACN/NH<sub>3</sub> 95/5/0.2 buffer) to afford the title compound (24 mg, 9%). <sup>1</sup>H NMR (400 MHz, CDCl<sub>3</sub>) δ 7.23 – 7.39 (m, 7H), 6.97 (t, *J* = 7.3 Hz, 1H), 6.88 (d, *J* = 7.9 Hz, 2H), 5.13 (s, 2H), 3.96 – 4.05 (m, 2H), 3.84 (br, *J* = 24.1 Hz, 1H), 3.54 – 3.67 (m, 2H), 3.4 – 3.53 (m, 2H), 2.28 – 2.62 (m, 2H), 1.77 (d, *J* = 13.0 Hz, 2H), 1.68 (d, *J* = 10.8 Hz, 2H), 1.61 (d, *J* = 13.1 Hz, 1H), 1.37 – 1.53 (m, 2H), 1.18 – 1.37 (m, 2H), 0.99 – 1.15 (m, 1H).

### General procedure B for catalytic hydrogenation (2.8a-j and 2.11a-e)

In a RBF, the Cbz-protected amides or sulfonamides (1.00 eq) and 5% Pd/C (0.05 eq) were suspended in MeOH (5 mL). The reaction was stirred for 12h at room temperature, under an atmosphere of H<sub>2</sub> (1 bar). The catalyst was removed by filtration through a plug of celite, and the filtrate was concentrated under vacuum. The compound was purified by preparative SFC (run time:15 minutes).

**3-(Cyclohexylamino)-*N*-(3,4-dimethoxyphenethyl)propanamide (2.8a).** Compound **2.8a** was synthesized from **2.7a**, according to general procedure B (purification conditions: 25-35% CO<sub>2</sub> in MeOH/H<sub>2</sub>O/NH<sub>3</sub> 97/3/50 mM buffer) to afford the title compound (13 mg, 24%). <sup>1</sup>H NMR (400 MHz, CDCl<sub>3</sub>) δ 7.93 (bs, 1H), 6.69 – 6.81 (m, 3H), 3.86 (s, 3H), 3.85 (s, 3H), 3.50 (q, *J* = 6.9 Hz, 2H), 2.78 – 2.84 (m, 2H), 2.75 (t, *J* = 7.0 Hz, 2H), 2.24 – 2.36 (m, 3H), 1.71 – 1.82 (m, 2H), 1.62 – 1.71 (m, 2H), 1.54 – 1.62 (m, 1H), 1.03 – 1.29 (m, 3H), 0.82 – 0.98 (m, 2H). <sup>13</sup>C NMR (101 MHz, CDCl<sub>3</sub>) δ 172.97, 149.08, 147.71, 131.86, 120.71, 112.00, 111.32, 56.48, 55.98, 42.69, 40.24, 36.13, 35.36, 33.47, 26.12, 25.01. HRMS (ESI) *m/z* [M + H]<sup>+</sup> calcd for C<sub>19</sub>H<sub>30</sub>N<sub>2</sub>O<sub>3</sub>: 335.2335, found: 335.2332. Purity: 97%.

***N*-(4-Aminophenethyl)-3-(cyclohexylamino)propanamide (2.8b).** Compound **2.8b** was synthesized from **2.7b**, according to general procedure B (purification conditions: 25-35% CO<sub>2</sub> in MeOH/H<sub>2</sub>O/NH<sub>3</sub> 97/3/50 mM buffer) to afford the title compound (43 mg, 64%). <sup>1</sup>H NMR (400 MHz, CDCl<sub>3</sub>) δ 7.79 (br, 1H), 6.93 – 6.99 (m, 2H), 6.56 – 6.64 (m, 2H), 3.58 (br, 2H), 3.44 (q, *J* = 6.8 Hz, 2H), 2.76 – 2.83 (m, 2H), 2.67 (t, *J* = 7.0 Hz, 2H), 2.23 – 2.37 (m, 3H), 1.73 – 1.81 (m, 2H), 1.62 – 1.72 (m, 2H), 1.53 – 1.62 (m, 1H), 1.42 (br, 1H), 1.04 – 1.29 (m, 3H), 0.86 – 1 (m, 2H). <sup>13</sup>C NMR

## CHAPTER 2

(101 MHz, CDCl<sub>3</sub>)  $\delta$  172.86, 144.87, 129.58, 129.06, 115.35, 56.42, 42.66, 40.41, 36.18, 34.83, 33.47, 26.13, 25.02. HRMS (ESI)  $m/z$  [M + H]<sup>+</sup> calcd for C<sub>17</sub>H<sub>27</sub>N<sub>3</sub>O: 290.2232, found: 290.2230. Purity: 89%.

**3-(Cyclohexylamino)-*N*-(2,2-diphenylethyl)propanamide (2.8c).** Compound **2.8c** was synthesized from **2.7c**, according to general procedure B (purification conditions: 20-30% CO<sub>2</sub> in MeOH/H<sub>2</sub>O/NH<sub>3</sub> 97/3/50 mM buffer) to afford the title compound (26 mg, 32%). <sup>1</sup>H NMR (400 MHz, CDCl<sub>3</sub>)  $\delta$  8.18 (s, 1H), 7.17 – 7.34 (m, 10H), 4.20 (t,  $J$  = 8.0 Hz, 1H), 3.90 (dd,  $J$  = 8.0, 5.7 Hz, 2H), 2.67 – 2.74 (m, 2H), 2.21 – 2.29 (m, 2H), 2.14 (tt,  $J$  = 10.6, 3.3 Hz, 1H), 1.53 – 1.71 (m, 5H), 1.02 – 1.25 (m, 4H), 0.67 – 0.84 (m, 2H). <sup>13</sup>C NMR (101 MHz, CDCl<sub>3</sub>)  $\delta$  173.11, 142.35, 128.71, 128.53, 128.45, 128.32, 128.18, 126.96, 126.74, 56.27, 50.83, 43.58, 42.52, 36.07, 33.34, 26.06, 25.04. HRMS (ESI)  $m/z$  [M + H]<sup>+</sup> calcd for C<sub>23</sub>H<sub>30</sub>N<sub>2</sub>O: 351.2436, found: 351.2436. Purity: 97%.

**3-(Cyclohexylamino)-*N*-(4-phenylbutyl)propanamide (2.8d).** Compound **2.8d** was synthesized from **2.7d**, according to general procedure B (purification conditions: 20-30% CO<sub>2</sub> in MeOH/H<sub>2</sub>O/NH<sub>3</sub> 97/3/50 mM buffer) to afford the title compound (62 mg, 31%). <sup>1</sup>H NMR (400 MHz, CDCl<sub>3</sub>)  $\delta$  8.12 (bs, 1H), 7.31 – 7.4 (m, 2H), 7.26 (t,  $J$  = 7.0 Hz, 3H), 3.34 (q,  $J$  = 6.7 Hz, 2H), 2.95 (t,  $J$  = 5.8 Hz, 2H), 2.72 (t,  $J$  = 7.6 Hz, 2H), 2.49 (tt,  $J$  = 10.3, 3.7 Hz, 1H), 2.35 – 2.44 (m, 2H), 1.87 – 2.01 (m, 2H), 1.67 – 1.86 (m, 5H), 1.57 – 1.67 (m, 2H), 1.44 (br, 1H), 1.18 – 1.4 (m, 3H), 1.04 – 1.18 (m, 2H). <sup>13</sup>C NMR (101 MHz, CDCl<sub>3</sub>)  $\delta$  172.83, 142.21, 128.38, 128.30, 125.77, 56.44, 42.74, 38.85, 36.07, 35.57, 33.58, 29.19, 28.92, 26.09, 24.94. HRMS (ESI)  $m/z$  [M + H]<sup>+</sup> calcd for C<sub>19</sub>H<sub>30</sub>N<sub>2</sub>O: 303.2436, found: 303.2430. Purity: 93%.

**3-(Cyclohexylamino)-*N*-phenethylpropanamide (2.8e).** Compound **2.8e** was synthesized from **2.7e**, according to general procedure B (purification conditions: 20-30% CO<sub>2</sub> in MeOH/H<sub>2</sub>O/NH<sub>3</sub> 97/3/50 mM buffer) to afford the title compound (31 mg, 31%). <sup>1</sup>H NMR (400 MHz, CDCl<sub>3</sub>)  $\delta$  8.04 (br, 1H), 7.3 – 7.39 (m, 2H), 7.2 – 7.3 (m, 3H), 3.58 (q,  $J$  = 6.7 Hz, 2H), 2.81 – 2.91 (m, 4H), 2.28 – 2.41 (m, 3H), 1.79 (d,  $J$  = 12.5 Hz, 2H), 1.68 – 1.76 (m, 2H), 1.58 – 1.68 (m, 1H), 1.1 – 1.36 (m, 4H), 0.86 – 1.02 (m, 2H). <sup>13</sup>C NMR (101 MHz, CDCl<sub>3</sub>)  $\delta$  172.98, 139.49, 139.36, 128.82, 128.70, 128.57, 126.40, 56.39, 42.65, 40.11, 36.16, 35.74, 33.48, 26.11, 25.01. HRMS (ESI)  $m/z$  [M + H]<sup>+</sup> calcd for C<sub>17</sub>H<sub>26</sub>N<sub>2</sub>O: 275.2123, found: 275.2123. Purity: 86%.

**3-(Cyclohexylamino)-*N*-isobutylpropanamide (2.8f).** Compound **2.8f** was synthesized from **2.7f**, according to general procedure B (purification conditions: 20-30% CO<sub>2</sub> in MeOH/H<sub>2</sub>O/NH<sub>3</sub> 97/3/50 mM buffer) to afford the title compound (34 mg, 43%). <sup>1</sup>H NMR (500 MHz, CDCl<sub>3</sub>)  $\delta$  8.10 (br, 1H), 3.01 – 3.08 (m, 2H), 2.83 – 2.91 (m, 2H), 2.40 (tt,  $J$  = 10.4, 3.7 Hz, 1H), 2.29 – 2.34 (m, 2H), 1.83 – 1.92 (m, 2H), 1.66 – 1.78 (m, 3H), 1.59 (dt,  $J$  = 12.6, 3.6 Hz, 1H), 1.50 (br, 1H), 1.24 (qt,  $J$  = 12.9, 3.2 Hz, 2H), 1.14 (qt,  $J$  = 12.5, 3.3 Hz, 1H), 1.03 (qd,  $J$  = 12.6, 3.3 Hz, 2H), 0.85 – 0.93 (m, 6H). <sup>13</sup>C NMR (126 MHz, CDCl<sub>3</sub>)  $\delta$  172.96, 56.57, 46.57, 42.84, 36.12, 33.65, 28.49, 26.15, 25.03, 20.33. HRMS (ESI)  $m/z$  [M + H]<sup>+</sup> calcd for C<sub>13</sub>H<sub>26</sub>N<sub>2</sub>O: 227.2123, found: 227.2133. Purity: 90%.

**3-(Cyclohexylamino)-*N*-(3-phenylpropyl)propanamide (2.8g).** Compound **2.8g** was synthesized from **2.7g**, according to general procedure B (purification conditions: 15-25% CO<sub>2</sub> in MeOH/H<sub>2</sub>O/NH<sub>3</sub> 97/3/50 mM buffer) to afford the title compound (36 mg, 37%). <sup>1</sup>H NMR (500 MHz, CDCl<sub>3</sub>)  $\delta$  8.05 (bs, 1H), 7.23 – 7.3 (m, 2H), 7.12 – 7.21 (m, 3H), 3.25 (q,  $J$  = 6.9 Hz, 2H), 2.81 – 2.9 (m, 2H), 2.59 – 2.69 (m, 2H), 2.41 (tt,  $J$  = 10.3, 3.7 Hz, 1H), 2.26 – 2.33 (m, 2H), 1.85 – 1.92 (m, 2H), 1.77 – 1.84 (m, 2H), 1.71 (dt,  $J$  = 12.7, 3.4 Hz, 2H), 1.60 (dt,  $J$  = 12.6, 3.6 Hz, 1H), 1.43 (br,

## CHAPTER 2

1H), 1.25 (qt,  $J = 12.7, 3.2$  Hz, 2H), 1.15 (qt,  $J = 12.5, 3.3$  Hz, 1H), 1.04 (qd,  $J = 12.6, 3.3$  Hz, 2H).  $^{13}\text{C}$  NMR (126 MHz,  $\text{CDCl}_3$ )  $\delta$  172.95, 141.66, 128.47, 128.43, 125.97, 56.52, 42.76, 38.70, 36.09, 33.66, 33.46, 31.26, 26.13, 25.00. HRMS (ESI)  $m/z$   $[\text{M} + \text{H}]^+$  calcd for  $\text{C}_{18}\text{H}_{28}\text{N}_2\text{O}$ : 289.2280, found: 289.2296. Purity: 90%.

**3-(Cyclohexylamino)-*N*-(3,3-diphenylpropyl)propanamide (2.8h).** Compound **2.8h** was synthesized from **2.7h**, according to general procedure B (purification conditions: 20-30%  $\text{CO}_2$  in  $\text{MeOH}/\text{H}_2\text{O}/\text{NH}_3$  97/3/50 mM buffer) to afford the title compound (141 mg, 61%).  $^1\text{H}$  NMR (500 MHz,  $\text{CDCl}_3$ )  $\delta$  8.00 (s, 1H), 7.23 – 7.33 (m, 8H), 7.15 – 7.22 (m, 2H), 3.99 (t,  $J = 7.8$  Hz, 1H), 3.22 (q,  $J = 6.6$  Hz, 2H), 2.8 – 2.9 (m, 2H), 2.38 – 2.49 (m, 1H), 2.22 – 2.34 (m, 4H), 1.86 – 1.94 (m, 2H), 1.67 – 1.81 (m, 3H), 1.57 – 1.67 (m, 1H), 1.23 – 1.34 (m, 2H), 1.13 – 1.23 (m, 1H), 1 – 1.13 (m, 2H).  $^{13}\text{C}$  NMR (126 MHz,  $\text{CDCl}_3$ )  $\delta$  172.81, 144.33, 128.52, 127.77, 126.29, 56.43, 48.97, 42.63, 37.79, 35.99, 35.20, 33.53, 26.07, 24.93. HRMS (ESI)  $m/z$   $[\text{M} + \text{H}]^+$  calcd for  $\text{C}_{24}\text{H}_{32}\text{N}_2\text{O}$ : 365.2593, found: 365.2589. Purity: 97%.

**3-(Cyclohexylamino)-*N*-ethylpropanamide (2.8i).** Compound **2.8i** was synthesized from **2.7i**, according to general procedure B (purification conditions: 20-30%  $\text{CO}_2$  in  $\text{MeOH}/\text{H}_2\text{O}/\text{NH}_3$  97/3/50 mM buffer) to afford the title compound (54 mg, 55%).  $^1\text{H}$  NMR (500 MHz,  $\text{CDCl}_3$ )  $\delta$  7.85 (br, 1H), 3.17 (qd,  $J = 7.3, 5.6$  Hz, 2H), 2.72 – 2.86 (m, 2H), 2.34 (tt,  $J = 10.3, 3.7$  Hz, 1H), 2.19 – 2.28 (m, 2H), 1.76 – 1.85 (m, 2H), 1.64 (dt,  $J = 12.5, 3.4$  Hz, 2H), 1.48 – 1.58 (m, 2H), 0.91 – 1.25 (m, 8H).  $^{13}\text{C}$  NMR (126 MHz,  $\text{CDCl}_3$ )  $\delta$  172.65, 56.37, 42.68, 36.02, 33.84, 33.48, 26.04, 24.87, 14.74. HRMS (ESI)  $m/z$   $[\text{M} + \text{H}]^+$  calcd for  $\text{C}_{11}\text{H}_{22}\text{N}_2\text{O}$ : 199.1810, found: 199.1814. Purity: NV.

**3-(Cyclohexylamino)-*N*-(2-phenoxyethyl)propanamide (2.8j).** Compound **2.8j** was synthesized from **2.7j**, according to general procedure B (purification conditions: 20-30%  $\text{CO}_2$  in  $\text{MeOH}/\text{H}_2\text{O}/\text{NH}_3$  97/3/50 mM buffer) to afford the title compound (5 mg, 31%).  $^1\text{H}$  NMR (500 MHz,  $\text{CDCl}_3$ )  $\delta$  8.47 (br, 1H), 7.26 – 7.32 (m, 2H), 6.95 (t,  $J = 7.4$  Hz, 1H), 6.86 – 6.91 (m, 2H), 4.04 (t,  $J = 5.1$  Hz, 2H), 3.65 (q,  $J = 5.4$  Hz, 2H), 2.84 – 2.96 (m, 2H), 2.33 – 2.48 (m, 3H), 1.83 – 1.92 (m, 2H), 1.68 (dt,  $J = 13.0, 3.5$  Hz, 3H), 1.53 – 1.63 (m, 1H), 1.17 – 1.28 (m, 2H), 1 – 1.16 (m, 3H).  $^{13}\text{C}$  NMR (126 MHz,  $\text{CDCl}_3$ )  $\delta$  173.21, 158.70, 129.63, 121.11, 114.54, 66.88, 56.58, 42.58, 38.72, 35.84, 33.38, 29.89, 29.85, 26.08, 25.00. HRMS (ESI)  $m/z$   $[\text{M} + \text{H}]^+$  calcd for  $\text{C}_{17}\text{H}_{26}\text{N}_2\text{O}_2$ : 291.2072, found: 291.2084. Purity: 93%.

### **2-(((Benzyloxy)carbonyl)(cyclohexyl)amino)ethane-1-sulfonic acid (2.9)**

In a RBF, to a solution of 2-(cyclohexylamino)ethane-1-sulfonic acid (**2.2**, CHES, 297 mg, 1.43 mmol) in  $\text{H}_2\text{O}$  (5 mL), potassium carbonate (218 mg, 1.58 mmol) was added. The resulting mixture was cooled at 0 °C. Benzyl carbonochloridate (0.237 mL, 1.58 mmol) was dissolved in 1,4-dioxane (5.00 mL) and added dropwise. The resulting mixture was allowed to stir at room temperature until complete conversion was observed (5hr, monitored by LC-MS). The reaction was quenched by addition of aq. HCl (3 M), then the crude mixture was poured into a separatory funnel and extracted with EtOAc. The collected organic layers were dried using a phase separator and solvent was removed under reduced pressure, to afford the title compound, used for the next step without further purification.

### **General procedure C for the preparation of Cbz-sulfonamides (2.10a-e)**

In a vial, to a solution of **2.9** (1.00 eq) in dry DCM (5mL), oxalyl dichloride (2.50 eq) and few drops of DMF were slowly added. The resulting mixture was allowed to stir at room temperature overnight.

## CHAPTER 2

Volatiles were removed and the residue was co-evaporated with DCM (3x). To the crude mixture in DCM (10 mL), the corresponding amine (1.10 eq) was added at 0 °C under inert atmosphere. The reaction mixture was allowed to warm to room temperature and stirred overnight. The reaction mixture was quenched with H<sub>2</sub>O, then washed twice with brine. The organic layer was dried using a phase separator and solvent removed under reduced pressure. The crude product was purified by preparative HPLC (run time: 20 min; flow rate: 19 mL/min).

**2-(Cyclohexylamino)-N-(3,3-diphenylpropyl)ethane-1-sulfonamide (2.10a).** Compound **2.10a** was synthesized from 3,3-diphenylpropan-1-amine (392 mg, 1.80 mmol), according to general procedure C (purification conditions: 55-95% ACN in H<sub>2</sub>O/ACN/NH<sub>3</sub> 95/5/0.2 buffer), to afford the title compound (120 mg, 14%). <sup>1</sup>H NMR (400 MHz, CDCl<sub>3</sub>) δ 7.03 – 7.55 (m, 15H), 5.12 (s, 1H), 3.74 – 4.22 (m, 2H), 3.37 – 3.7 (m, 2H), 2.74 – 3.36 (m, 4H), 2.11 – 2.43 (m, 2H), 1.18 – 1.9 (m, 10H), 0.95 – 1.15 (m, 1H).

**Benzyl cyclohexyl(2-(N-(3-phenylpropyl)sulfamoyl)ethyl)carbamate (2.10b).** Compound **2.10b** was synthesized from 3-phenylpropan-1-amine (0.399 mL, 2.80 mmol), according to general procedure C (purification conditions: 50-90% ACN in H<sub>2</sub>O/ACN/NH<sub>3</sub> 95/5/0.2 buffer), to afford the title compound (139 mg, 12%). MS (ES<sup>+</sup>) *m/z* [M + H]<sup>+</sup> calcd for C<sub>25</sub>H<sub>34</sub>N<sub>2</sub>O<sub>4</sub>S: 459.2, found: 459.3.

**Benzyl cyclohexyl(2-(N-(2-phenoxyethyl)sulfamoyl)ethyl)carbamate (2.10c).** Compound **2.10c** was synthesized from 2-phenoxyethan-1-amine (0.140 mL, 1.07 mmol), according to general procedure C (purification conditions: 45-85% ACN in H<sub>2</sub>O/ACN/NH<sub>3</sub> 95/5/0.2 buffer), to afford the title compound (227 mg, 51%). <sup>1</sup>H NMR (400 MHz, CDCl<sub>3</sub>) δ 7.22 – 7.46 (m, 7H), 6.98 (t, *J* = 7.3 Hz, 1H), 6.75 – 6.93 (m, 2H), 5.14 (s, 2H), 4.01 – 4.2 (m, 1H), 3.76 – 4.03 (m, 2H), 3.43 – 3.71 (m, 3H), 3.13 – 3.43 (m, 3H), 1.56 – 1.87 (m, 5H), 1.19 – 1.51 (m, 4H), 0.95 – 1.19 (m, 1H).

**Benzyl cyclohexyl(2-(N-(3,4-dimethoxyphenethyl)sulfamoyl)ethyl) carbamate (2.10d).** Compound **2.10d** was 2-(3,4-dimethoxyphenyl)ethan-1-amine (0.190 mL, 1.13 mmol), according to general procedure C (purification conditions: 35-75% ACN in H<sub>2</sub>O/ACN/NH<sub>3</sub> 95/5/0.2 buffer), to afford the title compound (179 mg, 35%). <sup>1</sup>H NMR (400 MHz, CDCl<sub>3</sub>) δ 7.29 (m, 5H), 6.57 – 6.86 (m, 3H), 5.12 (s, 2H), 3.84 (s, 6H), 3 – 3.6 (m, 6H), 2.56 – 2.88 (m, 2H), 1.54 – 1.88 (m, 6H), 1.17 – 1.52 (m, 4H), 0.93 – 1.16 (m, 1H).

**Benzyl cyclohexyl(2-(N-isobutylsulfamoyl)ethyl) carbamate (2.10e).** Compound **2.10e** was 2-methylpropan-1-amine (0.112 mL, 1.13 mmol), according to general procedure C (purification conditions: 40-80% ACN in H<sub>2</sub>O/ACN/NH<sub>3</sub> 95/5/0.2 buffer) to afford the title compound (173 mg, 43%). <sup>1</sup>H NMR (400 MHz, CDCl<sub>3</sub>) δ 7.28 – 7.43 (m, 5H), 5.15 (bs, 2H), 3.74 – 4.07 (m, 1H), 3.46 – 3.7 (m, 2H), 3.08 – 3.37 (m, 2H), 2.54 – 3.03 (m, 2H), 1.55 – 1.92 (m, 7H), 1.21 – 1.5 (m, 4H), 1.01 – 1.19 (m, 1H), 0.72 – 1.01 (m, 6H).

**2-(Cyclohexylamino)-N-(3,3-diphenylpropyl)ethane-1-sulfonamide (2.11a).** Compound **2.11a** was synthesized from **2.10a**, according to general procedure B (purification conditions: 15-25% CO<sub>2</sub> in MeOH/H<sub>2</sub>O/NH<sub>3</sub> 97/3/50 mM buffer) to afford the title compound (49 mg, 54%). <sup>1</sup>H NMR (400 MHz, CDCl<sub>3</sub>) δ 7.23 – 7.34 (m, 8H), 7.17 – 7.23 (m, 2H), 4.06 (t, *J* = 7.9 Hz, 1H), 2.98 – 3.16 (m, 6H), 2.24 – 2.48 (m, 3H), 1.8 – 1.91 (m, 2H), 1.68 – 1.78 (m, 2H), 1.57 – 1.68 (m, 1H), 1.09 – 1.34 (m, 3H), 0.92 – 1.07 (m, 2H). <sup>13</sup>C NMR (101 MHz, CDCl<sub>3</sub>) δ 143.87, 128.74, 127.83, 126.59, 56.54,

## CHAPTER 2

51.68, 48.43, 41.74, 41.26, 36.22, 33.59, 26.07, 24.99. HRMS (ESI)  $m/z$   $[M + H]^+$  calcd for  $C_{23}H_{32}N_2O_2S$ : 401.2263, found: 401.2283. Purity: 96%.

**2-(Cyclohexylamino)-*N*-(3-phenylpropyl)ethane-1-sulfonamide (2.11b).** Compound **2.11b** was synthesized from **2.10b**, according to general procedure B (purification conditions: 15-25%  $CO_2$  in MeOH/ $H_2O$ / $NH_3$  97/3/50 mM buffer), to afford the title compound (80 mg, 81%).  $^1H$  NMR (500 MHz, DMSO)  $\delta$  7.35 (s, 1H), 7.22 (t,  $J = 7.4$  Hz, 2H), 7.06 – 7.18 (m, 3H), 3.31 – 3.49 (m, 2H), 3.08 – 3.25 (m, 2H), 2.97 (t,  $J = 6.2$  Hz, 2H), 2.77 – 2.93 (m, 1H), 2.61 (t,  $J = 7.6$  Hz, 2H), 1.99 (d,  $J = 10.2$  Hz, 2H), 1.68 – 1.84 (m, 4H), 1.60 (d,  $J = 12.6$  Hz, 1H), 1.03 – 1.39 (m, 5H).  $^{13}C$  NMR (126 MHz, DMSO)  $\delta$  140.95, 127.98, 127.93, 125.45, 56.17, 53.99, 47.55, 41.79, 38.74, 32.12, 31.24, 29.04, 24.62, 23.83. HRMS (ESI)  $m/z$   $[M + H]^+$  calcd for  $C_{17}H_{28}N_2O_2S$ : 325.1949, found: 325.1928. Purity: 90%.

**2-(Cyclohexylamino)-*N*-(2-phenoxyethyl)ethane-1-sulfonamide (2.11c).** Compound **2.11c** was synthesized from **2.10c**, according to general procedure B, pure after filtration (156 mg, 97%).  $^1H$  NMR (500 MHz, MeOD)  $\delta$  7.26 (ddq,  $J = 9.8, 6.8, 2.3$  Hz, 2H), 6.85 – 7 (m, 3H), 4.06 (t,  $J = 5.3$  Hz, 2H), 3.49 (t,  $J = 5.3$  Hz, 2H), 3.39 (t,  $J = 6.8$  Hz, 2H), 3.22 (t,  $J = 6.8$  Hz, 2H), 2.71 (tt,  $J = 10.7, 3.7$  Hz, 1H), 1.92 – 2 (m, 2H), 1.75 – 1.83 (m, 2H), 1.66 (dt,  $J = 12.9, 3.1$  Hz, 1H), 1.1 – 1.34 (m, 5H).  $^{13}C$  NMR (126 MHz, MeOD)  $\delta$  159.22, 130.22, 121.91, 115.14, 67.85, 57.74, 50.76, 43.10, 40.66, 31.56, 26.05, 25.27. HRMS (ESI)  $m/z$   $[M + H]^+$  calcd for  $C_{16}H_{26}N_2O_3S$ : 327.1742, found: 327.1758. Purity: 89%.

**2-(Cyclohexylamino)-*N*-(3,4-dimethoxyphenethyl)ethane-1-sulfonamide (2.11d).** Compound **2.11d** was synthesized from **2.10d**, according to general procedure B, pure after filtration (126 mg, 96%).  $^1H$  NMR (500 MHz, MeOD)  $\delta$  6.85 – 6.92 (m, 2H), 6.79 (dd,  $J = 8.1, 2.0$  Hz, 1H), 3.83 (s, 3H), 3.80 (s, 3H), 3.28 (t,  $J = 7.2$  Hz, 2H), 3.09 (t,  $J = 6.8$  Hz, 2H), 2.92 (t,  $J = 6.8$  Hz, 2H), 2.78 (t,  $J = 7.2$  Hz, 2H), 2.43 (tt,  $J = 10.8, 3.7$  Hz, 1H), 1.82 – 1.92 (m, 2H), 1.7 – 1.81 (m, 2H), 1.6 – 1.69 (m, 1H), 1.24 – 1.37 (m, 2H), 1.12 – 1.23 (m, 1H), 0.99 – 1.11 (m, 2H).  $^{13}C$  NMR (126 MHz, MeOD)  $\delta$  150.47, 149.21, 133.02, 122.28, 113.92, 113.15, 57.47, 56.50, 56.42, 52.02, 45.57, 41.59, 37.23, 33.62, 27.07, 25.99. HRMS (ESI)  $m/z$   $[M + H]^+$  calcd for  $C_{18}H_{30}N_2O_4S$ : 371.2004, found: 371.1999. Purity: 95%.

**2-(Cyclohexylamino)-*N*-isobutylethane-1-sulfonamide (2.11e).** Compound **2.11e** was synthesized from **2.10e**, according to general procedure B, pure after filtration (107 mg, 93%).  $^1H$  NMR (500 MHz, MeOD)  $\delta$  3.25 (t,  $J = 6.9$  Hz, 2H), 3.12 (t,  $J = 6.9$  Hz, 2H), 2.87 (d,  $J = 6.8$  Hz, 2H), 2.64 (tt,  $J = 10.9, 3.7$  Hz, 1H), 1.92 – 2.02 (m, 2H), 1.71 – 1.86 (m, 3H), 1.62 – 1.71 (m, 1H), 1.27 – 1.39 (m, 2H), 1.1 – 1.26 (m, 3H), 0.96 (s, 3H), 0.94 (s, 3H).  $^{13}C$  NMR (126 MHz, MeOD)  $\delta$  57.83, 51.42, 51.22, 41.38, 32.91, 30.26, 26.86, 25.88, 20.30. HRMS (ESI)  $m/z$   $[M + H]^+$  calcd for  $C_{12}H_{26}N_2O_2S$ : 263.1793, found: 263.1815. Purity: 96%.

### General procedure D for the preparation of alkyl bromides (2.12a-c).

In a RBF, to a stirred solution of alcohol (1.00 eq) in dry DCM (10 mL), tribromophosphane (0.50 eq) was added at 0 °C. The reaction mixture was stirred for 2 h, then other 0.50 eq of tribromophosphane were added. Ice bath was removed, and the reaction was allowed to stir overnight. The reaction was quenched by slow addition of  $H_2O$ . The resulting mixture was poured into a separatory funnel and further washed with  $H_2O$  and brine. The organic layer was dried using

## CHAPTER 2

a phase separator and concentrated under reduced pressure. The residue was purified via flash chromatography (Hept/EtOAc 100:0 to 0:100) to give the desired product.

**(3-Bromopropane-1,1-diyl)dibenzene (2.12a).** Compound **2.12a** was prepared from 3,3-diphenylpropan-1-ol (750 mg, 3.53 mmol) according to general procedure D, to afford the title compound (714 mg, 74%). <sup>1</sup>H NMR (400 MHz, CDCl<sub>3</sub>) δ 7.23 – 7.34 (m, 8H), 7.16 – 7.23 (m, 2H), 4.21 (t, *J* = 7.7 Hz, 1H), 3.31 (t, *J* = 6.7 Hz, 2H), 2.57 (q, *J* = 6.8 Hz, 2H).

**(3-Bromopropyl)benzene (2.12b).** Compound **2.12b** was prepared from 3-phenylpropan-1-ol (1.50 g, 11.01 mmol) according to general procedure D, to afford the title compound (1200 mg, 54%).

**4-(2-Bromoethyl)-1,2-dimethoxybenzene (2.12c).** Compound **2.12c** was prepared from 2-(3,4-dimethoxyphenyl)ethan-1-ol (400 mg, 2.20 mmol) according to general procedure D, to afford the title compound (460 mg, 86%). <sup>1</sup>H NMR (400 MHz, CDCl<sub>3</sub>) δ 6.82 (d, *J* = 8.1 Hz, 1H), 6.7 – 6.78 (m, 2H), 3.88 (s, 3H), 3.86 (s, 3H), 3.54 (t, *J* = 7.7 Hz, 2H), 3.10 (t, *J* = 7.7 Hz, 2H).

**N-(2-((3,3-Diphenylpropyl)thio)ethyl)cyclohexanamine (2.13a).** In a vial, to a stirred solution of (3-bromopropane-1,1-diyl)dibenzene (**2.12a**, 374 mg, 1.36 mmol) in degassed DMF (5 mL), 2-mercaptoethan-1-amium chloride (185 mg, 1.63 mmol) and potassium carbonate (263 mg, 1.90 mmol) were added. The reaction mixture was stirred at room temperature until no further product formation was observed. After solvent removal, the crude mixture was diluted with H<sub>2</sub>O and extracted with DCM (3x). The combined organic layers were dried using a phase separator and solvent was removed under reduced pressure. The intermediate (21 mg, 0.08 mmol) was dissolved in a DCM/MeOH (2:3) mixture and cyclohexanone (0.009 ml, 0.09 mmol) was slowly added, under N<sub>2</sub>. After stirring for 20 min, sodium triacetoxhydroborate (19 mg, 0.09 mmol) was added and the reaction was allowed to stir at room temperature overnight. After solvent removal, the crude mixture was suspended in DCM (15 mL) and washed with H<sub>2</sub>O (3x) and brine. The organic layer was dried using a phase separator, the solvent was removed under vacuum. The compound was purified by preparative HPLC (gradient of 55-95% acetonitrile in H<sub>2</sub>O/ACN/NH<sub>3</sub> 95/5/0.2 buffer over 15 minutes with a flow of 19 mL/min). Collected fractions were freeze-dried, to afford the title compound over two steps (19 mg, 4%). <sup>1</sup>H NMR (400 MHz, CDCl<sub>3</sub>) δ 7.23 – 7.35 (m, 8H), 7.16 – 7.22 (m, 2H), 4.10 (t, *J* = 7.7 Hz, 1H), 2.77 (t, *J* = 6.5 Hz, 2H), 2.66 (t, *J* = 6.5 Hz, 2H), 2.25 – 2.53 (m, 5H), 1.68 – 1.92 (m, 5H), 1.55 – 1.67 (m, 1H), 1.13 – 1.33 (m, 3H), 0.98 – 1.13 (m, 2H). <sup>13</sup>C NMR (101 MHz, CDCl<sub>3</sub>, 26°C) δ 144.31, 128.67, 127.98, 126.46, 56.60, 50.09, 45.50, 35.55, 33.63, 32.60, 30.15, 26.25, 25.16. HRMS (ESI) *m/z* [M + H]<sup>+</sup> calcd for C<sub>23</sub>H<sub>31</sub>NS: 354.2255, found: 354.2266. Purity: 94%.

**N-(2-((3-Phenylpropyl)thio)ethyl)cyclohexanamine (2.13b)** In a MW vial, to a suspension of (3-bromopropyl)benzene (**2.12b**, 400 mg, 2.01 mmol) and 2-mercaptoethan-1-amium chloride (285 mg, 2.51 mmol) in degassed DMF (4 mL) under N<sub>2</sub>, N-ethyl-N-isopropylpropan-2-amine (0.875 ml, 5.02 mmol) was slowly added. The resulting mixture was heated at 100 °C for 5 min in a single node microwave reactor. Then pressure monitored was 1 atm. After solvent removal, the crude product was dissolved in DCM (15 mL), washed with NaOH 1 M (3x) and brine. The organic layer was dried using a phase separator and solvent removed under reduced pressure. The intermediate was dissolved in a DCM/MeOH (2:3) mixture and cyclohexanone (0.237 ml, 2.29 mmol) was slowly added, under N<sub>2</sub>. After stirring for 20 min, sodium triacetoxhydroborate (490 mg, 2.31 mmol) was added and the reaction was allowed to stir at room temperature overnight. After solvent removal,

## CHAPTER 2

the crude mixture was suspended in DCM (15 mL) and washed with H<sub>2</sub>O (3x) and brine. The organic layer was dried using a phase separator, the solvent was removed under vacuum. The compound was purified by preparative SFC (gradient of 15-25% CO<sub>2</sub> in MeOH/H<sub>2</sub>O/NH<sub>3</sub> 97/3/50 mM buffer over 15 minutes). Collected fractions were dried, to afford the title compound over two steps (110 mg, 20%). <sup>1</sup>H NMR (400 MHz, CDCl<sub>3</sub>) δ 7.23 – 7.32 (m, 2H), 7.14 – 7.22 (m, 3H), 2.80 (t, *J* = 6.6 Hz, 2H), 2.69 – 2.75 (m, 2H), 2.66 (t, *J* = 6.5 Hz, 2H), 2.49 – 2.56 (m, 2H), 2.37 – 2.46 (m, 1H), 1.81 – 1.97 (m, 4H), 1.68 – 1.79 (m, 2H), 1.54 – 1.68 (m, 2H), 0.99 – 1.33 (m, 5H). <sup>13</sup>C NMR (101 MHz, CDCl<sub>3</sub>) δ 141.46, 128.46, 128.37, 125.91, 56.49, 45.54, 34.77, 33.62, 32.68, 31.24, 31.20, 26.17, 25.06. HRMS (ESI) *m/z* [M + H]<sup>+</sup> calcd for C<sub>17</sub>H<sub>27</sub>N S: 278.1942, found: 278.1954. Purity: 89%.

***N*-(2-((2-Phenoxyethyl)thio)ethyl)cyclohexanamine (2.13c).** In a MW vial, to a suspension of (2-bromoethoxy)benzene (400 mg, 1.95 mmol) and 2-mercaptoethan-1-aminium chloride (266 mg, 2.34 mmol) in degassed DMF (4 mL) under N<sub>2</sub>, *N*-ethyl-*N*-isopropylpropan-2-amine (0.849 mL, 4.87 mmol) was slowly added. The resulting mixture was heated at 100 °C for 10 min in a single node microwave reactor. Then pressure monitored was 1 atm. After solvent removal, the crude product was dissolved in DCM (15 mL), washed with NaOH 1 M (3x) and brine. The organic layer was dried using a phase separator and solvent removed under reduced pressure. The intermediate (92 mg, 0.47 mmol) was dissolved in a DCM/MeOH (2:3) mixture and cyclohexanone (0.056 mL, 0.54 mmol) was slowly added, under N<sub>2</sub>. After stirring for 30min, sodium triacetoxhydroborate (114 mg, 0.54 mmol) was added and the reaction was allowed to stir at room temperature overnight. After solvent removal, the crude mixture was suspended in DCM (15 mL) and washed with H<sub>2</sub>O (3x) and brine. The organic layer was dried using a phase separator, the solvent was removed under vacuum. The compound was purified by preparative SFC (gradient of 15-25% CO<sub>2</sub> in MeOH/H<sub>2</sub>O/NH<sub>3</sub> 97/3/50 mM buffer over 15 minutes). Collected fractions were dried, to afford the title compound over two steps (22 mg, 4%). <sup>1</sup>H NMR (500 MHz, CDCl<sub>3</sub>) δ 7.22 – 7.33 (m, 2H), 6.92 – 6.99 (m, 1H), 6.83 – 6.92 (m, 2H), 4.13 (t, *J* = 6.8 Hz, 2H), 2.90 (t, *J* = 6.8 Hz, 2H), 2.83 – 2.88 (m, 2H), 2.73 – 2.81 (m, 2H), 2.42 (tt, *J* = 10.4, 3.7 Hz, 1H), 1.8 – 1.92 (m, 2H), 1.67 – 1.77 (m, 2H), 1.57 – 1.65 (m, 1H), 1.52 (br, 1H), 1.2 – 1.31 (m, 2H), 1.13 – 1.2 (m, 1H), 1.02 – 1.12 (m, 2H). <sup>13</sup>C NMR (126 MHz, CDCl<sub>3</sub>) δ 158.53, 129.61, 121.12, 114.68, 67.81, 56.62, 45.80, 33.75, 33.46, 30.97, 26.25, 25.14. HRMS (ESI) *m/z* [M + H]<sup>+</sup> calcd for C<sub>16</sub>H<sub>25</sub>N O S: 280.1735, found: 280.1740. Purity: 89%.

***N*-(2-((3,4-Dimethoxyphenethyl)thio)ethyl)cyclohexanamine (2.13d).** In a RBF, sodium hydroxide (204 mg, 5.10 mmol) and 2-mercaptoethan-1-aminium chloride (232 mg, 2.04 mmol) were dissolved in degassed MeOH (20 mL) under N<sub>2</sub>. After stirring 30 min, 4-(2-bromoethyl)-1,2-dimethoxybenzene (**2.12c**, 500 mg, 2.04 mmol) was added and the resulting mixture was stirred at room temperature overnight. The crude mixture was filtered, and the filtrate was concentrated under reduced pressure. The crude product was dissolved in diethyl ether, filtered and the solvent evaporated. The intermediate was dissolved in a DCM/MeOH (2:3) mixture and cyclohexanone (0.243 mL, 2.35 mmol) was slowly added, under N<sub>2</sub>. After stirring for 30min, sodium triacetoxhydroborate (497 mg, 2.35 mmol) was added and the reaction was allowed to stir at room temperature overnight. After solvent removal, the crude mixture was suspended in DCM (15 mL) and washed with H<sub>2</sub>O (3x) and brine. The organic layer was dried using a phase separator, the solvent was removed under vacuum. The compound was purified by preparative SFC (gradient of 20-30% CO<sub>2</sub> in MeOH/H<sub>2</sub>O/NH<sub>3</sub> 97/3/50 mM buffer over 15 minutes). Collected fractions were dried, to afford the title compound over two steps (107 mg, 16%). <sup>1</sup>H NMR (500 MHz, CDCl<sub>3</sub>) δ 6.79 (d, *J* = 8.1 Hz, 1H), 6.69 – 6.75 (m, 2H), 3.86 (s, 3H), 3.84 (s, 3H), 2.78 – 2.84 (m, 4H), 2.71 – 2.77 (m, 2H), 2.68 (t, *J* = 6.6 Hz, 2H), 2.36 – 2.45 (m, 1H), 1.81 – 1.9 (m, 2H), 1.63 – 1.77 (m, 3H), 1.55 –

## CHAPTER 2

1.63 (m, 1H), 1.19 – 1.29 (m, 2H), 1.11 – 1.19 (m, 1H), 1 – 1.11 (m, 2H). <sup>13</sup>C NMR (126 MHz, CDCl<sub>3</sub>) δ 148.93, 147.63, 133.18, 120.42, 111.82, 111.27, 56.60, 55.98, 55.92, 45.62, 36.12, 33.77, 33.66, 32.98, 26.21, 25.11. HRMS (ESI) *m/z* [M + H]<sup>+</sup> calcd for C<sub>18</sub>H<sub>29</sub>NO<sub>2</sub>S: 324.1997, found: 324.1998. Purity: 89%.

***N*-2-(Isobutylthio)ethylcyclohexanamine (2.13e).** In a RBF, sodium hydroxide (642 mg, 16.06 mmol) and 2-mercaptoethan-1-aminium chloride (829 mg, 7.30 mmol) were dissolved in degassed DMF (10 mL) under N<sub>2</sub>. After stirring 30 min, 1-bromo-2-methylpropane (0.794 mL, 7.30 mmol) was added and the resulting mixture was stirred at room temperature overnight. The crude mixture was filtered, then cyclohexanone (0.870 mL, 8.39 mmol) was added under N<sub>2</sub>. After stirring for 15 min, sodium triacetoxyhydroborate (1.779 g, 8.39 mmol) was added and the reaction was allowed to stir at room temperature overnight. After solvent removal, the crude mixture was redissolved in DCM and washed with H<sub>2</sub>O (3x) and brine, dried using a phase separator and concentrated under reduced pressure. The compound was purified by preparative SFC (gradient of 15-25% CO<sub>2</sub> in MeOH/H<sub>2</sub>O/NH<sub>3</sub> 97/3/50 mM buffer over 15 minutes). Collected fractions were dried, to afford the title compound over two steps (392 mg, 25%). <sup>1</sup>H NMR (400 MHz, CDCl<sub>3</sub>) δ 2.80 (t, *J* = 6.5 Hz, 2H), 2.64 (t, *J* = 6.6 Hz, 2H), 2.35 – 2.46 (m, 3H), 1.5 – 1.91 (m, 7H), 1 – 1.32 (m, 5H), 0.94 – 1 (m, 6H). <sup>13</sup>C NMR (101 MHz, CDCl<sub>3</sub>) δ 56.65, 45.74, 41.37, 33.72, 33.44, 28.83, 26.27, 25.17, 22.14. MS (ES<sup>+</sup>) *m/z* [M + H]<sup>+</sup> calcd for C<sub>12</sub>H<sub>25</sub>NS: 216.2, found: 216.3.

### General procedure E for the preparation of the sulfoxides (2.14a-e)

In a vial, to a solution of thioether (**2.13a-e**, 1.00 eq) in glacial AcOH (4 mL), hydrogen peroxide 30% (4.00 eq) was added. The reaction was stirred at room temperature until complete consumption of the starting material (50 min). After solvent removal, the crude mixture was dissolved in DCM and washed with H<sub>2</sub>O (3x) and brine. The organic layer was dried using a phase separator and concentrated under reduced pressure. The enantiomers were separated by chiral column chromatography.

**(+) and (-)-*N*-2-((3,3-Diphenylpropyl)sulfinyl)ethylcyclohexanamine (2.14a enantiomers 1 and 2).** Compound **2.14a** was prepared from *N*-2-((3,3-diphenylpropyl)thio)ethylcyclohexanamine (**2.13a**, 44 mg, 0.12 mmol), according to general procedure E, to afford the title compound (34 mg, 75%). <sup>1</sup>H NMR (500 MHz, CDCl<sub>3</sub>) δ 7.17 – 7.33 (m, 10H), 4.05 (t, *J* = 7.7 Hz, 1H), 3.11 – 3.19 (m, 1H), 3.04 – 3.11 (m, 1H), 2.81 – 2.89 (m, 1H), 2.67 – 2.79 (m, 2H), 2.41 – 2.66 (m, 4H), 1.68 – 1.76 (m, 1H), 1.56 – 1.64 (m, 1H), 0.98 – 1.37 (m, 8H), 0.77 – 0.93 (m, 1H). <sup>13</sup>C NMR (126 MHz, CDCl<sub>3</sub>) δ 143.60, 143.34, 128.86, 128.83, 127.92, 127.87, 126.80, 126.77, 56.88, 52.50, 51.20, 50.38, 40.48, 33.20, 33.11, 28.47, 26.05, 25.01, 24.99.

The enantiomers of **2.14a** were separated by chiral column chromatography on a Lux C4 (250x20 mm, 5 μm) column. 1.00 mL (25 mg/mL in EtOH/DCM 75:25) were injected and eluted with 32% EtOH/DEA 100/0.5 in CO<sub>2</sub>, 140 bar at 40 °C, a flow rate of 70 mL/min and detected at 220 nm. The first eluted compound was collected and evaporated to afford **2.14a enantiomer 1** (7.4 mg, 99.8% ee). HRMS (ESI) *m/z* [M + H]<sup>+</sup> calcd for C<sub>23</sub>H<sub>31</sub>NOS: 370.2205, found: 370.2209. The second eluted compound was collected and evaporated to afford **2.14a enantiomer 2** (11 mg, 95.4% ee). HRMS (ESI) *m/z* [M + H]<sup>+</sup> calcd for C<sub>23</sub>H<sub>31</sub>NOS: 370.2205, found: 370.2202.

**(+) and (-)-*N*-2-((3-Phenylpropyl)sulfinyl)ethylcyclohexanamine ((2.14b enantiomers 1 and 2).** Compound **2.14b** was prepared from *N*-2-((2-phenoxyethyl)thio)ethylcyclohexanamine (**2.13b**, 110 mg, 0.40 mmol), according to general procedure E, to afford the title compound (89 mg, 76%).



## CHAPTER 2

<sup>1</sup>H NMR (500 MHz, CDCl<sub>3</sub>) δ 7.25 – 7.33 (m, 2H), 7.13 – 7.23 (m, 3H), 3.28 – 3.36 (m, 1H), 3.17 – 3.25 (m, 1H), 2.91 – 3.04 (m, 2H), 2.74 – 2.85 (m, 3H), 2.6 – 2.72 (m, 2H), 2.03 – 2.18 (m, 2H), 1.9 – 1.97 (m, 2H), 1.72 – 1.81 (m, 2H), 1.58 – 1.66 (m, 1H), 1.1 – 1.33 (m, 6H). <sup>13</sup>C NMR (126 MHz, CDCl<sub>3</sub>) δ 140.39, 128.70, 128.56, 126.46, 56.98, 52.03, 49.82, 39.97, 34.69, 31.58, 31.48, 25.63, 24.81, 24.27.

The enantiomers of **2.14b** were separated by chiral column chromatography on a Lux A1 (250x30 mm, 5 μm) column. 0.700 mL (44.5 mg/mL in EtOH) were injected and eluted with 25% EtOH/DEA 100/0.5 in CO<sub>2</sub>, 130 bar at 40 °C, a flow rate of 130 mL/min and detected at 220 nm. The first eluted compound was collected and evaporated to afford **2.14b enantiomer 1** (30 mg, 97.8% ee). HRMS (ESI) *m/z* [M + H]<sup>+</sup> calcd for C<sub>17</sub>H<sub>27</sub>NOS: 294.1891, found: 294.1908. Purity: 94%. The second eluted compound was collected and evaporated to afford **2.14b enantiomer 2** (30 mg, 99.0% ee). HRMS (ESI) *m/z* [M + H]<sup>+</sup> calcd for C<sub>17</sub>H<sub>27</sub>NOS: 294.1891, found: 294.1898. Purity: 87%.

### **(+) and (-)-N-(2-((2-Phenoxyethyl)sulfinyl)ethyl)cyclohexanamine (2.14c enantiomers 1 and 2)**

Compound **2.14c** was prepared from N-(2-((2-phenoxyethyl)thio)ethyl)cyclohexanamine (**2.13c**, 32 mg, 0.11 mmol), according to general procedure E, to afford the title compound (33 mg, 98%). <sup>1</sup>H NMR (400 MHz, CDCl<sub>3</sub>) δ 7.21 – 7.31 (m, 2H), 6.93 (t, *J* = 7.4 Hz, 1H), 6.88 (d, *J* = 7.9 Hz, 2H), 4.12 (t, *J* = 6.8 Hz, 2H), 2.8 – 2.93 (m, 4H), 2.73 – 2.79 (m, 2H), 2.41 (tt, *J* = 10.4, 3.7 Hz, 1H), 1.8 – 1.92 (m, 2H), 1.66 – 1.77 (m, 2H), 1.53 – 1.66 (m, 2H), 0.97 – 1.31 (m, 5H). <sup>13</sup>C NMR (101 MHz, CDCl<sub>3</sub>) δ 158.51, 129.59, 121.10, 114.66, 67.79, 56.60, 45.76, 33.69, 33.40, 30.95, 26.22, 25.12.

The enantiomers of **2.14c** were separated by chiral column chromatography on a YMC SA (250x20 mm, 5 μm) column. 0.700 mL (24 mg/mL in EtOH/DCM 1:1) were injected and eluted with 30% EtOH/DEA 100/0.5 in CO<sub>2</sub>, 130 bar at 40 °C, a flow rate of 75 mL/min and detected at 270 nm. The first eluted compound was collected and evaporated to afford **2.14c enantiomer 1** (11 mg, 93% ee). HRMS (ESI) *m/z* [M + H]<sup>+</sup> calcd for C<sub>16</sub>H<sub>25</sub>NO<sub>2</sub>S: 296.1684, found: 296.1687. Purity: 90%. The second eluted compound was collected and evaporated to afford **2.14c enantiomer 2** (13 mg, 97% ee). HRMS (ESI) *m/z* [M + H]<sup>+</sup> calcd for C<sub>16</sub>H<sub>25</sub>NO<sub>2</sub>S: 296.1684, found: 296.1682. Purity: 89%.

### **(+) and (-)-N-(2-((3,4-Dimethoxyphenethyl)sulfinyl)ethyl)cyclohexanamine (2.14d enantiomers 1 and 2)**

Compound **2.14d** was prepared from N-(2-((3,4-dimethoxyphenethyl)thio)ethyl)cyclohexanamine (**2.13d**, 90 mg, 0.28 mmol), according to general procedure E, to afford the title compound (52 mg, 55%). <sup>1</sup>H NMR (500 MHz, CDCl<sub>3</sub>) δ 6.72 – 6.86 (m, 3H), 3.81 – 3.9 (m, 6H), 2.67 – 3.32 (m, 8H), 2.39 – 2.56 (m, 1H), 1.89 (d, *J* = 9.7 Hz, 2H), 1.72 (d, *J* = 12.8 Hz, 2H), 1.56 – 1.64 (m, 1H), 0.97 – 1.37 (m, 6H). <sup>13</sup>C NMR (126 MHz, CDCl<sub>3</sub>) δ 149.22, 147.97, 131.45, 120.61, 111.90, 111.52, 56.87, 56.05, 56.02, 54.62, 52.94, 40.52, 33.37, 33.28, 28.57, 26.09, 25.03, 25.02.

The enantiomers of **2.14d** were separated by chiral column chromatography on a Chiralpak (250x20 mm, 5 μm) column. 0.500 mL (25 mg/mL in EtOH) were injected and eluted with 22% IPA/DEA 100/0.5 in CO<sub>2</sub>, 120 bar at 40 °C, a flow rate of 70 mL/min and detected at 220 nm. The first eluted compound was collected and evaporated to afford **2.14d enantiomer 1** (12.6 mg, 99.2% ee). HRMS (ESI) *m/z* [M + H]<sup>+</sup> calcd for C<sub>18</sub>H<sub>29</sub>NO<sub>3</sub>S: 340.1946, found: 340.1952. Purity: 96%. The second eluted compound was collected and evaporated to afford **2.14d enantiomer 2** (17.2 mg, 97.6% ee). HRMS (ESI) *m/z* [M + H]<sup>+</sup> calcd for C<sub>18</sub>H<sub>29</sub>NO<sub>3</sub>S: 340.1946, found: 340.1936. Purity: 89%.

**(+) and (-)-N-(2-(Isobutylsulfinyl)ethyl)cyclohexanamine ((+) and (-)-2.14e)**. Compound **2.14e** was prepared from N-(2-(isobutylthio)ethyl)cyclohexanamine (**2.13e**, 392 mg, 1.82 mmol), according to general procedure E, to afford the title compound (377 mg, 90%). <sup>1</sup>H NMR (500 MHz,

## CHAPTER 2

$\text{CDCl}_3$ )  $\delta$  2.98 – 3.14 (m, 2H), 2.63 – 2.79 (m, 3H), 2.31 – 2.43 (m, 2H), 2.09 – 2.22 (m, 1H), 1.77 – 1.86 (m, 2H), 1.59 – 1.76 (m, 3H), 1.48 – 1.58 (m, 1H), 0.93 – 1.24 (m, 11H).  $^{13}\text{C}$  NMR (126 MHz,  $\text{CDCl}_3$ )  $\delta$  62.29, 56.66, 53.74, 40.36, 33.48, 33.40, 26.04, 24.93, 24.92, 23.89, 22.88, 21.66.

The enantiomers of **2.14e** were separated by chiral column chromatography on a Lux A1 (250x30 mm, 5  $\mu\text{m}$ ) column. 0.900 mL (75 mg/mL in EtOH) were injected and eluted with 20% EtOH/ $\text{NH}_3$  100/0.5 in  $\text{CO}_2$ , 120 bar at 40  $^\circ\text{C}$ , a flow rate of 130 mL/min and detected at 220 nm. The first eluted compound was collected and evaporated to afford (-)-**2.14e** (151 mg, 99.6% ee).  $[\alpha]_{\text{D}}^{20}$ : -15 ( $c = 1$ , ACN). HRMS (ESI)  $m/z$   $[\text{M} + \text{H}]^+$  calcd for  $\text{C}_{12}\text{H}_{25}\text{NOS}$ : 232.1735, found: 232.1719. The second eluted compound was collected and evaporated to afford (+)-**2.14e** (149 mg, 99.4% ee).  $[\alpha]_{\text{D}}^{20}$ : +14 ( $c = 1$ , ACN). HRMS (ESI)  $m/z$   $[\text{M} + \text{H}]^+$  calcd for  $\text{C}_{12}\text{H}_{25}\text{NOS}$ : 232.1735, found: 232.1728.

### General procedure F for the preparation of the sulfones (2.15a-c,e)

In a vial, to a solution of thioether (**2.13a-c,e**, 1.00 eq) and in glacial AcOH (4 mL), hydrogen peroxide 30% (4.00 eq) was added. The reaction was stirred overnight at room temperature. The reaction was quenched by addition of NaOH 1M, then the residue was extracted with DCM (3x). The organic layers were dried using a phase separator and concentrated under reduced pressure. The compound was purified by preparative HPLC.

**N-(2-((3,3-Diphenylpropyl)sulfonyl)ethyl)cyclohexanamine (2.15a)**. Compound **2.15a** was prepared from N-(2-((3,3-diphenylpropyl)thio)ethyl)cyclohexanamine (**2.13a**, 19 mg, 0.05 mmol), according to general procedure E, to afford the title compound (6 mg, 40%).  $^1\text{H}$  NMR (500 MHz,  $\text{CDCl}_3$ )  $\delta$  7.27 – 7.34 (m, 4H), 7.17 – 7.25 (m, 6H), 4.02 (t,  $J = 8.0$  Hz, 1H), 2.99 – 3.14 (m, 6H), 2.53 – 2.64 (m, 2H), 2.33 – 2.43 (m, 1H), 1.77 – 1.88 (m, 2H), 1.66 – 1.75 (m, 2H), 1.53 – 1.66 (m, 2H), 1.07 – 1.31 (m, 4H), 0.92 – 1.04 (m, 2H).  $^{13}\text{C}$  NMR (126 MHz,  $\text{CDCl}_3$ )  $\delta$  143.09, 128.93, 127.82, 126.94, 56.67, 53.58, 53.02, 50.07, 40.05, 33.44, 27.61, 26.12, 25.01. HRMS (ESI)  $m/z$   $[\text{M} + \text{H}]^+$  calcd for  $\text{C}_{23}\text{H}_{31}\text{NO}_2\text{S}$ : 386.2154, found: 386.2171. Purity: 91%.

**N-(2-((3-Phenylpropyl)sulfonyl)ethyl)cyclohexanamine (2.15b)**. Compound **2.15b** was prepared from N-(2-((3-phenylpropyl)thio)ethyl)cyclohexanamine (**2.13b**, 100 mg, 0.36 mmol), according to general procedure F (purification conditions: 5-95% ACN in 0.2%  $\text{NH}_3$ ) to afford the title compound (8 mg, 7%). MS ( $\text{ES}^+$ )  $m/z$   $[\text{M} + \text{H}]^+$  calcd for  $\text{C}_{17}\text{H}_{27}\text{NO}_2\text{S}$ : 310.4, found: 310.2. Purity: 75%.

**N-(2-((2-Phenoxyethyl)sulfonyl)ethyl)cyclohexanamine (2.15c)**. Compound **2.15c** was prepared from N-(2-((2-phenoxyethyl)thio)ethyl)cyclohexanamine (**2.13c**, 57 mg, 0.20 mmol), according to general procedure F (purification conditions: 5-95% ACN in 0.2%  $\text{NH}_3$ ) to afford the title compound (5 mg, 8%). MS ( $\text{ES}^+$ )  $m/z$   $[\text{M} + \text{H}]^+$  calcd for  $\text{C}_{16}\text{H}_{25}\text{NO}_3\text{S}$ : 312.4, found: 312.2. Purity: 52%.

**N-(2-(Isobutylsulfonyl)ethyl)cyclohexanamine (2.15e)**. Compound **2.15e** was prepared from N-(2-(isobutylthio)ethyl)cyclohexanamine (**2.13e**, 65 mg, 0.30 mmol), according to general procedure F (purification conditions: 5-95% ACN in 0.2%  $\text{NH}_3$ ) to afford the title compound (24 mg, 32%). MS ( $\text{ES}^+$ )  $m/z$   $[\text{M} + \text{H}]^+$  calcd for  $\text{C}_{12}\text{H}_{25}\text{NO}_2\text{S}$ : 248.4, found: 248.2. Purity: 92%.

## CHAPTER 2

### 2.6 REFERENCES

1. Nishizawa, R.; Saino, T.; Takita, T.; Suda, H.; Aoyagi, T.; Umezawa, H. Synthesis and structure-activity relations of bestatin analogs, inhibitors of aminopeptidase B. *J. Med. Chem.* **1977**, *20* (4), 510-515.
2. Richter, A.; Hedberg, C. A Practical and Convenient Synthesis of the Protease Inhibitor Epibestatin. *Synthesis* **2010**, *2010* (12), 2039-2042.
3. Umezawa, H.; Aoyagi, T.; Suda, H.; Hamada, M.; Takeuchi, T. Bestatin, an inhibitor of aminopeptidase B, produced by actinomycetes. *J. Antibiot.* **1976**, *29* (1), 97-99.
4. Rose, R.; Erdmann, S.; Bovens, S.; Wolf, A.; Rose, M.; Hennig, S.; Waldmann, H.; Ottmann, C. Identification and structure of small-molecule stabilizers of 14-3-3 protein-protein interactions. *Angew. Chem. Int. Ed. Engl.* **2010**, *49* (24), 4129-4132.
5. Ottmann, C.; Marco, S.; Jaspert, N.; Marcon, C.; Schauer, N.; Weyand, M.; Vandermeeren, C.; Duby, G.; Boutry, M.; Wittinghofer, A.; Rigaud, J.-L.; Oecking, C. Structure of a 14-3-3 Coordinated Hexamer of the Plant Plasma Membrane H<sup>+</sup>-ATPase by Combining X-Ray Crystallography and Electron Cryomicroscopy. *Molecular Cell* **2007**, *25* (3), 427-440.
6. Wurtele, M.; Jelich-Ottmann, C.; Wittinghofer, A.; Oecking, C. Structural view of a fungal toxin acting on a 14-3-3 regulatory complex. *EMBO J.* **2003**, *22* (5), 987-94.
7. Andrei, S. A. Engineering stabilizers of 14-3-3 protein-protein interactions. Technische Universiteit Eindhoven, Eindhoven, 2019.
8. Jhoti, H.; Cleasby, A.; Verdonk, M.; Williams, G. Fragment-based screening using X-ray crystallography and NMR spectroscopy. *Curr. Opin. Chem. Biol.* **2007**, *11* (5), 485-493.
9. Milroy, L.-G.; Bartel, M.; Henen, M. A.; Leysen, S.; Adriaans, J. M. C.; Brunsveld, L.; Landrieu, I.; Ottmann, C. Stabilizer-Guided Inhibition of Protein-Protein Interactions. *Angew. Chem. Int. Ed.* **2015**, *54* (52), 15720-15724.
10. Andrei, S. A.; Meijer, F. A.; Neves, J. F.; Brunsveld, L.; Landrieu, I.; Ottmann, C.; Milroy, L.-G. Inhibition of 14-3-3/Tau by Hybrid Small-Molecule Peptides Operating via Two Different Binding Modes. *ACS Chemical Neuroscience* **2018**, *9* (11), 2639-2654.
11. Rose, R.; Erdmann, S.; Bovens, S.; Wolf, A.; Rose, M.; Hennig, S.; Waldmann, H.; Ottmann, C. Identification and structure of small-molecule stabilizers of 14-3-3 protein-protein interactions. *Angew. Chem. Int. Ed.* **2010**, *49* (24), 4129-32.
12. Yen, C.-F.; Hu, C.-K.; Chou, M.-C.; Tseng, C.-T.; Wu, C.-H.; Huang, Y.-H.; Chen, S.-J.; King, C.-H. R. Preparation of 2-aminopyrimidine compounds having affinity to chemokine receptors. US20090143302A1, 2009.

# CHAPTER 3

## Design Of Drug-Like Protein-Protein Interaction Stabilizers Guided By Chelation-Controlled Bioactive Conformation Stabilization

### Abstract

The protein-protein interactions (PPIs) of 14-3-3 proteins are a model system for studying PPI stabilization. The complex natural product Fusicoccin A stabilizes many 14-3-3 PPIs but is not amenable for use in SAR studies, motivating the search for more drug-like chemical matter. However, drug-like 14-3-3 PPI stabilizers enabling such study have remained elusive. An X-ray crystal structure of a PPI in complex with an extremely low potency stabilizer uncovered an unexpected non-protein interacting, ligand-chelated  $Mg^{2+}$  leading to the discovery of metal ion-dependent 14-3-3 PPI stabilization potency. This originates from a novel chelation-controlled bioactive conformation stabilization effect. Metal chelation has been associated with pan-assay interference compounds (PAINS) and frequent hitter behavior, but chelation can evidently also lead to true potency gains and find use as a medicinal chemistry strategy to guide compound optimization. To demonstrate this, we exploited the effect to design the first potent, selective and drug-like 14-3-3 PPI stabilizers.

## 3.1 INTRODUCTION

Protein-protein interactions (PPIs) are a major class of macromolecular interactions which control the function of many proteins.<sup>[1]</sup> The protein interactome is crucial to many biological processes, is implicated in many diseases<sup>[2-4]</sup> and contains many promising intervention points for development of therapeutics.<sup>[5-6]</sup> Inhibition is the most advanced mode of action for PPI modulation, with several rationally-designed PPI inhibitors in clinical testing or approved as drugs.<sup>[7]</sup> In contrast, PPI stabilization is comparatively unexplored.<sup>[8]</sup> Several natural products have been shown post hoc to operate by stabilization of PPIs,<sup>[9]</sup> but there are few examples of rationally designed small-molecule, drug-like PPI stabilizers. This is partly due to incomplete understanding of the structural and kinetic principles driving stabilization, making robust screen design difficult and resulting in a paucity of tractable starting points for PPI stabilizer development.<sup>[10-12]</sup>

14-3-3 proteins are non-enzymatic adapter proteins that bind as dimers to phosphorylated client proteins, controlling client activity and cellular fate.<sup>[13-14]</sup> They are involved in many cellular processes such as cell cycle regulation and apoptosis,<sup>[15]</sup> subcellular localization<sup>[16]</sup> and enzymatic activity regulation.<sup>[17]</sup> There are 7 human 14-3-3 isoforms, structurally composed of 9 helices forming an amphipathic binding groove which binds 14-3-3 consensus motifs on phosphorylated client proteins.<sup>[13]</sup> The natural product Fusicoccin A (**1**, Figure 1a) and related fusicoccanes<sup>[18]</sup> stabilize 14-3-3 PPIs with many phosphorylated partners.<sup>[19-20]</sup> Ternary complex crystal structures show that they occupy a well-defined binding pocket (“FC pocket”) at the interface between 14-3-3 and the binding partner (Figure 3.1b). The fusicoccanes’ synthetic complexity makes them unsuitable for a molecular matched pair approach<sup>[21]</sup> to generate structure-activity relationship (SAR) principles or to study PPI stabilization selectivity. We therefore aimed to identify synthetically tractable, drug-like small-molecule starting points for systematic investigation of 14-3-3 PPI stabilization. In the course of this, we also discovered a novel chelation-controlled ligand conformational stabilization effect which had profound effects on compound potency, resulting in metal ion-assisted small molecule PPI stabilization. Chelation of metals by ligands of interest has been associated with assay interference and frequent hitter behavior, especially in PPI inhibition assays based on AlphaScreen technology.<sup>[22]</sup> Based on this observation, compounds containing potential chelating moieties tend to be filtered out from screening collections either prior to screening or in order to triage large screening data sets prior to data analysis, as an extension to the originally-reported PAINS filters.<sup>[23]</sup>

In this report, we show that metal ion chelation may in some cases lead to true potency gains and allow identification of hits that otherwise would be discarded as of insufficient potency. In our case, this manifested itself as a metal-ion assisted PPI

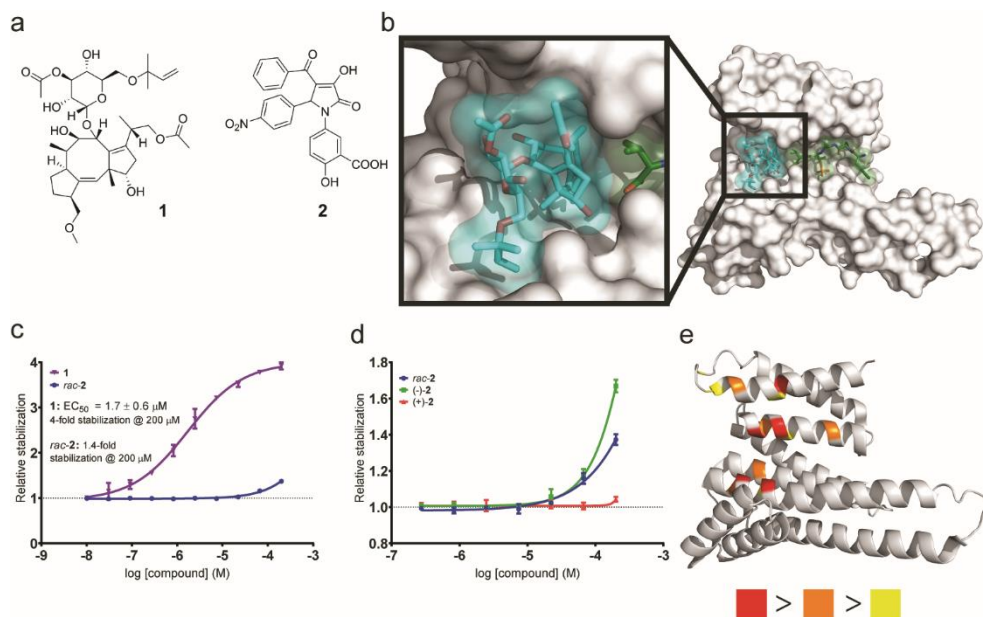


**Figure 3.1** | Identification of **2** as a low potency 14-3-3/ER $\alpha$  PPI stabilizer. (a) Chemical structures of Fusicoccin **1** and Pyrrolidone **2**. (b) Crystal structure of the ternary complex between 14-3-3 $\sigma$  (white surface), ER $\alpha$  pT<sup>594</sup> phosphopeptide **3** (green sticks) and **1** (blue sticks) rendered from PDB 4JDD and highlighting the “FC pocket”. (c) Comparison of 14-3-3 $\zeta$ /ER $\alpha$ (pT<sup>594</sup>) PPI stabilization activity of **1** (purple inverse triangles) and *rac*-**2** (blue circles) in an FP assay, using 50 nM 14-3-3 $\zeta$  and 10 nM ER $\alpha$ (pT<sup>594</sup>) phosphopeptide FITC-**3**. “Relative stabilization” (y-axis) is the mean fold-increase of FP signal over baseline (i.e. interaction between 14-3-3 $\zeta$  and FITC-**3** alone). The error bars in all plots indicate  $\pm$  SD ( $n = 3$ ). (d) Comparison of PPI stabilization activity of *rac*-**2**, (-)-**2** (green squares) and (+)-**2** (red triangles) in 14-3-3/ER $\alpha$ (pT<sup>594</sup>) FP assay. (e) The <sup>1</sup>H-<sup>15</sup>N TROSY-HSQC peak intensities most affected by binding of (-)-**2** correspond to 14-3-3 residues lining the FC pocket (mapped on the crystal structure of 14-3-3 $\sigma$  rendered from PDB 1YZ5). The 5 most affected residues are colored red, the next 5 orange and the next 5 yellow.  $I/I_0$  values and color coding is provided in Fig S3.6.

stabilization, where the addition of bivalent metal ions led to up to two orders of magnitude increase in compound potency.

We furthermore exploited this effect to design metal-independent PPI stabilizers by mimicking the chelation with intramolecular hydrogen bonds, leading to compounds with high PPI stabilization potency and which are insensitive to metal ion concentration. The resulting compounds enable the systematic investigation of 14-3-3 PPI stabilization SAR and selectivity and further development of small-molecule 14-3-3 PPI stabilizers with potency rivaling that of the natural product **1**. We also propose that this type of ligand-specific conformational effect is a potential source of false negatives and should be considered when analyzing screening data and interpreting SAR for chelation-competent ligands as well as during the analysis and triage of high-throughput screen output.

## 3.2 RESULTS

**Racemic Pyrrolidone1 (*rac*-2) is a weak stabilizer of the canonical 14-3-3/ER $\alpha$ (pT<sup>594</sup>) PPI**

Binding of 14-3-3 to the ER $\alpha$  pT<sup>594</sup> phosphosite has been shown to prevent estradiol-induced activation of ER $\alpha$  by preventing ER $\alpha$  dimerisation.<sup>[24]</sup> By stabilizing the 14-3-3/ER $\alpha$  interaction, **1** was shown to enhance the 14-3-3-mediated inhibition of ER $\alpha$  activity and therefore the 14-3-3/ER $\alpha$  interaction is of interest as a potential target for development of ER $\alpha$ -dependent breast cancer therapies. To test compounds for 14-3-3 PPI stabilization, we selected the ER $\alpha$  pT<sup>594</sup> phosphosite (ER $\alpha$ (pT<sup>594</sup>)) as the phosphorylated 14-3-3 binding partner, due to the availability of a ternary X-ray crystal structure with **1**. Pyrrolidone1 (**2**, Figure 3.1a) has previously been reported as a low potency stabilizer of the PPI between 14-3-3 and the plant plasma membrane H<sup>+</sup>-ATPase 2 (PMA2).<sup>[25]</sup> Since **1** stabilizes both the 14-3-3/PMA2 and 14-3-3/ER $\alpha$ (pT<sup>594</sup>) PPIs<sup>[24, 26]</sup> and **2** binds to the FC pocket of the non-canonical 14-3-3/PMA2 complex (the PMA2 peptide used was non-phosphorylated), we decided to investigate **2** as a potential stabilizer of the 14-3-3/ER $\alpha$ (pT<sup>594</sup>) complex. We developed fluorescence polarization (FP) and surface plasmon resonance (SPR) assays based on 14-3-3 $\zeta$  and ER $\alpha$  pT<sup>594</sup> phosphopeptides (**3** or FITC-**3**, sequence AEGFPApT<sup>594</sup>V-COOH).

The  $K_d$  of the 14-3-3/**3** interaction was  $227 \pm 14$  nM (Figure S3.1) as measured by SPR. In a 14-3-3/ER $\alpha$ (pT<sup>594</sup>) FP assay (based on a labelled derivative of **3**, FITC-**3**), **2** showed very low activity (1.4-fold stabilization at 200  $\mu$ M, Fig. 3.1c) compared to **1** (EC<sub>50</sub>  $1.7 \pm 0.6$   $\mu$ M, 4-fold stabilization at 200  $\mu$ M). In the 14-3-3/ER $\alpha$ (pT<sup>594</sup>) SPR assay, a comparable EC<sub>50</sub> was determined for **1** (EC<sub>50</sub>  $1.8 \pm 0.2$   $\mu$ M), while the PPI stabilization effect of **2** was undetectable, with only binding of **2** to 14-3-3 protein being observed (Figure S3.2, S3.3). The enantiomers of **2** were then separated by chiral HPLC. In the 14-3-3/ER $\alpha$ (pT<sup>594</sup>) FP and SPR assays, (-)-**2** was found to be more active than *rac*-**2** and (+)-**2** was shown to be inactive (Figure 3.1d and S3.9). (-)-**2** was shown to be stable with respect to epimerization under basic conditions (see Supporting Information).

NMR experiments were conducted using 14-3-3 $\sigma\Delta$ C<sup>[27]</sup> and **3** to determine if (-)-**2** binds to the FC pocket of the 14-3-3/ER $\alpha$ (pT<sup>594</sup>) complex. WaterLOGSY experiments<sup>[28]</sup> were performed with (-)-**2** in the presence and absence of either 14-3-3 $\sigma\Delta$ C or the 14-3-3 $\sigma\Delta$ C/**3** complex. Positively phased <sup>1</sup>H signals for (-)-**2** confirmed binding to 14-3-3 $\sigma\Delta$ C alone (Figure S3.4, red spectrum) and the 14-3-3 $\sigma\Delta$ C/**3** complex (Figure S3.4, green spectrum). Protein-based NMR experiments were then carried out to determine the binding site of (-)-**2** on 14-3-3 $\sigma\Delta$ C. By observing changes in the intensity ratio ( $I/I_0$ ) of resonances in the fully-assigned <sup>1</sup>H-<sup>15</sup>N TROSY-HSQC

spectrum of 14-3-3 $\sigma\Delta$ C<sup>[29]</sup> in the presence (*I*) or absence (*I*<sub>0</sub>) of (-)-**2** (Figure S3.5, S3.6), a mapping of the residues most affected by (-)-**2** binding (Figure 3.1e) was generated, indicating that the binding site of (-)-**2** corresponds to the FC pocket.<sup>[25]</sup> Phosphopeptide **3** induced significant chemical shift perturbations in the 14-3-3 $\sigma\Delta$ C <sup>1</sup>H-<sup>15</sup>N TROSY-HSQC spectrum, with some resonances showing characteristics of a slow exchange regime on the NMR time scale (Figure S3.7), which is compatible with the high affinity observed by SPR. These strong chemical shift perturbations prevented a comprehensive determination of the binding site of (-)-**2** to the 14-3-3 $\sigma\Delta$ C/**3** complex by NMR. Nonetheless, two resonances with chemical shifts minimally but specifically affected by the presence of (-)-**2** were identified. These signals, corresponding to G171 and I219 (Figure S3.8), lie in the FC pocket and were already affected by the presence of (-)-**2** alone, indicating that (-)-**2** binds to the FC pocket of both 14-3-3 $\sigma\Delta$ C alone and in the 14-3-3 $\sigma\Delta$ C/**3** complex.

### **(R)-2 is the active enantiomer of 2: reassignment of binding mode and absolute configuration by X-ray crystallography**

Having confirmed by NMR that (-)-**2** binds to the FC pocket of the 14-3-3/ER $\alpha$ (pT<sup>594</sup>) complex, we set out to obtain an X-ray crystal structure of the 14-3-3 $\sigma$ /ER $\alpha$ (pT<sup>594</sup>) phosphopeptide **3**/(-)-**2** ternary complex. By co-crystallization, we obtained crystals which diffracted reproducibly at a resolution of 1.85 Å. The 3.25 Å X-ray crystal structure of the ternary complex of (*S*)-**2** bound to the *Nicotiana tabacum* 14-3-3 like protein C/PMA2 complex<sup>[25]</sup> (Figure 3.2a, magenta sticks) was initially used to model the binding orientation of **2**. However, it was not possible to model (*S*)-**2** into the observed ligand-derived electron density of the 14-3-3 $\sigma\Delta$ C/**3**/(-)-**2** ternary complex. The 1.85 Å resolution was sufficient to model the ligand *ab initio*, confirming that (-)-**2** binds to the FC pocket as well as unambiguously assigning the (*R*) absolute configuration to (-)-**2** (Figure 3.2a, yellow sticks). This assignment agreed with that obtained by vibrational circular dichroism on (+)-**2** (assigned (*S*), see Figure S23). Testing of (-)-**2** and (+)-**2** by SPR on the 14-3-3e/PMA2 PPI (Figure S3.10) showed that only (-)-**2** stabilized this complex, as was the case for 14-3-3/ER $\alpha$ (pT<sup>594</sup>). The fact that only (-)-**2** stabilizes both PPIs, together with the higher resolution of the 14-3-3 $\sigma\Delta$ C/**3**/(-)-**2** ternary complex crystal structure compared to the published 14-3-3e/PMA2/**2** structure supports our revised binding mode of **2** (Figure 3.2a) and reassignment of the absolute configuration for the active 14-3-3 PPI stabilizing enantiomer of **2** as (*R*) (from this point in the text, (-)-**2** and (+)-**2** will be referred to as (*R*)-**2** and (*S*)-**2** respectively).

Overall, (*R*)-**2** binds in a T-shaped conformation, with each of its phenyl rings pointing into separate sub-pockets (Figure 3.2b) and with all three phenyl rings oriented orthogonally to the pyrrolidone ring. The salicylate moiety of (*R*)-**2** occupies



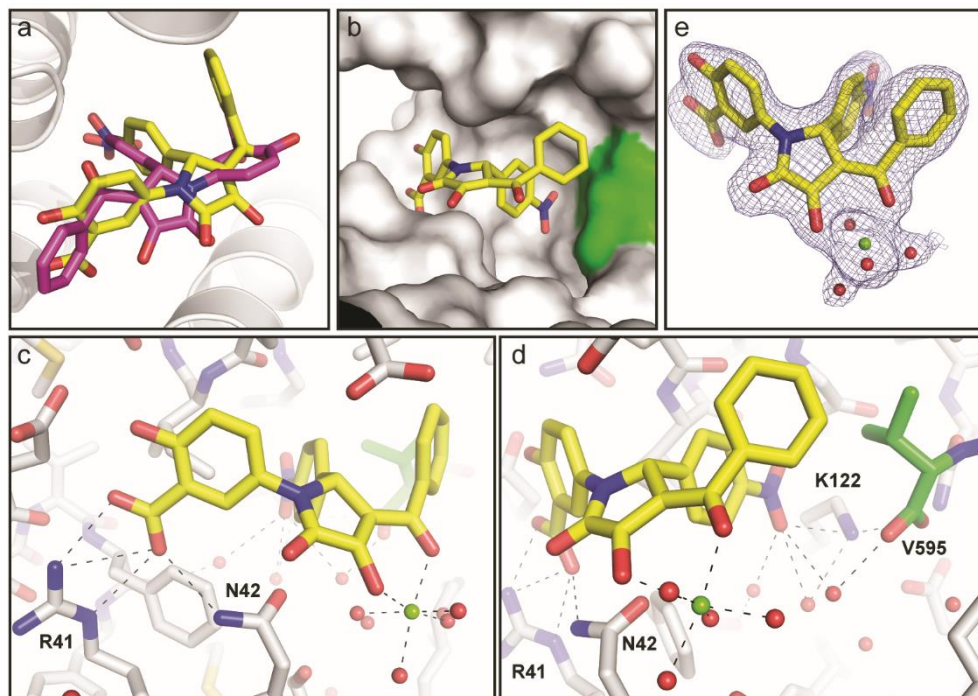


**Figure 3.2** | X-ray crystal structure of 14-3-3/ER $\alpha$ (pT<sup>594</sup>)/(*R*)-2 ternary complex and identification of (*R*)-2-chelated Mg<sup>2+</sup> ion. (a) Comparison of binding mode of **2** from 3.25 Å 14-3-3/PMA2 complex structure (magenta sticks, assigned as (*S*), rendered from PDB 3M51) with revised binding mode derived from the 1.85 Å 14-3-3/ER $\alpha$ (pT<sup>594</sup>) complex structure (yellow sticks, assigned (*R*) absolute configuration, PDB 6TJM). (b) Binding mode of (*R*)-2 in the FC pocket, showing surface contributions from 14-3-3 (grey surface) and ER $\alpha$ (pT<sup>594</sup>) phosphopeptide **3** (green surface). (c) Details of interactions of salicylate moiety of (*R*)-2. (d) Details of interactions of nitrophenyl moiety of (*R*)-2, showing the nitro group acting as H-bond acceptor from 14-3-3 Lys122 and water-mediated interaction with the C-terminus of ER $\alpha$ (pT<sup>594</sup>) phosphopeptide **3** (green). (e) Additional ligand-associated electron density ( $2F_{\text{obs}} - F_{\text{cal}}$  map contoured at 1  $\sigma$ ) corresponding to a fully-hydrated Mg<sup>2+</sup> ion (shown in green) chelated by the vinylogous carboxylate moiety of (*R*)-2

a narrow, largely negatively charged cleft (Figure 3.2c) not exploited by **1** (Figure S3.11). The carboxylate group participates in a bidentate interaction with Arg41 and accepts a H-bond from Asn42. The carbonyl of the pyrrolidone ring participates in an attractive antiparallel interaction with the sidechain of Asn42.<sup>[30]</sup> The nitro group accepts a H-bond from Lys122 (Figure 3.2d) which is also in direct contact with the C-terminus of **3**, thus (*R*)-2 bridges 14-3-3 and **3** via polar interactions. Unexpectedly, additional electron density was observed in conjunction with the ligand (Figure 3.2e), corresponding to a fully hydrated Mg<sup>2+</sup> ion (presumably derived from the Mg<sup>2+</sup>-containing crystallization buffer) chelated by the vinylogous carboxylate moiety of (*R*)-2. A pK<sub>a</sub> of 3.2 was measured (see Supporting Information) for the vinylogous

carboxylate moiety of *rac-2*, supporting the observation of the magnesium vinylogous carboxylate salt in the ternary complex.

### **(R)-2 but not 1 stabilizes the 14-3-3/CaMKK2(pS<sup>100</sup>) PPI**

Given the relatively high affinity of the 14-3-3/3 interaction, we sought a 14-3-3 binding partner with a binary complex of similar overall structure to the 14-3-3/ER $\alpha$ (pT<sup>594</sup>) structure (i.e. with a vacant FC pocket) but with lower 14-3-3 affinity, in order to investigate the dynamic range of PPI stabilization. We reasoned that such an interaction would also be useful to evaluate the 14-3-3 PPI stabilization specificity of (*R*)-**2**. pS<sup>100</sup> of calcium/calmodulin-dependent kinase kinase 2 (CaMKK2)<sup>[31]</sup> was identified as a suitable candidate. Unlike the pT<sup>594</sup> ER $\alpha$  phosphosite from which phosphopeptide **3** is derived, the N-terminal domain of CaMKK2 pS<sup>100</sup> phosphosite is not a canonical mode III 14-3-3 binder.<sup>[32]</sup> However, the crystal structure of 14-3-3 $\zeta$  in complex with a phosphopeptide derived from the CaMKK2 pS<sup>100</sup> site (sequence RKLpS<sup>100</sup>LQER, PDB ID: 6EWW) indicates that it mimics a canonical mode III binder and that the FC pocket in this complex is largely unoccupied and available for potential binding of stabilizers such as (*R*)-**2**.<sup>[31]</sup>

We determined the binding affinity of CaMKK2 pS<sup>100</sup> 13-mer phosphopeptide **4**<sup>[31]</sup> to 14-3-3 $\zeta$  by SPR (estimated  $K_d$  112  $\pm$  14  $\mu$ M, Figure S3.12) and found it significantly lower than for 14-3-3 $\zeta$ /**3** ( $K_d$  227  $\pm$  14 nM). An FP assay was then developed based on a FAM-labelled derivative of **4** (FAM-**4**). The stabilization of the 14-3-3/CaMKK2(pS<sup>100</sup>) PPI by *rac*-, (*R*)- and (*S*)-**2** and natural product **1** was then determined using by FP and SPR assays (Figure 3.3a and S3.13). Interestingly, despite an apparently vacant FC pocket, **1** exhibited only borderline statistically significant stabilization of the 14-3-3/CaMKK2(pS<sup>100</sup>) PPI by FP (p 0.060) and SPR (p 0.038) at 200  $\mu$ M (purple inverted triangles). Following the same stereochemical dependence as for the 14-3-3/ER $\alpha$ (pT<sup>594</sup>) PPI, (*R*)-**2** was a more effective stabilizer of the 14-3-3/CaMKK2(pS<sup>100</sup>) PPI than **1** (green squares), while (*S*)-**2** showed no significant stabilization activity (red triangles).

### **(R)-2 exhibits metal ion-dependent 14-3-3 PPI stabilization potency**

With stabilization by (*R*)-**2** confirmed in two 14-3-3 PPIs, we investigated a potential role for the crystallographically-observed Mg<sup>2+</sup> chelation by (*R*)-**2**. Performing the FP and SPR assays in the presence of Mg<sup>2+</sup> led to an apparent increase in stabilization potency and maximum efficacy of (*R*)-**2** in both the 14-3-3/ER $\alpha$ (pT<sup>594</sup>) and 14-3-3/CaMKK2(pS<sup>100</sup>) PPIs (Figure 3.3b and S3.14, S3.15). We then carried out Mg<sup>2+</sup> concentration-response experiments in the 14-3-3/ER $\alpha$ (pT<sup>594</sup>) and 14-3-3/CaMKK2(pS<sup>100</sup>) FP assays at a fixed concentration (10  $\mu$ M) of *rac-2*, (*R*)-**2**, (*S*)-**2** and **1** (Figure 3.3c). The 14-3-3/ER $\alpha$ (pT<sup>594</sup>) PPI stabilization efficacy of (*R*)-**2** and *rac-2* (green squares and blue circles respectively) and 14-3-3/CaMKK2(pS<sup>100</sup>)

## CHAPTER 3

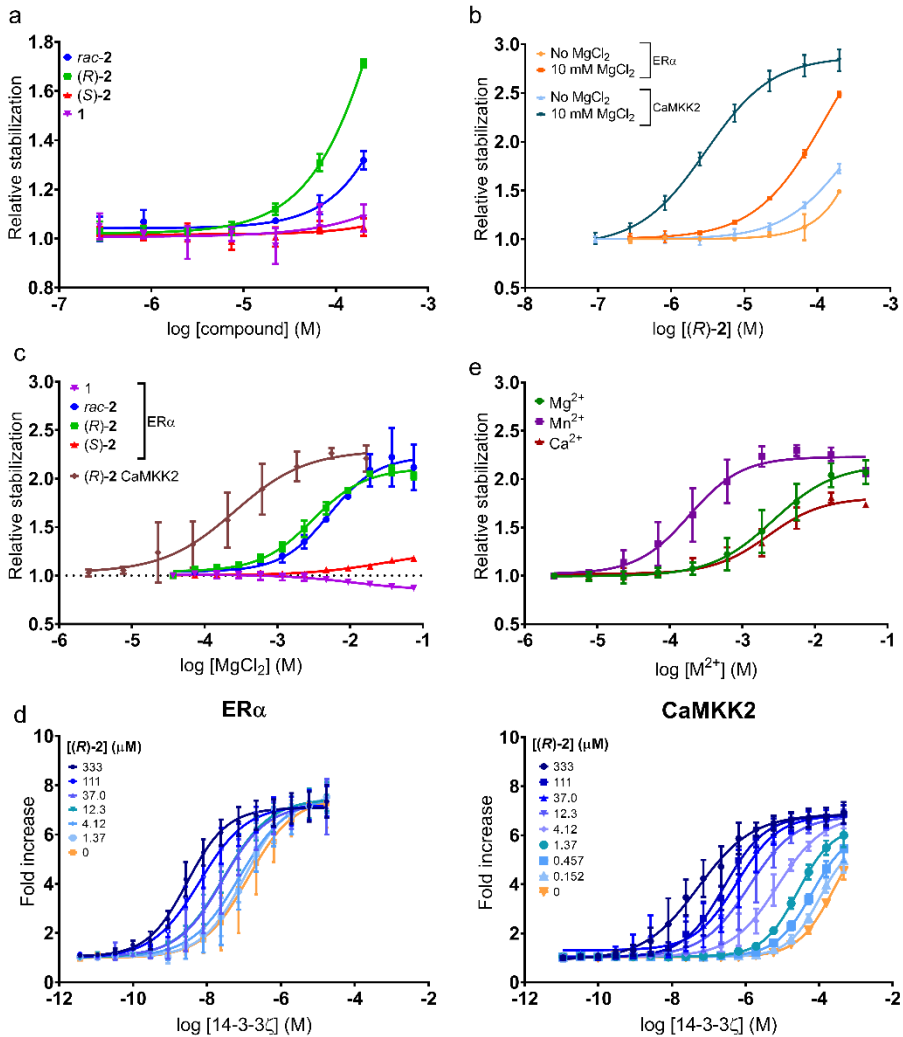


**Figure 3.3** | Metal ion-dependent stabilization of 14-3-3/ER $\alpha$ (pT<sup>594</sup>) and 14-3-3/CaMKK2(pS<sup>100</sup>) PPIs by (R)-2. (a) Stabilization of the 14-3-3/CaMKK2(pS<sup>100</sup>) PPI measured in FP assay. *Rac-2* (blue circles), (R)-2 (green squares) are stabilizers while (S)-2 (red triangles) and 1 (purple inverse triangles) are not. (b) The addition of 10 mM MgCl<sub>2</sub> increases the apparent potency of (R)-2 for 14-3-3/ER $\alpha$ (pT<sup>594</sup>) (light orange circles vs dark orange squares) and 14-3-3/CaMKK2(pS<sup>100</sup>) (light blue triangles vs dark blue inverse triangles) PPI stabilization. “Relative stabilization” (y-axis, panels a, b and c) is defined in Figure 1. (c) Mg<sup>2+</sup> increases PPI stabilization efficacy of 10  $\mu$ M *rac-2* (blue dots) and (R)-2 (green squares) whereas 1 and (S)-2 are unaffected (50 nM 14-3-3/10 nM FITC-3 or 30  $\mu$ M 14-3-3/10 nM FAM-4). “Relative stabilization” (y-axis) is mean fold-increase of signal at a given [Mg<sup>2+</sup>] over baseline (no added Mg<sup>2+</sup>). (d) Increase in apparent K<sub>d</sub> of 14-3-3/ER $\alpha$ (pT<sup>594</sup>) (10 nM FITC-3, left panel) or 14-3-3/CaMKK2(pS<sup>100</sup>) (10 nM FAM-4, right panel) PPIs by FP with increasing (R)-2 concentration, in the presence of 10 mM Mg<sup>2+</sup>. “Fold increase” (y-axis) is the mean fold-increase of signal over baseline (no (R)-2). (e) Ca<sup>2+</sup> (red triangles) and Mn<sup>2+</sup> (purple squares) also increase apparent efficacy of (R)-2 in 14-3-3/ER $\alpha$ (pT<sup>594</sup>) FP assay.

PPI stabilization efficacy of (*R*)-**2** (brown diamonds) was shown to be magnesium concentration-dependent. (*S*)-**2** is not a PPI stabilizer and hence was unaffected by  $Mg^{2+}$  concentration (red triangles). The 14-3-3/ $ER\alpha(pT^{594})$  PPI stabilization effect of **1** (purple inverse triangles) was also unaffected by varying  $Mg^{2+}$  concentration, indicating that the  $Mg^{2+}$  effect is ligand-specific and not due to effects on 14-3-3 protein or the phosphopeptide (see also Figure S3.16, S3.17).

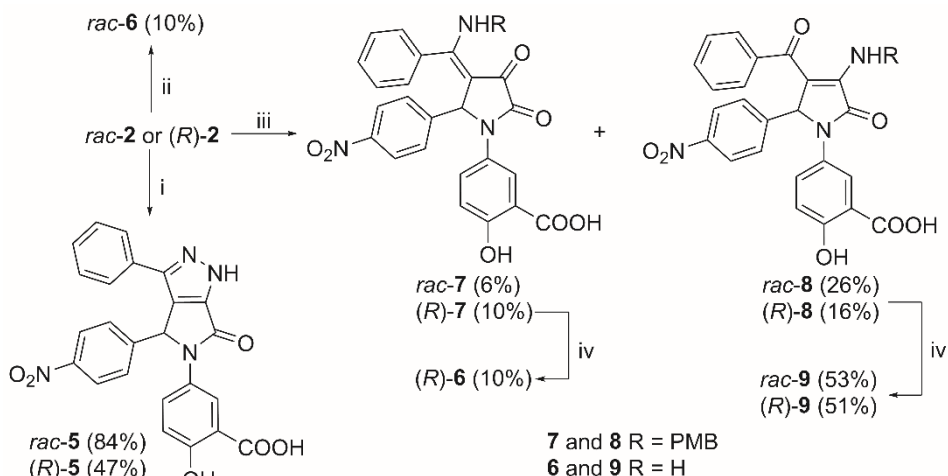
The addition of 10 mM  $MgCl_2$  afforded full concentration-response curves for (*R*)-**2**, allowing the determination of apparent  $EC_{50}$  values. In the 14-3-3/ $CaMKK2(pS^{100})$  FP assay, adding 10 mM  $MgCl_2$  led to an apparent  $EC_{50}$  of  $3.2 \pm 0.3 \mu M$  and 2.9-fold stabilization (Figure 3.3b). The PPI stabilizing potency and efficacy of the  $Mg^{2+}$  salt of (*R*)-**2** on the 14-3-3/ $CaMKK2(pS^{100})$  PPI is comparable to that of **1** on the 14-3-3/ $ER\alpha(pT^{594})$  PPI ( $EC_{50}$   $1.7 \pm 0.6 \mu M$ , 3.9-fold stabilization, Figure 3.1c). Taking the relative stabilization effect of (*R*)-**2** at 200  $\mu M$  in the absence of added  $Mg^{2+}$  as a baseline (1.5- and 1.7-fold for 14-3-3/ $ER\alpha(pT^{594})$  and 14-3-3/ $CaMKK2(pS^{100})$  PPIs respectively), the addition of 10 mM  $Mg^{2+}$  leads to 7-fold and 99-fold increases in apparent potency (Figure 3.3b). Exploiting the potentiating effect of  $Mg^{2+}$  on the PPI stabilization potency of (*R*)-**2**, we investigated the apparent affinity increase between 14-3-3 and phosphorylated binding partners induced by increasing concentrations of (*R*)-**2** in the 14-3-3/ $ER\alpha(pT^{594})$  and 14-3-3/ $CaMKK2(pS^{100})$  FP assays (Figure 3.3d). At the highest concentration of (*R*)-**2** tested (333  $\mu M$ ), the observed affinity of the 14-3-3/ $ER\alpha(pT^{594})$  PPI (left panel) was increased 57-fold and 3,700-fold for the 14-3-3/ $CaMKK2(pS^{100})$  PPI (right panel).

To assess whether this metal ion-assisted 14-3-3 PPI stabilization effect was specific to  $Mg^{2+}$ , we tested by FP the effect of adding increasing concentrations of  $MnCl_2$ ,  $CaCl_2$  and  $ZnCl_2$  to a fixed concentration of 14-3-3, FITC-**3** and (*R*)-**2** on the overall 14-3-3/ $ER\alpha(pT^{594})$  PPI stabilization efficacy (Figure 3.3e and S3.17). The potency of the assistance effect of  $Mg^{2+}$  and  $Ca^{2+}$  were comparable, while  $Mn^{2+}$  was approximately 15-fold more effective, with its maximum assistance effect achieved at less than 1 mM  $MnCl_2$ .<sup>[33]</sup> All three metals show similar overall stabilization efficacy in this setting, affording approximately 2-fold stabilization of the interaction. Addition of  $Zn^{2+}$  caused precipitation of phosphopeptide FITC-**3** precluding measurement of its effects.

### **Mimicry of the chelate by cyclization or intramolecular H-bonds affords metal independent 14-3-3 PPI stabilizers**

Based on the 14-3-3/ $ER\alpha(pT^{594})$ /*(R)*-**2** ternary complex crystal structure, the origin of the metal ion potentiation effect on the PPI stabilization potency of **2** was assumed to be due to solution phase stabilization of the crystallographically observed binding conformation of (*R*)-**2**. To test this hypothesis, we decided to mimic

the conformational restriction of the  $Mg^{2+}$  chelate of (*R*)-**2** by moieties that would not depend on the chelation of metal ions. Cyclisation of *rac*-**2** and its analogues to afford pyrazole derivatives such as **5** has previously been reported as a strategy to improve their 14-3-3 PPI stabilization activity.<sup>[34]</sup> However, this was based on a binding mode (Figure 2a, magenta sticks) determined from a low-resolution crystal structure that we have now shown to be erroneous. *Rac*-**5** was reported to be a better stabilizer of the 14-3-3/PMA2 complex than *rac*-**2**. A crystal structure of a similar bicyclic analogue of **5** in the 14-3-3/PMA2 complex was reported, however (*S*)-**2** (the inactive absolute configuration) was used to model **5** into the observed electron density, leading to difficulties in interpreting SAR due to incorrect stereochemistry and binding mode assumptions.



**Scheme 3.1** | Synthesis of conformationally-restricted analogues of **2**. i)  $H_2NNH_2$ , AcOH, 2 h, 120 °C. ii) aq.  $NH_3$ , AcOH, 2 h, 120 °C. iii)  $PMBNH_2$ , 2 h, 120 °C. iv) TFA, 30 min, 120 °C.

In addition, based on the 6-membered  $Mg^{2+}$ -containing chelate ring observed (Figure 3.2e), we reasoned that an intramolecular hydrogen bond contained in a 6-membered pseudo-ring, such as in the regioisomeric vinylogous amides **6** and **9**, would be a better chelate mimic than the 5-membered pyrazole ring. Reaction of *rac*-**2** with aqueous ammonia in acetic acid under microwave heating afforded only vinylogous amide *rac*-**6** in 20% yield, with no *rac*-**9** observed (Scheme 1). This contrasts with literature reports that 4-aryl substituents favor regioselective endocyclic nucleophilic attack by sterically unencumbered amines to afford the regioisomers corresponding to **9**.<sup>[35-40]</sup> Reaction of *rac*-**2** with *p*-methoxybenzylamine under microwave heating afforded *rac*-**7** (6%) and *rac*-**8** (26%). Removal of the PMB group of *rac*-**8** using TFA afforded *rac*-**9** in 53% yield. The single enantiomers (*R*)-**6** and (*R*)-**9** were prepared analogously to *rac*-**9**. Treatment of (*R*)-**2** with *p*-

methoxybenzylamine yielded the two regioisomeric PMB-protected vinylogous amides (*R*-7 (10%) and (*R*-8 (16%), which on deprotection with TFA afforded (*R*-6 and (*R*-9 in 10% and 51% yield, respectively. (*R*-5 was prepared in 47% yield from (*R*-2 by reaction with hydrazine.

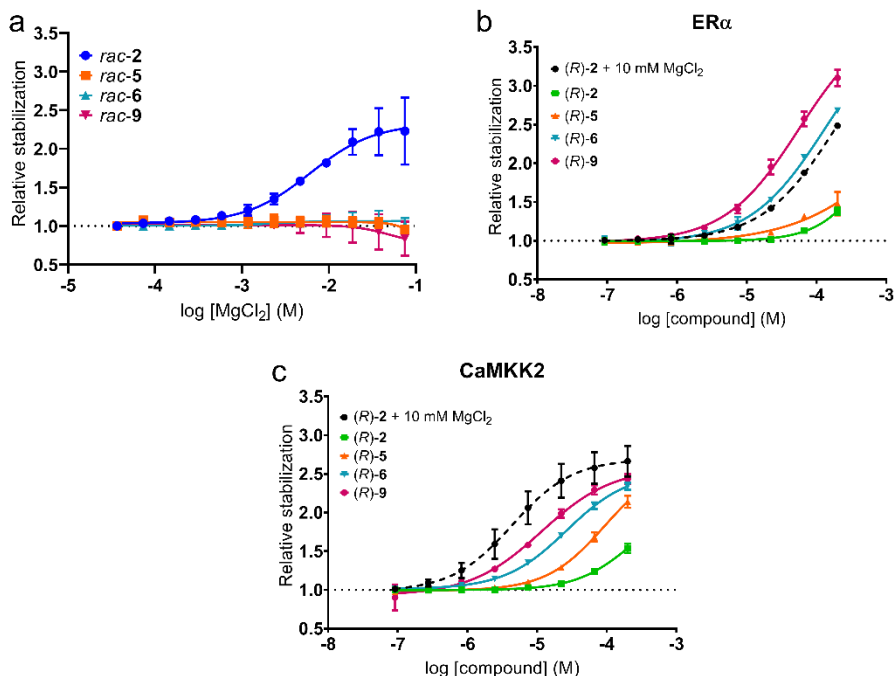


**Figure 3.4 |** Metal ion-independent 14-3-3 PPI stabilizers. (a, b) Stabilization of the 14-3-3/ER $\alpha$ (pT<sup>594</sup>) and 14-3-3/CaMKK2(pS<sup>100</sup>) PPIs by (*R*-6 and -9 as measured by FP. “Relative stabilization” (y-axes) is defined in Figure 1. (c) Mg<sup>2+</sup> concentration-response in 14-3-3/ER $\alpha$ (pT<sup>594</sup>) FP assay (50 nM 14-3-3 $\zeta$ /10 nM FITC-3 and 100  $\mu$ M *rac*-2, -5, -6 or -9), showing no effect of Mg<sup>2+</sup> on activity of *rac*-5, -6 or -9 (orange squares, pale blue triangles and inverted pink triangles respectively). “Relative stabilization” (y-axis) refers to mean fold increase of FP signal of a given [Mg<sup>2+</sup>] over signal observed in absence of added [Mg<sup>2+</sup>].

(*R*-5, (*R*-6 and (*R*-9 were then tested by FP and SPR for their 14-3-3/ER $\alpha$ (pT<sup>594</sup>) and 14-3-3/CaMKK2(pS<sup>100</sup>) PPI stabilization effect (Figure 3.4a,b and S3.19). Gratifyingly, (*R*-6 (inverted blue triangles) and (*R*-9 (pink circles) were more potent and efficacious stabilizers of both PPIs than (*R*-2 (without added Mg<sup>2+</sup>, green squares). Pyrazole (*R*-5 (orange triangles) was somewhat more potent and efficacious than (*R*-2 alone but was less active than either (*R*-6 or (*R*-9, suggesting that a 6-membered ring is preferable to a 5-membered ring. In the 14-3-3/CaMKK2(pS<sup>100</sup>) PPI, (*R*-2+10 mM Mg<sup>2+</sup> is still the most potent, suggesting that the ordered water molecules of the Mg<sup>2+</sup>-(*R*-2 chelate may contribute to binding affinity/PPI stabilization in this case. As expected, increasing concentrations of Mg<sup>2+</sup>

did not affect the 14-3-3/ER $\alpha$ (pT<sup>594</sup>) PPI stabilization efficacy of *rac*-**5**, **6** or **9** (Figure 3.4c, see Figure S3.18 for PPI stabilization data in absence of Mg<sup>2+</sup>) as they lack the chelation-competent vinylogous carboxylate moiety. The salicylate moiety of **2**, **5**, **6** and **9** can potentially chelate metals, but the fact that **5**, **6** or **9** did not show metal-dependent potency (Figure 3.4c) suggests that the salicylate moiety does not affect the potency of these compounds in our system. Therefore the effect of chelation by the salicylate moiety can be discounted for our purposes.

### Potency increase upon metal chelation is due to stabilization of bioactive conformation

In the 14-3-3/ER $\alpha$ (pT<sup>594</sup>)-bound conformation of **2** (Figure 3.2b), the O<sup>-</sup> and carbonyl oxygen of the vinylogous carboxylate moiety are in a *syn* relationship (*syn*-(*R*)-**2**, Figure 3.5a). In solution, and in the absence of chelatable metal ions, repulsive electrostatic allylic strain was expected to disfavor this conformation relative to the *anti* conformation (*anti*-(*R*)-**2**, Figure 3.5a). Comparing the DFT calculated gas phase free energies of *syn*- and *anti*-(*R*)-**2** (see Supporting Information) shows the protein-bound and chelation-stabilized *syn*-(*R*)-**2** conformation to be significantly higher energy. Accounting for solvation effects by using two different implicit solvation models for water reduced the energy difference between *syn*- and *anti*-(*R*)-**2** (Table 1).

**Table 3.1** | Calculated relative energies for *syn* and *anti*-conformations of (*R*)-**2**, -**6** and -**9**.

Cpd	Conformation of exocyclic carbonyl <sup>a</sup>	Free energies in water	
		B3LYP-D3 PBF <sup>b</sup>	M06-2X-D3 SM6 <sup>c</sup>
( <i>R</i> )- <b>2</b>	<i>syn</i>	0	2.2
( <i>R</i> )- <b>2</b>	<i>anti</i>	0.4	0
( <i>R</i> )- <b>6</b>	<i>syn</i>	0.0	0.0
( <i>R</i> )- <b>6</b>	<i>anti</i>	5.9	7.5
( <i>R</i> )- <b>9</b>	<i>syn</i>	0.0	0.0
( <i>R</i> )- <b>9</b>	<i>anti</i>	2.9	2.6

[a] The conformation of the salicylate was selected according to the crystal structure of (*R*)-**2** (Figure 5).

[b] PBF = Poisson Boltzmann Finite element method; a solvation model. [c] SM6 = Solvation Model 6

Both confirm that the *syn*-(*R*)-**2** conformation is not favored in water. Therefore, the *anti*-(*R*)-**2** conformation is predicted to be present in significant amounts in the solution phase in the absence of Mg<sup>2+</sup> or other metals. For the vinylogous amides (*R*)-**6** and (*R*)-**9**, both solvation models favor the corresponding *syn*- conformations (i.e. corresponding to the protein bound conformation of **2**) as the lowest energy

solution conformation, as expected and as borne out by their increased, metal ion-independent 14-3-3 PPI stabilization compared to (*R*)-**2**.

To confirm the calculations, 1D ROE difference NMR experiments were performed on *rac*-**2**, *rac*-**6** and *rac*-**9** (Figures S3.20-S3.22) to determine their preferred solution conformations. Irradiation of protons of either the benzoyl or nitrophenyl rings of *rac*-**2** showed only a small resonance transfer between these rings, suggesting that they prefer not to be in close spatial proximity and corresponding to the *anti* conformation (Figure 3.5a). On the other hand, strong resonance transfer was observed between the protons of the benzoyl and nitrophenyl rings for both *rac*-**6** and *rac*-**9**, indicating close spatial proximity suggestive of the *syn* conformation induced by intramolecular hydrogen bonding. Precipitation precluded determination by NMR of the conformational effects of Mg<sup>2+</sup> on *rac*-**2**, but these may be inferred from the X-ray crystal structure (Figure 3.5b)

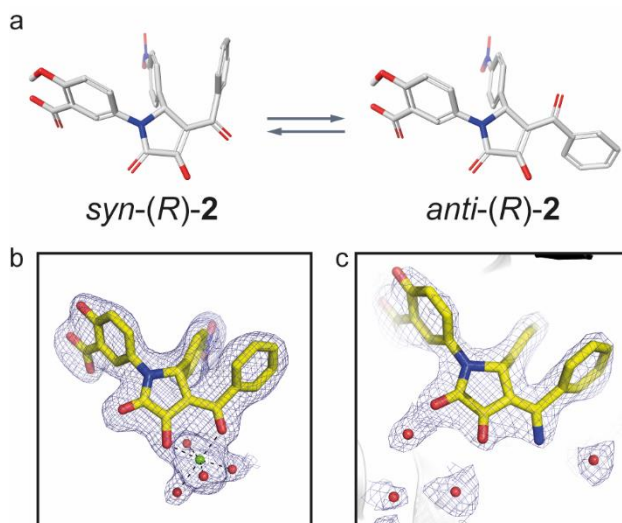


**Figure 3.5** | Conformational analysis of **2** and binding mode of (*R*)-**6** in 14-3-3/ER $\alpha$ (pT<sup>594</sup>) complex. (a) Comparison of *syn* and *anti* conformations of the vinylogous carboxylate moiety of (*R*)-**2**. Calculated free energies of (*R*)-**2** conformations show that protein-bound conformation *syn*-(*R*)-**2** is not favored in solution. (b) and (c) Binding modes and 2F<sub>obs</sub>-F<sub>cal</sub> electron density (contoured at 1  $\sigma$ ) of the magnesium complex of (*R*)-**2** (panel b, PDB 6TJM) and (*R*)-**6** (panel c, PDB 6TL3), shown in the same orientation of the 14-3-3/ER $\alpha$ (pT<sup>594</sup>) complex, indicating absence of chelated metal ion in (*R*)-**6** structure and intramolecular hydrogen bond-stabilized conformation of (*R*)-**6** that mimics *syn*-(*R*)-**2** conformation

*Rac*-**6** was then selected for crystallization studies in the 14-3-3/ER $\alpha$ (pT<sup>594</sup>) complex. A 2.45 Å resolution X-ray crystal structure of the ternary 14-3-3 $\sigma$  $\Delta$ C/**3**/*(R)*-**6** complex was obtained (Figure 3.5c), confirming the absolute configuration of the active enantiomer as (*R*) and a binding mode analogous to (*R*)-**2**. No additional



## CHAPTER 3

ligand-associated electron density attributable to a chelated metal ion was observed, indicating that the intramolecular hydrogen bond successfully stabilizes the *syn* conformation as demonstrated computationally.

### 3.3 DISCUSSION

Ligand conformational restriction is a widely used strategy to increase potency, and minimizes the entropic loss observed on ligand binding if the preferred solution and bound conformations differ.<sup>[41-43]</sup> This is typically achieved by cyclisation, introducing intramolecular hydrogen-bonding or by exploiting steric/stereoelectronic effects. Ligand chelation by solution phase metal ions can now be added to this list of strategies. However, given the lack of control over metal ion concentration in medically-relevant settings (e.g. intracellularly) and the requirement that the binding site accommodate a metal ion and associated ordered water molecules, it may prove to be difficult to easily and reliably exploit this effect in drug substances.

On the other hand, metal contamination has been reported to be a cause of false positives due to assay interference<sup>[44]</sup> or by ligands complexing to bioactive metal centers.<sup>[45]</sup> To our knowledge, no incidences of such ligand-specific conformational effects due to metal ions have been reported. Given that many assays require the presence of metal ions (such as  $\text{Ca}^{2+}$ ,  $\text{Mg}^{2+}$  or  $\text{Zn}^{2+}$ ) and high intracellular concentrations of some of these metals, such conformational effects should be considered as a potential cause of difficult to interpret assay data for chelation competent ligands. In principle, such behavior could lead to false negatives in screening campaigns and should be considered when analyzing screening data, especially in the case of conflicting results from samples that may have been subjected to more or less rigorous purification procedures which could result in different metal ion content. This effect could also be at play if unexpected discrepancies are observed between potencies in biochemical and cellular assays, where there may be differences in metal ion concentration. It has been proposed that chelating moieties should be used in substructure alerts to filter out compounds with potential to cause assay interference and frequent hitters.<sup>[22]</sup> However, the application of such filters needs to be considered on a case by case basis, with the assay technology and particular target in question taken into account. As we have shown, in some cases metal chelation can act as a ligand conformational probe and provide valuable hints as to the optimizability of low potency hits.

### 3.4 CONCLUSION

We have shown that by leveraging the serendipitously discovered  $\text{Mg}^{2+}$ -chelate and resulting chelation-controlled stabilization of bioactive ligand conformation, (*R*)-**2** can be optimized to afford stabilizers of canonical 14-3-3 PPIs with potency rivaling

## CHAPTER 3

natural product **1**. We also show that this metal-assisted PPI stabilization effect is due to solution phase stabilization of the bioactive conformation of **2** and can be mimicked by an intramolecular H-bond to afford metal-independent PPI stabilizers such as (*R*)-**6** and (*R*)-**9**. Compared to **1**, these compounds have the advantage of higher synthetic tractability and stabilize a 14-3-3 PPI that is refractive to stabilization by **1** and they should be useful tool compounds for the study of 14-3-3 PPI stabilization. This work gives new insights into the SAR of small molecule, non-natural product-derived 14-3-3 PPI stabilization and provides opportunities for structure-based drug design to identify new, small molecule 14-3-3 PPI stabilizers. More broadly, this work indicates that ligand-specific conformational effects due to metal ion chelation should be considered during the interpretation of assay and screening data, especially for chelation-competent ligands.

### Author Contribution

G.O'M., F.B. and C.O. conceived the idea. G.O'M. and F.B. designed experiments and analyzed data. F.B. performed chemical synthesis, FP and SPR and conformational analysis by NMR. S.A. performed crystallography. A.G. performed SPR experiments. J.F.N. and I.L. performed and analyzed NMR experiments on 14-3-3 complexes. P.B. performed computational analysis of conformational energies. F.B. and G.O'M. wrote the manuscript. All authors have contributed to manuscript editing and have given approval to the final version of the manuscript.

## 3.5 EXPERIMENTAL SECTION

## 3.5.1 Chemistry section

*General Information*

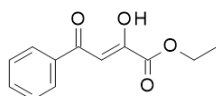
All solvents and reagents were obtained from commercially available sources and used without further purification. The microwave syntheses were performed in a Biotage Initiator with an external surface IR probe. Flash column chromatography was carried out on prepacked silica gel columns supplied by Biotage and using Biotage automated flash systems with UV detection.

UHPLC-MS experiments were performed using a Waters Acquity UHPLC system combined with a SQD mass spectrometer. The UHPLC system was equipped with both a BEH C18 column 1.7  $\mu\text{m}$  2.1 $\times$ 50 mm in combination with a 46 mM  $(\text{NH}_4)_2\text{CO}_3/\text{NH}_3$  buffer at pH 10 and a HSS C18 column 1.8  $\mu\text{m}$  2.1 $\times$ 50 mm in combination with 10 mM formic acid or 1 mM ammonium formate buffer at pH 3. The mass spectrometer used ESI+/- as ion source. UPLC was also carried out using a Waters UPLC fitted with Waters QDa mass spectrometer (Column temp 40 $^\circ\text{C}$ , UV = 190–400 nm, MS = ESI with pos/neg switching) equipped with a Waters Acquity BEH 1.7  $\mu\text{m}$  2.1 $\times$ 100 mm in combination with either 0.1% formic acid in water, 0.05% TFA in water or 0.04%  $\text{NH}_3$  in water. The flow rate was 1 mL/min.

Preparative HPLC was performed by Waters Fraction Lynx with ZQ MS detector on either a Waters Xbridge C18 OBD 5  $\mu\text{m}$  column (19 $\times$ 150 mm, flow rate 30 mL/min or 30 $\times$ 150 mm, flow rate 60 mL/min) using a gradient of 5–95% MeCN with 0.2%  $\text{NH}_3$  at pH 10 or a Waters SunFire C18 OBD 5  $\mu\text{m}$  column (19 $\times$ 150 mm, flow rate 30 mL/min or 30 $\times$ 150 mm, flow rate 60 mL/min) using a gradient of 5–95% MeCN with 0.1 M formic acid or on a Gilson Preparative HPLC with a UV/VIS detector 155 on a Kromasil C8 10  $\mu\text{m}$  column (20  $\times$  250 mm, flow rate 19 mL/min, or 50  $\times$  250 mm, flow rate 100 mL/min) using a varying gradient of ACN with 0.1% formic acid (FA) in water or 0.2% trifluoroacetic acid (TFA) in water or 0.2% acetic acid (AcOH) in water or 0.2% ammonia ( $\text{NH}_3$ ) in water. Molecular mass (HR-ESI-MS) was recorded using a Shimadzu LCMS-2020 instrument (ESI+). Purity of all test compounds was determined by LCMS. All screening compounds had a purity >95%.

General  $^1\text{H}$  NMR spectra were recorded on a Bruker Avance II, III, AV300, AV400 or AVIII500 spectrometer at a proton frequency of 400, 500 or 600 MHz at 25  $^\circ\text{C}$  or at a temperature and frequency stated in each experiment.  $^{13}\text{C}$  NMR spectra were recorded at 101 MHz or 126 MHz.

The chemical shifts ( $\delta$ ) are reported in parts per million (ppm) with residual solvent signal used as a reference ( $\text{CD}_2\text{Cl}_2$  at 5.32 ppm for  $^1\text{H}$  NMR and 53.84 ppm for  $^{13}\text{C}$  NMR,  $(\text{CD}_3)_2\text{SO}$  at 2.50 ppm for  $^1\text{H}$  NMR and 39.52 ppm for  $^{13}\text{C}$  NMR,  $\text{CDCl}_3$  at 7.26 ppm for  $^1\text{H}$  NMR and 77.16 ppm for  $^{13}\text{C}$  NMR). Coupling constants (J) are reported as Hz. NMR abbreviations are used as follows: br = broad, s = singlet, d = doublet, t = triplet, q = quartet, m = multiplet. Protons on heteroatoms such as  $\text{COOH}$  protons are only reported when detected in NMR and can therefore be missing.

*Synthetic procedures and compound characterization***Ethyl 2,4-dioxo-4-phenylbutanoate.**

In a 250 mL round-bottomed flask, acetophenone (2.9 mL, 25.0 mmol) was dissolved in THF (100 mL) and the resulting solution cooled to 0  $^\circ\text{C}$ . Sodium ethanolate (14 mL, 37.5 mmol) was then

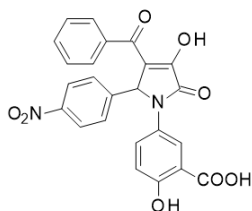
## CHAPTER 3

added dropwise and the reaction allowed to stir for 15 min at 0 °C. Diethyl oxalate (3.7 mL, 27.5 mmol) was finally added dropwise, the cooling bath removed, and the reaction allowed to stir overnight at rt.

The reaction was quenched with 1M HCl (50 mL). The resulting suspension was poured into a separatory funnel and the crude product was extracted with DCM (3x). The combined organic layers were dried using a phase separator and solvent was removed under reduced pressure.

The crude product was purified by preparative HPLC (40-80% ACN in H<sub>2</sub>O/ACN/AcOH 95/5/0.2 buffer over 20 minutes). Collected fractions were freeze-dried, to give ethyl 2,4-dioxo-4-phenylbutanoate (4.25 g, 77%) as a yellow solid.

<sup>1</sup>H NMR (400 MHz, CDCl<sub>3</sub>) δ 7.99 (d, J = 7.4 Hz, 2H), 7.60 (t, J = 7.4 Hz, 1H), 7.50 (t, J = 7.6 Hz, 2H), 7.07 (s, 1H), 4.39 (q, J = 7.1 Hz, 2H), 1.41 (t, J = 7.1 Hz, 3H). <sup>13</sup>C NMR (101 MHz, CDCl<sub>3</sub>) δ 190.82, 169.89, 162.29, 135.00, 133.89, 129.00, 127.99, 98.05, 62.72, 14.21. Matches with a previously reported characterization.<sup>[34]</sup>

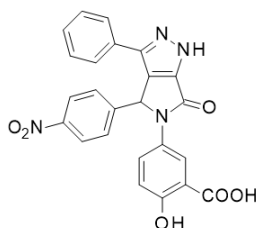


### 5-[3-Benzoyl-4-hydroxy-2-(4-nitrophenyl)-5-oxo-2H-pyrrol-1-yl]-2-hydroxybenzoic acid (**2**).

In a 20 mL vial, to a solution of ethyl 2,4-dioxo-4-phenylbutanoate (603 mg, 2.74 mmol) in AcOH (7 mL), 4-nitrobenzaldehyde (422 mg, 2.74 mmol) and 5-amino-2-hydroxybenzoic acid (441 mg, 2.74 mmol) were added. The vial was capped and heated at 120 °C for 180 min in a single node microwave reactor. The pressure monitored was 1 bar.

The mixture was diluted with diethyl ether and filtered. The filtered solid was washed with diethyl ether and dried under reduced pressure to give compound **2** (543 mg, 43%) as a pale yellow solid.

<sup>1</sup>H NMR (400 MHz, DMSO) δ 7.97 – 8.18 (m, 3H), 7.66 – 7.77 (m, 5H), 7.52 – 7.61 (m, 1H), 7.45 (t, J = 7.6 Hz, 2H), 6.91 (d, J = 8.9 Hz, 1H), 6.46 (s, 1H). <sup>13</sup>C NMR (101 MHz, DMSO) δ 189.01, 171.17, 164.47, 158.76, 151.04, 147.20, 144.40, 137.87, 132.70, 130.55, 129.26, 128.71, 128.17, 127.49, 124.91, 123.51, 119.08, 117.57, 113.01, 60.83. HRMS (ESI) *m/z* [M + H]<sup>+</sup> calcd for C<sub>24</sub>H<sub>16</sub>N<sub>2</sub>O<sub>8</sub>: 461.0985, found: 461.0974. Matches with a previously reported characterization.<sup>[34]</sup>

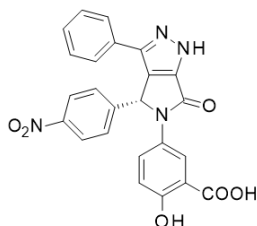


### 2-Hydroxy-5-[4-(4-nitrophenyl)-6-oxo-3-phenyl-1,4-dihydropyrrolo[3,4-c]pyrazol-5-yl]benzoic acid (**5**).

In 20 mL vial, compound **2** (98 mg, 0.21 mmol) was suspended in AcOH (6 mL). Hydrazine (35% in water) (0.025 mL, 0.28 mmol) was added, while stirring at room temperature. The vial was capped and heated at 120 °C for 120 min in a single node microwave reactor. The pressure monitored was

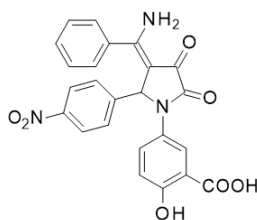
1 bar. After solvent removal, the crude mixture was dissolved in EtOAc and washed with HCl aq 1M (3x). The organic layer was dried using a phase separator and concentrated under reduced pressure. The residue was purified by preparative HPLC (15-35% acetonitrile in H<sub>2</sub>O/ACN/NH<sub>3</sub> 95/5/0.2 buffer over 20 minutes), to give compound **5** (82 mg, 84.0%) as an off-white solid.

<sup>1</sup>H NMR (500 MHz, DMSO) δ 8.07 (d, *J* = 8.7 Hz, 2H), 7.97 (d, *J* = 2.6 Hz, 1H), 7.61 – 7.71 (m, 3H), 7.59 (d, *J* = 7.5 Hz, 2H), 7.37 (t, *J* = 7.5 Hz, 2H), 7.29 (t, *J* = 7.3 Hz, 1H), 7.02 (s, 1H), 6.93 (d, *J* = 8.9 Hz, 1H). <sup>13</sup>C NMR (126 MHz, DMSO) δ 171.30, 161.19, 159.21, 150.07, 147.35, 144.55, 136.83, 130.95, 129.28, 129.04, 128.78, 128.04, 127.54, 125.93, 124.87, 123.92, 117.19, 114.57, 59.33. HRMS (ESI) *m/z* [M + H]<sup>+</sup> calcd for C<sub>24</sub>H<sub>16</sub>N<sub>4</sub>O<sub>6</sub>: 457.1148, found: 457.1147. Matches with a previously reported characterization.<sup>[34]</sup>



**(*R*)-2-Hydroxy-5-[4-(4-nitrophenyl)-6-oxo-3-phenyl-1,4-dihydropyrrolo[3,4-c]pyrazol-5-yl]benzoic acid ((*R*)-5).**

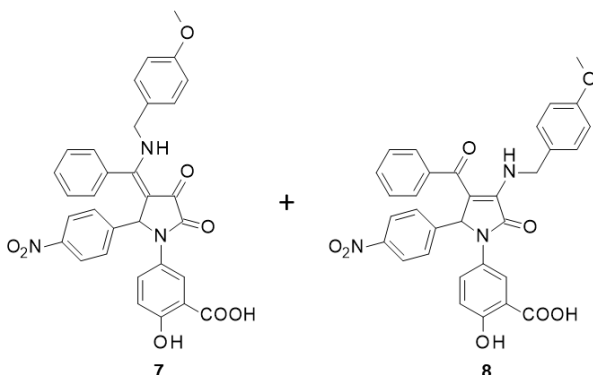
In 5 mL vial, compound (***R***-2) (110 mg, 0.24 mmol) was suspended in AcOH (3 mL). Hydrazine (35% in water) (0.028 mL, 0.31 mmol) was added, while stirring at room temperature. The vial was capped and heated at 120 °C for 120 min in a single node microwave reactor. The pressure monitored was 1 bar. After solvent removal, the residue was purified by preparative HPLC (25-65% acetonitrile in H<sub>2</sub>O/ACN/FA 95/5/0.2 buffer over 20 minutes), to give compound (*R*)-5 (51 mg, 46.8 %) as an off-white solid. <sup>1</sup>H NMR (500 MHz, DMSO) δ 8.02 – 8.11 (m, 2H), 7.94 (d, *J* = 2.7 Hz, 1H), 7.6 – 7.69 (m, 3H), 7.58 (d, *J* = 7.4 Hz, 2H), 7.39 (br, 2H), 7.25 – 7.35 (br, 1H), 7.02 (s, 1H), 6.92 (d, *J* = 8.9 Hz, 1H). <sup>13</sup>C NMR (126 MHz, DMSO) δ 171.31, 161.13, 158.70, 149.91, 147.34, 144.46, 136.75, 131.55, 129.24, 129.07, 128.83, 128.58, 127.46, 125.89, 125.71, 124.80, 123.91, 117.47, 113.08, 59.16. HRMS (ESI) *m/z* [M + H]<sup>+</sup> calcd for C<sub>24</sub>H<sub>16</sub>N<sub>4</sub>O<sub>6</sub>: 457.1148, found: 457.1158. [α]<sub>D</sub><sup>20</sup>: +20.0 (c 0.125, MeOH).



**5-[3-[Amino(phenyl)methylene]-2-(4-nitrophenyl)-4,5-dioxo-pyrrolidin-1-yl]-2-hydroxybenzoic acid (6).**

In a 5 mL vial, to a suspension of **2** (100 mg, 0.22 mmol) in AcOH (3 mL), ammonium hydroxide (0.328 mL, 2.17 mmol) was added. The vial was capped and heated at 120 °C for 120 min in a single node microwave reactor. The pressure monitored was 1 bar. After solvent removal, the residue was purified by preparative HPLC (10-50% acetonitrile in H<sub>2</sub>O/ACN/FA 95/5/0.2 buffer over 20 minutes), to give compound **6** (20 mg, 20.0 %) as a yellow solid.

$^1\text{H}$  NMR (500 MHz, DMSO)  $\delta$  10.18 (d,  $J$  = 3.3 Hz, 1H, H36), 9.02 (d,  $J$  = 3.3 Hz, 1H, H35), 7.93 (d,  $J$  = 2.7 Hz, 1H, H10), 7.72 (d,  $J$  = 8.7 Hz, 2H, H18 and H20), 7.60 (dd,  $J$  = 9.0, 2.7 Hz, 1H, H6), 7.41 – 7.49 (m, 1H, H31), 7.3 – 7.39 (m, 4H, H29, H30, H32 and H33), 6.92 (d,  $J$  = 8.5 Hz, 2H, H17 and H21), 6.85 (d,  $J$  = 9.0 Hz, 1H, H7), 6.36 (s, 1H, H15).  $^{13}\text{C}$  NMR (151 MHz, DMSO)  $\delta$  178.00, 171.13, 164.05, 163.17, 158.93, 146.64, 146.27, 133.49, 130.86, 130.52, 128.56, 128.44, 127.85, 127.63, 125.25, 122.77, 117.31, 113.11, 105.53, 58.89. HRMS (ESI)  $m/z$  [ $M + \text{H}$ ] $^+$  calcd for  $\text{C}_{24}\text{H}_{17}\text{N}_3\text{O}_7$ : 460.1145, found: 460.1147.

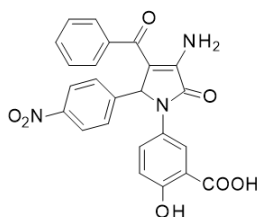


**2-Hydroxy-5-[3-[[4-(4-methoxyphenyl)methylamino]-phenyl-methylene]-2-(4-nitrophenyl)-4,5-dioxo-pyrrolidin-1-yl]benzoic acid (7) and 5-[3-benzoyl-4-[[4-(4-methoxyphenyl)methylamino]-2-(4-nitrophenyl)-5-oxo-2H-pyrrol-1-yl]-2-hydroxy-benzoic acid (8)**

In a 20 mL vial, to compound **2** (536 mg, 1.16 mmol) in AcOH (5 mL), (4-methoxyphenyl)methanamine (1.1 mL, 8.15 mmol) was added. The vial was capped and heated at 120 °C for 120 min in a single node microwave reactor. The pressure monitored was 1 bar. After solvent removal, the residue was purified by preparative HPLC (45-85% acetonitrile in  $\text{H}_2\text{O}/\text{ACN}/\text{TFA}$  95/5/0.2 buffer over 20 minutes), to afford compound **7** (40 mg, 5.9%) and compound **8** (174 mg, 25.8%), both as yellow solids.

**7:**  $^1\text{H}$  NMR (500 MHz, DMSO)  $\delta$  11.33 (t,  $J$  = 6.2 Hz, 1H), 7.88 (d,  $J$  = 2.7 Hz, 1H), 7.73 (d,  $J$  = 8.7 Hz, 2H), 7.62 (br, 2H), 7.55 (dd,  $J$  = 9.0, 2.7 Hz, 1H), 7.45 (t,  $J$  = 7.5 Hz, 1H), 7.07 (d,  $J$  = 8.6 Hz, 3H), 6.89 (d,  $J$  = 8.6 Hz, 2H), 6.75 – 6.85 (m, 3H), 6.51 (br, 1H), 6.05 (s, 1H), 4.31 (dd,  $J$  = 15.0, 5.3 Hz, 1H), 4.19 (dd,  $J$  = 14.9, 7.2 Hz, 1H), 3.73 (s, 3H).  $^{13}\text{C}$  NMR (126 MHz, DMSO)  $\delta$  177.19, 171.19, 164.30, 163.32, 158.85, 158.80, 146.47, 146.33, 130.99, 130.14, 129.07, 128.79, 128.38, 128.10, 127.92, 126.97, 125.23, 122.93, 117.41, 114.12, 112.83, 106.90, 104.55, 59.09, 55.12, 47.10. HRMS (ESI)  $m/z$  [ $M + \text{H}$ ] $^+$  calcd for  $\text{C}_{32}\text{H}_{25}\text{N}_3\text{O}_8$ : 580.1720, found: 580.1722.

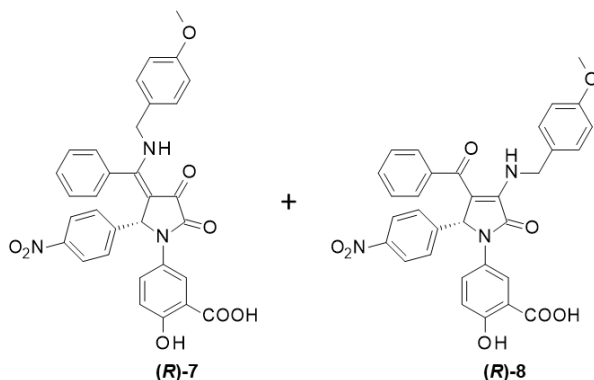
**8:**  $^1\text{H}$  NMR (600 MHz, DMSO)  $\delta$  8.96 (br, 1H), 7.93 (d,  $J$  = 2.7 Hz, 1H), 7.80 (d,  $J$  = 8.7 Hz, 2H), 7.58 (dd,  $J$  = 9.0, 2.7 Hz, 1H), 7.37 – 7.45 (m, 3H), 7.32 (t,  $J$  = 7.6 Hz, 2H), 7.25 (br, 2H), 7.07 (d,  $J$  = 8.7 Hz, 2H), 6.90 (d,  $J$  = 8.4 Hz, 2H), 6.85 (d,  $J$  = 8.9 Hz, 1H), 6.47 (s, 1H), 4.55-5.19 (br d, 2H), 3.73 (s, 3H).  $^{13}\text{C}$  NMR (126 MHz, DMSO)  $\delta$  190.23, 171.08, 163.78, 159.12, 158.48, 146.59, 145.24, 140.16, 131.23, 130.82, 129.02, 128.94, 128.16, 127.13, 126.98, 125.85, 123.00, 117.35, 113.90, 113.39, 111.37, 62.05, 55.07, 45.10. HRMS (ESI)  $m/z$  [ $M - \text{H}$ ] $^-$  calcd for  $\text{C}_{32}\text{H}_{25}\text{N}_3\text{O}_8$ : 578.1564, found: 578.1559.



**5-[4-Amino-3-benzoyl-2-(4-nitrophenyl)-5-oxo-2H-pyrrol-1-yl]-2-hydroxybenzoic acid (9).**

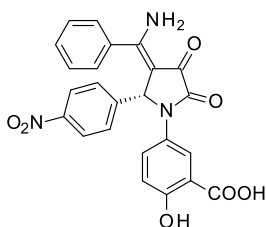
In a 5 mL vial, compound **8** (50 mg, 0.09 mmol) was dissolved in trifluoroacetic acid (1 mL, 0.09 mmol). The vial was capped and heated at 120 °C for 30 min in a single node microwave reactor. The pressure monitored was 3 bar. After solvent removal, the residue was purified by automated flash chromatography on a Biotage® KP-SIL 10 g column (40-100% heptane in EtOAc + 2% FA over 18CV), to give compound **9** (21 mg, 53.0%) as a pale yellow solid.

<sup>1</sup>H NMR (500 MHz, DMSO) δ 11.15 (br, 1H, H32), 7.98 (d, J = 2.5 Hz, 1H, H26), 7.80 (d, J = 8.4 Hz, 2H, H18 and H20), 7.76 (br, 2H, H34), 7.65 (dd, J = 8.9, 2.5 Hz, 1H, H22), 7.48 (d, J = 7.7 Hz, 2H, H12 and H16), 7.43 (t, J = 7.1 Hz, 1H, H14), 7.34 (t, J = 7.5 Hz, 2H, H13 and H15), 7.13 (d, J = 8.5 Hz, 2H, H17 and H21), 6.89 (d, J = 8.9 Hz, 1H, H23), 6.58 (s, 1H, H2). <sup>13</sup>C NMR (126 MHz, DMSO) δ 190.40, 171.19, 163.75, 158.92, 148.27, 146.61, 145.29, 140.12, 131.26, 130.73, 128.99, 128.23, 127.31, 126.88, 125.48, 123.05, 117.54, 112.96, 110.22, 62.13. HRMS (ESI) *m/z* [M + H]<sup>+</sup> calcd for C<sub>24</sub>H<sub>17</sub>N<sub>3</sub>O<sub>7</sub>: 460.1145, found: 460.1137.



**(R)-2-Hydroxy-5-[3-[[4-methoxyphenyl)methylamino]-phenyl-methylene]-2-(4-nitrophenyl)-4,5-dioxo-pyrrolidin-1-yl]benzoic acid ((R)-7) and (R)-5-[3-benzoyl-4-[[4-methoxyphenyl)methylamino]-2-(4-nitrophenyl)-5-oxo-2H-pyrrol-1-yl]-2-hydroxybenzoic acid ((R)-8).**

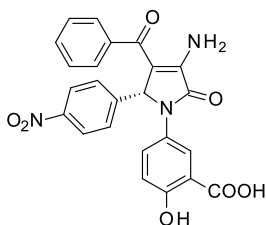
In a 20 mL vial, to compound (R)-2 (78 mg, 0.17 mmol) in AcOH (2 mL), (4-methoxyphenyl)methanamine (0.16 mL, 1.19 mmol) was added. The vial was capped and heated at 120 °C for 120 min in a single node microwave reactor. The pressure monitored was 1 bar. After solvent removal, the residue was purified by preparative HPLC (45-85% acetonitrile in H<sub>2</sub>O/ACN/TFA 95/5/0.2 buffer over 30 minutes). Collected fractions were freeze-dried, to give compounds (R)-7 (10 mg, 10.2%) and (R)-8 (16 mg, 16.3%), both as yellow solids. (R)-7: *m/z* (ESI-MS): [M+H]<sup>+</sup> calculated mass = 580.2, observed = 580.4. (R)-8: *m/z* (ESI-MS): [M+H]<sup>+</sup> calculated mass = 578.2, observed = 578.3 Compounds were not further characterized but used directly for the next step.



**(R)-5-[3-[Amino(phenyl)methylene]-2-(4-nitrophenyl)-4,5-dioxo-pyrrolidin-1-yl]-2-hydroxy-benzoic acid ((R)-6).**

In a 5 mL vial, compound (*R*)-7 (10 mg, 0.02 mmol) was dissolved in trifluoroacetic acid (1 mL, 0.09 mmol). The vial was capped and heated at 120 °C for 30 min in a single node microwave reactor. The pressure monitored was 2 bar. After solvent removal, the residue was purified by preparative HPLC (25-50% acetonitrile in H<sub>2</sub>O/ACN/TFA 95/5/0.2 buffer over 20 minutes). Collected fractions were freeze-dried, to afford compound (*R*)-6 (3.2 mg, 40.5%, 91.8% ee) as a pale yellow solid.

<sup>1</sup>H NMR (600 MHz, DMSO) δ 11.11 (br, 1H), 10.18 (br, 1H), 8.99 (br, 1H), 7.93 (d, J = 2.7 Hz, 1H), 7.72 (d, J = 8.4 Hz, 2H), 7.61 (dd, J = 9.0, 2.7 Hz, 1H), 7.42 – 7.48 (m, 1H), 7.3 – 7.39 (m, 4H), 6.93 (br, J = 5.9 Hz, 2H), 6.86 (d, J = 9.0 Hz, 1H), 6.35 (s, 1H). <sup>13</sup>C NMR (151 MHz, DMSO) δ 177.92, 171.14, 164.01, 163.18, 158.82, 146.61, 146.28, 133.48, 130.98, 130.52, 128.56, 128.42, 127.95, 127.65, 125.22, 122.78, 117.36, 112.82, 105.49, 58.85. HRMS (ESI) *m/z* [M + H]<sup>+</sup> calcd for C<sub>24</sub>H<sub>17</sub>N<sub>3</sub>O<sub>7</sub>: 460.1145, found: 460.1156.

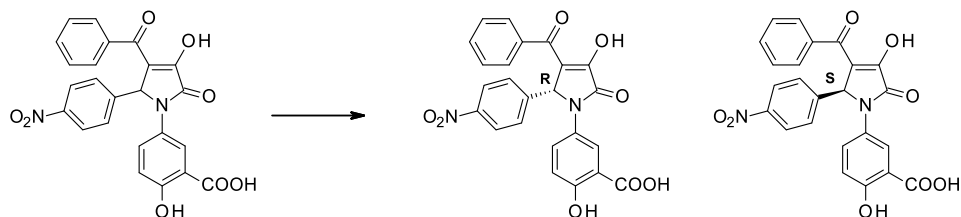


**(R)-5-[4-Amino-3-benzoyl-2-(4-nitrophenyl)-5-oxo-2H-pyrrol-1-yl]-2-hydroxy-benzoic acid ((R)-9).**

In a 5 mL vial, compound (*R*)-8 (16 mg, 0.03 mmol) was dissolved in trifluoroacetic acid (1 mL, 0.09 mmol). The vial was capped and heated at 120 °C for 30 min in a single node microwave reactor. The pressure monitored was 2 bar. After solvent removal, the residue was purified by preparative HPLC (35-65% acetonitrile in H<sub>2</sub>O/ACN/TFA 95/5/0.2 buffer over 20 minutes). Collected fractions were freeze-dried, to afford compound (*R*)-9 (6.4 mg, 50.5%, 89.8% ee) as a pale yellow solid.

<sup>1</sup>H NMR (600 MHz, DMSO) δ 11.13 (br, 1H), 7.97 (d, J = 2.7 Hz, 1H), 7.81 (d, J = 8.8 Hz, 2H), 7.73 (br, 2H), 7.65 (dd, J = 9.0, 2.7 Hz, 1H), 7.46 – 7.5 (m, 2H), 7.43 (t, J = 7.4 Hz, 1H), 7.34 (t, J = 7.6 Hz, 2H), 7.13 (d, J = 8.8 Hz, 2H), 6.89 (d, J = 9.0 Hz, 1H), 6.57 (s, 1H). <sup>13</sup>C NMR (151 MHz, DMSO) δ 190.36, 171.11, 163.71, 158.87, 148.19, 146.60, 145.25, 140.08, 131.21, 130.67, 128.95, 128.18, 127.28, 126.83, 125.45, 123.00, 117.49, 112.94, 110.21, 62.13. HRMS (ESI) *m/z* [M + H]<sup>+</sup> calcd for C<sub>24</sub>H<sub>17</sub>N<sub>3</sub>O<sub>7</sub>: 460.1145, found: 460.1153.



*Chiral separation, VCD analysis and racemization studies of 2***Chiral separation**

**(-) and (+)-5-[3-Benzoyl-4-hydroxy-2-(4-nitrophenyl)-5-oxo-2H-pyrrol-1-yl]-2-hydroxybenzoic acid ((-)-2 and (+)-2).**

The enantiomers of *rac*-**2** (1.2 g, 2.61 mmol) were separated by chiral column chromatography on a Chiralpak IC (250x20 mm, 5  $\mu$ m) column. 50 mg (50 mg/mL in EtOH/TEA 10:0.1) were injected and eluted with 100% EtOH/TEA (100:0.1), 120 bar at 25  $^{\circ}$ C, a flow rate of 12 mL/min and detected at 270 nm. The first eluted compound was collected and evaporated to afford (-)-**2** (759 mg, 97.3% ee) as a yellow solid.  $[\alpha]_D^{20}$ : -96.8 (c 0.5, MeOH).  $^1\text{H NMR}$  (500 MHz, DMSO)  $\delta$  8.01 – 8.11 (m, 3H), 7.68 – 7.77 (m, 5H), 7.52 – 7.59 (m, 1H), 7.44 (t,  $J$  = 7.7 Hz, 2H), 6.92 (d,  $J$  = 8.9 Hz, 1H), 6.47 (s, 1H).  $^{13}\text{C NMR}$  (126 MHz, DMSO)  $\delta$  189.13, 171.32, 164.58, 158.88, 151.15, 147.28, 144.48, 137.95, 132.80, 130.64, 129.35, 128.82, 128.26, 127.58, 124.99, 123.61, 119.18, 117.68, 113.08, 60.92. HRMS (ESI)  $m/z$   $[M + H]^+$  calcd for  $\text{C}_{24}\text{H}_{16}\text{N}_2\text{O}_8$ : 461.0985, found: 461.0966.

The second eluted compound was collected and evaporated to afford (+)-**2** (644 mg, 99.6% ee) as a yellow solid.  $[\alpha]_D^{20}$ : +103.6 (c 0.5, MeOH).  $^1\text{H NMR}$  (500 MHz, DMSO)  $\delta$  8.02 – 8.08 (m, 3H), 7.67 – 7.77 (m, 5H), 7.56 (tt,  $J$  = 7.0, 1.3 Hz, 1H), 7.41 – 7.49 (m, 2H), 6.91 (d,  $J$  = 8.9 Hz, 1H), 6.47 (s, 1H).  $^{13}\text{C NMR}$  (126 MHz, DMSO)  $\delta$  189.10, 171.32, 164.60, 158.91, 151.27, 147.27, 144.53, 137.97, 132.77, 130.56, 129.34, 128.82, 128.24, 127.54, 125.00, 123.61, 119.12, 117.64, 113.23, 60.92. HRMS (ESI)  $m/z$   $[M + H]^+$  calcd for  $\text{C}_{24}\text{H}_{16}\text{N}_2\text{O}_8$ : 461.0985, found: 461.0987.

## CHAPTER 3

SSL Report                      Request type                      Separation of isomers

### Sample Information

Sample ID	EN Number	Incoming amount	Compound name	Project name
Rac-2		1.2 g		

### Preparative Conditions

<b>Incoming</b> <i>rac-2</i>				
<b>Column</b>	<b>Dimensions (mm)</b>	<b>Particle Size (µm)</b>		
Chiralpak IC	250 x 20	5		
<b>Mobile Phase</b>		<b>Gradient</b>		
EtOH/TEA 100/0.1				
<b>Flow (ml/min)</b>	<b>Detection (nm)</b>	<b>Temperature (C)</b>		
12	270	RT		
<b>Injected Amount</b>	<b>Injection Volume</b>	<b>Cycle time (min)</b>		
50 mg	1 ml			
<b>Sample Conc. (mg/ml)</b>	<b>Instrument</b>	<b>Operator</b>		
50 mg/ml in EtOH/TEA	Semi 3			
<b>Date</b>				
2019-02-07 10:25:28				
<b>Comment</b>				
<b>Outgoing</b> Peak 1 (P1) and peak 2 (P2)				

## CHAPTER 3

### Analytical Conditions

<b>Column</b>	<b>Dimension (mm)</b>	<b>Particle Size (<math>\mu\text{m}</math>)</b>
Chiralpak IB-N3	150 x 4.6	3
<b>Mobile Phase</b>		
25% EtOH/DEA 100/20mM in CO <sub>2</sub> , 120 bar		
<b>Flow (ml/min)</b>	<b>Detection (nm)</b>	<b>Temperature (C)</b>
3.5	247	40
<b>Gradient</b>	<b>Instrument</b>	<b>Sample concentration (mg/ml)</b>

Sample ID	Purity	Chiral purity	Weight
Peak:1		97.3 ee	700 mg

Sample ID	Purity	Chiral purity	Weight
Peak:2		99.6 ee	600 mg

# CHAPTER 3

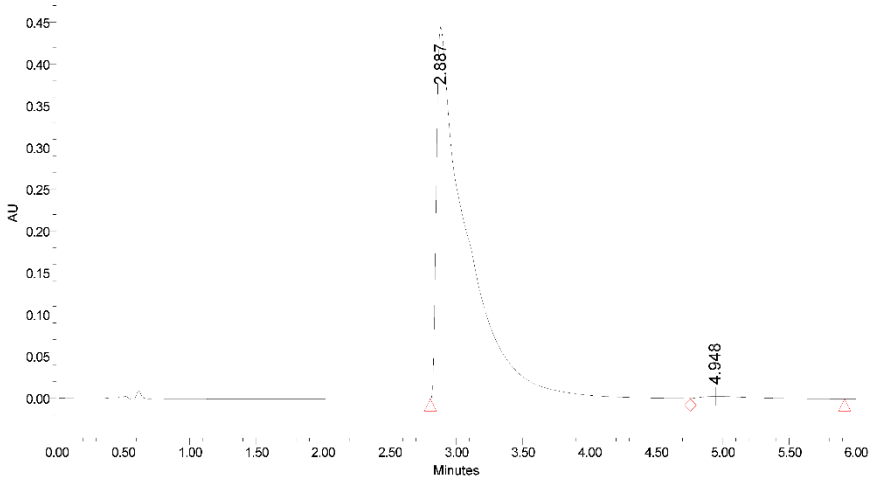
1 of 1

Sample Name: P1

Date Acquired: 2019-02-07 11:04:32

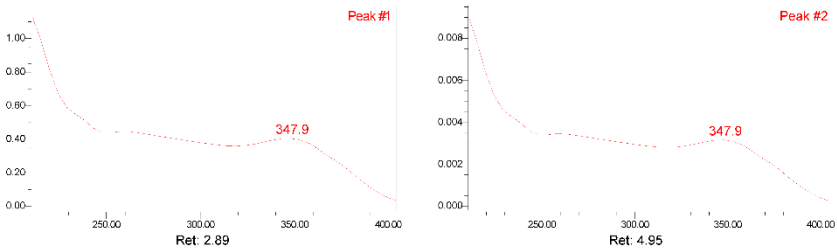
**Column:** Chiralpak IB N-3  
**Mobile Phase A:** CO<sub>2</sub>  
**Mobile Phase B:** EtOH/DEA 100/20mM  
**Gradient:** 25% B, 120 bar  
  
**Temperature:** 40°C  
**Sample Concentration:** Sample in EtOH

**Column ID:**  
**Column Dimension:** 150 \* 4.6  
**Particle Size:** 3  
**Injection volume:** 2.00 ul  
**Flow:** 3.5 ml/min  
**Wav elength:** PDA Spectrum PDA  
**Vial:** 1:F:6



	Retention Time	Area	% Area	k'	N	USP Resolution
1	2.887	7119325	98.63	0.000	778.5	
2	4.948	98593	1.37	0.714	763.8	3.042

ee = 97.3



Report Method: ee\_spektrum  
Acq Method Set: 120bar\_B2\_25\_40deg

Injection Id 6700

# CHAPTER 3

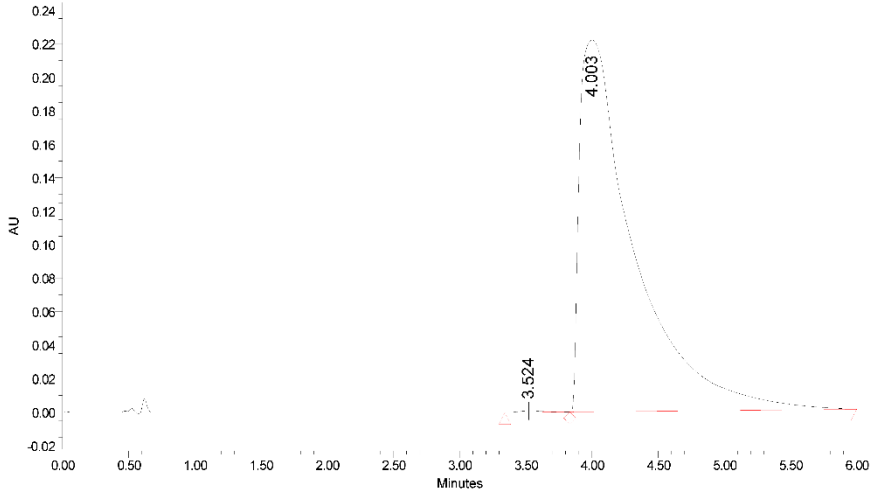
1 of 1

Sample Name: P2

Date Acquired: 2019-02-07 10:58:08

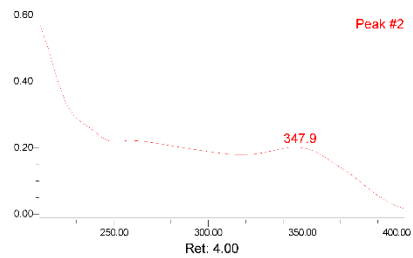
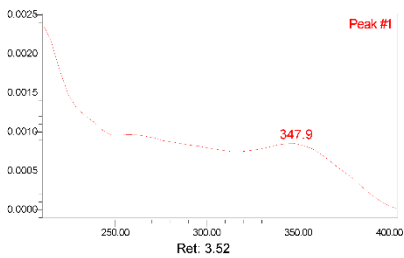
**Column:** Chiralpak IB N-3  
**Mobile Phase A:** CO<sub>2</sub>  
**Mobile Phase B:** EtOH/DEA 100/20mM  
**Gradient:** 25% B, 120 bar  
  
**Temperature:** 40°C  
**Sample Concentration:** Sample in EtOH

**Column ID:**  
**Column Dimension:** 150 \* 4.6  
**Particle Size:** 3  
**Injection volume:** 2.00 ul  
**Flow:** 3.5 ml/min  
**Wav elength:** PDA Spectrum PDA  
**Vial:** 1:F,7



	Retention Time	Area	% Area	k'	N	USP Resolution
1	3.524	11990	0.19	0.000	1627.9	
2	4.003	6374643	99.81	0.136	598.5	0.878

ee = 99.6



Report Method: ee\_spektrum  
Acq Method Set: 120bar\_B2\_25\_40deg

Injection Id 6693

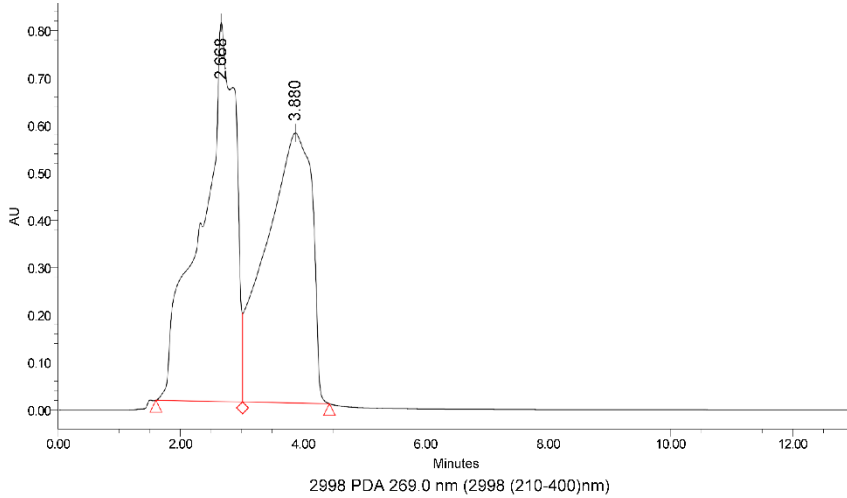
# CHAPTER 3

Sample Name: *rac-2*

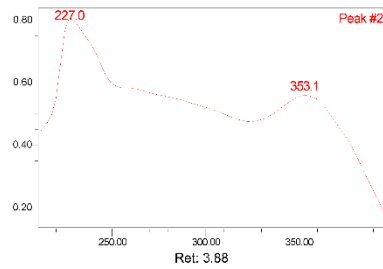
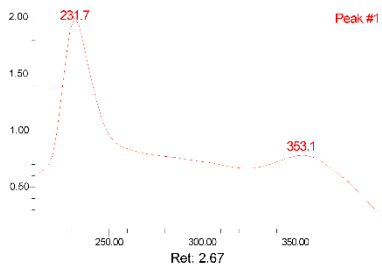
Date Acquired: 2019-01-31 09:49:02

Column: Chiralpak IC  
 Mobile Phase A:  
 Mobile Phase B: EtOH/TEA 100/0.1  
 Gradient: 100%B  
 Temperature: 25°C  
 Sample Concentration: Sample in EtOH

Column ID:  
 Column Dimension: 150\*4.6 mm  
 Particle Size: 3  
 Injection volume: 15.00 ul  
 Flow: 0.8 ml/min  
 Wav elength: 2998 PDA 269.0 nm  
 Vial: 2:a,1



	Retention Time	Area	% Area	K'	N	USP Resolution	Width @ 50%
1	2.668	30714976	50.92	0.000	103.7		5.238618e-001
2	3.680	29604704	49.08	0.454	93.3	0.760	9.176087e-001



Report Method: normal\_spektrum  
 Acq Method Set: C\_25C\_08ml

Injection Id 1556

# CHAPTER 3

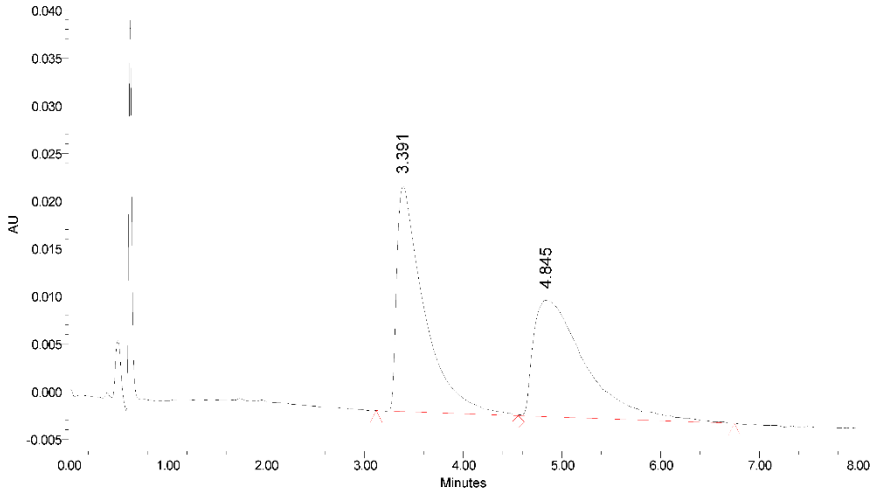
1 of 1

Sample Name: *rac-2*

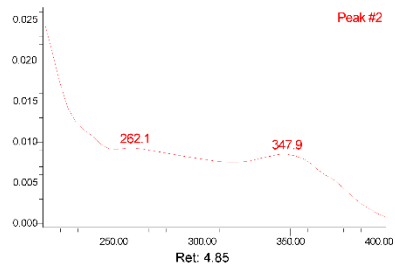
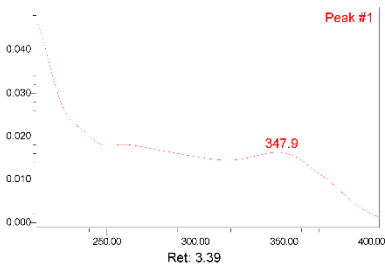
Date Acquired: 2019-02-07 10:39:18

**Column:** Chiralpak IB N-3  
**Mobile Phase A:** CO<sub>2</sub>  
**Mobile Phase B:** EtOH/DEA 100/20mM  
**Gradient:** 25% B, 120 bar  
  
**Temperature:** 40°C  
**Sample Concentration:** Sample in EtOH

**Column ID:**  
**Column Dimension:** 150 \* 4.6  
**Particle Size:** 3  
**Injection volume:** 5.00 ul  
**Flow:** 3.5 ml/min  
**Wav length:** PDA Spectrum PDA  
**Vial:** 1:f,5



	Retention Time	Area	% Area	k'	N	USP Resolution	Width @ 50%
1	3.391	457983	50.68	0.000	743.8		2.710256e-001
2	4.845	445739	49.32	0.429	545.1	2.015	5.344113e-001



Report Method: normal\_spektrum  
Acq Method Set: 120bar\_B2\_25\_40deg

Injection Id 6677

## CHAPTER 3

### **Vibrational Circular Dichroism (VCD)**

*Summary.* VCD analysis was performed on (+)-**2** only. The data collected suggest that (+)-**2** is likely to be the (S) enantiomer. All spectra, experimental and simulated, are shown in Figure 1.

*Experimental.* (+)-**2** (5.0 mg) was dissolved in 110  $\mu\text{L}$   $\text{CDCl}_3$ . Approximately 90  $\mu\text{L}$  of the solution was transferred to a 0.100 mm  $\text{BaF}_2$  cell and VCD spectra acquired for 12 hours in a Biotools ChiralIR2X instrument. The resolution was  $4\text{ cm}^{-1}$ . A VCD spectrum was collected on a  $\text{CDCl}_3$  blank in the same cell to act as a baseline reference and subtracted from the experimental spectrum.

*Computational Spectral Simulation.* A Monte Carlo molecular mechanics search for low energy geometries was conducted for the S enantiomer. MacroModel within the Maestro graphical interface (Schrödinger Inc.) was used to generate 123 starting coordinates for conformers. All conformers within 5 kcal/mol of the lowest energy conformer were used as starting point for density functional theory (DFT) minimizations within Gaussian09. Optimized structures, harmonic vibrational frequencies/intensities, VCD rotational strengths, and free energies at STP (including zero-point energies) were determined at B3LYP/6-31G\* level of theory. Three conformations were found that contributed over 10% to the Boltzmann distribution. An in-house built program was used to fit Lorentzian line shapes ( $12\text{ cm}^{-1}$  line width) to the computed spectrum of a Boltzmann distributed average thereby allowing direct comparisons between simulated and experimental spectra. Comparison of the calculated and experimental spectra is illustrated in Figure S3.23.



## CHAPTER 3

### Racemization studies on (*R*)-2

Sample was dissolved in EtOH, then triethylamine (TEA, 10 eq) was added and the resulting solution was stirred overnight at room temperature. The reaction mixture was then transferred into a vial and analyzed directly.

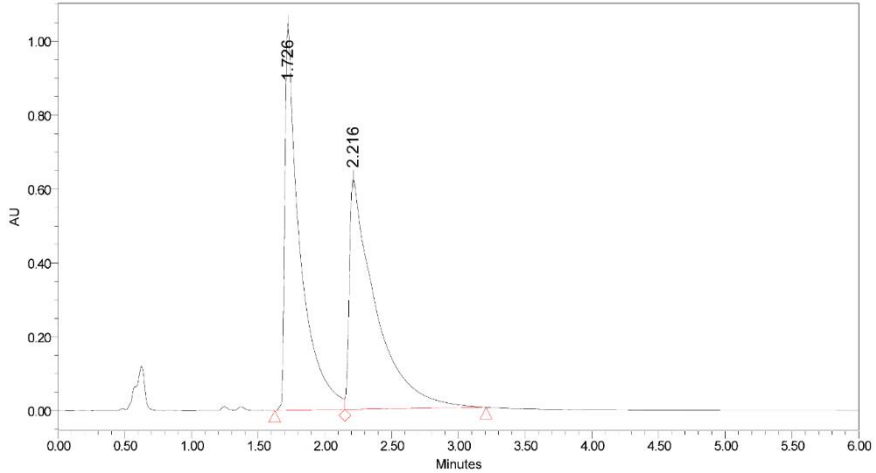
SSL Report	Request type	Racemisation test		
<b>Sample Information</b>				
Sample ID	EN Number	Incoming amount	Compound name	Project name
<i>rac</i> -2, ( <i>R</i> )-2		2 mg		
<b>Analytical Conditions</b>				
Column	Dimension (mm)	Particle Size (µm)		
Chiralpak IB-N3	150 x 4.6	3		
<b>Mobile Phase</b>				
30% EtOH/DEA 100/20mM in CO <sub>2</sub> , 120 bar				
Flow (ml/min)	Detection	Temperature (C)		
3,5		40		
Gradient	Instrument	Sample concentration (mg/ml)		
<b>Sample ID</b>	<b>Purity</b>	<b>Chiral Purity</b>	<b>Weight</b>	
Peak 1 ( <i>R</i> )-2				
<b>Comments</b>				
Peak 2 ( <i>S</i> )-2				
<b>Comments</b>				

# CHAPTER 3

Sample Name: *rac-2*

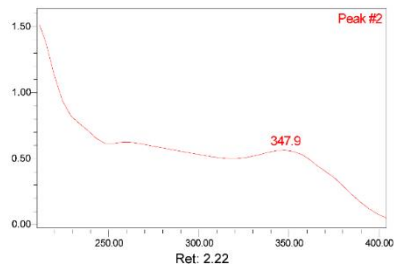
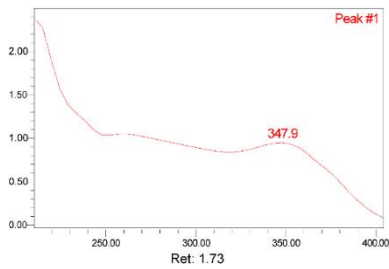
Column: Chiralpak IB N-3 CO2  
 Mobile Phase A: EtOH/DEA 100/20mM  
 Mobile Phase B: 30% B, 120 bar  
 Gradient: 40°C  
 Temperature:  
 Sample Concentration: Sample in EtOH

Column ID:  
 Column Dimension: 150 \* 4.6  
 Particle Size: 3  
 Injection volume: 10.00 ul  
 Flow: 3.5 ml/min  
 Wavelength: PDA Spectrum PDA  
 Vial: 1:b,3



Channel PDA Spectrum; Channel Description PDA Spectrum (210-400)nm

	Retention Time	Area	% Area	k'	N	USP Resolution	Width @ 50%
1	1.726	8200105	49.19	0.000	1321.5		9.595719e-002
2	2.216	8469435	50.81	0.284	518.2	1.692	1.805067e-001



Report Method: normal\_spektrum\_x  
 Acq Method Set: 120bar\_B2\_30\_40deg

Injection Id 29152

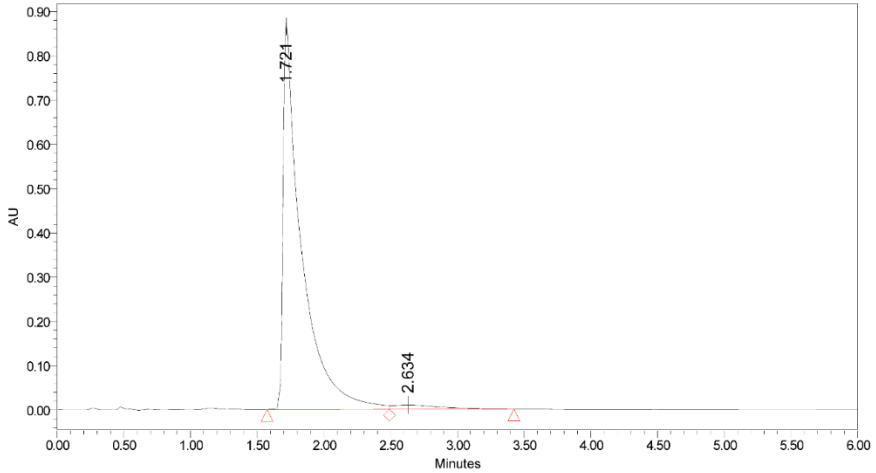
# CHAPTER 3

Sample Name: (R)-2

**Column:** Chiralpak IB N-3  
**Mobile Phase A:** CO2  
**Mobile Phase B:** EtOH/DEA 100/20mM  
**Gradient:** 30% B, 120 bar

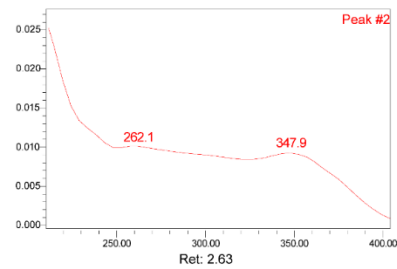
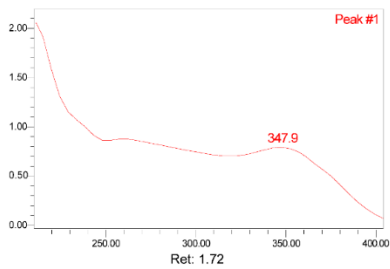
**Column ID:**  
**Column Dimension:** 150 \* 4.6  
**Particle Size:** 3  
**Injection volume:** 10.00 ul  
**Flow :** 3.5 ml/min  
**Wav length:** PDA Spectrum PDA  
**Vial:** 1:b,1

**Temperature:** 40°C  
**Sample Concentration:** Sample in EtOH



Channel PDA Spectrum; Channel Description PDA Spectrum (210-400)nm

	Retention Time	Area	% Area	K'	N	USP Resolution	Width @ 50%
1	1.721	8292807	97.21	0.000	957.5		1.155378e-001
2	2.634	237826	2.79	0.530			

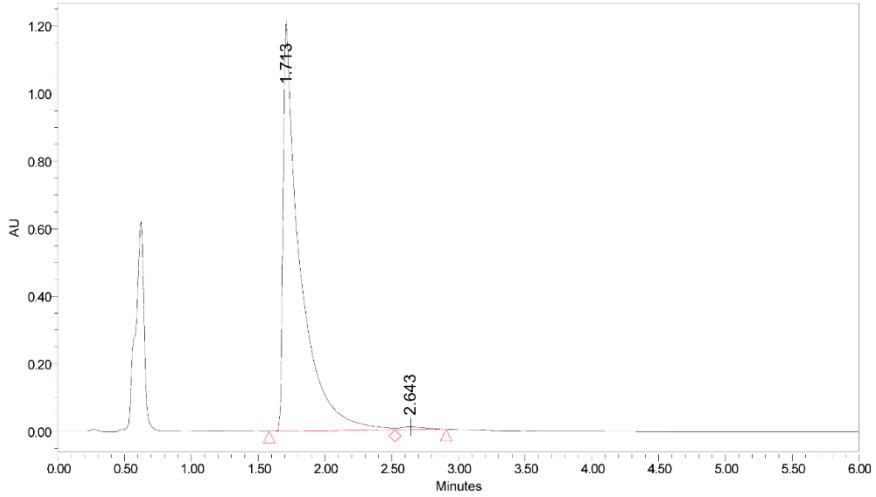


# CHAPTER 3

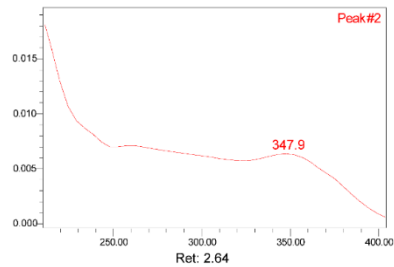
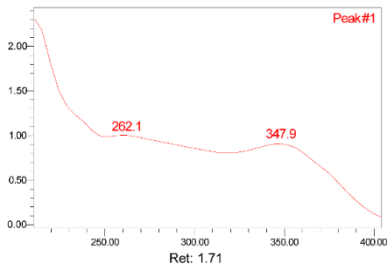
Sample Name: (R)-2 + TEA

**Column:** Chiralpak IB N-3  
**Mobile Phase A:** CO2  
**Mobile Phase B:** EtOH/DEA 100/20mM  
**Gradient:** 30% B, 120 bar  
  
**Temperature:** 40°C  
**Sample Concentration:** Sample in EtOH

**Column ID:**  
**Column Dimension:** 150 \* 4.6  
**Particle Size:** 3  
**Injection v olume:** 10.00 ul  
**Flow :** 3.5 ml/min  
**Wav elength:** PDA Spectrum PDA  
**Vial:** 1:B,2



	Retention Time	Area	% Area	k'	N	USP Resolution	Width @ 50%
1	1.713	10566923	98.90	0.000	1178.8		1.036627e-001
2	2.643	117647	1.10	0.543			



Report Method: normal\_spektrum  
 Acq Method Set: 120bar\_B2\_30\_40deg

Injection Id 29094

*Peptide synthesis and characterization*

ER $\alpha$ (pT<sup>594</sup>) phosphopeptide **3** (AEGFPapTV-COOH), CaMKK2(pS<sup>100</sup>) phosphopeptide **4** (GSLSARKLpSLQER) and fluorescein-labelled CaMKK2(pS<sup>100</sup>) phosphopeptide FAM-**4** were purchased from Chinese Peptide Company Inc. (Hangzhou, China). FITC-labeled ER $\alpha$ (pT<sup>594</sup>) phosphopeptide FITC-**3** was synthesized according to a standard solid-phase peptide synthesis (Fmoc SPPS) procedure. PMA2 C-terminal 52-mer (corresponding to PMA2 amino acids 905-956) was prepared according to ref<sup>[25]</sup>.

**FITC-labeled ER $\alpha$ (pT<sup>594</sup>) phosphopeptide 3 synthesis (FITC-3)**

*General information.* Fmoc-amino acids were purchased from Chem-Impex International, Inc., with the following side-chain protection: Fmoc-Ala-OH, Fmoc-Glu(OtBu)-OH, Fmoc-Gly-OH, Fmoc-Phe-OH, Fmoc-Pro-OH, Fmoc-Thr(PO(OBzl)OH)-OH, Fmoc-Val-OH. L-Amino acids were used in every case. Fluorescein 5-isothiocyanate (5-FITC) was purchased from Sigma-Aldrich. Diisopropylethylamine (DIPEA) was purchased from Sigma-Aldrich, 1-[bis(dimethylamino)methylene]-1H-1,2,3-triazolo[4,5-b]pyridinium 3-oxide hexafluorophosphate (HATU) was purchased from Chem-Impex International, Inc. 2-Chlorotrityl chloride resin (200-400 mesh) was purchased from Chem-Impex International, Inc. Peptide synthesis was monitored by reversed-phase (RP) ultra-performance liquid chromatography tandem mass spectrometer (UPLC-MS). Analytical RP-UPLC-MS was performed on a Waters Acquity UPLC system (PDA, sample manager, sample organizer, column oven modules) and Waters SQD2 mass spectrometer using the following column: Waters Acquity CSH C18 column, 130 Å, 1.7  $\mu$ m, 50 x 2.1 mm at a flow rate of 0.5 mL/min at 45 °C. A linear gradient of mobile phase: A = H<sub>2</sub>O + 10 mM formic acid (FA), 1 mM ammonia and 0.03% trifluoroacetic acid (TFA) and B = ACN/H<sub>2</sub>O 95/5 (vol/vol-%) + 10 mM FA, 1 mM ammonia and 0.03% TFA was used with detection at 220 nm.

*Resin loading.* In a peptide reactor 2-chlorotrityl chloride resin 0.8 mmol/g (0.2 mmol, 250 mg) was swollen in CH<sub>2</sub>Cl<sub>2</sub> for 10 min, then the solvent was drained. Fmoc-L-Val-OH (1 eq) was dissolved in CH<sub>2</sub>Cl<sub>2</sub> and DIPEA (3 eq) was added. The clear solution was added to the resin which was agitated for 10 min. Additional DIPEA (7 eq) was added and the resin was agitated for further 45 min. The remaining trityl groups were capped adding MeOH (0.8  $\mu$ L/mg of resin), the resin was agitated for 10 min. The mixture was drained and the resin beads washed with DMF (3 x) and CH<sub>2</sub>Cl<sub>2</sub> (3 x).

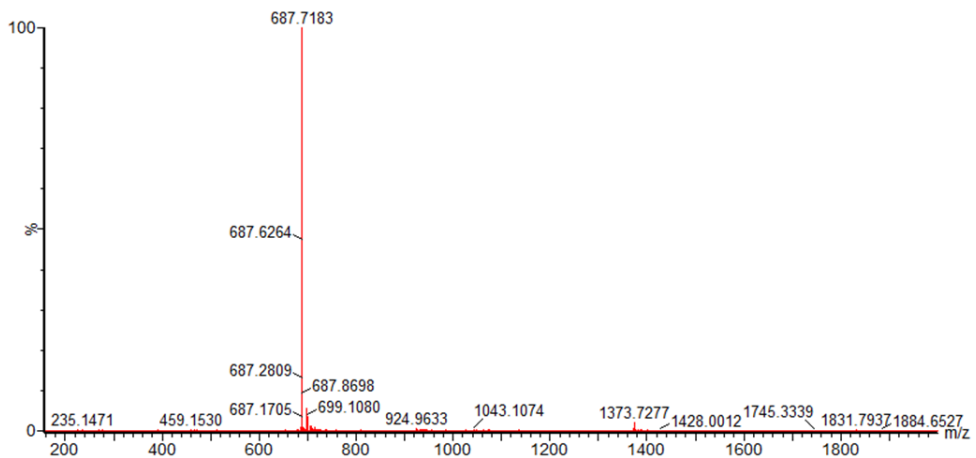
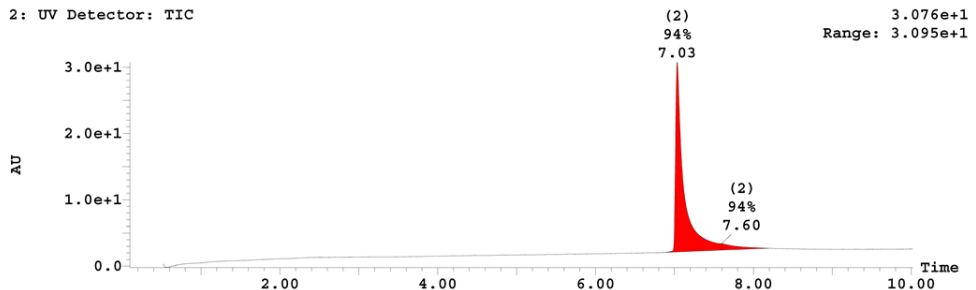
*Fmoc cleavage.* The N-terminal Fmoc protecting group was removed with a 20% solution of piperidine in DMF (2 x 5 min). The mixture was drained and the resin beads washed with DMF (3 x) and CH<sub>2</sub>Cl<sub>2</sub> (3 x).

*Peptide elongation.* Fmoc-L-AA-OH (4 eq) and HATU (4 eq) were dissolved in DMF, then DIPEA (6 eq) was added. After a pre-activation period of 2 min, the mixture was added to the resin, which was agitated for 45-60 min. The mixture was drained and the resin beads washed with DMF (3 x) and CH<sub>2</sub>Cl<sub>2</sub> (3 x). Successful coupling was indicated by ninhydrin test. Coupling of the spacer Fmoc-6-aminohexanoic acid (Fmoc-6-Ahx-OH, 4 eq) was performed using the same procedure as above. The peptide was finally reacted with Fluorescein-5-isothiocyanate (5-FITC, 4 eq) and DIPEA (6 eq) for 2h in the dark to yield fluorescent-immobilized peptidyl-resin.

*Cleavage from resin.* The resin-bound peptide was cleaved from resin using a solution of TFA/TIS/H<sub>2</sub>O/EDT (94:1:2.5:2.5). After shaking for 60 min, the TFA solution was filtered and the reaction mixture was poured into cold diethyl ether. Upon precipitation, the suspension was centrifuged, the precipitate dissolved in ACN/H<sub>2</sub>O and lyophilized.

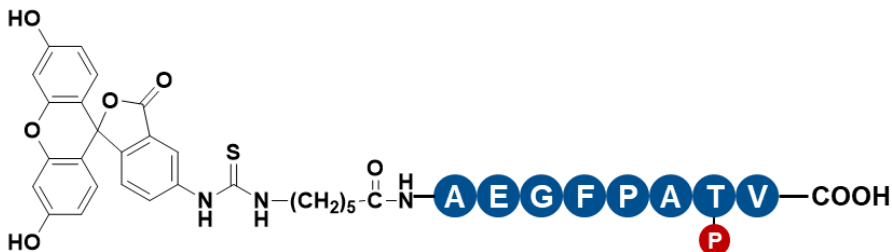
## CHAPTER 3

**Purification.** The compound was purified by preparative HPLC on a Kromasil C8 column (10  $\mu\text{m}$  250x20 ID mm) using a gradient of 43-63% ACN in H<sub>2</sub>O/ACN/FA 95/5/0.2 buffer, over 20 minutes with a flow of 19 mL/min. The compounds were detected by UV at 220 nm. Collected fractions were lyophilized, to yield the purified peptide FITC-3 (26 mg, 9.47%) as a yellow solid, in ca. 95% purity as estimated by analytical UPLC.



$R_t = 7.03$  min (3-60% B over 10 min, 0.5 mL/min).  $m/z$  (ESI-MS):  $[M+2H]^{2+}$  calculated mass = 687.2, observed = 697.7

Final sequence: 5-FITC-Ahx- AEGFPaPTV-OH (FITC-3)

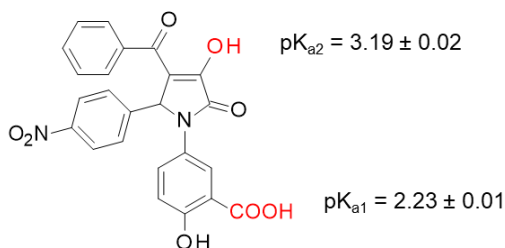


## CHAPTER 3

FAM-4 sequence: 5-FAM-GSLSARKLpSLQER-OH



### *pK<sub>a</sub> determination*



*Protocol summary.*  $pK_a$ s were determined using the SiriusT3 instrument from Sirius Analytical by performing an acid/base titration. The technique uses an *in situ* UV probe to measure the UV absorbance profile of the compound at each pH point during the titration. Measured  $pK_a$  values are reported as mean  $\pm$  SEM.

*Experimental procedure.* The sample  $pK_a$ s are investigated using the fast UV-metric method. This involves measuring the UV absorbance profile at each pH point during an acid/base titration using an *in situ* UV probe in the titration cell of a SiriusT3 instrument. Each sample is titrated in a triple titration over a nominal pH range of 2 to 12 in approximately 50, 40, 30 % methanol. Sample concentrations are typically in the range 35 -15  $\mu$ M. All titrations are carried out at 25 °C.

The  $pK_a$ (s) were determined by monitoring the change in UV absorbance with pH as the compound undergoes ionization. This information is used to produce a 3D matrix of pH vs. Wavelength vs. Absorbance data. A mathematical technique called Target Factor Analysis is applied to the matrix to produce molar absorbance profiles for the different light absorbing species present in solution and also a "Distribution of Species" plot showing how the proportion of each species varies with pH. Sample  $pK_a$ s are extrapolated to aqueous conditions using the Yasuda-Shedlovsky method.

The method requires that the sample compound possesses a chromophore and that changes in ionization influence the absorbance spectrum of the compound. This procedure will measure  $pK_a$  values in the range 2-12.

### 3.5.2 NMR data

*Production of  $^{15}N^2H$ -labeled 14-3-3 $\sigma\Delta$ C for  $^1H$ - $^{15}N$  TROSY-HSQC NMR spectroscopy.* The  $^{15}N^2H$ -labeled 14-3-3 $\sigma\Delta$ C ( $\Delta$ C17, cleaved after T231) for NMR studies was expressed in *E. coli* BL21 (DE3) cells transformed with a pProExHtb vector carrying the cDNA to express an N-terminally

## CHAPTER 3

His<sub>6</sub>-tagged human 14-3-3 $\sigma$  $\Delta$ C. Bacterial cells were grown in 1 L of deuterated M9 minimal medium supplemented with 2 g/L <sup>12</sup>C<sub>6</sub>H<sub>7</sub> glucose, 1 g/L <sup>15</sup>N ammonium chloride, 0.4 g/L Isogro <sup>15</sup>N<sup>12</sup>C<sup>2</sup>H Powder – Growth Medium (Sigma Aldrich) and 100  $\mu$ g/mL ampicillin. The recombinant protein was then purified from the bacterial extract by affinity chromatography using a Ni-NTA column (GE Healthcare). The His<sub>6</sub>-tag was further cleaved by the TEV protease. The protein was finally dialyzed overnight at 4 °C against NMR buffer (100 mM sodium phosphate, pH 6.8, 50 mM NaCl), concentrated, aliquoted, flash frozen and stored at -80 °C. A detailed protocol was previously published can be found at ref<sup>[29]</sup>.

*<sup>1</sup>H-<sup>15</sup>N TROSY-HSQC NMR experiments* <sup>1</sup>H-<sup>15</sup>N TROSY-HSQC (Transverse Relaxation Optimized Spectroscopy - Heteronuclear Single Quantum Coherence Spectroscopy) spectra were acquired at 32 °C in 3 mm tubes (sample volume 200  $\mu$ L) using a 900 MHz Bruker Avance Neo spectrometer, equipped with a cryoprobe. All samples were prepared in a buffer containing 100 mM sodium phosphate, 50 mM NaCl, pH 6.8, 4% (v/v) DMSO-*d*<sub>6</sub>, 1 mM DTT, EDTA-free protease inhibitor cocktail (Roche, Basel, Switzerland) and 10% (v/v) D<sub>2</sub>O. The experiments were recorded with 3072 complex data points in the direct dimension and 128 complex data points in the indirect dimension, with 184 scans per increment. For the evaluation of the binding of (-)-**2** to 14-3-3 $\sigma$  $\Delta$ C, spectra of 100  $\mu$ M <sup>15</sup>N<sup>2</sup>H-labeled 14-3-3 $\sigma$  $\Delta$ C were recorded in the presence and absence of 2000  $\mu$ M (-)-**2**. For the evaluation of the binding of (-)-**2** to the 14-3-3 $\sigma$  $\Delta$ C/ER $\alpha$  complex, spectra of <sup>15</sup>N<sup>2</sup>H-labeled 14-3-3 $\sigma$  $\Delta$ C 100  $\mu$ M with 60  $\mu$ M ER $\alpha$ (pT<sup>594</sup>) phosphopeptide **3** were recorded in the presence and absence of 1000  $\mu$ M and 2000  $\mu$ M (-)-**2**. For the evaluation of the binding of (+)-**2** to 14-3-3 $\sigma$  $\Delta$ C, spectra of 100  $\mu$ M <sup>15</sup>N<sup>2</sup>H-labelled 14-3-3 $\sigma$  $\Delta$ C were recorded in the presence and absence of 2000  $\mu$ M (+)-**2**. The reference for the <sup>1</sup>H chemical shift was relative to TMSP (trimethylsilylpropanoic acid) while <sup>15</sup>N chemical shift values were referenced indirectly. Assignments of the backbone resonances of <sup>15</sup>N<sup>2</sup>H-labeled 14-3-3 $\sigma$  $\Delta$ C have previously been reported.<sup>[29]</sup> Spectra were collected and processed with Topspin 4.0 (Bruker Biospin, Karlsruhe, Germany) and analysed with Sparky 3.12 (T. D. Goddard and D. G. Kneller, SPARKY 3, University of California, San Francisco).

*WaterLOGSY NMR experiments.* WaterLOGSY spectra were acquired at 16 °C in 5 mm tubes (sample volume 530  $\mu$ L) using a 600 MHz Bruker Avance III HD spectrometer equipped with a CPQCI cryogenic probe. The spectra were recorded with 32768 complex data points, with 384 scans per increment and with a mixing time of 1.7 s (acquisition time of 35 minutes). All samples were prepared in a buffer containing 100 mM sodium phosphate, 50 mM NaCl, pH 6.8 and 10% (v/v) D<sub>2</sub>O. The final concentration of DMSO-*d*<sub>6</sub> was 2% (v/v) and was kept constant for all experiments. To examine the binding of both (-)-**2** and (+)-**2** to either 14-3-3 $\sigma$  $\Delta$ C alone or in complex to the ER $\alpha$ (pT<sup>594</sup>) phosphopeptide **3**, WaterLOGSY spectra were recorded on solutions containing each of the enantiomers of **2** at 500  $\mu$ M in the presence of 25  $\mu$ M 14-3-3 $\sigma$  $\Delta$ C alone or together with 35  $\mu$ M ER $\alpha$ (pT<sup>594</sup>) phosphopeptide **3**, respectively. A <sup>1</sup>H spectrum with water-suppression was additionally recorded for each sample. The reference for the <sup>1</sup>H chemical shift was relative to TMSP (trimethylsilylpropanoic acid). Spectra were collected, processed and analyzed with Topspin 3.6 (Bruker Biospin, Karlsruhe, Germany).

### 3.5.3 Protein expression & purification and X-ray crystallography

*Protein expression & purification.* Proteins were expressed and purified as previously reported.<sup>[46]</sup>

*Purification protocol.* Prior to purification, the cell pellets were thawed and resuspended in 10 mL/g pellet lysis buffer (25 mM Tris, pH = 8.0, 150 mM NaCl, 5% v/v glycerol, 10 mM imidazole, 4 mM



## CHAPTER 3

BME and 1 mM PMSF). The cells were then lysed twice by homogenization using an EmulsiFlex-C3 homogenizer. The lysate was incubated with benzonase (Merck Millipore) for 15 minutes and then centrifuged at 20000 g for 15 minutes. The supernatant was applied in overnight circulation at 4 °C to a 5 mL HisTrap column pre-equilibrated with 20 column volumes (CV) lysis buffer. The column was then washed with 20 CV wash buffer (25 mM Tris, pH = 8.0, 300 mM NaCl, 5% v/v glycerol, 25 mM imidazole and 4 mM BME) and the protein eluted with 40 mL elution buffer (20 mM HEPES, pH 8.0, 100 mM NaCl, 5% v/v glycerol, 250 mM imidazole and 4 mM BME). The protein was then pipetted into a SpectrumLabs Spectra/Por 10000 Da MWCO dialysis bag and dialysed overnight at 4 °C against dialysis buffer (25 mM HEPES, pH = 8.0, 100 mM NaCl, 4 mM BME, 2 mM MgCl<sub>2</sub>). For 14-3-3σΔC, 1:500 mg/mg TEV protease was added to the dialysis bag. The full length proteins were then concentrated to ~50 mg/mL using 10000 Da MWCO Amicon spinfilters, aliquoted, flash frozen in liquid nitrogen and stored at -80 °C until further usage. The 14-3-3σΔC protein was instead applied to a 5 mL HisTrap column pre-equilibrated with 20 CV dialysis buffer. The flowthrough was captured and concentrated to ~50 mg/mL using 10000 Da MWCO Amicon spinfilters. The concentrated 14-3-3σΔC protein was then applied to a HiLoad superdex 75 16/60 SEC column using an Äkta FPLC apparatus. The fractions containing protein were then pooled, concentrated to ~50 mg/mL protein, flash frozen in liquid nitrogen and stored at -80 °C until further use.

*X-ray crystallography.* Crystals of the ternary complexes were grown by mixing 12.5 mg/mL 14-3-3σΔC with **3** in a molar ratio of 1:2 in 10 mM HEPES pH 7.4, 150 mM NaCl, 2 mM BME and 2 mM of the compound of interest and incubating overnight at 277 K. The formed complex was then set up for crystallization by mixing 1:1 (v/v) 0.1 M Tris, pH 7.0, 0.2 M magnesium chloride hexahydrate and 10 % v/v PEG 8000 and incubating in a sitting drop at 277 K. Crystals grew within a week and were cryoprotected by adding a grain of sucrose to the crystallization drop and incubating for 10 minutes. Crystals were then fished and stored in liquid nitrogen. Data collection and processing are described in the Supporting Information. The crystal structures were deposited in the Protein Data Bank (PDB ID 6TJM and 6TL3).

*Data collection and analysis.* X-ray diffraction data for the 14-3-3σΔC/ERα(pT<sup>594</sup>) phosphopeptide **3/(R)-2** complex was collected at 100 K at the p11 beamline of the PETRA-III synchrotron of the DESY facility in Hamburg, Germany using a Pilatus 6M-F detector.<sup>[47-48]</sup> X-ray diffraction data for the 14-3-3σΔC/ERα(pT<sup>594</sup>) phosphopeptide **3/(R)-6** complex was collected at 100 K on a Rigaku Micromax-003 sealed tube X-ray source and a Dectris Pilatus 200K detector. The data was indexed, integrated, scaled and merged using xia2 DIALS.<sup>[49]</sup> Phasing was done by molecular replacement using Phaser<sup>[50]</sup> and PDB 4JC3 as a starting model and was followed by iterative rounds of refinement and manual model building using Phenix.Refine<sup>[51]</sup> and Coot<sup>[52]</sup>, respectively. Model validation was performed using MolProbity.<sup>[53]</sup> Figures were created using PyMol. See Table S3.1 for data collection and refinement statistics.

## CHAPTER 3

**Table S3.1.** XRD statistics

	<b>14-3-3<math>\sigma</math><math>\Delta</math>C /ER<math>\alpha</math>/(R)-2</b>	<b>14-3-3<math>\sigma</math><math>\Delta</math>C /ER<math>\alpha</math>/(R)-6</b>
PDB code	6TJM	6TL3
<b>Data collection</b>		
Resolution (Å) <sup>[a]</sup>	1.85 (1.85 – 1.88)	2.46 (2.50 – 2.45)
Space group	C222	C222
Cell parameters (Å) <sup>[b]</sup>	a = 62.84, b = 152.31, c = 76.79 $\alpha = \beta = \gamma = 90^\circ$	a = 63.69, b = 152.23, c = 76.26 $\alpha = \beta = \gamma = 90^\circ$
Rmerge <sup>[a,b]</sup>	0.042 (1.17)	0.17 (0.64)
Average $I/\sigma(I)$ <sup>[a,b]</sup>	24.0 (1.0)	7.72 (2.03)
CC1/2 (%) <sup>[a,b,c]</sup>	100 (80.3)	99.1 (86.3)
Completeness (%) <sup>[a,b]</sup>	99.9 (99.1)	99.8 (100)
Redundancy <sup>[a,b]</sup>	12.5 (11.6)	6.2 (6.6)
<b>Refinement</b>		
Number of protein/solvent/ligand atoms	3770/127/50	3749/194/49
Rwork/Rfree (%)	19.7/21.8	21.0/25.9
Unique reflections used in refinement	31888	13882
R.m.s. deviations from ideal values bond lengths (Å) / bond angles (°)	0.006/0.617	0.006/0.600
Average protein/solvent/ligand B-factor (Å <sup>2</sup> )	52.5/55.7/47.7	36.4/40.7/34.21
Ramachandran favored (%)	98.22	97.25
Ramachandran allowed (%)	1.78	2.75
Ramachandran outliers (%)	0	0

[a] Number in parentheses is for the highest resolution shell [b] As reported by xia2 DIALS. [c] CC<sub>1/2</sub> = Pearson's intradataset correlation coefficient, as described by Karplus and Diederichs.<sup>[54]</sup>

### 3.5.4 Fluorescence Polarization (FP)

For affinity measurements, fluorescently-labeled peptides FITC-**3** or FAM-**4** were dissolved in FP buffer (10 mM HEPES, 150 mM NaCl, 0.05% TWEEN 20, pH 7.4) to a final concentration of 10 nM. Dilution series of 14-3-3 $\zeta$  protein were made in black, flat-bottomed 384-well microplates (Greiner Bio-One, model n. 784076) in a final sample volume of 12  $\mu$ L. Following 1 h incubation at room temperature, plates were read on an PHERAstar plate reader (BMG Labtech, Ortenberg, Germany) for FP signal (filter set  $\lambda_{\text{ex}}$  485 nm,  $\lambda_{\text{em}}$  520 nm). For PPI stabilization experiments, dilution series of compounds (10 mM DMSO stock solution) were added to a solution of FITC-**3** or FAM-**4** (10 nM) and 14-3-3 $\zeta$  protein (50 nM for ER $\alpha$ (pT<sup>594</sup>)/FITC-**3** and 30  $\mu$ M for CaMKK2(pS<sup>100</sup>)/FAM-**4**, corresponding to approximately 20% occupancy of 14-3-3 by FITC-**3** or FAM-**4**). Final DMSO concentration was 2% (vol/vol). All experiments were performed in triplicate ( $n = 3$ ), unless otherwise stated. Data reported are at end point.  $K_d$  and  $EC_{50}$  values were obtained from fitting the data with a four-parameter logistic model (4PL) using GraphPad Prism version 8.3.0 for Windows, GraphPad Software, San Diego, California USA, www.graphpad.com. Errors bars indicate standard deviation of individual measurements.

### 3.5.5 Surface Plasmon Resonance (SPR)

Unless otherwise stated, SPR measurements were performed on a Biacore 3000 (GE Healthcare) using as running buffer 10 mM HEPES, 150 mM NaCl, 0.05% TWEEN 20, pH 7.4. 14-3-3 $\zeta$  protein was immobilized on a CMD200M Biacore Sensor Chip (XanTec Bioanalytics GmbH, Düsseldorf, Germany) at approximately 4000 RUs using EDC/NHS coupling chemistry. Phosphopeptides **3** or **4** (50 nM and 30  $\mu$ M respectively in running buffer) and test compounds **2**, **5**, **6** or **9** (dissolved in running buffer and prepared from 10 mM DMSO stock solution to afford final test concentration and 1% final DMSO concentration) were premixed and injected at a flowrate of 20  $\mu$ L/min and 20 °C for 60 s or 120 s in running buffer. All experiments were performed in triplicate ( $n = 3$ ) unless otherwise stated. For each curve, the values at equilibrium response (*i.e.* binding coverage) were extracted and fitted using a four-parameter logistic model (4PL) using GraphPad Prism version 8.3.0 for Windows, GraphPad Software, San Diego, California USA, www.graphpad.com. Errors bars indicate standard deviation of individual measurements.

### 3.5.6 Computational details

All calculations were performed within the Schrödinger Small-Molecule Drug Discovery Suite 2019-2.<sup>[55]</sup> Initial geometries were derived from MCMM<sup>[56]</sup> conformational searches in MacroModel version 12.4 using the OPLS3e<sup>[57]</sup> force field in combination with the GB/SA continuum solvation model for water.<sup>[58]</sup> Density functional theory calculations were performed using Jaguar version 10.4.<sup>[59]</sup> Structures were optimized using the B3LYP-D3<sup>[60]</sup> *a posteriori*-corrected hybrid functional<sup>[61]</sup> with the 6-31G\*\*+ basis set and the PBF solvation model<sup>[62]</sup> for water. Normal-mode analysis were used to estimate the Gibbs free energies. Final energies were calculated using B3LYP-D3/6-311G\*\*+ with the PBF solvation model for water and with M06-2X-D3/6-31\*\*+ together with SM6.<sup>[63-64]</sup> M06-2X-D3/6-311\*\*+ together with PBF (water) energies were calculated to compare the two functionals. For comparative purposes, some combinations were also included.

For each compound, six different conformations were examined in detail starting from the conformation as found for (*R*)-**2** in the crystal structure. The torsion changed next was then the bond to the exocyclic carbonyl in combination with the attached phenyl group resulting in two different anti-conformations. For these three variants the salicylate was also rotated 180°. Structures of the optimized conformations are illustrated in Figure S3.24.

## 3.5.7 Supporting Figures

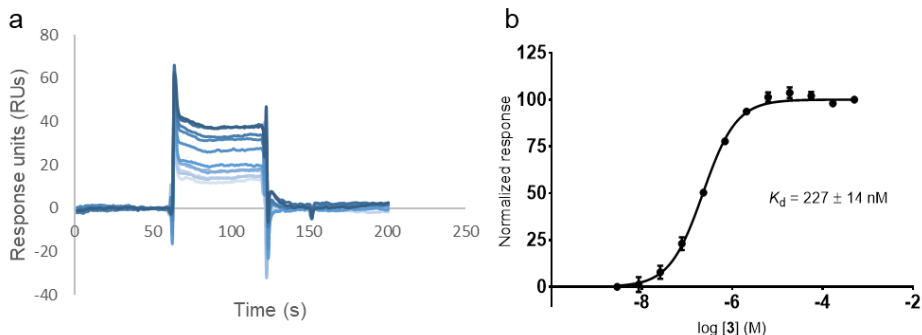


**Figure S3.1. Determination of affinity ER $\alpha$ (pT<sup>594</sup>) phosphopeptide 3 for 14-3-3 $\zeta$  by SPR.** (a) Representative example of an SPR sensorgram in which increasing concentrations of 3 were flowed over immobilized 14-3-3 $\zeta$ . The response units (RUs) achieved (y axis) are presented as a function of time in seconds (x axis). For each curve, the RU values at equilibrium response were extracted and fitted in a dose-response curve using a four-parameter logistic model (4PL), shown in (b), against the log of the molar concentration of 3 (mean  $\pm$  SD,  $n = 3$ ). To account for the variations in protein immobilization between runs, the equilibrium RU values were normalized to a 0-100 % interval, where 0% is baseline response and 100% is the mean curve plateau value. Experiment was performed in 1:3 dilution series from an initial concentration of 3 of 500  $\mu$ M.

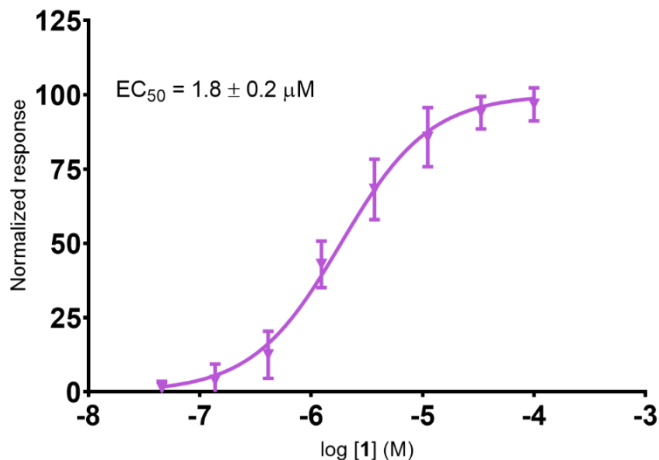


**Figure S3.2. Stabilization of the 14-3-3/ER $\alpha$ (pT<sup>594</sup>) complex by Fusicoccin A (1) measured by SPR.** 1 was titrated (1:3 dilution series, initial concentration 100  $\mu$ M) in the presence of 50 nM ER $\alpha$ (pT<sup>594</sup>) phosphopeptide 3 and surface-immobilized 14-3-3 $\zeta$ . Binding affinity was estimated to be  $EC_{50} = 1.8 \pm 0.2$   $\mu$ M by curve fitting using a four-parameter logistic model (4PL). Error bars show standard deviation from the mean for each data point ( $n = 3$ ). To account for the variations in protein immobilization between runs, the equilibrium RU values were normalized to a 0-100 % interval, where 0% is baseline response and 100% is the mean curve plateau value.

## CHAPTER 3

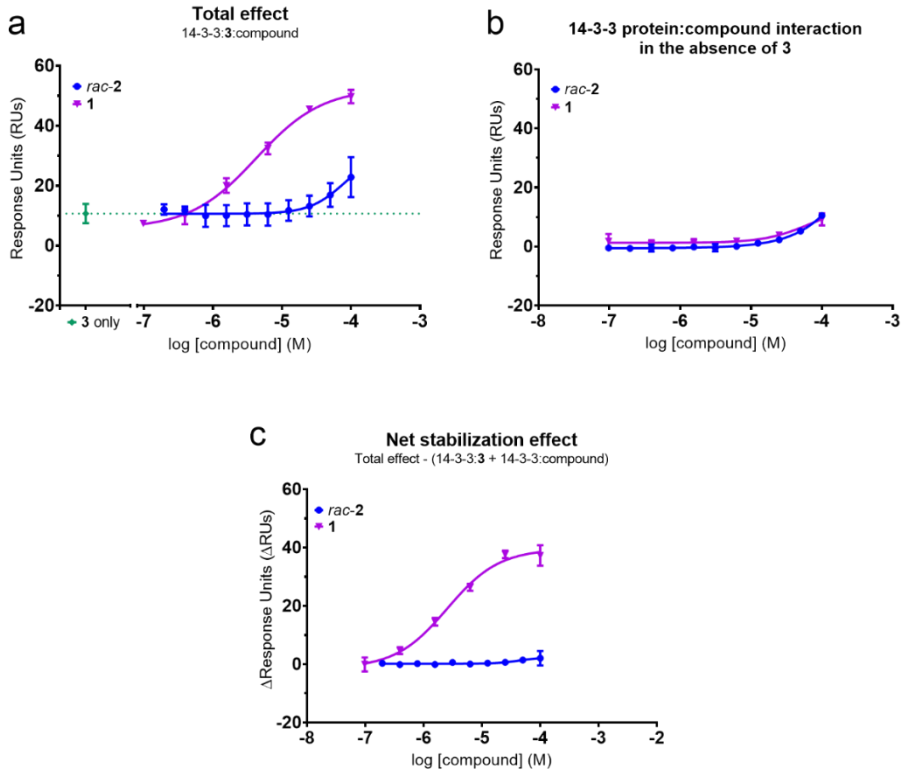


**Figure S3.3. Comparison of the stabilization effect of *rac-2* and 1 on the 14-3-3/ER $\alpha$ (pT<sup>594</sup>) complex measured by SPR (in the absence of added Mg<sup>2+</sup>).** Compound (*rac-2* or 1) concentration (x axis) is plotted as the log of the molar compound concentration. (a) “Total effect” is the total RU obtained by adding compound (*rac-2* or 1) to immobilised 14-3-3 $\zeta$  in the presence of 50 nM ER $\alpha$ (pT<sup>594</sup>) phosphopeptide **3**, i.e. (affinity for 14-3-3 $\zeta$  + affinity for 14-3-3 $\zeta$ /**3** complex + stabilization of 14-4-4 $\zeta$ /**3** interaction). RU obtained from 14-3-3 $\zeta$ /**3** interaction (“**3** only”) indicated by dashed line (10.7  $\pm$  2.6 RU). (b) Determination of contribution of compound affinity for immobilized 14-3-3 $\zeta$  protein in the absence of ER $\alpha$ (pT<sup>594</sup>) phosphopeptide **3**. (c) “Net stabilization effect” ( $\Delta$ RU, y-axis) is defined as (total RU from 14-3-3 $\zeta$ /**3**/compound interactions)-(RU from 14-3-3 $\zeta$ /**3** interaction)+(RU from 14-3-3 $\zeta$ /compound interaction)).

## CHAPTER 3

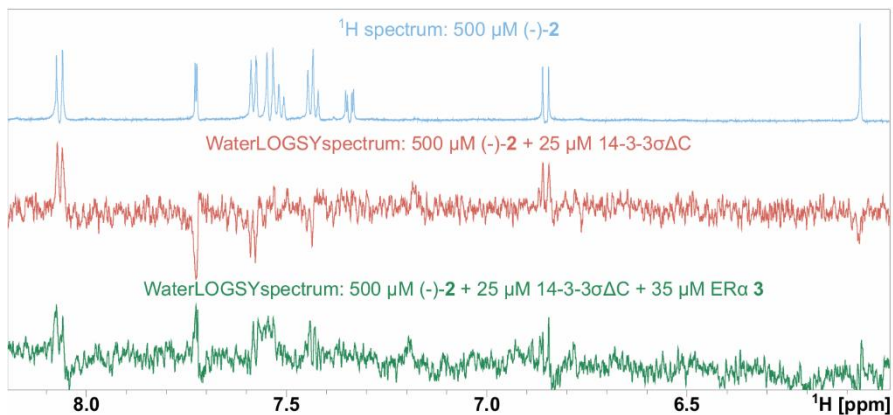


**Figure S3.4.** WaterLOGSY NMR experiments indicate that (-)-(*R*)-2 binds to 14-3-3 $\sigma$  $\Delta$ C both in the absence and presence of ER $\alpha$ (pT<sup>594</sup>) phosphopeptide 3. <sup>1</sup>H spectrum (blue) and WaterLOGSY spectra of 500  $\mu$ M (-)-2 in the presence of either 25  $\mu$ M 14-3-3 $\sigma$  $\Delta$ C (red) or 25  $\mu$ M 14-3-3 $\sigma$  $\Delta$ C+35  $\mu$ M ER $\alpha$ (pT<sup>594</sup>) phosphopeptide 3 (green).

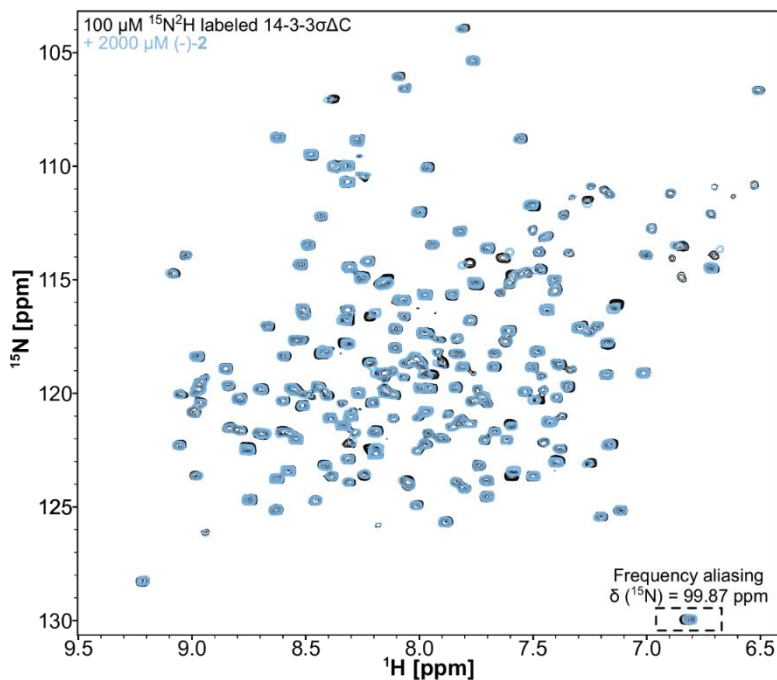


**Figure S3.5.** <sup>1</sup>H-<sup>15</sup>N TROSY-HSQC spectra of 100  $\mu$ M <sup>15</sup>N<sup>2</sup>H labeled 14-3-3 $\sigma$  $\Delta$ C alone (black), or in the presence of 2000  $\mu$ M (-)-2 (superimposed in blue).

## CHAPTER 3

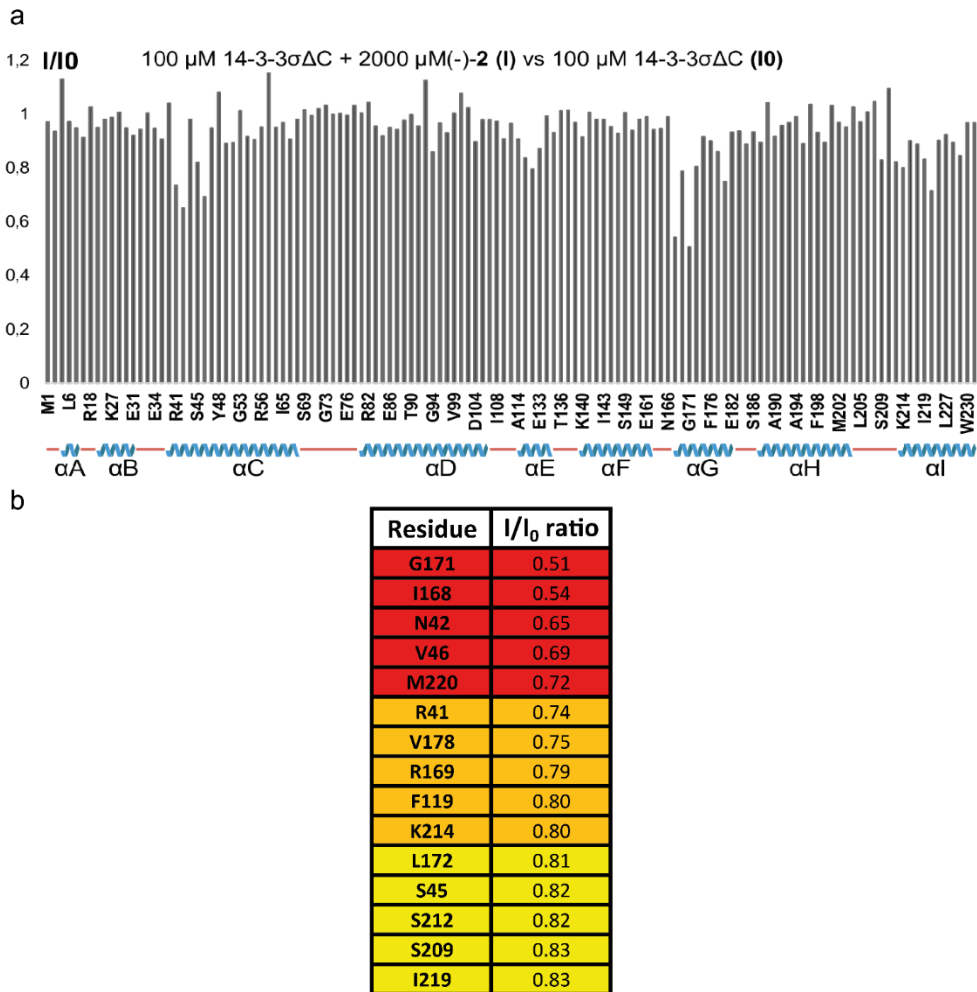


**Figure S3.6. Determination of (-)-(R)-2 binding site on 14-3-3 by chemical shift mapping.** (a) The binding site of (-)-(R)-2 on 14-3-3 $\sigma\Delta\text{C}$  was identified by determining the intensity ratio ( $I/I_0$ ) for each pair of corresponding resonances in the 14-3-3 $\sigma\Delta\text{C}$  spectrum in the presence of (-)-(R)-2 (I) compared to the absence of (-)-(R)-2 ( $I_0$ ). Plot of the  $I/I_0$  values of  $^1\text{H}$ - $^{15}\text{N}$  correlation peak intensities in the spectrum of 100  $\mu\text{M}$   $^{15}\text{N}^2\text{H}$ -labeled 14-3-3 $\sigma\Delta\text{C}$  in the presence of 2000  $\mu\text{M}$  (-)-(R)-2 (I), compared to corresponding resonances in the reference spectrum of 100  $\mu\text{M}$  14-3-3 $\sigma\Delta\text{C}$  ( $I_0$ ) (y axis) versus 14-3-3 $\sigma\Delta\text{C}$  amino acid sequence (x axis, not proportional to sequence length). A total of 131 correlation peak intensity ratios are shown. The helices of 14-3-3 $\sigma\Delta\text{C}$  are identified below the x axis as blue cartoons, while disordered regions are represented by red lines. (b) Ranking of the most affected residues of 14-3-3 $\sigma\Delta\text{C}$  by the binding of (-)-(R)-2. The 5 most affected residues are colored red, the next 5 orange and the next 5 yellow.

CHAPTER 3

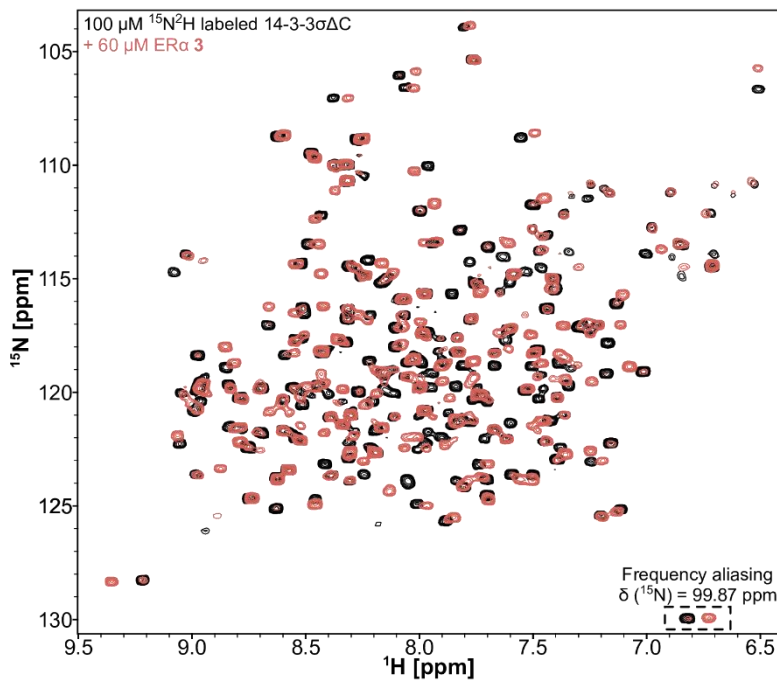


**Figure S3.7.**  $^1\text{H}$ - $^{15}\text{N}$  TROSY-HSQC spectra of 100  $\mu\text{M}$   $^{15}\text{N}^2\text{H}$ -labeled 14-3-3 $\sigma\Delta\text{C}$  alone (black), or in the presence of 60  $\mu\text{M}$  ER $\alpha$ (pT $^{594}$ ) phosphopeptide **3** (superimposed in red). Note that for some resonances, both the free and the bound form are observed, suggesting a slow exchange regime on the NMR time scale.



CHAPTER 3

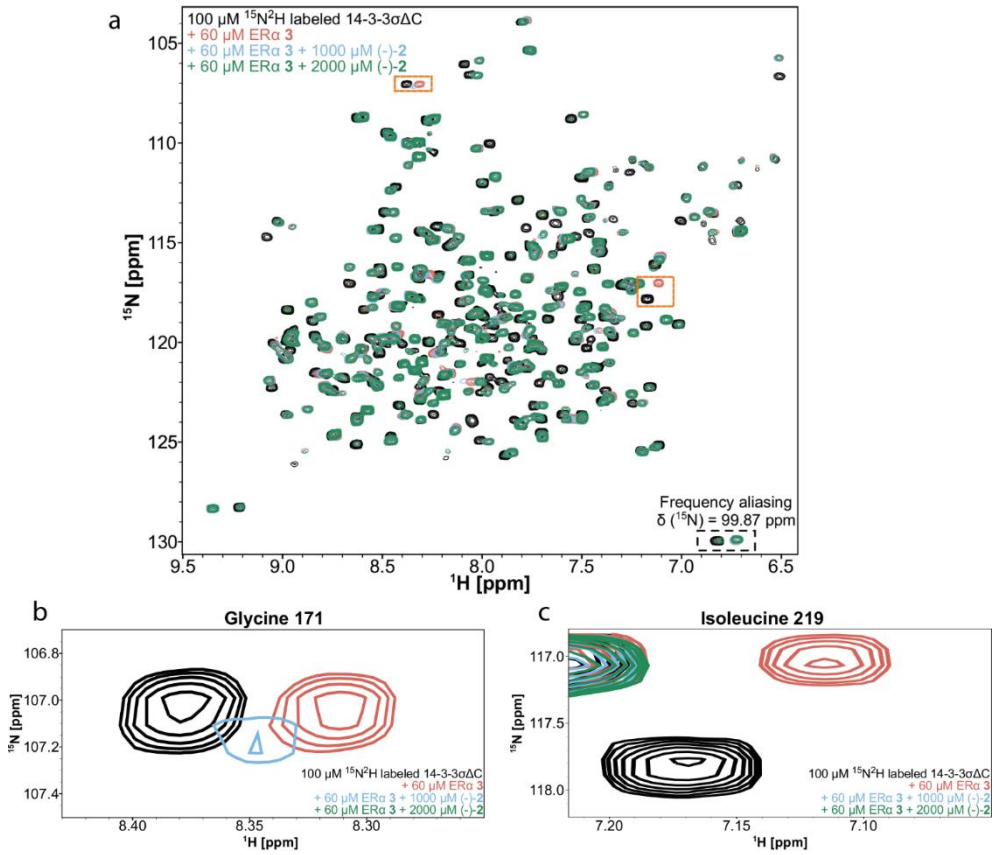


**Figure S3.8.**  $^1\text{H}$ - $^{15}\text{N}$  TROSY-HSQC experiments show that  $(-)-(R)$ -2 binds in the FC pocket. (a)  $^1\text{H}$ - $^{15}\text{N}$  TROSY-HSQC spectra of  $100\ \mu\text{M}$   $^{15}\text{N}^2\text{H}$ -labeled 14-3-3 $\sigma\Delta\text{C}$  alone (black), or in the presence of  $60\ \mu\text{M}$  ER $\alpha$ (pT $^{594}$ ) phosphopeptide **3** (superimposed in red),  $60\ \mu\text{M}$  ER $\alpha$ (pT $^{594}$ ) phosphopeptide **3**+ $1000\ \mu\text{M}$   $(-)-(R)$ -2 (superimposed in blue) or  $60\ \mu\text{M}$  ER $\alpha$ (pT $^{594}$ ) phosphopeptide **3**+ $2000\ \mu\text{M}$   $(-)-(R)$ -2 (superimposed in green). The spectral regions delimited by orange dashes are enlarged in b and c. (b, c) Overlaid enlarged spectral regions showing the resonances corresponding to G171 (b) and I219 (c).  $1000\ \mu\text{M}$   $(-)-(R)$ -2 induced broadening beyond detection of the resonance of G171 (blue spectrum), while  $2000\ \mu\text{M}$   $(-)-(R)$ -2 induced broadening beyond detection of the resonance (green spectrum). For I219, broadening beyond detection of the resonance (blue spectrum) was observed already at  $1000\ \mu\text{M}$   $(-)-(R)$ -2.

## CHAPTER 3

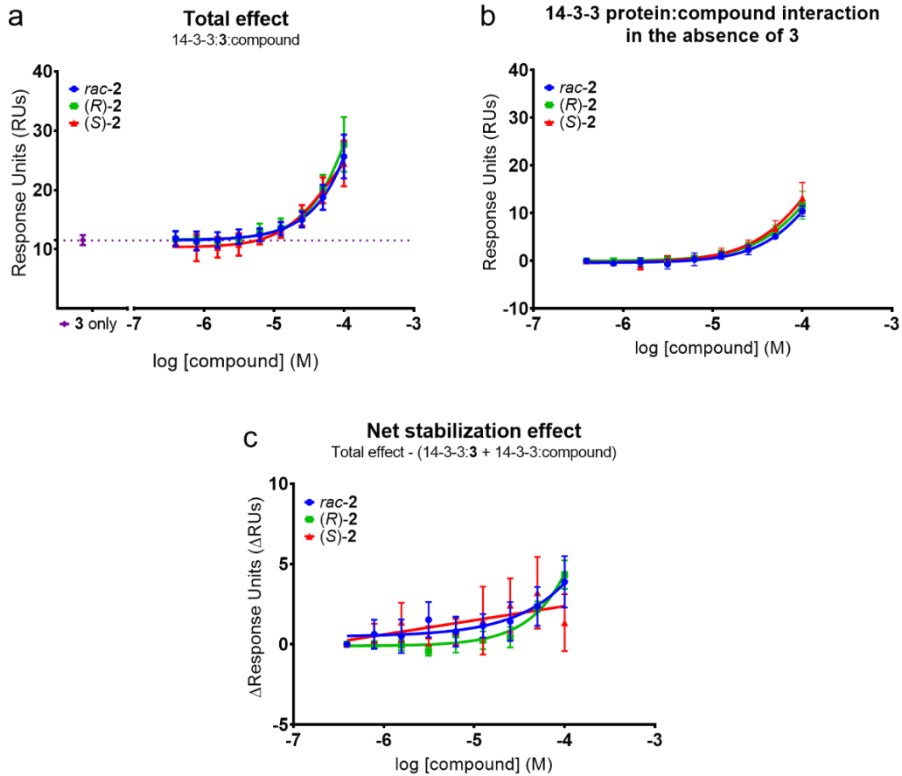


**Figure S3.9. Comparison of the stabilization effect of *rac*-2, (*R*)-2 and (*S*)-2 on the 14-3-3/ ER $\alpha$ (pT<sup>594</sup>) complex measured by SPR (in the absence of added Mg<sup>2+</sup>).** Compound (*rac*-, (*R*)- or (*S*)-2) concentration (x axis) is plotted as the log of the molar compound concentration. (a) “Total effect” is the total RUs afforded by adding compound (*rac*-, (*R*)- or (*S*)-2) to immobilized 14-3-3 $\zeta$  in the presence of 50 nM ER $\alpha$ (pT<sup>594</sup>) phosphopeptide **3**, i.e. (affinity for 14-3-3 $\zeta$  + affinity for 14-3-3 $\zeta$ /**3** complex + stabilization of 14-4-4 $\zeta$ /**3** interaction). RUs obtained from 14-3-3 $\zeta$ /**3** interaction (“**3** only”) indicated by dashed line (11.5  $\pm$  0.9 RUs). (b) Determination of compound (*rac*-, (*R*)- or (*S*)-2) affinity for immobilized 14-3-3 $\zeta$  protein in the absence of ER $\alpha$ (pT<sup>594</sup>) phosphopeptide **3**. (c) “Net stabilization effect” ( $\Delta$ RUs, y axis) is defined as (total RUs from 14-3-3 $\zeta$ /**3**/compound interactions)-((RUs from 14-3-3 $\zeta$ /**3** interaction)+(RUs from 14-3-3 $\zeta$ /compound interaction)).

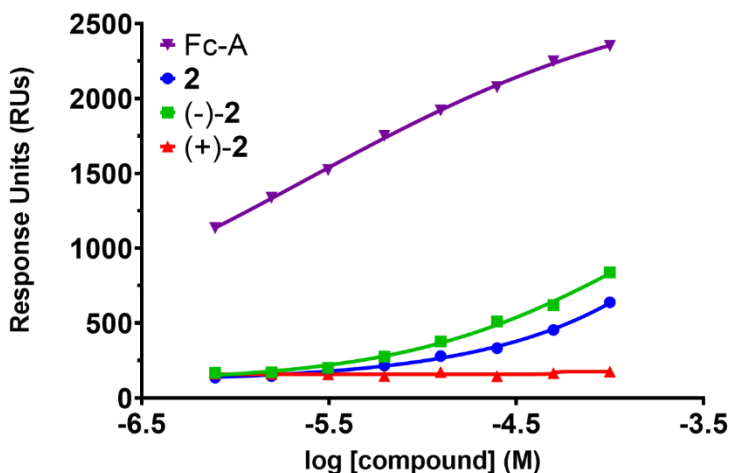


**Figure S3.10.** (-)-2 but not (+)-2 stabilizes the 14-3-3/PMA2 PPI. Measurement by SPR of the stabilization of the 14-3-3 $\eta$ /PMA2 PPI by *rac*-2 (blue dots), (-)-2 (green squares), (+)-2 (red triangles) and 1 (purple inverse triangles), in the presence of 10 mM MgCl<sub>2</sub>. PMA2 peptide was immobilised on a CMD200M chip via EDC/NHS coupling chemistry, at 8000 RUs. 14-3-3 $\eta$  (10  $\mu$ M) and increasing concentrations of compound (1:2 dilution series, 100  $\mu$ M initial concentration, n = 1) were premixed and injected at a flowrate of 20  $\mu$ L/min at 20  $^{\circ}$ C for 120 s in running buffer, followed by a single injection of 0.5% SDS for 60 s as regeneration step between concentrations.

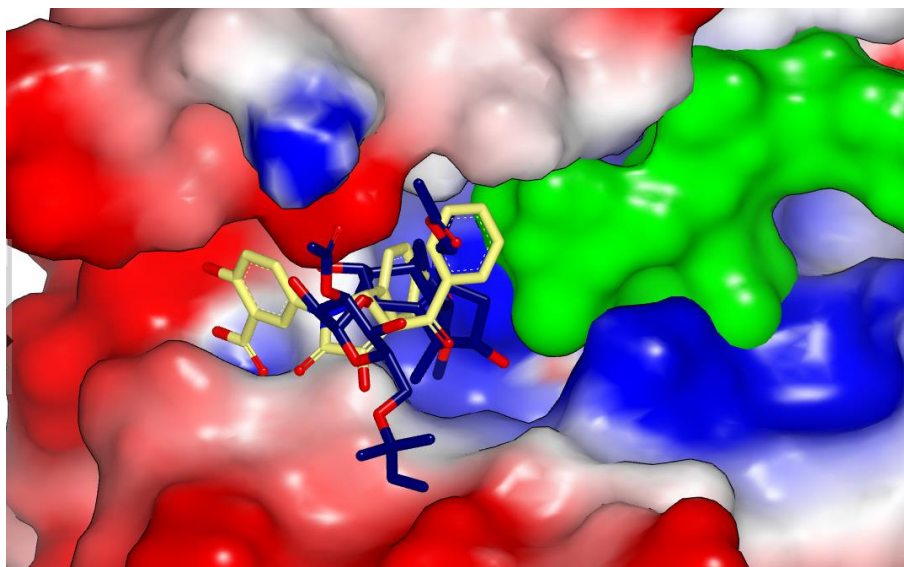


**Figure S3.11.** The salicylate moiety of (*R*)-2 occupies a subpocket not utilized by Fusicoccin A. Comparison of the binding modes in the FC pocket of Fusicoccin A 1 (dark blue sticks, rendered from PDB 4JDD) and (*R*)-2 (yellow sticks, rendered from PDB 6TJM) in 14-3-3 $\sigma\Delta$ C/ER $\alpha$ (pT<sup>594</sup>) phosphopeptide 3 complex (rendered from PDB 4JDD, 14-3-3  $\sigma\Delta$ C protein surface coloured according to electrostatic potential, ER $\alpha$ (pT<sup>594</sup>) phosphopeptide 3 surface coloured green).

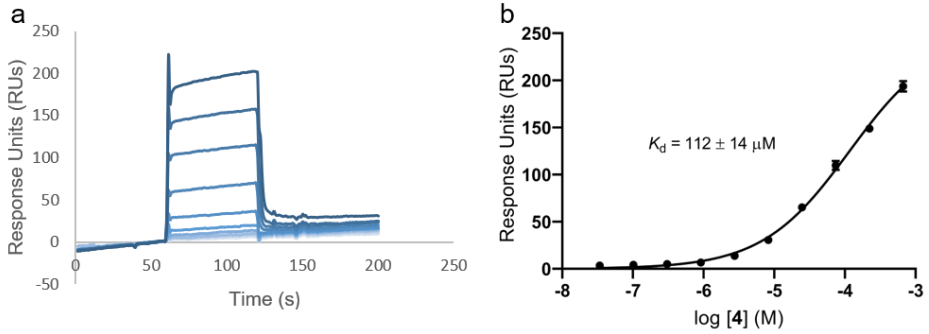


**Figure S3.12. Estimation of affinity of CaMKK2(pS<sup>100</sup>) phosphopeptide 4 for 14-3-3 $\zeta$  by SPR.** (a) Representative example of an SPR sensorgram in which increasing concentrations of 4 were flowed over immobilized 14-3-3 $\zeta$ . The Response Units (RUs) achieved (y axis) are presented as a function of time in seconds (x axis). For each curve, the values at equilibrium response (i.e. binding coverage) were extrapolated and fitted in a dose-response curve using a four-parameter logistic model (4PL), shown in (b), against the log of the molar concentration of 4 (mean  $\pm$  SD, n = 3). Titration was performed in 1:3 dilution series from an initial concentration of 4 of 667  $\mu\text{M}$ . Unspecific binding at higher concentrations of 4 precluded determination of a full dose-response curve.

## CHAPTER 3

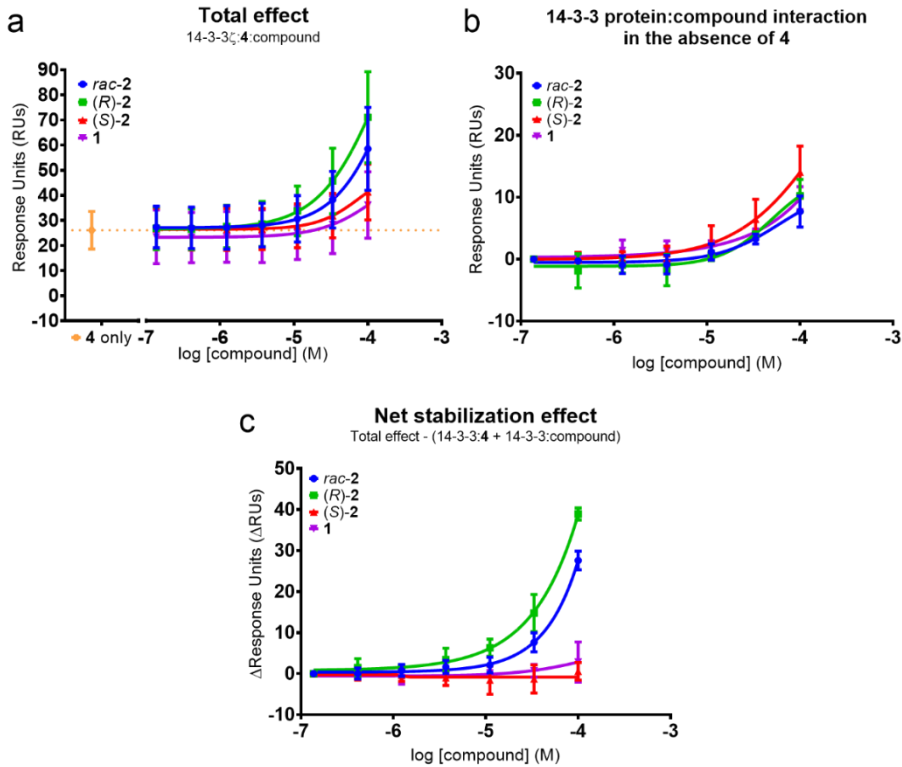


**Figure S3.13. Comparison of the stabilization effect of 1 and *rac*-, (*R*)- or (*S*)-2 on the 14-3-3/CaMKK2(pS<sup>100</sup>) complex measured by SPR (in the absence of added Mg<sup>2+</sup>).** Compound concentration (x axis) is plotted as the log of the compound concentration in molar. (a) "Total effect" is the total RUs afforded by adding compound (1, *rac*-, (*R*)- or (*S*)-2) to immobilised 14-3-3 $\zeta$  in the presence of 30  $\mu$ M CaMKK2(pS<sup>100</sup>) phosphopeptide 4, i.e. (affinity for 14-3-3 $\zeta$  + affinity for 14-3-3 $\zeta$ /4 complex + stabilization of 14-3-3 $\zeta$ /4 interaction). RUs obtained from 14-3-3 $\zeta$ /4 interaction ("4 only") indicated by dashed line (26.1  $\pm$  7.5 RUs). (b) Determination of contribution of compound affinity for immobilized 14-3-3 $\zeta$  protein in the absence of phosphopeptide 4. (c) "Net stabilization effect" ( $\Delta$ RUs, y axis) is defined as (total RUs from 14-3-3 $\zeta$ /4/compound interaction)-(RUs from 14-3-3 $\zeta$  /4 interaction)+(RUs from 14-3-3 $\zeta$ /compound interaction)).

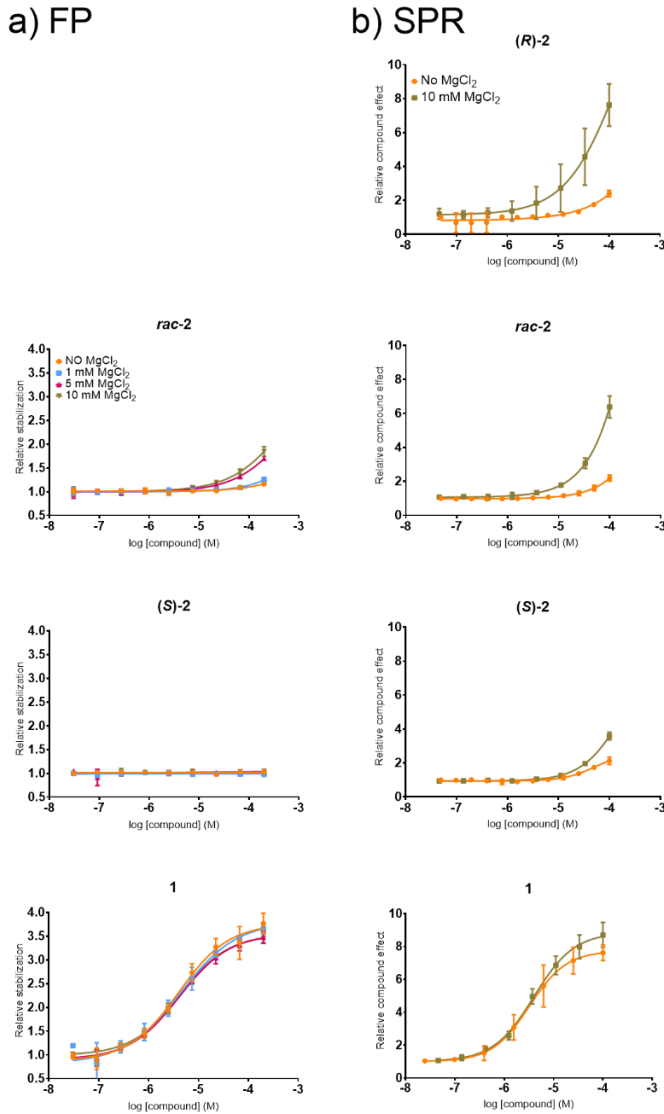


**Figure S3.14. Determination by FP and SPR of the effect of  $\text{MgCl}_2$  on the stabilization of *rac-2*, (*R*)-2, (*S*)-2 and 1 towards the 14-3-3/ $\text{ER}\alpha(\text{pT}^{594})$  complex.** (a) Concentration-response of compounds in FP assay (10 nM FITC-3 and 50 nM 14-3-3 $\zeta$ ) in the absence of  $\text{MgCl}_2$  (orange circles), 1 mM  $\text{MgCl}_2$  (light blue squares), 5 mM  $\text{MgCl}_2$  (red triangles) or 10 mM  $\text{MgCl}_2$  (gold inverse triangles). “Relative stabilization” (y axis) is the mean fold-increase of FP signal over baseline (i.e. FP signal from interaction between 14-3-3 $\zeta$  and  $\text{ER}\alpha(\text{pT}^{594})$  phosphopeptide FITC-3 alone). (b) Concentration-response of compounds in SPR assay in the absence of  $\text{MgCl}_2$  (orange circles) or with 10 mM  $\text{MgCl}_2$  (gold squares). Compound titration was performed in the presence of 50 nM  $\text{ER}\alpha(\text{pT}^{594})$  phosphopeptide 3. “Relative compound effect” is the mean fold-increase of SPR signal over baseline (without correcting for compound binding to 14-3-3 $\zeta$  alone). The error bars indicate +/- SD (n=3).

a) FP

b) SPR

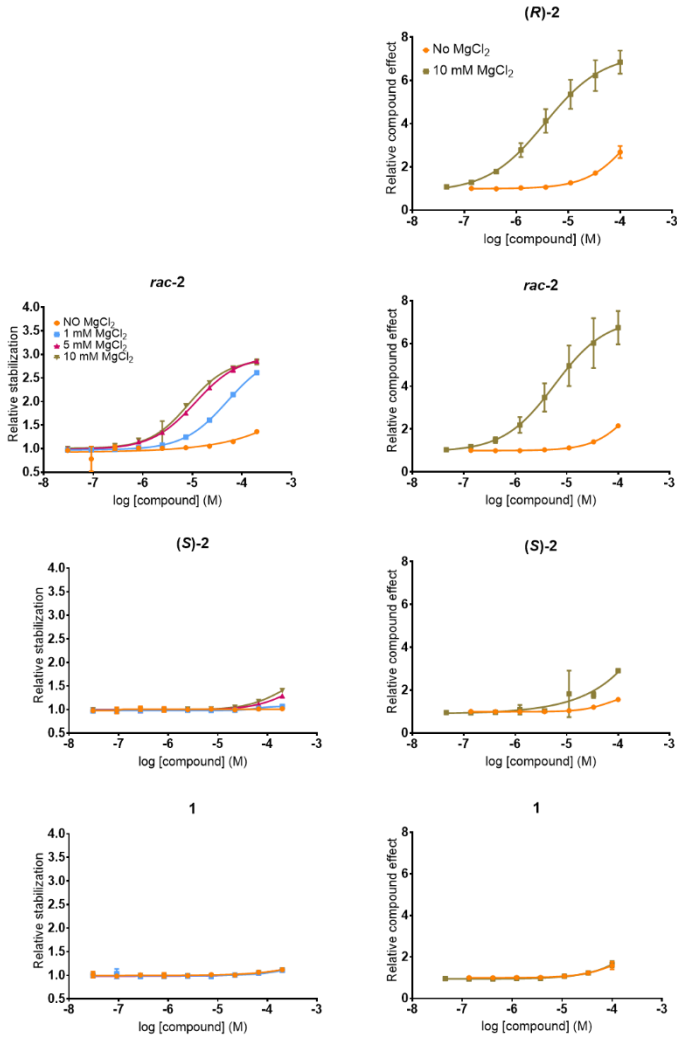


**Figure S3.15. Determination by FP and SPR of the effect of MgCl<sub>2</sub> on the stabilization of 2, (S)-2 and 1 towards the 14-3-3/CaMKK2(pS<sup>100</sup>) complex.** (a) Concentration-response of compounds in FP assay (10 nM FAM-labelled CaMKK2(pS<sup>100</sup>) phosphopeptide FAM-4 and 30 μM 14-3-3ζ) in the absence of MgCl<sub>2</sub> (orange circles), 1 mM MgCl<sub>2</sub> (light blue squares), 5 mM MgCl<sub>2</sub> (red triangles) or 10 mM MgCl<sub>2</sub> (gold inverse triangles). “Relative stabilization” (y axis) is the mean fold-increase of FP signal over baseline (i.e. FP signal from interaction between 14-3-3ζ and labelled CaMKK2(pS<sup>100</sup>) phosphopeptide FAM-4 alone). (b) Concentration-response of compounds in SPR assay in the absence of MgCl<sub>2</sub> (orange circles) or with 10 mM MgCl<sub>2</sub> (gold squares). Compound titration was performed in the presence of 30 μM CaMKK2(pS<sup>100</sup>) phosphopeptide 4. “Relative compound effect” is the mean fold-increase of SPR signal over baseline (without correcting for compound binding to 14-3-3ζ alone). The error bars indicate +/- SD (n=3).

CHAPTER 3

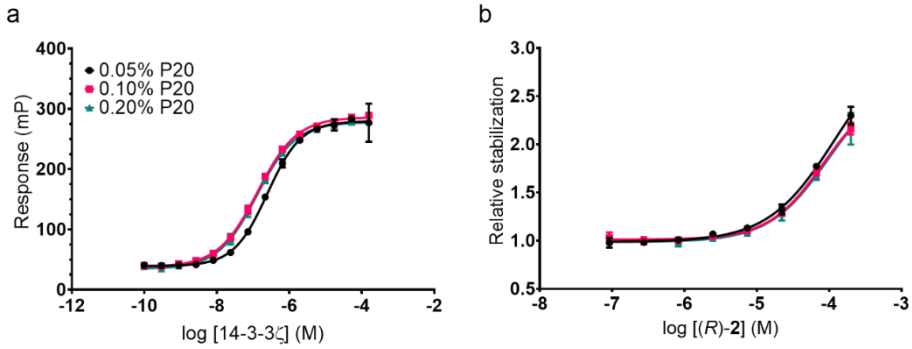
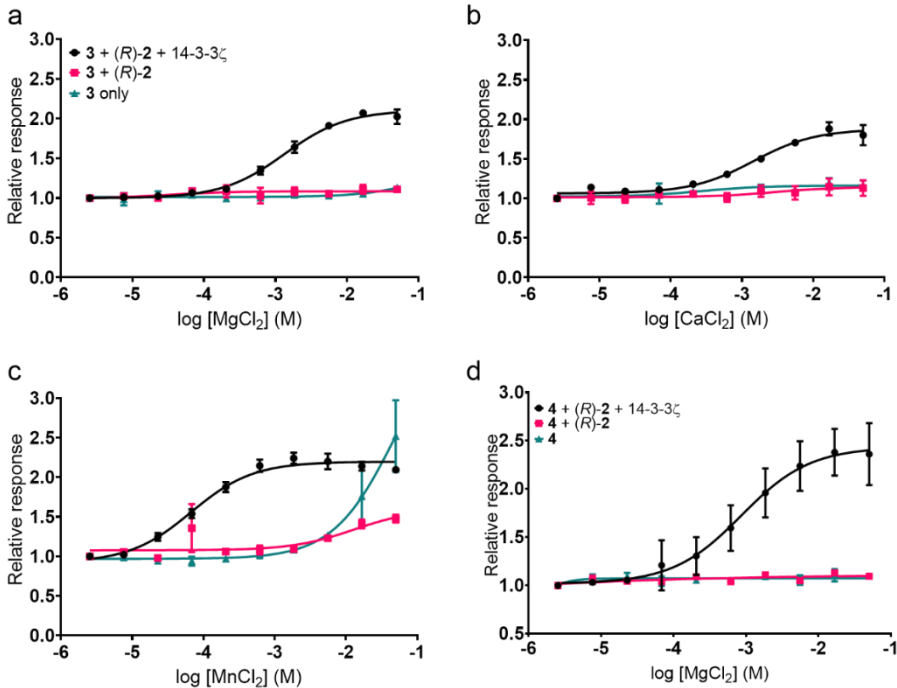


**Figure S3.16. Detergent tolerability test to discount assay interference due to potential aggregation behavior.** Determination of effect of different detergent (Tween20 – P20) concentrations on the affinity of the ER $\alpha$ (pT<sup>594</sup>) phosphopeptide FITC-3 for 14-3-3 $\zeta$  (panel a) and on the stabilization effect promoted by (R)-2 for the 14-3-3 $\zeta$ /ER $\alpha$ (pT<sup>594</sup>) complex (panel b) measured by FP and in the presence of 10 mM Mg<sup>2+</sup>. (a) The FP response (mP, y axis) plotted against the log of the 14-3-3 $\zeta$  concentration (in molar) at different detergent concentrations: 0.05% (black dots), 0.10% (pink squares) and 0.20% (teal triangles). (b) “Relative stabilization” (expressed as mean fold-increase of FP signal over baseline, i.e. interaction between 14-3-3 $\zeta$  and ER $\alpha$ (pT<sup>594</sup>) phosphopeptide FITC-3 alone) plotted versus increasing concentrations of (R)-2. The error bars indicate +/- SD (n=3).





## CHAPTER 3

**Figure S3.17. Effect of bivalent metal ions on stabilization of 14-3-3/ER $\alpha$ (pT<sup>594</sup>) and 14-3-3/CaMKK2(pS<sup>100</sup>) PPIs by (R)-2 in FP assay and various counterscreens.** “Relative response” (y axes) is the mean fold-increase of FP signal over baseline (i.e. interaction between 14-3-3 $\zeta$  and labelled phosphopeptides FITC-3 or FAM-4 alone). Relative response (black circles) plotted versus metal ion concentration (1:3 dilution series, 50 mM initial concentration) at fixed concentrations of (R)-2 (10  $\mu$ M), phosphopeptide (10 nM FITC-3 in panels a-c and FAM-4 in panel d) and 14-3-3 $\zeta$  (50 nM in panels a-c, 30  $\mu$ M in panel d). For the 14-3-3 $\zeta$ /ER $\alpha$ (pT<sup>594</sup>) complex magnesium (panel a), calcium (panel b) and manganese (panel c) were tested, while for the 14-3-3 $\zeta$ /CaMKK2(pS<sup>100</sup>) complex only magnesium was tested (panel d). To rule out protein independent effects, and/or unspecific binding, counterscreens with compound + phosphopeptide only (pink squares) and compound alone (teal triangles) were performed.

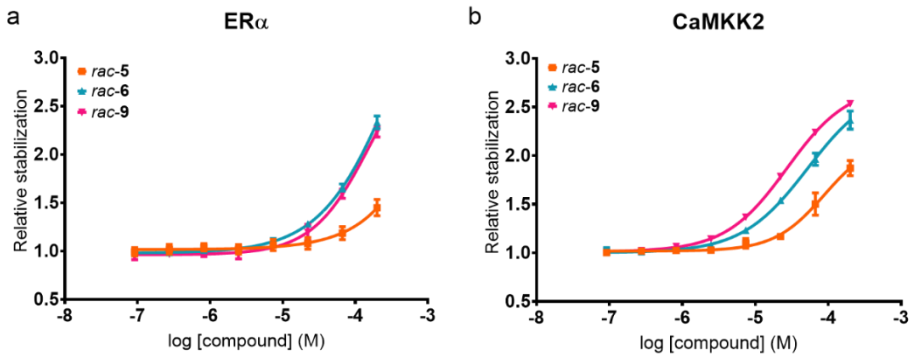


**Figure S3.18. *rac-5*, *rac-6* and *rac-9* stabilize the 14-3-3/ER $\alpha$ (pT<sup>594</sup>) and 14-3-3/CaMKK2(pS<sup>100</sup>) PPIs in the absence of bivalent metal ions.** Stabilization effects of *rac-5*, *rac-6* and *rac-9* measured in FP assays in the absence of added MgCl<sub>2</sub>. (a) Stabilization of the 14-3-3/ER $\alpha$ (pT<sup>594</sup>) PPI (10 nM FITC-3, 50 nM 14-3-3 $\zeta$ ). (b) Stabilization of the 14-3-3/CaMKK2(pS<sup>100</sup>) PPI (10 nM FAM-4, 30  $\mu$ M 14-3-3 $\zeta$ ). “Relative stabilization” (y axis) refers to mean fold increase of FP signal at a given compound concentration over signal observed in absence of compound. The error bars indicate  $\pm$  SD (n=3).

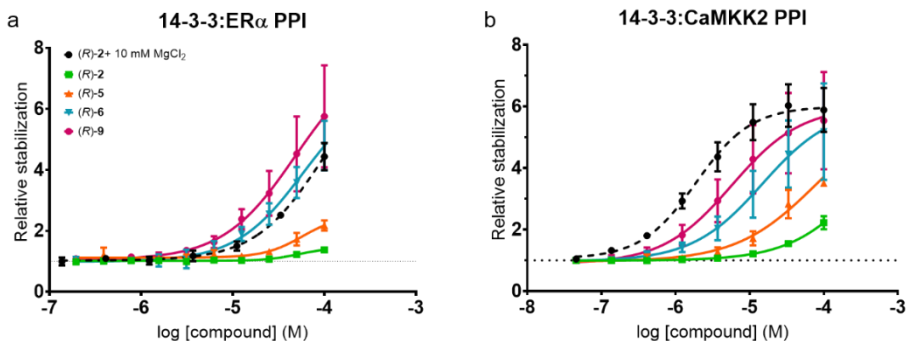


**Figure S3.19. Stabilization of the 14-3-3/ER $\alpha$ (pT<sup>594</sup>) PPI (panel a) and 14-3-3/CaMKK2(pS<sup>100</sup>) PPI (panel b), measured by SPR assay.** “Relative stabilization” (y axes) is defined as ((RUs from 14-3-3 $\zeta$ /3 or 4/compound interactions)-(RUs from 14-3-3 $\zeta$ /compound interaction))/((RUs from 14-3-3 $\zeta$ /3 or 4 interaction).



CHAPTER 3

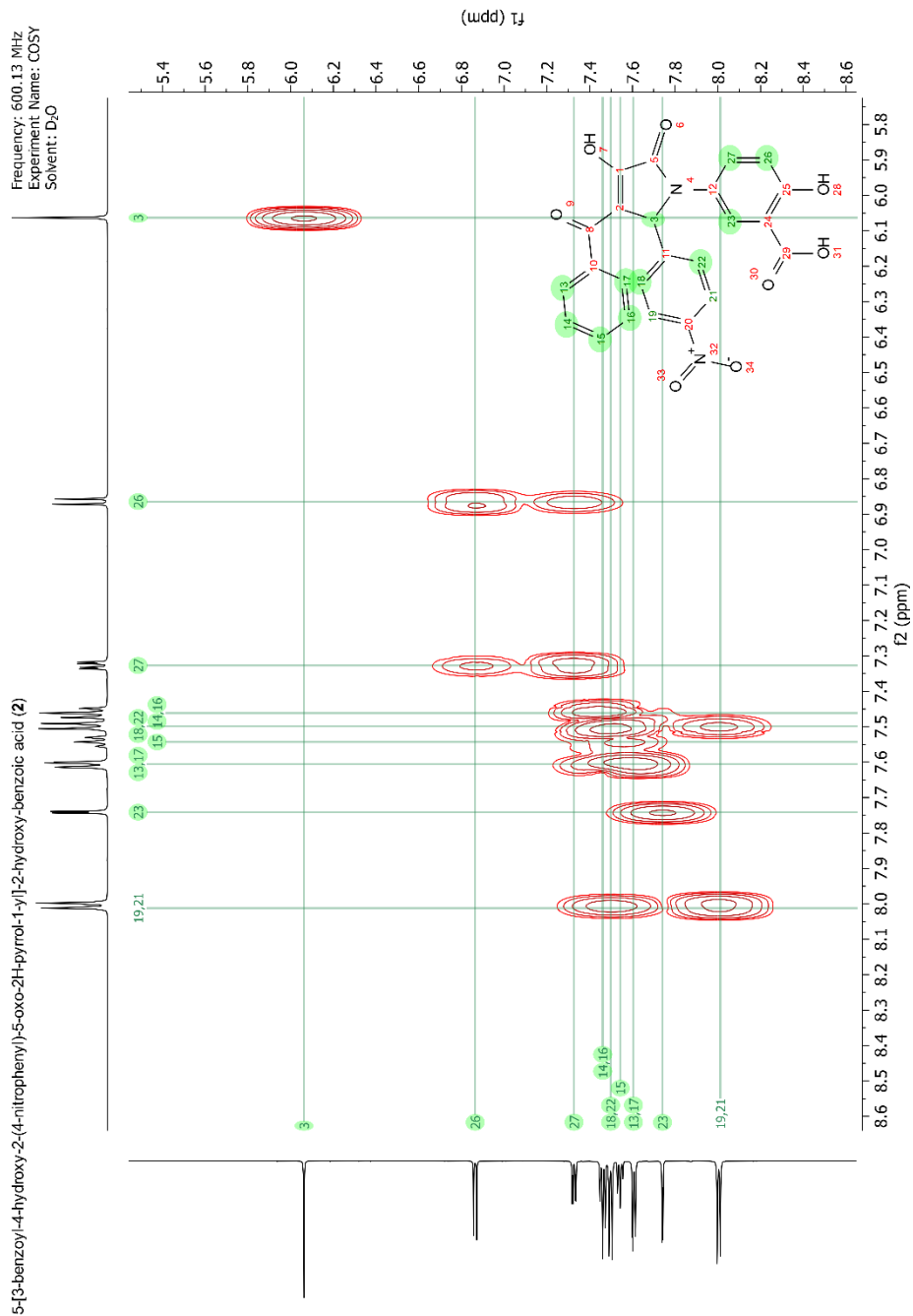


Figure S3.20b. <sup>1</sup>H-<sup>1</sup>H COSY spectrum of *rac*-2.

CHAPTER 3

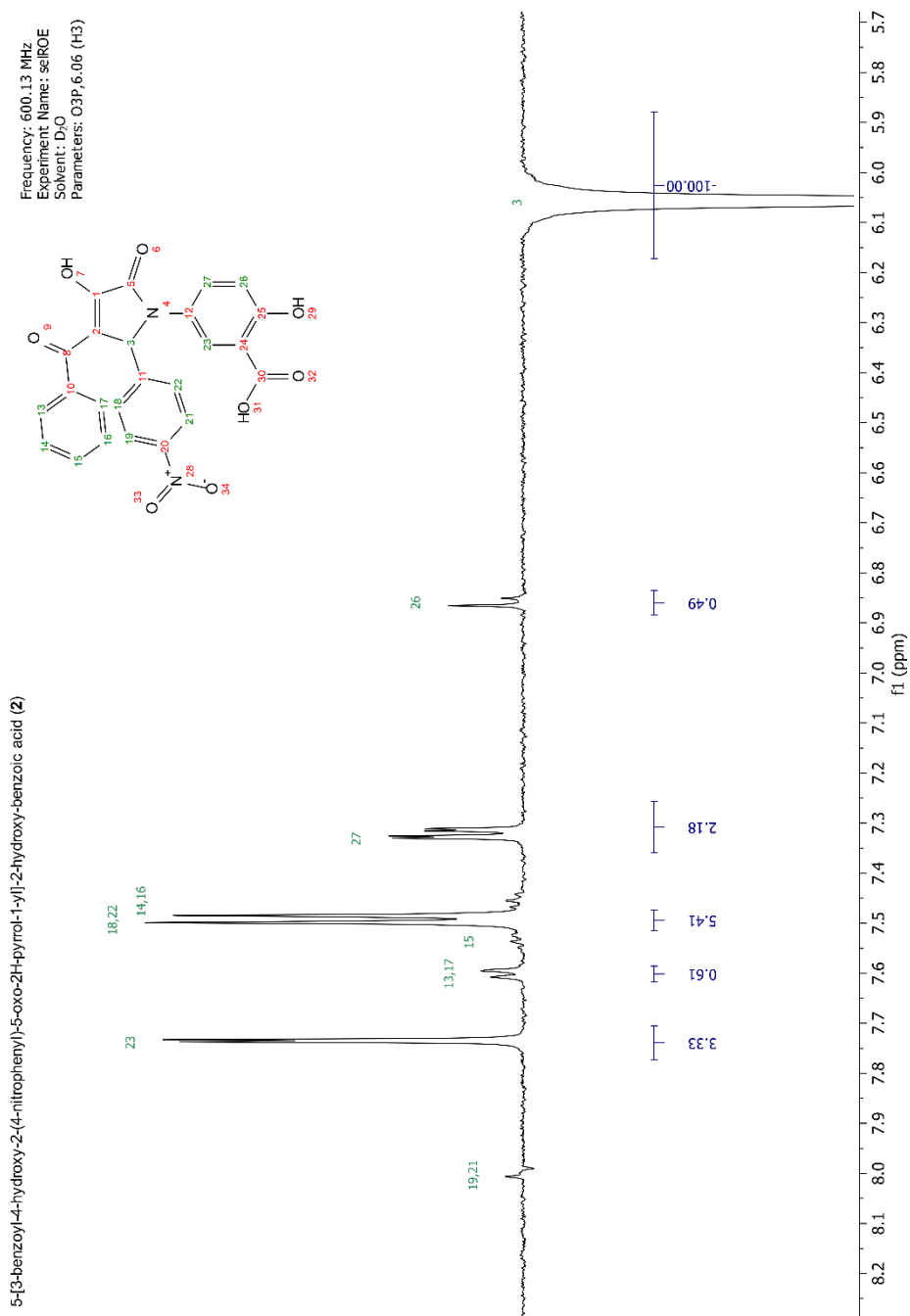
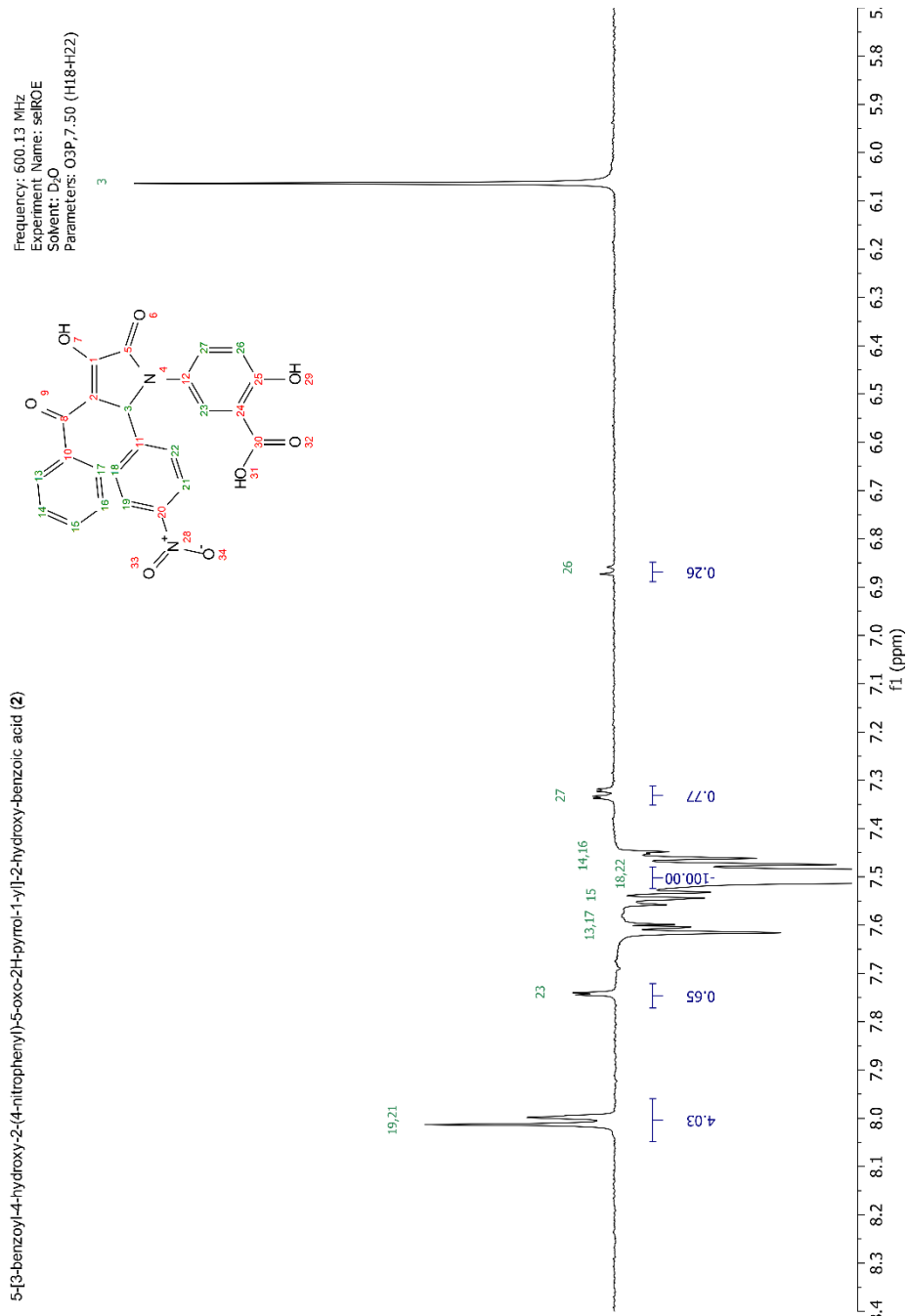
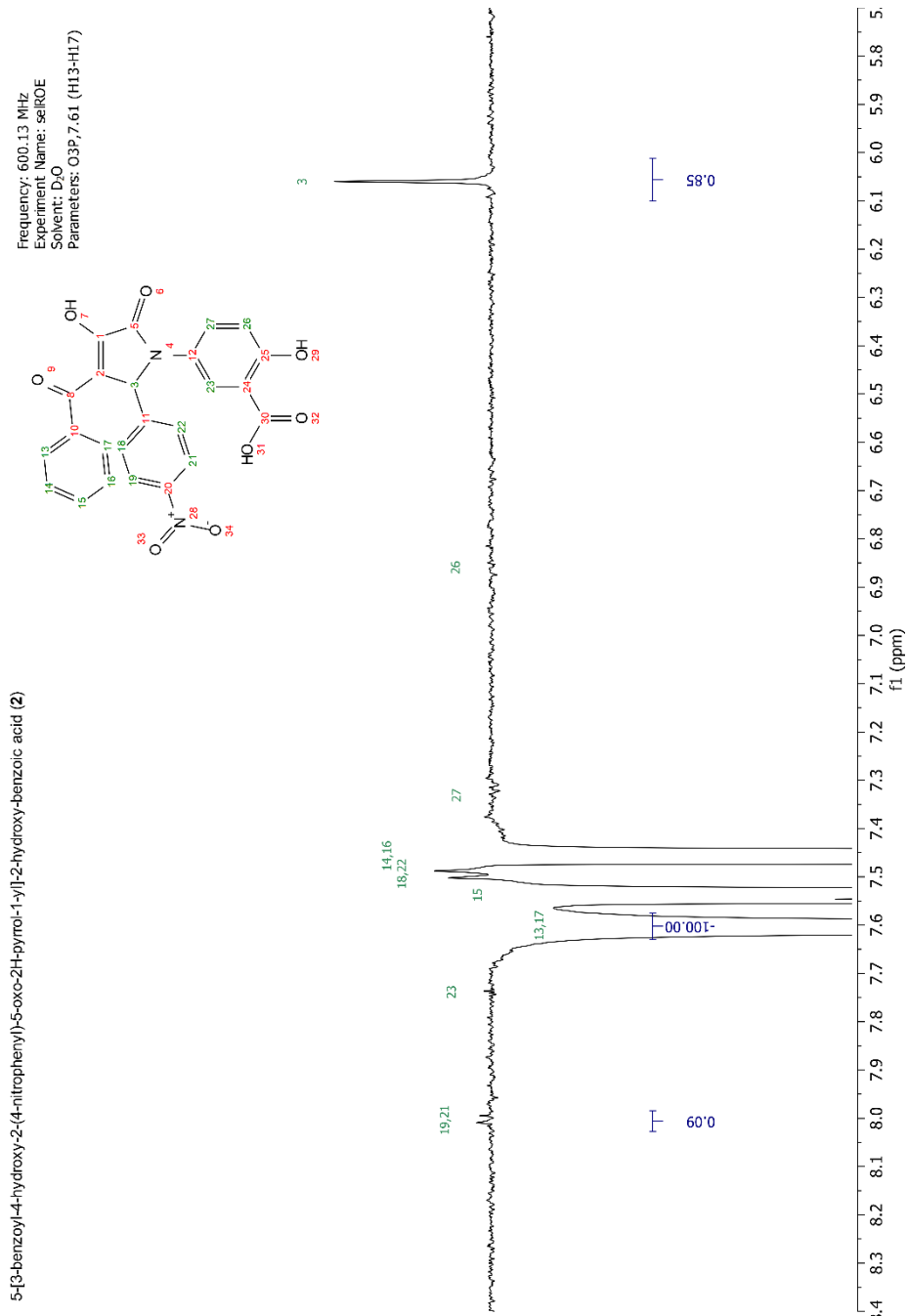


Figure S3.20c. 1D selective ROESY of *rac*-**2** (excitation of H3, 6.06 ppm).



**Figure S3.20d.** 1D selective ROESY of *rac*-**2** (excitation of H18-H22, 7.50 ppm).

CHAPTER 3



**Figure S3.20e.** 1D selective ROESY of *rac*-**2** (excitation of H13-H17, 7.61 ppm).

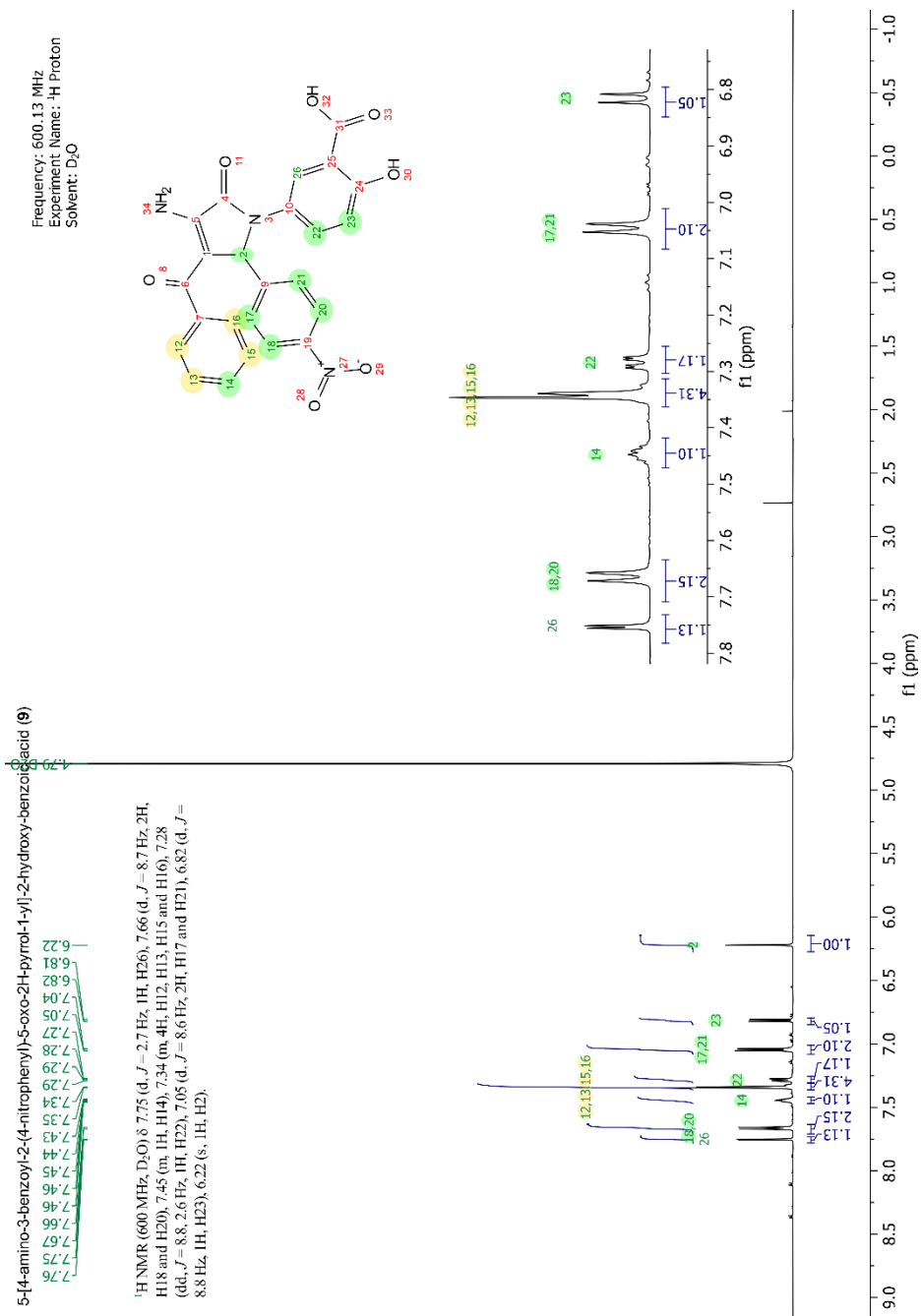


**Figure S3.21a.** <sup>1</sup>H NMR spectrum of *rac*-**9** in D<sub>2</sub>O, with assignments. *Rac*-**9** (3.0 mg, 6.53 μmol) was dissolved in 1 mM NaOH in D<sub>2</sub>O (131 μL, 13.06 μmol) transferred into a 3 mm NMR tube and D<sub>2</sub>O was added to bring final volume to 160 μL.

CHAPTER 3

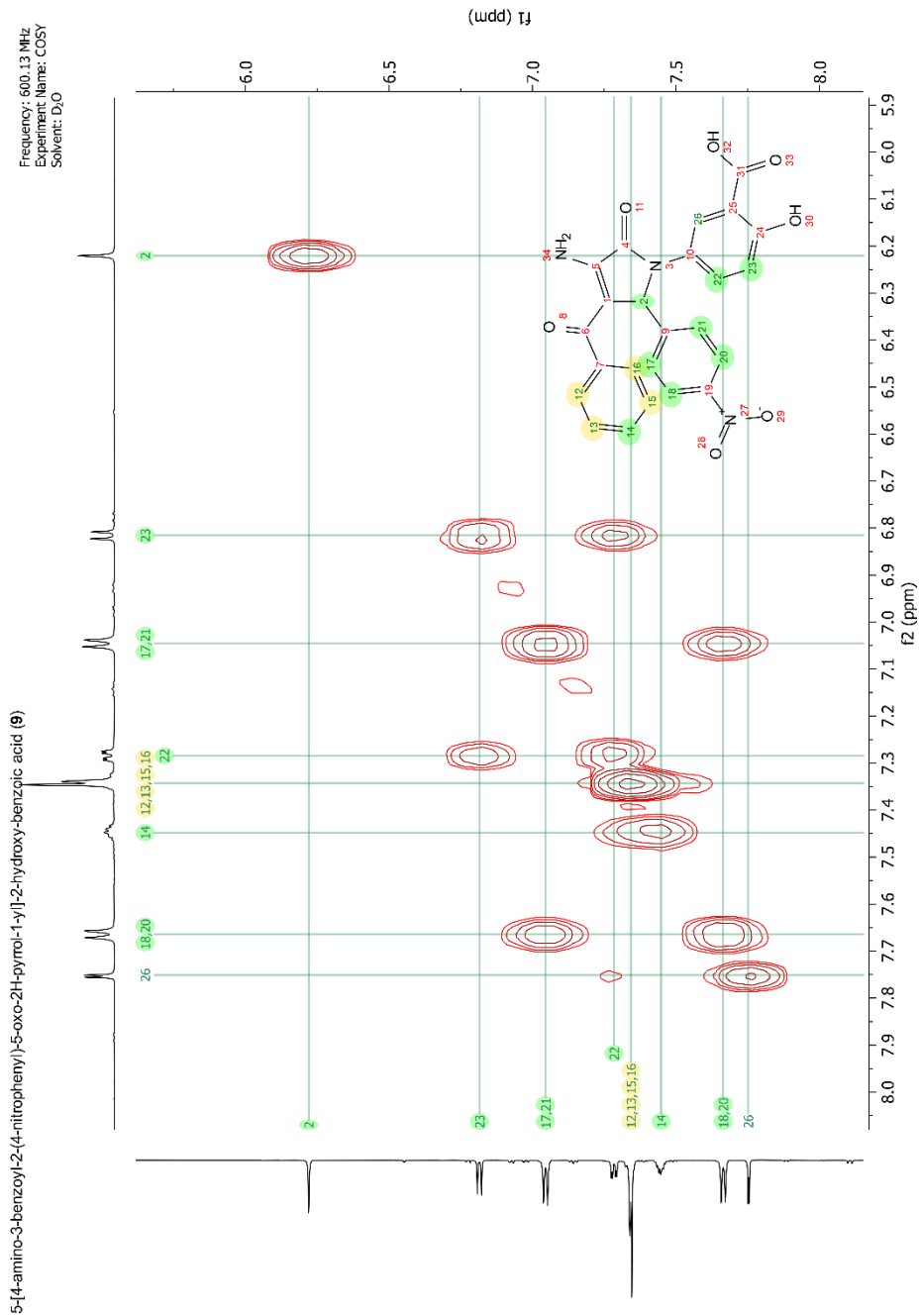
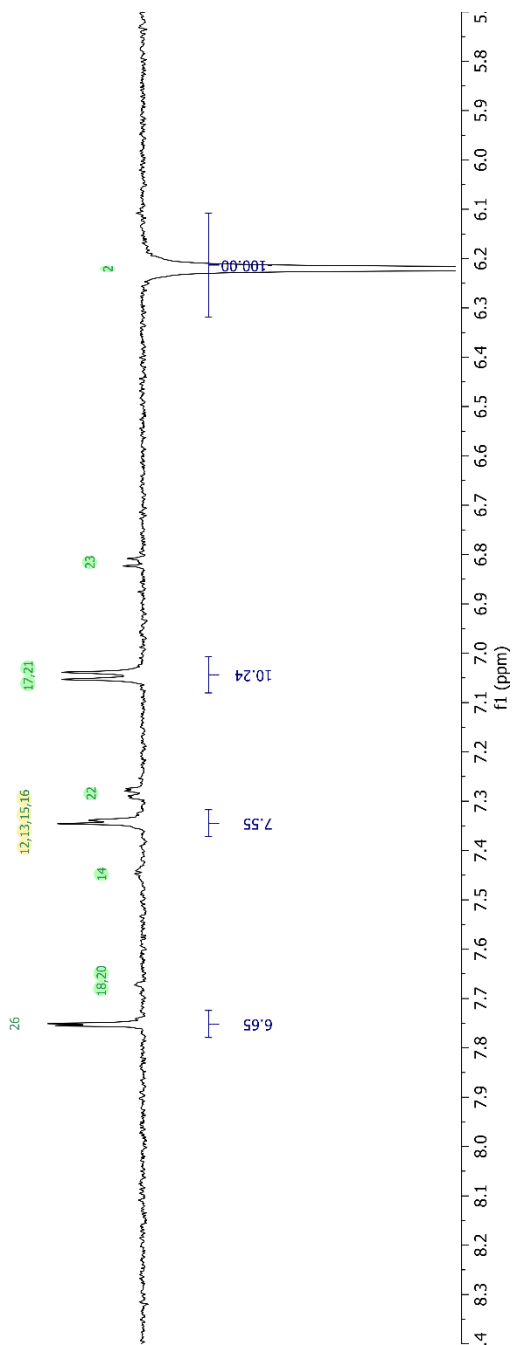
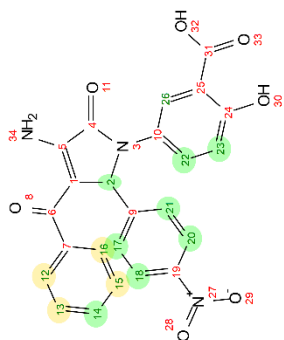


Figure S3.21b. <sup>1</sup>H-<sup>1</sup>H COSY spectrum of *rac*-**9**.



5-[4-amino-3-benzoyl-2-(4-nitrophenyl)-5-oxo-2H-pyridol-1-yl]-2-hydroxy-benzoic acid (**9**)

Frequency: 600.13 MHz  
 Experiment Name: selROE  
 Solvent: D<sub>2</sub>O  
 Parameters: O3P,6.22 (H2)



**Figure S3.21c.** 1D selective ROESY of *rac*-**9** (excitation of H2, 6.22 ppm).

CHAPTER 3

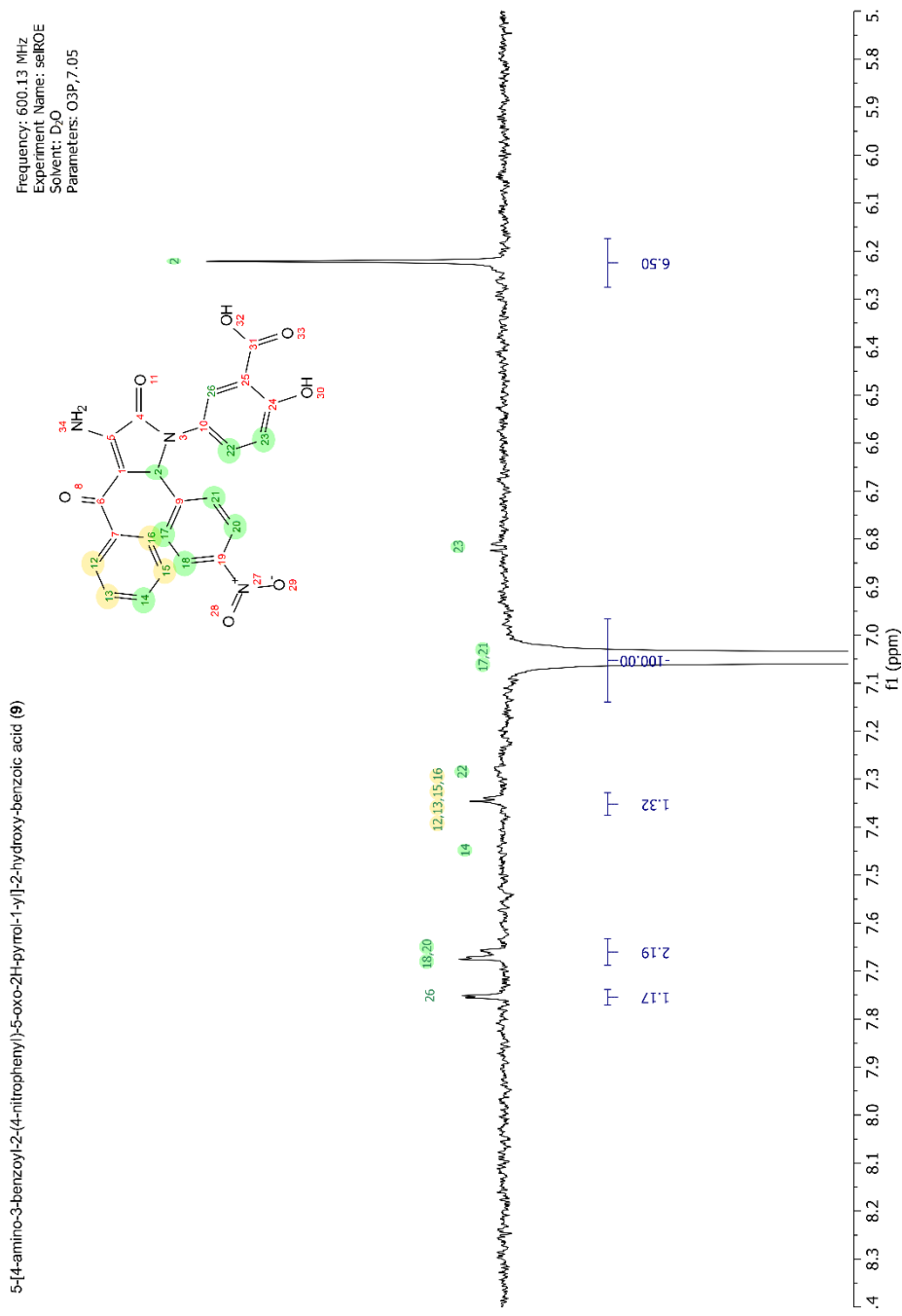
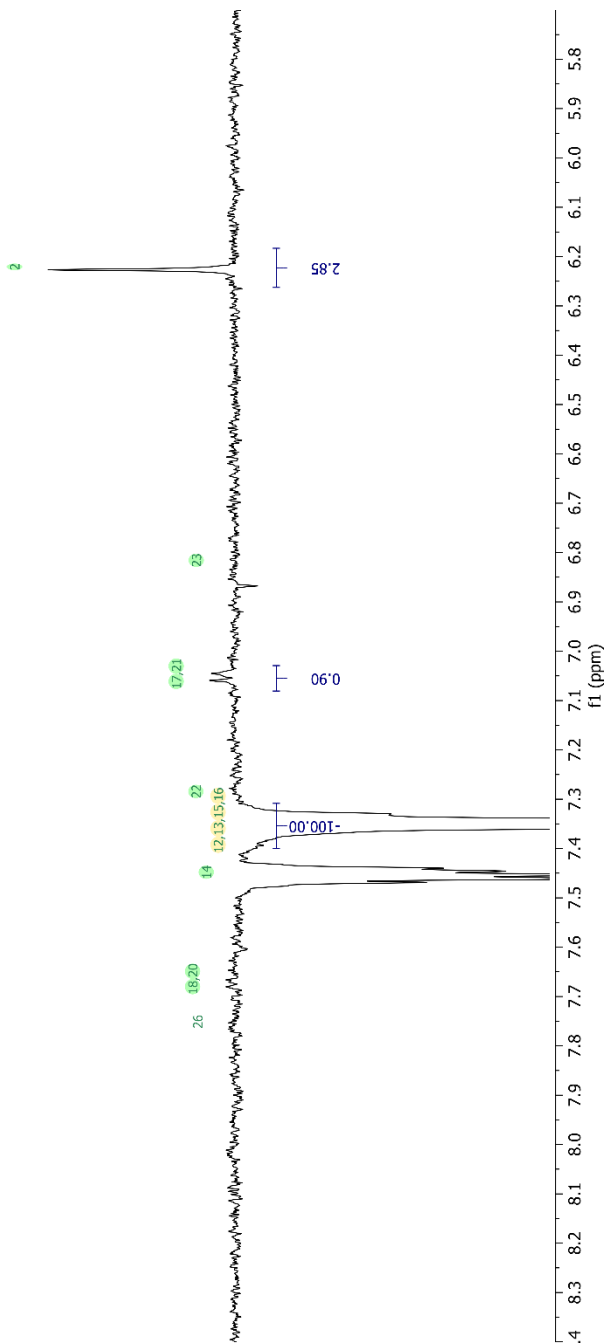
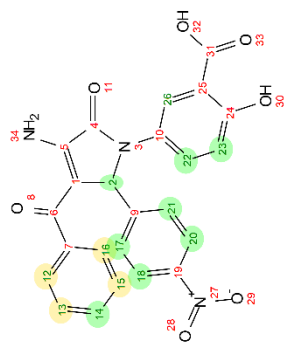


Figure S3.21d. 1D selective ROESY of *rac*-**9** (excitation of H17-H21, 7.05 ppm).

5-[4-amino-3-benzoyl-2-(4-nitrophenyl)-5-oxo-2H-pyridol-1-yl]-2-hydroxy-benzoic acid (**9**)

Frequency: 600.13 MHz  
 Experiment Name: selROE  
 Solvent: D<sub>2</sub>O  
 Parameters: O3P,7.34



**Figure S3.21e.** 1D selective ROESY of *rac*-**9** (excitation of H12-H16, H13-H15 overlapping, 7.34 ppm).



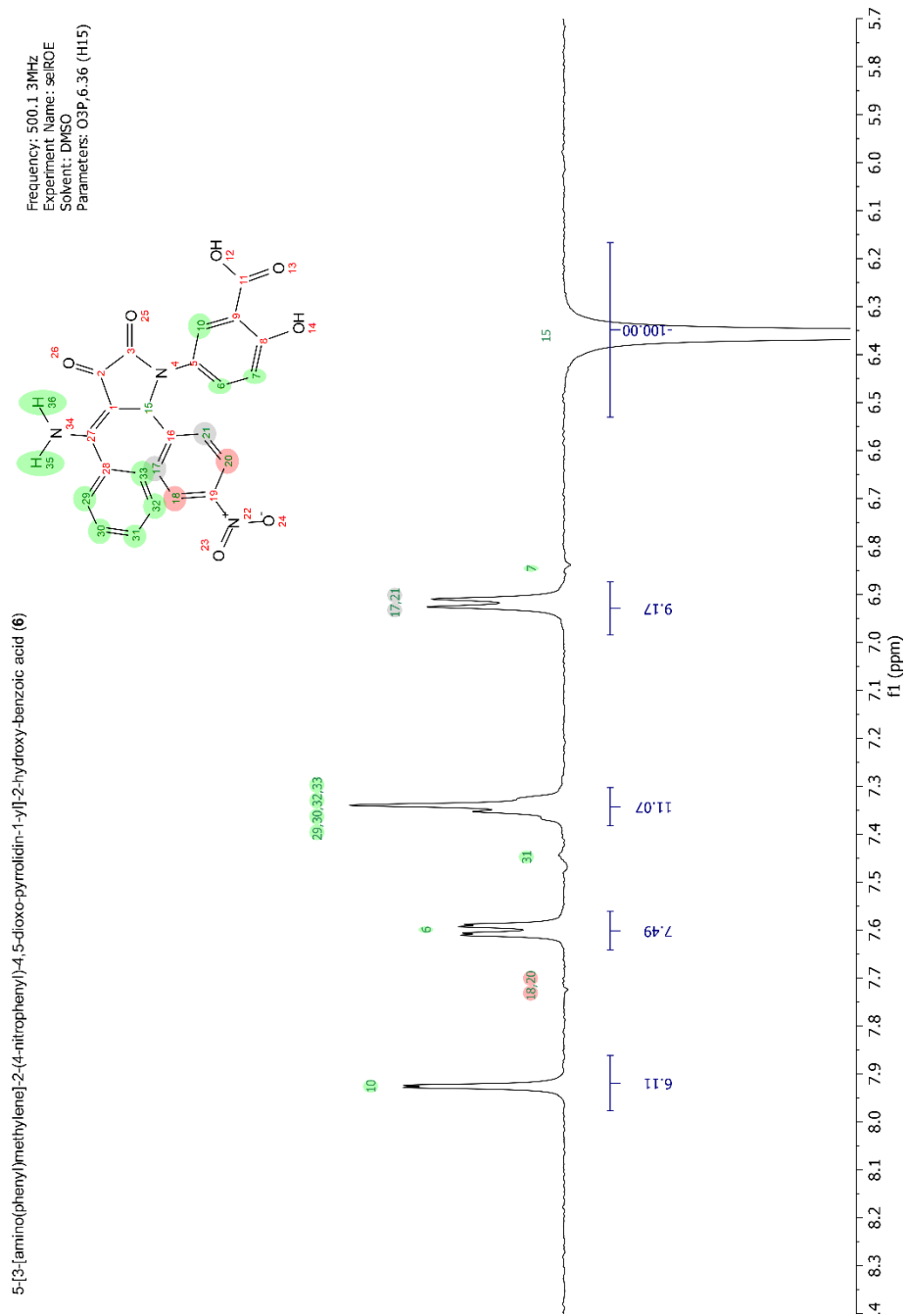


**Figure S3.22b.** 1D selective ROESY of *rac*-**6** (excitation of H15, 6.36 ppm).

CHAPTER 3

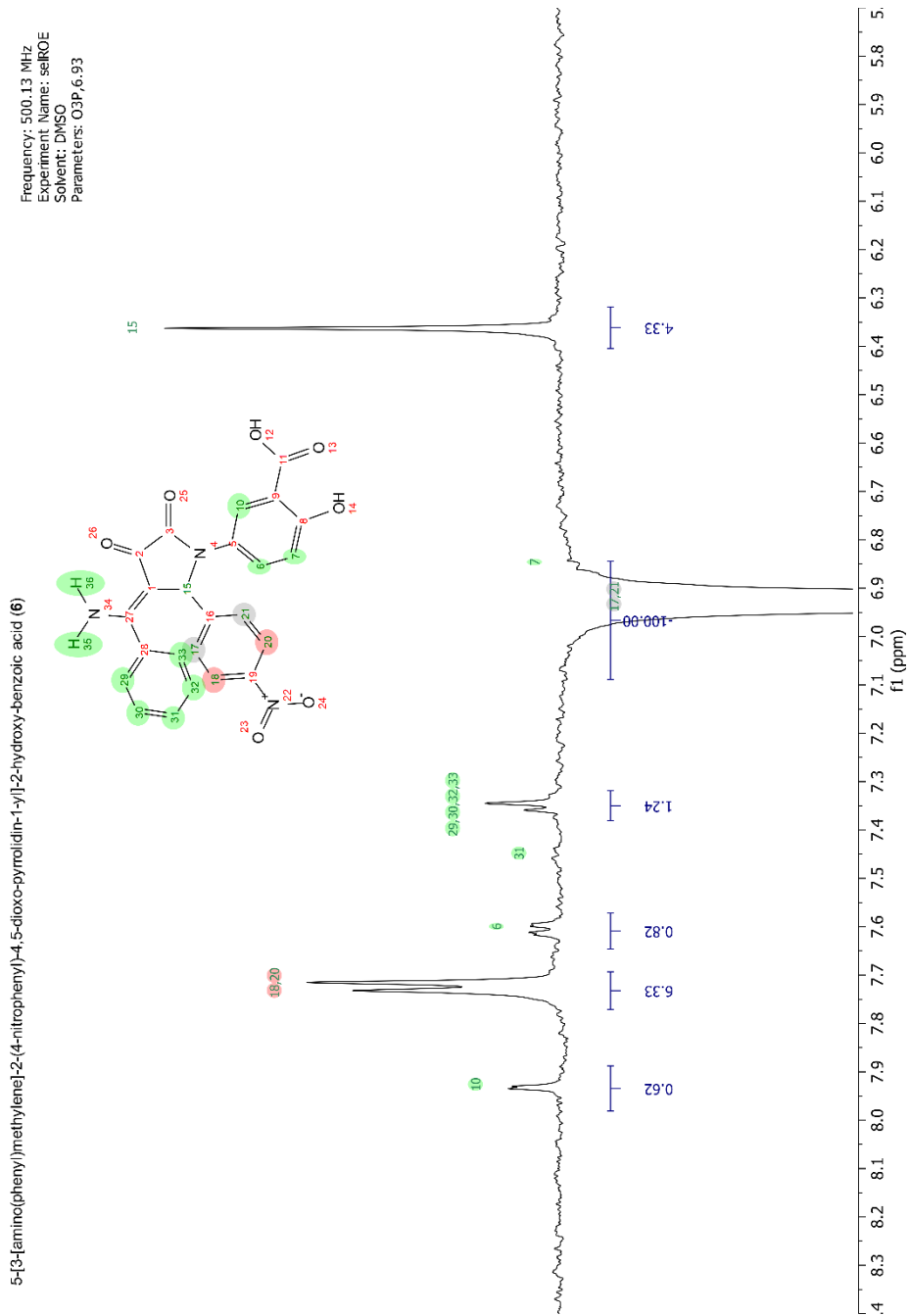
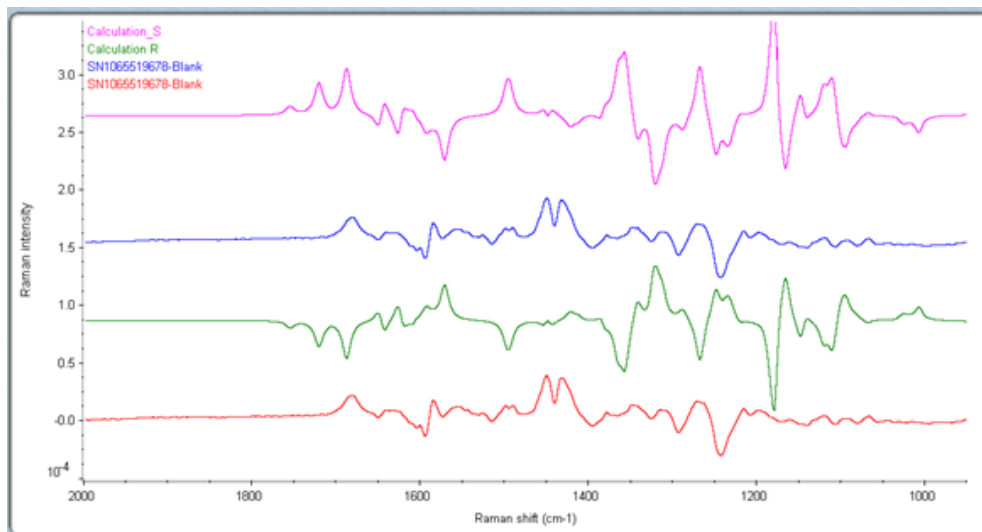
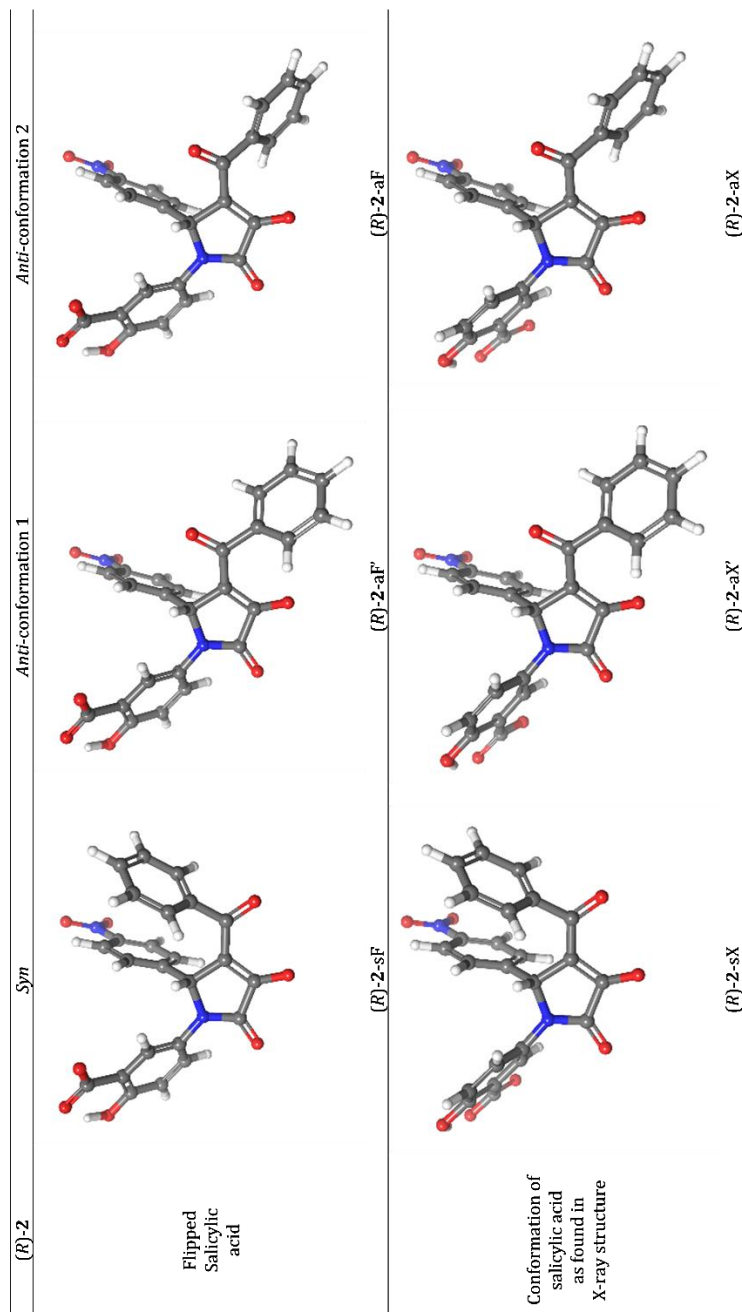


Figure S3.22c. 1D selective ROESY of *rac*-**6** (excitation of H17-H21, 6.93 ppm).

## CHAPTER 3



**Figure S3.23.** Comparison of calculated and experimental spectra: the calculated spectrum for the (*S*) enantiomer is shown in pink and the (*R*) enantiomer (by inversion) in green. There is a reasonable, but not high certainty match between the experimental spectrum of (+)-**2** and the calculated spectrum for the (*S*) enantiomer, particularly in the region 1200-1300 cm<sup>-1</sup>.



**Figure S3.24.** Optimized geometries of the 6 conformations of *(R)*-2 studied in detail illustrating the naming scheme also employed for compounds *(R)*-6 and *(R)*-9.



## CHAPTER 3

**NOTE.** Computational tables reporting conformational energies for ligands (*R*)-**2**, (*R*)-**6**, (*R*)-**9**, the coordinates in Angstrom of the structures optimized by B3LYP-D3/6-31G\*\*+ in combination with the PBF model for water and spectroscopic data of all product can be found at [chem202001608-sup-0001-misc\\_information.pdf](http://chem202001608-sup-0001-misc_information.pdf)

### 3.6 REFERENCES

- [1] J. A. Wells, C. L. McClendon, *Nature* **2007**, *450*, 1001-1009.
- [2] J. Menche, A. Sharma, M. Kitsak, S. D. Ghiassian, M. Vidal, J. Loscalzo, A. L. Barabasi, *Science* **2015**, *347*, 1257601.
- [3] M. Vidal, M. E. Cusick, A. L. Barabasi, *Cell* **2011**, *144*, 986-998.
- [4] T. Ideker, R. Sharan, *Genome Res.* **2008**, *18*, 644-652.
- [5] G. Zinzalla, D. E. Thurston, *Future Med. Chem.* **2009**, *1*, 65-93.
- [6] S. Jaeger, P. Aloy, *IUBMB Life* **2012**, *64*, 529-537.
- [7] D. E. Scott, A. R. Bayly, C. Abell, J. Skidmore, *Nat. Rev. Drug Discovery* **2016**, *15*, 533-550.
- [8] P. Thiel, M. Kaiser, C. Ottmann, *Angew. Chem. Int. Ed.* **2012**, *51*, 2012-2018.
- [9] F. Giordanetto, A. Schafer, C. Ottmann, *Drug Discov Today* **2014**, *19*, 1812-1821.
- [10] V. Azzarito, K. Long, N. S. Murphy, A. J. Wilson, *Nat. Chem.* **2013**, *5*, 161-173.
- [11] E. Sijbesma, K. K. Hallenbeck, S. Leysen, P. J. de Vink, L. Skora, W. Jahnke, L. Brunsveld, M. R. Arkin, C. Ottmann, *J. Am. Chem. Soc.* **2019**, *141*, 3524-3531.
- [12] S. Surade, T. L. Blundell, *Chem. Biol.* **2012**, *19*, 42-50.
- [13] A. Aitken, *Semin. Cancer Biol.* **2006**, *16*, 162-172.
- [14] H. Fu, R. R. Subramanian, S. C. Masters, *Annu. Rev. Pharmacool. Toxicol.* **2000**, *40*, 617-647.
- [15] H. Hermeking, A. Benzinger, *Semin. Cancer Biol.* **2006**, *16*, 183-192.
- [16] A. J. Muslin, H. Xing, *Cell. Signalling* **2000**, *12*, 703-709.
- [17] T. Obsil, R. Ghirlando, D. C. Klein, S. Ganguly, F. Dyda, *Cell* **2001**, *105*, 257-267.
- [18] L. M. Stevers, E. Sijbesma, M. Botta, C. MacKintosh, T. Obsil, I. Landrieu, Y. Cau, A. J. Wilson, A. Karawajczyk, J. Eickhoff, J. Davis, M. Hann, G. O'Mahony, R. G. Doveston, L. Brunsveld, C. Ottmann, *J. Med. Chem.* **2018**, *61*, 3755-3778.
- [19] M. B. Yaffe, K. Rittinger, S. Volinia, P. R. Caron, A. Aitken, H. Leffers, S. J. Gamblin, S. J. Smerdon, L. C. Cantley, *Cell* **1997**, *91*, 961-971.
- [20] B. Coblitz, M. Wu, S. Shikano, M. Li, *FEBS Lett.* **2006**, *580*, 1531-1535.
- [21] P. W. Kenny, J. Sadowski, in *Cheminformatics in Drug Discovery* (Eds.: R. Mannhold, H. Kubinyi, G. Folkers, T. I. Oprea), Wiley VCH, **2005**, pp. 271-285.
- [22] K. Schorpp, I. Rothenaigner, E. Salmina, J. Reinshagen, T. Low, J. K. Brenke, J. Gopalakrishnan, I. V. Tetko, S. Gul, K. Hadian, *J. Biomol. Screening* **2014**, *19*, 715-726.
- [23] J. B. Baell, G. A. Holloway, *J. Med. Chem.* **2010**, *53*, 2719-2740.
- [24] I. J. De Vries-van Leeuwen, D. da Costa Pereira, K. D. Flach, S. R. Piersma, C. Haase, D. Bier, Z. Yalcin, R. Michalides, K. A. Feenstra, C. R. Jimenez, T. F. de Greef, L. Brunsveld, C. Ottmann, W. Zwart, A. H. de Boer, *Proc. Natl. Acad. Sci. U. S. A.* **2013**, *110*, 8894-8899.
- [25] R. Rose, S. Erdmann, S. Bovens, A. Wolf, M. Rose, S. Hennig, H. Waldmann, C. Ottmann, *Angew. Chem. Int. Ed.* **2010**, *49*, 4129-4132.
- [26] M. Wurtele, C. Jelich-Ottmann, A. Wittinghofer, C. Oecking, *EMBO J.* **2003**, *22*, 987-994.

## CHAPTER 3

- [27] V. Obsilova, P. Herman, J. Vecer, M. Sulc, J. Teisinger, T. Obsil, *J. Biol. Chem.* **2004**, *279*, 4531-4540.
- [28] C. Dalvit, G. Fogliatto, A. Stewart, M. Veronesi, B. Stockman, *J. Biomol. NMR* **2001**, *21*, 349-359.
- [29] J. F. Neves, I. Landrieu, H. Merzougui, E. Boll, X. Hanouille, F. X. Cantrelle, *Biomol. NMR Assignments* **2019**, *13*, 103-107.
- [30] F. H. Allen, C. A. Baalham, J. P. M. Lommerse, P. R. Raithby, *Acta Crystallogr. Sect. B: Struct. Sci.* **1998**, *54*, 320-329.
- [31] K. Psenakova, O. Petrvalska, S. Kylarova, D. Lentini Santo, D. Kalabova, P. Herman, V. Obsilova, T. Obsil, *Biochim. Biophys. Acta Gen. Subj.* **2018**, *1862*, 1612-1625.
- [32] S. Ganguly, J. L. Weller, A. Ho, P. Chemineau, B. Malpoux, D. C. Klein, *Proc. Natl. Acad. Sci. U. S. A.* **2005**, *102*, 1222-1227.
- [33] C. W. Bock, A. K. Katz, G. D. Markham, J. P. Glusker, *J. Am. Chem. Soc.* **1999**, *121*, 7360-7372.
- [34] A. Richter, R. Rose, C. Hedberg, H. Waldmann, C. Ottmann, *Chem. – Eur. J.* **2012**, *18*, 6520-6527.
- [35] M. N. Armisheva, N. A. Kornienko, V. L. Gein, M. I. Vakhrin, *Russ. J. Gen. Chem.* **2011**, *81*, 1893-1895.
- [36] L. F. Gein, V. L. Gein, I. A. Kylosova, Z. G. Aliev, *Russ. J. Org. Chem.* **2010**, *46*, 252-254.
- [37] V. L. Gein, M. N. Armisheva, N. A. Kornienko, L. F. Gein, *Russ. J. Gen. Chem.* **2014**, *84*, 2270-2272.
- [38] V. L. Gein, N. L. Fedorova, E. B. Levandovskaya, M. I. Vakhrin, *Russ. J. Org. Chem.* **2011**, *47*, 95-99.
- [39] V. L. Gein, N. N. Kasimova, *Russ. J. Gen. Chem.* **2005**, *75*, 254-260.
- [40] V. L. Gein, N. N. Kasimova, Z. G. Aliev, M. I. Vakhrin, *Russ. J. Org. Chem.* **2010**, *46*, 875-883.
- [41] Z. Fang, Y. Song, P. Zhan, Q. Zhang, X. Liu, *Future Med. Chem.* **2014**, *6*, 885-901.
- [42] A. D. G. Lawson, M. MacCoss, J. P. Heer, *J. Med. Chem.* **2018**, *61*, 4283-4289.
- [43] Y. Zheng, C. M. Tice, S. B. Singh, *Bioorg. Med. Chem. Lett.* **2017**, *27*, 2825-2837.
- [44] J. C. Hermann, Y. Chen, C. Wartchow, J. Menke, L. Gao, S. K. Gleason, N. E. Haynes, N. Scott, A. Petersen, S. Gabriel, B. Vu, K. M. George, A. Narayanan, S. H. Li, H. Qian, N. Beatini, L. Niu, Q. F. Gan, *ACS Med. Chem. Lett.* **2013**, *4*, 197-200.
- [45] F. E. Morreale, A. Testa, V. K. Chaugule, A. Bortoluzzi, A. Ciulli, H. Walden, *J. Med. Chem.* **2017**, *60*, 8183-8191.
- [46] S. A. Andrei, P. de Vink, E. Sijbesma, L. Han, L. Brunsveld, N. Kato, C. Ottmann, Y. Higuchi, *Angew. Chem. Int. Ed.* **2018**, *57*, 13470-13474.
- [47] A. Burkhardt, T. Pakendorf, B. Reime, J. Meyer, P. Fischer, N. Stübe, S. Panneerselvam, O. Lorbeer, K. Stachnik, M. Warmer, P. Rödiger, D. Göries, A. Meents, *Eur. Phys. J. Plus* **2016**, *131*, 56.
- [48] A. Meents, B. Reime, N. Stuebe, P. Fischer, M. Warmer, D. Goeries, J. Roever, J. Meyer, J. Fischer, A. Burkhardt, I. Vartiainen, P. Karvinen, C. David, *Development of an in-vacuum x-ray microscope with cryogenic sample cooling for beamline P11 at PETRA III*, Vol. 8851, SPIE, **2013**.
- [49] G. Winter, *J. Appl. Crystallogr.* **2009**, *43*, 186-190.
- [50] A. J. McCoy, R. W. Grosse-Kunstleve, P. D. Adams, M. D. Winn, L. C. Storoni, R. J. Read, *J. Appl. Crystallogr.* **2007**, *40*, 658-674.

## CHAPTER 3

- [51] P. D. Adams, P. V. Afonine, G. Bunkoczi, V. B. Chen, I. W. Davis, N. Echols, J. J. Headd, L. W. Hung, G. J. Kapral, R. W. Grosse-Kunstleve, A. J. McCoy, N. W. Moriarty, R. Oeffner, R. J. Read, D. C. Richardson, J. S. Richardson, T. C. Terwilliger, P. H. Zwart, *Acta Crystallogr. Sect. D: Biol. Crystallogr.* **2010**, *66*, 213-221.
- [52] P. Emsley, K. Cowtan, *Acta Crystallogr. Sect. D: Biol. Crystallogr.* **2004**, *60*, 2126-2132.
- [53] V. B. Chen, W. B. Arendall, 3rd, J. J. Headd, D. A. Keedy, R. M. Immormino, G. J. Kapral, L. W. Murray, J. S. Richardson, D. C. Richardson, *Acta Crystallogr. Sect. D: Biol. Crystallogr.* **2010**, *66*, 12-21.
- [54] P. A. Karplus, K. Diederichs, *Science* **2012**, *336*, 1030-1033.
- [55] *Small-Molecule Drug Discovery Suite 2019-2*, Schrödinger, LLC, New York, NY, **2019**
- [56] G. Chang, W. C. Guida, W. C. Still, *J. Am. Chem. Soc.* **1989**, *111*, 4379-4386.
- [57] K. Roos, C. Wu, W. Damm, M. Reboul, J. M. Stevenson, C. Lu, M. K. Dahlgren, S. Mondal, W. Chen, L. Wang, R. Abel, R. A. Friesner, E. D. Harder, *J. Chem. Theory Comput.* **2019**, *15*, 1863-1874.
- [58] W. C. Still, A. Tempczyk, R. C. Hawley, T. Hendrickson, *J. Am. Chem. Soc.* **1990**, *112*, 6127-6129.
- [59] A. D. Bochevarov, E. Harder, T. F. Hughes, J. R. Greenwood, D. A. Braden, D. M. Philipp, D. Rinaldo, M. D. Halls, J. Zhang, R. A. Friesner, *Int. J. Quantum Chem.* **2013**, *113*, 2110-2142.
- [60] S. Grimme, J. Antony, S. Ehrlich, H. Krieg, *J. Chem. Phys.* **2010**, *132*, 154104.
- [61] A. D. Becke, *J. Chem. Phys.* **1993**, *98*, 5648-5652.
- [62] B. Marten, K. Kim, C. Cortis, R. A. Friesner, R. B. Murphy, M. N. Ringnalda, D. Sitkoff, B. Honig, *J. Phys. Chem.* **1996**, *100*, 11775-11788.
- [63] C. P. Kelly, C. J. Cramer, D. G. Truhlar, *J. Chem. Theory Comput.* **2005**, *1*, 1133-1152.
- [64] Y. Zhao, D. G. Truhlar, *Theor. Chem. Acc.* **2007**, *120*, 215-241

# CHAPTER 4

## Synthetic Strategies For The Development Of Six-Membered Bicyclic Rigid Analogues Of Pyrrolidone1

### **Abstract**

In order to further explore the enhanced potency and stabilization observed upon addition of bivalent metal ions, a different strategy was envisaged for the mimicry of the ligand conformational restriction imposed by the chelation of such ions. The approach aimed at obtaining six-membered rigid analogues of Pyr1 rather than six-membered pseudo-rings by intramolecular H-bonding. Multiple synthetic routes implementing different sets of reagents and reaction conditions were investigated. A viable synthetic route was established but characterization of the desired product has not been fully elucidated yet due to complex NMR data interpretation. As of today, further experiments are still required in order to achieve the desired six-membered bicyclic rigid analogues of Pyr1.

## CHAPTER 4

### 4.1 CONFORMATIONAL RESTRICTION IN DRUG DISCOVERY

Conformational restriction of flexible ligands is a widely employed synthetic strategy in medicinal chemistry.<sup>1</sup> Indeed, application of conformational control by introducing some degree of structural constraints can potentially lead to an improvement in potency, selectivity and/or physicochemical properties by improvement of metabolic stability or cell/membrane penetration.

For ligands with rotatable bonds, a number of different low energy conformations are typically allowed when free (unbound), in solution. However, the conformation assumed by a ligand upon binding to its target (bioactive conformation), very often does not correspond to the conformation when free in solution (solution conformation).<sup>2</sup> In energetic terms, these ligands suffer an entropic penalty upon binding because of the shift and subsequent lock into an energetically less favorable conformation. Hence, molecules that instead are purposely designed to prefer the bioactive conformation in solution will account for higher affinities, due to their conformational pre-organization. This pre-organization reduces the conformational entropy penalty payout for the transition from the ligand's unbound conformation(s) to its bioactive one.<sup>3-4</sup>

Different conformational control features can be applied in order to bias the conformational preference of the free ligand towards its bioactive conformation. Among them, we find: steric or stereoelectronic effects, intramolecular hydrogen-bonding and cyclization.<sup>5</sup> For our purposes, we opted to employ the cyclization strategy.

### 4.2 BACKGROUND

As discussed in chapter 3, it was demonstrated, both computationally and experimentally, that the bioactive conformation (*syn*) the O- and carbonyl oxygen of the vinylogous carboxylate of (*R*)-**2** (from here on named (*R*)-**4.1**) differs from the lower energy conformation (*anti*), preferred in solution due to repulsive electrostatic allylic strain (Figure 4.1a). Addition of bivalent metal ions led to stabilization of the bioactive ligand conformation by chelation. Mimicry of this effect was successfully exploited by intramolecular H-bonding, yielding regioisomeric compounds (*R*)-**6** and (*R*)-**9**, whose 14-3-3 PPI stabilization potency was metal-independent.

Mimicry of this metal ion effect by cyclization using hydrazine to obtain 5-membered rigid analogues was also achieved,<sup>6</sup> but was much less efficient in terms of 14-3-3 PPI stabilization potency. This was most probably related to different orientation of the phenyl ring of the benzoyl moiety, if compared with the 6-membered pseudo-ring formed upon addition of Mg<sup>2+</sup>. It was reasoned that a 6-membered ring would better mimic the hexagonal geometry induced by bivalent

metal ions and therefore a synthetic route towards 6-membered bicyclic rigid analogues of (*R*)-**4.1** was sought (Figure 4.1b).

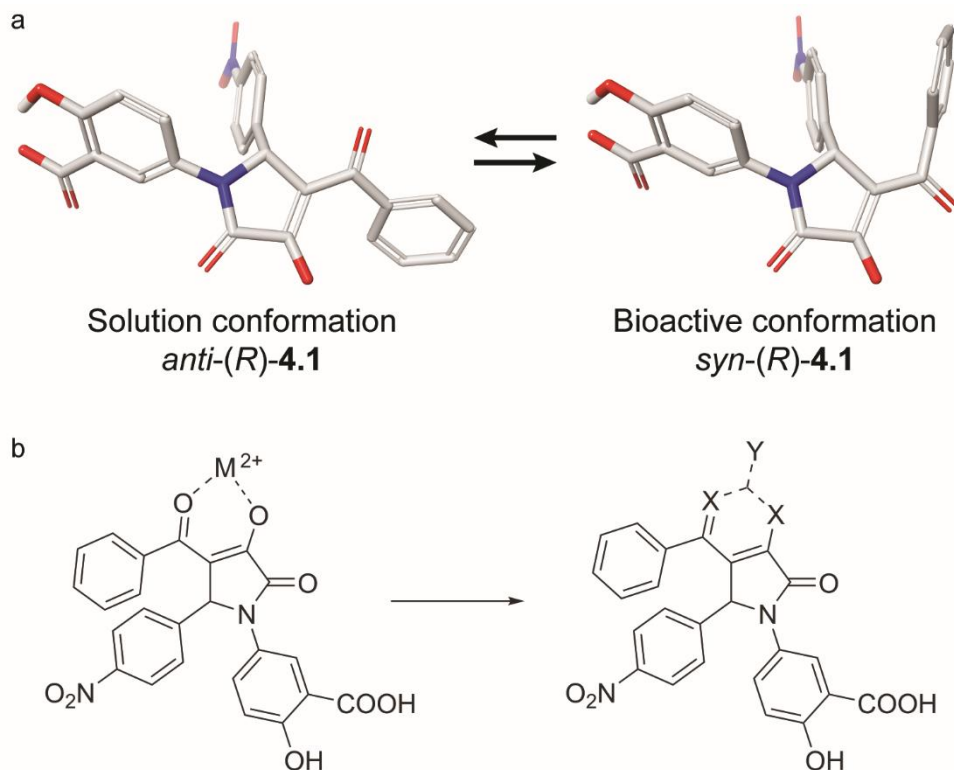


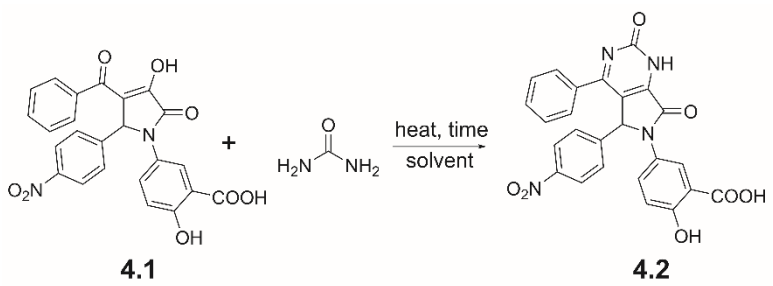
**Figure 4.1** | Mimicry of the  $M^{2+}$  effect. (a) Comparison between the solution conformation (*anti*) and bioactive conformation (*syn*) of (*R*)-**4.1**. (b) Cyclization of the vinylogous carboxylate moiety as a synthetic strategy for the mimicry of the  $Mg^{2+}$  effect.

Due to the time-consuming chiral separation procedure, all the reactions performed in this chapter made use of racemic **4.1** (*rac*-**4.1**, from this point on simply referred to as **4.1**). In order to obtain a 6-membered bicyclic derivative of **4.1** (**4.2**), namely a 5,6-dihydro-1H-pyrrolo[3,4-d]pyrimidine-2,7-dione, urea was initially chosen as reactant. Upon reaction of **4.1** with an excess of urea (5 eq) under the same conditions used previously for the synthesis of the 1,4-dihydropyrrolo[3,4-c]pyrazole 5-membered rigid analogue **5** (microwave heating, 120 °C, 3 h in AcOH), only starting material was recovered. In the attempt to gauge the feasibility of the reaction, different reaction conditions were therefore evaluated, varying solvent, reaction times and temperatures (Table 4.1).

Increasing reaction times or temperatures in AcOH (entries 1-3), as well as shifting to polar aprotic solvents such as dimethylformamide (4-7) or acetonitrile (8-

10), afforded only traces (< 2% conversion, monitored by LC-MS, Figure S4.1) to no product, even under harsher conditions (entries 6-7). Use of polar protic solvents under neutral (entries 11-12) or basic (entry 13) conditions, also led to unsatisfactory outcomes, with only traces observed at best (isopropanol, 11, Figure S4.2). It was reasoned that the much lower nucleophilicity of urea, compared to the hydrazine used for the synthesis of **5**, represented the main issue for such negative results. Therefore, it was decided to attempt the reaction using O-methylisourea and guanidine in place of urea, to obtain derivatives 2-methoxy-5,7-dihydro-6H-pyrrolo[3,4-d]pyrimidin-7-one (**4.3**) and 2-amino-5,7-dihydro-6H-pyrrolo[3,4-d]pyrimidin-7-one (**4.4**), respectively (Figure 4.2).

**Table 4.1** | Test reactions for the synthesis of **4.2**.<sup>(a)</sup>



Entry	Solvent	Temperature (°C)	Time (min)	Conversion (%) <sup>(b)</sup>
1	AcOH	120	300	0
2	AcOH	160	20	0
3	AcOH	reflux <sup>(c)</sup>	ON	0
4	DMF	130	30	0
5	DMF	160	15	0
6	DMF	220	5	0
7	DMF	220	15	0
8	ACN	100	60	traces
9	ACN	100	180	0
10	ACN + HCl cat.	100	120	0
11	IPA	120	180	traces
12	EtOH	100	180	0
13	EtONa (21% in EtOH)	100	120	0

(a) Reactions were performed using 30 mg of **4.1**, an excess of urea (5.00 eq) and a total volume of 3 mL, in a sealed vial under microwave heating (unless otherwise noted).

(b) Conversion rates were monitored by LC-MS.

(c) Reaction was performed using conventional heating.

## CHAPTER 4

A summary of the test reactions performed is reported in Table 4.2. Unfortunately, in both cases, only starting material was recovered and no product was observed. Due to the repeated failures, an in-depth literature investigation was conducted, together with a more careful investigation of the possible reaction mechanism(s) involved.

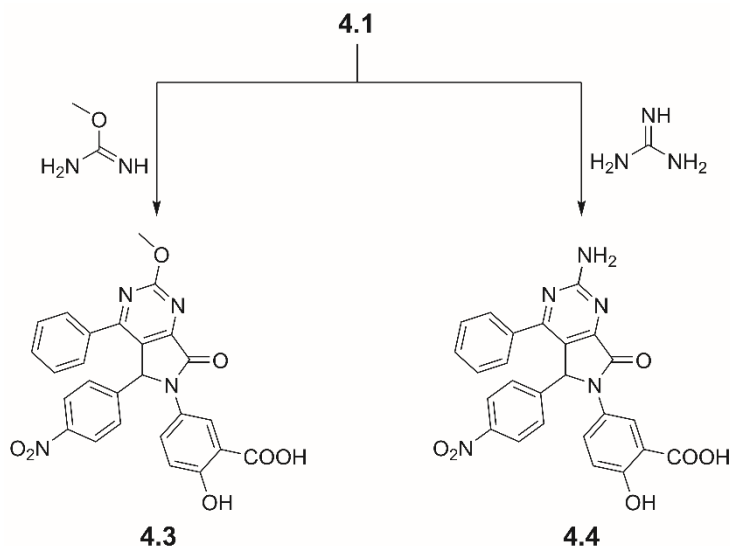


**Figure 4.2** | Use of more nucleophilic reagents than urea to achieve 6-membered rigid analogues of **4.1**: O-methylisourea, to synthesize **4.3** (left) and guanidine, to synthesize **4.4** (right).

Literature research focused on cyclization reactions between vinylogous carboxylic acids or corresponding esters and substrates such as ureas and thioureas. It was found that for vinylogous carboxylic acids, reactions were conducted under either neutral or acidic conditions, while for vinylogous esters reactions were performed under basic conditions. Each case and the relative attempts made to synthesize the desired cyclized product will be discussed in the next sections.

**Table 4.2** | Test reactions for the synthesis of **4.2**.<sup>(a)</sup>

Entry	Reagent	Solvent	Temperature (°C)	Time (min)	Conversion (%) <sup>(b)</sup>
14	O-methylisourea	AcOH	120	180	0
15	O-methylisourea	AcOH	120	300	0
16	O-methylisourea	DMF	130	60	0
17	O-methylisourea	ACN	100	60	0
18	O-methylisourea	IPA	120	180	0

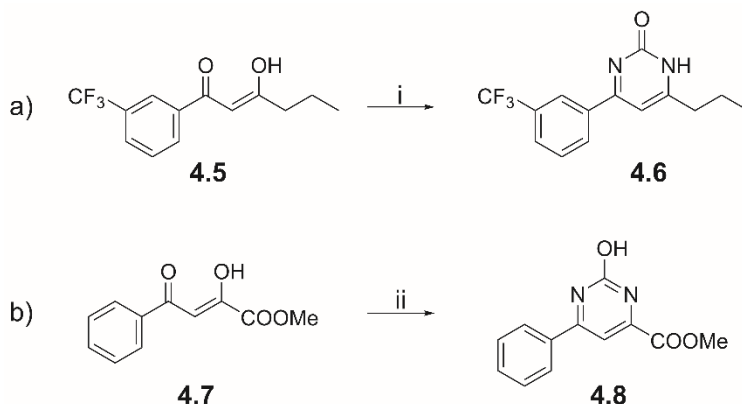


<b>19</b>	O-methylisourea	EtONa (21% in EtOH)	100	120	0
<b>20</b>	guanidine	AcOH	120	120	0
<b>21</b>	guanidine	AcOH	190	10	0
<b>22</b>	guanidine	DMF	130	60	0
<b>23</b>	guanidine	ACN	100	60	0
<b>24</b>	guanidine	IPA	120	180	0

- (a) Reactions were performed using 30 mg of **4.1**, an excess of urea (5.00 eq) and a total volume of 3 mL, under microwave heating (unless otherwise noted).  
 (b) Conversion rates were monitored by LC-MS.

### 4.3 VINYLOGOUS CARBOXYLIC ACIDS AS SUBSTRATES

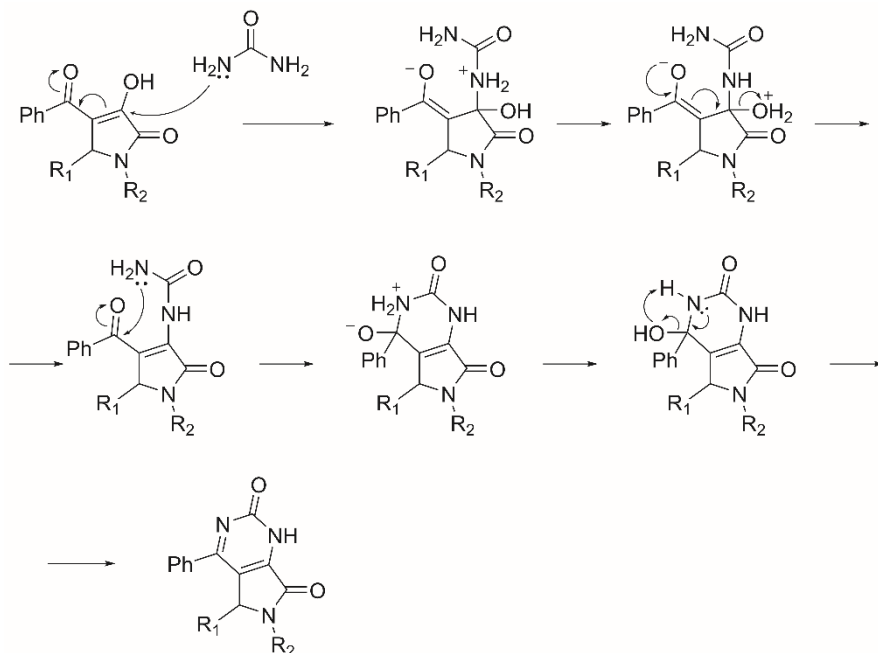
Reactions involving vinylogous carboxylic acids were found to be conducted either under acidic or neutral conditions. For acidic conditions, the use of strong acids such as hydrochloric acid (HCl)<sup>7-8</sup> or sulfuric acid (H<sub>2</sub>SO<sub>4</sub>)<sup>9</sup> was reported (Scheme 4.1a and b). In the former case, HCl was used stoichiometrically, added in two portions over 40 hours to give **4.6** in 73% yield.<sup>7</sup> In the latter, H<sub>2</sub>SO<sub>4</sub> was added in catalytic amount to obtain **4.8** in 78% yield.<sup>9</sup>



**Scheme 4.1** | Examples of urea cyclization in the presence of strong acids. i) Urea (1.50 eq), HCl (5 M, 0.75 eq), EtOH, 16 h, reflux. Then further addition of urea (1.00 eq) and HCl (5 M, 0.75 eq), EtOH, 24 h, reflux. ii) Urea (2.50 eq), H<sub>2</sub>SO<sub>4</sub> cat., MeOH, o/n, reflux.

Chapter 3 highlighted how, for this type of substrates, the regiochemistry of the nucleophilic attack was hard to predict and rationalize. Indeed, reaction of **4.1** (named **2** in chapter 3) with aqueous ammonia afforded only vinylogous amide **6** (chapter 3), the 1,2-addition product (exocyclic nucleophilic attack on the carbonyl group), and no vinylogous amide **9** (chapter 3), the 1,4-addition product (endocyclic nucleophilic attack) was observed. On the other hand, reaction of **4.1** with *p*-methoxybenzylamine (and other primary amines not reported) afforded a mixture of

both 1,2- and 1,4-addition products. Nevertheless, we hypothesized a reaction mechanism as depicted in Scheme 4.2, starting with a 1,4 conjugate addition of urea to **4.1**. Proton transfer to the hydroxyl of the vinylogous carboxylic acid and subsequent rearrangement causes the release of a water molecule. A second nucleophilic attack of the urea onto the carbonyl group generates a tetrahedral intermediate which, upon proton transfer and following dehydration, leads to the desired cyclized product.



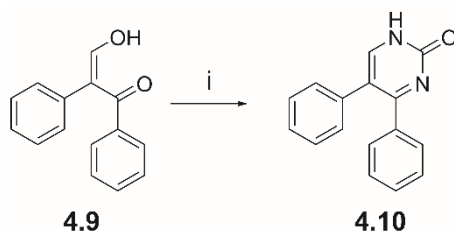
**Scheme 4.2** | Proposed reaction mechanism for the possible condensation of urea with **4.1** under acidic conditions. R<sub>1</sub> = 4-nitrophenyl; R<sub>2</sub> = 3-carboxy-4-hydroxyphenyl; Ph = phenyl.

Under strongly acidic conditions, both the carboxylic acid of the salicylate ring and the vinylogous carboxylic acid of **4.1** will be protonated. The presence of strong acids might also help the dehydration steps and/or might promote protonation of the oxygen of the benzoyl group in addition to protonation of the vinylogous carboxylate, thus making it more susceptible to nucleophilic attack from urea, and therefore pushing the reaction forward. On the other hand, urea is known to protonate in strong acidic media<sup>10</sup>, therefore decreasing even more its nucleophilic character and possibly compromise the reaction initiation. As such, it is difficult to predict if stoichiometric amounts of strong acids would allow the reaction to start.

The only procedure found that made use of neutral conditions was reported by Coppola *et al.*<sup>11</sup> Here, 3-hydroxy-1,2-diphenyl-2-propen-1-one (**4.9**) was reacted with

## CHAPTER 4

an excess of urea in dimethylacetamide (DMA) for one hour at 150-160 °C, to obtain the desired 2-pyrimidinone product (**4.10**), in 37% yield (Scheme 4.3). Under neutral conditions, the vinylogous carboxylate of **4.1** will be deprotonated. In this specific case, it might be that the electrostatic repulsion of the negative charge on the vinylogous carboxylate oxygen and the nucleophile lone pair could favor the 1,2-addition to the carbonyl over 1,4 conjugate addition. It is also true, however, that the negative charge will be delocalized over the two oxygens, thus making more difficult to predict the favored addition position.



**Scheme 4.3** | Urea cyclization reaction under neutral conditions. i) urea (3.70 eq), DMA, 1 h, 150-160 °C.

As previously discussed in section 4.2, attempts both under neutral and acidic conditions did not yield any desired 6-membered rigid analogue. Hence, based on the proposed reaction mechanism, two possible points of intervention that would potentially help in driving the reaction forward were identified. The first was the addition of a Lewis acid in order to make the carbonyl group more electrophilic and therefore promoting the second nucleophilic attack of urea and subsequent cyclization. The second was to convert the hydroxyl group of the vinylogous carboxylic acid into a vinylogous ester and thus provide a better leaving group as well as circumvent the electrostatic repulsion between the nucleophile and the charged vinylogous carboxylate.

Lewis acids, compounds capable of accepting a pair of electrons, have a widespread use in organic synthesis.<sup>12</sup> One of their common applications is the activation of carbonyl groups. In fact, coordination of the Lewis acid to a lone electron pair on the carbonyl oxygen induces a greater polarization of the C=O bond, effectively enhancing the carbonyl susceptibility to nucleophilic attack.<sup>13</sup>

For our purpose, we found literature reports for the synthesis of pyrimidinones starting from urea that made use of Lewis acids such as boron trifluoride diethyl etherate (BF<sub>3</sub>·OEt<sub>2</sub>)<sup>14</sup> and chlorotrimethylsilane (TMSCl), either alone<sup>15-16</sup> or in combination with catalytic amount of cupric chloride (CuCl<sub>2</sub>).<sup>17</sup> BF<sub>3</sub>·OEt<sub>2</sub> was used in catalytic amount to promote the reaction of β-methoxyvinyl trifluoromethyl ketones with urea. Reactions were carried out in IPA and stirred for 20 h at reflux to obtain the desired cyclized products in moderate to good yield. TMSCl or the combination

**Table 4.3** | Test reactions for the synthesis of **4.2** or **4.3** using different Lewis acids.<sup>(a)</sup>

Entry	Lewis acid (eq) <sup>(b)</sup>	Solvent	Temperature (°C)	Time (min)	Conversion (%) <sup>(c)</sup>
25	BF <sub>3</sub> OEt <sub>2</sub> (0.10)	IPA	130	100	0
26	BF <sub>3</sub> OEt <sub>2</sub> (0.10)	IPA	reflux <sup>(d)</sup>	ON	0
27 <sup>(e)</sup>	BF <sub>3</sub> OEt <sub>2</sub> (0.10)	IPA	130	100	0
28 <sup>(e)</sup>	BF <sub>3</sub> OEt <sub>2</sub> (0.10)	IPA	reflux <sup>(d)</sup>	ON	0
29	TMSCl (2.00)	ACN/DMF (1:2)	90 <sup>(d)</sup>	ON	0
30	TMSCl (2.00)	ACN/DMF (1:2)	150	110	0
31	TMSCl (2.00)	DMF	220	15	0
32	TMSCl + CuCl <sub>2</sub> (1.00/10% mol)	ACN	reflux <sup>(d)</sup>	360	0
33	TMSCl + CuCl <sub>2</sub> (1.00/10% mol)	ACN	130	140	traces
34	TMSCl + CuCl <sub>2</sub> (1.00/10% mol)	ACN	160	20	0

(a) Reactions were performed using 30 mg of **4.1**, an excess of urea (2.50 eq) and a total volume of 3 mL, under microwave heating (unless otherwise noted).

(b) Number of equivalents in respect to **4.1**.

(c) Conversion rates were monitored by LC-MS.

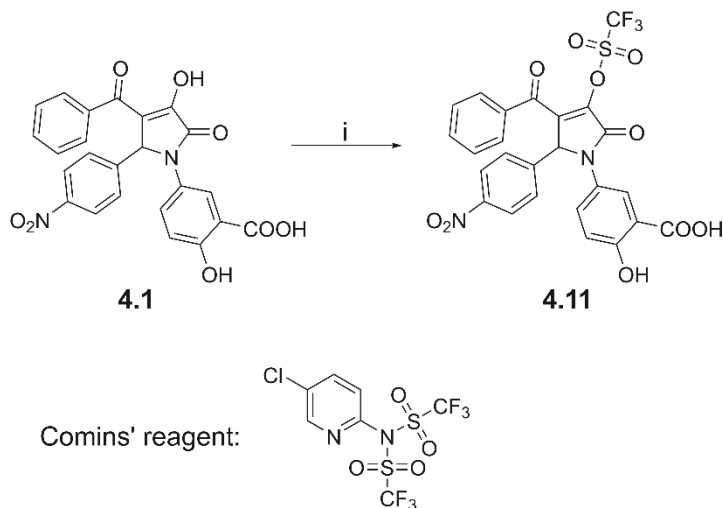
(d) Reaction was performed using conventional heating

(e) Reaction was performed using O-methylisourea (2.50 eq).

of TMSCl/CuCl<sub>2</sub> was instead used to promote chemical activation of ketones involved in Biginelli reactions, formally a one-pot multicomponent reaction of an aldehyde, a β-ketoester and urea to synthesize dihydropyrimidinones.<sup>18-19</sup> TMSCl has also been reported to function as water scavenger, thus effectively promoting dehydration reactions and could therefore potentially be twice as helpful in our reactions.<sup>20-21</sup> A summary of the reactions performed on **4.1** in the presence of Lewis acids is reported in Table 4.3. The use of BF<sub>3</sub>-OEt<sub>2</sub> did not give any desired product with urea, but a peak of unknown product with MW of 488 Da (expected mass for desired product: 498 Da) was observed for O-methylisourea (35% conversion). The unknown compound was not characterized. A possible explanation for the failure of these reactions was that BF<sub>3</sub>-OEt<sub>2</sub> could potentially have formed a stable chelate or carboxylate complex, rather than coordinating to the carbonyl oxygen, therefore causing the reaction to stall and to not give product. TMSCl alone also did not yield

any product, but traces were observed when tested in combination with  $\text{CuCl}_2$  (Figure S4.3).

In parallel, in pursuing the strategy to have a better leaving group, it was decided to convert the vinylogous carboxylic acid into a triflate by means of Comins' reagent (Scheme 4.4). Comins' reagent, formally a *N*-(5-chloro-2-pyridyl)triflimide, has been reported to be an efficient reagent for conversion of ketone enolates or dienolates into the corresponding vinyl triflates.<sup>22-23</sup>



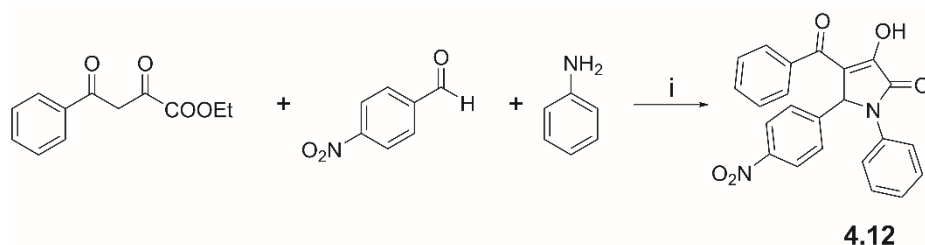
**Scheme 4.4** | Application of Comins' reagent to generate a better leaving group for **4.1**. i) a) LiHMDS, dry THF,  $-78\text{ }^\circ\text{C}$ , 30 min, b) Comins' reagent,  $-78\text{ }^\circ\text{C}$  to RT, o/n.

**4.1** was initially reacted with lithium bis(trimethylsilyl)amide (LiHMDS) for 30 min at  $-78\text{ }^\circ\text{C}$  under nitrogen. Upon addition of one equivalent of Comins' reagent, the initial brownish suspension turned into orange. Addition of another equivalent turned the suspension into a clear solution. After 3 hours, 31% of product was observed (monitored by LC-MS). However, the reaction did not progress any further even after overnight stirring at room temperature. After purification by flash column chromatography, **4.11** was subsequently reacted with either urea or *O*-methylisourea under microwave conditions. LC-MS for both test reactions did not show formation of any desired product (**4.2** or **4.3**, respectively). However, a peak of mass equal to 488 Da was observed in both chromatograms, which could suggest that some side-reaction might have taken place instead. It needs to be noted that **4.11** was characterized by LC-MS (Figure S4.4) but not by NMR. The lack of full structural characterization for **4.11**, together with the two unknown by-products with equal mass from two independent and different reactions, could potentially indicate that **4.11** was not the desired triflated product to begin with. Characterization of the above-mentioned unknown by-products (MW 488 Da) was then attempted. The

unknown by-product from the urea reaction was successfully isolated, however a malfunction in the HPLC machine prevented the isolation of the one from the O-methylisourea reaction. NMR characterization resulted to be complex, and without further information it was not possible to elucidate the structure of such products. Another possible reason for the reaction failure might involve steric aspects. Indeed, the bulky triflate group might hinder the nucleophilic addition of urea at the conjugate position, thus preventing the reaction to follow the proposed mechanism. Due to time restrictions and more fruitful outcomes using vinylogous carboxylate esters under basic conditions (which will be discussed in the next paragraph), this synthetic route was not pursued any further.

#### 4.4 VINYLOGOUS CARBOXYLATE ESTERS AS SUBSTRATES

For the reaction investigation under basic conditions, a “simplified” version of **4.1**, **4.12**, was used (Scheme 4.5). **4.12** was synthesized from ethyl 2,4-dioxo-4-phenylbutanoate, 4-nitrobenzaldehyde and aniline under microwave heating in fair yields (55%).



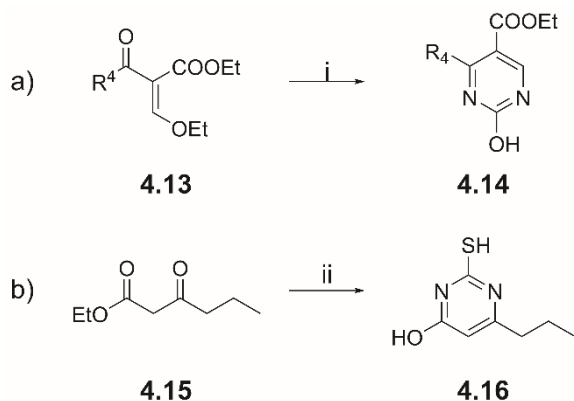
**Scheme 4.5** | Synthesis of **4.12**. i) AcOH, 120 °C, 3 h, MW.

It was reasoned that the lack of both the carboxylate and phenol functional groups would minimize possible competing side-reactions and improve solubility in organic solvents as well as simplify the overall work-up and purification procedures.

Literature research showed that these cyclization reactions are performed starting from the vinylogous carboxylates (Scheme 4.6a)<sup>24</sup> or  $\beta$ -keto esters (Scheme 4.6b).<sup>8</sup> In the former case, **4.14** was prepared from the ethyl vinylogous carboxylate **4.13** and urea in the presence of sodium ethoxide (NaOEt) in ethanol under heating. In the latter, **4.15** was reacted with thiourea and sodium methoxide in methanol under heating to give **4.16**.

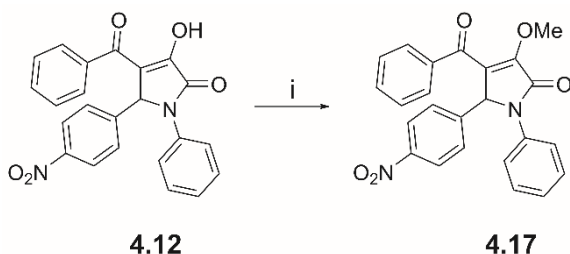
Under basic conditions, the vinylogous carboxylic acid of **4.12** would be deprotonated and the presence of a negative charge would most probably prevent a nucleophilic attack at the conjugate position. Moreover, OH<sup>-</sup> is a poor leaving group and its loss after initial urea attack would be unlikely to happen. Based on these observations as well as literature reports, **4.12** was then converted into its

## CHAPTER 4



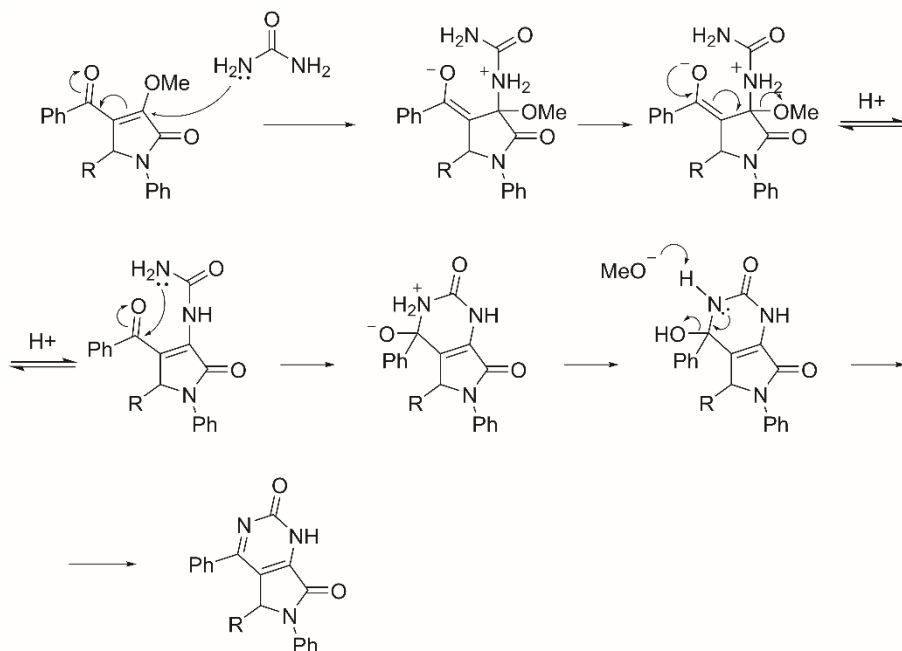
**Scheme 4.6** | Examples of pyrimidine formation by cyclization under basic conditions. i) urea, NaOEt, EtOH, reflux, N<sub>2</sub> ii) thiourea, NaOMe, MeOH, 0 °C to reflux.

corresponding methyl ester **4.17** in good yields (76%) by reaction with trimethylsilyldiazomethane (TMS-CHN<sub>2</sub>).



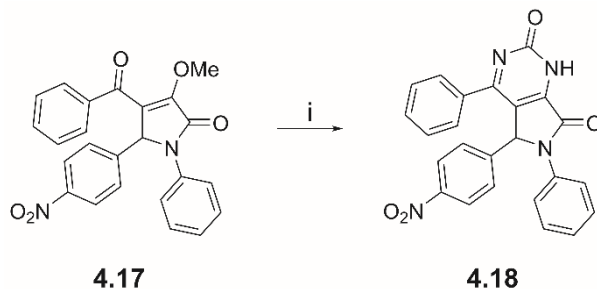
**Scheme 4.7** | Synthesis of vinylogous methyl ester **4.17**. i) TMSCHN<sub>2</sub>, MeOH/ACN (1:4), RT, 30 min, N<sub>2</sub>

In addition, a different mechanism was proposed for such reaction when performed under basic conditions (Scheme 4.8). Here, addition of urea at the conjugate position leads to an intermediate transition state which results in the elimination of the alkoxide molecule (MeO<sup>-</sup>). Afterwards, abstraction of a proton from the urea NH<sub>2</sub><sup>+</sup> is followed by the second nucleophilic attack onto the electrophilic carbon of the carbonyl group. Proton transfer and subsequent aromatization by dehydration lead to the final cyclized product.



**Scheme 4.8** | Proposed mechanism for cyclization of urea and **4.17** under basic conditions. R = 4-nitrophenyl; Ph = phenyl

Next, the reaction of **4.17** in the presence of urea was carried out, using sodium methanolate 30% solution as reaction medium (Scheme 4.9). After refluxing the reaction overnight, the crude product was purified and isolated in 8% yield (**4.18**).



**Scheme 4.9** | Synthesis of 6-membered rigid analogue **4.18**. i) urea, NaOMe, reflux, o/n,  $\text{N}_2$ .

LC-MS analysis returned the correct expected mass for the product (424.12 Da), both in positive ( $m/z$   $[\text{M} + \text{H}]^+ = 425.08$  Da) and negative ( $m/z$   $[\text{M} - \text{H}]^- = 423.06$  Da) ionization mode. An additional peak of twice the mass of **4.18** was also observed (849.34 Da and 847.24, respectively in positive and negative ionization mode), suggesting that a dimer could be present in solution (Figure 4.3). It is worth pointing



## CHAPTER 4

out that the impurity peak present ( $R_t = 1.13$  min,  $m/z [M + H]^+ = 385.09$  Da) does not belong to either **4.17** ( $R_t = 1.34$  min) or **4.12** ( $R_t = 1.21$  min).

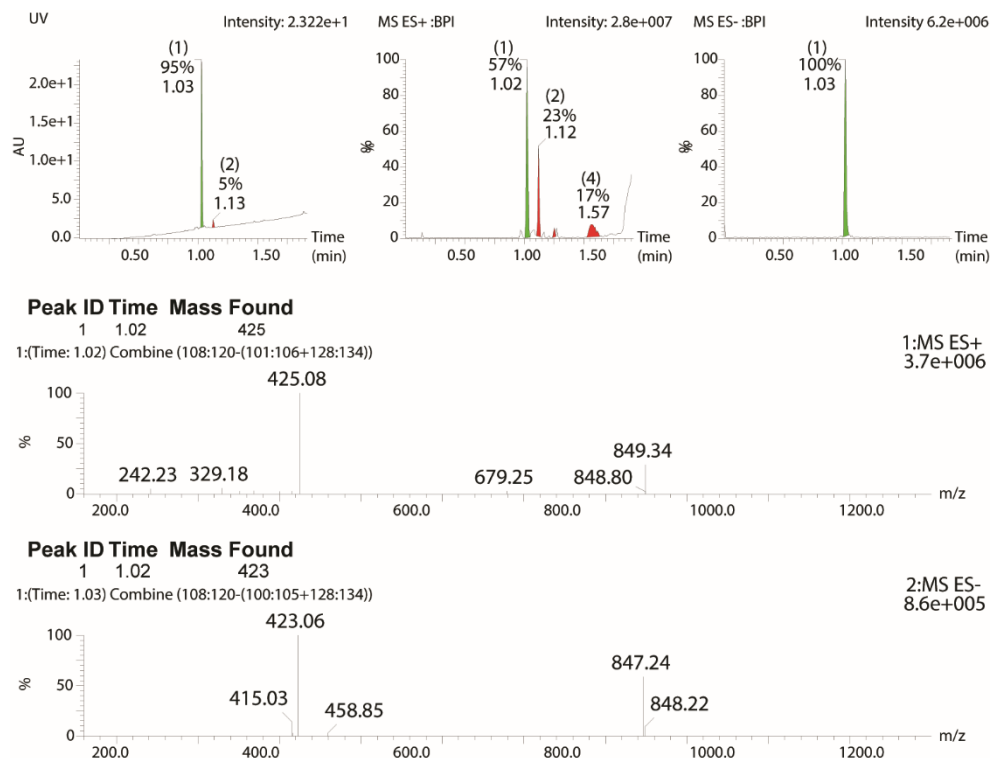


**Figure 4.3** | LC-MS analysis of purified compound **4.18**. Top: UV trace (left panel) and base peak intensity (BPI) chromatograms in positive (ES+, middle panel) and negative (ES-, right panel) ionization detection mode. Peak intensities are reported at the top right-hand corner of each panel. Method: ACN/H<sub>2</sub>O (pH = 3), 20:80 – 90:10 over 2 min. AU = absorbance units. Bottom: mass traces in positive and negative ionization mode of **4.18**.  $m/z [M + H]^+ = 425.08$  Da;  $m/z [2M + H]^+ = 849.34$  Da;  $m/z [M - H]^- = 423.06$  Da;  $m/z [2M - H]^- = 847.24$  Da.

Structure characterization became puzzling when NMR analysis was performed. In fact, the <sup>1</sup>H NMR spectrum of **4.18** did not show the characteristic singlet peak around 6.5 ppm belonging to the chiral proton (Figure S4.5), which was clearly visible in the <sup>1</sup>H spectrum of **4.17** (Figure S4.6). On the other hand, the singlet integrating three protons from the methoxy group of **4.17** at 3.96 ppm was not visible in the spectrum of **4.18**, also confirming that starting material **4.17** was not present in the sample. The aromatic region of **4.18** presents a high base line, with rather broadened peaks and what appears to be background noise, which contrasts with the sharp and well separated peaks of **4.17** (Figure S4.7) It was speculated that the origin of high background noise could be related to the 5% impurity observed in the LC-MS chromatogram. However, this hypothesis was later discarded as the UV peak of such

## CHAPTER 4

impurity was much lower intensity when compared to the peak of **4.17**, and a high UV absorbance would be expected from a sample whose peaks have a chemical shift in the aromatic region (6.5 ppm to 8.5 ppm).

Pyrimidinones and closely related pyridones can exist in tautomeric equilibrium with their respective enolic form. The preference for one form over the other is strictly dependent on the regioisomer in study and the experimental conditions (gas vs condensed phase).<sup>25</sup> Moreover, pyrimidinones and pyridones are also known to exist as hydrogen-bonded dimers and that significant amounts of dimers can also be present in solution.<sup>17, 26</sup> Although it has been reported that interconversion of these species is rapid in solution and only averaged signals are observed in <sup>1</sup>H NMR even at low temperatures (-120 °C),<sup>26</sup> it was speculated that for our substrate this might not be the case and that **4.18** might exist in a relatively stable form with its tautomers and/or dimers.

### 4.5 CONCLUSIONS

The aim of this chapter was to find an alternative conformational restriction strategy for the mimicry of the ligand-specific conformational effect induced by bivalent metal ions. With this intent, multiple synthetic routes towards the synthesis of six-membered bicyclic rigid analogues of **4.1** were explored.

Reactions involving the vinylogous carboxylate **4.1** and different reactants such as urea, O-methylisourea and guanidine were performed. Different reaction conditions were screened, varying solvent, temperature, time and pH. The implementation of Lewis acids was also evaluated, but none of the conditions tested afforded the desired bicyclic products in satisfactory amounts.

On the other hand, the use of vinylogous carboxylate ester **4.17**, reacted with urea under basic conditions seemed to be more successful. However, structural characterization resulted to be complex. LC-MS analysis showed the presence of a peak with twice the exact mass of the desired product **4.18**. <sup>1</sup>H NMR analysis revealed the absence of the characteristic singlet peak of the chiral proton and a marked background noise around the aromatic region. It was speculated that **4.18** could exist in solution as a stable dimer, but further investigation is required to elucidate the structure of the reaction product.

# CHAPTER 4

## 4.6 EXPERIMENTAL SECTION

### 4.6.1 Supporting Figures

Sample: **4.2** Reaction conditions: ACN, 100 °C, 60 min

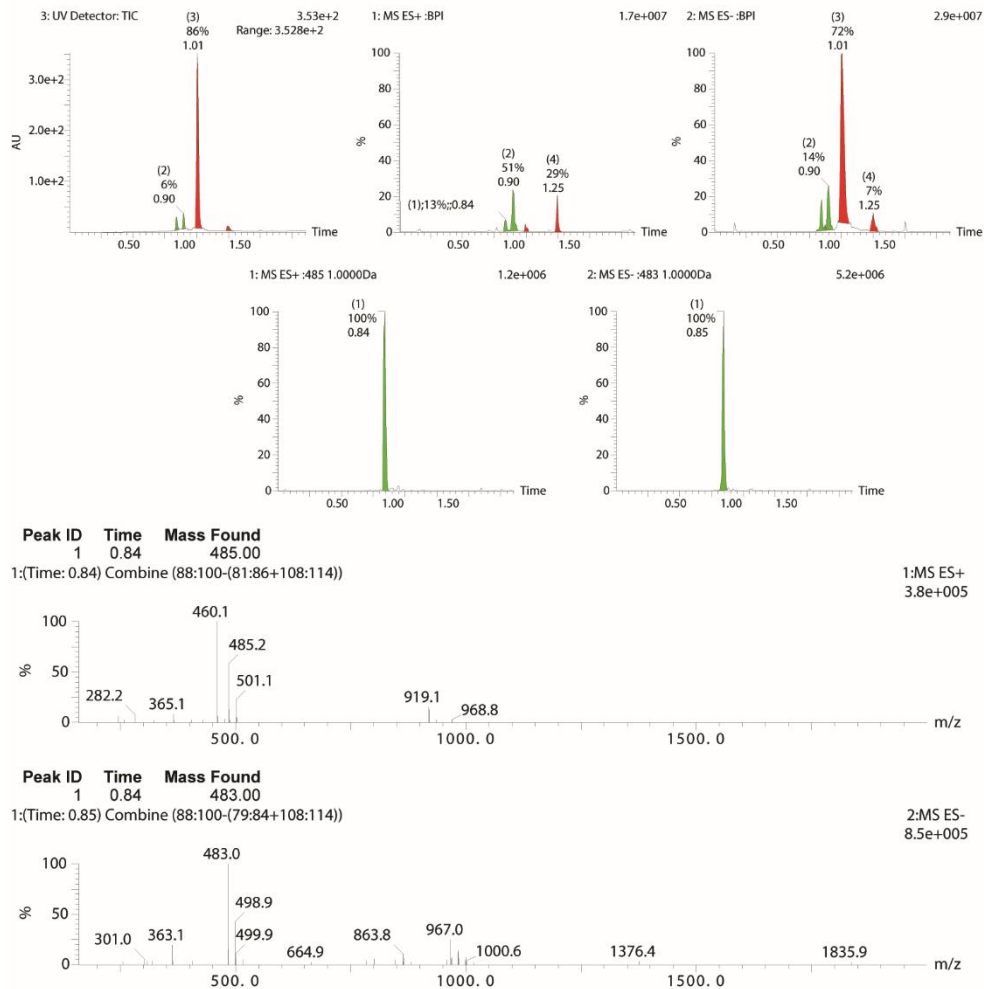


**Figure S4.1** | LC-MS analysis of **4.2**, entry 33. Green peak ( $R_t = 0.84$  min) exhibits the correct mass both in positive and negative ionization mode. Expected mass for **4.2**: 484.1;  $m/z [M + H]^+ = 485.2$  Da;  $m/z [M - H]^- = 483.0$  Da. The red peak ( $n^\circ 3$ ,  $R_t = 1.01$  min) corresponds to **4.1**.

# CHAPTER 4

Sample: **4.2** Reaction conditions: IPA, 120 °C, 180 min

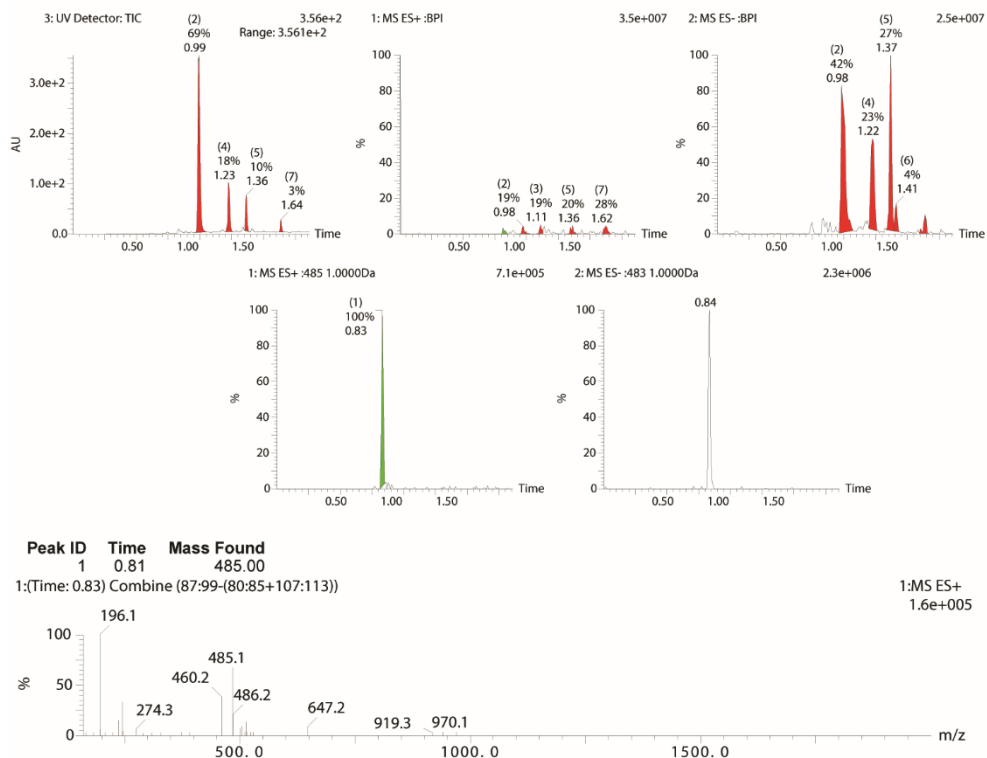


**Figure S4.2** | LC-MS analysis of **4.2**, entry 11. Green peak ( $R_t = 0.83$  min) exhibits the correct mass in positive ionization mode. Expected mass for **4.2**: 484.1;  $m/z [M + H]^+ = 485.1$  Da. The red peak ( $n^\circ 2$ ,  $R_t = 0.99$  min) corresponds to **4.1**.

# CHAPTER 4

Sample: **4.2** Reaction conditions: TMSCl/CuCl<sub>2</sub>, ACN, 130 °C, 140 min

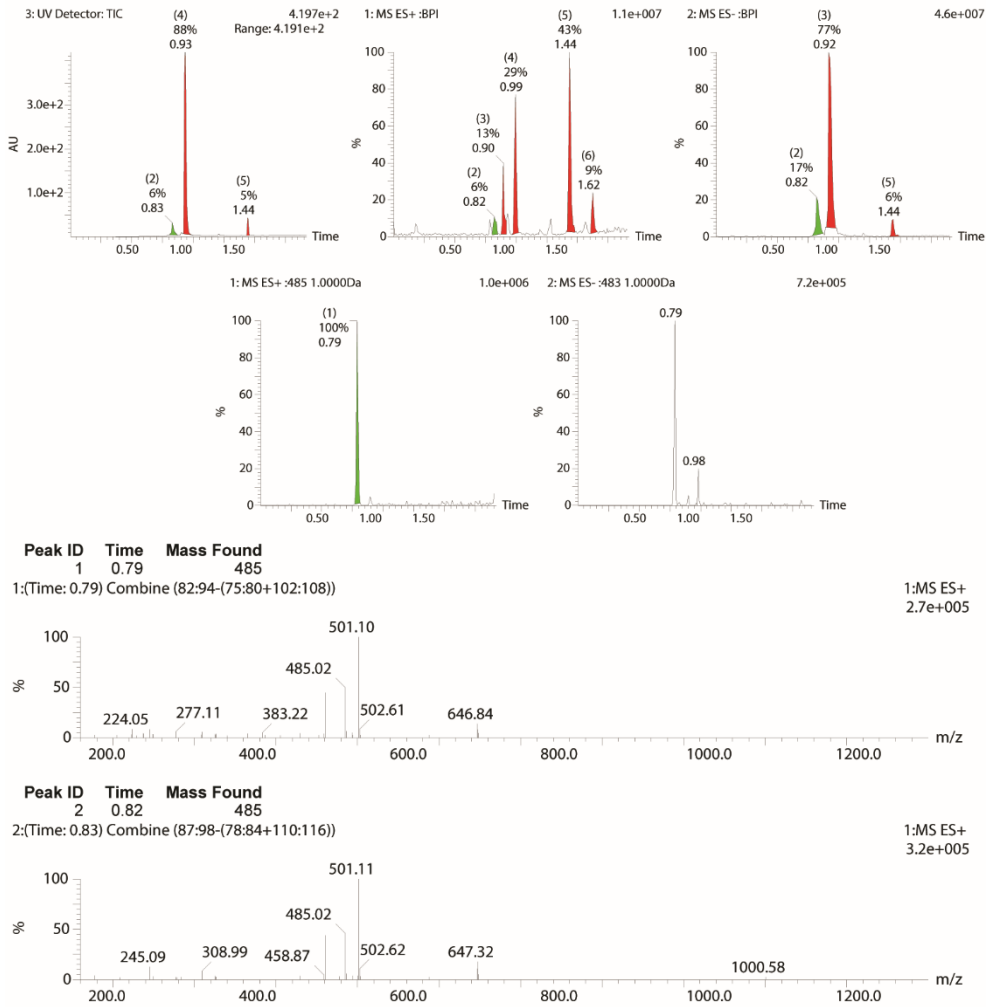


**Figure S4.3** | LC-MS analysis of **4.2**, entry 33. Green peak ( $R_t = 0.83$  min) shows the correct mass in positive ionization mode. Expected mass for **4.2**: 484.1;  $m/z [M + H]^+ = 485.0$  Da. The red peak ( $n^\circ 4$ ,  $R_t = 0.93$  min) corresponds to **4.1**.

# CHAPTER 4

Sample: 4.11

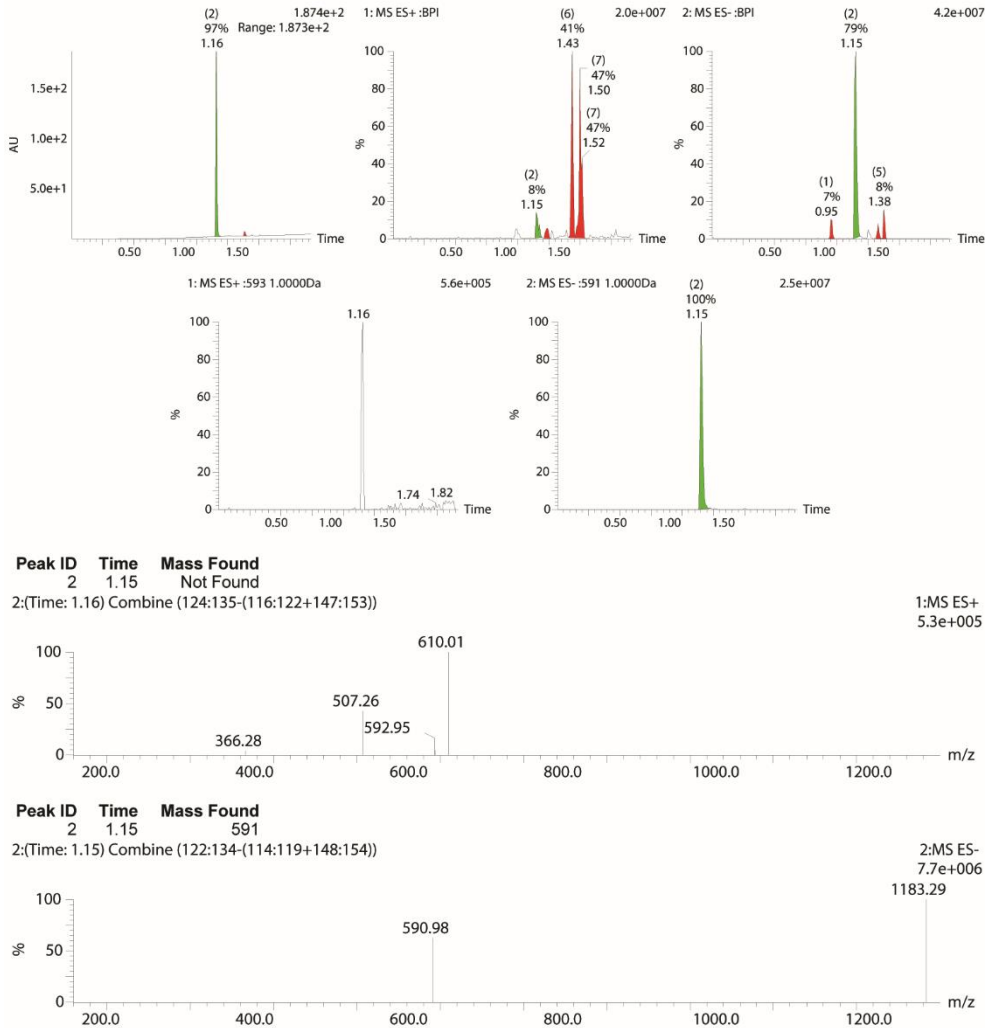


**Figure S4.4** | LC-MS analysis of 4.11. Green peak ( $R_t = 1.16$  min) exhibits the correct mass both in positive and negative ionization mode. Expected mass for 4.11: 592.04;  $m/z$   $[M + H]^+ = 592.95$  Da;  $m/z$   $[M - H]^- = 590.98$  Da.

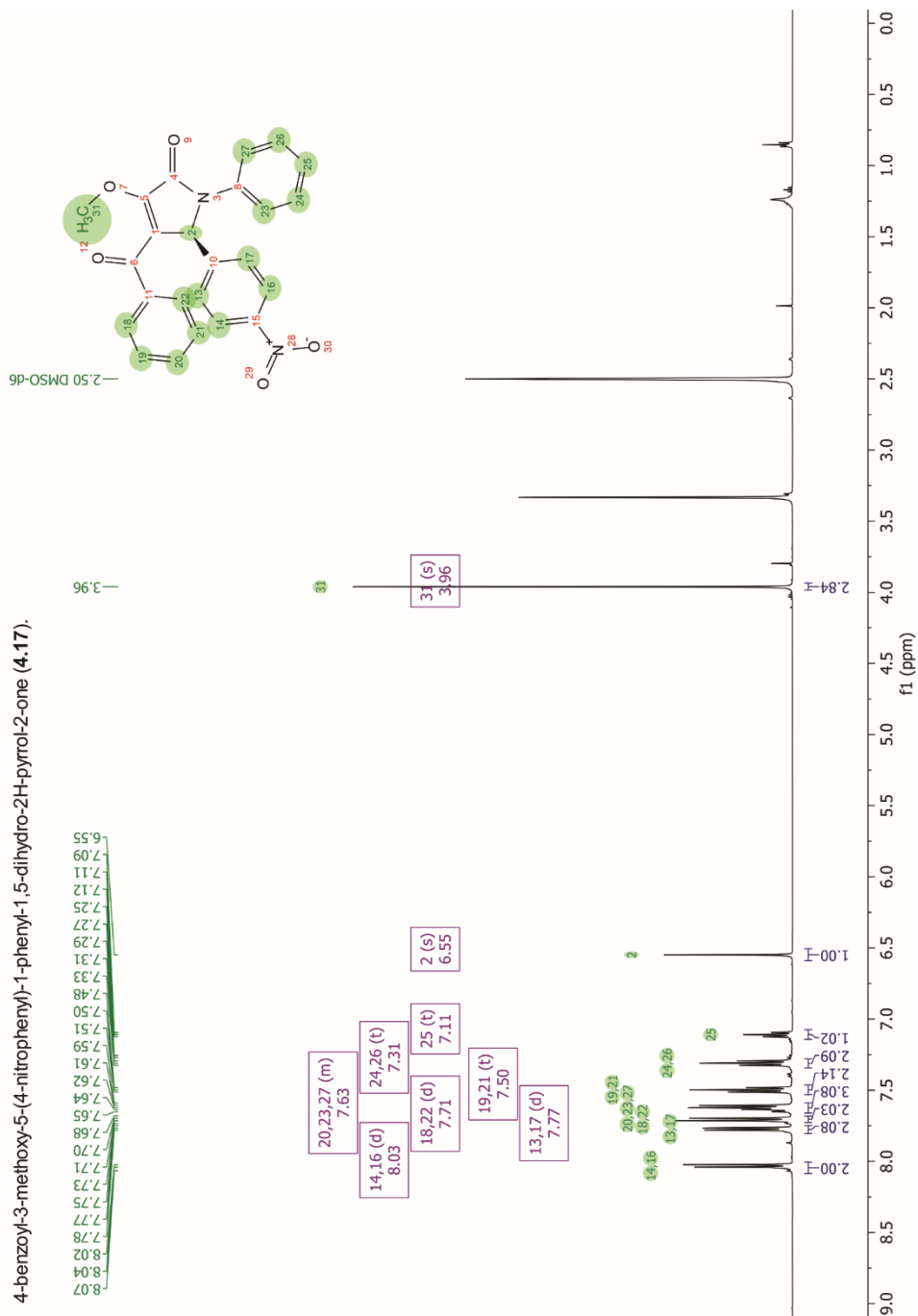


Figure S4.5 | <sup>1</sup>H NMR spectra in DMSO-d<sub>6</sub> of 4.17 with relative assignments.

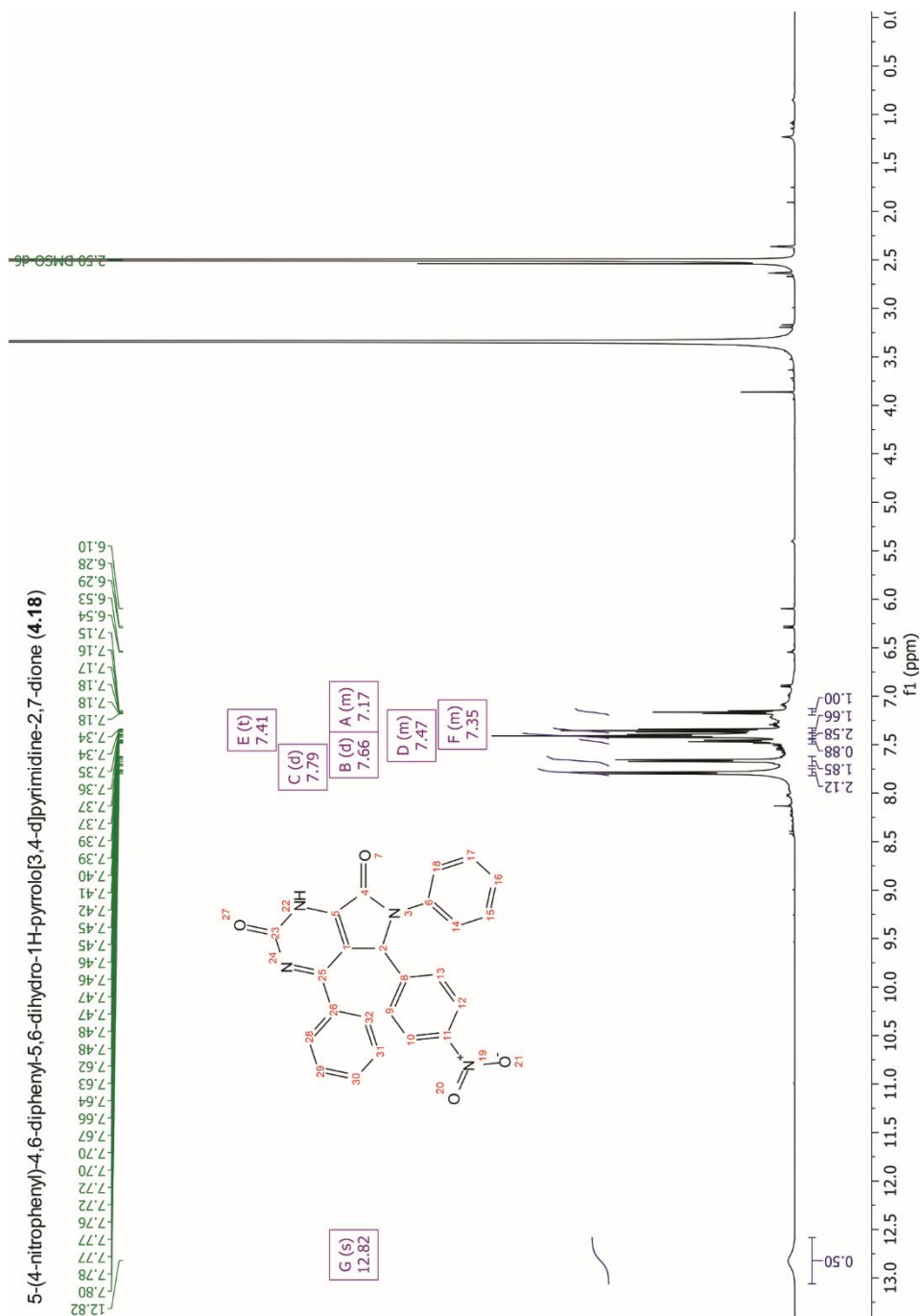


Figure S4.6 |  $^1\text{H}$  NMR spectra in DMSO- $d_6$  of 4.18.



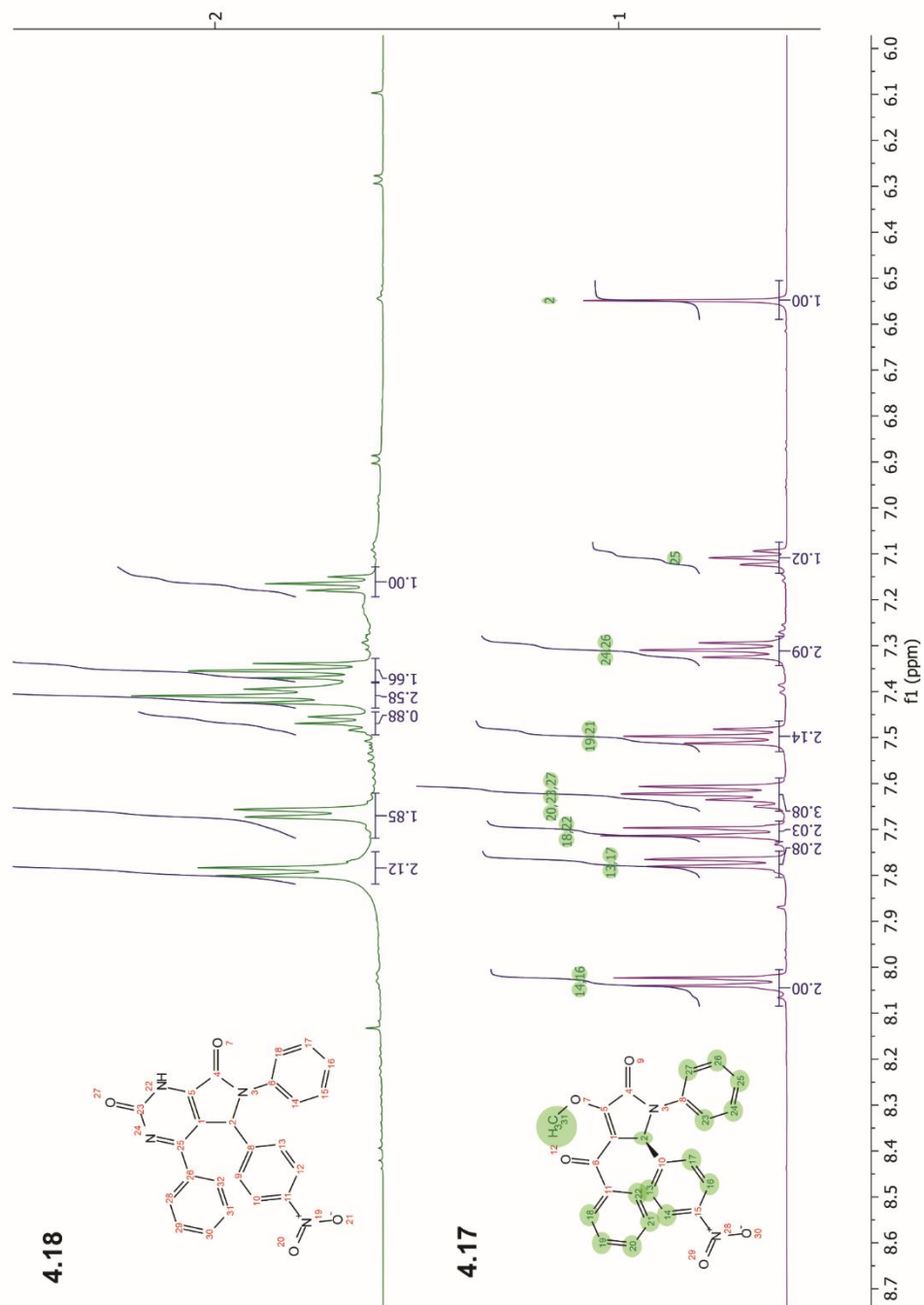


Figure S4.7 | Stacked <sup>1</sup>H NMR spectra of **4.17** (bottom, purple) and **4.18** (top, green).

## 4.6.2 Chemistry

### *General Information*

All solvents and reagents were obtained from commercially available sources and used without further purification. The microwave syntheses were performed in a Biotage Initiator with an external surface IR probe. Flash column chromatography was carried out on prepacked silica gel columns supplied by Biotage and using Biotage automated flash systems with UV detection.

UHPLC-MS experiments were performed using a Waters Acquity UHPLC system combined with a SQD mass spectrometer. The UHPLC system was equipped with a HSS C18 column 1.8  $\mu\text{m}$  2.1 $\times$ 50 mm in combination with 10 mM formic acid or 1 mM ammonium formate buffer at pH 3. The mass spectrometer used ESI+/- as ion source. UPLC was also carried out using a Waters UPLC fitted with Waters QDa mass spectrometer (Column temp 40°C, UV = 190–400 nm, MS = ESI with pos/neg switching) equipped with a Waters Acquity BEH 1.7  $\mu\text{m}$  2.1 $\times$ 100 mm in combination with either 0.1% formic acid in water, 0.05% TFA in water or 0.04%  $\text{NH}_3$  in water. The flow rate was 1 mL/min.

Preparative HPLC was performed by Waters Fraction Lynx with ZQ MS detector on either a Waters Xbridge C18 OBD 5  $\mu\text{m}$  column (19 $\times$ 150 mm, flow rate 30 mL/min or 30 $\times$ 150 mm, flow rate 60 mL/min) using a gradient of 5–95% ACN with 0.2%  $\text{NH}_3$  at pH 10 or a Waters SunFire C18 OBD 5  $\mu\text{m}$  column (19 $\times$ 150 mm, flow rate 30 mL/min or 30 $\times$ 150 mm, flow rate 60 mL/min) using a gradient of 5–95% ACN with 0.1 M formic acid or on a Gilson Preparative HPLC with a UV/VIS detector 155 on a Kromasil C8 10  $\mu\text{m}$  column (20  $\times$  250 mm, flow rate 19 mL/min, or 50  $\times$  250 mm, flow rate 100 mL/min) using a varying gradient of ACN with 0.1% formic acid (FA) in water or 0.2% trifluoroacetic acid (TFA) in water or 0.2% acetic acid (AcOH) in water or 0.2% ammonia ( $\text{NH}_3$ ) in water. Molecular mass (HR-ESI-MS) was recorded using a Shimadzu LCMS-2020 instrument (ESI+). Purity of all test compounds was determined by LCMS. All screening compounds had a purity >95%.

General  $^1\text{H}$  NMR spectra were recorded on a Bruker Avance II, III, AV300, AV400 or AVIII500 spectrometer at a proton frequency of 500 MHz at 25 °C or at a temperature and frequency stated in each experiment.  $^{13}\text{C}$  NMR spectra were recorded at 126 MHz.

The chemical shifts ( $\delta$ ) are reported in parts per million (ppm) with residual solvent signal used as a reference (( $\text{CD}_3$ ) $_2\text{SO}$  at 2.50 ppm for  $^1\text{H}$  NMR and 39.52 ppm for  $^{13}\text{C}$  NMR). Coupling constants ( $J$ ) are reported as Hz. NMR abbreviations are used as follows: br = broad, s = singlet, d = doublet, t = triplet, q = quartet, m = multiplet. Protons on heteroatoms such as  $\text{COOH}$  protons are only reported when detected in NMR and can therefore be missing.

### *Synthetic procedures and compound characterization*

**5-(3-Benzoyl-2-(4-nitrophenyl)-5-oxo-4-(((trifluoromethyl)sulfonyl)oxy)-2,5-dihydro-1H-pyrrol-1-yl)-2-hydroxybenzoic acid (4.11).** To a suspension of **4.1** (150 mg, 0.33 mmol) in anhydrous THF (3 mL) at -78 °C, lithium bis(trimethylsilyl)amide (0.977 ml, 0.98 mmol) was added. The reaction mixture was stirred for 30min at -78°C under inert atmosphere. Subsequently, N-(5-chloropyridin-2-yl)-1,1,1-trifluoro-N-((trifluoromethyl)sulfonyl)methanesulfonamide (154 mg, 0.39 mmol) (Comins' reagent), previously dissolved in anhydrous THF (1 mL), was added dropwise. The resulting mixture was allowed to warm up at room temperature while stirring, over two hours. Another equivalent of Comin's reagent was then added, which turned the suspension into a clear orange solution. After solvent removal, the residue was purified by automated flash chromatography on a Biotage® KP-SIL 10g column. A gradient from 0% to 20% of MeOH + 10% formic acid in  $\text{CH}_2\text{Cl}_2$  over 20CV was used as mobile phase. The product was collected using the wavelength 254

## CHAPTER 4

nm. Product fractions were collected, to afford the title compound (18 mg, 9 %) as pale yellow solid. MS (ESI)  $m/z$   $[M + H]^+$  calcd for  $C_{25}H_{15}F_3N_2O_{10}S$ : 593.05, found: 592.95. Purity: 97%.  $R_t$  = 1.16 min

**4-Benzoyl-3-hydroxy-5-(4-nitrophenyl)-1-phenyl-1,5-dihydro-2H-pyrrol-2-one (4.12).** In vial, to a solution of ethyl 2,4-dioxo-4-phenylbutanoate (430 mg, 1.95 mmol) in AcOH (6 mL), 4-nitrobenzaldehyde (295 mg, 1.95 mmol) and aniline (0.178 mL, 1.95 mmol) were added. The vial was capped and heated at 120 °C for 180 min in a single node microwave reactor. The pressure monitored was 1 bar. The mixture was diluted with diethyl ether and filtered. The filtered solid was washed with diethyl ether and dried under reduced pressure to give the title product (425 mg, 54%) as an off-white solid.  $^1H$  NMR (500 MHz, DMSO)  $\delta$  12.20 (bs, 1H), 8.04 (d,  $J$  = 8.8 Hz, 2H), 7.69 – 7.78 (m, 4H), 7.65 (d,  $J$  = 7.8 Hz, 2H), 7.57 (t,  $J$  = 7.4 Hz, 1H), 7.45 (t,  $J$  = 7.7 Hz, 2H), 7.32 (t,  $J$  = 7.9 Hz, 2H), 7.12 (t,  $J$  = 7.4 Hz, 1H), 6.52 (s, 1H).  $^{13}C$  NMR (126 MHz, DMSO)  $\delta$  189.08, 164.60, 150.98, 147.15, 144.63, 137.88, 136.05, 132.77, 129.27, 128.90, 128.76, 128.21, 125.67, 123.47, 122.52, 119.15, 60.33. HRMS (ESI)  $m/z$   $[M + H]^+$  calcd for  $C_{23}H_{16}N_2O_5$ : 401.1137, found: 401.1128. Purity: 99%.  $R_t$  = 1.21 min.

**4-Benzoyl-3-methoxy-5-(4-nitrophenyl)-1-phenyl-1,5-dihydro-2H-pyrrol-2-one (4.17).** In a vial, to a suspension of **4.12** (200 mg, 0.50 mmol) in MeOH/ACN (1:4), (diazomethyl)trimethylsilane (0.325 mL, 0.65 mmol) was added portion-wise over 10 min while stirring at room temperature, under inert atmosphere. The reaction was monitored by LC-MS until complete consumption of the starting material was observed. Reaction was quenched by addition of few drops of acetic acid, then volatiles were removed under reduced pressure. The residue was purified by automated flash chromatography on a Biotage® KP-SIL 10g column. A gradient from 30% to 70% of EtOAc in heptane over 15CV was used as mobile phase. The product was collected using the wavelength 254 nm. Product fractions were collected, to afford the title compound (157 mg, 76 %) as a off-white solid.  $^1H$  NMR (500 MHz, DMSO)  $\delta$  8.03 (d,  $J$  = 8.7 Hz, 2H), 7.77 (d,  $J$  = 7.4 Hz, 2H), 7.71 (d,  $J$  = 8.7 Hz, 2H), 7.63 (dd,  $J$  = 14.3, 7.8 Hz, 3H), 7.50 (t,  $J$  = 7.7 Hz, 2H), 7.31 (t,  $J$  = 7.9 Hz, 2H), 7.11 (t,  $J$  = 7.4 Hz, 1H), 6.55 (s, 1H), 3.96 (s, 3H). MS (ESI)  $m/z$   $[M + H]^+$  calcd for  $C_{24}H_{18}N_2O_5$ : 415.1, found: 415.4. Purity: 100%.  $R_t$  = 1.34 min.

**5-(4-Nitrophenyl)-4,6-diphenyl-5,6-dihydro-1H-pyrrolo[3,4-d]pyrimidine-2,7-dione (4.18).** In a vial, **4.17** (50 mg, 0.12 mmol) and urea (72.5 mg, 1.21 mmol) were dissolved in sodium methanolate 30% solution in MeOH (3 mL) at room temperature under inert atmosphere. The reaction was refluxed overnight. Volatiles were removed, then the crude mixture was re-dissolved in DMSO and purified directly. The compound was purified by preparative HPLC (25-65% ACN in  $H_2O$ /ACN/FA 95/5/0.2 buffer, over 20 min), to give the title compound (4 mg, 8 %) as a pale orange solid. MS (ESI)  $m/z$   $[M + H]^+$  calcd for  $C_{24}H_{16}N_4O$ : 425.13, found: 425.06. Purity: 95%.  $R_t$  = 1.03 min.

## CHAPTER 4

### 4.7 REFERENCES

1. Fang, Z.; Song, Y. n.; Zhan, P.; Zhang, Q.; Liu, X. Conformational restriction: an effective tactic in 'follow-on'-based drug discovery. *Future Med. Chem.* **2014**, *6* (8), 885-901.
2. Perola, E.; Charifson, P. S. Conformational Analysis of Drug-Like Molecules Bound to Proteins: An Extensive Study of Ligand Reorganization upon Binding. *J. Med. Chem.* **2004**, *47* (10), 2499-2510.
3. Boström, J.; Norrby, P. O.; Liljefors, T. Conformational energy penalties of protein-bound ligands. *J. Comput. Aided Mol. Des.* **1998**, *12* (4), 383-96.
4. Blundell, C. D.; Packer, M. J.; Almond, A. Quantification of free ligand conformational preferences by NMR and their relationship to the bioactive conformation. *Biorg. Med. Chem.* **2013**, *21* (17), 4976-4987.
5. Zheng, Y.; Tice, C. M.; Singh, S. B. Conformational control in structure-based drug design. *Biorg. Med. Chem. Lett.* **2017**, *27* (13), 2825-2837.
6. Richter, A.; Rose, R.; Hedberg, C.; Waldmann, H.; Ottmann, C. An Optimised Small-Molecule Stabiliser of the 14-3-3–PMA2 Protein–Protein Interaction. *Chem. – Eur. J.* **2012**, *18* (21), 6520-6527.
7. Cai, J.; Rankovic, Z.; Moir, J. H. Preparation of 4-phenylpyridine-2-carbonitrile derivs. as inhibitors of cathepsin K and cathepsin S. WO2005121106A1, 2005.
8. Rankovic, Z.; Cai, J.; Kerr, J.; Fradera, X.; Robinson, J.; Mistry, A.; Hamilton, E.; McGarry, G.; Andrews, F.; Caulfield, W.; Cumming, I.; Dempster, M.; Waller, J.; Scullion, P.; Martin, I.; Mitchell, A.; Long, C.; Baugh, M.; Westwood, P.; Kinghorn, E.; Bruin, J.; Hamilton, W.; Uitdehaag, J.; Zeeland, M. v.; Potin, D.; Saniere, L.; Fouquet, A.; Chevallier, F.; Deronzier, H.; Dorleans, C.; Nicolai, E. Design and optimization of a series of novel 2-cyano-pyrimidines as cathepsin K inhibitors. *Biorg. Med. Chem. Lett.* **2010**, *20* (5), 1524-1527.
9. PAZ, C.; PETER, M. G.; SCHMIDT, B.; BECERRA, J.; GUTIÉRREZ, M.; ASTUDILLO, L.; SILVA, M. SYNTHESIS AND AChE INHIBITING ACTIVITY OF 2, 4 SUBSTITUTED 6-PHENYL PYRIMIDINES. *J. Chil. Chem. Soc.* **2012**, *57*, 1292-1294.
10. Wen, N.; Brooker, M. H. Urea protonation: Raman and theoretical study. *The Journal of Physical Chemistry* **1993**, *97* (33), 8608-8616.
11. Coppola, G. M.; Fraser, J. D.; Hardtmann, G. E.; Huegi, B. S.; Kathawala, F. G. Pyrimidones 1. Synthesis of some 1-substituted-5-aryl- and (4,5-diaryl)-2(1H)pyrimidones. *J. Heterocycl. Chem.* **1979**, *16* (3), 545-554.
12. *Lewis Acids in Organic Synthesis*. WILEY-VCH Verlag GmbH: 2000.
13. Román-Leshkov, Y.; Davis, M. E. Activation of Carbonyl-Containing Molecules with Solid Lewis Acids in Aqueous Media. *ACS Catalysis* **2011**, *1* (11), 1566-1580.
14. Bonacorso, H. G.; Costa, M. B.; Lopes, I. S.; Oliveira, M. R.; Drekenner, R. L.; Martins, M. A. P.; Zanatta, N.; Flores, A. F. C. Synthesis of Tetrahydro-2(1H)quinazolinones, Cyclopenta[d]-2(1H)pyrimidinones, and Their Thioxo Analogs from 2-Trifluoroacetyl-1-methoxycycloalkenes. *Synth. Commun.* **2005**, *35* (23), 3055-3064.
15. Wang, C.; Xu, H.; Xie, Z.; Wang, X.; Zhang, Z.; Sun, Q. Chlorotrimethylsilane-promoted one-pot synthesis of steroidal[17,16-d]pyrimidines. *Steroids* **2010**, *75* (12), 1033-1038.
16. Azizian, J.; Mirza, B.; Mojtahedi, M. M.; Abaee, M. S.; Sargordan, M. Biginelli reaction for synthesis of novel trifluoromethyl derivatives of bis(tetrahydropyrimidinone)benzenes. *J. Fluorine Chem.* **2008**, *129* (11), 1083-1089.

## CHAPTER 4

17. Mirza-Aghayan, M.; Moradi, A.; Bolourtchian, M.; Boukherroub, R. Cheap and Efficient Protocol for the Synthesis of Tetrahydroquinazolinone, Dihydropyrimidinone, and Pyrimidinone Derivatives. *Synth. Commun.* **2009**, *40* (1), 8-20.
18. Kappe, C. O. A Reexamination of the Mechanism of the Biginelli Dihydropyrimidine Synthesis. Support for an N-Acyliminium Ion Intermediate<sup>1</sup>. *J. Org. Chem.* **1997**, *62* (21), 7201-7204.
19. Oliver Kappe, C. 100 years of the biginelli dihydropyrimidine synthesis. *Tetrahedron* **1993**, *49* (32), 6937-6963.
20. Chlorotrimethylsilane. In *Encyclopedia of Reagents for Organic Synthesis*.
21. Izumi, M.; Fukase, K.; Kusumoto, S. TMSCl as a Mild and Effective Source of Acidic Catalysis in Fischer Glycosidation and Use of Propargyl Glycoside for Anomeric Protection. *Bioscience, Biotechnology, and Biochemistry* **2002**, *66* (1), 211-214.
22. Comins, D. L.; Dehghani, A. Pyridine-derived triflating reagents: An improved preparation of vinyl triflates from metallo enolates. *Tetrahedron Lett.* **1992**, *33* (42), 6299-6302.
23. Tasber, E. S.; Garbaccio, R. M. Thermodynamic equilibration of dihydropyridone enolates: application to the total synthesis of (+/-)-epiuleine. *Tetrahedron Lett.* **2003**, *44* (51), 9185-9188.
24. Palanki, M. S. S.; Erdman, P. E.; Gayo-Fung, L. M.; Shevlin, G. I.; Sullivan, R. W.; Goldman, M. E.; Ransone, L. J.; Bennett, B. L.; Manning, A. M.; Suto, M. J. Inhibitors of NF- $\kappa$ B and AP-1 Gene Expression: SAR Studies on the Pyrimidine Portion of 2-Chloro-4-trifluoromethylpyrimidine-5-[N-(3',5'-bis(trifluoromethyl)phenyl)carboxamide]. *J. Med. Chem.* **2000**, *43* (21), 3995-4004.
25. Galvão, T. L. P.; Rocha, I. M.; Ribeiro da Silva, M. D. M. C.; Ribeiro da Silva, M. A. V. From 2-Hydroxypyridine to 4(3H)-Pyrimidinone: Computational Study on the Control of the Tautomeric Equilibrium. *The Journal of Physical Chemistry A* **2013**, *117* (47), 12668-12674.
26. Gallant, M.; Phan Viet Minh, T.; Wuest, J. D. Hydrogen-bonded dimers. Direct study of the interconversion of pyridone dimers and hydroxypyridine monomers by low-temperature nuclear magnetic resonance spectroscopy. *J. Am. Chem. Soc.* **1991**, *113* (2), 721-723.

# CHAPTER 5

## Optimization Of Pyrrolidone-Based Druglike Molecules For The Stabilization Of 14-3-3 Protein-Protein Interactions: Achieving Full-Length PPI Stabilization

### **Abstract**

Stabilization of protein-protein interactions (PPIs) has recently emerged as a promising, yet still relatively unexplored, drug discovery strategy. Progress is hampered by the paucity of available high-quality chemical starting points for the rational study of PPI stabilization. In this regard, the PPI of 14-3-3 adapter proteins with phosphorylated binding partners represent a model system for the study of PPI stabilization. The synthetically tractable Pyrrolidone<sup>1</sup> and a number of its derivatives have been previously shown to selectively stabilize different 14-3-3 PPIs. Starting from these compounds, an expanded library of Pyrrolidone<sup>1</sup> analogues was synthesized and characterized by means of two biophysical assay. Structure-activity relationship analysis was performed, highlighting new selective stabilizers. A crystal structure of two of the synthesized derivatives was obtained, revealing new structural insights of these class of stabilizers. Moreover, we report for the first time the stabilization of a 14-3-3 PPI with a full-length binding partner, proving the feasibility of the use of phosphopeptides as 14-3-3 binding partner mimics. The work presented in this chapter demonstrates the potential of rational design approaches in the development of selective PPI stabilizers and provides new insights for a more in-depth understanding of the structural drivers underlying 14-3-3 PPIs.

## 5.1 INTRODUCTION

Stabilisation of protein-protein interactions (PPIs) by small molecules has emerged as an interesting strategy in drug discovery over the past decade. Testimony to the feasibility of this approach comes both from nature and from a growing number of synthetic molecules reported in literature<sup>1</sup>. However, the *ab initio* discovery of druglike, small molecule PPI stabilizers remains elusive, as most of the reported ones were discovered serendipitously.<sup>2</sup> The reason for this needs to be mostly ascribed to the lack of high-quality starting points. This paucity of chemical probes limits, on one hand, the druggability assessment of the desired PPI target and, on the other, complicates the evaluation of the possible biological effects associated to that PPI target.<sup>3</sup>

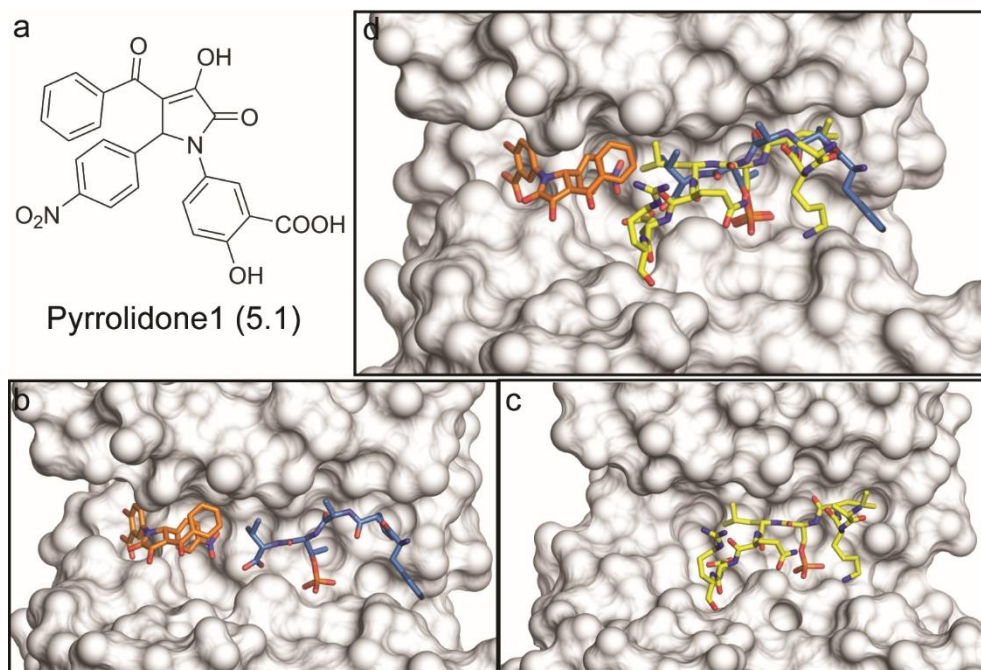


**Figure 5.1** | (*R*)-Pyrrolidone1 (*R*-5.1) stabilizes different 14-3-3 PPIs. (a) Chemical structure of 5.1. (b) Crystal structure of 14-3-3 $\sigma$  (pink surface), ER $\alpha$ (pT<sup>594</sup>) (5.2, blue sticks) and (*R*)-5.1 (orange sticks) (PDB 6TJM) ternary complex. (c) Crystal structure of 14-3-3 $\zeta$  (pink surface) and CaMKK2(pS<sup>100</sup>) (5.3, yellow sticks) binary complex. (d) Superimposition of the 14-3-3 $\sigma$ :5.2:(*R*)-5.1 and 14-3-3 $\zeta$ :5.3.

In this context, the 14-3-3 proteins represent a viable platform for the development of new conceptual approaches to study the principles of PPI stabilization.<sup>4</sup> 14-3-3s are ubiquitously expressed adapter proteins, comprising seven human isoforms ( $\beta$ ,  $\epsilon$ ,  $\gamma$ ,  $\eta$ ,  $\sigma$ ,  $\tau$ , and  $\zeta$ ), that act by binding to phosphorylated consensus motifs through their highly conserved amphipathic groove.<sup>5</sup> Upon binding

## CHAPTER 5

to their protein partners, 14-3-3s regulate protein localization, protein folding and modulation of other PPIs.<sup>6</sup> Several hundreds of potential 14-3-3 binding partners have been identified,<sup>7</sup> of which many are relevant to disease, and therefore targeting these PPIs represents a potentially attractive strategy for therapeutic purposes.<sup>8-9</sup>

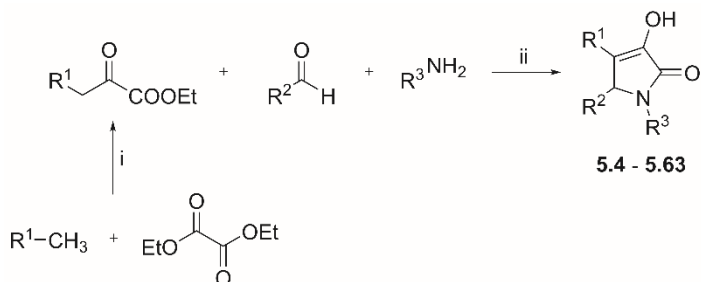
Chapters 3 dealt with the synthetic molecule pyrrolidone1 (**5.1**, Figure 5.1a) and a number of its derivatives that act as stabilizers of different 14-3-3 PPI partners, highlighting principles of selectivity and potential scope for SAR investigation. Moreover, Chapter 3 described the metal ion-dependent 14-3-3 PPI stabilization potency of **5.1**, whereby addition of  $Mg^{2+}$  and other bivalent metal ions to the assay buffer resulted in up to a 100-fold increase in stabilization potency.<sup>10</sup> This was due to preferential stabilization of the bioactive conformation by chelation of bivalent metal ions by the vinylogous carboxylate moiety, which eventually lead to an improved assay window and wider dynamic range of stabilization. The effect could be recapitulated by installing an intramolecularly H-bonding vinylogous amide. But this was at the expense of additional synthetic steps and therefore, in this chapter, the chelation effect was exploited to carry out SAR analysis to explore the effect of varying of  $R^1$ - $R^3$  in the synthetically more accessible vinylogous carboxylates (Scheme 5.1).

The two 14-3-3 binding partners initially presented in chapter 3, namely estrogen receptor alpha ( $ER\alpha$ ) and calcium/calmodulin-dependent protein kinase kinase 2 (CaMKK2) (Figure 5.1c-d) were selected for this purpose. In this study, we report the synthesis and SAR characterization of novel pyrrolidone derivatives and their biophysical evaluation against both targets using assays based on truncated phosphopeptides derived from  $ER\alpha$  and CaMKK2. Furthermore, we show that **5.1** is able to stabilize the interaction between 14-3-3 and full-length CaMKK2, hence proving that the use of phosphopeptides seems to be predictive of stabilization for full-length proteins as well as that the applicability of this class of compounds can be extended to the study of full-length PPIs.

### 5.2 LIBRARY SYNTHESIS AND ASSAY SET-UP

The racemic pyrrolidones **5.4** - **5.63** were synthesized in parallel fashion via a Biginelli-type reaction, a one-pot multicomponent condensation reaction involving  $\alpha$ -ketoesters, amines and aldehydes as starting materials, reacted in acetic acid under microwave heating (Scheme 5.1).<sup>10</sup> Non-commercially available  $\alpha$ -ketoesters **5.5** and **5.9** were prepared by Claisen condensation starting from the corresponding methyl ketone and diethyl oxalate.<sup>11</sup>





**Scheme 5.1** | Synthesis of pyrrolidone-based derivatives of **5.1**. i) EtONa, THF, 0 °C – RT, o/n. ii) AcOH, 3 h, 120 °C.

For the evaluation of compound stabilization effect we established fluorescence polarization (FP) and surface plasmon resonance (SPR) assays based on 14-3-3 $\zeta$  and ER $\alpha$ - and CaMKK2-derived phosphopeptides, namely ER $\alpha$ (pT<sup>594</sup>) (**5.2**, sequence AEGFPaPT<sup>594</sup>V-COOH)<sup>12</sup> and CaMKK2(pS<sup>100</sup>) (**5.3**, sequence: GSLSARKLpS<sup>100</sup>LQER)<sup>13</sup>, with pT<sup>594</sup> and pS<sup>100</sup> denoting the threonine and serine phosphosites (Figure 5.1).

All vinylogous carboxylates were tested in both FP and SPR assays in the presence of 10 mM MgCl<sub>2</sub>, the concentration at which the maximum metal-promoted stabilization effect is achieved for **5.1**. Moreover, due to laborious chiral separation procedures, all the final pyrrolidones here presented were tested as racemates.

For most of the compounds discussed herein, a full concentration-response curve could not be obtained. Therefore, for the FP assay, we defined the parameter “EC<sub>1.2</sub>” to be used for SAR analysis and comparison among the different compounds instead of the more customary EC<sub>50</sub>. EC<sub>1.2</sub> is defined as the concentration of compound, expressed in  $\mu$ M, that causes a 1.2-fold increase in stabilization of the 14-3-3/phosphopeptide complex. For compounds which did not reach 1.2-fold stabilization, an EC<sub>1.2</sub> is not reported. For compounds that achieved a full concentration-response curve, both EC<sub>50</sub> and EC<sub>1.2</sub> were reported. For **5.1**, the potency and stabilization effect of the 14-3-3/ER $\alpha$ (pT<sup>594</sup>) and 14-3-3/CaMKK2(pS<sup>100</sup>) PPIs were found to be in accordance with previously reported data in chapter 3. In SPR assay, for 14-3-3/CaMKK2(pS<sup>100</sup>)/**5.1**, a EC<sub>50</sub> value of 4.2  $\mu$ M could be determined (Figure S5.1). From this point in the text, 14-3-3/ER $\alpha$ (pT<sup>594</sup>) and 14-3-3/CaMKK2(pS<sup>100</sup>) PPIs will be simply referred as by their respective 14-3-3 binding partners, ER $\alpha$  and CaMKK2.

### 5.3 STRUCTURE-ACTIVITY RELATIONSHIP (SAR)

**Modifications to R<sup>1</sup>** (Table 5.1, Figure 5.3). Based on our published crystal structure of **5.1** in complex with 14-3-3/ER $\alpha$  (PDB 6TJM),<sup>10</sup> the benzoyl moiety of

(*R*)-**5.1** points mainly toward a hydrophobic pocket formed by Leu218, Ile219 and Leu222 of 14-3-3 $\sigma$  (residues numbering based on 6TJM) and also partly faces Val595 of the phosphopeptide **5.2** (residues numbering based on full length ER $\alpha$ ,<sup>12</sup> Figure 5.2). Therefore, we reasoned that modifications to R<sup>1</sup> would be beneficial for two main reasons. Firstly, additional affinity for 14-3-3 protein can be gained by introducing non-polar interactions with the hydrophobic residues. Secondly, selectivity against different 14-3-3 PPI client partners could be conferred by introducing specific compound-phosphopeptide interactions.

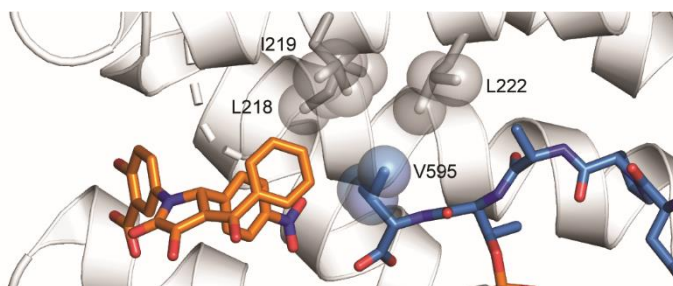


**Figure 5.2** | Binding mode of (*R*)-**5.1** in ER $\alpha$ (pT<sup>594</sup>). The phenyl ring of (*R*)-**5.1** points towards hydrophobic residues Leu218, Ile219 and Leu222 and faces Val595 of the ER $\alpha$ (pT<sup>594</sup>) peptide.

2-Chlorobenzoyl (**5.4**) afforded an EC<sub>1.2</sub> of 65  $\mu$ M for ER $\alpha$ , and 8  $\mu$ M for CaMKK2. 2-Bromobenzoyl (**5.5**) led to an improvement in both potency (EC<sub>1.2</sub> 39  $\mu$ M) and stabilization effect at 200  $\mu$ M (1.65-fold versus 1.40-fold for **5.4**) in ER $\alpha$ . **5.5** was also more potent than **5.4** for CaMKK2 (EC<sub>1.2</sub> 5.4  $\mu$ M), but not in maximum stabilization effect at 200  $\mu$ M (2.45-fold vs 2.40-fold for **5.4**). Due to greater overall potency for CaMKK2 compared to ER $\alpha$ , EC<sub>50</sub> values for both **5.4** (55  $\mu$ M) and **5.5** (41  $\mu$ M) could be generated for CaMKK2, showing an analogous trend as for the EC<sub>1.2</sub>.

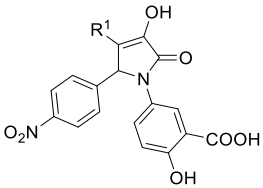
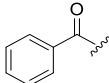
A 2-acetylpyrid-1-yl (**5.9**) moiety introduces polarity at the 2 position relative to the carbonyl, which appears to be tolerated, with EC<sub>1.2</sub> 48  $\mu$ M for ER $\alpha$  and EC<sub>1.2</sub> 7  $\mu$ M and EC<sub>50</sub> 33  $\mu$ M for CaMKK2, with similar stabilization effect to **5.4** and **5.5** (1.60-fold for ER $\alpha$  and 2.42-fold for CaMKK2). SPR testing of **5.9** did not show a clear stabilization effect for ER $\alpha$ , but confirmed the FP data for CaMKK2 (Figure S5.2). Difluoromethoxy substitution at the meta position of the phenyl ring (**5.6**), was detrimental for ER $\alpha$ , with the stabilization effect dropping below 1.2-fold (1.17-fold), but was tolerated by CaMKK2 (EC<sub>1.2</sub> 17  $\mu$ M). The tolerance of both lipophilic and polar substituents at this position, with no marked differences in terms of potency and stabilization effect among them, is presumably ascribed to the fact that such substituents are pointing towards a solvent-exposed space.

6-chlorobenzoyl analogue **5.7** was as potent as **5.1** for ER $\alpha$  in the FP and SPR assay, both in terms of potency and stabilization effect. For CaMKK2, in FP **5.7**

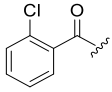
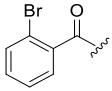
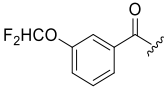
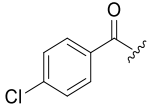
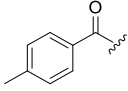
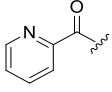
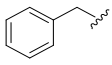
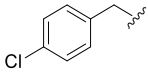
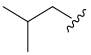
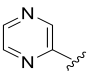
exhibited analogous potency to **5.1** ( $EC_{50}$  8.9 vs 8.6  $\mu\text{M}$ ) and slightly higher stabilization effect (2.95-fold vs 2.74-fold). In SPR, although a strong stabilization effect was measured at the highest concentration tested (4.42-fold at 100  $\mu\text{M}$ ), an  $EC_{50}$  value could not be determined due to the lack of a full concentration response curve (Figure S5.2). Replacement of the chlorine atom with a methyl substituent (**5.8**) resulted in a slight loss in both potency ( $EC_{1.2}$  52  $\mu\text{M}$  for  $ER\alpha$  and  $EC_{50}$  14  $\mu\text{M}$  for CaMKK2) and stabilization effect (1.68-fold for  $ER\alpha$  and 2.68-fold for CaMKK2) in FP assay.

Replacement of the carbonyl with a methylene (compounds **5.10** – **5.12**) was shown to be detrimental in both  $ER\alpha$  and CaMKK2. Interestingly, comparison of compounds **5.10** and **5.12** shows how a phenyl ring (**5.10**) is still preferred over smaller alkyl groups such as isopropyl (**5.12**). Also, comparison of **5.10** with its 4-chloro analogue **5.11** highlights an inverted trend compared to their corresponding benzoyl analogues (**5.1** and **5.7**, respectively). Replacement of the carbonyl by a methylene introduces significant variations to the molecule. Flexibility is increased due to the lack of chelatable moiety but also due to loss of conjugation. The loss of conjugation indeed makes the molecule more flexible even in the absence of bivalent metal ions and will also affect the  $pK_a$  of the vinylogous OH and hence the electronics of the whole pyrrolidone ring. The higher flexibility probably also results in a steric clash of the bulkier 4-chlorobenzyl group of **5.11** (when compared to the benzyl group of **5.10**) with the protein. Overall, these combined effects led to a drastic drop in potency ( $EC_{1.2}$  could not be defined), as well as stabilization effect (1.10-fold for  $ER\alpha$  and 1.19 for CaMKK2).

**Table 5.1** | Stabilization effect of compounds **5.4** - **5.13** on 14-3-3/ $ER\alpha$ (pT<sup>594</sup>) and 14-3-3/CaMKK2(pS<sup>100</sup>)

					
Cpd	R <sup>1</sup>	FP		SPR	
		Stabilization effect <sup>a</sup>		Total activity <sup>d</sup>	
		EC <sub>1.2</sub> ( $\mu\text{M}$ ) <sup>b</sup>		Net stabilization effect <sup>e</sup>	
EC <sub>50</sub> ( $\mu\text{M}$ ) <sup>c</sup>		ER $\alpha$	CaMKK2	ER $\alpha$	CaMKK2
<b>5.1</b>		1.90 $\pm$ 0.05 28 (25 to 31) - <sup>f</sup>	2.74 $\pm$ 0.05 1.1 (1.0 to 1.2) 8.6 (7.9 to 9.4) <sup>c</sup>	6.49 $\pm$ 0.42 3.99 $\pm$ 0.26 -	7.41 $\pm$ 1.13 7.15 $\pm$ 0.13 4.2 (3.7 to 4.7)

## CHAPTER 5

<b>5.4</b>		1.40 ± 0.15 65 (39 to 96) -	2.40 ± 0.02 8 (6 to 10) 55 (34 to 163) <sup>c</sup>		
<b>5.5</b>		1.65 ± 0.12 39 (25 to 57) -	2.45 ± 0.01 5.4 (4.7 to 5.2) 41 (34 to 53)		
<b>5.6</b>		1.17 ± 0.04 - -	2.05 ± 0.13 17 (10 to 25) -		
<b>5.7</b>		2.09 ± 0.07 20 (18 to 24) -	2.95 ± 0.09 1.0 (0.7 to 1.3) 8.9 (7.2 to 11.2)	5.25 4.02 -	4.90 4.41 -
<b>5.8</b>		1.68 ± 0.05 52 (37 to 71) -	2.68 ± 0.01 2.2 (1.7 to 2.7) 14 (12 to 19)		
<b>5.9</b>		1.60 ± 0.02 48 (45 to 52) -	2.42 ± 0.14 7 (5 to 10) 33 (25 to 54)	3.95 2.09 -	4.18 3.18 -
<b>5.10</b>		1.23 ± 0.10 173 (136 to 200+) -	1.81 ± 0.09 27 (18 to 40) -		
<b>5.11</b>		1.10 ± 0.15 - -	1.19 ± 0.20 - -		
<b>5.12</b>		1.06 ± 0.07 - -	1.27 ± 0.26 90 (22 to 200+) -		
<b>5.13</b>		1.18 ± 0.12 - -	1.34 ± 0.34 77 (18 to 200+) -		

(a) The stabilization effect is expressed as the mean fold-increase of FP signal over baseline (i.e. interaction between 14-3-3ζ and FITC-**2** or FAM-**3** alone). Measurements were performed in the presence of 50 nM 14-3-3ζ /10 nM FITC-**2** or 30 μM 14-3-3ζ/10 nM FAM-**3**. Values are reported as mean ± SD (n ≥ 2).

(b) EC<sub>1.2</sub> (μM). 95% confidence interval (CI) is reported for each value, in brackets.

(c) EC<sub>50</sub> (μM) values were reported for those compounds where a full concentration-response curve was observed, otherwise the symbol “-” was used, meaning that the value could not be determined. 95% confidence interval (CI) is reported for each value, in brackets.

(d) “Total activity” is defined as the ratio between the “Total effect” and “peptide effect”. “Total effect” corresponds to the total signal obtained by adding compound to immobilized 14-3-3ζ in the presence of phosphopeptides **2** or **3**, i.e. (intrinsic affinity for 14-3-3ζ + affinity for 14-3-3ζ:**2** or **3** complex + stabilization

of 14-3-3 $\zeta$ :**2** or **3** interaction). The “peptide effect” is the signal relative to the affinity of the corresponding phosphopeptide for the protein (i.e. 14-3-3 $\zeta$ :**2** or **3** binary complex interaction). Measurements were performed with ~ 4000 RUs of immobilized 14-3-3 $\zeta$  and 50 nM of **2** or 30  $\mu$ M of **3**. Values are reported as mean  $\pm$  SD ( $n \geq 2$ ). Values without a SD were performed in singlicates.

(e) The net stabilization effect is defined as: (“Total effect” – “compound effect”)/“peptide effect”. “Total effect” and “peptide effect” are defined in point d. “Compound effect” is the compound intrinsic affinity for 14-3-3 $\zeta$  in the absence of phosphopeptide (i.e. 14-3-3 $\zeta$ :compound interaction). Measurements were performed with ~ 4000 RUs of immobilized 14-3-3 $\zeta$  and 50 nM of **2** or 30  $\mu$ M of **3**. Values are reported as mean  $\pm$  SD ( $n \geq 2$ ). Values without a SD were performed in singlicates. Blank cells mean that the compound was not tested in that particular assay.

Taken together, these results confirm our previously reported observations regarding the role of the vinylogous carboxylic acid chelatable moiety and overall conformation in the pyrrolidone scaffold in driving the stabilization potency of these class of compounds for these two 14-3-3 PPIs.

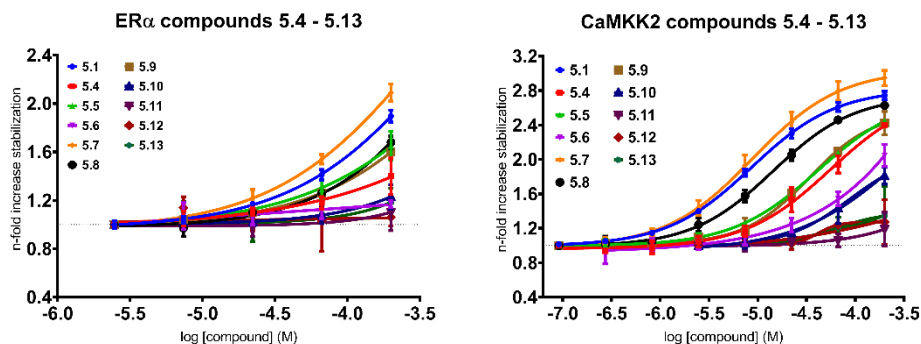


**Figure 5.3** | Stabilization of 14-3-3 $\zeta$ /ER $\alpha$ (pT<sup>594</sup>) (left panel) and 14-3-3 $\zeta$ /CaMKK2(pS<sup>100</sup>) (right panel) PPIs by compounds **5.1** and **5.4** – **5.13** measured by FP. “n-fold increase stabilization” (y-axes) is the mean fold-increase of FP signal over baseline (i.e. interaction between 14-3-3 $\zeta$  and either ER $\alpha$ (pT<sup>594</sup>) or CaMKK2(pS<sup>100</sup>) alone). The error bars in all plots indicate  $\pm$  SD ( $n \geq 2$ ).

**Modifications R<sup>2</sup>** (Table 5.2, Figure 5.6). The crystal structure of (*R*)-**5.1** in complex with 14-3-3 $\zeta$  and ER $\alpha$ (pT<sup>594</sup>) (PDB 6JTM) shows that the nitro group of **5.1** acts as a H-bond acceptor from Lys122 of 14-3-3 $\zeta$  and makes polar contact with the C-terminal Val595 of **2** by a water-bridge (Figure 5.4). Nitro groups are less-than ideal H-bond acceptors, are known to be highly metabolized and to induce severe toxicity.<sup>14</sup> Although they have found useful application, especially as antineoplastic or antibiotic agents,<sup>15</sup> their use in medicinal chemistry is usually avoided.<sup>14</sup> Therefore, alternative groups able to exploit this H-bond interaction were sought.

The importance of this H-bond in driving both the affinity and the stabilization effect of this class of compounds was highlighted when reduction of the nitro functionality to the corresponding amine (**5.14**), removal of either the nitro group

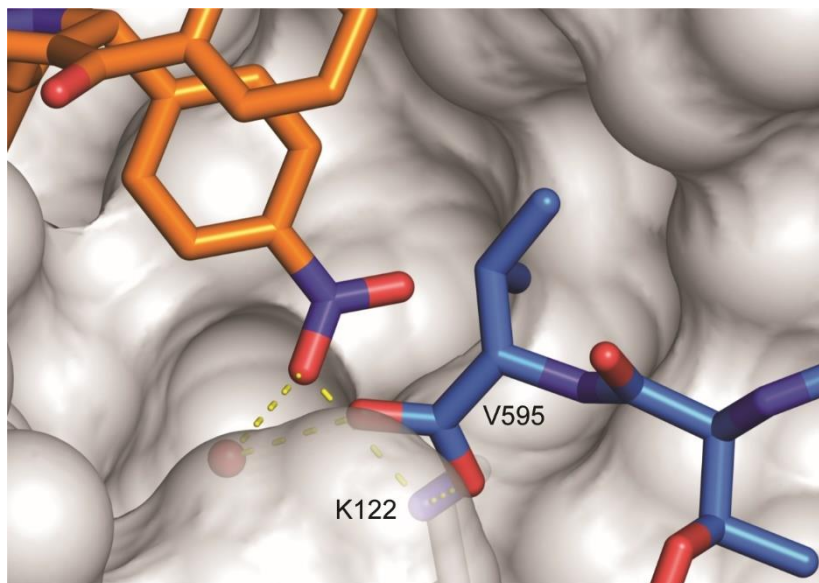


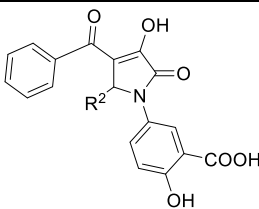
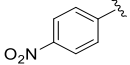
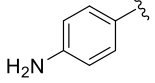
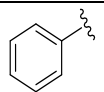
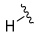
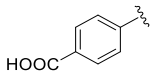
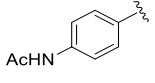
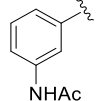
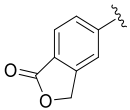
**Figure 5.4** | The nitro group of (*R*)-**5.1** accepts and H-bond from Lys122 of 14-3-3 protein and interacts with Val595 of ER $\alpha$ (pT<sup>594</sup>) via a molecule of water.

**(5.15)** or the entire nitrophenyl ring (**5.16**), as well as its substitution with a carboxyl group (**5.17**), completely abrogated compound activity (EC<sub>1.2</sub> could not be defined in either ER $\alpha$  or CaMKK2). Introduction of an acetamido group at either the para or meta position of the phenyl ring (**5.18** and **5.19**) was detrimental in the CaMKK2 system, but showed a similar, moderate stabilization effect in ER $\alpha$  (1.21-fold and 1.29 fold, respectively), with a preference for the para position in terms of potency (EC<sub>1.2</sub> 191  $\mu$ M for **5.18** and 131  $\mu$ M for **5.19**). SPR assay performed **5.19** also showed only a weak net stabilization effect, with major contribution to the total activity deriving only from the intrinsic affinity of the compound for 14-3-3 $\zeta$  (Figure S3).

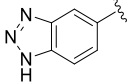
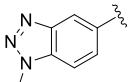
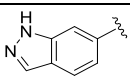
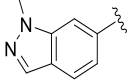
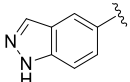
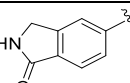
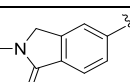
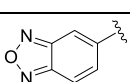
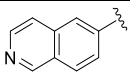
Next, the nitrophenyl moiety was replaced by a number of oxygen- and/or nitrogen-containing heterocyclic aromatic substituents (**5.20** – **5.29**). Benzolactone **5.20** was found to be well-tolerated in ER $\alpha$ , with potency (EC<sub>1.2</sub> 76  $\mu$ M) and stabilization effect (1.56-fold) similar to the nitro derivative **5.1**. Analogously, in CaMKK2, an equal stabilization effect at 200  $\mu$ M to that of **5.1** was achieved, with a two-fold lower EC<sub>50</sub> (16  $\mu$ M vs 8.6  $\mu$ M of **5.1**). In the SPR assays, **5.20** showed similar net stabilization effect in both systems (2.47-fold in ER $\alpha$  and 2.67-fold in CaMKK2, Figure S3). For benzotriazole **5.21** and its *N*-methyl isomer **5.22**, in the ER $\alpha$  system, no EC<sub>1.2</sub> was found, having both a maximum stabilization effect below 1.2-fold. On the other hand, both promoted stabilization of CaMKK2. **5.21** registered an EC<sub>1.2</sub> of 22  $\mu$ M and a stabilization effect at 200  $\mu$ M of 1.61-fold, while *N*-methylation (**5.22**) resulted in a loss of both potency (EC<sub>1.2</sub> 150  $\mu$ M) and stabilization effect (1.34-fold).

## CHAPTER 5

**Table 5.2** | Stabilization effect of compounds **5.14** - **5.29** on 14-3-3/ER $\alpha$ (pT<sup>594</sup>) and 14-3-3/CaMKK2(pS<sup>100</sup>).

					
Cpd	R <sup>2</sup>	FP		SPR	
		Stabilization effect <sup>a</sup>		Total activity <sup>d</sup>	
		EC <sub>1.2</sub> ( $\mu$ M) <sup>b</sup>		Net stabilization effect <sup>e</sup>	
EC <sub>50</sub> ( $\mu$ M) <sup>c</sup>		ER $\alpha$	CaMKK2	ER $\alpha$	CaMKK2
<b>1</b>		1.90 $\pm$ 0.05 28 (25 to 31) -	2.74 $\pm$ 0.05 1.1 (1.0 to 1.2) 8.6 (7.9 to 9.4) <sup>c</sup>	6.49 $\pm$ 0.42 3.99 $\pm$ 0.26 -	7.41 $\pm$ 1.13 7.15 $\pm$ 0.13 4.2 (3.7 to 4.7)
<b>5.14</b>		1.00 $\pm$ 0.08 - -	1.08 $\pm$ 0.11 - -		
<b>5.15</b>		1.02 $\pm$ 0.01 - -	1.04 $\pm$ 0.14 - -		
<b>5.16</b>		0.93 $\pm$ 0.02 - -	1.12 $\pm$ 0.07 - -		
<b>5.17</b>		1.02 $\pm$ 0.03 - -	1.02 $\pm$ 0.07 - -		
<b>5.18</b>		1.21 $\pm$ 0.03 191 (174 to 200+) -	1.08 $\pm$ 0.33 - -		
<b>5.19</b>		1.29 $\pm$ 0.14 131 (93 to 169) -	1.09 $\pm$ 0.11 - -	2.95 $\pm$ 0.75 (1.19 $\pm$ 0.40) -	1.54 $\pm$ 0.05 (1.18 $\pm$ 0.03) -
<b>5.20</b>		1.56 $\pm$ 0.06 73 (65 to 82) -	2.63 $\pm$ 0.13 2.4 (1.9 to 2.9) 16 (13 to 20) <sup>c</sup>	3.72 $\pm$ 0.37 (2.47 $\pm$ 0.33) -	3.00 $\pm$ 0.09 (2.67 $\pm$ 0.09) -

## CHAPTER 5

5.21		1.08 ± 0.02 - -	1.61 ± 0.07 22 (10 to 50) -		
5.22		1.15 ± 0.02 - -	1.34 ± 0.29 150 (59 to 200+) -		
5.23		1.24 ± 0.06 169 (146 to 195) -	1.48 ± 0.17 48 (19 to 98) -	4.00 ± 0.03 (1.54 ± 0.05) -	3.15 ± 0.49 (2.16 ± 0.11) -
5.24		0.96 ± 0.04 - -	1.53 ± 0.41 23 (0 to 75) -	3.20 ± 0.26 (1.13 ± 0.07) -	3.93 ± 1.00 (2.65 ± 0.55) -
5.25		1.13 ± 0.03 - -	1.18 ± 0.02 - -		
5.26		1.00 ± 0.02 - -	1.21 ± 0.17 - -		
5.27		0.99 ± 0.02 - -	1.05 ± 0.04 - -		
5.28		1.19 ± 0.02 - -	1.82 ± 0.18 61 (33 to 101) -	4.62 ± 0.25 (1.32 ± 0.20) -	3.76 ± 1.30 (2.29 ± 0.33) -
5.29		1.16 ± 0.08 - -	1.45 ± 0.12 115 (73 to 152) -	6.29 ± 0.20 (1.10 ± 0.09) -	3.19 ± 0.48 (1.57 ± 0.25) -

(a) – (e) are defined in Table 5.1. Values are reported as mean ± SD ( $n \geq 2$ ). Values without a SD were performed in singlicates. Blank cells mean that the compound was not tested in that particular assay. .

Indazoles **5.24** – **5.26** also showed only weak to null stabilization effect in ER $\alpha$ , with **5.23** reporting an EC<sub>1.2</sub> of 169  $\mu$ M, while the other two did not show stabilization above 1.2-fold. A similar outcome was observed in SPR, where **5.23** showed a better net stabilization effect than **5.24** (1.54-fold and 1.13-fold, respectively). In CaMKK2, **5.23** and **5.24** both registered about 1.5-fold stabilization in FP, while **5.25** only 1.18-fold. Conversely to what has been observed for benzotriazoles **5.21** and **5.22**, *N*-methylation here improved the EC<sub>1.2</sub> by approximately two-fold (23  $\mu$ M for **5.24** vs 48  $\mu$ M for **5.23**). This improvement was also observed in SPR, where **5.24** showed a



2.65-fold net stabilization effect compared to 2.16-fold for **5.23** (Figure S3 and S4). *N*-methylation, on the other hand, had no influence on either system for lactams **5.26** and **5.27**, which showed only a very marginal stabilization effect.

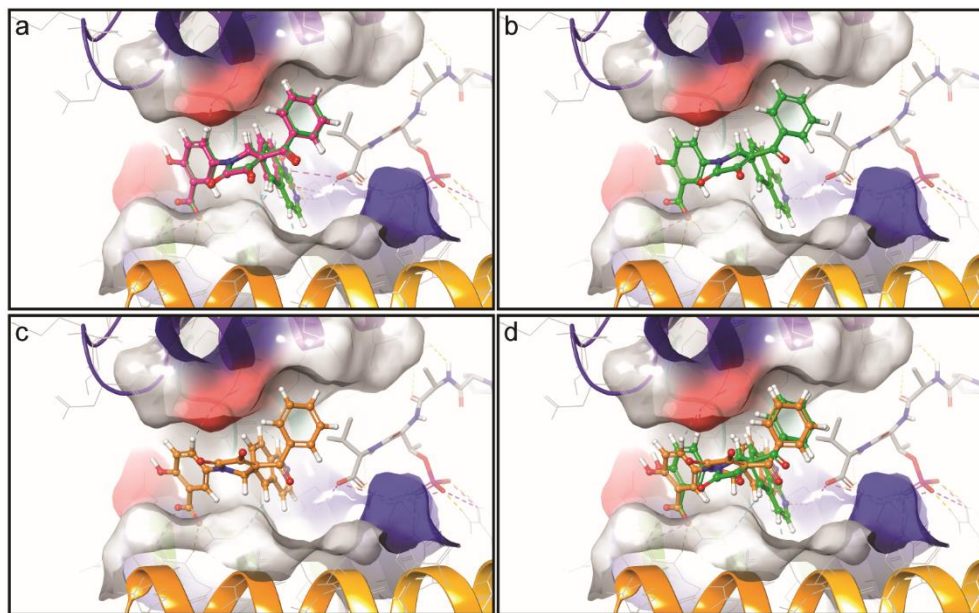


**Figure 5.5** | Dockings of the enantiomers of isoquinoline **5.29** in 14-3-3 $\sigma\Delta$ C/ER $\alpha$ (pT<sup>594</sup>) (PDB 6JTM). (a) Overlay of (*R*)-**5.1** (pink sticks) and (*R*)-**5.29** (green sticks), showing analogous binding poses. (b) Binding pose of (*R*)-**5.29** (green sticks) with its nitrogen forming a H-bond interaction with Lys122. (c) Binding pose of (*S*)-**5.29** (beige sticks) similar to the one of (*R*)-**5.29**, but due to inverted stereochemistry, no H-bond contact of the nitrogen with Lys122 is observed. (d) overlay of (*R*)-**5.29** (green sticks) and (*S*)-**5.29** (beige sticks) highlighting the different orientation of the isoquinoline substituent due to opposed stereochemistry. In all panels, ER $\alpha$ (pT<sup>594</sup>) is shown in grey sticks and 14-3-3 $\sigma\Delta$ C surface is coloured based on charge (red for acidic residues, blue for basic residues).

Finally, neither 2,1,3-benzoxadizole **5.28** nor isoquinoline **5.29** showed stabilization above 1.2-fold towards ER $\alpha$ , but were moderately active towards CaMKK2, with **5.28** being the second best of the series in terms of stabilization effect (1.82-fold), but not in terms of potency (EC<sub>1.2</sub> 61  $\mu$ M). Interestingly, in CaMKK2, **5.29** exhibited only a minimal net stabilization effect by SPR in agreement with FP data (1.10-fold in ER $\alpha$  and 1.57-fold in CaMKK2), but displayed about three times higher affinity for 14-3-3 $\zeta$  alone than any other compound tested (Figure S5.4, red curves). The isoquinoline nitrogen of **5.29** is a better H-bond acceptor than a nitro group but the lower stabilization effect observed might suggest that a stronger affinity for the protein can make the compound a better 14-3-3 binder, but also negatively impact its stabilization effect.

Another hypothesis relies on the fact that **5.29** was tested as a racemate. In chapter 3 it was shown that (*S*)-**5.1**, although not a stabilizer of either 14-3-3/ER $\alpha$  or 14-3-3/CaMKK2 PPI, binds to 14-3-3 alone with comparable affinity to the active PPI stabilizer (*R*)-**5.1**. It was then speculated that (*S*)-**5.29** may also equally bind to 14-3-3, thus negatively affecting the stabilization effect of its corresponding racemate. To test this supposition, a docking protocol was established for the enantiomers of **5.29** in both 14-3-3 PPIs, in the presence and absence of the respective phosphopeptide. In ER $\alpha$ , (*R*)-**5.1** gave a docking score of -7.0 (Figure 5.5a). The predicted binding pose of (*R*)-**5.29** matched the crystal structure binding pose of (*R*)-**5.1**, with its isoquinoline nitrogen engaging Lys122 via a H-bond, and also displayed a similar docking score (- 6.9, Figure 5.5a and b). Due to the inverted stereochemistry, (*S*)-**5.29** did not form a H-bond with Lys122 (Figure 5.5c). Despite the lack of the H-bond interaction, (*S*)-**5.29** reported a docking score of -6.4, only slightly lower than (*R*)-**5.29**, thus suggesting that it still docks relatively well into the binding pocket. It is worth pointing out, however, that the vinylogous carboxylate of (*S*)-**5.29** is in a low energy conformation (not in the *syn*- conformation as for (*R*)-**5.1** and (*R*)-**5.29**), which has probably influenced the docking score obtained (Figure 5.5c).

Docking of (*R*)- and (*S*)-**5.29** in the 14-3-3/CaMKK2 crystal structure (PDB 6EWW) returned binding poses that did not match the experimentally and computationally demonstrated *syn*- conformation of the vinylogous carboxylate (chapter 3, section 3.2). A clash of **5.29** with the CaMKK2(pS<sup>100</sup>) peptide was also observed. However, it was not possible to verify the accuracy of these docking poses due to the lack of structural data about the conformation assumed by the CaMKK2(pS<sup>100</sup>) peptide in a ternary complex. Dockings using 14-3-3 apo structure were also wrong, as the enantiomers were docked in correspondence of the phospho-binding pocket. This was not surprising, as given the size and open nature of the phospho-binding pocket compared to the Fc pocket, it could be expected that the docking protocol would try to satisfy some polar interactions.

Taken together, these dockings point at the fact that the (*S*)-**5.29** could indeed affect the overall stabilization effect of *rac*-**5.29**. Nonetheless, confirmation of this through separation of the enantiomers and subsequent SPR testing for their intrinsic affinity towards the 14-3-3 protein (in the absence of compound) is still required.

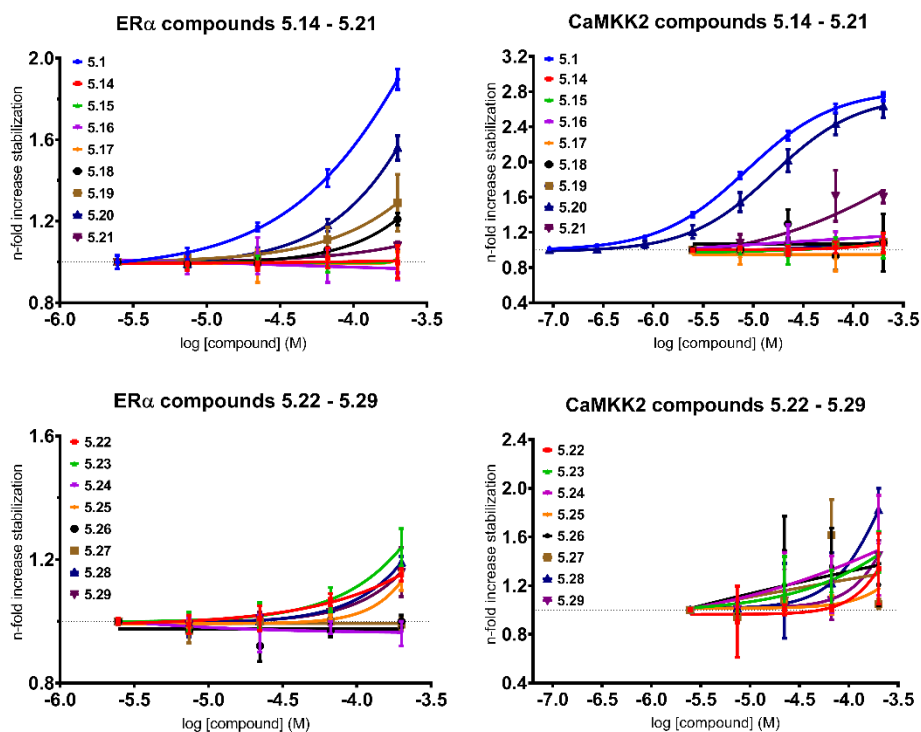


**Figure 5.6** | Stabilization of 14-3-3 $\zeta$ /ER $\alpha$ (pT<sup>594</sup>) (left panel) and 14-3-3 $\zeta$ /CaMKK2(pS<sup>100</sup>) (right panel) PPIs by compounds **5.1** and **5.14** – **5.29**. “n-fold increase stabilization” (y-axes) is defined in Figure 5.2. The error bars in all plots indicate  $\pm$  SD ( $n \geq 2$ ).

**Modifications to R<sup>3</sup>** (Table 5.3, Figure 5.8). The choice of the R<sup>3</sup> variations was performed before obtaining the high resolution crystal structure of (*R*)-**5.1** (PDB 6JTM, Figure 5.7a). The rationale behind the design of this library was therefore based on the incorrect binding pose observed in the low resolution (3.25 Å) X-ray crystal structure of the ternary complex of (*S*)-**5.1** bound to the *Nicotiana tabacum* 14-3-3 like protein C/PMA2 complex (PDB 3M51, Figure 5.7b).<sup>16</sup> In that structure, the salicylate ring of **5.1** points towards the PMA2 peptide, with no polar interactions with 14-3-3 observed. Hence, the initial design strategy focused on replacing the salicylate moiety with non-polar groups, thereby avoiding the overall desolvation penalty incurred by the salicylate group not making productive, polar interactions in the PPI complex.

The salicylate moiety was first replaced by various monosubstituted phenyl derivatives at the *ortho*-, *meta*- and *para*- positions. Halogen-bearing phenyl rings at the *ortho* position were not well-tolerated in ER $\alpha$ , with an EC<sub>1.2</sub> of 169  $\mu$ M for the 2-Cl derivative (**5.30**) and 99  $\mu$ M for the 2-F (**5.31**). In terms of stabilization effect, **5.30**

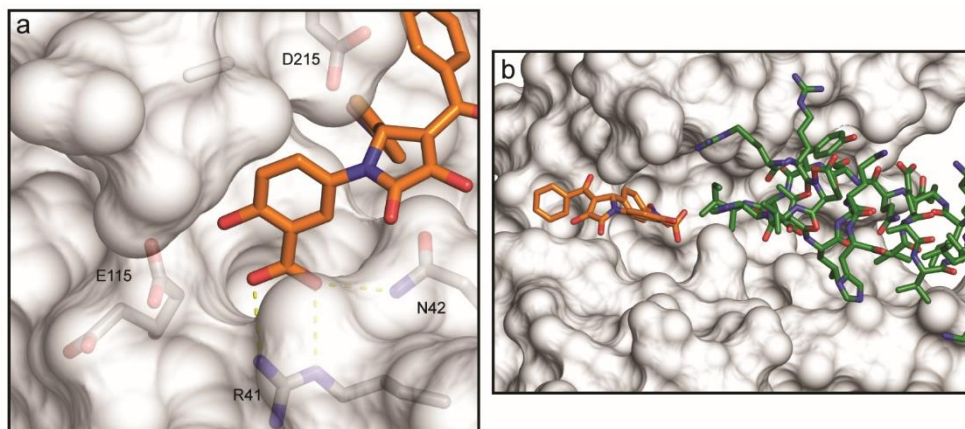


**Figure 5.7** | Comparison of binding mode of **5.1** (orange sticks), from two different resolution data sets with different absolute stereochemistry. (a) **5.1** modelled as (*R*), with the carboxylate of the salicylate ring of forming a bidentate interaction with Arg41 and Asn42 (PDB 6JTM). (b) **5.1** modelled as (*S*), with the salicylate ring pointing towards the PMA2 peptide (green sticks) and not interacting with any protein residue (PDB 3M51).

showed a 1.87-fold increase, while **5.31** 1.29-fold increase. For **5.30**, the concentration-response curve raised from the baseline only at the highest concentration point, and very steeply (Figure 5.8 red squares), while **5.31** showed a linear increase (Figure 5.8, green triangles), which could suggest that they might be false positives for ER $\alpha$ . SPR counter-test showed that both **5.30** and **5.31** have an intrinsic affinity for 14-3-3 protein alone (red curves, Figure S5.5) but do not elicit a stabilization effect above the 1.2-fold threshold on the 14-3-3/ER $\alpha$  complex (0.87-fold for **5.30** and 1.17-fold for **5.31**). On the other hand, for CaMKK2, both compounds showed high potency (**5.30** 11  $\mu$ M and **5.31** 16  $\mu$ M) and stabilization effect (2.32-fold and 2.19-fold, respectively). SPR testing confirmed the comparable total activity (3.79-fold and 3.60-fold) and net stabilization effect (2.61-fold and 2.83-fold). These two derivatives displayed a clear preference for the CaMKK2 PPI over the ER $\alpha$  one, showing a good degree of selectivity, without heavily affecting the potency (about ten-fold loss in EC $_{1.2}$  when compared to **5.1**).

2-CN (**5.32**) and 2-NO $_2$  (**5.33**) were not able to stabilize ER $\alpha$  but showed potency in the range of 30 to 50  $\mu$ M for CaMKK2. In ER $\alpha$ , the 2-COOH derivative (**5.34**) displayed only a two-fold loss in EC $_{1.2}$  (52  $\mu$ M vs 28  $\mu$ M) when compared to **5.1** in FP assay, but did not show stabilization by SPR (0.82-fold). When tested in CaMKK2, **5.34** showed a hundred-fold loss in EC $_{1.2}$  (104  $\mu$ M vs 1.1  $\mu$ M for **5.1**) and also did not show stabilization by SPR (0.97-fold, Figure S5.5) 2-OH (**5.35**) was shown to be a good stabilizer of both systems. In FP, **5.35** displayed a EC $_{1.2}$  of 99  $\mu$ M and 1.39-fold stabilization effect in ER $\alpha$  and of 9.4  $\mu$ M and 2.31-fold in CaMKK2.

Its stabilization effect was confirmed by SPR (1.81-fold for ER $\alpha$  and 3.06-fold for CaMKK2). Methylation of the hydroxy group (**5.36**) negatively impacted potency and stabilization effect in both systems. This detrimental effect was presumably due to the loss of the H-bond interaction with Asn42. Indeed, etherification nullifies the HBD ability of the hydroxyl group and could also potentially hinder or prevent the HBA interaction from Asn42 (discussed in section 5.5).

For ER $\alpha$ , of the electron-withdrawing groups at the *meta*- position (**5.39** – **5.43**), only the trifluoromethyl substituent (**5.41**) showed an EC<sub>1.2</sub> below 150  $\mu$ M (73  $\mu$ M), with a good stabilization effect at 200  $\mu$ M (2.26-fold). SPR analysis showed a net stabilization effect of 1.88-fold at 100  $\mu$ M, but the curve was otherwise flat, thus suggesting that is probably a very weak stabilizer for ER $\alpha$ . A similar profile was observed for CaMKK2 in both FP and SPR assays.

Carboxylic acid **5.42** (a matched pair of **5.1** which lacks the salicylate hydroxyl group), showed only a minimal stabilization effect in FP for ER $\alpha$  (1.20-fold), which was confirmed in the SPR assay (1.08-fold vs 4.10 of **5.1**). On the other hand, in the CaMKK2 system, **5.42** was found to be the best compound among the electron-withdrawing substituents at the *meta*- position in the FP assay, with an EC<sub>1.2</sub> of 18  $\mu$ M and stabilization effect of 1.99-fold, which was then confirmed by SPR, with a net stabilization effect of 2.31-fold at 100  $\mu$ M (Figure S5.7).

Substituents at the *para*- position (**5.46** – **5.50**) were not well tolerated in ER $\alpha$ , all displaying EC<sub>1.2</sub> above 100  $\mu$ M. 4-CN derivative **5.46** showed a stabilization effect only at the highest concentration in FP, and with high variability (1.90  $\pm$  0.54). SPR was performed to ascertain if it was a true hit or simply an artifact due to high concentration. This showed only weak net stabilization effect (1.17-fold) and high variability as well in the CR curve, therefore suggesting that **5.46** might not be a true stabilizer of the 14-3-3/ER $\alpha$  interaction (Figure S5.7). Derivatives **5.46** – **5.50** exhibited a better potency when tested in CaMKK2, with only compound **5.48** having an EC<sub>1.2</sub> above 100  $\mu$ M in FP and minimal stabilization effect in SPR (1.24-fold, Figure S5.8). Sulfonamide derivative **5.50** was the best of the *para*- substituted derivatives (EC<sub>1.2</sub> 32  $\mu$ M and stabilization effect of 1.87-fold in FP).

Compound **5.51**, the 4-hydroxyl matched pair of **5.1** which lacks the salicylate carboxylate function, was found to be still active in both ER $\alpha$  and CaMKK2, and its stabilization effect was confirmed in SPR (~ 2-fold in both ER $\alpha$  and CaMKK2, Figure S5.8). For CaMKK2, an EC<sub>50</sub> of 25  $\mu$ M was found.

An unsubstituted phenyl ring (**5.52**) showed a good degree of stabilization effect and potency for both ER $\alpha$  and CaMKK2 in both assay platforms (Figure 5.8 and S5.8). In FP, a EC<sub>1.2</sub> of 55  $\mu$ M and 1.64-fold stabilization effect was found for ER $\alpha$ , and of 17  $\mu$ M and 2.09-fold for CaMKK2. Notably, while for CaMKK2 no difference

in either potency or stabilization effect was observed when comparing **5.52** with the 3-COOH derivative (**5.42**), for ER $\alpha$  the absence of the carboxylate moiety resulted in a better stabilization effect (1.51-fold vs 1.20-fold) as well as higher potency (EC<sub>1.2</sub> 55  $\mu$ M vs nd). Removal of the 4-OH (**5.42**) is more detrimental than removal of the 3-COOH (**5.51**), both in terms of potency and stabilization effect. When comparing 3-COOH derivative **5.42** with its unsubstituted phenyl ring matched pair (**5.52**), neither potency nor stabilization effect is affected in CaMKK2 and it is indeed beneficial for ER $\alpha$ . These observations suggest a particular role for the 4-OH. It could mask the negative charge on the 3-carboxylate by intramolecular hydrogen bonding, thus reducing the electrostatic repulsion experienced by the salicylate moiety upon penetration into a negatively charged pocket prior to bidentate bond formation with Arg41 and H-bond interaction with Asn42.

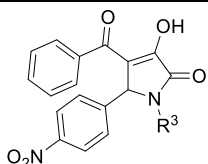
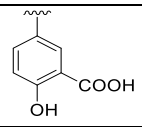
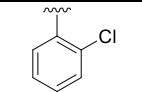
We then studied the effects adding linkers of various lengths between the phenyl ring and the pyrrolidone scaffold of **5.51**: methylene (**5.53**), ethylene (**5.54**), propylene (**5.55**) and ethoxy (**5.56**). In CaMKK2, increasing linker length led to a marked drop in both stabilization effect and potency when compared to **5.52**, with only ethylene linker (**5.54**) showing at least 1.2-fold stabilization effect (1.24-fold), which was confirmed by SPR (1.16-fold net stabilization effect). On the other hand, although a clear trend was not identified, ER $\alpha$  was found to be less susceptible to increasing linker lengths, with **5.55** being the best compound (EC<sub>1.2</sub> 75  $\mu$ M and 2.00-fold stabilization effect by FP). When compared to **5.52**, **5.55** shows a higher stabilization (2.00-fold vs 1.64-fold) effect but slightly lower potency (75  $\mu$ M vs 55  $\mu$ M).

Replacement of the phenyl ring with an isopropyl group (**5.57**) or a 4-pyridinyl group (**5.58**) was found to be detrimental in both systems. Isonicotinic acid derivative **5.59** was synthesized in an attempt to pick up a polar interaction with the side chain of Asp215 on 14-3-3 $\zeta$  (Figure 5.7a). 2,4-dimethoxyphenyl derivative (**5.60**) showed good potency (49  $\mu$ M for ER $\alpha$  and 38  $\mu$ M for CaMKK2) and stabilization in both systems (1.68-fold and 2.22-fold). Compared to its mono methoxy analogue **5.36**, **5.60** showed improved potency and stabilization in ER $\alpha$ , but only better stabilization effect in CaMKK2 (2.22-fold vs 1.87-fold). Modification of the salicylate ring by introduction of a methylene spacer at the *meta*- position in between the ring and the carboxylate function (**5.61**) resulted in an almost total loss of potency and stabilization effect when compared to its match pair **5.1**, probably due to a steric clash with the 14-3-3 protein surface.

Finally, bulkier substituents such as 3-biphenyl (**5.62**) and 1-naphthyl (**5.63**) were also synthesized. **5.62** showed a high stabilization effect in ER $\alpha$  (1.93-fold) and fairly good potency (EC<sub>1.2</sub> 64  $\mu$ M). Similar potency was found in CaMKK2 (60  $\mu$ M) but lower stabilization effect (1.41-fold). However, when tested by SPR, only a minimal

stabilization effect was observed, about 1.15-fold in both systems, but a pronounced affinity for 14-3-3 was detected, roughly twice as much as most of the synthesized derivative (~ 40 RUs vs ~ 15 – 25 RUs, Figure S9, red curves). **5.63** showed peculiar behavior when tested against ER $\alpha$  by FP. In both runs, high raw data were observed, but only at the highest concentration point (200  $\mu$ M). In brief, FP works by exciting a fluorescent sample by polarized light, and emission intensities are measured in both the parallel ( $I_{||}$ ) and perpendicular ( $I_{\perp}$ ) planes (to the excitation light). These measurements, i.e. the raw data, can then be used to calculate the final FP values. An arbitrary cut-off value of  $\pm$  3000 units in respect to the averaged  $I_{||}$  recorded for the fluorescein labelled **5.2** peptide (FITC-**5.2**) alone at assay concentration (10 nM), was set to define outliers. The values recorded for **5.63** at 200  $\mu$ M in the two independent runs were above 10000 units. This behavior was not observed when **5.63** was tested against CaMKK2, thus suggesting that is not due to a ligand-specific effect (ie auto-fluorescence) but rather to a possible aggregation with FITC-**5.2** at the tested concentration. For this reason, the stabilization effect was calculated at the second highest concentration point, where the raw data were within the cut-off range (66.7  $\mu$ M, Figure 5.7). When measured in CaMKK2, a EC<sub>50</sub> of 22  $\mu$ M could be defined. In SPR, a similar total activity was found in the two systems (5.22-fold for ER $\alpha$  and 5.33-fold for CaMKK2), but the net stabilization effect was almost two-fold higher for CaMKK2 (4.07-fold vs 2.59-fold).

**Table 5.3.** Stabilization effect of compounds **5.30** – **5.63** on 14-3-3/ER $\alpha$ (pT<sup>594</sup>) and 14-3-3/ CaMKK2(pS<sup>100</sup>).

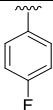
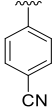
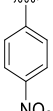
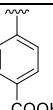
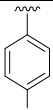
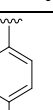
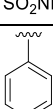
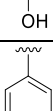
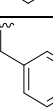
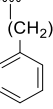
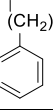
					
Cpd	R <sup>3</sup>	FP		SPR	
		Stabilization effect <sup>a</sup>		Total activity <sup>d</sup>	
		EC <sub>1.2</sub> ( $\mu$ M) <sup>b</sup>		Net stabilization effect <sup>e</sup>	
		ER $\alpha$	CaMKK2	ER $\alpha$	CaMKK2
<b>5.1</b>		1.90 $\pm$ 0.05 28 (25 to 31) -	2.74 $\pm$ 0.05 1.1 (1.0 to 1.2) 8.6 (7.9 to 9.4)	6.49 $\pm$ 0.42 3.99 $\pm$ 0.26 -	7.41 $\pm$ 1.13 7.15 $\pm$ 0.13 4.2 (3.7 to 4.7)
<b>5.30</b>		1.87 $\pm$ 0.11 169 (63 to 200) -	2.32 $\pm$ 0.03 11 (9 to 13) -	3.07 (0.87) -	3.79 (2.61) -

## CHAPTER 5

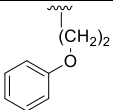
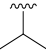
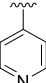
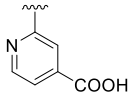
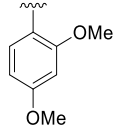
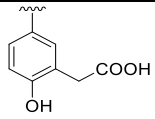
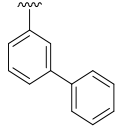
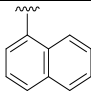
5.31		1.29 ± 0.09 99 (59 to 150) -	2.19 ± 0.03 16 (14 to 18) -	2.66 (1.17) -	3.60 (2.83) -
5.32		0.72 ± 0.53 - -	1.80 ± 0.22 32 (24 to 41) -		
5.33		1.04 ± 0.37 - -	1.42 ± 0.22 50 (21 to 96) -		
5.34		1.60 ± 0.11 52 (38 to 70) -	1.38 ± 0.27 104 (50 to 170) -	2.78 ± 0.05 (0.82 ± 0.33) -	1.41 ± 0.22 (0.97 ± 0.11) -
5.35		1.39 ± 0.09 99 (79 to 118) -	2.31 ± 0.09 9.4 (7.9 to 11.1) -	4.26 ± 0.44 (1.81 ± 0.17) -	5.03 ± 1.03 (3.06 ± 0.60) -
5.36		1.27 ± 0.01 193 (70 to 200+) -	1.87 ± 0.04 29 (23 to 36) -		
5.37		1.86 ± 0.13 172 (68 to 200) -	1.71 ± 0.06 33 (25 to 43) -	4.79 (2.35) -	3.45 (1.65) -
5.38		1.16 ± 0.38 - -	1.97 ± 0.06 22 (17 to 27) -		
5.39		1.66 ± 0.03 174 (65 to 200) -	1.71 ± 0.05 34 (29 to 40) -		
5.40		1.46 ± 0.03 184 (67 to 200) -	1.68 ± 0.05 41 (35 to 48) -		
5.41		2.26 ± 0.37 73 (40 to 129) -	1.42 ± 0.18 84 (52 to 119) -	3.17 (1.88) -	2.45 (1.81) -
5.42		1.20 ± 0.02 - -	1.99 ± 0.11 18 (15 to 21) -	2.68 ± 0.38 (1.08 ± 0.25) -	2.65 ± 0.24 (2.31 ± 0.13) -
5.43		1.03 ± 0.06 - -	1.73 ± 0.05 42 (27 to 60) -		
5.44		1.36 ± 0.12 126 (59 to 186) -	1.73 ± 0.11 37 (24 to 56) -		



## CHAPTER 5

5.45		1.18 ± 0.14 - -	2.00 ± 0.01 24 (22 to 28) -	2.25 (0.95) -	3.00 (2.32) -
5.46		1.90 ± 0.54 136 (58 to 196) -	1.59 ± 0.06 57 (42 to 73) -	2.85 (1.17) -	2.53 (1.62) -
5.47		1.62 ± 0.46 180 (65 to 200) -	1.51 ± 0.13 61 (41 to 83) -		
5.48		1.22 ± 0.23 178 (96 to 200+) -	1.30 ± 0.04 133 (114 to 151) -	2.27 ± 0.36 (0.86 ± 0.19) -	1.57 ± 0.06 (1.24 ± 0.12) -
5.49		1.01 ± 0.33 - -	1.34 ± 0.10 88 (49 to 137) -		
5.50		1.46 ± 0.11 123 (54 to 180) -	1.87 ± 0.12 32 (20 to 51) -		
5.51		1.57 ± 0.05 41 (35 to 49) -	2.35 ± 0.13 5.7 (4.6 to 7.1) 25 (21 to 33)	4.32 ± 0.86 (2.03 ± 0.19) -	2.36 ± 0.10 (2.07 ± 0.12) -
5.52		1.64 ± 0.05 55 (46 to 65) -	2.09 ± 0.01 17 (15 to 20) -	2.98 ± 0.07 (1.22 ± 0.07) -	3.25 ± 0.44 (2.36 ± 0.12) -
5.53		1.51 ± 0.13 145 (79 to 189) -	1.12 ± 0.06 - -		
5.54		1.34 ± 0.01 104 (71 to 139) -	1.24 ± 0.10 168 (109 to 200+) -	3.32 (1.22) -	2.06 (1.16) -
5.55		2.00 ± 0.23 75 (44 to 116) -	1.07 ± 0.08 - -		

## CHAPTER 5

<b>5.56</b>		1.54 ± 0.30 114 (50 to 169) -	1.14 ± 0.11 - -		
<b>5.57</b>		0.53 ± 0.31 - -	1.23 ± 0.15 142 (59 to 200+) -		
<b>5.58</b>		1.10 ± 0.02 - -	1.33 ± 0.04 113 (81 to 145) -		
<b>5.59</b>		1.44 ± 0.03 86 (74 to 98) -	1.40 ± 0.20 91 (49 to 139) -		
<b>5.60</b>		1.68 ± 0.08 49 (40 to 60) -	2.22 ± 0.04 38 (0 to 84) -		
<b>5.61</b>		1.03 ± 0.01 - -	1.13 ± 0.04 - -		
<b>5.62</b>		1.93 ± 0.36 64 (38 to 102) -	1.41 ± 0.15 60 (26 to 109) -	4.83 (1.17) -	2.86 (1.11) -
<b>5.63</b>		2.20 ± 0.01* 3.5 (2.5 to 4.8) -	2.67 ± 0.07 4.8 (3.0 to 7.3) 22 (17 to 35) <sup>c</sup>	5.22 (2.59) -	5.33 (4.07) -

(a) – (e) are defined in Table 5.1. Values are reported as mean ± SD (n ≥ 2). Values without a SD were performed in singicates. Blank cells mean that the compound was not tested in that particular assay. . \* Stabilization effect calculated on the second highest concentration point (66 μM).

### 5.4 SELECTIVITY BETWEEN ER $\alpha$ AND CAMKK2

In terms of selectivity, overall, the synthesized derivatives were more potent in the 14-3-3/CaMKK2(pS<sup>100</sup>) PPI. This can be due to the lower intrinsic affinity of phosphopeptide **5.3** for 14-3-3 ( $K_d = 112 \pm 14 \mu\text{M}$ ) compared to **5.2** ( $K_d = 227 \pm 14 \text{ nM}$ ), which presumably accounts for a wider range of stabilization allowed.<sup>10</sup> Selectivity ratios of CaMKK2 over ER $\alpha$  for all compounds tested are reported in Table 5.4.

## CHAPTER 5

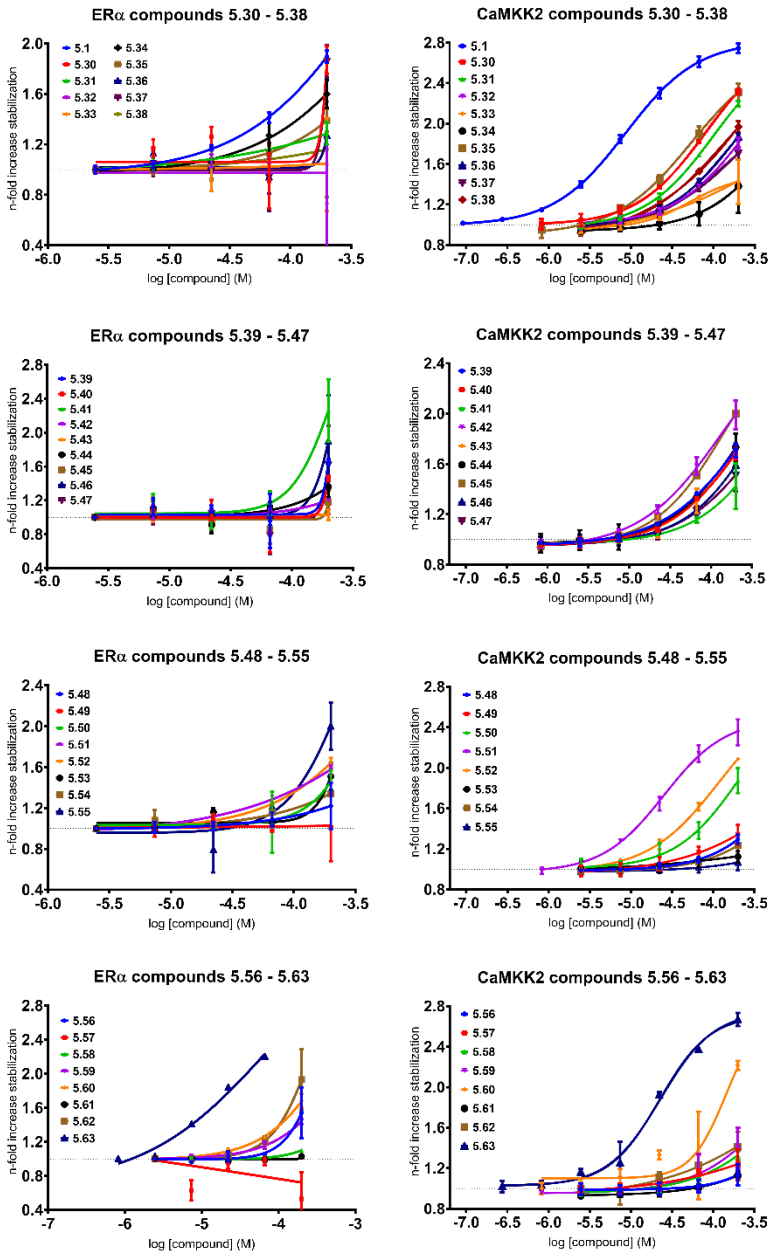


**Figure 5.8** | Stabilization of 14-3-3 $\zeta$ /ER $\alpha$ (pT<sup>594</sup>) (left panel) and 14-3-3 $\zeta$ /CaMKK2(pS<sup>100</sup>) (right panel) PPIs by compounds **5.1** and **5.30** – **5.63**. “n-fold increase stabilization” (y-axes) is defined in Figure 5.2. The error bars in all plots indicate +/- SD (n ≥ 2).

CHAPTER 5

**Table 5.4** | EC<sub>1.2</sub> and selectivity ratios of compounds **5.1** and **5.4 - 5.63** on 14-3-3/ER $\alpha$ (pT<sup>594</sup>) and 14-3-3/CaMKK2(pS<sup>100</sup>).<sup>a</sup>

Cpd	ER $\alpha$ EC <sub>1.2</sub> ( $\mu$ M)	CaMKK2 EC <sub>1.2</sub> ( $\mu$ M)	Fold selectivity CaMKK2: ER $\alpha$
5.1	28	1.1	25
5.4	65	7.8	8
5.5	39	5.4	7
5.6	>200	17	> 12
5.7	20	1.0	20
5.8	52	2.2	24
5.9	48	7.3	7
5.10	173	27	6
5.11	-	-	-
5.12	>200	90	> 2
5.13	>200	77	> 3
5.14	-	-	-
5.15	-	-	-
5.16	-	-	-
5.17	-	-	-
5.18	191	>200	< 1
5.19	131	>200	< 0.7
5.20	73	2.4	31
5.21	>200	22	> 9
5.22	>200	150	> 1
5.23	169	48	4
5.24	>200	23	> 9
5.25	-	-	-
5.26	-	-	-
5.27	-	-	-
5.28	>200	61	> 3
5.29	>200	115	> 2
5.30	169	11	15
5.31	99	16	6
5.32	>200	32	> 6
5.33	>200	50	> 4

5.34	52	104	0.5
5.35	99	9.4	11
5.36	193	29	7
5.37	172	33	5
5.38	>200	22	> 9
5.39	174	34	5
5.40	184	41	4
5.41	73	84	1
5.42	>200	18	> 11
5.43	>200	42	> 5
5.44	126	37	3
5.45	>200	24	> 8
5.46	136	57	2
5.47	180	61	3
5.48	178	133	1
5.49	>200	88	> 2
5.50	123	32	4
5.51	41	5.7	7
5.52	55	17	3
5.53	145	>200	< 0.7
5.54	104	168	0.6
5.55	75	>200	< 0.4
5.56	114	>200	< 0.6
5.57	>200	142	> 1
5.58	>200	113	> 2
5.59	86	91	1
5.60	49	38	1
5.61	-	-	-
5.62	64	60	1
5.63	3.5	4.8	1

## CHAPTER 5

(a) Selectivity ratios have been calculated from FP EC<sub>1,2</sub> data. For those compounds whose EC<sub>1,2</sub> could not be defined due to stabilization effect lower than 1.2-fold, the value ">200" has been reported, meaning that the EC<sub>1,2</sub> is higher than 200  $\mu$ M and their respective selectivity ratios are preceded by the > or < symbols.

For the R<sup>1</sup> variations, 4-chlorophenyl **5.7** and 4-methylphenyl **5.8** showed a preference, respectively, of 20-fold and 24-fold for CaMKK2 over ER $\alpha$ , which is comparable to the one of **5.1** (25-fold). 3-Difluoromethoxyphenyl (**5.6**) also showed a good degree of selectivity, of at least 12-fold. None of the R<sup>1</sup> variations showed an increased selectivity when compared to **5.1**. This can be presumably ascribed to the fact that the substituents on the benzoyl ring are still too far from **5.2** or **5.3** to engage in additional interactions that can confer selectivity towards either of the phosphopeptides.

Within the R<sup>2</sup> variations, benzolactone **5.20** was the most selective of all compounds for CaMKK2, with a 31-fold ratio. The other nitro replacements (R<sup>2</sup>) showed a 9-fold difference at best instead.

As for the R<sup>3</sup> derivatives, 2-chlorophenyl **5.30** demonstrated high selectivity (15-fold) for CaMKK2 over ER $\alpha$ . The 3-carboxylate **5.42**, match pair of **5.1**, preserved a good degree of selectivity (> 11-fold vs 25-fold). The 2-OH-Ph derivative **5.35**, also displayed at least a ten-fold selectivity ratio (11). 1-Naphtyl **5.63**, although potent in both systems (EC<sub>1,2</sub> < 5  $\mu$ M), did not show any preference.

Only few of the synthesized compounds exhibited selectivity towards ER $\alpha$ , albeit minimal. 4-phenylacetamide **5.18** and its matched pair 3-phenylacetamide **5.19** (R<sup>2</sup>) had a preference for ER $\alpha$  slightly higher than 1.1-fold and 1.5-fold respectively, while phenethyl **5.54**, phenylpropyl **5.55** and ethyloxyphenyl **5.56** (R<sup>3</sup>) showed at least a 1.8-fold selectivity.

### 5.5 CRYSTAL STRUCTURES OF DERIVATIVES 5.20 AND 5.35

Due to their good potency and selectivity, benzolactone **5.20** and 2-OH **5.35** were selected for crystallization studies. By co-crystallization, crystal structures of the ternary 14-3-3 $\sigma$  $\Delta$ C/ER $\alpha$ (pT<sup>594</sup>)/**5.20** (yet to be submitted to PDB) and 14-3-3 $\sigma$  $\Delta$ C/ER $\alpha$ (pT<sup>594</sup>)/**5.35** (PDB 6YSM) complexes were obtained at a resolution of 2.50 Å and 2.38 Å, respectively (Figure 5.9a and b). The crystal structure of 14-3-3 $\sigma$  $\Delta$ C/ER $\alpha$ (pT<sup>594</sup>)/(R)-**5.1** (PDB 6TJM) was used as initial model for refinement.

Compounds **5.20** and **5.35** were unequivocally modelled with (R) absolute configuration, therefore they have the same stereochemical dependence as (R)-**5.1**. Additional ligand-associated electron density allowed to also model a Mg<sup>2+</sup> ion chelated by their vinylogous carboxylate moieties, thus further confirming the ligand-specific, metal ion induced conformational restriction previously described in chapter

3. No major differences in orientation or spatial localization were observed when compared to the binding mode of (*R*)-**5.1**, with the three molecules nicely overlapping

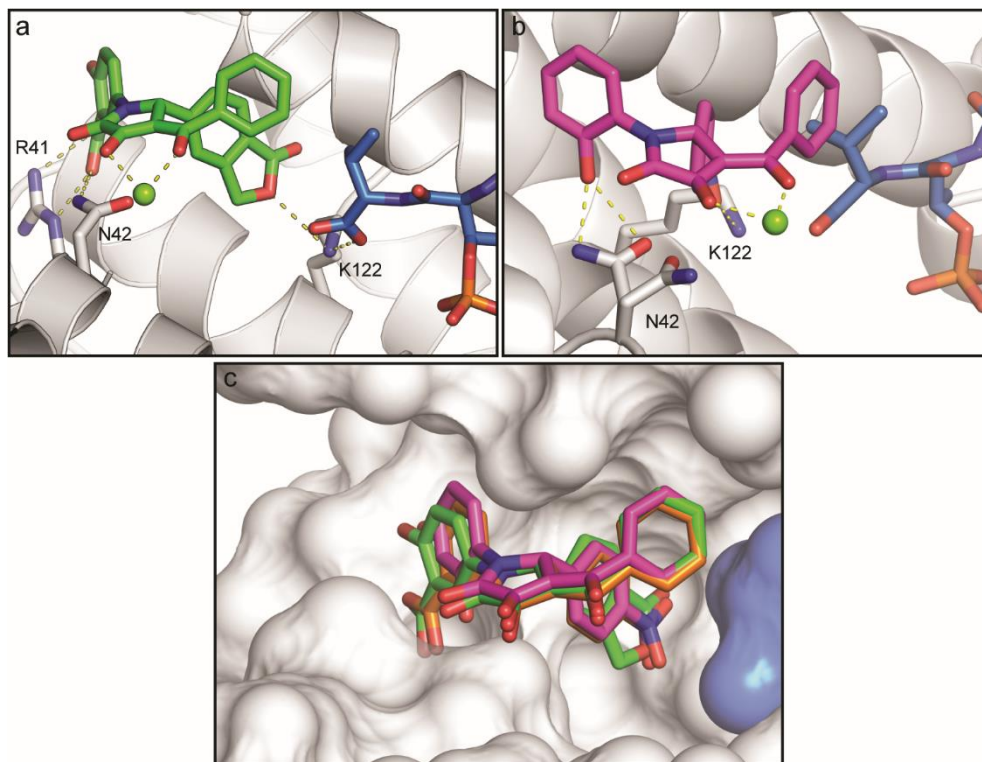


**Figure 5.9** | X-ray crystal structure of 14-3-3 $\sigma$ /ER $\alpha$ (pT<sup>594</sup>)/**5.20** and 14-3-3 $\sigma$ /ER $\alpha$ (pT<sup>594</sup>)/**5.35** (PDB 6YSM) ternary complexes. (a) Binding mode and details of interactions between **5.20** (modelled as (*R*), green sticks) and 14-3-3 $\sigma$  (white helices). (b) Binding mode and details of interactions between **5.35** (modelled as (*R*), pink sticks) and 14-3-3 $\sigma$  $\Delta$ C (white helices). The vinylogous carboxylate of both **5.20** and **5.35** chelates a Mg<sup>2+</sup> ion (green sphere) (c) Overlay of (*R*)-**5.1**, (*R*)-**5.20** and (*R*)-**5.35** showing analogous binding modes. 14-3-3 $\sigma$  is shown as white surface, while ER $\alpha$ (pT<sup>594</sup>) as blue surface.

with one another. As for (*R*)-**5.1**, (*R*)-**5.20** and *R*-**5.35** bind in a T-shaped conformation with their three phenyl rings pointing towards three different sub-pockets (Figure 5.9c). The endocyclic oxygen of the benzolactone ring of (*R*)-**5.20** accepts a H-bond from Lys122 and its salicylate moiety exhibits the same polar interactions observed for (*R*)-**5.1** (Figure 5.8a). The phenolic OH of (*R*)-**5.35** forms a H-bond interaction with Arg42, interestingly a novel interaction not made by any other compounds in the series. Arg42 was modelled in two possible different conformations, possibly suggesting a less productive H-bond when compared to the salicylate moiety.

## 5.6 STABILIZATION OF PPI BETWEEN FULL-LENGTH CaMKK2 AND 14-3-3

In the context of studying 14-3-3 PPIs at a molecular level, the use of synthetic phosphopeptides derived from the main phosphorylated motifs of the 14-3-3 client proteins is a commonly employed approach. In fact, for phosphorylation-dependent 14-3-3 PPIs, these short phosphorylated sequences recapitulate the main interactions of the PPI, and mutation of the single phosphorylation site can significantly impact their intrinsic affinity, both *in vitro* and *in vivo*.<sup>8</sup> Moreover, from a merely practical standpoint, the use of short synthetic phosphopeptides considerably simplifies the biophysical and biochemical study of these PPIs, as expression, purification and implementation in assays of either long protein constructs or full-length proteins is very often complex and time-consuming, especially for the ones that are site-specifically phosphorylated.

This is supported by the paucity of structural data reported for 14-3-3 complexes with full length proteins or longer constructs.<sup>17-20</sup> Notably, the interaction between tobacco 14-3-3cΔC (deleted of its C-terminal 18 amino acids) and the entire 14-3-3 binding motif of PMA2 H<sup>+</sup>-ATPase comprising 52 amino acids (PMA2-CT52, residues 905–956) is, to date, the only successful case where Fc-A mediated stabilization has been investigated in more complex systems.

(*R*)-**5.1** has been shown to effectively stabilize the 14-3-3/CaMKK2(pS<sup>100</sup>) complex (chapter 3), with an EC<sub>50</sub> of about 3 μM and a 3,700-fold increase in apparent *K<sub>d</sub>*.<sup>10</sup> We therefore aimed at evaluating its stabilizing effect on a larger CaMKK2 construct. Our collaborators in the Obšil group have reported the expression and isolation of phosphorylated human CaMKK2 (residues 93 – 517), comprising its two known 14-3-3 binding motifs, located around pS<sup>100</sup> and pS<sup>511</sup>, the kinase domain and the Ca<sup>2+</sup>/CaM binding region (from here on referred to as FL-pCaMKK2, Figure 5.10) and show the formation of a stable complex with 14-3-3γ.<sup>13</sup>

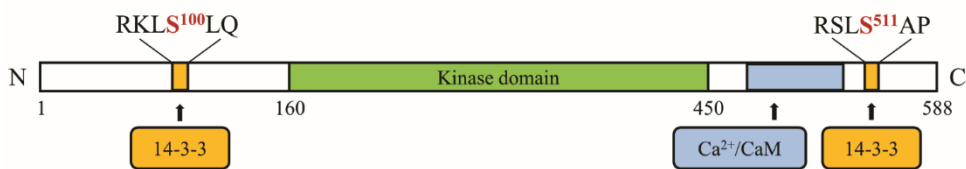


**Figure 5.10** | Domain structure of human CaMKK2. The 14-3-3 binding motifs (gold), the kinase domain (green) and the CaM binding region (light blue) are highlighted.

In order to investigate the potential stabilization effect of (*R*)-**5.1** towards the 14-3-3γ/FL-pCaMKK2 complex, sedimentation velocity analytical ultracentrifugation (SV-AUC) experiments were performed in collaboration with the Obšil laboratory.

SV-AUC is an analytical ultracentrifugation method that measures the rate at which molecules move in response to centrifugal force generated in a centrifuge, when spun at high speed (usually 40,000 – 60,000 rpm). Mass will redistribute in the gravitational field forming a boundary starting from the center of the rotor (corresponding to the meniscus region at the air/test solution interface), which progressively moves towards the outside over time. The rate at which the sedimentation boundary moves is a measure of the sedimentation coefficient ( $S$ ) of the protein. The sedimentation coefficient depends on the molecular weight (larger proteins sediment more quickly) and also on molecular shape.<sup>21-22</sup>

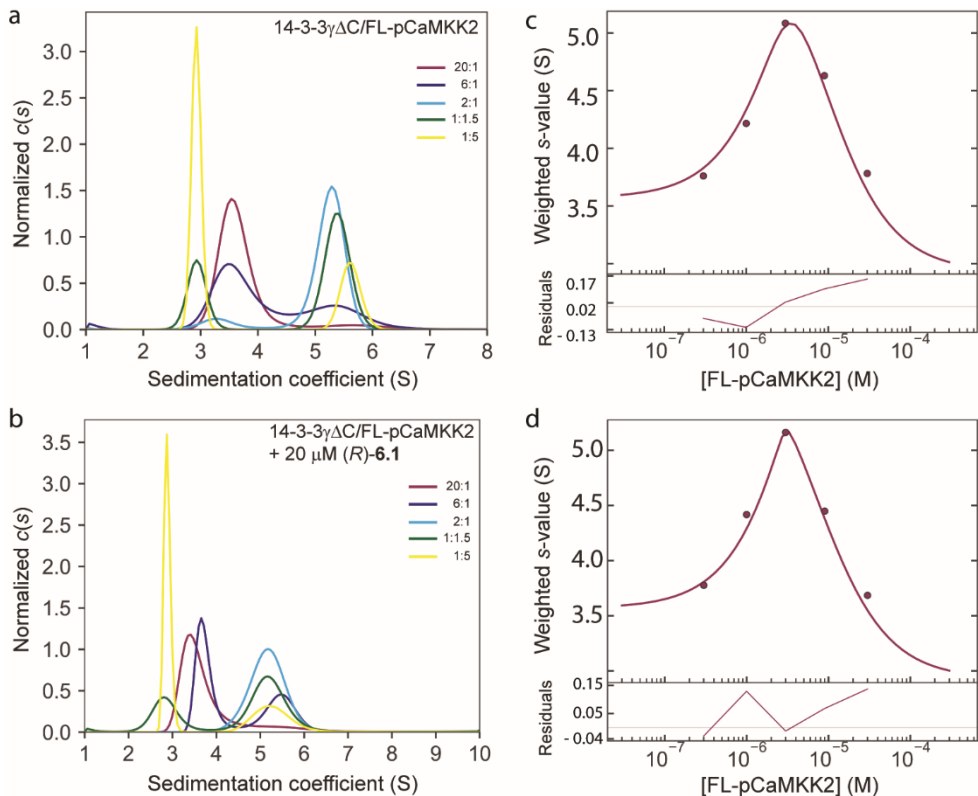


**Figure 5.11** | Human CaMKK2 construct FL-pCaMKK2 forms a stable complex with 14-3-3 $\gamma$  in the presence of (R)-5.1. (a and b) Series of area-normalized  $c(s)$  distributions of mixtures of FL-pCaMKK2 and 14-3-3 $\gamma$  at various molar ratios, using 6  $\mu$ M 14-3-3 $\gamma$  and 0.3–30  $\mu$ M FL-pCaMKK2 in the absence (panel a) or presence (panel b) of (R)-5.1 (20  $\mu$ M). (c and d) Isotherms of weight-averaged sedimentation coefficients  $s_w$ , obtained from SV AUC, used for estimation of dissociation constant values ( $K_d$ ) for 14-3-3 $\gamma$ /FL-pCaMKK2 in the absence (panel c) and presence (panel d) of (R)-5.1 (20  $\mu$ M).

A range of different molar ratios of 14-3-3 $\gamma$ /FL-pCaMKK2 were examined. The normalized continuous sedimentation coefficient distributions  $c(s)$  showed that,



when 14-3-3 $\gamma$  and FL-pCaMKK2 are in high molar excess, they form single peaks with a weight-averaged sedimentation coefficient ( $s_w$ ) of  $\sim 3.5$  S (purple curve) and  $\sim 3.1$  S (yellow curve), respectively (Figure 5.11a). Intermediate 14-3-3 $\gamma$ : FL-pCaMKK2 ratios (navy blue, cyan and green curves) show the presence of a complex with a  $s_w$  of  $\sim 5.5$  S. Notably, when in a molar ratio of 2:1 (cyan curve), the peak corresponding to the complex is almost the only visible one, thus suggesting a 2:1 M stoichiometry for 14-3-3 $\gamma$ /FL-pCaMKK2. SV-AUC analysis was then performed in an analogous way in the presence of (R)-**5.1** (20  $\mu$ M) as depicted in Figure 5.11b. Data revealed the formation of a complex with a  $s_w$  of  $\sim 5.2$  S. This  $s_w$  value corresponds to a molar ratio of 2:1 (cyan curve) as well, thus suggesting that the 2:1 M stoichiometry of the complex is maintained when (R)-**5.1** is present. Subsequently, equilibrium dissociation constants ( $K_d$ ) were estimated by analyzing the isotherms of weight-averaged sedimentation coefficients ( $s_w$  isotherms) derived from the SV-AUC distributions as a function of FL-pCaMKK2 concentration (Figure 5.11c and d). The direct modeling<sup>23-24</sup> of the  $s_w$  values using the Lamm equation<sup>23-24</sup> returned a  $K_d$  of  $250 \pm 20$  nM for the binary 14-3-3 $\gamma$ : FL-pCaMKK2 interaction, whereas for the ternary complex 14-3-3 $\gamma$ /FL-pCaMKK2:(R)-**5.1** a  $K_d$  of  $9 \pm 1$  nM was found, corresponding to a  $\sim 27$ -fold stabilization of the 14-3-3 $\gamma$ /FL-pCaMKK2 in the presence of 20  $\mu$ M (R)-**5.1**. When Fc-A was tested against 14-3-3 $\gamma$ /FL-pCaMKK2, a very weak stabilization effect was observed only at very high Fc-A concentration,<sup>25</sup> therefore confirming the FP and SPR data generated in chapter 3 using the corresponding phosphopeptide CaMKK2(pS<sup>100</sup>).

## 5.7 CONCLUSION

The main aim of this chapter was to explore the structure activity relationship of pyrrolidone-based 14-3-3 PPI stabilizers, evaluating potency, stabilization effect and selectivity against two 14-3-3 PPIs, namely 14-3-3/ER $\alpha$ (pT<sup>594</sup>) and 14-3-3/CaMKK2(pS<sup>100</sup>). A number of derivatives of starting compound **5.1** was synthesized (**5.4** - **5.63**), varying each of the three positions on the pyrrolidone scaffold (R<sup>1</sup>, R<sup>2</sup> and R<sup>3</sup>, scheme 5.1). Each compound was initially tested in FP assay, and SPR was used as secondary assay for the most interesting compounds. In terms of potency and stabilization effect, 4-chlorophenyl **5.7** for R<sup>1</sup>, benzolactone **5.20** for R<sup>2</sup> and 1-naphthyl **5.63** for R<sup>3</sup> were shown to be the best substituents. It is also worth pointing out that the isoquinoline derivative **5.29** (R<sup>2</sup>) showed more than three times the affinity for 14-3-3 protein (alone) than any other derivative when tested by SPR. This was, however, at the expense of potency and stabilization.

In terms of selectivity, overall, the synthesized derivatives were more potent in the 14-3-3/CaMKK2(pS<sup>100</sup>) PPI. Specifically, 4-chlorophenyl **5.7** (20-fold) and 4-methylphenyl **5.8** (24-fold) for R<sup>1</sup>, the benzolactone **5.20** (31-fold) for R<sup>2</sup> and the 2-

chlorophenyl **5.30** (15-fold) for R<sup>3</sup> exhibited the highest degree of selectivity for 14-3-3/CaMKK2(pS<sup>100</sup>) over 14-3-3/ER $\alpha$ (pT<sup>594</sup>). In this sense, **5.20** was even more selective than **5.1** (25-fold). On the other hand, phenylpropyl **5.55** (R<sup>3</sup>), was the only derivative with at least a 2-fold selectivity (2.7-fold) for ER $\alpha$ (pT<sup>594</sup>).

X-ray crystal structures of the 14-3-3 $\sigma$ /ER $\alpha$ (pT<sup>594</sup>)/**5.20** and 14-3-3 $\sigma$ /ER $\alpha$ (pT<sup>594</sup>)/**5.35** ternary complexes were obtained, showing how the nitro and the salicylate groups can be successfully be replaced, while maintaining good potency and selectivity between 14-3-3 PPIs.

Finally, the stabilization effect of compound (*R*)-**5.1** was tested against full-length doubly phosphorylated CaMKK2 (14-3-3 $\gamma$ /FL-pCaMKK2), displaying a 27-fold stabilization at 20  $\mu$ M. This result, together with others,<sup>26</sup> show how short phosphopeptides can recapitulate key interactions between 14-3-3 and the full-length phosphorylated client partner, therefore providing a valuable proof-of-concept for the study of 14-3-3 PPIs.

As next steps, it will be of great importance to obtain a x-ray crystal structure of the ternary complex 14-3-3/CaMKK2(pS<sup>100</sup>)/(*R*)-**5.1** in order to gain structural insight on this PPI, to synthesize a new derivative bearing all the most relevant modifications here described, that combine the R<sup>1</sup> - R<sup>3</sup> modifications together to check if the observed SAR is additive, and to further investigate the 14-3-3 $\gamma$ /FL-pCaMKK2 PPI with metal-insensitive pyrrolidone-based stabilizers.

### Author contribution

Prof. Dr. Tomáš Obšil is greatly is thanked for the fruitful discussion and help in SV-AUC experiments. Olivia Petrvalska performed SV-AUC data collection and analysis on (*R*)-**5.1**. Dr. Sebastian Andrei performed X-ray crystallography on compounds **5.20** and **5.35**. Dr. Jakob Pallensen performed the docking procedure on **5.29**.

## 5.8 EXPERIMENTAL SECTION

## 5.8.1 Supporting Figures

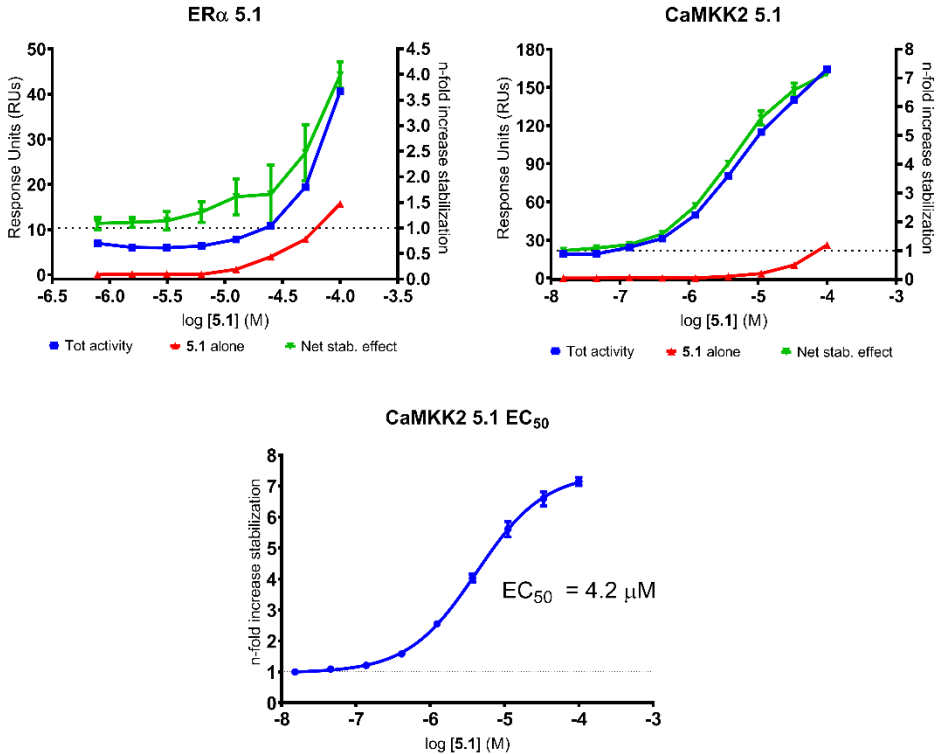


**Figure S5.1** | Total activity and net stabilization effect for compound **5.1**, measured by SPR assay in ER $\alpha$  (left panel) and CaMKK2 (right panel). Compound concentration (x-axis) is plotted as the log of the molar compound concentration. Three curves are defined. “Tot activity” (total activity, blue curve) is the total RUs (left y-axis) afforded by adding **5.1** to immobilized 14-3-3 $\zeta$  in the presence of either 50 nM **5.2** (ER $\alpha$ (pT<sup>594</sup>), left panel) or 30  $\mu$ M **5.3** (CaMKK2(pS<sup>100</sup>), right panel). It corresponds to the affinity for 14-3-3 $\zeta$  + affinity for 14-3-3 $\zeta$ /**5.2** or **5.3** complex + stabilization of 14-4-4 $\zeta$ /**5.2** or **5.3** interaction). “**5.1** alone” (red curve) is the RUs (left y-axis) obtained from **5.1** affinity for immobilized 14-3-3 $\zeta$  protein in the absence **5.2** (or **5.3**). “Net stab. effect” (Net stabilization effect, expressed as n-fold, green curve, right y-axis) is defined as (“Total activity” - “Compound alone”)/ (“Peptide effect”). “Peptide effect” is the RUs obtained from the 14-3-3 $\zeta$ :**5.2** (or **5.3**) interaction, using a fixed concentration of phosphopeptide **5.2** (50 nM) or **5.3** (30  $\mu$ M), corresponding approximately to 20% occupancy of 14-3-3 by **5.2** or **5.3**. The lines connecting the concentration points do not represent a fitted curve. Bottom panel: as saturation could be observed for the 14-3-3 $\zeta$ : CaMKK2(pS<sup>100</sup>):**5.1**, an EC<sub>50</sub> (4.2  $\mu$ M, 3.7 to 4.7  $\mu$ M 95% CI) value was obtained from fitting the data with a four-parameter logistic model (4PL) using GraphPad Prism.

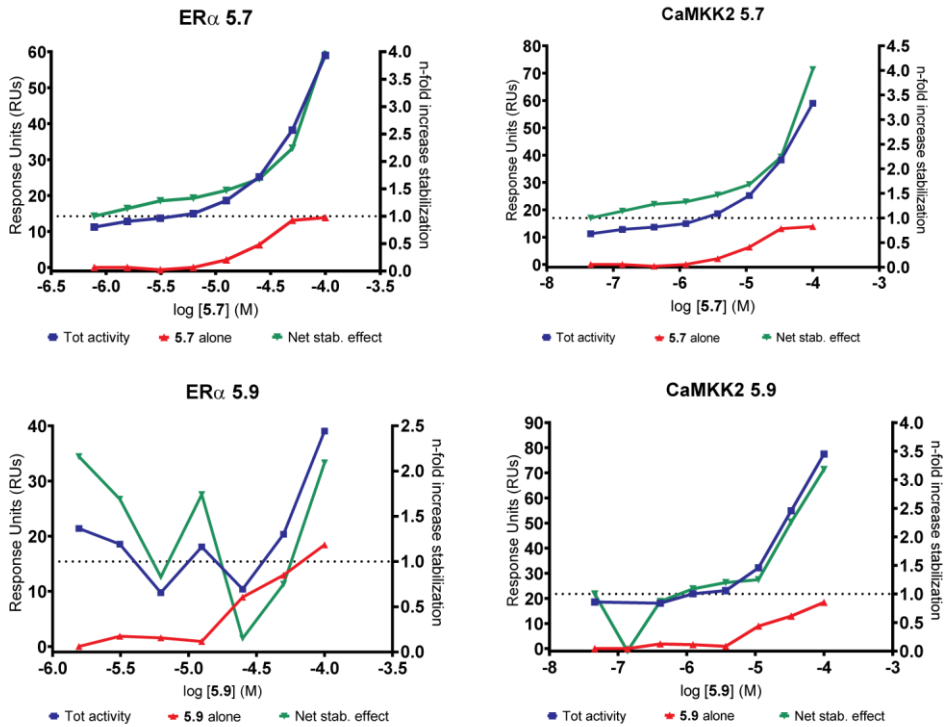


**Figure S5.2** | Total activity and net stabilization effect for compounds **5.7** and **5.9** ( $R^1$ ), measured by SPR assay in ER $\alpha$  (left panels) and CaMKK2 (right panels). Compound concentration (x-axis) is plotted as the log of the molar compound concentration. For each compound, three curves are defined. “Tot activity” (total activity, blue curve) is the total RUs (left y-axis) afforded by adding the specific compound to immobilized 14-3-3 $\zeta$  in the presence of either 50 nM **5.2** (ER $\alpha$ (pT<sup>594</sup>), left panels) or 30  $\mu$ M **5.3** (CaMKK2(pS<sup>100</sup>), right panels). It corresponds to the affinity for 14-3-3 $\zeta$  + affinity for 14-3-3 $\zeta$ /**5.2** or **5.3** complex + stabilization of 14-4-4 $\zeta$ /**5.2** or **5.3** interaction. “Compound alone” (red curve) is the RUs (left y-axis) obtained from compound affinity for immobilized 14-3-3 $\zeta$  protein in the absence **5.2** (or **5.3**). “Net stab. effect” (Net stabilization effect, expressed as n-fold, green curve, right y-axis) is defined as (“Total activity” - “Compound alone”)/ (“Peptide effect”). “Peptide effect” is the RUs obtained from the 14-3-3 $\zeta$ :**5.2** (or **5.3**) interaction, using a fixed concentration of phosphopeptide **5.2** (50 nM) or **5.3** (30  $\mu$ M), corresponding approximately to 20% occupancy of 14-3-3 by **5.2** or **5.3**. The lines connecting the concentration points do not represent a fitted curve.

CHAPTER 5

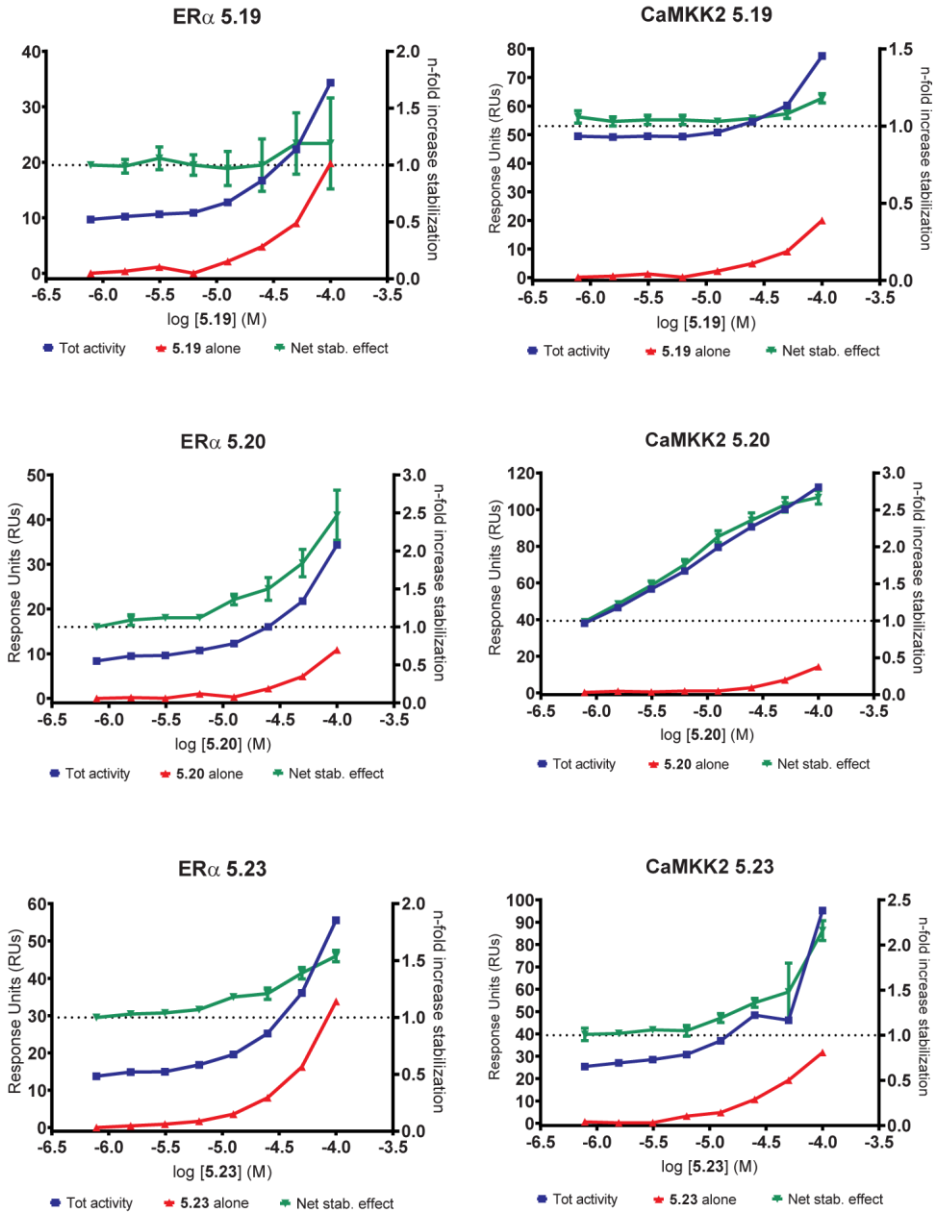


**Figure S5.3** | Total activity and net stabilization effect for compounds **5.19**, **5.20** and **5.23** ( $R^2$ ), measured by SPR assay in ER $\alpha$  (left panels) and CaMKK2 (right panels). Figure description as in Figure S5.2.

CHAPTER 5

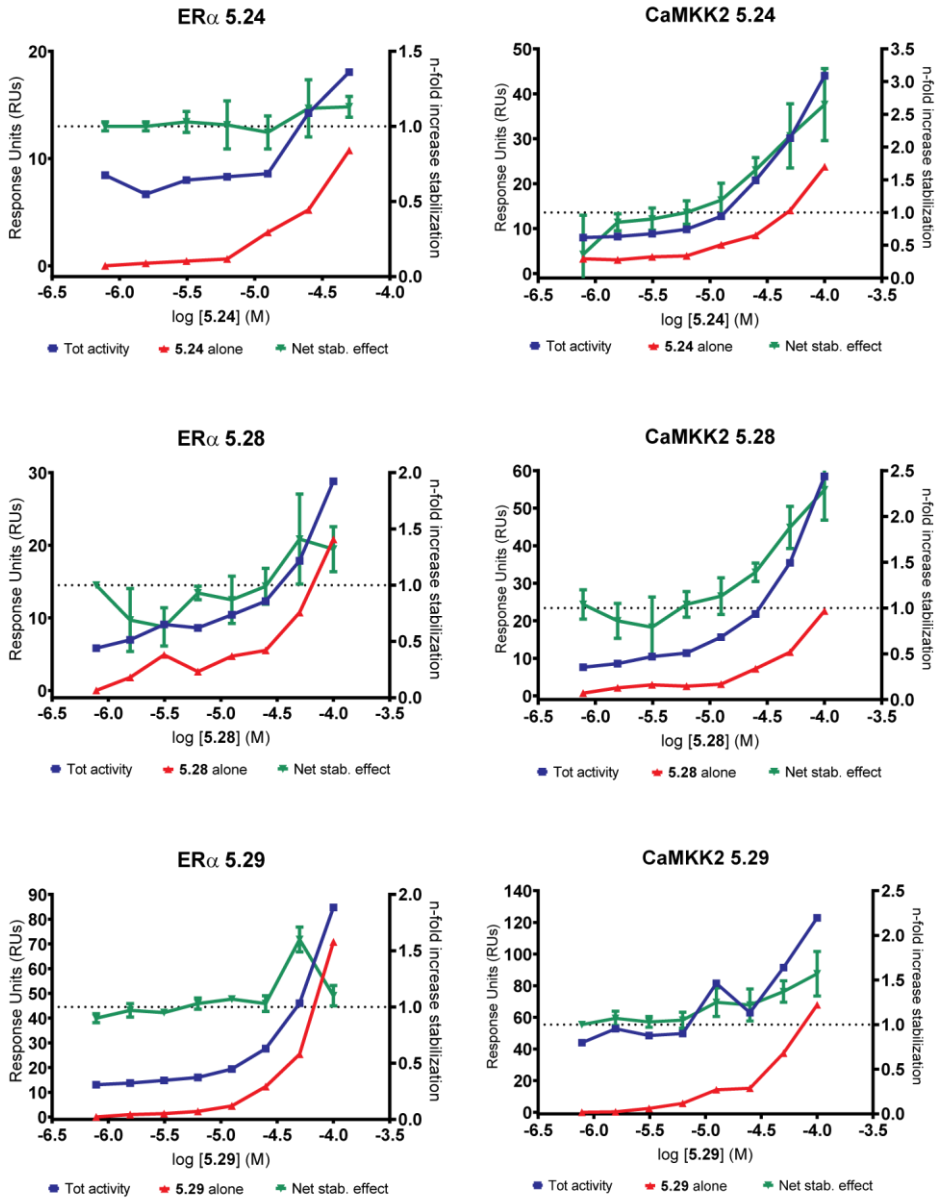


**Figure S5.4** | Total activity and net stabilization effect for compounds **5.24**, **5.28** and **5.29** ( $R^2$ ), measured by SPR assay in ER $\alpha$  (left panels) and CaMKK2 (right panels). Figure description as in Figure S5.2.

CHAPTER 5

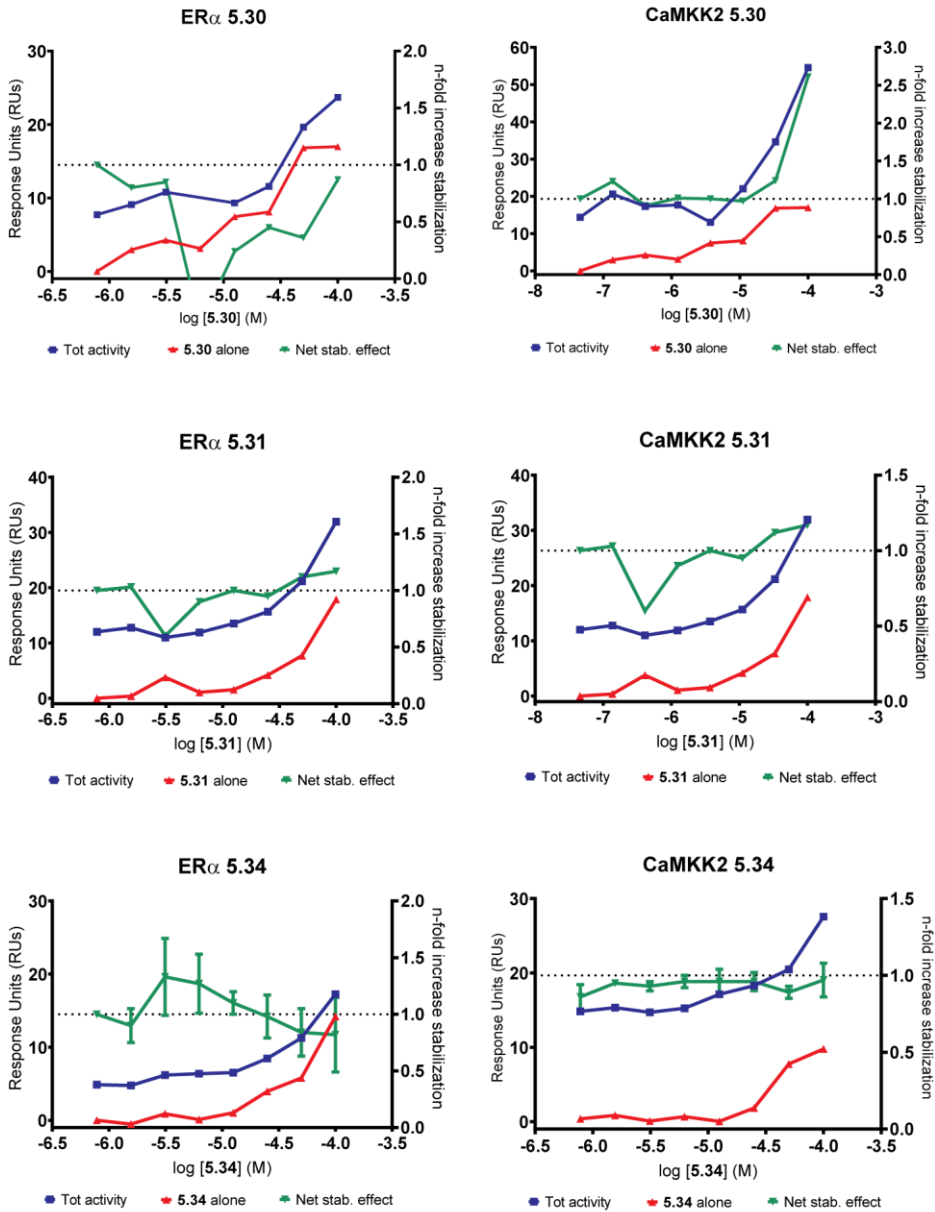


**Figure S5.5** | Total activity and net stabilization effect for compounds **5.30**, **5.31** and **5.34** ( $R^3$ ), measured by SPR assay in ER $\alpha$  (left panels) and CaMKK2 (right panels). Figure description as in Figure S5.2.

CHAPTER 5

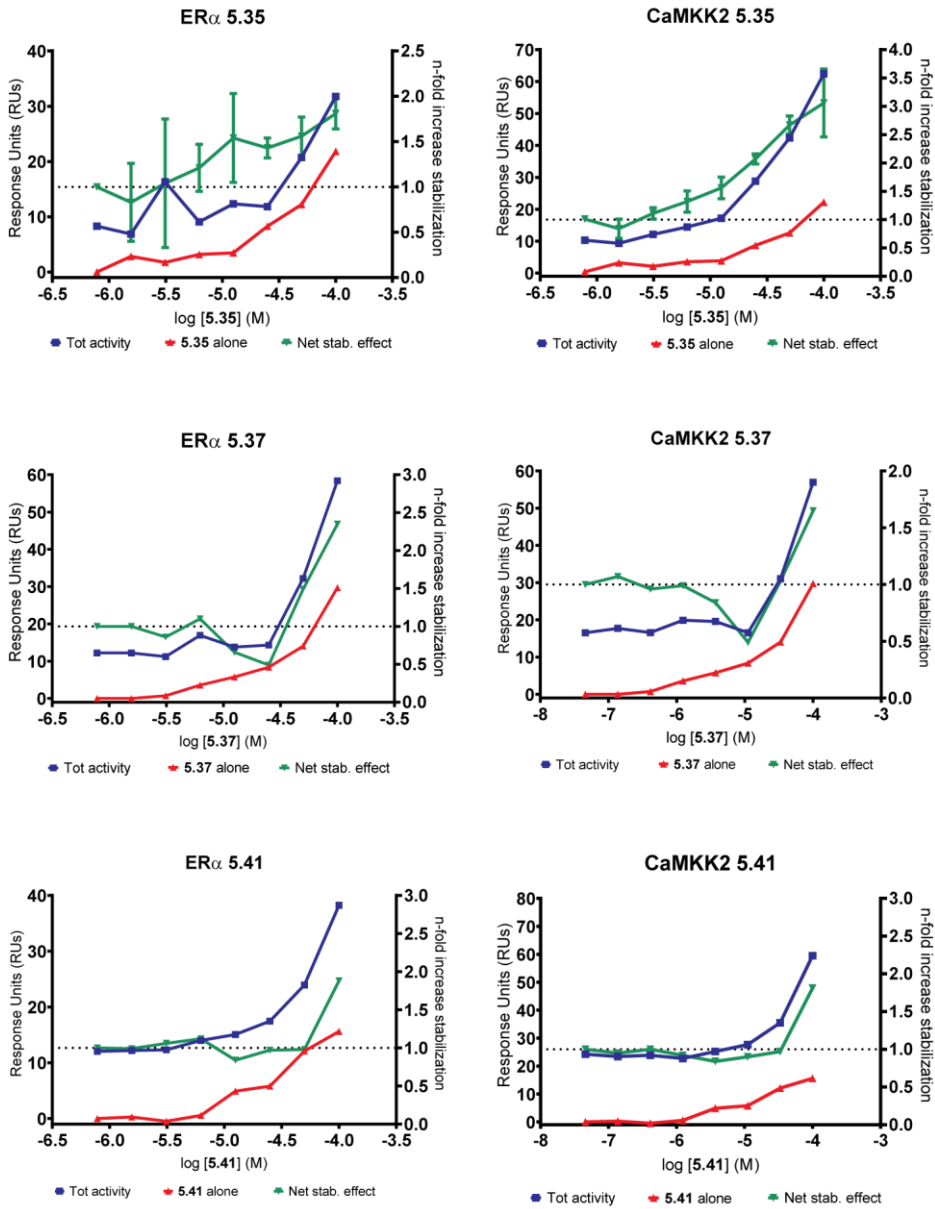


**Figure S5.6** | Total activity and net stabilization effect for compounds **5.35**, **5.37** and **5.41** ( $R^3$ ), measured by SPR assay in ER $\alpha$  (left panels) and CaMKK2 (right panels). Figure description as in Figure S2.



CHAPTER 5

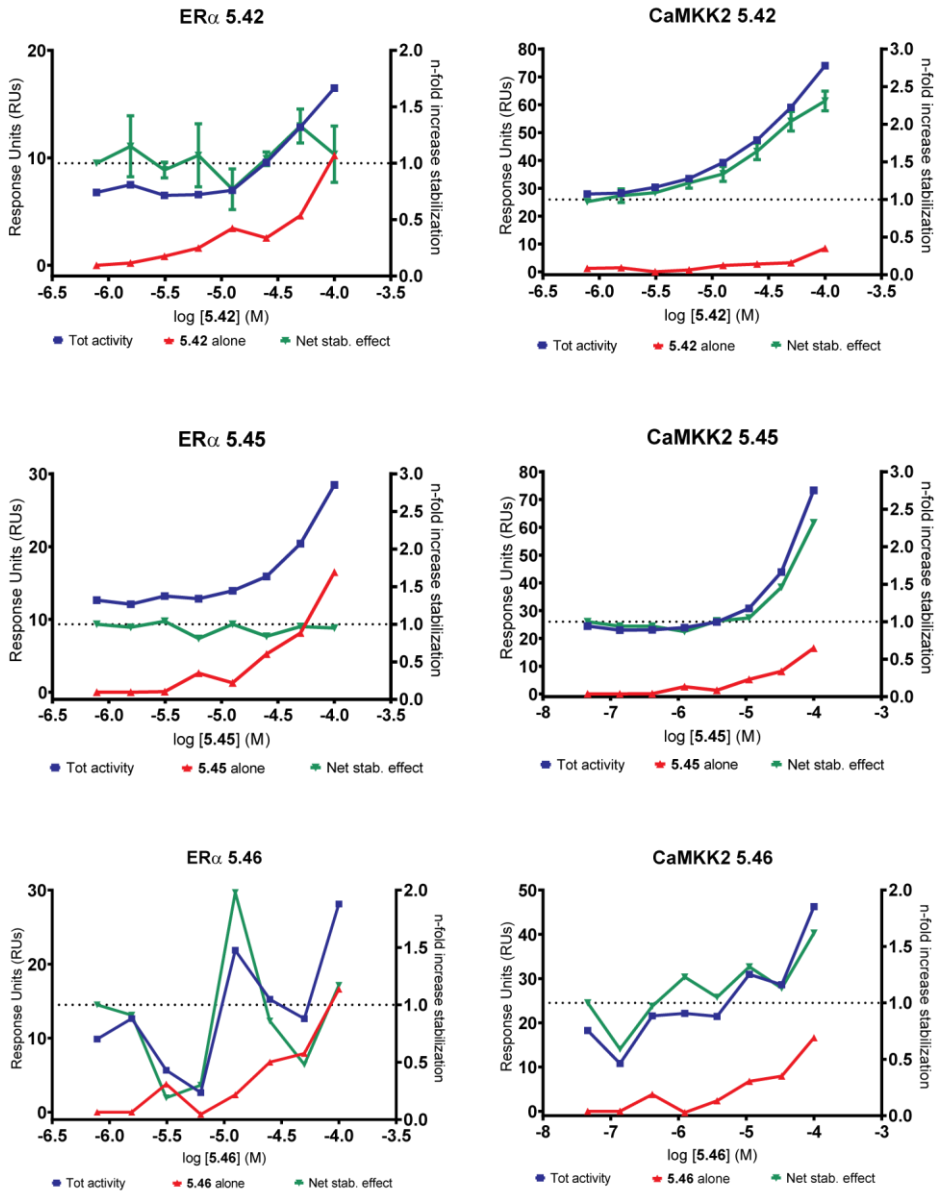


**Figure S5.7** | Total activity and net stabilization effect for compounds **5.42**, **5.45** and **5.46** ( $R^3$ ), measured by SPR assay in ER $\alpha$  (left panels) and CaMKK2 (right panels). Figure description as in Figure S2.

CHAPTER 5

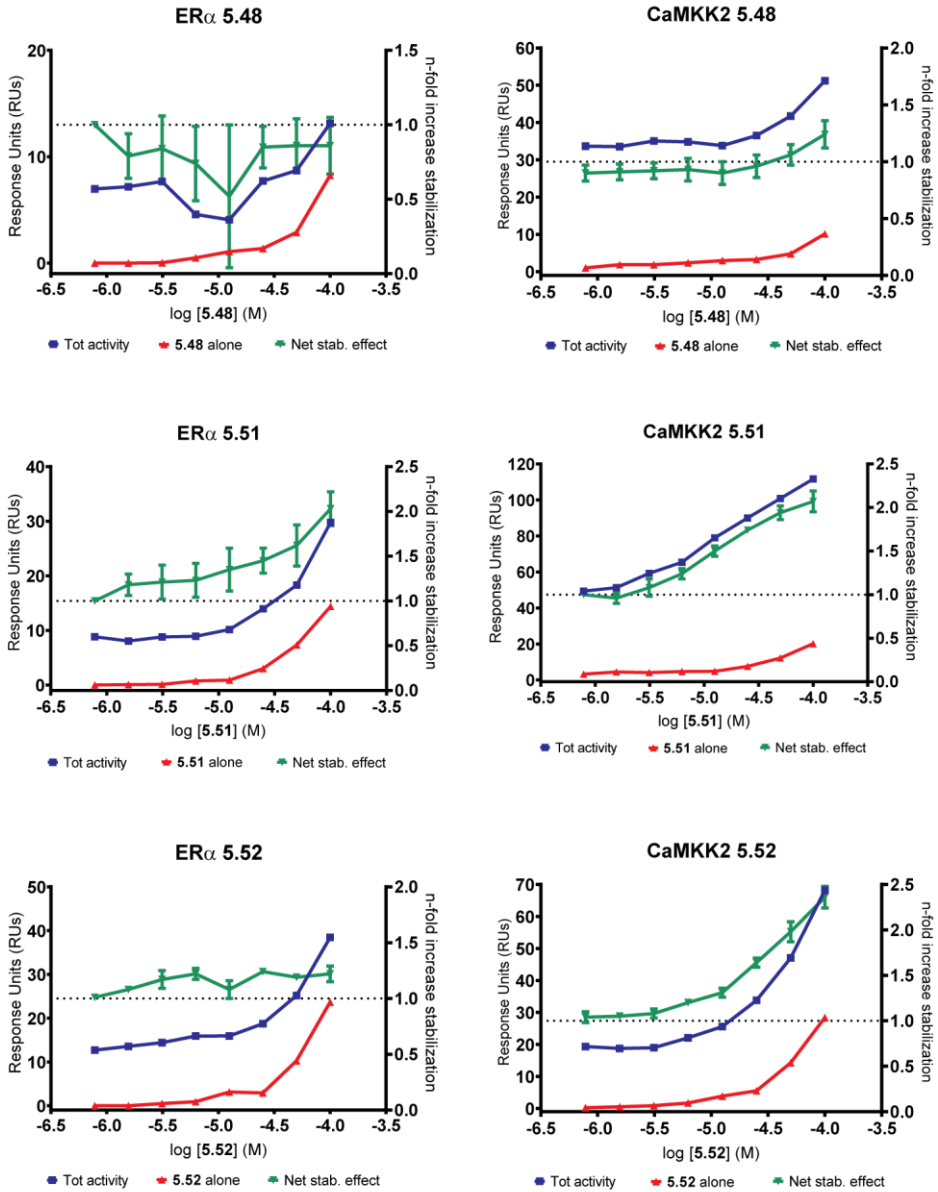


**Figure S5.8** | Total activity and net stabilization effect for compounds **5.48**, **5.51** and **5.52** ( $R^3$ ), measured by SPR assay in ER $\alpha$  (left panels) and CaMKK2 (right panels). Figure description as in Figure S2.

CHAPTER 5

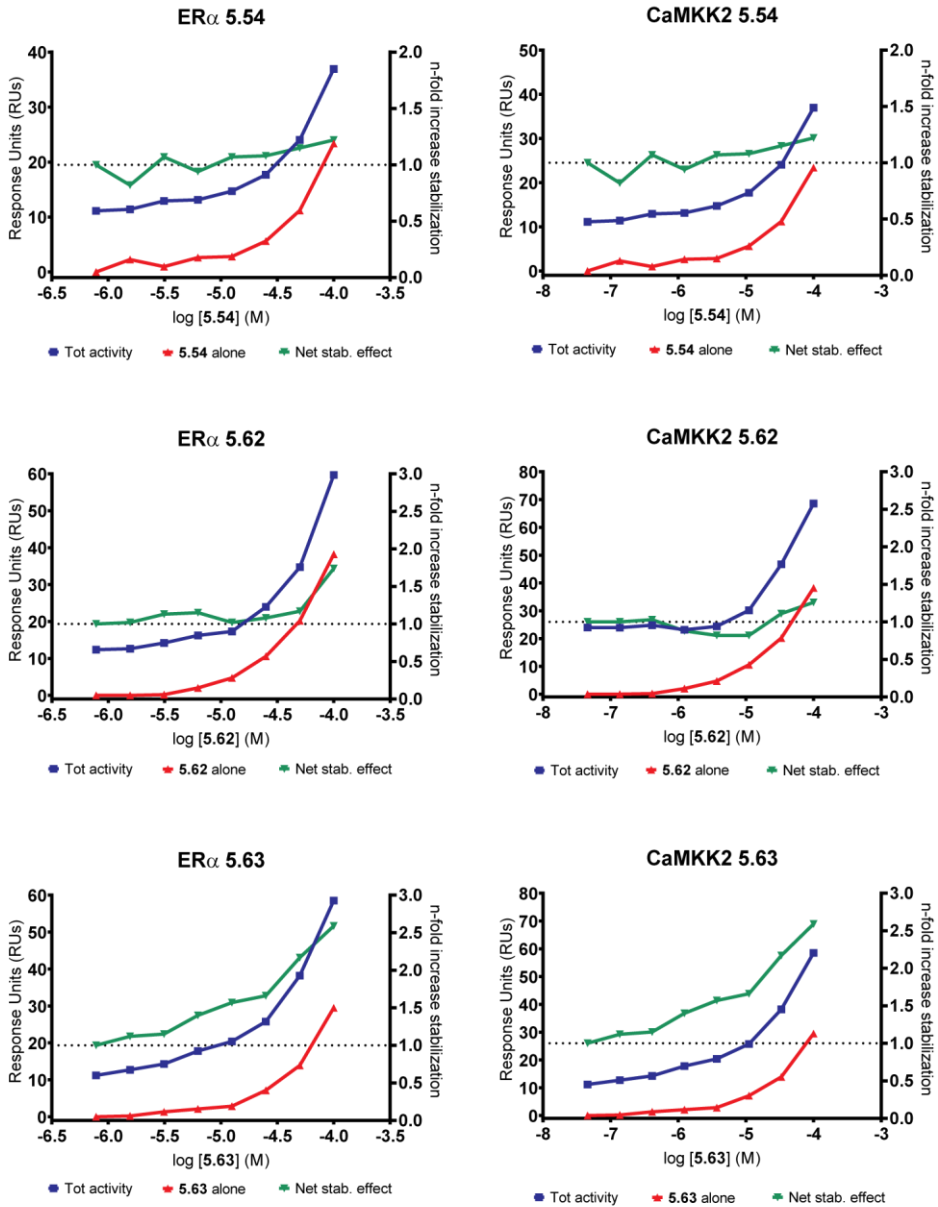


**Figure S5.9** | Total activity and net stabilization effect for compounds **5.54**, **5.62** and **5.63** ( $R^3$ ), measured by SPR assay in ER $\alpha$  (left panels) and CaMKK2 (right panels). Figure description as in Figure S2.

## 5.8.2 Chemistry section

### *General Information*

All solvents and reagents were obtained from commercially available sources and used without further purification. The microwave syntheses were performed in a Biotage Initiator with an external surface IR probe. Flash column chromatography was carried out on prepacked silica gel columns supplied by Biotage and using Biotage automated flash systems with UV detection.

UHPLC-MS experiments were performed using a Waters Acquity UHPLC system combined with a SQD mass spectrometer. The UHPLC system was equipped with both a BEH C18 column 1.7  $\mu\text{m}$  2.1 $\times$ 50 mm in combination with a 46 mM  $(\text{NH}_4)_2\text{CO}_3/\text{NH}_3$  buffer at pH 10 and a HSS C18 column 1.8  $\mu\text{m}$  2.1 $\times$ 50 mm in combination with 10 mM formic acid or 1 mM ammonium formate buffer at pH 3. The mass spectrometer used ESI+/- as ion source. UPLC was also carried out using a Waters UPLC fitted with Waters QDa mass spectrometer (Column temp 40 $^\circ\text{C}$ , UV = 190–400 nm, MS = ESI with pos/neg switching) equipped with a Waters Acquity BEH 1.7  $\mu\text{m}$  2.1 $\times$ 100 mm in combination with either 0.1% formic acid in water, 0.05% TFA in water or 0.04%  $\text{NH}_3$  in water. The flow rate was 1 mL/min.

Preparative HPLC was performed by Waters Fraction Lynx with ZQ MS detector on either a Waters Xbridge C18 OBD 5  $\mu\text{m}$  column (19 $\times$ 150 mm, flow rate 30 mL/min or 30 $\times$ 150 mm, flow rate 60 mL/min) using a gradient of 5–95% MeCN with 0.2%  $\text{NH}_3$  at pH 10 or a Waters SunFire C18 OBD 5  $\mu\text{m}$  column (19 $\times$ 150 mm, flow rate 30 mL/min or 30 $\times$ 150 mm, flow rate 60 mL/min) using a gradient of 5–95% MeCN with 0.1 M formic acid or on a Gilson Preparative HPLC with a UV/VIS detector 155 on a Kromasil C8 10  $\mu\text{m}$  column (20  $\times$  250 mm, flow rate 19 mL/min, or 50  $\times$  250 mm, flow rate 100 mL/min) using a varying gradient of ACN with 0.1% formic acid (FA) in water or 0.2% trifluoroacetic acid (TFA) in water or 0.2% acetic acid (AcOH) in water or 0.2% ammonia ( $\text{NH}_3$ ) in water. Molecular mass (HR-ESI-MS) was recorded using a Shimadzu LCMS-2020 instrument (ESI+). Purity of all test compounds was determined by LCMS. All screening compounds had a purity >95%.

General  $^1\text{H}$  NMR spectra were recorded on a Bruker Avance II, III, AV300, AV400 or AVIII500 spectrometer at a proton frequency of 400, 500 or 600 MHz at 25  $^\circ\text{C}$  or at a temperature and frequency stated in each experiment.  $^{13}\text{C}$  NMR spectra were recorded at 101 MHz or 126 MHz.

The chemical shifts ( $\delta$ ) are reported in parts per million (ppm) with residual solvent signal used as a reference ( $\text{CD}_2\text{Cl}_2$  at 5.32 ppm for  $^1\text{H}$  NMR and 53.84 ppm for  $^{13}\text{C}$  NMR,  $(\text{CD}_3)_2\text{SO}$  at 2.50 ppm for  $^1\text{H}$  NMR and 39.52 ppm for  $^{13}\text{C}$  NMR,  $\text{CDCl}_3$  at 7.26 ppm for  $^1\text{H}$  NMR and 77.16 ppm for  $^{13}\text{C}$  NMR). Coupling constants (J) are reported as Hz. NMR abbreviations are used as follows: br = broad, s = singlet, d = doublet, t = triplet, q = quartet, m = multiplet. Protons on heteroatoms such as  $\text{COOH}$  protons are only reported when detected in NMR and can therefore be missing.

### *Synthetic procedures and compound characterization*

**Ethyl 2,4-dioxo-4-phenyl-butanoate.** Synthesized as described in ref.<sup>10</sup> Matches with previously reported characterization.

#### **Ethyl 4-(2-bromophenyl)-2,4-dioxobutanoate (5.5a).**

In a RBF, 1-(2-bromophenyl)ethan-1-one (2.03 mL, 15.1 mmol) was dissolved in THF (100 mL) and the resulting solution cooled to 0  $^\circ\text{C}$ . Sodium ethanolate (8.4 mL, 22.6 mmol) was then added dropwise and the reaction allowed to stir for 15 min at 0  $^\circ\text{C}$ . Diethyl oxalate (2.25 mL, 15.6 mmol) was finally added dropwise, the cooling bath removed, and the reaction allowed to stir overnight at rt. The reaction was quenched with 1M HCl (50 mL). The resulting suspension was poured into a

separatory funnel and the crude product was extracted with DCM (3x). The combined organic layers were dried using a phase separator and solvent was removed under reduced pressure. The residue was purified by automated flash chromatography on a Biotage® KP-SIL 10g column. A gradient from 0 to 10% of EtOAc in heptane over 20 CV was used as mobile phase. Collected fractions were dried under reduced pressure, to give ethyl 4-(2-bromophenyl)-2,4-dioxobutanoate (3.25 g, 72.1 %) as a dark red solid. <sup>1</sup>H NMR (400 MHz, CDCl<sub>3</sub>) δ 7.67 (dd, *J* = 7.9, 1.1 Hz, 1H), 7.57 (dd, *J* = 7.6, 1.8 Hz, 1H), 7.42 (td, *J* = 7.5, 1.2 Hz, 1H), 7.35 (td, *J* = 7.7, 1.8 Hz, 1H), 5.89 (s, 1H), 4.39 (q, *J* = 7.1 Hz, 2H), 1.39 (t, *J* = 7.1 Hz, 3H). <sup>13</sup>C NMR (101 MHz, CDCl<sub>3</sub>) δ 194.33, 167.43, 161.97, 138.13, 134.34, 132.79, 130.20, 127.74, 120.28, 103.15, 62.83, 14.21.

**Ethyl 2,4-dioxo-4-(pyridin-2-yl)butanoate (5.9a).**

In a RBF, 1-(pyridin-2-yl)ethan-1-one (2.78 mL, 24.8 mmol) was dissolved in THF (50 mL) and the resulting solution cooled to 0 °C. Sodium ethanolate (13.9 mL, 37.2 mmol) was then added dropwise and the reaction allowed to stir for 15 min at 0 °C. Diethyl oxalate (3.70 mL, 27.2 mmol) was finally added dropwise, the cooling bath removed, and the reaction allowed to stir overnight at rt. The reaction was quenched with 1M HCl (50 mL). The resulting suspension was poured into a separatory funnel and the crude product was extracted with DCM (3x). The combined organic layers were dried using a phase separator and solvent was removed under reduced pressure. The residue was purified by automated flash chromatography on a Biotage® KP-SIL 10g column. A gradient from 0 to 10% of EtOAc in heptane over 20 CV was used as mobile phase. Collected fractions were dried under reduced pressure, to give ethyl 2,4-dioxo-4-(pyridin-2-yl)butanoate (2.015 g, 35.8 %) as a yellow solid. <sup>1</sup>H NMR (400 MHz, CDCl<sub>3</sub>) δ 8.68 – 8.79 (m, 1H), 8.17 (d, *J* = 7.9 Hz, 1H), 7.90 (td, *J* = 7.8, 1.7 Hz, 1H), 7.61 (br, 1H), 7.51 (ddd, *J* = 7.6, 4.8, 1.2 Hz, 1H), 4.39 (q, *J* = 7.1 Hz, 2H), 1.40 (t, *J* = 7.1 Hz, 3H). <sup>13</sup>C NMR (101 MHz, CDCl<sub>3</sub>) δ 190.55, 162.29, 151.95, 149.25, 137.53, 127.57, 123.00, 99.51, 62.68, 14.25.

**General procedure for the synthesis of compounds 5.1, 5.4 – 5.63.**

In a 20 mL vial, to a solution of methyl/ethyl 2,4-dioxobutanoate analogue (1.0 equiv) in ACOH (2.5–5.0 mL/mmol), the corresponding aldehyde (1.0 equiv) and amine (1.0 equiv) were added. The vial was capped and heated at 120 °C for 180 min in a single node microwave reactor. The pressure monitored was 1 bar.

**Rac- and (R)- 5-[3-Benzoyl-4-hydroxy-2-(4-nitrophenyl)-5-oxo-2H-pyrrol-1-yl]-2-hydroxybenzoic acid (5.1 and (R)-5.1).** Synthesized as described in ref.<sup>10</sup> Matches with previously reported characterization.

**5-(3-(2-Chlorobenzoyl)-4-hydroxy-2-(4-nitrophenyl)-5-oxo-2,5-dihydro-1H-pyrrol-1-yl)-2-hydroxybenzoic acid (5.4).** Prepared from methyl 4-(2-chlorophenyl)-2,4-dioxobutanoate (130 mg, 0.54 mmol), 4-nitrobenzaldehyde (83 mg, 0.54 mmol) and 5-amino-2-hydroxybenzoic acid (87 mg, 0.54 mmol). After solvent removal, the crude product was purified by preparative HPLC (5–95% ACN with 0.1 M FA, flow rate 30 mL/min). Collected fractions were freeze-dried, to give the title compound (99 mg, 37.1%) as an off-white solid. <sup>1</sup>H NMR (600 MHz, DMSO) δ 8.10 (d, *J* = 8.8 Hz, 2H), 7.99 (d, *J* = 2.7 Hz, 1H), 7.61 – 7.71 (m, 3H), 7.39 – 7.49 (m, 2H), 7.33 – 7.39 (m, 1H), 7.27 (d, *J* = 7.2 Hz, 1H), 5.87 (d, *J* = 8.9 Hz, 1H), 5.36 (s, 1H). HRMS (ESI) *m/z* [M + H]<sup>+</sup> calcd for C<sub>24</sub>H<sub>15</sub>ClN<sub>2</sub>O<sub>8</sub>: 495.0595, found: 495.0583. Purity: 99%.

**5-(3-(2-Bromobenzoyl)-4-hydroxy-2-(4-nitrophenyl)-5-oxo-2,5-dihydro-1H-pyrrol-1-yl)-2-hydroxybenzoic acid (5.5).** Prepared from **5.5a** (350 mg, 1.04 mmol), 4-nitrobenzaldehyde (157 mg, 1.04 mmol) and 5-amino-2-hydroxybenzoic acid (159 mg, 1.04 mmol). After solvent removal, the crude product was purified by preparative HPLC (5–95% ACN in 0.1 M FA, with a flow rate of 60 mL/min). The collected fractions were freeze-dried, to give the title compound (133 mg, 24%) as a yellow solid. <sup>1</sup>H NMR (600 MHz, DMSO) δ 8.10 (d, *J* = 8.7 Hz, 2H), 8.00 (d, *J* = 2.7 Hz, 1H), 7.63 – 7.69 (m, 3H), 7.60 (d, *J* = 8.0 Hz, 1H), 7.42 (t, *J* = 7.5 Hz, 1H), 7.35 (t, *J* = 7.7 Hz, 1H), 7.24 (d, *J* = 7.5 Hz, 1H), 5.89 (d, *J* = 8.9 Hz, 1H), 5.38 (s, 1H). HRMS (ESI) *m/z* [M + H]<sup>+</sup> calcd for C<sub>24</sub>H<sub>15</sub>BrN<sub>2</sub>O<sub>8</sub>: 539.0090, found: 539.0073. Purity: 98%.

**5-(3-(3-(Difluoromethoxy)benzoyl)-4-hydroxy-2-(4-nitrophenyl)-5-oxo-2,5-dihydro-1H-pyrrol-1-yl)-2-hydroxybenzoic acid (5.6).** Prepared from methyl 4-(3-(difluoromethoxy)phenyl)-2,4-dioxobutanoate (120 mg, 0.44 mmol), 4-nitrobenzaldehyde (68.0 mg, 0.44 mmol) and 5-amino-2-hydroxybenzoic acid (71.1 mg, 0.44 mmol). After solvent removal, the crude product was purified by preparative HPLC (5–95% ACN with 0.1 M FA, flow rate 30 mL/min). Collected fractions were freeze-dried, to give compound the title compound (42 mg, 18.1%) as a off-white solid. HRMS (ESI) *m/z* [M + H]<sup>+</sup> calcd for C<sub>25</sub>H<sub>16</sub>F<sub>2</sub>N<sub>2</sub>O<sub>9</sub>: 527.0902, found: 527.0887.

**5-(3-(4-Chlorobenzoyl)-4-hydroxy-2-(4-nitrophenyl)-5-oxo-2,5-dihydro-1H-pyrrol-1-yl)-2-hydroxybenzoic acid (5.7).**

Prepared from methyl 4-(4-chlorophenyl)-2,4-dioxobutanoate (150 mg, 0.62 mmol), 4-nitrobenzaldehyde (96 mg, 0.62 mmol) and 5-amino-2-hydroxybenzoic acid (100 mg, 0.62 mmol). The mixture was diluted with diethyl ether and filtered. The solid residue was washed with diethyl ether and dried under reduced pressure to give the title compound (60.0 mg, 19.5%) as a yellow solid. <sup>1</sup>H NMR (400 MHz, DMSO) δ 8 – 8.11 (m, 3H), 7.65 – 7.77 (m, 5H), 7.48 – 7.57 (m, 2H), 5.91 (d, *J* = 8.9 Hz, 1H), 5.44 (s, 1H). <sup>13</sup>C NMR (101 MHz, DMSO) δ 187.77, 171.14, 164.34, 158.78, 151.71, 147.21, 144.36, 137.47, 135.62, 130.56, 129.28, 128.31, 127.43, 124.94, 123.50, 118.66, 117.58, 113.01, 60.75. HRMS (ESI) *m/z* [M + H]<sup>+</sup> calcd for C<sub>24</sub>H<sub>15</sub>ClN<sub>2</sub>O<sub>8</sub>: 495.0595, found: 495.0577.

**2-Hydroxy-5-(3-hydroxy-4-(4-methylbenzoyl)-5-(4-nitrophenyl)-2-oxo-2,5-dihydro-1H-pyrrol-1-yl)benzoic acid (5.8).** Prepared from methyl 2,4-dioxo-4-(*p*-tolyl)butanoate (250 mg, 1.14 mmol), 4-nitrobenzaldehyde (175 mg, 1.14 mmol) and 5-amino-2-hydroxybenzoic acid (183 mg, 1.14 mmol). After solvent removal, the crude product was purified by preparative HPLC (5–95% ACN with 0.1 M FA, flow rate 30 mL/min). Collected fractions were freeze-dried, to give compound **xx1** (14 mg, 3%) as a off-white solid. HRMS (ESI) *m/z* [M + H]<sup>+</sup> calcd for C<sub>25</sub>H<sub>18</sub>N<sub>2</sub>O<sub>8</sub>: 475.1141, found: 475.1125.

**2-Hydroxy-5-(3-hydroxy-5-(4-nitrophenyl)-2-oxo-4-picolinoyl-2,5-dihydro-1H-pyrrol-1-yl)benzoic acid (5.9).** Prepared from **5.9a** (150 mg, 0.64 mmol), 4-nitrobenzaldehyde (97 mg, 0.64 mmol) and 5-amino-2-hydroxybenzoic acid (99 mg, 0.64 mmol). After solvent removal, the crude product was purified by preparative HPLC (5–95% ACN in 0.1 M FA, flow rate 60 mL/min). The collected fractions were freeze-dried, to give the title compound (29 mg, 10%) as a pale yellow solid. <sup>1</sup>H NMR (600 MHz, DMSO) δ 8.99 (d, *J* = 4.4 Hz, 1H), 8.36 (td, *J* = 7.9, 1.6 Hz, 1H), 8.15 (d, *J* = 8.0 Hz, 1H), 7.97 – 8.08 (m, 4H), 7.57 – 7.72 (m, 3H), 5.86 (d, *J* = 8.9 Hz, 1H), 5.35 (s, 1H). HRMS (ESI) *m/z* [M + H]<sup>+</sup> calcd for C<sub>23</sub>H<sub>15</sub>N<sub>3</sub>O<sub>8</sub>: 462.0937, found: 462.0941. Purity: 100%

**5-(3-Benzyl-4-hydroxy-2-(4-nitrophenyl)-5-oxo-2,5-dihydro-1H-pyrrol-1-yl)-2-hydroxybenzoic acid (5.10).** Prepared from ethyl 2-oxo-4-phenylbutanoate (250 mg, 1.21 mmol), 4-nitrobenzaldehyde (183 mg, 1.21 mmol) and 5-amino-2-hydroxybenzoic acid (186 mg, 1.21 mmol). After solvent removal, the crude mixture was purified by preparative SFC (MeOH/NH<sub>3</sub> 20 mM). The collected fractions were dried under reduced pressure, to give the title compound (10 mg, 2%) as a pale yellow solid. HRMS (ESI)  $m/z$  [M + H]<sup>+</sup> calcd for C<sub>24</sub>H<sub>18</sub>N<sub>2</sub>O<sub>7</sub>: 447.1192, found: 447.1169. Purity: 96%.

**5-(3-(4-Chlorobenzyl)-4-hydroxy-2-(4-nitrophenyl)-5-oxo-2,5-dihydro-1H-pyrrol-1-yl)-2-hydroxybenzoic acid (5.11).** Prepared from ethyl 4-(4-chlorophenyl)-2-oxobutanoate (274 mg, 1.14 mmol), 4-nitrobenzaldehyde (172 mg, 1.14 mmol) and 5-amino-2-hydroxybenzoic acid (175 mg, 1.14 mmol) After solvent removal, the reaction mixture was triturated with diethyl ether. The solid residue was washed with diethyl ether and subsequently purified by preparative HPLC (5-95% ACN in 0.2% NH<sub>3</sub>, flow rate 60 mL/min). The collected fractions were freeze-dried, to give the title compound (119 mg, 18%) as a HRMS (ESI)  $m/z$  [M + H]<sup>+</sup> calcd for C<sub>24</sub>H<sub>17</sub>ClN<sub>2</sub>O<sub>7</sub>: 481.0802, found: 481.0808. Purity: 86%.

**2-Hydroxy-5-(3-hydroxy-4-isobutyl-5-(4-nitrophenyl)-2-oxo-2,5-dihydro-1H-pyrrol-1-yl)benzoic acid (5.12).** Prepared from ethyl 5-methyl-2-oxohexanoate (196 mg, 1.14 mmol), 4-nitrobenzaldehyde (172 mg, 1.14 mmol) and 5-amino-2-hydroxybenzoic acid (175 mg, 1.14 mmol) After solvent removal, the reaction mixture was triturated with diethyl ether. The solid residue was washed with diethyl ether and subsequently purified by preparative HPLC (5-95% ACN in 0.2% NH<sub>3</sub>, flow rate 60 mL/min). The collected fractions were freeze-dried, to give the title compound (141 mg, 27%) as a HRMS (ESI)  $m/z$  [M + H]<sup>+</sup> calcd for C<sub>21</sub>H<sub>20</sub>N<sub>2</sub>O<sub>7</sub>: 413.1349, found: 413.1360. Purity: 100%

**2-Hydroxy-5-(3-hydroxy-5-(4-nitrophenyl)-2-oxo-4-(pyrazin-2-yl)-2,5-dihydro-1H-pyrrol-1-yl)benzoic acid (5.13).** Prepared from ethyl 2-oxo-3-(pyrazin-2-yl)propanoate (221 mg, 1.14 mmol), 4-nitrobenzaldehyde (172 mg, 1.14 mmol) and 5-amino-2-hydroxybenzoic acid (175 mg, 1.14 mmol) After solvent removal, the reaction mixture was triturated with diethyl ether. The solid residue was washed with diethyl ether and subsequently purified by preparative HPLC (5-95% ACN in 0.2% NH<sub>3</sub>, flow rate 60 mL/min). The collected fractions were freeze-dried, to give the title compound (180 mg, 36%) as an off-white solid. HRMS (ESI)  $m/z$  [M + H]<sup>+</sup> calcd for C<sub>21</sub>H<sub>14</sub>N<sub>4</sub>O<sub>7</sub>: 435.0941, found: 435.0960. Purity: 86%.

**5-(2-(4-Aminophenyl)-3-benzoyl-4-hydroxy-5-oxo-2,5-dihydro-1H-pyrrol-1-yl)-2-hydroxybenzoic acid (5.14).** In a RBF, **5.1** (100 mg, 0.22 mmol) and Pd/C 5% (45 mg, 0.011 mmol) were suspended in MeOH (5 mL). The reaction was allowed to stir at RT under an atmosphere of H<sub>2</sub> (1 bar) until complete consumption of starting material (6 hr). The catalyst was removed by filtration through a plug of celite, the filtrate was concentrated under vacuum and the resulting solid was purified by preparative HPLC (5-95% ACN in 0.1 M FA, flow rate 60 mL/min). The collected fractions were freeze-dried, to give the title compound (8 mg, 9%) as an off-white solid. HRMS (ESI)  $m/z$  [M + H]<sup>+</sup> calcd for C<sub>24</sub>H<sub>18</sub>N<sub>2</sub>O<sub>6</sub>: 431.1243, found: 431.1245. Purity: 97%.

**5-(3-Benzoyl-4-hydroxy-5-oxo-2-phenyl-2,5-dihydro-1H-pyrrol-1-yl)-2-hydroxybenzoic acid (5.15).** Prepared from ethyl 2,4-dioxo-4-phenylbutanoate (300 mg, 1.36 mmol), benzaldehyde (0.138 mL, 1.36 mmol) and 5-amino-2-hydroxybenzoic acid (209 mg, 1.36 mmol) After solvent

removal, the reaction mixture was triturated with diethyl ether. The solid residue was washed with diethyl ether and subsequently purified by preparative HPLC (2-94% ACN in 0.2% NH<sub>3</sub>, flow rate 60 mL/min). The collected fractions were freeze-dried, to give the title compound (124 mg, 22%) as an off-white solid. HRMS (ESI)  $m/z$  [M + H]<sup>+</sup> calcd for C<sub>24</sub>H<sub>17</sub>NO<sub>6</sub>: 415.1134, found: 415.1127. Purity: 95%.

**5-(4-Benzoyl-3-hydroxy-2-oxo-2,5-dihydro-1H-pyrrol-1-yl)-2-hydroxybenzoic acid (5.16).**

Prepared from ethyl 2,4-dioxo-4-phenylbutanoate (71 mg, 0.32 mmol), formaldehyde (30  $\mu$ l, 0.32 mmol), and 5-amino-2-hydroxybenzoic acid (52.0 mg, 0.32 mmol). After solvent removal, the crude product was purified by preparative HPLC (5-95% ACN with 0.1 M FA, flow rate 30 mL/min). Collected fractions were freeze-dried, to give the title compound (23 mg, 21.0%) as an off-white solid. <sup>1</sup>H NMR (600 MHz, DMSO)  $\delta$  8.23 (d,  $J$  = 2.8 Hz, 1H), 7.93 (dd,  $J$  = 9.0, 2.8 Hz, 1H), 7.78 – 7.84 (m, 2H), 7.60 (t,  $J$  = 7.4 Hz, 1H), 7.50 (t,  $J$  = 7.7 Hz, 2H), 7.01 (d,  $J$  = 9.0 Hz, 1H), 4.64 (s, 2H). HRMS (ESI)  $m/z$  [M + H]<sup>+</sup> calcd for C<sub>18</sub>H<sub>13</sub>NO<sub>6</sub>: 340.0821, found: 340.0802. Purity: 100%.

**5-(3-Benzoyl-2-(4-carboxyphenyl)-4-hydroxy-5-oxo-2,5-dihydro-1H-pyrrol-1-yl)-2-hydroxybenzoic acid (5.17).**

Prepared from ethyl 2,4-dioxo-4-phenylbutanoate (300 mg, 1.36 mmol), 4-formylbenzoic acid (205 mg, 1.36 mmol) and 5-amino-2-hydroxybenzoic acid (209 mg, 1.36 mmol). After solvent removal, the reaction mixture was triturated with diethyl ether. The solid residue was washed with diethyl ether and subsequently purified by preparative HPLC (5-95% ACN in 0.1 M FA, flow rate 60 mL/min). The collected fractions were freeze-dried, to give title compound (58 mg, 9%) as an off-white solid. <sup>1</sup>H NMR (400 MHz, DMSO)  $\delta$  8.01 (d,  $J$  = 2.7 Hz, 1H), 7.77 (d,  $J$  = 8.3 Hz, 2H), 7.66 – 7.73 (m, 3H), 7.57 (t,  $J$  = 7.4 Hz, 1H), 7.4 – 7.52 (m, 4H), 5.90 (d,  $J$  = 8.9 Hz, 1H), 5.35 (s, 1H). HRMS (ESI)  $m/z$  [M + H]<sup>+</sup> calcd for C<sub>25</sub>H<sub>17</sub>NO<sub>8</sub>: 460.1032, found: 460.1029. Purity: 96%.

**5-(2-(4-Acetamidophenyl)-3-benzoyl-4-hydroxy-5-oxo-2,5-dihydro-1H-pyrrol-1-yl)-2-hydroxybenzoic acid (5.18).**

Prepared from ethyl 2,4-dioxo-4-phenylbutanoate (250 mg, 1.14 mmol), *N*-(4-formylphenyl)acetamide (185 mg, 1.14 mmol) and 5-amino-2-hydroxybenzoic acid (174 mg, 1.14 mmol). After solvent removal, the crude product was purified by preparative HPLC (5-95% ACN in 0.2% NH<sub>3</sub>, flow rate 60 mL/min). The collected fractions were freeze-dried, to give the title compound (21 mg, 4%) as a yellow solid. HRMS (ESI)  $m/z$  [M + H]<sup>+</sup> calcd for C<sub>26</sub>H<sub>20</sub>N<sub>2</sub>O<sub>7</sub>: 473.1349, found: 473.1338. Purity: 95%.

**5-(2-(3-Acetamidophenyl)-3-benzoyl-4-hydroxy-5-oxo-2,5-dihydro-1H-pyrrol-1-yl)-2-hydroxybenzoic acid (5.19).**

Prepared from ethyl 2,4-dioxo-4-phenylbutanoate (256 mg, 1.16 mmol), *N*-(3-formylphenyl)acetamide (190 mg, 1.16 mmol) and 5-amino-2-hydroxybenzoic acid (178 mg, 1.16 mmol). After solvent removal, the reaction mixture was triturated with diethyl ether. The filtrate was evaporated under reduced pressure and purified by preparative HPLC (0-20% acetonitrile in H<sub>2</sub>O/ACN/FA 95/5/0.2 buffer, over 15 minutes with a flow rate of 19 mL/min.). The collected fractions were freeze-dried, to give the title compound (46 mg, 8%) as a yellow solid. HRMS (ESI)  $m/z$  [M + H]<sup>+</sup> calcd for C<sub>26</sub>H<sub>20</sub>N<sub>2</sub>O<sub>7</sub>: 473.1349, found: 473.1334. Purity: 69%.

**5-(3-Benzoyl-4-hydroxy-5-oxo-2-(1-oxo-1,3-dihydroisobenzofuran-5-yl)-2,5-dihydro-1H-pyrrol-1-yl)-2-hydroxybenzoic acid (5.20).**

Prepared from ethyl 2,4-dioxo-4-phenylbutanoate (250 mg, 1.14 mmol), 1-oxo-1,3-dihydroisobenzofuran-5-carbaldehyde (185 mg, 1.14 mmol) and 5-amino-2-hydroxybenzoic acid (174 mg, 1.14 mmol). After solvent removal, the reaction mixture was



trituated with diethyl ether. The solid residue was washed with diethyl ether and subsequently purified by preparative HPLC (5-95% ACN in 0.1 M FA, flow rate 60 mL/min). The collected fractions were freeze-dried, to give the title compound (192 mg, 35%) as a yellow solid. <sup>1</sup>H NMR (500 MHz, DMSO) δ 8.02 (d, *J* = 2.8 Hz, 1H), 7.67 – 7.75 (m, 4H), 7.65 (dd, *J* = 8.9, 2.7 Hz, 1H), 7.62 (d, *J* = 8.0 Hz, 1H), 7.53 – 7.59 (m, 1H), 7.44 (t, *J* = 7.7 Hz, 2H), 5.86 (d, *J* = 8.9 Hz, 1H), 5.42 (s, 1H), 5.28 (s, 2H). <sup>13</sup>C NMR (126 MHz, DMSO) δ 188.90, 171.19, 170.01, 164.65, 159.03, 147.55, 143.75, 138.03, 132.62, 130.23, 128.77, 128.15, 127.33, 125.02, 124.94, 124.85, 122.35, 119.17, 117.41, 113.77, 69.70, 61.38. HRMS (ESI) *m/z* [M + H]<sup>+</sup> calcd for C<sub>26</sub>H<sub>17</sub>NO<sub>8</sub>: 472.1032, found: 472.1045. Purity: 97%.

**5-(2-(1H-Benzo[d][1,2,3]triazol-5-yl)-3-benzoyl-4-hydroxy-5-oxo-2,5-dihydro-1H-pyrrol-1-yl)-2-hydroxybenzoic acid (5.21).** Prepared from ethyl 2,4-dioxo-4-phenylbutanoate (250 mg, 1.14 mmol), 1H-benzo[d][1,2,3]triazole-5-carbaldehyde (177 mg, 1.14 mmol) and 5-amino-2-hydroxybenzoic acid (174 mg, 1.14 mmol) After solvent removal, the reaction mixture was trituated with diethyl ether. The solid residue was washed with diethyl ether and subsequently purified by preparative HPLC (5-95% ACN in 0.1 M FA, flow rate 60 mL/min). The collected fractions were freeze-dried, to give the title compound (173 mg, 33%) as a yellow solid. HRMS (ESI) *m/z* [M + H]<sup>+</sup> calcd for C<sub>24</sub>H<sub>16</sub>N<sub>4</sub>O<sub>6</sub>: 457.1148, found: 457.1141. Purity: 97%.

**5-(3-Benzoyl-4-hydroxy-2-(1-methyl-1H-benzo[d][1,2,3]triazol-5-yl)-5-oxo-2,5-dihydro-1H-pyrrol-1-yl)-2-hydroxybenzoic acid (5.22).** Prepared from ethyl 2,4-dioxo-4-phenylbutanoate (250 mg, 1.14 mmol), 1-methyl-1H-benzo[d][1,2,3]triazole-5-carbaldehyde (193 mg, 1.14 mmol) and 5-amino-2-hydroxybenzoic acid (174 mg, 1.14 mmol) After solvent removal, the reaction mixture was trituated with diethyl ether. The solid residue was washed with diethyl ether and dried under reduced pressure, to give the title compound (167 mg, 31%) as a yellow solid. <sup>1</sup>H NMR (600 MHz, DMSO) δ 8.07 (s, 1H), 8.00 (d, *J* = 2.6 Hz, 1H), 7.73 (d, *J* = 7.3 Hz, 2H), 7.62 – 7.68 (m, 2H), 7.54 (t, *J* = 7.4 Hz, 1H), 7.49 (d, *J* = 8.8 Hz, 1H), 7.43 (t, *J* = 7.7 Hz, 2H), 5.80 (d, *J* = 8.9 Hz, 1H), 5.43 (s, 1H), 4.16 (s, 3H). HRMS (ESI) *m/z* [M + H]<sup>+</sup> calcd for C<sub>25</sub>H<sub>18</sub>N<sub>4</sub>O<sub>6</sub>: 471.1304, found: 471.1299. Purity: 96%.

**5-(3-Benzoyl-4-hydroxy-2-(1H-indazol-6-yl)-5-oxo-2,5-dihydro-1H-pyrrol-1-yl)-2-hydroxybenzoic acid (5.23).** Prepared from ethyl 2,4-dioxo-4-phenylbutanoate (250 mg, 1.14 mmol), 1H-indazole-6-carbaldehyde (170 mg, 1.14 mmol) and 5-amino-2-hydroxybenzoic acid (174 mg, 1.14 mmol) After solvent removal, the reaction mixture was trituated with diethyl ether. The solid residue was washed with diethyl ether and subsequently purified by preparative HPLC (5-90% ACN in 0.2% NH<sub>3</sub>, flow rate 60 mL/min). The collected fractions were freeze-dried, to give the title compound (128 mg, 24%) as a off-white solid. <sup>1</sup>H NMR (500 MHz, DMSO) δ 12.99 (s, 1H), 7.99 (d, *J* = 2.7 Hz, 1H), 7.88 – 7.93 (m, 1H), 7.68 – 7.73 (m, 2H), 7.65 (dd, *J* = 8.9, 2.6 Hz, 1H), 7.51 – 7.59 (m, 3H), 7.44 (t, *J* = 7.7 Hz, 2H), 5.94 – 7.04 (m, 1H), 5.81 (d, *J* = 8.9 Hz, 1H), 5.37 (s, 1H). <sup>13</sup>C NMR (126 MHz, DMSO) δ 189.28, 171.19, 164.48, 158.88, 150.23, 139.60, 137.88, 134.16, 133.28, 132.72, 130.36, 128.78, 128.22, 127.59, 124.90, 122.52, 120.81, 119.92, 118.52, 117.24, 113.47, 110.77, 62.01. HRMS (ESI) *m/z* [M + H]<sup>+</sup> calcd for C<sub>25</sub>H<sub>17</sub>N<sub>3</sub>O<sub>6</sub>: 455.1195, found: 455.1198. Purity: 97%.

**5-(3-Benzoyl-4-hydroxy-2-(1-methyl-1H-indazol-6-yl)-5-oxo-2,5-dihydro-1H-pyrrol-1-yl)-2-hydroxybenzoic acid (5.24).** Prepared from ethyl 2,4-dioxo-4-phenylbutanoate (250 mg, 1.14 mmol), 1-methyl-1H-indazole-6-carbaldehyde (187 mg, 1.14 mmol) and 5-amino-2-hydroxybenzoic

acid (174 mg, 1.14 mmol). After solvent removal, the reaction mixture was triturated with diethyl ether. Purified by recrystallization from 1,4-dioxane, to give the title compound (61 mg, 11%) as a yellow solid.  $^1\text{H}$  NMR (500 MHz, DMSO)  $\delta$  8.03 (d,  $J$  = 2.7 Hz, 1H), 7.86 – 7.89 (m, 1H), 7.69 – 7.77 (m, 4H), 7.52 – 7.6 (m, 2H), 7.44 (t,  $J$  = 7.7 Hz, 2H), 7.07 (dd,  $J$  = 8.4, 1.2 Hz, 1H), 5.87 (d,  $J$  = 8.9 Hz, 1H), 5.37 (s, 1H), 3.97 (s, 3H).  $^{13}\text{C}$  NMR (126 MHz, DMSO)  $\delta$  189.36, 171.25, 164.53, 158.69, 150.25, 139.41, 137.90, 134.40, 132.71, 132.19, 130.73, 128.84, 128.21, 127.79, 125.05, 123.19, 120.89, 119.98, 119.43, 117.36, 112.94, 109.80, 62.15, 35.34. HRMS (ESI)  $m/z$  [ $M + H$ ] $^+$  calcd for C<sub>26</sub>H<sub>19</sub>N<sub>3</sub>O<sub>6</sub>: 470.1352, found: 470.1345. Purity: 99%.

**5-(3-Benzoyl-4-hydroxy-2-(1H-indazol-5-yl)-5-oxo-2,5-dihydro-1H-pyrrol-1-yl)-2-**

**hydroxybenzoic acid (5.25).** Prepared from ethyl 2,4-dioxo-4-phenylbutanoate (272 mg, 1.14 mmol), 1H-indazole-5-carbaldehyde (174 mg, 1.14 mmol) and 5-amino-2-hydroxybenzoic acid (174 mg, 1.14 mmol). After solvent removal, the reaction mixture was triturated with diethyl ether. The filtrate was evaporated under reduced pressure and the crude product was purified by preparative HPLC (5-95% ACN in 0.1 M FA, flow rate 60 mL/min). The collected fractions were freeze-dried, to give the title compound (40 mg, 7%) as a pale yellow solid. HRMS (ESI)  $m/z$  [ $M + H$ ] $^+$  calcd for C<sub>25</sub>H<sub>17</sub>N<sub>3</sub>O<sub>6</sub>: 455.1195, found: 455.1208. Purity: 84%.

**5-(3-Benzoyl-4-hydroxy-5-oxo-2-(1-oxoisindolin-5-yl)-2,5-dihydro-1H-pyrrol-1-yl)-2-**

**hydroxybenzoic acid (5.26).** Prepared from ethyl 2,4-dioxo-4-phenylbutanoate (250 mg, 1.14 mmol), 1-oxoisindoline-5-carbaldehyde (184 mg, 1.14 mmol) and 5-amino-2-hydroxybenzoic acid (174 mg, 1.14 mmol). After solvent removal, the reaction mixture was triturated with diethyl ether. The solid residue was washed with diethyl ether and subsequently purified by preparative HPLC ( ). The collected fractions were freeze-dried, to give the title compound (43 mg, 8%) as an orange solid. HRMS (ESI)  $m/z$  [ $M + H$ ] $^+$  calcd for C<sub>26</sub>H<sub>18</sub>N<sub>2</sub>O<sub>7</sub>: 471.1192, found: 471.1188. Purity: 82%.

**5-(3-Benzoyl-4-hydroxy-2-(2-methyl-1-oxoisindolin-5-yl)-5-oxo-2,5-dihydro-1H-pyrrol-1-yl)-2-**

**2-hydroxybenzoic acid (5.27).** Prepared from ethyl 2,4-dioxo-4-phenylbutanoate (250 mg, 1.14 mmol), 2-methyl-1-oxoisindoline-5-carbaldehyde (200 mg, 1.14 mmol) and 5-amino-2-hydroxybenzoic acid (174 mg, 1.14 mmol). After solvent removal, the reaction mixture was triturated with diethyl ether. The solid residue was washed with diethyl ether and dried under reduced pressure, to give the title compound (300 mg, 55%) as a pale yellow solid.  $^1\text{H}$  NMR (400 MHz, DMSO)  $\delta$  8.02 (d,  $J$  = 2.6 Hz, 1H), 7.65 – 7.75 (m, 3H), 7.53 – 7.62 (m, 2H), 7.4 – 7.52 (m, 4H), 5.89 (d,  $J$  = 8.9 Hz, 1H), 5.37 (s, 1H), 4.32 (s, 2H), 2.96 (s, 3H).  $^{13}\text{C}$  NMR (101 MHz, DMSO)  $\delta$  189.11, 171.18, 165.62, 164.48, 158.69, 150.50, 141.87, 139.89, 137.90, 132.65, 132.42, 130.55, 128.72, 128.16, 127.65, 127.53, 124.89, 122.60, 122.51, 119.70, 117.42, 113.00, 61.60, 51.14, 28.84. HRMS (ESI)  $m/z$  [ $M + H$ ] $^+$  calcd for C<sub>27</sub>H<sub>20</sub>N<sub>2</sub>O<sub>7</sub>: 485.1349, found: 485.1339. Purity: 97%.

**5-(2-(Benzo[c][1,2,5]oxadiazol-5-yl)-3-benzoyl-4-hydroxy-5-oxo-2,5-dihydro-1H-pyrrol-1-yl)-2-**

**2-hydroxybenzoic acid (5.28).** Prepared from ethyl 2,4-dioxo-4-phenylbutanoate (250 mg, 1.14 mmol), benzo[c][1,2,5]oxadiazole-5-carbaldehyde (174 mg, 1.14 mmol) and 5-amino-2-hydroxybenzoic acid (174 mg, 1.14 mmol). After solvent removal, the reaction mixture was triturated with diethyl ether. The solid residue was washed with diethyl ether and dried under reduced pressure, to give the title compound (167 mg, 32%) as an off-white solid.  $^1\text{H}$  NMR (500 MHz, DMSO)  $\delta$  8.22 (s, 1H), 8.06 (d,  $J$  = 2.7 Hz, 1H), 7.86 – 7.91 (m, 1H), 7.7 – 7.78 (m, 3H), 7.53 – 7.63 (m, 2H), 7.45 (t,  $J$  = 7.7 Hz, 2H), 5.91 (d,  $J$  = 8.9 Hz, 1H), 5.45 (s, 1H).  $^{13}\text{C}$  NMR (126 MHz, DMSO)  $\delta$  189.09, 171.15, 164.50, 158.85, 152.05, 148.61, 148.48, 141.51, 137.89, 132.71, 131.14, 130.66,

128.78, 128.17, 127.29, 125.13, 117.57, 117.45, 115.70, 115.40, 113.10, 61.09. HRMS (ESI)  $m/z$   $[M + H]^+$  calcd for C<sub>24</sub>H<sub>15</sub>N<sub>3</sub>O<sub>7</sub>: 458.0988, found: 458.0980. Purity: 97%.

**5-(3-Benzoyl-4-hydroxy-2-(isoquinolin-6-yl)-5-oxo-2,5-dihydro-1H-pyrrol-1-yl)-2-hydroxybenzoic acid (5.29).** Prepared from ethyl 2,4-dioxo-4-phenylbutanoate (268 mg, 1.22 mmol), isoquinoline-6-carbaldehyde (201 mg, 1.22 mmol) and 5-amino-2-hydroxybenzoic acid (186 mg, 1.22 mmol). After solvent removal, the reaction mixture was triturated with diethyl ether. The solid residue was washed with diethyl ether, then taken up in 1,4-dioxane and stirred for 15 min. The resulting suspension was filtered, the filtrate was evaporated under reduced pressure and purified by preparative HPLC (5-95% ACN in 0.1 M FA, flow rate 60 mL/min). The collected fractions were freeze-dried, to give the title compound (20 mg, 4%) as a yellow solid. <sup>1</sup>H NMR (500 MHz, CD<sub>3</sub>OD)  $\delta$  9.09 (s, 1H), 8.34 (d,  $J$  = 5.9 Hz, 1H), 7.97 (d,  $J$  = 8.0 Hz, 3H), 7.71 – 7.8 (m, 3H), 7.60 (d,  $J$  = 8.7 Hz, 1H), 7.43 – 7.53 (m, 2H), 7.38 (t,  $J$  = 7.5 Hz, 2H), 5.73 (d,  $J$  = 8.8 Hz, 1H), 5.31 (s, 1H). HRMS (ESI)  $m/z$   $[M + H]^+$  calcd for C<sub>27</sub>H<sub>18</sub>N<sub>2</sub>O<sub>6</sub>: 467.1243, found: 467.1241. Purity: 99%.

**4-Benzoyl-1-(2-chlorophenyl)-3-hydroxy-5-(4-nitrophenyl)-1,5-dihydro-2H-pyrrol-2-one (5.30).** Prepared from ethyl 2,4-dioxo-4-phenylbutanoate (200 mg, 0.91 mmol), 4-nitrobenzaldehyde (137 mg, 0.91 mmol) and 2-(trifluoromethyl)aniline (0.114 mL, 0.91 mmol). After solvent removal, the crude mixture was dissolved in DCM and washed with aq. HCl 1 M (3x). The crude was then back-extracted with NaOH 1 M (3x). The combined aqueous layers were made acidic with aq. HCl 3 M, extracted with DCM (3x) and then the solvent was removed under vacuum. The resulting solid was purified by preparative HPLC (5-95% ACN in 0.2% NH<sub>3</sub>, flow rate 60 mL/min). Collected fractions were freeze-dried, to give the title compound (24 mg, 5.1%) as a pale yellow solid. <sup>1</sup>H NMR (600 MHz, DMSO)  $\delta$  8.02 (d,  $J$  = 8.8 Hz, 2H), 7.75 – 7.83 (m, 2H), 7.56 (d,  $J$  = 8.4 Hz, 2H), 7.45 (d,  $J$  = 7.1 Hz, 1H), 7.39 (d,  $J$  = 7.4 Hz, 1H), 7.33 (t,  $J$  = 7.5 Hz, 2H), 7.23 – 7.3 (m, 2H), 5.99 – 7.22 (m, 1H), 5.98 (s, 1H). HRMS (ESI)  $m/z$   $[M + H]^+$  calcd for C<sub>23</sub>H<sub>15</sub>CIN<sub>2</sub>O<sub>5</sub>: 435.0748, found: 435.0739. Purity: 95%.

**4-Benzoyl-1-(2-fluorophenyl)-3-hydroxy-5-(4-nitrophenyl)-1,5-dihydro-2H-pyrrol-2-one (5.31).** Prepared from ethyl 2,4-dioxo-4-phenylbutanoate (200 mg, 0.91 mmol), 4-nitrobenzaldehyde (137 mg, 0.91 mmol) and 2-fluoroaniline (101 mg, 0.91 mmol). After solvent removal, the crude product was purified by preparative HPLC (5-95% ACN with 0.1 M FA, flow rate 30 mL/min). Collected fractions were freeze-dried, to give the title compound (84 mg, 22.0%) as a off-white solid. <sup>1</sup>H NMR (600 MHz, DMSO)  $\delta$  8.05 (d,  $J$  = 8.6 Hz, 2H), 7.76 (d,  $J$  = 7.3 Hz, 2H), 7.64 (d,  $J$  = 8.4 Hz, 2H), 7.60 (t,  $J$  = 7.3 Hz, 1H), 7.55 (t,  $J$  = 7.3 Hz, 1H), 7.45 (t,  $J$  = 7.6 Hz, 2H), 7.27 – 7.32 (m, 1H), 7.21 – 7.26 (m, 1H), 7.19 (t,  $J$  = 7.6 Hz, 1H), 5.28 (s, 1H). HRMS (ESI)  $m/z$   $[M + H]^+$  calcd for C<sub>23</sub>H<sub>15</sub>FN<sub>2</sub>O<sub>5</sub>: 419.1043, found: 419.1014.

**2-(3-Benzoyl-4-hydroxy-2-(4-nitrophenyl)-5-oxo-2,5-dihydro-1H-pyrrol-1-yl)benzonitrile (5.32).** Prepared from ethyl 2,4-dioxo-4-phenylbutanoate (300 mg, 1.36 mmol), 4-nitrobenzaldehyde (206 mg, 1.36 mmol) and 2-aminobenzonitrile (161 mg, 1.36 mmol). After solvent removal, the reaction mixture was diluted with aq HCl (1M) and extracted with EtOAc (3x). The combined organic layers were dried using a phase separator and solvent was removed under reduced pressure. The crude product was purified by preparative HPLC (5-95% ACN in 0.2% NH<sub>3</sub>, flow rate 60 mL/min). Collected fractions were freeze-dried, to give the title compound (14 mg, 2.4%) as a pale yellow solid. <sup>1</sup>H NMR (600 MHz, DMSO)  $\delta$  8.07 (d,  $J$  = 8.8 Hz, 2H), 7.8 – 7.83 (m, 1H), 7.76 – 7.79 (m, 3H), 7.7 – 7.76 (m, 1H), 7.65 (d,  $J$  = 8.6 Hz, 2H), 7.48 – 7.58 (m, 1H), 7.4 –

7.46 (m, 3H), 5.42 (s, 1H). HRMS (ESI)  $m/z$   $[M + H]^+$  calcd for C<sub>24</sub>H<sub>15</sub>N<sub>3</sub>O<sub>5</sub>: 425.1090, found: 425.1067. Purity: 99%.

**4-Benzoyl-3-hydroxy-1-(2-nitrophenyl)-5-(4-nitrophenyl)-1,5-dihydro-2H-pyrrol-2-one (5.33).**

Prepared from ethyl 2,4-dioxo-4-phenylbutanoate (300 mg, 1.36 mmol), 4-nitrobenzaldehyde (206 mg, 1.36 mmol) and 2-nitroaniline (188 mg, 1.36 mmol). After solvent removal, the crude product was purified by preparative HPLC (5-95% ACN in 0.2% NH<sub>3</sub>, flow rate 30 mL/min). Collected fractions were freeze-dried, to give the title compound (4 mg, 1%) as a yellow solid. <sup>1</sup>H NMR (600 MHz, DMSO)  $\delta$  8.07 – 8.12 (m, 2H), 7.9 – 7.95 (m, 1H), 7.8 – 7.85 (m, 3H), 7.74 – 7.78 (m, 2H), 7.69 – 7.74 (m, 1H), 7.55 (t,  $J$  = 7.5 Hz, 1H), 7.45 (t,  $J$  = 7.7 Hz, 3H), 5.54 (s, 1H). HRMS (ESI)  $m/z$   $[M + H]^+$  calcd for C<sub>23</sub>H<sub>15</sub>N<sub>3</sub>O<sub>7</sub>: 445.0988, found: 445.1008. Purity: 99%.

**2-(3-Benzoyl-4-hydroxy-2-(4-nitrophenyl)-5-oxo-2,5-dihydro-1H-pyrrol-1-yl)benzoic acid (5.34).**

Prepared from ethyl 2,4-dioxo-4-phenylbutanoate (300 mg, 1.36 mmol), 4-nitrobenzaldehyde (206 mg, 1.36 mmol), and 2-aminobenzoic acid (187 mg, 1.36 mmol). After solvent removal, the reaction mixture was triturated with diethyl ether. The filtrate was evaporated under reduced pressure and the crude product was purified by preparative HPLC (30-70% ACN in H<sub>2</sub>O/ACN/TFA 95/5/0.2 buffer over 20 minutes with a flow of 100 mL/min). Collected fractions were freeze-dried, to give the title compound (20 mg, 1.6%) as an off-white solid. HRMS (ESI)  $m/z$   $[M + H]^+$  calcd for C<sub>24</sub>H<sub>16</sub>N<sub>2</sub>O<sub>7</sub>: 445.1036, found: 445.1039.

**4-Benzoyl-3-hydroxy-1-(2-hydroxyphenyl)-5-(4-nitrophenyl)-1,5-dihydro-2H-pyrrol-2-one (5.35).**

In a RBF, to a solution of ethyl 2,4-dioxo-4-phenylbutanoate (1000 mg, 4.54 mmol) in AcOH (20 mL), 4-nitrobenzaldehyde (686 mg, 4.54 mmol) and 2-aminophenol (496 mg, 4.54 mmol) were added. The reaction mixture was stirred at RT for 3 days. After filtration, the solid residue was purified by preparative HPLC (25-65% ACN in H<sub>2</sub>O/ACN/FA 95/5/0.2 over 20 min, flowrate of 100 mL/min). Collected fractions were freeze-dried, to give the title compound (743 mg, 39%) as a white solid. <sup>1</sup>H NMR (500 MHz, DMSO)  $\delta$  = 10.00 (s, 1H), 8.01 – 8.07 (m, 2H), 7.71 – 7.77 (m, 2H), 7.61 – 7.67 (m, 2H), 7.54 – 7.61 (m, 1H), 7.42 – 7.5 (m, 2H), 7.14 (dd,  $J$  = 7.9, 1.7, 1H), 7.06 (ddd,  $J$  = 8.2, 7.3, 1.7, 1H), 5.86 (dd,  $J$  = 8.1, 1.4, 1H), 5.72 (td,  $J$  = 7.6, 1.4, 1H), 5.24 (s, 1H). <sup>13</sup>C NMR (126 MHz, DMSO)  $\delta$  189.28, 164.69, 152.86, 151.78, 147.26, 144.51, 137.94, 132.80, 129.38, 128.94, 128.92, 128.85, 128.82, 128.27, 123.45, 122.53, 119.21, 119.15, 118.19, 115.67, 61.58. HRMS (ESI)  $m/z$   $[M + H]^+$  calcd for C<sub>23</sub>H<sub>16</sub>N<sub>2</sub>O<sub>6</sub>: 417.1086, found: 417.1079.

**4-Benzoyl-3-hydroxy-1-(2-methoxyphenyl)-5-(4-nitrophenyl)-1,5-dihydro-2H-pyrrol-2-one (5.36).**

Prepared from ethyl 2,4-dioxo-4-phenylbutanoate (200 mg, 0.91 mmol), 4-nitrobenzaldehyde (137 mg, 0.91 mmol) and 2-methoxyaniline (0.103 mL, 0.91 mmol). After solvent removal, the crude mixture was dissolved in DCM and washed with aq. HCl 1 M (3x). The crude was then back-extracted with NaOH 1 M (3x). The combined aqueous layers were made acidic with aq. HCl 3 M, extracted with DCM (3x) and then the solvent was removed under vacuum. The resulting solid was purified by preparative HPLC (5-95% ACN in 0.2% NH<sub>3</sub>, flow rate 60 mL/min). Collected fractions were freeze-dried, to give the title compound (54 mg, 13.7%) as an off-white solid. <sup>1</sup>H NMR (400 MHz, DMSO)  $\delta$  8.03 (d,  $J$  = 8.8 Hz, 2H), 7.71 – 7.77 (m, 2H), 7.61 (d,  $J$  = 8.8 Hz, 2H), 7.54 – 7.59 (m, 1H), 7.46 (t,  $J$  = 7.6 Hz, 2H), 7.18 – 7.27 (m, 2H), 7.02 – 7.1 (m, 1H), 5.83 – 5.92 (m, 1H), 5.18 (s, 1H), 3.80 (s, 3H). <sup>13</sup>C NMR (126 MHz, DMSO)  $\delta$  189.06, 164.69, 154.55, 147.19, 144.36, 137.96, 132.64, 129.31, 129.22, 128.80, 128.74, 128.17, 123.86, 123.31,

120.46, 112.53, 61.92, 55.81. HRMS (ESI)  $m/z$   $[M + H]^+$  calcd for C<sub>24</sub>H<sub>18</sub>N<sub>2</sub>O<sub>6</sub>: 431.1243, found: 431.1254. Purity: 99%.

**4-Benzoyl-1-(3-chlorophenyl)-3-hydroxy-5-(4-nitrophenyl)-1,5-dihydro-2H-pyrrol-2-one**

**(5.37).** Prepared from ethyl 2,4-dioxo-4-phenylbutanoate (200 mg, 0.91 mmol), 4-nitrobenzaldehyde (137 mg, 0.91 mmol) and 3-chloroaniline (0.096 mL, 0.91 mmol). After solvent removal, the reaction mixture was triturated with diethyl ether. The solid residue was washed with diethyl ether and subsequently purified by preparative HPLC (30-70% ACN in H<sub>2</sub>O/ACN/FA 95/5/0.2 buffer, over 20 minutes with a flow of 19 mL/min). Collected fractions were freeze-dried, to give the title compound (95 mg, 24%) as a pale yellow solid. <sup>1</sup>H NMR (400 MHz, DMSO)  $\delta$  8.06 (d,  $J$  = 8.8 Hz, 2H), 7.82 – 7.87 (m, 1H), 7.76 (d,  $J$  = 8.8 Hz, 2H), 7.67 – 7.73 (m, 2H), 7.57 (t,  $J$  = 7.3 Hz, 2H), 7.45 (t,  $J$  = 7.6 Hz, 2H), 7.34 (t,  $J$  = 8.1 Hz, 1H), 7.13 – 7.24 (m, 1H), 5.54 (s, 1H). <sup>13</sup>C NMR (101 MHz, DMSO, 26°C)  $\delta$  188.91, 164.85, 147.20, 144.31, 137.80, 137.45, 133.17, 132.74, 130.48, 129.21, 128.71, 128.16, 125.40, 123.48, 121.99, 120.72, 119.28, 60.20. HRMS (ESI)  $m/z$   $[M + H]^+$  calcd for C<sub>23</sub>H<sub>15</sub>ClN<sub>2</sub>O<sub>5</sub>: 435.0748, found: 435.0725. Purity: 99%.

**4-Benzoyl-1-(3-fluorophenyl)-3-hydroxy-5-(4-nitrophenyl)-1,5-dihydro-2H-pyrrol-2-one**

**(5.38).** Prepared from ethyl 2,4-dioxo-4-phenylbutanoate (200 mg, 0.91 mmol), 4-nitrobenzaldehyde (137 mg, 0.91 mmol) and 3-fluoroaniline (0.088 mL, 0.91 mmol). After solvent removal, the crude mixture was dissolved in DCM and washed with aq. HCl 1 M (3x). The crude was then back-extracted with NaOH 1 M (3x). The combined aqueous layers were made acidic with aq. HCl 3 M, extracted with DCM (3x) and then the solvent was removed under vacuum. The resulting solid was purified by preparative SFC (MeOH/H<sub>2</sub>O/NH<sub>3</sub> 97/3/50 mM. Column: Waters BEH 5 $\mu$ m 30x250mm). Collected fractions were dried under reduced pressure, to give the title compound (40 mg, 11%) as a pale yellow solid. HRMS (ESI)  $m/z$   $[M + H]^+$  calcd for C<sub>23</sub>H<sub>15</sub>FN<sub>2</sub>O<sub>5</sub>: 419.1043, found: 419.1029. Purity: 98%.

**3-(3-Benzoyl-4-hydroxy-2-(4-nitrophenyl)-5-oxo-2,5-dihydro-1H-pyrrol-1-yl)benzotrile**

**(5.39).** Prepared from ethyl 2,4-dioxo-4-phenylbutanoate (200 mg, 0.91 mmol), 4-nitrobenzaldehyde (137 mg, 0.91 mmol), and 3-aminobenzotrile (108 mg, 0.91 mmol). After solvent removal, the reaction mixture was triturated with diethyl ether. The filtrate was evaporated under reduced pressure and the crude product was purified by preparative SFC (MeOH/H<sub>2</sub>O/NH<sub>3</sub> 97/3/50 mM). Collected fractions were dried under reduced pressure, to give the title compound (78 mg, 20%) as an off-white solid. <sup>1</sup>H NMR (600 MHz, DMSO)  $\delta$  8.21 (s, 1H), 8.03 (d,  $J$  = 8.5 Hz, 2H), 7.94 (d,  $J$  = 7.8 Hz, 1H), 7.73 (d,  $J$  = 7.3 Hz, 2H), 7.66 (d,  $J$  = 8.4 Hz, 2H), 7.44 – 7.54 (m, 2H), 7.39 (t,  $J$  = 7.2 Hz, 1H), 7.31 (t,  $J$  = 7.6 Hz, 2H), 5.95 – 7.26 (m, 3H), 5.30 (s, 1H). HRMS (ESI)  $m/z$   $[M + H]^+$  calcd for C<sub>24</sub>H<sub>15</sub>N<sub>3</sub>O<sub>5</sub>: 425.1090, found: 425.1075. Purity: 99%.

**4-Benzoyl-3-hydroxy-1-(3-nitrophenyl)-5-(4-nitrophenyl)-1,5-dihydro-2H-pyrrol-2-one (5.40).**

Prepared from ethyl 2,4-dioxo-4-phenylbutanoate (200 mg, 0.91 mmol), 4-nitrobenzaldehyde (137 mg, 0.91 mmol) and 3-nitroaniline (126 mg, 0.91 mmol). After solvent removal, the reaction mixture was triturated with diethyl ether. The solid residue was washed with diethyl ether and subsequently purified by preparative SFC (MeOH/H<sub>2</sub>O/NH<sub>3</sub> 97/3/50 mM). Collected fractions were dried under reduced pressure, to give the title compound (102 mg, 25%) as a yellow solid. <sup>1</sup>H NMR (500 MHz, DMSO)  $\delta$  12.32 (br, 1H), 8.70 (s, 1H), 8.06 (d,  $J$  = 8.2 Hz, 2H), 8.02 (d,  $J$  = 8.1 Hz, 1H), 7.96 (d,  $J$  = 8.1 Hz, 1H), 7.82 (d,  $J$  = 8.2 Hz, 2H), 7.73 (d,  $J$  = 7.3 Hz, 2H), 7.53 – 7.66 (m, 2H), 7.39 – 7.5 (m, 2H), 5.67 (s, 1H). <sup>13</sup>C NMR (126 MHz, DMSO)  $\delta$  189.04, 165.14, 150.38, 147.94, 147.29, 143.90,

137.69, 137.14, 132.90, 130.36, 129.35, 129.03, 128.92, 128.78, 128.24, 127.85, 123.60, 120.04, 119.65, 115.56, 60.28. HRMS (ESI)  $m/z$   $[M + H]^+$  calcd for C<sub>23</sub>H<sub>15</sub>N<sub>3</sub>O<sub>7</sub>: 445.0988, found:445.0983. Purity: 98%.

**4-Benzoyl-3-hydroxy-5-(4-nitrophenyl)-1-(3-(trifluoromethyl)phenyl)-1,5-dihydro-2H-pyrrol-2-one (5.41).** Prepared from ethyl 2,4-dioxo-4-phenylbutanoate (200 mg, 0.91 mmol), 4-nitrobenzaldehyde (137 mg, 0.91 mmol) and 3-(trifluoromethyl)aniline (0.114 mL, 0.91 mmol). After solvent removal, the reaction mixture was triturated with diethyl ether. The solid residue was washed with diethyl ether and subsequently purified by preparative SFC (MeOH/H<sub>2</sub>O/NH<sub>3</sub> 97/3/50 mM). Collected fractions were dried under reduced pressure, to give the title compound (18 mg, 4%) as a pale yellow solid. HRMS (ESI)  $m/z$   $[M + H]^+$  calcd for C<sub>24</sub>H<sub>15</sub>F<sub>3</sub>N<sub>2</sub>O<sub>5</sub>: 469.1011, found:469.0997. Purity: 99%.

**3-(3-Benzoyl-4-hydroxy-2-(4-nitrophenyl)-5-oxo-2,5-dihydro-1H-pyrrol-1-yl)benzoic acid (5.42).** Prepared from ethyl 2,4-dioxo-4-phenylbutanoate (200 mg, 0.91 mmol), 4-nitrobenzaldehyde (137 mg, 0.91 mmol) and 3-aminobenzoic acid (125 mg, 0.91 mmol). After solvent removal, the reaction mixture was triturated with diethyl ether. The solid residue was washed with diethyl ether and subsequently purified by preparative HPLC (5-95% ACN in 0.2% NH<sub>3</sub>, flow rate 60 mL/min). Collected fractions were freeze-dried, to give the title compound (90 mg, 22%) as a pale yellow solid. <sup>1</sup>H NMR (600 MHz, DMSO)  $\delta$  13.01 (br, 1H), 8.32 – 8.38 (m, 1H), 8.03 (d,  $J$  = 8.9 Hz, 2H), 7.78 – 7.84 (m, 1H), 7.73 – 7.78 (m, 2H), 7.65 (d,  $J$  = 8.8 Hz, 2H), 7.62 (d,  $J$  = 7.8 Hz, 1H), 7.38 – 7.43 (m, 2H), 7.33 (t,  $J$  = 7.6 Hz, 2H), 7.18 (br, 2H), 5.29 (s, 1H). <sup>1</sup>H NMR (600 MHz, DMSO)  $\delta$  13.01 (br, 1H), 8.32 – 8.38 (m, 1H), 8.03 (d,  $J$  = 8.9 Hz, 2H), 7.78 – 7.84 (m, 1H), 7.73 – 7.78 (m, 2H), 7.65 (d,  $J$  = 8.8 Hz, 2H), 7.62 (d,  $J$  = 7.8 Hz, 1H), 7.38 – 7.43 (m, 2H), 7.33 (t,  $J$  = 7.6 Hz, 2H), 7.18 (br, 3H), 5.29 (s, 1H). <sup>13</sup>C NMR (126 MHz, DMSO)  $\delta$  185.42, 168.92, 165.95, 149.14, 145.37, 140.42, 137.61, 131.27, 130.22, 129.02, 128.82, 128.74, 127.14, 125.41, 125.33, 123.02, 122.59, 60.10. HRMS (ESI)  $m/z$   $[M + H]^+$  calcd for C<sub>24</sub>H<sub>16</sub>N<sub>2</sub>O<sub>7</sub>: 445.1036, found:445.1025. Purity: 98%.

**3-(3-Benzoyl-4-hydroxy-2-(4-nitrophenyl)-5-oxo-2,5-dihydro-1H-pyrrol-1-yl)benzamide (5.43).** Prepared from ethyl 2,4-dioxo-4-phenylbutanoate (311 mg, 1.41 mmol), 4-nitrobenzaldehyde (213 mg, 1.41 mmol) and 3-aminobenzamide (192 mg, 1.41 mmol). After solvent removal, the reaction mixture was triturated with diethyl ether. The solid residue was washed with diethyl ether and dried under reduced pressure, to give the title compound (303 mg, 48%) as a yellow solid. <sup>1</sup>H NMR (500 MHz, DMSO)  $\delta$  12.22 (br, 1H), 8.14 (t,  $J$  = 1.8 Hz, 1H), 8.03 – 8.08 (m, 2H), 7.97 (br, 1H), 7.81 (dd,  $J$  = 8.1, 1.3 Hz, 1H), 7.7 – 7.78 (m, 4H), 7.64 (d,  $J$  = 7.8 Hz, 1H), 7.53 – 7.6 (m, 1H), 7.37 – 7.5 (m, 4H), 5.56 (s, 1H). <sup>13</sup>C NMR (126 MHz, DMSO)  $\delta$  189.08, 165.97, 164.65, 150.76, 147.21, 144.37, 137.79, 135.06, 134.91, 132.81, 129.18, 128.87, 128.77, 128.21, 125.27, 124.64, 123.51, 121.57, 119.32, 60.27. HRMS (ESI)  $m/z$   $[M + H]^+$  calcd for C<sub>24</sub>H<sub>17</sub>N<sub>3</sub>O<sub>6</sub>: 444.1195, found: 444.1183. Purity: 99%.

**4-Benzoyl-3-hydroxy-1-(3-methoxyphenyl)-5-(4-nitrophenyl)-1,5-dihydro-2H-pyrrol-2-one (5.44).** Prepared from ethyl 2,4-dioxo-4-phenylbutanoate (200 mg, 0.91 mmol), 4-nitrobenzaldehyde (137 mg, 0.91 mmol) and 3-methoxyaniline (0.105 mL, 0.91 mmol). After solvent removal, the reaction mixture was triturated with diethyl ether. The solid residue was washed with diethyl ether and subsequently purified by preparative HPLC (5-95% ACN in 0.2% NH<sub>3</sub>, flow rate 60 mL/min). Collected fractions were freeze-dried, to give the title compound (10 mg, 3%) as a off-

white solid.  $^1\text{H NMR}$  (600 MHz, DMSO)  $\delta$  8.03 (d,  $J$  = 8.7 Hz, 2H), 7.73 (d,  $J$  = 7.3 Hz, 2H), 7.66 (d,  $J$  = 8.4 Hz, 2H), 7.43 (t,  $J$  = 7.5 Hz, 1H), 7.34 (t,  $J$  = 7.5 Hz, 2H), 7.26 – 7.29 (m, 1H), 7.2 – 7.25 (m, 1H), 7.17 (t,  $J$  = 8.1 Hz, 1H), 5.64 (dd,  $J$  = 8.1, 2.4 Hz, 1H), 5.28 (s, 1H), 3.69 (s, 3H). HRMS (ESI)  $m/z$   $[\text{M} + \text{H}]^+$  calcd for  $\text{C}_{24}\text{H}_{18}\text{N}_2\text{O}_6$ : 431.1243, found: 431.1245. Purity: 98%.

**4-Benzoyl-1-(4-fluorophenyl)-3-hydroxy-5-(4-nitrophenyl)-1,5-dihydro-2H-pyrrol-2-one (5.45).** Prepared from ethyl 2,4-dioxo-4-phenylbutanoate (200 mg, 0.91 mmol), 4-nitrobenzaldehyde (137 mg, 0.91 mmol) and 4-fluoroaniline (101 mg, 0.91 mmol). After solvent removal, the crude mixture was dissolved in DCM and washed with aq. HCl 1 M (3x). The crude was then back-extracted with NaOH 1 M (3x). The combined aqueous layers were made acidic with aq. HCl 3 M, extracted with DCM (3x) and then the solvent was removed under vacuum. The resulting solid was purified by preparative HPLC (5-95% ACN in 0.2%  $\text{NH}_3$ , flow rate 60 mL/min). Collected fractions were freeze-dried, to give the title compound (52 mg, 14%) as a pale yellow solid.  $^1\text{H NMR}$  (600 MHz, DMSO)  $\delta$  8.03 (d,  $J$  = 8.8 Hz, 2H), 7.71 – 7.75 (m, 2H), 7.62 – 7.69 (m, 4H), 7.44 (t,  $J$  = 7.4 Hz, 1H), 7.35 (t,  $J$  = 7.6 Hz, 2H), 7.1 – 7.16 (m, 2H), 5.28 (s, 1H). HRMS (ESI)  $m/z$   $[\text{M} + \text{H}]^+$  calcd for  $\text{C}_{23}\text{H}_{15}\text{FN}_2\text{O}_5$ : 419.1043, found: 419.1065. Purity: 99%.

**4-(3-Benzoyl-4-hydroxy-2-(4-nitrophenyl)-5-oxo-2,5-dihydro-1H-pyrrol-1-yl)benzotrile (5.46).** Prepared from ethyl 2,4-dioxo-4-phenylbutanoate (200 mg, 0.91 mmol), 4-nitrobenzaldehyde (137 mg, 0.91 mmol) and 4-aminobenzotrile (108 mg, 0.91 mmol). After solvent removal, the crude mixture was purified by preparative SFC (MeOH/ $\text{NH}_3$  20 mM). The collected fractions were dried under reduced pressure, to give the title compound (25 mg, 6%) as a pale yellow solid.  $^1\text{H NMR}$  (500 MHz, DMSO)  $\delta$  8.03 – 8.09 (m, 2H), 7.87 – 7.93 (m, 2H), 7.76 – 7.84 (m, 4H), 7.69 – 7.74 (m, 2H), 7.53 – 7.58 (m, 1H), 7.41 – 7.47 (m, 2H), 5.58 (s, 1H).  $^{13}\text{C NMR}$  (126 MHz, DMSO)  $\delta$  188.72, 165.51, 151.69, 147.18, 144.44, 140.22, 137.89, 133.14, 132.68, 129.22, 128.77, 128.13, 123.51, 123.42, 121.89, 119.12, 118.50, 107.28, 59.92. HRMS (ESI)  $m/z$   $[\text{M} + \text{H}]^+$  calcd for  $\text{C}_{24}\text{H}_{15}\text{N}_3\text{O}_5$ : 425.1090, found: 425.1079. Purity: 98%.

**4-Benzoyl-3-hydroxy-1,5-bis(4-nitrophenyl)-1,5-dihydro-2H-pyrrol-2-one (5.47).** Prepared from ethyl 2,4-dioxo-4-phenylbutanoate (200 mg, 0.91 mmol), 4-nitrobenzaldehyde (137 mg, 0.91 mmol), and 4-nitroaniline (126 mg, 0.91 mmol). After solvent removal, the reaction mixture was triturated with diethyl ether. The filtrate was evaporated under reduced pressure and the crude product was purified by preparative SFC (MeOH/ $\text{NH}_3$  20mM). Collected fractions were dried under reduced pressure, to give the title compound (57 mg, 14%) as a off-white solid.  $^1\text{H NMR}$  (500 MHz, DMSO)  $\delta$  8.16 – 8.22 (m, 2H), 8.04 – 8.09 (m, 2H), 7.95 – 8.01 (m, 2H), 7.77 – 7.85 (m, 2H), 7.68 – 7.77 (m, 2H), 7.53 – 7.6 (m, 1H), 7.41 – 7.49 (m, 2H), 5.61 (s, 1H).  $^{13}\text{C NMR}$  (126 MHz, DMSO)  $\delta$  188.77, 165.65, 151.02, 147.22, 144.31, 143.69, 141.94, 137.84, 132.75, 130.04, 129.26, 128.97, 128.80, 128.70, 128.16, 124.56, 123.80, 123.56, 123.45, 121.64, 119.32, 60.11. HRMS (ESI)  $m/z$   $[\text{M} + \text{H}]^+$  calcd for  $\text{C}_{23}\text{H}_{15}\text{N}_3\text{O}_7$ : 445.0988, found: 445.0957. Purity: 99%.

**4-(3-Benzoyl-4-hydroxy-2-(4-nitrophenyl)-5-oxo-2,5-dihydro-1H-pyrrol-1-yl)benzoic acid (5.48).** Prepared from ethyl 2,4-dioxo-4-phenylbutanoate (200 mg, 0.91 mmol), 4-nitrobenzaldehyde (137 mg, 0.91 mmol) and 4-aminobenzoic acid (125 mg, 0.91 mmol). After solvent removal, the reaction mixture was triturated with diethyl ether. The solid residue was washed with diethyl ether and subsequently purified by preparative HPLC (2-94% ACN in 0.2%  $\text{NH}_3$ , flow rate 60 mL/min). The collected fractions were freeze-dried, to give the title compound (8 mg, 2%) as a pale yellow solid.  $^1\text{H NMR}$  (500 MHz, DMSO)  $\delta$  12.88 (s, 1H), 8.05 (d,  $J$  = 7.6 Hz,

2H), 7.86 (d,  $J = 7.7$  Hz, 2H), 7.81 (d,  $J = 7.7$  Hz, 2H), 7.76 (d,  $J = 7.6$  Hz, 2H), 7.72 (d,  $J = 7.7$  Hz, 2H), 7.55 (t,  $J = 7.1$  Hz, 1H), 7.43 (t,  $J = 7.3$  Hz, 2H), 5.54 (s, 1H).  $^{13}\text{C}$  NMR (126 MHz, DMSO)  $\delta$  187.45, 165.66, 145.83, 140.51, 138.90, 131.74, 130.05, 129.07, 128.78, 127.75, 125.84, 123.29, 121.11, 59.99. HRMS (ESI)  $m/z$   $[\text{M} + \text{H}]^+$  calcd for  $\text{C}_{24}\text{H}_{16}\text{N}_2\text{O}_7$ : 445.1036, found: 445.0993. Purity: 99%.

**4-Benzoyl-3-hydroxy-5-(4-nitrophenyl)-1-(4-(trifluoromethyl)phenyl)-1,5-dihydro-2H-pyrrol-2-one (5.49).** Prepared from ethyl 2,4-dioxo-4-phenylbutanoate (200 mg, 0.91 mmol), 4-nitrobenzaldehyde (137 mg, 0.91 mmol) and 4-(trifluoromethyl)aniline (0.114 mL, 0.91 mmol). After solvent removal, the reaction mixture was triturated with diethyl ether. The solid residue was washed with diethyl ether and subsequently purified by preparative HPLC (20-40% ACN in  $\text{H}_2\text{O}/\text{ACN}/\text{FA}$  95/5/0.2 buffer, over 20 minutes with a flow of 19 mL/min). Collected fractions were freeze-dried, to give the title compound (17 mg, 4%) as a off-white solid.  $^1\text{H}$  NMR (400 MHz, DMSO)  $\delta$  8.06 (d,  $J = 8.8$  Hz, 2H), 7.92 (d,  $J = 8.5$  Hz, 2H), 7.79 (d,  $J = 8.8$  Hz, 2H), 7.66 – 7.74 (m, 4H), 7.57 (t,  $J = 7.4$  Hz, 1H), 7.45 (t,  $J = 7.6$  Hz, 2H), 5.60 (s, 1H).  $^{13}\text{C}$  NMR (101 MHz, DMSO, 26°C)  $\delta$  189.01, 165.09, 150.46, 147.23, 144.13, 139.59, 137.72, 132.84, 129.21, 128.75, 128.20, 125.08, 125.04, 125.49, 125.31, 125.17, 123.54, 122.61, 122.09, 119.53, 60.07. HRMS (ESI)  $m/z$   $[\text{M} + \text{H}]^+$  calcd for  $\text{C}_{24}\text{H}_{15}\text{F}_3\text{N}_2\text{O}_5$ : 469.1011, found: 469.0990. Purity: 99%.

**4-(3-Benzoyl-4-hydroxy-2-(4-nitrophenyl)-5-oxo-2,5-dihydro-1H-pyrrol-1-yl)benzenesulfonamide (5.50).** Prepared from ethyl 2,4-dioxo-4-phenylbutanoate (200 mg, 0.91 mmol), 4-nitrobenzaldehyde (137 mg, 0.91 mmol) and 4-aminobenzenesulfonamide (157 mg, 0.91 mmol). After solvent removal, the crude mixture was purified by preparative HPLC (5-95% ACN in 0.1 M FA, flow rate 60 mL/min). The collected fractions were freeze-dried, to give the title compound (55 mg, 12%) as a pale yellow solid. HRMS (ESI)  $m/z$   $[\text{M} + \text{H}]^+$  calcd for  $\text{C}_{23}\text{H}_{17}\text{N}_3\text{O}_7\text{S}$ : 480.0865, found: 480.0842. Purity: 100%.

**4-Benzoyl-3-hydroxy-1-(4-hydroxyphenyl)-5-(4-nitrophenyl)-1,5-dihydro-2H-pyrrol-2-one (5.51).** Prepared from ethyl 2,4-dioxo-4-phenylbutanoate (480 mg, 2.18 mmol), 4-nitrobenzaldehyde (329 mg, 2.18 mmol) and 4-aminophenol (238 mg, 2.18 mmol). After solvent removal, the crude product was purified by preparative HPLC (25–65% ACN  $\text{H}_2\text{O}/\text{ACN}/\text{FA}$  95/5/0.2 buffer over 20 minutes with a flow of 100 mL/min). Collected fractions were freeze-dried, to give the title compound (48 mg, 5.3%) as an off-white solid.  $^1\text{H}$  NMR (500 MHz, DMSO)  $\delta$  12.13 (br, 1H), 9.48 (s, 1H), 8.02 – 8.08 (m, 2H), 7.69 – 7.73 (m, 2H), 7.64 – 7.69 (m, 2H), 7.53 – 7.59 (m, 1H), 7.44 (t,  $J = 7.7$  Hz, 2H), 7.34 – 7.4 (m, 2H), 5.65 – 5.7 (m, 2H), 5.36 (s, 1H).  $^{13}\text{C}$  NMR (126 MHz, DMSO)  $\delta$  188.98, 164.26, 163.09, 155.39, 147.11, 144.94, 138.02, 132.62, 129.25, 128.72, 128.15, 127.45, 124.71, 123.42, 118.66, 115.33, 60.92. HRMS (ESI)  $m/z$   $[\text{M} + \text{H}]^+$  calcd for  $\text{C}_{23}\text{H}_{16}\text{N}_2\text{O}_6$ : 417.1086, found: 417.1089.

**4-Benzoyl-3-hydroxy-5-(4-nitrophenyl)-1-phenyl-1,5-dihydro-2H-pyrrol-2-one (5.52).** Prepared from ethyl 2,4-dioxo-4-phenylbutanoate (430 mg, 1.95 mmol), 4-nitrobenzaldehyde (295 mg, 1.36 mmol) and aniline (0.178 mL, 1.95 mmol) After solvent removal, the reaction mixture was triturated with diethyl ether. The solid residue was washed with diethyl ether and dried under reduced pressure, to give the title compound (425 mg, 55%) as a off-white solid.  $^1\text{H}$  NMR (500 MHz, DMSO)  $\delta$  12.20 (br, 1H), 8.04 (d,  $J = 8.8$  Hz, 2H), 7.69 – 7.78 (m, 4H), 7.65 (d,  $J = 7.8$  Hz, 2H), 7.57 (t,  $J = 7.4$  Hz, 1H), 7.45 (t,  $J = 7.7$  Hz, 2H), 7.32 (t,  $J = 7.9$  Hz, 2H), 7.12 (t,  $J = 7.4$  Hz, 1H), 5.52 (s, 1H).  $^{13}\text{C}$  NMR (126 MHz, DMSO)  $\delta$  189.08, 164.60, 150.98, 147.15, 144.63, 137.88,



135.05, 132.77, 129.27, 128.90, 128.76, 128.21, 125.67, 123.47, 122.52, 119.15, 60.33. HRMS (ESI)  $m/z$  [M + H]<sup>+</sup> calcd for C<sub>23</sub>H<sub>16</sub>N<sub>2</sub>O<sub>5</sub>: 401.1137, found: 401.1128. Purity: 99%.

**4-Benzoyl-1-benzyl-3-hydroxy-5-(4-nitrophenyl)-1,5-dihydro-2H-pyrrol-2-one (5.53).** Prepared from ethyl 2,4-dioxo-4-phenylbutanoate (250 mg, 1.14 mmol), 4-nitrobenzaldehyde (172 mg, 1.14 mmol) and phenylmethanamine (0.125 mL, 1.14 mmol). After solvent removal, the reaction mixture was triturated with diethyl ether. The solid residue was washed with diethyl ether and subsequently purified by preparative HPLC (5-95% ACN in 0.1 M FA, flow rate 60 mL/min). The collected fractions were freeze-dried, to give the title compound (269 mg, 57%) as a pale yellow solid. <sup>1</sup>H NMR (600 MHz, DMSO)  $\delta$  8.09 (d,  $J$  = 8.3 Hz, 2H), 7.65 (d,  $J$  = 7.7 Hz, 2H), 7.44 – 7.5 (m, 3H), 7.36 (t,  $J$  = 7.6 Hz, 2H), 7.2 – 7.31 (m, 3H), 7.02 – 7.1 (m, 2H), 5.29 (s, 1H), 4.81 (d,  $J$  = 15.2 Hz, 1H), 3.84 (d,  $J$  = 15.2 Hz, 1H). HRMS (ESI)  $m/z$  [M + H]<sup>+</sup> calcd for C<sub>24</sub>H<sub>18</sub>N<sub>2</sub>O<sub>5</sub>: 415.1294, found: 415.1305. Purity: 98%.

**4-Benzoyl-3-hydroxy-5-(4-nitrophenyl)-1-phenethyl-1,5-dihydro-2H-pyrrol-2-one (5.54).** Prepared from ethyl 2,4-dioxo-4-phenylbutanoate (200 mg, 0.91 mmol), 4-nitrobenzaldehyde (110 mg, 0.73 mmol), and 2-phenylethan-1-amine (114  $\mu$ L, 0.91 mmol). After solvent removal, the crude product was purified by preparative SFC (MeOH/H<sub>2</sub>O/NH<sub>3</sub> 97/3/50mM). Collected fractions were dried, to give the title compound (20 mg, 5.2%) as a off-white solid. <sup>1</sup>H NMR (400 MHz, DMSO)  $\delta$  8.16 (d,  $J$  = 8.8 Hz, 2H), 7.62 – 7.69 (m, 2H), 7.59 (d,  $J$  = 8.8 Hz, 2H), 7.53 (t,  $J$  = 7.4 Hz, 1H), 7.41 (t,  $J$  = 7.6 Hz, 2H), 7.24 – 7.33 (m, 2H), 7.18 – 7.24 (m, 1H), 7.11 – 7.17 (m, 2H), 5.49 (s, 1H), 3.8 – 3.94 (m, 1H), 2.85 (dq,  $J$  = 10.9, 5.7 Hz, 2H), 2.67 – 2.8 (m, 1H). <sup>13</sup>C HRMS (ESI)  $m/z$  [M + H]<sup>+</sup> calcd for C<sub>25</sub>H<sub>20</sub>N<sub>2</sub>O<sub>5</sub>: 429.1450, found: 429.1441.

**4-Benzoyl-3-hydroxy-5-(4-nitrophenyl)-1-(3-phenylpropyl)-1,5-dihydro-2H-pyrrol-2-one (5.55).** Prepared from ethyl 2,4-dioxo-4-phenylbutanoate (250 mg, 1.14 mmol), 4-nitrobenzaldehyde (172 mg, 1.14 mmol) and 3-phenylpropan-1-amine (0.162 mL, 1.14 mmol). After solvent removal, the reaction mixture was triturated with diethyl ether. The solid residue was washed with diethyl ether and subsequently purified by preparative HPLC (2-94% ACN in 0.2% NH<sub>3</sub>, flow rate 60 mL/min). The collected fractions were freeze-dried, to give the title compound (191 mg, 38%) as a pale yellow solid. <sup>1</sup>H NMR (600 MHz, DMSO)  $\delta$  8.13 (d,  $J$  = 8.6 Hz, 2H), 7.65 (d,  $J$  = 7.0 Hz, 2H), 7.60 (d,  $J$  = 8.3 Hz, 2H), 7.52 (t,  $J$  = 7.4 Hz, 1H), 7.41 (t,  $J$  = 7.7 Hz, 2H), 7.20 (t,  $J$  = 7.5 Hz, 2H), 7.07 – 7.15 (m, 3H, H<sub>4</sub>), 5.59 (s, 1H), 2.73 (ddd,  $J$  = 13.8, 8.2, 5.4 Hz, 1H), 2.42 – 2.48 (m, 1H), 1.73 (dp,  $J$  = 14.1, 7.3 Hz, 1H), 1.65 (dp,  $J$  = 14.7, 7.5 Hz, 1H). HRMS (ESI)  $m/z$  [M + H]<sup>+</sup> calcd for C<sub>26</sub>H<sub>22</sub>N<sub>2</sub>O<sub>5</sub>: 443.1607, found: 443.1618. Purity: 99%.

**4-Benzoyl-3-hydroxy-5-(4-nitrophenyl)-1-(2-phenoxyethyl)-1,5-dihydro-2H-pyrrol-2-one (5.56).** Prepared from ethyl 2,4-dioxo-4-phenylbutanoate (250 mg, 1.14 mmol), 4-nitrobenzaldehyde (172 mg, 1.14 mmol) and 2-phenoxyethan-1-amine (0.149 mL, 1.14 mmol). After solvent removal, the reaction mixture was triturated with diethyl ether. The solid residue was washed with diethyl ether and subsequently purified by preparative HPLC (5-95% ACN in 0.2% NH<sub>3</sub>, flow rate 60 mL/min). The collected fractions were freeze-dried, to give the title compound (190 mg, 38%) as a pale yellow solid. <sup>1</sup>H NMR (600 MHz, DMSO)  $\delta$  8.12 (d,  $J$  = 8.7 Hz, 2H), 7.65 (d,  $J$  = 7.1 Hz, 2H), 7.58 (d,  $J$  = 8.3 Hz, 2H), 7.45 (t,  $J$  = 7.1 Hz, 1H), 7.35 (t,  $J$  = 7.6 Hz, 2H), 7.25 (t,  $J$  = 7.9 Hz, 2H), 5.92 (t,  $J$  = 7.3 Hz, 1H), 5.85 (d,  $J$  = 8.1 Hz, 2H), 5.62 (s, 1H), 3.97 – 4.09 (m, 2H), 3.89 – 3.96 (m, 1H), 2.99 – 3.07 (m, 1H). HRMS (ESI)  $m/z$  [M + H]<sup>+</sup> calcd for C<sub>25</sub>H<sub>20</sub>N<sub>2</sub>O<sub>6</sub>: 445.1400, found: 445.1407. Purity: 99%.

**4-Benzoyl-3-hydroxy-1-isopropyl-5-(4-nitrophenyl)-1,5-dihydro-2H-pyrrol-2-one (5.57).**

Prepared from ethyl 2,4-dioxo-4-phenylbutanoate (250 mg, 1.14 mmol), 4-nitrobenzaldehyde (172 mg, 1.14 mmol) and propan-2-amine (0.10 mL, 1.14 mmol). After solvent removal, the crude mixture was dissolved in DCM and washed with aq. HCl 1 M (3x). The crude was then back-extracted with NaOH 1 M (3x). The combined aqueous layers were made acidic with aq. HCl 3 M, extracted with DCM (3x) and then the solvent was removed under vacuum. The resulting solid was purified by preparative HPLC (5-95% ACN in 0.2% NH<sub>3</sub>, flow rate 60 mL/min). Collected fractions were freeze-dried, to give the title compound (8 mg, 2%) as a pale yellow solid. HRMS (ESI)  $m/z$  [M + H]<sup>+</sup> calcd for C<sub>20</sub>H<sub>18</sub>N<sub>2</sub>O<sub>5</sub>: 367.1294, found: 367.1285. Purity: 98%.

**4-Benzoyl-3-hydroxy-5-(4-nitrophenyl)-1-(pyridin-4-yl)-1,5-dihydro-2H-pyrrol-2-one (5.58).**

Prepared from ethyl 2,4-dioxo-4-phenylbutanoate (250 mg, 1.14 mmol), 4-nitrobenzaldehyde (172 mg, 1.14 mmol) and pyridin-4-amine (107 mg, 1.14 mmol). After solvent removal, the crude mixture was purified by preparative HPLC (5-95% ACN in 0.1 M FA, flow rate 60 mL/min). The collected fractions were freeze-dried, to give the title compound (3 mg, 1%) as a pale yellow solid. HRMS (ESI)  $m/z$  [M + H]<sup>+</sup> calcd for C<sub>22</sub>H<sub>15</sub>N<sub>3</sub>O<sub>5</sub>: 402.1090, found: 402.1073. Purity: 99%.

**2-(3-Benzoyl-4-hydroxy-2-(4-nitrophenyl)-5-oxo-2,5-dihydro-1H-pyrrol-1-yl)isonicotinic acid (5.59).**

Prepared from ethyl 2,4-dioxo-4-phenylbutanoate (250 mg, 1.14 mmol), 4-nitrobenzaldehyde (172 mg, 1.14 mmol) and 2-aminoisonicotinic acid (157 mg, 1.14 mmol). After solvent removal, the reaction mixture was triturated with diethyl ether. The filtrate was evaporated under reduced pressure and the crude product was purified by preparative HPLC (5-95% ACN in 0.2% NH<sub>3</sub>, flow rate 60 mL/min). The collected fractions were freeze-dried, to give the title compound (42 mg, 8%) as a pale yellow solid. HRMS (ESI)  $m/z$  [M + H]<sup>+</sup> calcd for C<sub>23</sub>H<sub>15</sub>N<sub>3</sub>O<sub>7</sub>: 445.0988, found: 445.0994. Purity: 97%.

**4-Benzoyl-1-(2,4-dimethoxyphenyl)-3-hydroxy-5-(4-nitrophenyl)-1,5-dihydro-2H-pyrrol-2-one (5.60).**

Prepared from ethyl 2,4-dioxo-4-phenylbutanoate (250 mg, 1.14 mmol), 4-nitrobenzaldehyde (172 mg, 1.14 mmol) and 2,4-dimethoxyaniline (0.167 mL, 1.14 mmol). After solvent removal, the reaction mixture was triturated with diethyl ether. The solid residue was washed with diethyl ether and subsequently purified by preparative HPLC (5-95% ACN in 0.2% NH<sub>3</sub>, flow rate 60 mL/min). The collected fractions were freeze-dried, to give the title compound (278 mg, 53%) as a pale yellow solid. <sup>1</sup>H NMR (400 MHz, DMSO)  $\delta$  8.05 (d,  $J$  = 8.8 Hz, 2H), 7.7 – 7.77 (m, 2H), 7.54 – 7.64 (m, 3H), 7.46 (t,  $J$  = 7.6 Hz, 2H), 7.10 (d,  $J$  = 8.7 Hz, 1H), 5.58 (d,  $J$  = 2.6 Hz, 1H), 5.44 (dd,  $J$  = 8.7, 2.6 Hz, 1H), 5.07 (s, 1H), 3.78 (s, 3H), 3.71 (s, 3H). HRMS (ESI)  $m/z$  [M + H]<sup>+</sup> calcd for C<sub>25</sub>H<sub>20</sub>N<sub>2</sub>O<sub>7</sub>: 461.1349, found: 461.1330. Purity: 99%.

**2-(3-(3-Benzoyl-4-hydroxy-2-(4-nitrophenyl)-5-oxo-2,5-dihydro-1H-pyrrol-1-yl)phenyl)acetic acid (5.61).**

Prepared from ethyl 2,4-dioxo-4-phenylbutanoate (200 mg, 0.91 mmol), 4-nitrobenzaldehyde (110 mg, 0.73 mmol) and 2-(3-aminophenyl)acetic acid (137 mg, 0.91 mmol). After solvent removal, the crude product was purified by preparative HPLC (5–95% ACN with 0.2 M NH<sub>3</sub>, flow rate 30 mL/min). Collected fractions were freeze-dried, to give the title compound (111 mg, 25.7%) as an off-white solid. HRMS (ESI)  $m/z$  [M + H]<sup>+</sup> calcd for C<sub>25</sub>H<sub>18</sub>N<sub>2</sub>O<sub>7</sub>: 459.1192, found: 459.1193.

**1-([1,1'-Biphenyl]-3-yl)-4-benzoyl-3-hydroxy-5-(4-nitrophenyl)-1,5-dihydro-2H-pyrrol-2-one (5.62).** Prepared from ethyl 2,4-dioxo-4-phenylbutanoate (250 mg, 1.14 mmol), 4-nitrobenzaldehyde (172 mg, 1.14 mmol) and [1,1'-biphenyl]-3-amine (193 mg, 1.14 mmol). After solvent removal, the reaction mixture was triturated with diethyl ether. The solid residue was washed with diethyl ether and subsequently purified by preparative HPLC (5-95% ACN in 0.2% NH<sub>3</sub>, flow rate 60 mL/min). The collected fractions were freeze-dried, to give the title compound (131 mg, 24%) as a pale yellow solid. <sup>1</sup>H NMR (600 MHz, DMSO) δ 8.02 (d, *J* = 8.4 Hz, 2H), 7.91 (s, 1H), 7.65 – 7.77 (m, 4H), 7.53 – 7.64 (m, 3H), 7.41 – 7.49 (m, 3H), 7.32 – 7.41 (m, 5H), 5.43 (s, 1H). HRMS (ESI) *m/z* [M + H]<sup>+</sup> calcd for C<sub>29</sub>H<sub>20</sub>N<sub>2</sub>O<sub>5</sub>: 477.1450, found: 477.1449. Purity: 99%.

**4-Benzoyl-3-hydroxy-1-(naphthalen-1-yl)-5-(4-nitrophenyl)-1,5-dihydro-2H-pyrrol-2-one (5.63).** Prepared from ethyl 2,4-dioxo-4-phenylbutanoate (250 mg, 1.14 mmol), 4-nitrobenzaldehyde (172 mg, 1.14 mmol) and naphthalen-1-amine (163 mg, 1.14 mmol). After solvent removal, the crude mixture was dissolved in DCM and washed with aq HCl 1 M (3x). The crude was then back-extracted with NaOH 1M (3x). The combined aqueous layers were made acidic with aq HCl 1 M, extracted with DCM (3x) and then solvent was removed under vacuum. The solid residue was subsequently purified by preparative HPLC (5-95% ACN in 0.2% NH<sub>3</sub>, flow rate 60 mL/min). The collected fractions were freeze-dried, to give the title compound (2 mg, 0.5%) as a pale yellow solid. HRMS (ESI) *m/z* [M + H]<sup>+</sup> calcd for C<sub>27</sub>H<sub>18</sub>N<sub>2</sub>O<sub>5</sub>: 451.1294, found: 451.1284. Purity: 99%.

### 5.8.3 Fluorescence Polarization (FP)

PPI stabilization measurements were performed in FP buffer (10 mM HEPES, 150 mM NaCl, 0.05% TWEEN 20, pH 7.4), using black, flat-bottomed 384-well microplates (Greiner Bio-One, model n. 784076) in a final sample volume of 12 μL. Following 1 h incubation at room temperature, plates were read on an PHERAstar plate reader (BMG Labtech, Ortenberg, Germany) for FP signal (filter set λ<sub>ex</sub> 485 nm, λ<sub>em</sub> 520 nm). Dilution series of compounds (10 mM DMSO stock solution) were added to a solution of FITC-**5.2** or FAM-**5.3** (10 nM) and 14-3-3ζ protein (50 nM for ERα(pT<sup>594</sup>)/FITC-**5.2** and 30 μM for CaMKK2(pS<sup>100</sup>)/FAM-**5.3**, corresponding to approximately 20% occupancy of 14-3-3 by FITC-**5.2** or FAM-**5.3**). Final DMSO concentration was 2% (vol/vol). All experiments were performed in two or more independent replicates (*n* ≥ 2), unless otherwise stated. Data reported are at end point. EC<sub>1,2</sub> and EC<sub>50</sub> values were obtained from fitting the data with a four-parameter logistic model (4PL). With the exception of compounds for which a EC<sub>50</sub> could be defined, for all the others a top value was set to 3.92-fold for ERα (corresponding to the saturation value, i.e. the max stabilization value, of Fusicoccin-A at 200 μM) and to 2.75-fold (corresponding to the saturation value, i.e. the max stabilization value, of (*R*)-**5.1** at 200 μM).<sup>10</sup> The software used for model fitting was GraphPad Prism version 8.3.0 for Windows, GraphPad Software, San Diego, California USA, www.graphpad.com. Error bars indicate standard deviation of individual measurements. 95% confidence intervals (CI) were reported as calculated from GraphPad Prism.

### 5.8.4 Surface Plasmon Resonance (SPR)

Unless otherwise stated, SPR measurements were performed on a Biacore 3000 (GE Healthcare) using as running buffer 10 mM HEPES, 150 mM NaCl, 0.05% TWEEN 20, pH 7.4. 14-3-3ζ protein was immobilized on a CMD200M Biacore Sensor Chip (XanTec Bioanalytics GmbH, Düsseldorf, Germany) at approximately 4000 RUs using EDC/NHS coupling chemistry. Phosphopeptides **5.2** or **5.3** (50 nM and 30 μM respectively in running buffer) and test compounds (dissolved in running

## CHAPTER 5

buffer and prepared from 10 mM DMSO stock solution to afford final test concentration and 1% final DMSO concentration) were premixed and injected at a flowrate of 20  $\mu\text{L}/\text{min}$  and 20  $^{\circ}\text{C}$  for 60 s or 120 s in running buffer. All experiments were performed in at least two independent replicates ( $n \geq 2$ ), unless otherwise stated. For each curve, the values at equilibrium response (*i.e.* binding coverage) were extracted and fitted using a four-parameter logistic model (4PL) using GraphPad Prism version 8.3.0 for Windows, GraphPad Software, San Diego, California USA, [www.graphpad.com](http://www.graphpad.com). Error bars indicate standard deviation of individual measurements.

### 5.8.5 Analytical ultracentrifugation

Sedimentation velocity (SV) experiments were performed using a ProteomLab<sup>TM</sup> XL-I analytical ultracentrifuge (Beckman Coulter). Samples were dialyzed against buffer containing 50 mM Tris-HCl (pH 7.5), 150 mM NaCl, and 1 mM tris(2-carboxyethyl) phosphine (TCEP) before analysis. For experiments in the presence of (R)-5.1 (20  $\mu\text{M}$ ), 10 mM  $\text{MgCl}_2$  was added to the above-mentioned buffer. Buffer density, viscosity, and partial specific volume of all proteins were estimated using the program SEDNTERP (<http://sednterp.unh.edu/>). SV experiments were conducted in charcoal-filled Epon centerpieces with 12-mm optical path length, at 20  $^{\circ}\text{C}$ , and at 42,000 rpm rotor speed (An-50 Ti rotor, Beckman Coulter), and all sedimentation profiles were recorded with interference and absorption optics (280 nm).

The analysis of mixtures of FL-pCaMKK2 and 14-3-3 $\gamma$  at various molar ratios was performed with 0.3–30  $\mu\text{M}$  FL-pCaMKK2 and 6  $\mu\text{M}$  14-3-3 $\gamma$ . The sedimentation coefficients  $c(s)$  distributions were calculated from the raw interference data using SEDFIT software package. The procedure was followed by integration of calculated distributions to establish the weight-average  $s$ -values ( $s_w$ ). Calculated  $s_w$  values were plotted as a function of FL-pCaMKK2 concentration to construct  $s_w$  isotherms. Obtained isotherms were fitted with  $A + B \rightleftharpoons AB$  model as implemented in the SEDPHAT software package with previously known  $s$  values of each component. Resulting parameters were verified and loading concentrations were corrected using global Lamm equation modelling also implemented in the SEDPHAT software.<sup>23-24</sup>

### 5.8.6 Protein expression and purification

14-3-3 $\zeta$  was expressed and purified as previously reported.<sup>27</sup>

14-3-3 $\gamma$  was expressed and purified as previously reported.<sup>13</sup>

CaMKK2 (residues 93 – 517, FL-pCaMKK2), was expressed and purified and phosphorylated at the pS<sup>100</sup> and pS<sup>511</sup> sites as previously reported.<sup>13</sup>

### 5.8.7 Peptide synthesis and characterization

ER $\alpha$ (pT<sup>594</sup>) phosphopeptide **5.2** (AEGFPApTV-COOH), CaMKK2(pS<sup>100</sup>) phosphopeptide **5.3** (GSLSARKLpSLQER) and fluorescein-labelled CaMKK2(pS<sup>100</sup>) phosphopeptide FAM-**5.3** were purchased from Chinese Peptide Company Inc. (Hangzhou, China). FITC-labeled ER $\alpha$ (pT<sup>594</sup>) phosphopeptide FITC-**5.2** was synthesized according to ref.<sup>10</sup>

### 5.8.8 In silico experiments

In silico experiments were performed using Schrödinger's Maestro software (version 11.4). X-ray crystal structures of 14-3-3 crystallized with ER $\alpha$ (pT<sup>594</sup>) or CaMKK2(pS<sup>100</sup>) was obtained from the PDB bank (PDB ID: 6TJM and 6EWW, respectively).

## CHAPTER 5

*Protein preparation.* Protein Preparation Wizard with default settings was used to prepare the imported X-ray crystal structures. Standard procedures for the preprocessing was carried out (preprocessed by assigning bond orders, adding hydrogens, maintaining all waters within 15 Å from het groups, and generating het states using Epik at pH 7.0±2.0). Magnesium ion in the binding pocket of the 6TJM-structure was removed.

*Ligand Preparation.* Ligands were prepared for modeling using LigPrep with default settings. OPLS3e was used for ligand optimization and all possible states generated at pH 7.0±2.0 using Epik with desalting and generation of tautomers. Chiralities were retained or varied (generating all possible stereoisomeric combinations).

*Docking Grid Generation.* The Receptor Grid Generation tool in Maestro with default settings was used for docking grid generation. The ligand was identified in the complex. Van der Waals radius scaling was performed with a scaling factor of 1.0 and partial charge cutoff of 0.25. The center and size of the enclosing box were defined based on the centroid and size of the ligand.

*Docking and Scoring.* Glide with default settings was used for ligand docking and scoring. Prepared ligands were selected and van der Waals radi scaled to 0.80 with a partial charge cutoff of 0.15. Precision mode was set to SP (standard precision). Ligand sampling was set to flexible, with sampling of nitrogen inversion and ring conformations. Epik state penalties were added to the docking score. Docking minimization was performed on 10 poses per ligand. Glide docking performed with a receptor and ligand van der Waals scaling of 0.50, the number of poses set to 5-10, and residues within 5.0 Å of the ligand pose refined and side chains optimized. The highest scoring pose (selected by Glide based on DScore and Emodel) was used for evaluation of docking results, but the remaining poses were also analyzed.

### 5.8.9 X-ray crystallography

*X-ray crystallography.* Crystals of the ternary complexes were grown by mixing 12.5 mg/mL 14-3-3 $\sigma\Delta$ C with **5.2** in a molar ratio of 1:2 in 10 mM HEPES pH 7.4, 150 mM NaCl, 2 mM BME and 2 mM of the compound of interest and incubating overnight at 277 K. The formed complex was then set up for crystallization by mixing 1:1 (v/v) 0.1 M Tris, pH 7.0, 0.2 M magnesium chloride hexahydrate and 10 % v/v PEG 8000 and incubating in a sitting drop at 277 K. Crystals grew within a week and were cryoprotected by adding a grain of sucrose to the crystallization drop and incubating for 10 minutes. Crystals were then fished and stored in liquid nitrogen. Data collection and processing are described in the next section. The crystal structure of **5.35** was deposited in the Protein Data Bank (PDB ID 6YSM).

*Data collection and analysis.* X-ray diffraction data for both complexes was collected at 100 K on a Rigaku Micromax-003 sealed tube X-ray source and a Dectris Pilatus 200K detector. The data was indexed, integrated, scaled and merged using xia2 DIALS.<sup>29</sup> Phasing was done by molecular replacement using Phaser<sup>30</sup> and PDB 4JC3 as a starting model and was followed by iterative rounds of refinement and manual model building using Phenix.Refine<sup>31</sup> and Coot,<sup>32</sup> respectively. Model validation was performed using MolProbity.<sup>33</sup> Figures were created using PyMol. See Table S5.1 for data collection and refinement statistics.

**Table S5.1.** XRD statistics

	<b>14-3-3<math>\sigma</math><math>\Delta</math>C/ER<math>\alpha</math>/5.35</b>	<b>14-3-3<math>\sigma</math><math>\Delta</math>C/ER<math>\alpha</math>/5.20</b>
PDB code	6YSM	-
<b>Data collection</b>		
Resolution ( $\text{\AA}$ ) <sup>a</sup>	2.38 (2.42 – 2.38)	2.50 (2.54 – 2.50)
Space group	C222	C222
Cell parameters ( $\text{\AA}$ ) <sup>b</sup>	a = 63.84, b = 151.08, c = 77.72  $\alpha = \beta = \gamma = 90^\circ$	A = 64.17, b = 151.62, c = 78.95  $\alpha = \beta = \gamma = 90^\circ$
$R_{\text{merge}}$ <sup>a,b</sup>	0.148 (0.488)	0.153 (0.579)
Average $I/\sigma(I)$ <sup>a,b</sup>	5.98 (1.52)	6.02 (1.71)
$CC_{1/2}$ (%) <sup>a,b,c</sup>	98.2 (92.8)	98.4 (89.9)
Completeness (%) <sup>a,b</sup>	98.4 (99.0)	98.4 (92.1)
Redundancy <sup>a,b</sup>	5.7 (5.2)	6.0 (6.2)
<b>Refinement</b>		
Number of protein/solvent/ligand atoms	1869/224/31	1827/161/35
$R_{\text{work}}/R_{\text{free}}$ (%)	22.8/25.35	27.53/32.96
Unique reflections used in refinement	15977	13480
R.m.s. deviations from ideal values bond lengths ( $\text{\AA}$ ) / bond angles ( $^\circ$ )	0.008/0.850	0.002/0.450
Average protein/solvent/ligand B-factor ( $\text{\AA}^2$ )	46398/45.81/77.76	53.66/53.08/77.39
Ramachandran favored (%)	96.40	97.31
Ramachandran allowed (%)	3.60	2.24
Ramachandran outliers (%)	0	0.45

(a) Number in parentheses is for the highest resolution shell

(b) As reported by xia2 DIALS.

(c)  $CC_{1/2}$  = Pearson's intradataset correlation coefficient, as described by Karplus and Diederichs.

## CHAPTER 5

### 5.9 REFERENCES

1. Andrei, S. A.; Sijbesma, E.; Hann, M.; Davis, J.; O'Mahony, G.; Perry, M. W. D.; Karawajczyk, A.; Eickhoff, J.; Brunsveld, L.; Doveston, R. G.; Milroy, L.-G.; Ottmann, C. Stabilization of protein-protein interactions in drug discovery. *Expert Opinion on Drug Discovery* **2017**, *12* (9), 925-940.
2. Andrei, S. A.; Sijbesma, E.; Hann, M.; Davis, J.; O'Mahony, G.; Perry, M. W. D.; Karawajczyk, A.; Eickhoff, J.; Brunsveld, L.; Doveston, R. G.; Milroy, L. G.; Ottmann, C. Stabilization of protein-protein interactions in drug discovery. *Expert Opin. Drug Discovery* **2017**, *12* (9), 925-940.
3. Surade, S.; Blundell, T. L. Structural Biology and Drug Discovery of Difficult Targets: The Limits of Ligandability. *Chem. Biol.* **2012**, *19* (1), 42-50.
4. Stevers, L. M.; Sijbesma, E.; Botta, M.; MacKintosh, C.; Obsil, T.; Landrieu, I.; Cau, Y.; Wilson, A. J.; Karawajczyk, A.; Eickhoff, J.; Davis, J.; Hann, M.; O'Mahony, G.; Doveston, R. G.; Brunsveld, L.; Ottmann, C. Modulators of 14-3-3 Protein-Protein Interactions. *J. Med. Chem.* **2018**, *61* (9), 3755-3778.
5. Aitken, A. 14-3-3 proteins: A historic overview. *Semin. Cancer Biol.* **2006**, *16* (3), 162-172.
6. Fu, H.; Subramanian, R. R.; Masters, S. C. 14-3-3 proteins: structure, function, and regulation. *Annu. Rev. Pharmacool. Toxicol.* **2000**, *40* (1), 617-47.
7. Pozuelo Rubio, M.; Geraghty, K. M.; Wong, B. H.; Wood, N. T.; Campbell, D. G.; Morrice, N.; Mackintosh, C. 14-3-3-affinity purification of over 200 human phosphoproteins reveals new links to regulation of cellular metabolism, proliferation and trafficking. *Biochem. J* **2004**, *379* (Pt 2), 395-408.
8. Pennington, K. L.; Chan, T. Y.; Torres, M. P.; Andersen, J. L. The dynamic and stress-adaptive signaling hub of 14-3-3: emerging mechanisms of regulation and context-dependent protein-protein interactions. *Oncogene* **2018**, *37* (42), 5587-5604.
9. Foote, M.; Zhou, Y. 14-3-3 proteins in neurological disorders. *Int. J. Biochem. Mol Biol.* **2012**, *3* (2), 152-64.
10. Bosica, F.; Andrei, S. A.; Neves, J. F.; Brandt, P.; Gunnarsson, A.; Landrieu, I.; Ottmann, C.; O'Mahony, G. Design of Drug-Like Protein-Protein Interaction Stabilizers Guided By Chelation-Controlled Bioactive Conformation Stabilization. *Chem. – Eur. J.* **2020**, *26* (31), 7131-7139.
11. Richter, A.; Rose, R.; Hedberg, C.; Waldmann, H.; Ottmann, C. An Optimised Small-Molecule Stabiliser of the 14-3-3–PMA2 Protein-Protein Interaction. *Chem. – Eur. J.* **2012**, *18* (21), 6520-6527.
12. De Vries-van Leeuwen, I. J.; da Costa Pereira, D.; Flach, K. D.; Piersma, S. R.; Haase, C.; Bier, D.; Yalcin, Z.; Michalides, R.; Feenstra, K. A.; Jiménez, C. R.; de Greef, T. F. A.; Brunsveld, L.; Ottmann, C.; Zwart, W.; de Boer, A. H. Interaction of 14-3-3 proteins with the Estrogen Receptor Alpha F domain provides a drug target interface. *Proc. Natl. Acad. Sci.* **2013**, *110* (22), 8894-8899.
13. Psenakova, K.; Petivalska, O.; Kylarova, S.; Lentini Santo, D.; Kalabova, D.; Herman, P.; Obsilova, V.; Obsil, T. 14-3-3 protein directly interacts with the kinase domain of calcium/calmodulin-dependent protein kinase kinase (CaMKK2). *Biochim. Biophys. Acta Gen. Subj.* **2018**, *1862* (7), 1612-1625.
14. Nepali, K.; Lee, H.-Y.; Liou, J.-P. Nitro-Group-Containing Drugs. *J. Med. Chem.* **2019**, *62* (6), 2851-2893.
15. Avendano, C.; Menendez, J. C., In *Medicinal Chemistry of Anticancer Drugs 2nd edition*, Elsevier Science: 2015; p 768.

## CHAPTER 5

16. Rose, R.; Erdmann, S.; Bovens, S.; Wolf, A.; Rose, M.; Hennig, S.; Waldmann, H.; Ottmann, C. Identification and structure of small-molecule stabilizers of 14-3-3 protein-protein interactions. *Angew. Chem. Int. Ed.* **2010**, *49* (24), 4129-32.
17. Obsil, T.; Ghirlando, R.; Klein, D. C.; Ganguly, S.; Dyda, F. Crystal Structure of the 14-3-3z:Serotonin N-Acetyltransferase Complex: A Role for Scaffolding in Enzyme Regulation. *Cell* **2001**, *105* (2), 257-267.
18. Sluchanko, N. N.; Beelen, S.; Kulikova, A. A.; Weeks, S. D.; Antson, A. A.; Gusev, N. B.; Strelkov, S. V. Structural Basis for the Interaction of a Human Small Heat Shock Protein with the 14-3-3 Universal Signaling Regulator. *Structure* **2017**, *25* (2), 305-316.
19. Kondo, Y.; Ognjenović, J.; Banerjee, S.; Karandur, D.; Merk, A.; Kulhanek, K.; Wong, K.; Roose, J. P.; Subramaniam, S.; Kuriyan, J. Cryo-EM structure of a dimeric B-Raf:14-3-3 complex reveals asymmetry in the active sites of B-Raf kinases. *Science* **2019**, eaay0543.
20. Ottmann, C.; Marco, S.; Jaspert, N.; Marcon, C.; Schauer, N.; Weyand, M.; Vandermeeren, C.; Duby, G.; Boutry, M.; Wittinghofer, A.; Rigaud, J.-L.; Oecking, C. Structure of a 14-3-3 Coordinated Hexamer of the Plant Plasma Membrane H<sup>+</sup>-ATPase by Combining X-Ray Crystallography and Electron Cryomicroscopy. *Molecular Cell* **2007**, *25* (3), 427-440.
21. Cole, J. L.; Lary, J. W.; P. Moody, T.; Laue, T. M., Analytical Ultracentrifugation: Sedimentation Velocity and Sedimentation Equilibrium. In *Methods in Cell Biology*, Academic Press: 2008; Vol. 84, pp 143-179.
22. Zhao, H.; Brautigam, C. A.; Ghirlando, R.; Schuck, P. Overview of Current Methods in Sedimentation Velocity and Sedimentation Equilibrium Analytical Ultracentrifugation. *Current Protocols in Protein Science* **2013**, *71* (1), 20.12.1-20.12.49.
23. Schuck, P. Size-Distribution Analysis of Macromolecules by Sedimentation Velocity Ultracentrifugation and Lamm Equation Modeling. *Biophys. J.* **2000**, *78* (3), 1606-1619.
24. Dam, J.; Velikovskiy, C. A.; Mariuzza, R. A.; Urbanke, C.; Schuck, P. Sedimentation Velocity Analysis of Heterogeneous Protein-Protein Interactions: Lamm Equation Modeling and Sedimentation Coefficient Distributions  $c(s)$ . *Biophys. J.* **2005**, *89* (1), 619-634.
25. Bosica, F. Personal communication. **2020**.
26. Neves, J. F.; Petrvalská, O.; Bosica, F.; Cantrelle, F. X.; Merzougui, H.; O'Mahony, G.; Obšil, T.; Landrieu, I. Phosphorylated full-length Tau interacts with 14-3-3 proteins via two short phosphorylated sequences, each occupying a binding groove of 14-3-3 dimer. *FEBS J.* **2020**, *submitted*.
27. Andrei, S. A.; de Vink, P.; Sijbesma, E.; Han, L.; Brunsveld, L.; Kato, N.; Ottmann, C.; Higuchi, Y. Rationally Designed Semisynthetic Natural Product Analogues for Stabilization of 14-3-3 Protein-Protein Interactions. *Angew. Chem. Int. Ed.* **2018**, *57* (41), 13470-13474.
28. Madhavi Sastry, G.; Adzhigirey, M.; Day, T.; Annabhimoju, R.; Sherman, W. Protein and ligand preparation: parameters, protocols, and influence on virtual screening enrichments. *Journal of Computer-Aided Molecular Design* **2013**, *27* (3), 221-234.
29. Winter, G. xia2: an expert system for macromolecular crystallography data reduction. *J. Appl. Crystallogr.* **2010**, *43* (1), 186-190.
30. McCoy, A. J.; Grosse-Kunstleve, R. W.; Adams, P. D.; Winn, M. D.; Storoni, L. C.; Read, R. J. Phaser crystallographic software. *J. Appl. Crystallogr.* **2007**, *40* (4), 658-674.
31. Adams, P. D.; Afonine, P. V.; Bunkoczi, G.; Chen, V. B.; Davis, I. W.; Echols, N.; Headd, J. J.; Hung, L.-W.; Kapral, G. J.; Grosse-Kunstleve, R. W.; McCoy, A. J.; Moriarty, N. W.; Oeffner, R.; Read, R. J.; Richardson, D. C.; Richardson, J. S.; Terwilliger, T. C.; Zwart, P. H. PHENIX: a comprehensive Python-based system for macromolecular structure solution. *Acta Crystallographica Section D* **2010**, *66* (2), 213-221.



## CHAPTER 5

32. Emsley, P.; Cowtan, K. Coot: model-building tools for molecular graphics. *Acta Crystallographica Section D* **2004**, *60* (12 Part 1), 2126-2132.
33. Chen, V. B.; Arendall, W. B., III; Headd, J. J.; Keedy, D. A.; Immormino, R. M.; Kapral, G. J.; Murray, L. W.; Richardson, J. S.; Richardson, D. C. MolProbity: all-atom structure validation for macromolecular crystallography. *Acta Crystallographica Section D* **2010**, *66* (1), 12-21.

# CHAPTER 6

Epilogue

## CHAPTER 6

### 6.1 INTRODUCTION

Targeting protein-protein interactions (PPIs) for potential therapeutic intervention has recently drawn a great deal of attention and effort, in both academia and industry. Over the last twenty years, the long-standing 'one target, one drug' drug discovery paradigm has started to shift towards 'multispecifics',<sup>1</sup> drugs that can target multiple entities at a time. Hence, the once deemed 'undruggable' PPIs have now become attractive tractable targets for the development of innovative therapeutic strategies.

In this sense, the PPIs of the 14-3-3 protein family represent a viable platform and have been here presented as a case study for the exploration of the molecular principles governing, particularly, PPI stabilization.

The main aim of this chapter is to highlight the relevant achievements of this thesis and frame them in the broader context of 14-3-3 PPI stabilization. By analysing in turn the individual components of what constitute a stabilized 14-3-3 PPI ternary complex (i.e. 14-3-3, the protein partner and the stabilizer), some of the current challenges and future prospects of the field are also discussed.

### 6.2 THE 14-3-3 PROTEIN

As discussed in chapter 1, human 14-3-3 proteins exist in seven different isoforms.<sup>2</sup> These seven isoforms share about 50% amino acid identity, with the majority of conserved residues present in the amphipathic binding groove that serves as the phosphate-binding pocket.<sup>3</sup> Due to the high degree of homology, it was initially thought that 14-3-3 isoforms were redundant and that, in the absence of one isoform, the others would act as backups.<sup>4</sup>

However, while the highly conserved nature of 14-3-3 structure among eukaryotes speaks to their essential role in regulating vital cell functions, the divergence into so many isoforms suggests additional, more specific roles for each one of them.<sup>5</sup> Indeed, different studies have reported a tissue-specific expression of 14-3-3 isoforms as well as isoform-specific functions.<sup>6-7</sup> Moreover, as 14-3-3s exist in cells as homo- and hetero-dimers, it has also been suggested that 14-3-3s can elicit different functions based on the dimerization pattern.<sup>8</sup>

For example, the heterodimer of 14-3-3 $\epsilon$  with  $\gamma$  or  $\zeta$ , previously known as mitochondrial import stimulating factor (MSF) is a unique cytoplasmic chaperone responsible for the ATP-dependent transport of preproteins to the mitochondrial surface prior to their import.<sup>9</sup> 14-3-3 $\gamma$  and  $\epsilon$  are the only isoforms able to bind to phospholipids in vesicles and cell membranes.<sup>10-11</sup>

Isoform-specific functions have been also studied in the context of disease. 14-3-3 $\zeta$ , for example, is highly overexpressed in a variety of cancers, including breast, prostate, lung, and stomach cancers. It acts as a suppressor of apoptosis and plays

a crucial role in tumorigenesis and cancer progression.<sup>12</sup> 14-3-3 $\sigma$  has been shown to be a tumour suppressor protein whose downregulation has been frequently detected in many types of cancer. Conversely, its increased expression causes resistance to anticancer agents.<sup>13</sup> It is worth pointing out that the distinction in terms of pro-/anti-apoptotic role of these two isoforms is not always clear-cut, as 14-3-3 $\sigma$  is for example overexpressed in certain types of cancer, where it has been shown to drive cell survival.<sup>14</sup> Other isoforms, such as 14-3-3 $\beta$  and 14-3-3 $\tau$  have been implicated as positive regulators of cell-cycle progression and tumorigenesis.<sup>15-16</sup>

As 14-3-3s are highly expressed in the brain, accounting for about 1% of the total amount of soluble brain proteins, their role in neurological disorders and neurodegeneration has been extensively studied.<sup>17-18</sup> Multiple studies in 14-3-3 isoform-specific knock-out (K/O) mouse models have been very helpful in understanding 14-3-3 isoform-specific functions in the brain.<sup>6</sup> For example, K/O of 14-3-3 $\epsilon$  or 14-3-3 $\zeta$  has been associated with schizophrenic behaviour, impaired learning and memory,<sup>19-21</sup> while K/O of 14-3-3 $\gamma$  with hyperactive and depressive-like behaviour.<sup>22</sup>

Given the multitude of different mechanisms in which specific 14-3-3 isoforms are involved, in the context of medicinal chemistry, the question whether compounds that target 14-3-3 PPIs need to be isoform specific remains unanswered. In chapter 1, different modulators of 14-3-3 PPIs were discussed. Despite their use as either inhibitors or stabilizers, their isoform-specificity has not been investigated. Owing to the highly conserved phospho-binding pockets of 14-3-3 isoforms, it is difficult to imagine any isoform selectivity by targeting this pocket. However, 14-3-3 $\sigma$  is the only isoform that contains a native surface-exposed cysteine at the edge of this pocket, which can be specifically targeted with covalent molecules, as already demonstrated.<sup>23</sup> Another potential strategy is to design a molecule that targets the divergent C-terminal region of a specific 14-3-3 isoform, that is the region with the highest variability throughout the 14-3-3 isoforms.<sup>3, 24</sup>

Conversely, in a cancer setting, a non-isoform specific molecule may be potentially desirable. As discussed in the preceding paragraph, many cancers rely on high levels of 14-3-3 $\zeta$  expression, but given the functional overlap between different isoforms, targeting the  $\zeta$  isoform specifically may simply allow for compensation by other 14-3-3 isoforms. Thus, a compound that targets multiple 14-3-3 isoforms may be an advantage in this context.<sup>2</sup>

### 6.3 THE BINDING PARTNER

14-3-3 proteins interact with a large number of protein partners with figures as high as 1,000 protein partners, either identified or predicted.<sup>25</sup> This huge number of binding partners, together with their similarities in binding sequences (i.e. mode I, II

and III binding motifs, see chapter 1), makes achieving 14-3-3 PPI stabilizer selectivity a daunting challenge.

In addition to this, as the number of newly reported 14-3-3 binding partners has been growing steadily, the knowledge about the spatio-temporal organization of the surrounding 14-3-3 interactome and the possible implications deriving from the modulation of these 14-3-3 PPIs are very much lagging behind.

Another possible limitation to the current state-of-the-art in the 14-3-3 PPI stabilisation field, is the use of phosphopeptide mimics as surrogates for full-length 14-3-3 binding partners in assays and biophysical experiments. To date, the use of short synthetic phosphopeptides (10-40 amino acids) is a commonly employed strategy in the study of 14-3-3 PPIs. This approach is, in our opinion, indeed very useful, as long as the model and reagents being studied is validated. In order to do that, two key questions need to be addressed.

*What about phosphorylation?* Pure, synthetic phosphopeptides of known sequence can be easily prepared from phosphorylated amino acid building blocks, but production of full-length phosphoproteins relies on kinases. Here, the challenge is two-fold. As full-length proteins can have multiple phosphorylation sites, the first thing to do is to ascertain which one(s) preferentially bind to 14-3-3. To do that, one would need site-specific phosphorylations in order to accurately study the individual phosphorylation sites. However, the endogenous kinase is not always known or compatible with known *in vitro* techniques.<sup>26</sup>

*Is the phosphopeptide predictive of the full-length protein?* We (see chapter 5) and other groups<sup>27</sup> have shown that phosphopeptides can indeed be successfully used as *in vitro* surrogates of their corresponding full-length proteins for the study of 14-3-3 PPIs and their stabilization. This, however, might not always be the case: even though phosphorylation is usually the main driver of affinity for 14-3-3 binding, a peptide simply cannot reproduce, for example, secondary interactions in the protein structure which can be too weak on their own, but activated upon complex formation with 14-3-3.<sup>28</sup>

For this reason, structural data are particularly needed for understanding the structural basis of binding and, hence, selectivity of specific partners. To date, only a limited number of 14-3-3 crystal structures with larger protein partners is available. The main difficulty lies on the fact that the partner proteins themselves are often multidomain proteins and thus challenging to crystallize and that most of the 14-3-3 binding sequences are localized in intrinsically disordered regions (IDRs), therefore making crystallographic analysis very difficult.<sup>29</sup> To overcome these inherent limitations, the use of complementary approaches to crystallography such as cryo-EM, which has been recently shown to be a powerful technique,<sup>30</sup> might be of great help in providing additional structural information required for the validation of a given 14-3-3 PPI.

## 6.4 THE STABILIZER

The discovery of tractable, drug-like small molecule stabilizers of 14-3-3 PPIs represents a current bottleneck in this field. The natural product Fc-A and other members of the fusicoccane family have been shown to stabilize many 14-3-3 PPIs,<sup>31-32</sup> but their synthetic complexity makes them not amenable to medicinal chemistry SAR studies. With this in mind, more tractable starting points were sought. As widely discussed in this thesis, this has been a non-trivial challenge.

Studies carried out on epibestatin and CHES in chapter 2 showed how the first is an artefact and the second is neither a binder nor a stabilizer.

Extensive work has been performed on the Pyrrolidone1 scaffold. In chapter 3 Pyrrolidone1, a reported stabilizer of the 14-3-3/PMA2 interaction,<sup>33</sup> was shown to be able to stabilize the 14-3-3/ER $\alpha$  and 14-3-3/CaMKK2 derived-phosphopeptide complexes, and that its (*R*) enantiomer is solely responsible for the stabilization effect on these 14-3-3 PPIs. In chapters 3 and 4, the conformational restriction induced by bivalent metal ions observed for Pyrrolidone1 and its analogues was investigated. Mimicry of this by an intramolecular hydrogen bond contained in a 6-membered pseudo-ring resulted in regioisomeric vinylogous amide analogues, which exhibited higher potency and stabilization effect than their parent compound in ER $\alpha$ , but not CaMKK2. Attempts made towards the synthesis of six-membered bicyclic rigid analogues did not yield the desired product, proving that the chemistry around the pyrrolidone scaffold can be complex. SAR studies performed in chapter 5 reported the discovery of Pyrrolidone1 derivatives with equal potency and stabilization effect and better selectivity than Pyrrolidone1, and with improved physicochemical properties, paving the way towards cell permeable compounds. Finally, full-length stabilization of (*R*)-Pyrrolidone1 against 14-3-3/CAMKK2 PPI was described.

Pyrrolidone1 is, to date, the best non fusicoccin-based druglike small molecule that was shown to stabilize a 14-3-3 PPI. The urge for novel scaffolds for the stabilization of 14-3-3 PPI is therefore highly desirable. To achieve that, it will be crucial to combine traditional drug discovery approaches such as high-throughput screening (HTS),<sup>33</sup> fragment-based drug design<sup>34</sup> and *in silico* techniques<sup>35</sup> with approaches such as disulphide-<sup>23</sup> or imine-based 'tethering',<sup>36</sup> supramolecular ligands<sup>37</sup> and dynamic combinatorial chemistry,<sup>38</sup> whose use in the study of PPIs has just started to find application.

Finally, selectivity across different 14-3-3 PPI is still an open question, in spite of the progress reported here. The key factor will be to develop stabilizers able to selectively interact with a given 14-3-3 binding partner through specific compound/14-3-3 protein partner interactions.

## 6.5 CONCLUSION

The aim of this thesis was to generate new potent and selective druglike compounds that will find use in elucidating the structural drivers and SAR principles governing 14-3-3 PPI stabilization. These new compounds will serve as chemical probes to investigate the 14-3-3 interactome and its underlying biology, with the aim of achieving pharmacological modulation of specific 14-3-3 PPIs.

In this sense, (*R*)-Pyrrolidone1 and its vinylogous amide derivatives represent the first proof of concept of potent and selective druglike 14-3-3 PPI stabilizers. The SAR studies performed in the pyrrolidone series also demonstrate the chemical tractability of this class of compounds, highlighting principles of selectivity against different 14-3-3 PPIs.

In order to achieve fully functional chemical probes, however, further chemical optimization is still required. In order for these molecules to be attractive for cell-based assays, better potency is needed, together with a higher degree of selectivity towards a wider panel of 14-3-3 PPIs. To achieve that, the use of metal-insensitive analogues of Pyrrolidone1 will be crucial for two reasons. First, due to the lack of control over metal ion concentration in biologically-relevant settings, the use of the metal-ion induced bioactive conformation may prove hard to exploit. Second, both the vinylogous amides and the six-membered bicyclic rigid analogues provide new exit vectors for the grow of the molecule in different directions within the Fc binding pocket, which can potentially lead to increased potency and selectivity. Finally, a more thorough investigation of the benzoyl moiety is required, as that is the portion closest to the 14-3-3 binding partner and therefore potentially the best position from which confer selectivity via specific interaction with the 14-3-3 binding partner.

## CHAPTER 6

### 6.6 REFERENCES

1. Deshaies, R. J. Multispecific drugs herald a new era of biopharmaceutical innovation. *Nature* **2020**, *580* (7803), 329-338.
2. Pennington, K. L.; Chan, T. Y.; Torres, M. P.; Andersen, J. L. The dynamic and stress-adaptive signaling hub of 14-3-3: emerging mechanisms of regulation and context-dependent protein-protein interactions. *Oncogene* **2018**, *37* (42), 5587-5604.
3. Gardino, A. K.; Smerdon, S. J.; Yaffe, M. B. Structural determinants of 14-3-3 binding specificities and regulation of subcellular localization of 14-3-3-ligand complexes: A comparison of the X-ray crystal structures of all human 14-3-3 isoforms. *Semin. Cancer Biol.* **2006**, *16* (3), 173-182.
4. Steinacker, P.; Schwarz, P.; Reim, K.; Brechlin, P.; Jahn, O.; Kratzin, H.; Aitken, A.; Wiltfang, J.; Aguzzi, A.; Bahn, E.; Baxter, H. C.; Brose, N.; Otto, M. Unchanged survival rates of 14-3-3 $\gamma$  knockout mice after inoculation with pathological prion protein. *Mol. Cell. Biol.* **2005**, *25* (4), 1339-1346.
5. Paul, A.-L.; Denison, F. C.; Schultz, E. R.; Zupanska, A. K.; Ferl, R. J. 14-3-3 phosphoprotein interaction networks - does isoform diversity present functional interaction specification? *Frontiers in plant science* **2012**, *3*, 190-190.
6. Fan, X.; Cui, L.; Zeng, Y.; Song, W.; Gaur, U.; Yang, M. 14-3-3 Proteins Are on the Crossroads of Cancer, Aging, and Age-Related Neurodegenerative Disease. *Int. J. Mol. Sci.* **2019**, *20* (14), 3518.
7. Aghazadeh, Y.; Papadopoulos, V. The role of the 14-3-3 protein family in health, disease, and drug development. *Drug Discovery Today* **2016**, *21* (2), 278-287.
8. Aitken, A. Functional specificity in 14-3-3 isoform interactions through dimer formation and phosphorylation. Chromosome location of mammalian isoforms and variants. *Plant Mol. Biol.* **2002**, *50* (6), 993-1010.
9. Hachiya, N.; Komiya, T.; Alam, R.; Iwahashi, J.; Sakaguchi, M.; Omura, T.; Mihara, K. MSF, a novel cytoplasmic chaperone which functions in precursor targeting to mitochondria. *The EMBO Journal* **1994**, *13* (21), 5146-5154.
10. Roth, D.; Morgan, A.; Martin, H.; Jones, D.; Martens, G. J. M.; Aitken, A.; Burgoyne, R. D. Characterization of 14-3-3 proteins in adrenal chromaffin cells and demonstration of isoform-specific phospholipid binding. *Biochem. J* **1994**, *301* (1), 305-310.
11. Bustad, H. J.; Skjaerven, L.; Ying, M.; Halskau, Ø.; Baumann, A.; Rodriguez-Larrea, D.; Costas, M.; Underhaug, J.; Sanchez-Ruiz, J. M.; Martinez, A. The Peripheral Binding of 14-3-3 $\gamma$  to Membranes Involves Isoform-Specific Histidine Residues. *PLOS ONE* **2012**, *7* (11), e49671.
12. Yang, X.; Cao, W.; Zhang, L.; Zhang, W.; Zhang, X.; Lin, H. Targeting 14-3-3zeta in cancer therapy. *Cancer Gene Ther.* **2012**, *19* (3), 153-159.
13. Li, Z.; Liu, J.-Y.; Zhang, J.-T. 14-3-3sigma, the double-edged sword of human cancers. *Am. J. Transl. Res.* **2009**, *1* (4), 326-340.
14. Neupane, D.; Korc, M. 14-3-3 $\sigma$  Modulates Pancreatic Cancer Cell Survival and Invasiveness. *Clin. Cancer Res.* **2008**, *14* (23), 7614-7623.
15. Takihara, Y.; Matsuda, Y.; Hara, J. Role of the  $\beta$  isoform of 14-3-3 proteins in cellular proliferation and oncogenic transformation. *Carcinogenesis* **2000**, *21* (11), 2073-2077.
16. Martin, D.; Brown-Luedi, M.; Chiquet-Ehrismann, R. Tenascin-C signaling through induction of 14-3-3 tau. *J. Cell Biol.* **2003**, *160* (2), 171-5.
17. Steinacker, P.; Aitken, A.; Otto, M. 14-3-3 proteins in neurodegeneration. *Seminars in Cell & Developmental Biology* **2011**, *22* (7), 696-704.



## CHAPTER 6

18. Kaplan, A.; Ottmann, C.; Fournier, A. E. 14-3-3 adaptor protein-protein interactions as therapeutic targets for CNS diseases. *Pharmacol. Res.* **2017**, *125*, 114-121.
19. Ikeda, M.; Hikita, T.; Taya, S.; Uruguchi-Asaki, J.; Toyo-oka, K.; Wynshaw-Boris, A.; Ujike, H.; Inada, T.; Takao, K.; Miyakawa, T.; Ozaki, N.; Kaibuchi, K.; Iwata, N. Identification of YWHAE, a gene encoding 14-3-3epsilon, as a possible susceptibility gene for schizophrenia. *Hum. Mol. Genet.* **2008**, *17* (20), 3212-3222.
20. Cheah, P. S.; Ramshaw, H. S.; Thomas, P. Q.; Toyo-oka, K.; Xu, X.; Martin, S.; Coyle, P.; Guthridge, M. A.; Stomski, F.; van den Buuse, M.; Wynshaw-Boris, A.; Lopez, A. F.; Schwarz, Q. P. Neurodevelopmental and neuropsychiatric behaviour defects arise from 14-3-3ζ deficiency. *Molecular Psychiatry* **2012**, *17* (4), 451-466.
21. Ramshaw, H.; Xu, X.; Jaehne, E. J.; McCarthy, P.; Greenberg, Z.; Saleh, E.; McClure, B.; Woodcock, J.; Kabbara, S.; Wiszniak, S.; Wang, T.-Y.; Parish, C.; van den Buuse, M.; Baune, B. T.; Lopez, A.; Schwarz, Q. Locomotor hyperactivity in 14-3-3ζ KO mice is associated with dopamine transporter dysfunction. *Translational Psychiatry* **2013**, *3* (12), e327-e327.
22. Kim, D. E.; Cho, C. H.; Sim, K. M.; Kwon, O.; Hwang, E. M.; Kim, H. W.; Park, J. Y. 14-3-3γ Haploinsufficient Mice Display Hyperactive and Stress-sensitive Behaviors. *Exp Neurol* **2019**, *28* (1), 43-53.
23. Sijbesma, E.; Hallenbeck, K. K.; Leysen, S.; de Vink, P. J.; Skora, L.; Jahnke, W.; Brunsveld, L.; Arkin, M. R.; Ottmann, C. Site-Directed Fragment-Based Screening for the Discovery of Protein-Protein Interaction Stabilizers. *J. Am. Chem. Soc.* **2019**, *141* (8), 3524-3531.
24. Kobayashi, H.; Ogura, Y.; Sawada, M.; Nakayama, R.; Takano, K.; Minato, Y.; Takemoto, Y.; Tashiro, E.; Watanabe, H.; Imoto, M. Involvement of 14-3-3 proteins in the second epidermal growth factor-induced wave of Rac1 activation in the process of cell migration. *J. Biol. Chem.* **2011**, *286* (45), 39259-68.
25. Diallo, K.; Opong, A. K.; Lim, G. E. Can 14-3-3 proteins serve as therapeutic targets for the treatment of metabolic diseases? *Pharmacol. Res.* **2019**, *139*, 199-206.
26. Xue, L.; Tao, W. A. Current technologies to identify protein kinase substrates in high throughput. *Front. Biol.* **2013**, *8* (2), 216-227.
27. Neves, J. F.; Petrvalská, O.; Bosica, F.; Cantrelle, F. X.; Merzougui, H.; O'Mahony, G.; Obšil, T.; Landrieu, I. Phosphorylated full-length Tau interacts with 14-3-3 proteins via two short phosphorylated sequences, each occupying a binding groove of 14-3-3 dimer. *FEBS J.* **2020**, *submitted*.
28. Sluchanko, N. N. Association of Multiple Phosphorylated Proteins with the 14-3-3 Regulatory Hubs: Problems and Perspectives. *J. Mol. Biol.* **2018**, *430* (1), 20-26.
29. Bustos, D. M.; Iglesias, A. A. Intrinsic disorder is a key characteristic in partners that bind 14-3-3 proteins. *Proteins: Structure, Function, and Bioinformatics* **2006**, *63* (1), 35-42.
30. Kondo, Y.; Ognjenović, J.; Banerjee, S.; Karandur, D.; Merk, A.; Kulhanek, K.; Wong, K.; Roose, J. P.; Subramaniam, S.; Kuriyan, J. Cryo-EM structure of a dimeric B-Raf:14-3-3 complex reveals asymmetry in the active sites of B-Raf kinases. *Science* **2019**, eaay0543.
31. Andrei, S. A.; de Vink, P.; Sijbesma, E.; Han, L.; Brunsveld, L.; Kato, N.; Ottmann, C.; Higuchi, Y. Rationally Designed Semisynthetic Natural Product Analogues for Stabilization of 14-3-3 Protein-Protein Interactions. *Angew. Chem. Int. Ed.* **2018**, *57* (41), 13470-13474.
32. Stevers, L. M.; Sijbesma, E.; Botta, M.; MacKintosh, C.; Obsil, T.; Landrieu, I.; Cau, Y.; Wilson, A. J.; Karawajczyk, A.; Eickhoff, J.; Davis, J.; Hann, M.; O'Mahony, G.; Doveston, R. G.; Brunsveld, L.; Ottmann, C. Modulators of 14-3-3 Protein-Protein Interactions. *J. Med. Chem.* **2018**, *61* (9), 3755-3778.

## CHAPTER 6

33. Rose, R.; Erdmann, S.; Bovens, S.; Wolf, A.; Rose, M.; Hennig, S.; Waldmann, H.; Ottmann, C. Identification and structure of small-molecule stabilizers of 14-3-3 protein-protein interactions. *Angew. Chem. Int. Ed.* **2010**, *49* (24), 4129-32.
34. Guillory, X.; Wolter, M.; Leysen, S.; Neves, J. F.; Kuusk, A.; Genet, S.; Somsen, B.; Morrow, J. K.; Rivers, E.; van Beek, L.; Patel, J.; Goodnow, R.; Schoenherr, H.; Fuller, N.; Cao, Q.; Doveston, R. G.; Brunsveld, L.; Arkin, M. R.; Castaldi, P.; Boyd, H.; Landrieu, I.; Chen, H.; Ottmann, C. Fragment-based Differential Targeting of PPI Stabilizer Interfaces. *J. Med. Chem.* **2020**, *63* (13), 6694-6707.
35. Sijbesma, E.; Visser, E.; Plitzko, K.; Thiel, P.; Milroy, L.-G.; Kaiser, M.; Brunsveld, L.; Ottmann, C. Structure-based evolution of a promiscuous inhibitor to a selective stabilizer of protein-protein interactions. *Nat. Commun.* **2020**, *11* (1), 3954.
36. Ottmann, C.; Wolter, M.; Valenti, D.; Cossar, P. J.; Levy, L. M.; Hristeva, S.; Genski, T.; Hoffmann, T.; Brunsveld, L.; Tzalis, D. Fragment Based Protein-Protein Interaction Stabilizers via Imine-Based Tethering. *Angew. Chem. Int. Ed.* *n/a* (n/a).
37. Gigante, A.; Sijbesma, E.; Sánchez-Murcia, P. A.; Hu, X.; Bier, D.; Bäcker, S.; Knauer, S.; Gago, F.; Ottmann, C.; Schmuck, C. A Supramolecular Stabilizer of the 14-3-3 $\zeta$ /ER $\alpha$  Protein-Protein Interaction with a Synergistic Mode of Action. *Angew. Chem. Int. Ed.* **2020**, *59* (13), 5284-5287.
38. Hartman, A. M.; Elgaher, W. A. M.; Hertrich, N.; Andrei, S. A.; Ottmann, C.; Hirsch, A. K. H. Discovery of Small-Molecule Stabilizers of 14-3-3 Protein-Protein Interactions via Dynamic Combinatorial Chemistry. *ACS Med. Chem. Lett.* **2020**, *11* (5), 1041-1046.

## CHAPTER 6

# SUMMARY

Rational design of small molecule 14-3-3 protein-protein interaction stabilizers

## SUMMARY

For the past 50 years the 'one target, one drug' concept has dominated the drug discovery industry. However, over the last decade, the classical view of drug action and therapeutic targets has started to shift towards a more holistic approach, as very often biological systems and diseases are considerably more complex than a two-variable equation (i.e. a target and a drug).

The wealth of knowledge collected with the advent of the "-omics" era (genomics, transcriptomics, proteomics) has enabled scientists to study DNA, RNA and proteins not only as individual cell components, but also in the context of networks, that is how they are interconnected with each other and how this complex molecular interplay is regulated.

In this context, the study of the protein-protein interaction (PPI) network, known as interactome, is of crucial importance, as proteins are involved in almost every process within a living cell. As such, PPIs are also relevant in the context of diseases and therefore represent an attractive target for new therapeutic opportunities.

When trying to modulate the protein interactome, one must consider its intrinsic dynamic nature, as not all PPIs occur all the time at the same location under all conditions. In order to properly function, Nature has evolved a fine spatio-temporal control of protein localization, which involves the induction of protein proximity.

Proximity, or the physical closeness of molecules, is a ubiquitous and essential mechanism in biology. Scientists have exploited this concept of inducing proximity by the means of molecular entities (for example a small molecule or antibody), also known as chemical inducers of proximity (CIP), that promote the formation of a non-native or stabilize a native PPI. This approach has found widespread use in biology and medicine. Indeed, the use of CIPs has spanned from tools to solve biological quandaries to drugs with novel mechanism of action.

Despite the many promising examples, the study of PPIs as a therapeutic target class is still in its early stages. In the effort to expand the chemical repertoire of CIPs, we found the concept of stabilizing native PPI complexes, already endowed by Nature itself of a functional response, particularly interesting. In this regard, our research has focused on the study of a particular class of PPIs, that is the interactome of the 14-3-3 proteins as subject for small molecule PPI stabilization.

14-3-3 proteins are a family of highly conserved adapter proteins involved in many relevant biological processes and as such they are also implicated in human diseases. Hence, the modulation of 14-3-3 PPI represents an attractive strategy for potential therapeutic intervention.

The work performed in this thesis therefore aimed at the study of 14-3-3 PPIs through the development of small molecule, druglike compounds that will find use in elucidating the structural drivers and SAR principles governing 14-3-3 PPI stabilization.

## SUMMARY

To begin, chapter 2 deals with epibestatin, one the two reported small molecule stabilizers of the 14-3-3/PMA2 PPI. Lack of consistent results during the structural and biophysical evaluation of epibestatin, unequivocally invalidated it as 14-3-3 PPI stabilizer. The buffer component CHES was proposed as possible interfering compound. A library of 35 CHES derivatives was synthesized in order to potentially improve its putative weak activity, but none of them showed any stabilization activity.

Chapter 3 analyzes the role of the other reported 14-3-3/PMA2 small molecule stabilizer, the racemic compound pyrrolidone1 (Pyr1). Pyr1 was found to be active also towards the 14-3-3/ER $\alpha$  and the 14-3-3/CaMKK2 PPIs. Testing of Pyr1 enantiomers in biophysical assays showed that only one enantiomer contributes to PPI stabilisation activity. An X-ray crystal structure was obtained and an unexpected non-protein interacting, ligand-chelated Mg<sup>2+</sup> was also observed, the leading to the discovery of metal ion-dependent 14-3-3 PPI stabilization potency. This effect, also characteristic of other bivalent metal ions, afforded a ~ 100-fold increase in the apparent PPI stabilization potency of Pyr1. Mimicry of this effect by intramolecular H-bonds led to the first potent, drug-like 14-3-3 PPI stabilizers.

The subsequent chapter 4 further describes the efforts made towards the mimicry of the ligand-specific metal ion effect. Here, the strategy envisioned was to achieve conformational restriction via six-membered bicyclic rigid analogues of Pyr1. Of the multiple synthetic routes pursued, only one was found to be promising. However, full structural characterization of the putative six-membered bicyclic rigid analogue of Pyr1 resulted to be complex and further experiments to fully elucidate the synthesized compound and its underlying chemistry are still required today.

Chapter 5 continues with the exploration of the synthetically tractable Pyr1 scaffold. A structure-activity relationship study on 59 newly synthesized Pyr1 derivatives was performed. Potency, stabilization effect and selectivity towards two different 14-3-3 PPIs was evaluated. Crystal structures of two of these derivatives were obtained, showing analogous binding mode of Pyr1 and also the presence of the Mg<sup>2+</sup> ion. Finally, the stabilization effect of (R)-Pyr1 was evaluated in the 14-3-3/CaMKK2 PPI using full-length CaMKK2 protein. A 27-fold stabilization was measured, therefore demonstrating that phosphopeptides can be successfully used as surrogates of full-length proteins in the study of 14-3-3-mediated PPIs.

In conclusion, this thesis describes the relevant results achieved in the development of potent and selective stabilizers of 14-3-3 PPIs. In doing so, it also illustrates the current challenges and future perspectives in the field 14-3-3 PPI stabilization. Altogether, the data here reported provide a solid foundation for a more thorough understanding of the structural drivers underlying 14-3-3 PPIs and will help in the future development of new 14-3-3 PPIs stabilizers.

## SUMMARY

# BIOGRAPHY



Francesco Bosica was born on January 26<sup>th</sup>, 1991 in Turin (Italy). He obtained his 5-year Master of Science (MSc) in Pharmaceutical Chemistry and Technologies from the University of Turin (Italy). His MSc dissertation dealt with the synthesis of potential small molecule modulators of Ten-eleven Translocation (TET) enzymes and was performed under the supervision of Prof. Massimo Bertinaria. During his MSc studies, Francesco had two Erasmus Traineeship

experiences. In the first, he focused on hospital pharmacy practices at the Birmingham Children's Hospital (UK) under the supervision of Mr. Jeff Aston. In the second, he worked on cycloaddition reactions under continuous conditions via highly reactive dipolar intermediates at the Department of Chemistry of the University of Cambridge (UK), supervised by Prof. Steven V. Ley.

In October 2016, he started his PhD in Medicinal Chemistry as part of the TASPPI project funded by the H2020 Marie Curie Actions of the European Commission at AstraZeneca (Sweden) under the supervision of Dr. Gavin O'Mahony. In January 2020, he moved to the Eindhoven University of Technology (The Netherlands) to complete his doctoral studies under the guidance of Dr. Christian Ottmann. His work focuses on small molecule stabilization of protein-protein interactions and the most important results of his research are highlighted in this thesis.





# LIST OF PUBLICATIONS

Neves, J. F.; Petrválská, O.; Bosica, F.; Cantrelle, F. X.; Merzougui, H.; O'Mahony, G.; Obšil, T.; Landrieu, I. Phosphorylated full-length Tau interacts with 14-3-3 proteins via two short phosphorylated sequences, each occupying a binding groove of 14-3-3 dimer. *FEBS J.* **2020**, *accepted*.

Bosica, F.; Andrei, S. A.; Neves, J. F.; Brandt, P.; Gunnarsson, A.; Landrieu, I.; Ottmann, C.; O'Mahony, G. Design of Drug-Like Protein–Protein Interaction Stabilizers Guided By Chelation-Controlled Bioactive Conformation Stabilization. *Chem. – Eur. J.* **2020**, *26* (31), 7131-7139.

Battilocchio, C.; Bosica, F.; Rowe, S. M.; Abreu, B. L.; Godineau, E.; Lehmann, M.; Ley, S. V. Continuous Preparation and Use of Dibromoformaldoxime as a Reactive Intermediate for the Synthesis of 3-Bromoisoxazolines. *Org. Process Res. Dev.* **2017**, *21* (10), 1588-1594.



# ACKNOWLEDGEMENTS

Looking back at these four years, sometimes I can't still believe that I have done such many things and met so many incredible people who, in one way or another, have helped me through this long journey that is a PhD.

First and foremost, I would like to thank my supervisor, Dr. Gavin O'Mahony. Gavin, I will never stop saying to my family and friends how lucky I was to be supervised by you. I have always been amazed by your widespread knowledge and familiarity in most of the aspects of medicinal chemistry. Your enthusiasm in trying to understand how things work has been contagious. Also, thank you for always looking at the glass half full, compensating a bit for my "let's keep the expectations low".

I would like to thank you Dr. Christian Ottmann, for his immense knowledge of the 14-3-3 world, the fruitful (and challenging) discussions had over the years, both scientific and not. I did enjoy the evening beers altogether chatting and laughing at the TASPPI meetings.

A special thanks to Prof. Tomáš Obšil for his support on the SV-AUC experiments and to Dr. Isabelle Landrieu for having allowed me to go to Lille to perform the protein NMR experiments.

I would also like to acknowledge each of my Committee Members, prof. M. Merckx, prof. L. Brunsveld, dr. A. Bach, prof. M. Waring, prof. A.R.A. Palmans and dr. F. Eduati for having accepted to be the opponents during my PhD defence.

To all my TASPPI colleagues, Leire, Marianna, Blaz, Domenico, Madita, Joao, Sonja, Claire, Federica, Alice, Lorenzo e Dario. What an experience we had! Travelling across Europe for meetings, late-night homework and presentations rehearsals, dinners, beers, wine and nights out. I truly enjoyed every moment we spent together, even if we could meet only for few days every half a year. Thanks to Blaz for your lasagne and for the long chats we had over the week I spent at your place. Grazie Lorenzo per le nostre pause caffè durante il lockdown, mi hanno aiutato parecchio. Grazie Dario, per tutte le occasioni in cui abbiamo riso e ci siamo lamentati di tu sai chi assieme. Grazie Dome per il fantastico tour di Praga. Grazie Alice per avermi sopportato per questi quattro anni, sempre disponibile a rispondere alle mie domande e ascoltare le mie sfuriate.

A big thanks to all my Astra colleagues, and particularly Rouven, Tom, Giulia, Elisa, Walter, Mark, David. My time at Astra has been amazing also because of you. Also, thank you Sebastian for your help with the crystallography, you have always been available to my many questions and I believe we could make a good team.

Alla mia coinqui preferita, Carmen. Grazie di tutto. Hai allietato un anno e mezzo della mia vita svedese, non credo ce l'avrei fatta senza di te e sicuramente sarebbe stato molto meno divertente. Ricorderò sempre i nostri lamenti, le nostre chiacchierate post cena, le spese assieme, i tuoi consigli e il tuo incessante supporto per qualsiasi cosa.

A Omar, grazie per esserci sempre stato, per essere venuto così spesso a trovarmi, grazie per le nostre serate, per le nostre vacanze, insomma, grazie un po' per tutto in realtà. A Bert, grazie soprattutto per tutti i momenti passati assieme in Olanda con le nostre notti e grazie per quella scena epica con il buttafuori quella sera in Svezia. A Paolo, non sei mai venuto a trovarmi, non so se te la perdono (scherzo), ma anche vedendoci poco, non sei mai mancato quando ne ho avuto bisogno o per una lunga chiacchierata. A Edo, grazie per quel weekend a Berlino e per tutti i passaggi negli ultimi mesi, negli ultimi anni c'è stato un riavvicinamento di cui sono profondamente felice. A Mastro, grazie per avermi introdotto ad alcune delle più belle serie tv, grazie per avermi fatto sentire come se nulla fosse cambiato dopo questi quattro anni, sei un vero amico. A Rolf, grazie per le nostre vacanze di surf, grazie per il bel weekend a Copenhagen, un bel ricordo nel grigiore nordico. A Fla, grazie per il tuo incessante entusiasmo nel fare le cose, è stato bello potersi rivedere e riavvicinarsi dopo così tanto tempo. Grazie a Ussy, sempre carico, sempre sul pezzo, il nostro intermezzo svedese è stato un piacevole ritorno ai tempi universitari. Grazie ai soliti, vecchi amici di sempre: Gama, Maggio, Matti, Tod, Mirch, Gali per avermi fatto sempre sentire a casa le poche volte che tornavo in quel di Casta beach.

Alla mia famiglia, un grazie infinito. Papi e Marti, grazie per esserci sempre stati in questi anni, sempre disponibili, sempre pronti ad accogliermi con il sorriso all'aeroporto. Marti, grazie per avermi accompagnato in tutti i miei giri. Era bello sapere che, spostandosi in un posto completamente nuovo con la prospettiva di non tornare a casa per mesi, tu eri lì ad aiutarmi. Papi, grazie per le telefonate settimanali, per esserti preso cura di me anche a distanza con gli immancabili pacchi, per sopportare i miei sbalzi di umore. A entrambi, siamo stati distanti geograficamente, ma sempre vicini nel cuore. Ai miei zii, le occasioni per vedersi sono ahimè state poche, ma il piacere dei nostri pranzi assieme è sempre stato impagabile. Vi voglio bene.

A Cami, last but not least, of course. Ci sei sempre stata fin dall'inizio, con una forza e un commitment senza pari, non lo dimenticherò mai. Grazie per avermi aiutato in questo percorso, non sarei arrivato dove sono senza di te.